Novel Approaches for Targeted Protein Degradation of Histone Deacetylases: Beyond Conventional E3 Ligase Recruitment

Dissertation

zur

Erlangung des Doktorgrades (Dr. rer. nat.)

der

Mathematisch-Naturwissenschaftlichen Fakultät

der

Rheinischen Friedrich-Wilhelms-Universität Bonn

vorgelegt von

Felix Feller

aus

Mettingen

Bonn 2025

Angefertigt mit Genehmigung der Mathematisch-Naturwissenschaftlichen Fakultät

der Rheinischen Friedrich-Wilhelms-Universität Bonn

Gutachter/Betreuer: Prof. Dr. Finn K. Hansen

Gutachter: Prof. Dr. Gerd Bendas

Tag der Promotion: 16.01.2026

Erscheinungsjahr: 2026

Die vorliegende Arbeit wurde in der Zeit von Januar 2021 bis August 2025 unter der Leitung von Herrn Prof. Dr. Finn K. Hansen am Pharmazeutischen Institut der Rheinischen Friedrich-Wilhelms-Universität Bonn angefertigt.

Die vorliegende Arbeit wurde ohne unzulässige Hilfe Dritter und ohne Benutzung anderer als der von mir kenntlich gemachten Hilfsmittel angefertigt. Alle indirekten oder direkten Zitate aus fremden Quellen wurden als solche kenntlich gemacht.

Table of Contents

List of Abbreviations

2-CTC	2-Chlorotrityl chloride
β-TrCP1	β-Transducin-repeat-containing protein

A

aa	Amino acids
AbTAC	Antibody-based proteolysis targeting chimera
acetyl-CoA	Acetyl-coenzyme A
AF-2	Activity function domain 2
Apaf-1	Apoptotic peptidase activator factor 1
ApoE4	Apolipoprotein E4
AR	Adrogen receptor
ATP	Adenosine triphosphate
ATTEC	Autophagosome-tethering compound
AUTAC	Autophagy-targeting chimera
AUTOTAC	Autophagy-targeting chimera
AbTAC	Antibody-based proteolysis targeting chimera

B

Bak	Bcl-2 antagonist/killer
Bax	Bcl-2 associated X protein
Bcl	B-cell lymphoma protein
BET	Bromodomain and extra-terminal domain
Bim	Bcl-2 interacting mediator of cell death
BiP	Binding immunoglobulin protein
BIR	Baculovirus IAP repeats
Boc_3Arg	*tert*-Butyl carbamate-protected arginine
BRCA1	Suppressor breast cancer 1
BRD4	Bromodomain containing protein 4
BTK	Bruton tyrosine kinase

C

CBL	Casitas B-lineage lymphoma
CBP	CREB-binding protein
CCL	CC-motif chemokine ligand
CD	Catalytic domain
CDK	Cyclin-dependent kinase
CDOCA-Me	Methyl 2-cyano-3,11-dioxo-18β-olean-1,12-dien-30-oate
CHIP	C-terminus of HSP70 interacting protein
cIAP	Cellular inhibitor of apoptosis protein
CI-M6PR	Cation-independent mannose-6-phosphate receptor
CK1α	Casein kinase 1α
CoREST	Co-repressor of REST
CRABP	Cellular retinol- and retinoic acid-binding protein
CRBN	Cereblon

CREB	Cyclic adenosine monophosphate response element-binding protein
CRL	Cullin-RING ligase
CTCL	Cutaneous T-cell lymphoma

D

DC_{50}	Half maximal degradation concentration
DCAF	DDB1-CUL4 associated factor
DDB1	DNA damage-binding protein 1
DDR	DNA damage response
DFMO	Difluoromethyl-1,3,4-oxadiazole
D_{max}	Maximal degradation
DMD	Duchenne muscular dystrophy
DNA	Deoxyribonucleic acid
DNMT	DNA (cytosine-5)-methyltransferases
DSB	Double-strand break
DUB	Deubiquitinase

E

E2F	E2-promoter binding factor
E6AP	E6-associated protein
EC_{50}	Half maximal effective concentration
eDHFR	*Escherichia coli* dihydrofolate reductase
EGF	Epithermal growth factor
EGFP	Enhanced green fluorescent protein
EGFR	Epidermal growth factor receptor
EMA	European Medicines Agency
ER	Estrogen receptor
EZH2	Enhancer of zeste homolog 2

F

FAD	Flavin adenine dinucleotide
FBP	F-box protein
FDA	United States Food and Drug Administration
FEM1	Feminization-1
FEM1B	Feminization-1 homolog b
FKBP12	FK506-binding protein 12

G

Gal4	Galactose-responsive transcription factor 4
GSPT1	G1 to S phase transition 1
GST-α1	Glutathione-S-transferase-α1

H

HaloTag	Haloalkane dehalogenase tag
HAT	Histone acetyltransferase
Hda1	Histone deacetylase-A1
HDAC	Histone deacetylase
HDLP	Histone deacetylase-like protein
HECT	Homologous to the E6AP carboxyl terminus
HIF	Hypoxia-inducible factor
HMT	Histone methyl transferase
HPLC	High-performance liquid chromatography
HPV	Human papilloma virus

$HRAS^{G12V}$	Harvey rat sarcoma virus mutant G12V
HSC	Heat-shock cognate
HSP	Heat shock protein
HyT	Hydrophobic-tagged

I

IAP	Inhibitor of apoptosis protein
IBR	In between RING
IC_{50}	Half maximal inhibitory concentration
IFN	Interferon
IKZF	Ikaros family zinc finger protein
IL	Interleukin
IMiD	Immunomodulatory imide drug
IκBα	Inhibitor of NF-κB α

K

KDM	Histone lysine demethylase
KRAS	Kirsten rat sarcoma virus

L

LC3	1B-light chain 3
LSD1	Lysine-specific demethylase 1
LYTAC	Lysosome- targeting chimera

M

M6Pn	Multiple serine-O-mannose-6-phosphonate
$(M6Pn\text{-}co\text{-}Ala)_n$	M6Pn-alanine copolymers
mAb	Monoclonal antibody
MDM2	Mouse double minute 2
MEF2	Myocyte enhancer factor-2
MetAP-2	Methionine aminopeptidase-2
MG	Molecular glue
MIER	Mesoderm induction early response
MM	Multiple myeloma
MRE11	Meiotic recombination 11 homolog
mRNA	Messanger ribonucleic acid
Myc	Myelocytomatosis viral incogene homolog

N

NAD	Nicotinamide adenine dinucleotide
NAE	NEDD8-activating enzyme
NCoR	Nuclear receptor co-repressor
NEDD8	Neural precursor cell expressed developmentally downregulated protein 8
NEHJ	Nonhomologous end joining
NES	Nuclear export signals
NF-κB	Nuclear factor κ-light chain enhancer of activated B-cells
NLS	Nuclear localization sequences
NMPA	National Medical Products Administration of China
NuRD	Nucleosome remodeling and deacetylase

P

PARP	Poly(adenosine diphosphate-ribose) polymerase

PD-L1	Programmed death-ligand 1
PEG	Polyethylene glycol
PHD finger	Plant homeodomain
PI	Propidium iodide
POI	Protein of interest
PPI	Protein-protein interaction
PROTAC	Proteolysis targeting chimera
PTCL	Peripheral T-cell lymphoma
PTM	Posttranslational modification

R

RAS	Rat sarcoma virus protein
RB	Retinoblastoma protein
RBM39	RNA binding motif protein 39
RBR	RING-in between RING
RBX	RING box protein
REST	Repressor element-1 silencing transcription factor
RING	Really interesting new gene
RNA	Ribonucleic acid
RNF	Ring finger protein
RP	Regulatory particle
Rpd3	Reduced potassium dependency 3

S

SALL4	Sal-like protein 4
SARS-CoV-2	Severe acute respiratory syndrome coronavirus 2
SCF	Skp1/2, Cul1 and FBP complex
SERD	Selective estrogen receptor degrader
SHMT2	Serine hydroxymethyltransferase 2
Sin3	Switch-independent protein 3
SIRT	Sirtuin
Skp	S-phase-kinase-associated protein
SMRT	Silencing mediator for retinoid and thyroid receptors
SNIPER	Specific and nongenetic IAP-dependent protein erasers

T

TFMO	Trifluoromethyl-1,2,4-oxadiazole
TGF-α	Tumor growth factor α
TIR1	Transport inhibitor response 1
TNF	Tumor necrosis factor
TP53	Transformation-related protein 53
TPD	Targeted protein degradation
TRAIL	Tumor necrosis factor-related apoptosis-inducing ligand

U

U-4CR	Ugi four-component reaction
Ub	Ubiquitin
UBE2M	Ubiquitin conjugating enzyme E2 M
UGT	Uridine 5'-diphospho-glucuronosyltransferase

UPR	Unfolded protein response
UPS	Ubiquitin–proteasome system

V

VEGF	Vascular endothelial growth factor
VHL	Von Hippel-Lindau

W

WDR	WD40 repeat

X

XIAP	X chromosome-linked IAP

Z

ZBG	Zinc binding group
ZnF-UBD	Zinc finger ubiquitin binding domain

List of Appendices

1 Introduction

1.1 Cancer & Epigenetics

Cancer is the second leading cause of death worldwide, with 20.0 million cases and 9.7 million deaths recorded in 2022. Neoplastic diseases have already surpassed cardiovascular diseases in terms of mortality in western societies. Moreover, global cancer incidence is projected to rise to 27.5 million cases by 2040.[1,2] Thus, the development of new cancer drugs is imperative, and novel therapeutic approaches are required to address these tremendous numbers.

There are hundreds of different types of cancer, which can be found in various human organs. Derived from normal cells, their cancer counterparts undergo multiple genetic changes transforming in a series of premalignant stages.[3] In rodent cells, at least two genetic changes are required to reach an oncogenic stage, whereas in human cells, this transformation is more complex and less easily induced.[4] Despite the significant diversity among human cancer types, they share a set of common aberrancies considered as cancer hallmarks. These hallmarks can be acquired in multiple orders and by various mechanisms but need to be reached to gain fully malignant cancer properties. It includes self-sufficiency in growth signals, insensitivity to anti-growth signals, evasion of apoptosis, limitless replicative potential, sustained angiogenesis, reprogramming of energy metabolism, avoiding immune destruction, as well as tissue invasion and metastasis (Fig. 1). These hallmarks can be accomplished by genome instability and mutation, as well as tumor-promoting inflammation. As cancer research progresses, the number of hallmarks and detailed knowledge of these may further expand, as it has been in the past.[5,6]

Normal cells rely on external signals for mitogenic growth, whereas cancer cells became autonomous by producing growth factors, e.g. epidermal growth factor (EGF) or transforming growth factor α (TGF-α), for autocrine stimulation. In addition, overexpression of growth factor receptors and mutations in downstream mediators, such as the rat sarcoma protein (RAS), which is mutated in up to 25% of human cancers, represents the most common ways of cancer cells to accomplish self-sufficiency in growth signals.[7] Beside the stimulation of growth, cancer has to develop resilience to restriction of proliferation. Tumor suppressors like retinoblastoma protein (RB) and the transcription factor p53 are often disabled to avoid cell cycle arrest and subsequent induction of apoptosis.[8] Furthermore, cancer cells evade apoptosis by the upregulation of B-cell lymphoma protein 2 (Bcl-2), inhibiting Bcl-2 associated X protein (Bax) and Bcl-2 antagonist/killer

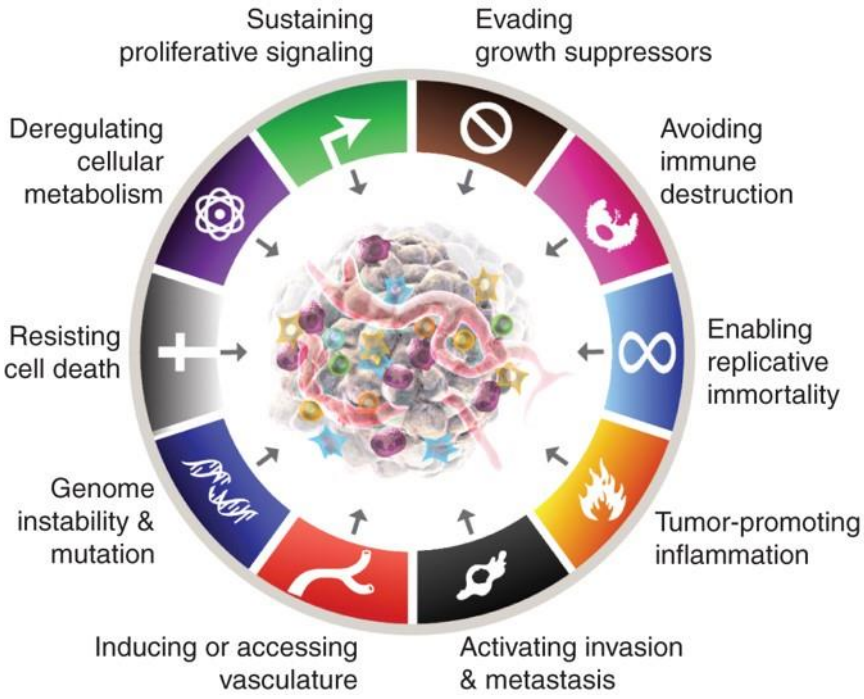

Figure 1. The hallmarks of cancer consisting of eight hallmark capabilities and two enabling characteristics (genome instability & mutation, and tumor-promoting inflammation), representing common cancer specifications to gain fully malignant cancer properties. Adapted and modified after D. Hanahan with permission of American Association for Cancer Research (License number 5995250718804).[6]

(Bak) and thereby apoptosis. Through upregulation of Bcl-2 inhibitor proteins (Noxa and Puma) p53 induces apoptosis, which offers additional targets for impaired function by mutations for tumorgenesis.[9] Another safety mechanism to prevent unlimited proliferation are telomeres protecting the ends of chromosomes. They determine proliferation success by their length as they erode through every cell division. Cancer cells encounter this issue by upregulation of telomerase, extending the telomeres, enabling immortalization.[10] This cancer mechanisms can lead to the macroscopic growth of neoplasms, which is limited to a diameter of approximately 1-2 mm, if the tumor is not able to stimulate angiogenesis. Like normal cells, tumor cells require nutrients and oxygen, but at a certain size diffusion is no longer sufficient to supply all the tumor cells. To overcome this, tumor cells tend to upregulate vascular endothelial growth factor A (VEGF-A) to induce the formation of new blood vessels for tumor vascularization. Starting with the permeabilization of nearby blood vessels, angiogenesis is highly regulated by multiple activators and inhibitors, as its usually quiescent in adult tissue, except in female reproductive organs or injured tissue.[11] Direct contact to blood vessels facilitates another cancer hallmark: tissue invasion and metastasis. By inactivation or downregulation of adhesion molecules like E-cadherin, cancer cells lose cell-to-cell contact, enabling the invasion into near blood vessels. However, N-cadherin is subject to increased expression as it promotes migration and interaction with stromal cells, enabling extravasation, the migration out of the vessel lumen into the surrounding tissues.[12,13]

Those and other mechanisms differ cancer cells from healthy tissue, driven by genetic instability, as well as aberrant epigenetic regulation. The consequences of genetic mutation are versatile and genetic instability is present in all stages of cancer. Most frequently effected is the tumor suppressor and DNA damage checkpoint gene tumor suppressor *TP53*, further supporting genetic instability, if its function is diminished.[14] However, oncogene upregulation and tumor suppressor gene silencing can occur without affecting the DNA sequence but by aberrant epigenetic changes that alter the accessibility of dedicated genes.

The term epigenetic or epigenotype was introduced in the 1940s by Conrad Waddington and first comprises the entire processing from the genotype into a specific phenotype.[15] The last 80 years of research elucidated the numerous machineries and processes translating the genotype into a phenotypic outcome, leading to a new definition. More recently, epigenetics is considered as the changes in gene function that are heritable through cell proliferation and do not change the DNA sequence, thereby determine gene expression patterns.[16]

Epigenetic changes can occur directly at the DNA. Methylation of cytosine to 5-methylcytosin exhibits the most frequently observed modification occurring to about 90% in the CpG dinucleotide (Fig. 2).[17] The methyl group is transferred by DNA (cytosine-5)-methyltransferases (DNMTs) and CpG dinucleotides can be clustered in islands. These CpG islands are located within promoters and recruit transcription factors. However, the methylation of cytosine leads to

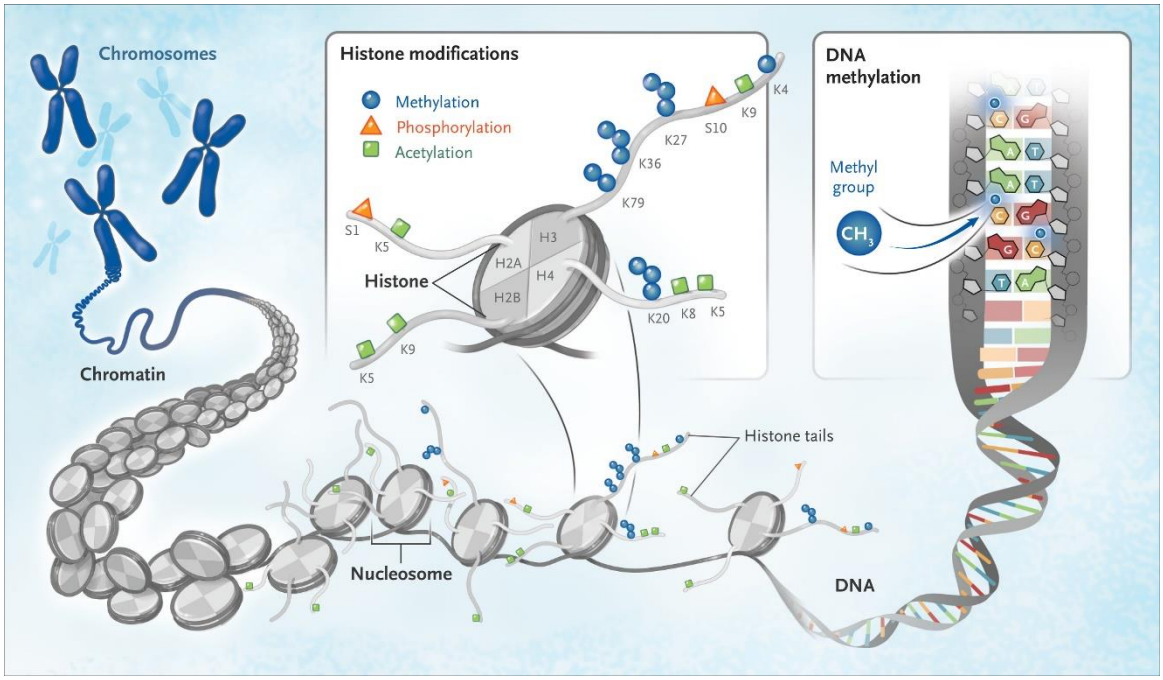

Figure 2. The DNA is wrapped in 1¾ turns around the histone core octamer (two copies of histones H2A, H2B, H3, and H4) forming the nucleosome with the linker DNA and histone H1 (not shown). Further condensation into chromatin-fibers result in the formation of chromosomes. Epigenetic modification can occur on DNA level in form of methylation of cytosine, or on histone level including, methylation, phosphorylation, and acetylation. PTMs of histones are located at the outstanding tail. Reproduced with permission from Bates,[22] Copyright Massachusetts Medical Society.

silencing of the related genes. Global hypomethylation in combination with local hypermethylation of tumor suppressors was observed in cancer cells.[18]

Since DNA is tightly packaged and associated with multiple proteins, various mechanisms can facilitate epigenetic modifications. The nucleosome is the basic packaging subunit and consists of a linker DNA, linker histone H1 and the core, which again is composed of the four core histones each in two copies and a 147 base pairs segment of DNA. The two copies of histones H2A, H2B, H3, and H4 arrange in a spool-like octamer and the DNA is wrapped in 1¾ turns around this core (Fig. 2). The histone octamer can compensate the negative charge of DNA due to the high content of basic amino acids, positively charged under physiological conditions, enabling electrostatic interactions that prevent transcription.[19,20] The linker histone H1 organizes DNA into a 30 nm chromatin-fiber, facilitating higher-order condensation through fiber-fiber interactions, ultimately leading to chromosome formation.[21] Most of the positively charged amino acids are located in the N-terminal tail of histones, standing out of the spool and are prone for posttranslational modifications (PTMs), including methylation, acetylation, phosphorylation, and ubiquitination. The enzymes that regulate these modifications are categorized into writers, readers, and erasers. Writers, including histone methyltransferases (HMTs) and histone acetyltransferases (HATs) add PTMs, which are subsequently recognized by readers like chromodomain, or bromodomain containing proteins. Histone lysine demethylases (KDMs) or histone deacetylases (HDACs) are considered erasers as they remove methyl or acetyl residues, enabling the reversibility of PTMs.[22] These distinct modifications can be viewed as part of a broader regulatory framework, as phosphorylation of histone H3S10 facilitates H3K14 acetylation and H3K4 methylation, leading to an open chromatin structure.[23] Furthermore, acetylation can inhibit other PTMs, by competing for ε-amino group of lysine. Hence, acetylation can stabilize a protein by preventing ubiquitination and subsequent proteasomal degradation.[24] HMTs can be recruited by special DNA patterns and function in multi-protein complexes. They are responsible for methylation of histones, which subsequently enables DNA methylation by DNMTs, indicating the integration of DNA modification in the interplay of epigenetic regulation.[25] The methylation of histones can occur at all basic amino acids, but most studied is the methylation of lysine, ranging from mono-, di-, and trimethylations. Depending on the methylation state and location, they are recognized by different proteins containing methyl binding domains like plant homeodomain (PHD) fingers or WD40 repeats (WDR). Moreover, readers can contain more than one distinct recognition domain, including the chromatin regulator tripartite motif-containing 24 that binds with a PHD and a bromodomain to the same histone tail.[26]

In contrast to methylation, histone acetylation occurs only at lysine residues. The acetyl residue neutralizes the positive charge of the amine group, preventing electrostatic interactions of histones to the DNA. Thereby the heterochromatin, consisting of histones and DNA, loosens and forms the more accessible euchromatin, representing the uncondensed DNA. An increased pore size in the chromatin from 10-20 nm to 60-100 nm is observable upon enhanced histone acetylation, illustrating better accessibility.[27] By using acetyl-coenzyme A (acetyl-CoA), HATs transfer the acetyl moiety to the ε-amino group of lysine residues. HATs do not bind directly to the DNA for transcription regulation but are recruited by transcriptions factors and function in association to multi-protein complexes. Their acetylation function is not only limited to histones but can modify transcription factors as well, including p53 and E2-promoter binding factor (E2F).[28] CREB-binding protein (CBP) and p300 belong to the most studied family of HATs. With more than 90% of homology in their HAT domain and overlapping cellular function, both proteins are closely related.[29] By acetylating all core histones, they activate transcription.[30] The acetylation of histones is recognized by bromodomains with a central deep hydrophobic cavity accompanied with an anchoring hydrogen bond to the acetyl carbonyl oxygen. Named after the *brahma* gene of Drosophila they consists of 110 conserved amino acids.[31,32] Multiple proteins contain bromodomains, including HATs, chromatin-remodeling complexes, HMTs, transcription factors, and the bromodomain and extra-terminal domain (BET) family, leading to versatile effects of acetyl recognition. The ability to regulate protein-protein interactions and the wide distribution in multiple cellular processes make them a promising drug target in neurological diseases, inflammation, and cancer.[33] However, the acetylation pattern is highly dynamic and reversible as HDACs facilitate the hydrolysis of acetyllysine residues of histones, resulting in a more condensed heterochromatin. They are involved in versatile cellular processes and dysregulated in cancer among other diseases, making them valuable drug targets.[34] Consequently, they depict the primary focus of this thesis and are further discussed in the following chapters.

1.2 Histone Deacetylases

The modification and regulation of chromatin is a versatile and immensely controlled process. In the 1960´s Allfrey *et al*. hypothesized that gene transcription is regulated by acetylation and methylation of histone residues.[35] The first enzymatic deacetylation of histones was discovered in calf thymus extract in 1969.[36] By affinity chromatography utilizing trapoxin, Taunton *et al*. identified the first human HDAC, designated HD1 and later HDAC1, with high sequence homology to reduced potassium dependency 3 (Rpd3), a yeast deacetylase.[37] HDACs can be distinguished

into four classes (see 1.2.2 Structural & Functional Aspects of HDAC Classes). Class III enzymes containing a nicotinamide adenine dinucleotide (NAD)/flavin adenine dinucleotide (FAD)-binding domain are NAD^+-dependent, while class I, II, and IV are zinc-dependent and belong to the arginase superfamily.[38] Despite low sequence homology to the arginase I, HDACs share the topology of eight β-sheets flanked by a number of α-helices to coordinate the metal ions.[39]

Since zinc-dependent class I, II, and IV isoforms differ from class III isoforms in both structure and function, the following chapters will focus on zinc-dependent HDACs. Unless otherwise specified, the term 'HDAC' will refer to these zinc-dependent isoforms.

1.2.1 Catalytic Mechanism

Determining protein structures is essential for understanding their function and for the rational design of small molecule binders. Structural insights enable the elucidation of catalytic mechanisms and the mode of action of targeted drugs.

The first proposed catalytic mechanism of a metal-dependent deacetylase was based on the crystal structure of the bacterial histone deacetylase-like protein (HDLP), exhibiting the α/β fold of arginases.[40] This mechanism was expanded by the data derived from the structure and enzymatic testing of HDAC8.[41] A narrow hydrophobic cleft was identified on the surface of HDACs, consisting of a tube-shaped cavity approximately 11 Å deep, with the catalytic core at the bottom.[42] This catalytic core contains the Zn^{2+}, which is coordinated by H180, D178, D267, and two water molecules (Fig. 3). When the substrate binds for amide bond hydrolysis, the lone pair of electrons on the amide carbonyl oxygen displaces a coordinated water molecule, interacting with the zinc ion and polarizing the carbonyl group. Y306 turns from an “out” to an “in” position and donates a hydrogen bound to the carbonyl for further polarization. This hydrogen bond enables nucleophilic attack of the carbonyl carbon by the zinc ion coordinated water molecule. Thereby, the zinc ion is important for correct orientation of the water molecule. In addition, H143 functions as a general base accepting the proton of the water molecule for the nucleophilic attack of the carbonyl carbon. The resulting tetrahedral transition state collapses as the carbonyl oxygen’s electron pair reverts, facilitating the liberation of the lysine amine, which is protonated by H143 acting as a general acid. This reaction yields the free protonated lysine and acetate as final products.[43,44] H142 and H143 can be considered as electrostatic directors, ensuring the optimal position of the zinc bound water for the nucleophilic attack.

HDACs not only carry one metal ion but contain two more metal-ion binding sites. A potassium ion is located in the close proximity of 7 Å to the catalytic Zn^{2+}, also supporting the position of the

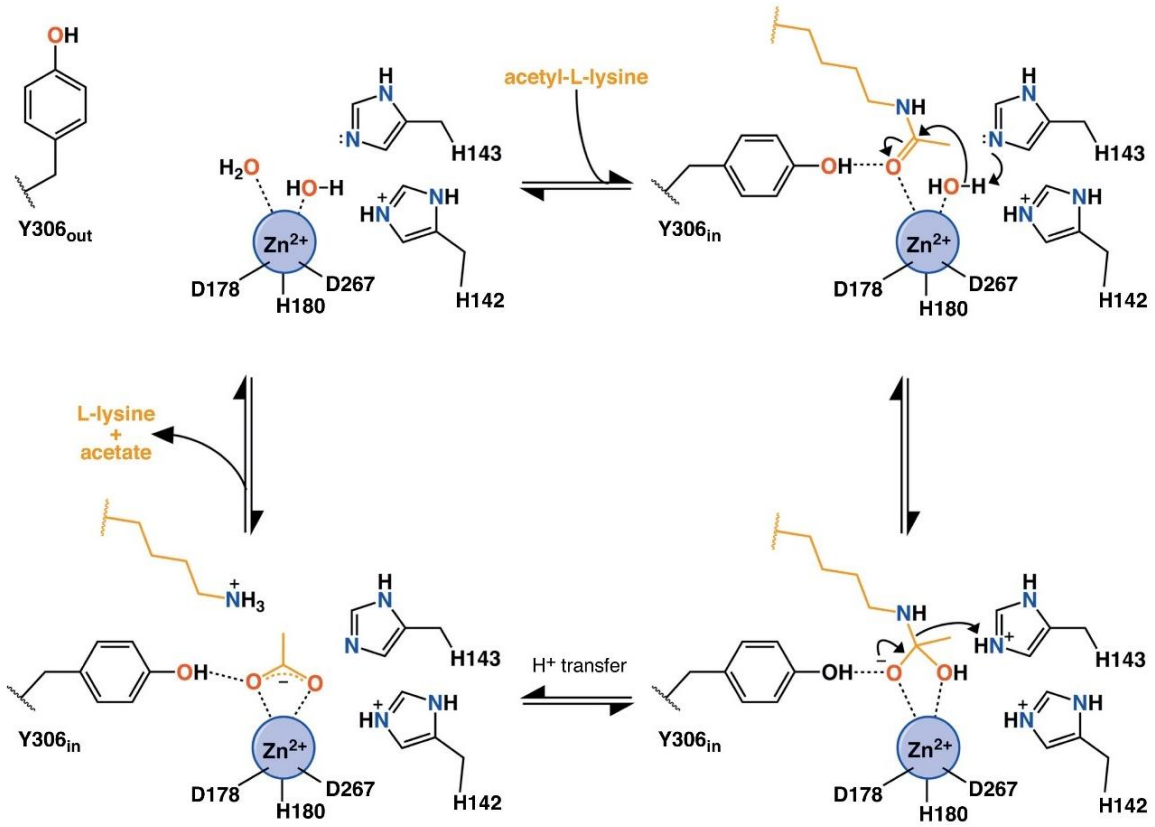

Figure 3. Proposed mechanism of acetyllysine hydrolysis of HDAC8. The acetyllysine binds by replacing a water molecule to coordinate the zinc ion and the carbonyl bond is polarized by the turned Y306$_{in}$. After the nucleophilic attack of the zinc bound water, the tetrahedral intermediate collapses liberating the amine, which gets protonated by H143. The resulting acetate, and free lysine leave the catalytic core, and the zinc ion is coordinated by water, ready for the next cycle of hydrolysis. Adapted and modified after N. J. Porter and D. W. Christianson with permission of Elsevier (License number 5995351107004).[43]

water molecule for nucleophile attack, as well as enhancing substrate binding and support for the tetrahedral transition state.[45] Additional, the substrate backbone amino-group of the +1 amino acid to *N*-acetyllysine in the substrate is stabilized by a dual hydrogen bond to the carboxylic acid of aspartate D101.[46] Switching to a proline at position +1 interrupts this connection and lead to reduced turnover.[47]

1.2.2 Structural & Functional Aspects of HDAC Classes

As previously mentioned, histone deacetylases are classified into four classes based on the sequence homology of the catalytic domain to yeast enzymes (Fig. 4). Class I HDACs (HDAC1, 2, 3, and 8) show sequence similarity to yeast Rpd3, class II (HDAC4, 5, 6, 7, 9, and 10) proved to have homology to yeast histone deacetylase-A1 (Hda1). Sequence homology of HDAC6 and 10 lead to sub-classification in class IIb additionally possessing an extended N-terminal regulatory domain, compared to class IIa.[49,50] Class III comprises the so-called sirtuins (SIRT1, 2, 3, 4, 5, 6, and 7) showing sequence homology to yeast Sir2 protein and class IV contains only HDAC11, which shares similarity to both class I and II.[51]

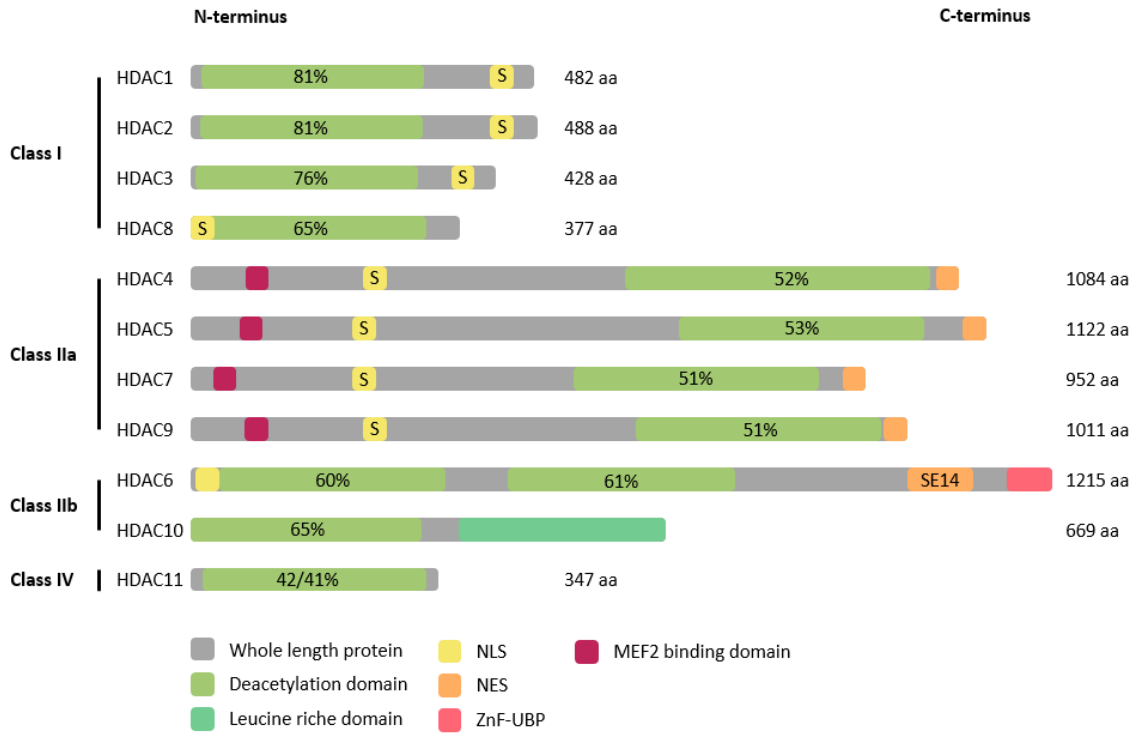

Figure 4. Domain structure of zinc-dependent HDACs. The similarity to Rpd3 for class I and Hda1 for class II is represented in percentage in the deacetylation domain. HDAC11 contains similarity to Rpd3/Hda1. The size of the whole length protein is represented on the right in amino acids (aa). Serine (S); SE14 repeats (SE14); Nuclear localization sequence (NLS); Nuclear export sequence (NES); zinc-finger ubiquitin binding domain (ZnF-UBD); Myocyte enhancer factor-2 (MEF2). Adapted from Li et al.[34] and Yang et al.[48]

Class I HDACs, comprising HDAC1-3, and HDAC8, are primarily localized in the nucleus and deacetylate all four core histones. However, their substrate specificity remains ambiguous, as the knockout of a specific HDAC can be functionally compensated by others.[51] The structure of the catalytic cleft and adjacent protein surface determines the substrate spectrum of the isoform. In addition, a 14 Å channel branches out at the catalytic core of HDAC class I enzymes. This so-called foot pocket is suggested to be the exit route for the acetate product. HDAC3 and 8 differ from HDAC1 and 2 in a smaller foot pocket as the space is occupied by tyrosine.[52,53] Full physiological function of HDAC class I is gained by incorporation in multi-protein complexes, including transcription factors, nuclear repressors, and epigenetic modifiers, like methyl-binding proteins, DNMTs, and HMTs.[54] More than 15 co-repressor complexes are known, differing in size (200 – 2,000 kDa) and number of subunits (3 to more than 14 subunits). Incorporation into a complex is essential to direct HDAC activity towards specific gene loci.[55] A well-studied interaction is the recruitment of HDAC1/2 to methylated DNA by the methyl CpG binding protein 2, which is recruited to hyper-methylated CpG islands. The interaction is mediated by the HDAC1/2 containing switch-independent protein 3 (Sin3) complex for further silencing of the respective genes.[56] In addition, HDAC1/2 can be accompanied by DNMT1, to maintain DNA hyper-methylation and gene silencing.[57] Furthermore, HDAC1/2-containing complexes include the

nucleosome remodeling and deacetylase (NuRD),[58] the co-repressor of REST (CoREST), which associates with lysine-specific demethylase 1 (LSD1) for histone demethylation,[59] and the mesoderm induction early response (MIER).[60] In case of Sin3, NuRD, and CoREST, inositol tetraphosphate acts as an adapter for HDAC binding.[61] In contrast, HDAC3 is exclusively recruited to the nuclear receptor co-repressor (NCoR)/silencing mediator for retinoid and thyroid receptors (SMRT) complex, which is responsible for the repressor function of unliganded nuclear hormone receptors.[62]

Class I HDACs also target non-histone substrates, regulating their abundance and activity. HDAC1 destabilizes p53, inactivates the cell cycle related transcription factor E2F1, and increases the demethylation activity of LSD1 upon deacetylation.[63–65] HDAC8 shows deacetylation activity of estrogen-related receptor α, supporting its function as transcription factor, and structural maintenance of chromosomes protein 3, which is important in cell cycle regulation.[66,67] HDAC1-3 knockout leads to embryonic or perinatal lethality in mice, proving the essential role of class I HDACs in development.[68]

Class II is separated into subgroups IIa and IIb. A particular feature of class IIa HDACs is the combination of nuclear localization sequences (NLS) and nuclear export signal (NES), which enable shuttling between cytoplasm and nucleus upon phosphorylation. The myocyte enhancer factor-2 (MEF2) binding domain promotes nuclear retention, while the chaperone 14-3-3-protein retains HDAC class IIa in the cytoplasm, after phosphorylation of several serine residues.[48]

Class IIa HDACs have reduced catalytic activity due to structural differences. The conserved tyrosine residue (e.g., Y306 in HDAC8) is replaced by a histidine that rotates out of the active site, weakening carbonyl polarization of the acetylated lysine. This results in up to 1000-fold lower activity compared to class I HDACs. Exchanging the histidine back to a tyrosine in HDAC4 restores the catalytic activity. However, trifluoroacetyllysine was found to be an effective substrate for HDAC4, indicating a low but measurable enzymatic activity.[69] Nevertheless, the substrate spectrum remains unclear. They rather function as scaffolding proteins for corepressor complexes or other transcription factors. By interacting with the SMRT/NCoR complex *via* their catalytic domain, class IIa HDACs activate the enzymatic function of HDAC3 within the complex.[70]

Class IIb consist of HDAC6 and 10. Even though HDAC6 contains NLS and NES, similar to class IIa HDACs, it remains cytoplasmic due to SE14 repeats, while HDAC10 can be found in the nucleus and cytoplasm, bearing only a leucine rich domain.[71,72] The most striking difference of HDAC6 to all the other HDACs is the existence of two catalytic domains (CDs). While CD2 exhibits a broad substrate spectrum, CD1 is highly specific for C-terminal acetyllysine substrates.[47] Furthermore,

HDAC6 contains a zinc-finger ubiquitin binding domain (ZnF-UBD) that is involved in the regulation of aggresome formation and autophagy.[48] Due to its cytoplasmic localization, HDAC6 primarily deacetylates non-histone substrates, such as α-tubulin and cortactin, which regulate the cytoskeleton and cell migration, ultimately stabilizing microtubules.[73] In addition, HDAC6 regulates stress response by heat shock protein (HSP) 90 deacetylation and retains the DNA end-joining protein Ku70 in the cytoplasm, preventing apoptosis induction by Bax.[74–76] HDAC10 exhibits a unique substrate specificity. A sterically restricted helix within the active site creates a long, narrow cleft that is largely inaccessible to proteins. Rather, small polyamines, such as N^8-acetylspermidine, are recognized as substrates. Additionally, the E274 functions as an electrostatic gatekeeper, recognizing positively charged secondary amines.[47] Nevertheless, there is not much known about specific substrates of HDAC10.

HDAC11 is the only member of class IV and localized in the nucleus but knowledge of its function remains limited.[77] More recent studies revealed that HDAC11 exhibits low deacetylation activity, but is highly efficient in hydrolysis of fatty acids like C10 decanoyllysine, C12 dodecanoyllysine, and C14 myristoyllysine.[78] Serine hydroxymethyltransferase 2 (SHMT2) is deacylated by HDAC11, thereby affecting the interferon (IFN) receptor regulation of SHMT2 and immune response.[79]

The first direct link between HDACs and transcriptional repression was established with the yeast histone deacetylase Rpd3, which is required for full repression and activation of target genes.[80] Further evidence was provided by fusion proteins combining HDAC isoforms (e.g., HDAC1) with the galactose-responsive transcription factor 4 (Gal4) DNA-binding domain, which lead to repressed transcription at Gal4-responsive genes.[81] HDACs are enriched at active genes, correlating with RNA polymerase II levels, and promote post-transcriptional formation of heterochromatin.[82] Rather than acting as a simple off-switch of transcription, HDACs are part of a dynamic equilibrium with HATs, modulating histone acetylation at both active and inactive genes. This results in transient acetylation of promoters, remaining the inactive state of genes, but enable transcription initiation upon additional activators. As the function of HDACs is still under study, HDAC inhibitors are known for multiple decades and were used as tools to study functions of HDACs. This revealed an increase of RNA-polymerase II in inactive promoter regions, upon treatment with HDAC inihibitors.[82] Additionally, extensive H3K27 methylation can suppress acetylation activity, contributing to stable gene silencing.[82]

The function of HDACs in gene transcription regulation goes even further, as shown by genome wide studies of HDAC-knockouts. HDAC3 knockout mice show both up- and downregulation of transcription.[83] Similarly, the comparison of inhibitor treated and untreated cells show equal

numbers of genes being up- or downregulated. This result can be explained by non-histone substrates and versatile functions of binding partners.[84,85] For example, in the PTM cross talk of acetylation and phosphorylation of RNA-polymerase II. The acetylation of lysine (K7) leads to decreasing phosphorylation of serine (S5), which results in reduced transcription elongation. HDAC1 mediates the deacetylation of K7 and the subsequent phosphorylation of S5 facilitates elongation of transcription.[86]

Since gene transcription and protein biosynthesis are crucial for all cellular processes, HDACs play a substantial role in regulating multiple cellular functions. Among these, the cell cycle is directly controlled by cyclins and cyclin-dependent kinases (CDKs) but also modulated by HDACs at a higher level. Cyclin A is deacetylated by HDAC3 affecting cell cycle progression in the S phase and G2/M transition.[83] Furthermore, HDAC10 is involved in G2/M transition, as its depletion leads to G2/M arrest, through indirect cyclin A2 downregulation.[87] In addition, key proteins of the spindle assembly checkpoint are regulated by HDAC2/3 to facilitate mitosis progression and respective HDAC inhibitor vorinostat promotes expression of the cell cycle inhibitor p21 by histone hyperacetylation in its promotor region, similarly the HDAC8-selective inhibitor PCI-34051 resulting in G2/M cell cycle arrest by increased p21 expression.[88–90] However, HDAC1 is involved in repression of E2F related genes important for cell cycle progression. HDACs can be found in a complex with the E2F binding-partner Rb for transcription repression and the DNA methyltransferase DNMT1, leading to gene silencing.[57]

Specific checkpoints in the cell cycle enable cells to prevent DNA damage or force cells into apoptosis. This is an important process to prevent cells from aberrant chromosomes or DNA damage.[91] HDACs play important roles in both processes, apoptosis and DNA damage response. HDAC1-3 downregulate p53, a major player in apoptosis induction, thereby the activation of pro-apoptotic genes like Bax is reduced.[92] Furthermore, HDAC1 inhibition can induce apoptosis, as this retains K120 acetylation of p53, thereby enabling the transcription factor to upregulate apoptotic peptidase activator factor 1 (Apaf-1) for sensitizing caspase activation and apoptosis.[93] In addition, further transcription factors are hyperacetylated upon HDAC inhibitor treatment, resulting in upregulation and stabilization of the proapoptotic protein Bcl-2 interacting mediator (Bim) of cell death.[94,95] The before mentioned mechanisms address the intrinsic mitochondrial pathway of apoptosis. However, HDAC inhibitors also activate the extrinsic pathway by restoring tumor necrosis factor- related apoptosis-inducing ligand (TRAIL) expression.[96]

In addition, HDAC isoforms 1/2 are involved in DNA damage response (DDR): The double-strand break (DSB) is the most challenging DNA damage that can lead to cell death and contributes to

cancer.[97] Eukaryotic cells repair DSB *via* two pathways: homologous recombination, which is restricted to the S and G2 phases and nonhomologous end joining (NHEJ), which occurs throughout the cell cycle.[98] To enable NHEJ, HDAC1/2 are rapidly recruited to the DNA damage site causing deacetylation of H3K56 and H4K16. The H3K56 acetylation pattern reflects DDR distribution across the cell cycle: H3K56Ac is absent in the G1 phase, where NHEJ is most active, but highest in the S phase, where homologous recombination is predominant.[99,100]

HDACs also play a key role in protein quality control, particularly in the degradation of misfolded proteins. These are prone to aggregation and must be eliminated before they form toxic aggregates. Therefore, these proteins are typically ubiquitinated and degraded by the proteasome.[101] HDACs interact with the ubiquitin–proteasome system. For instance, panobinostat upregulates the E3 ligase cellular inhibitor of apoptosis protein (cIAP) 2 in bladder cancer cells. Thus, meiotic recombination 11 homolog (MRE11) is degraded, which sensitizing tumor cells to DSB induced by radiotherapy, as the MRE11 complex control DSB repair.[102] Furthermore, HDAC1 suppresses von Hippel-Lindau (VHL) expression, stabilizes hypoxia-inducible factor 1α (HIF-1α), thereby promoting angiogenesis.[103] A direct participation by HDAC6 in the UPS was found by Zhang *et al.*[104] They prove *in vivo* ubiquitination of the DNA mismatch repair protein mutator S protein homolog 2 by the CD1 of HDAC6. However, when aggregates are to large or proteasome capacity is overwhelmed, HDAC6 facilitates their transport *via* dynein to aggresomes near the nucleus.[105] Furthermore, HDAC6 controls the aggresome clearance by autophagy, a lysosome-mediated degradation.[106] Similarly, HDAC10 promotes autophagy by deacetylating heat-shock cognate (HSC)/HSP70, leading to translocation of the targeted proteins to the lysosome. HDAC6 and 10 inhibition leads to accumulation of autophagosomes and lysosomes. Notably, HDAC10 depletion sensitizes tumor cells to doxorubicin by counteracting drug-induced autophagy.[107]

1.2.3 Pathophysiology & Drug Targets

HDACs can be found in different neoplastic and non-neoplastic diseases, which are associated with mutations or aberrant function. However, germline polymorphism or somatic mutations of HDACs associated with cancer are rare. Exceptions are the leader sequence of HDAC2, which exhibits an insertion in some cancer samples, and a polymorphism in the promoter region of HDAC10, resulting in an increased promoter activity, which is associated with the development of hepatocellular carcinoma.[108,109] Instead of mutations, aberrant HDAC expression is associated with multiple solid or hematological tumors and has been found in the brain, lung, gastrointestinal tract, liver, pancreas, breast, urogenital tract, skin as well as bone marrow and blood.[110]

Class I HDACs, especially HDAC1, are linked to poor prognosis in myeloma and bladder cancer,[111,112] while overexpression of class II HDACs correlates with poor survival in neuroblastoma and medulloblastoma to name only some.[113,114] In breast cancer, HDACs are involved in tumor progression. Initially, most breast cancer types are estrogen receptor (ER) dependent, but some lose ER expression during tumor progression.[115] HDAC1 was found to be overexpressed in MCF-7 cells with diminished ER expression and treatment with HDAC inhibitors recovered ER expression. A direct interaction of HDAC1 and ER-α is facilitated by the activity function domain 2 (AF-2) and suppresses the activity of the receptor.[116,117] In addition, the proto-oncogene myelocytomatosis viral oncogene homolog (Myc) is recruited by HDACs, resulting in altered gene expression and tumorgenesis.[118] Treatment with vorinostat and entinostat induced the acetylation of Myc, which led to a reduction of Myc levels. Subsequently, TRAIL repression is reduced and apoptosis induced.[96]

HDACs function as tumor drivers by multiple and isoform-dependent mechanisms (Fig. 5). The effects of class I HDACs on cell cycle progression and apoptosis mitigation classify them as tumor

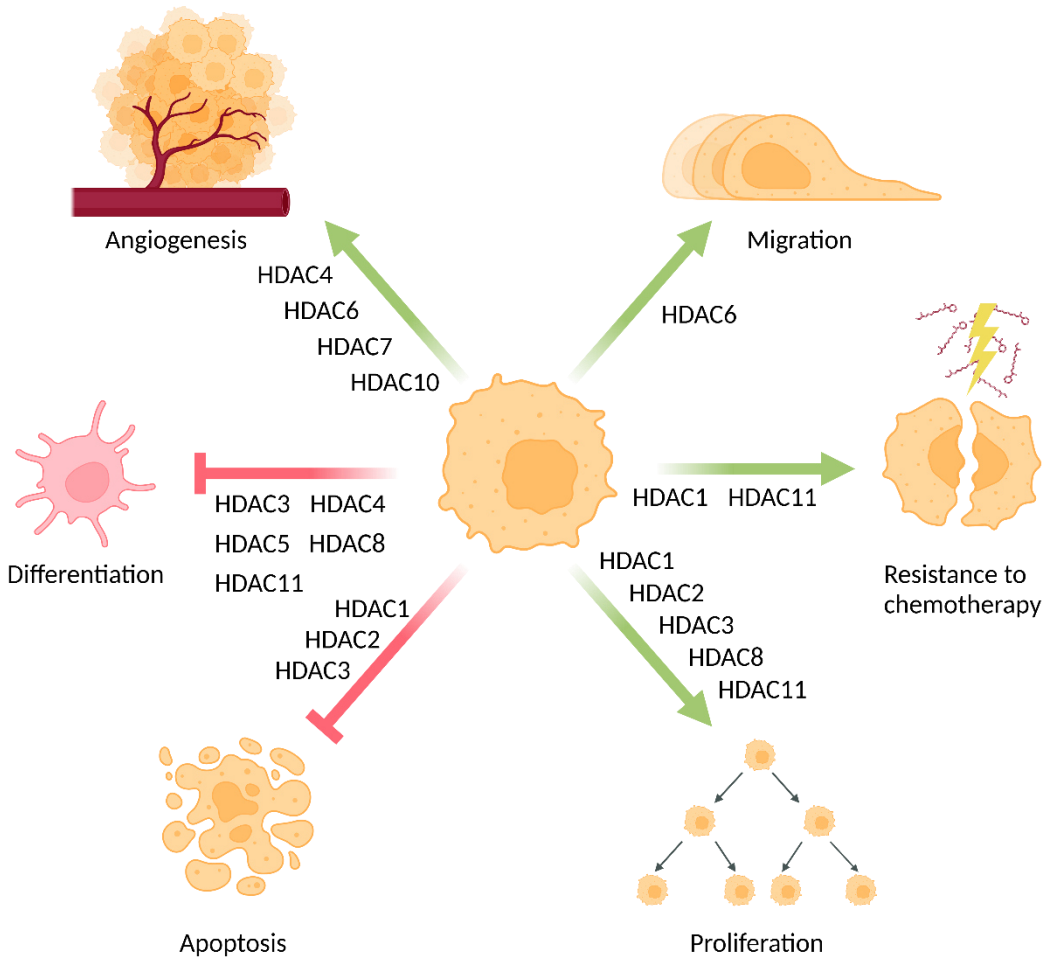

Figure 5. Function of HDAC isoforms as tumor drivers. The depicted isoforms increase angiogenesis, migration, resistance to chemotherapy and proliferation, while the respective isoforms suppress apoptosis and cell differentiation. Adapted from Witt et al.[68] Created with BioRender.com

drivers. Furthermore, HDAC1 overexpression is observed in chemotherapy resistant cancer cells and the knockdown sensitized the cells again for the chemotherapeutic drugs, including etoposide, melphalan, and carboplatin.[119] Comparable to HDAC1, the knockdown of HDAC2 by small interfering RNA promotes cell differentiation and inhibits proliferation in cervical or breast cancer cells.[120] Antiproliferative effects and increased differentiation were observed in acute promyelocytic leukemia cells for HDAC3 knockdown and in childhood neuroblastoma for HDAC8 knockdown.[113,121] Class IIa HDACs are often involved in cancer cell differentiation and angiogenesis.[122,123] Overexpression of HDAC6 leads to enhanced mobility in embryonic fibroblasts and can be targeted by selective HDAC6 inhibition, while knockout of both class IIb HDAC isoforms reduces VEGF receptor expression, leading to mitigation of angiogenesis.[124,125] The class IV isoform HDAC11 regulates multiple cancer processes like cell growth, differentiation, and resistance to chemotherapy.[126]

The role of HDACs in cancer is extensively studied and they represent a major clinical target, although aberrant HDAC activity is also implicated in non-neoplastic diseases. Impaired regulation of histone acetylation and hypoacetylation could be observed in many neurological diseases, while treatment with HDAC inhibitors results in hyperacetylation, neuroprotective effects, and neuronal differentiation.[127] Positive effects are also reported for Huntington´s disease, Parkinson´s disease, Alzheimer´s disease, and more.[128] Furthermore, HDAC inhibitors show promising results in psychiatric disorders like depression or schizophrenia.[127]

Additional applications for HDAC inhibitors are immune disorders, which is reasonable as cells of the adaptive immune system undergo drastic phenotypic changes after exposure to appropriate stimuli. Inhibitor treatment demonstrated promising results in several mouse inflammation models as well as in patient samples from autoimmune diseases.[129] Considering the broad range of inflammation-related diseases, including infectious diseases, arthritis, and digestive diseases, HDACs become an even more substantial target.[130] HDACs positively regulate diverse proinflammatory cytokines (e.g. IL-6, IL-12, TNF), chemokines (e.g. CCL2, CCL7), and other mediators.[131,132] Beyond the human immune system, HDAC inhibitors can also influence the metabolism of viruses: they can limit long-term presence of human immunodeficiency virus 1, reduce influenza virus assembly *via* HDAC6 inhibition, or downregulate angiotensin-converting enzyme 2, important for severe acute respiratory syndrome coronavirus 2 (SARS-CoV-2) infection.[133–135]

1.2.4 HDAC Inhibitors & Clinical Applications

The incorporation of HDACs in multiple pathogenic mechanisms made them subject to long years of drug discovery. In the beginning, this led to the identification of natural products as HDAC inhibitors and subsequently encouraged drug discovery to develop a huge number of HDAC inhibitors. In 1997, Jung *et al.*[136] established a three-part pharmacophore model, which mimics the natural substrate acetyllysine (Fig. 6A). Most HDAC inhibitors bear a chelator to coordinate the catalytic zinc ion in the catalytic core of the enzyme, the so-called zinc binding group (ZBG).

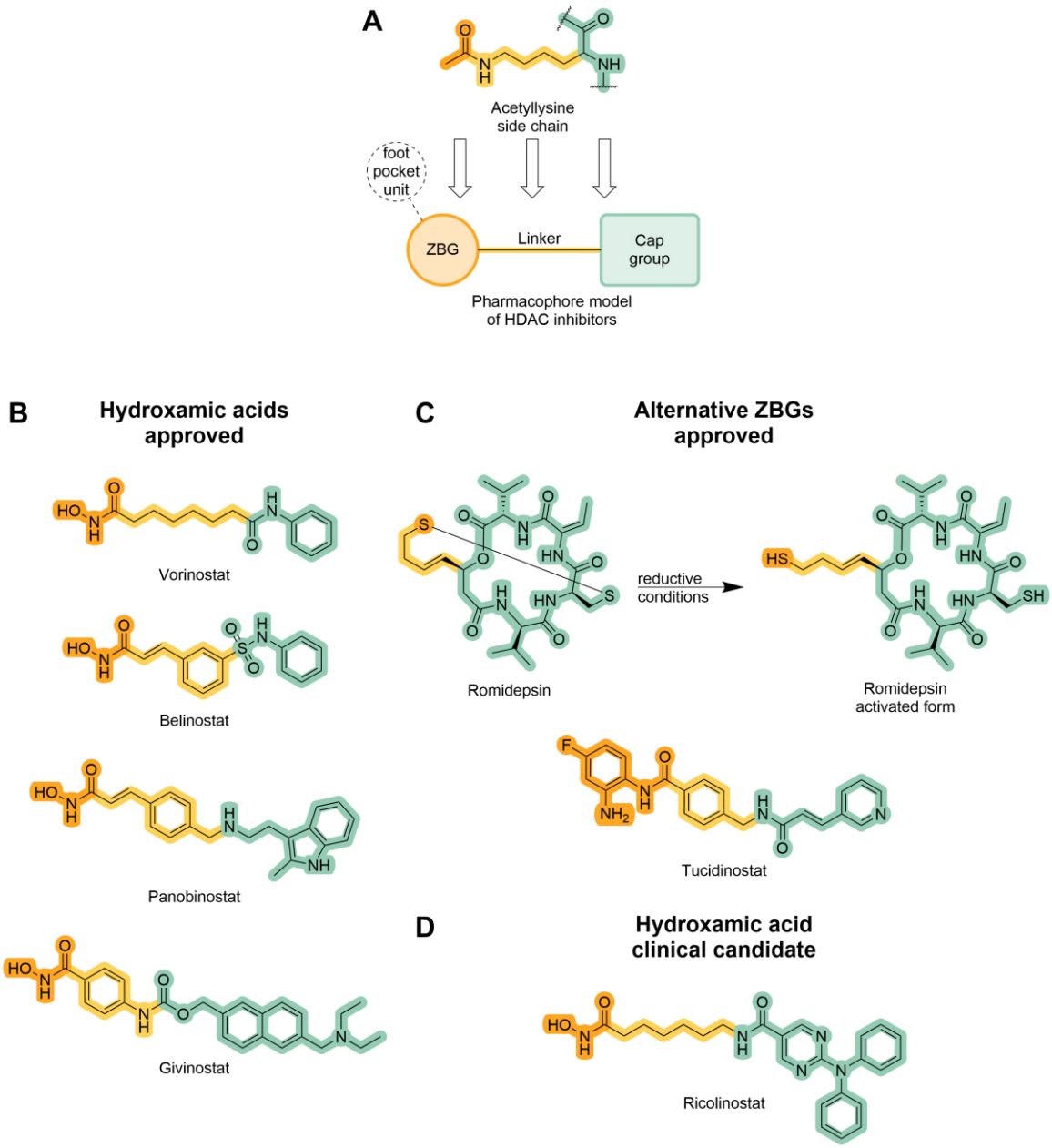

Figure 6. Pharmacophore model of HDAC inhibitors. (A) The pharmacophore model for HDAC inhibitors consisting of the zinc binding group (ZBG, orange), linker (yellow), and cap group (green). For further modifications, a foot pocket unit can be attached to the ZBG. The pharmacophore model shows similarity to the natural substrate acetyllysine. (B) Approved inhibitors based on hydroxamic acids. (C) Approved inhibitors based on alternative ZBGs. (D) Example for a hydroxamic acid-based inhibitor in clinical development.

Established ZBGs are hydroxamic acids, *ortho*-aminoanilides, and thiols among others. The ZBG is fused to the linker, which interacts with the hydrophobic residues of the catalytic channel. At the opening of the catalytic channel, the cap group comes into place, interacting with the surface residues surrounding the channel entrance.[137] Isoform selectivity can be fine-tuned by optimizing these three elements, with additional features such as a foot pocket unit further enhancing specificity. However, as the enzymatic catalytic core is highly conserved, the highest structural diversity can be observed in the cap group of inhibitors that occupies the protein´s surface.[138]

To date, there are seven HDAC inhibitors approved for the use in human (Fig. 6B, C), four approved by the U.S. Food and Drug Administration (FDA): Vorinostat (Zolinza) is approved for cutaneous T-cell lymphoma (CTCL), belinostat (Beleodaq) for peripheral T-cell lymphoma (PTCL), and romidepsin (Istodax) for CTCL and PTCL, as well as givinostat (Duvyzat) for the treatment of Duchenne muscular dystrophy (DMD). Furthermore, the European Medicines Agency (EMA) approved panobinostat (Farydak) for treating multiple myeloma in combination with dexamethasone and bortezomib.[139,140] In addition, the *ortho*-aminoanilides tucidinostat (Epidaza, Hiyasta) is approved by the National Medical Products Administration of China (NMPA) for the treatment of hormone receptor positive breast cancer and PTCL.[141,142]

While early-stage cutaneous T-cell lymphoma is typically limited to the skin and responds well to topical therapy, advanced stages show reduced survival and require systemic treatment, including HDAC inhibitors.[143] Like CTCL, peripheral T-cell lymphoma is a non-Hodgkin lymphoma but generally has poor prognosis.[144] Another major indication for HDAC inhibitors is multiple myeloma, characterized by uncontrolled proliferation of plasma cells in the bone marrow. Despite already established treatments like proteasome inhibitors, acquisition of drug-resistance remains a significant challenge, particularly in refractory patients. HDAC inhibitors show promising results in overcoming resistance to proteasome inhibitors and demonstrate synergistic effects when combined with those by blocking both the proteasomal and aggresome degradation pathways. This even led to the development of dual HDAC-proteasome inhibitors.[145,146] In solid tumors, HDAC inhibitors are approved only for hormone receptor-positive breast cancer. Tucidinostat, a class I-selective HDAC inhibitor, is used to counteract resistance to aromatase inhibitors, which is often driven by epigenetic reprogramming.[142] Overall, HDAC inhibitors are more effective in hematologic malignancies than in solid tumors. The only approved non-oncologic indication is DMD, an X-linked disorder causing progressive muscle degeneration by mutations in extracellular matrix proteins. The majority of patients die before the age of 20 years, predominantly due to respiratory failure and cardiomyopathy.[147] Givinostat, recently approved, helps to reduce inflammation and increase muscle mass, complementing corticosteroid therapy.[140]

Hydroxamic acid is the most common ZBG and is incorporated in approved HDAC inhibitors such as vorinostat, belinostat, panobinostat, and givinostat (Fig. 6B). This ZBG is characterized by nanomolar potency, and fast-on/fast-off binding kinetics.[139] As the approved hydroxamate-based inhibitors exhibit low nanomolar half maximal inhibitory concentration (IC_{50}) values for all of the zinc dependent HDAC isoforms, they are classified as pan-HDAC inhibitors (Table 1).[71] However, the effect on HDAC class IIa isoforms seems to be ambiguous, as other publications report low activity of hydroxamate-based HDAC inhibitors on class IIa HDACs, including vorinostat.[148,149] The potency of hydroxamates is significantly higher compared to short-chain fatty acids, which are also HDAC inhibitors but exhibit inhibition in the millimolar to high micromolar range.[150] In 2006, vorinostat became the first approved HDAC inhibitor. It is characterized by a bidentate binding mode in a trihedral bipyramidal geometry of the hydroxamate, as well as hydrogen bond interactions to conserved amino acids. This structural feature leads to poor isoform selectivity, resulting in a broad-spectrum pan-HDAC activity. Furthermore, the alkyl linker of vorinostat mimics the alkyl side chain of lysine.[151] However, hydroxamic acids come with certain limitations, as they are excellent chelators for metal ions like zinc, iron, and nickel, which are implemented in multiple biological processes. Mutagenicity represents a further issue, as vorinostat, belinostat, and panobinostat are Ames test positive and lead to chromosomal aberrations in rodent cells.[152] Lossen rearrangement is the proposed mechanism for the observed mutagenicity and genotoxicity (Fig. 7). Under basic conditions and *O*-activation of the hydroxamic acid, the nitrogen gets deprotonated. This anionic intermediate rearranging fast to the isocyanate.[153] Isocyanates are instable and prone to nucleophilic attack, e.g. by DNA bases.[154] However, the clinical safety profile of the approved hydroxamates showed predominantly mild adverse effects like

Table 1. Isoform selectivity profile of approved HDAC inhibitors and late-stage clinical candidates. HDAC isoform specific IC_{50} values of selected compounds, summarized as per Ho et al.[71]

HDAC class	HDAC isoform	Vorinostat[a] [nM]	Belinostat[a] [nM]	Panobinostat[a] [nM]	Givinostat [nM]	Romidepsin [nM]	Tucidinostat [nM]	Ricolinostat [nM]
Class I	1	60	26	3	133	1	95	58
	2	42	22	2	293	1	160	48
	3	36	19	2	136	1	67	51
	8	173	22	22	837	n.e.	733	100
Class IIa	4	20	15	1	n.e.	647	n.e.	n.e.
	5	36	25	1	532	n.e.	n.e.	n.e.
	7	129	51	2	524	n.e.	n.e.	n.e.
	9	49	24	1	512	n.e.	n.e.	n.e.
Class IIb	6	29	10	1	312	226	n.e.	5
	10	60	59	31	331	1	78	n.d.
Class IV	11	31	27	4	287	0.3	432	n.e.

[a]Ki values based on IC_{50} values and converted by Cheng-Prusoff equation, n.e.: no effect IC_{50} > 1000 nM, n.d.: not determined. As the results were obtained by different assays, comparison between different inhibitors might be inaccurate. This table is rather intended to display the isoform selectivity profile of the selected inhibitors.

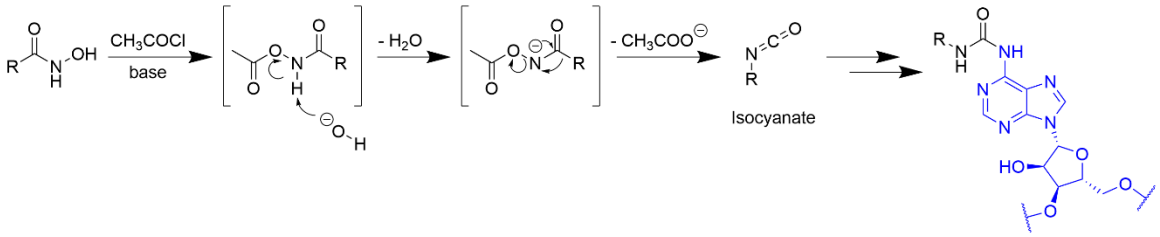

Figure 7. Hydroxamic acids are prone for decomposition by Lossen rearrangement, liberating genotoxic isocyanates. Adapted by Shen et al.[152]

gastrointestinal, hematologic and constitutional issues. Pulmonary embolism, cardiac abnormalities and hepatic failure have been reported as serious adverse effects under treatment of vorinostat or belinostat. For both treatments, uridine 5'-diphospho-glucuronosyltransferase (UGT) polymorphism induces the risk for serious adverse effects. Reports of panobinostat treatments have demonstrated more severe adverse effects.[139] Treatment with givinostat against DMD resulted in mainly mild adverse effects, e.g. gastrointestinal issues. Similar to other HDAC inhibitors, thrombocytopenia was reported as severe adverse event, but less pronounced.[155]

In contrast, the macrocyclic depsipeptide romidepsin represents a natural product produced by *Chromobacterium violaceum*. In the reductive cellular environment, the intramolecular disulfide of the prodrug is reduced to the thiol as the active inhibitor (Fig. 6C).[156] Romidepsin in its active thiol form exhibits inhibition of multiple isoforms with exception of HDAC8 and class IIa (Table 1). The selectivity profile of romidepsin is mostly determined by the branched cap group and there are even inhibitors known, sharing similar cap groups but lacking the ZBG.[157,158]

Tucidinostat is the only approved *ortho*-aminoanilide (Fig. 6C), a class of ZBGs that selectively inhibit HDAC1-3 while showing weak activity against HDAC8. This selectivity arises from their larger size compared to hydroxamic acids. *ortho*-Aminoanilides occupy a lateral cavity present in HDAC1-2 but blocked in HDAC3 and HDAC8 by tyrosine.[52,138,159] Introducing a suitable moiety, like a (hetero)aromatic group, at position 5 at the 2-aminoanilide ZBG allows engagement of the 14 Å internal foot pocket in HDAC1/2, thereby enhancing selectivity over HDAC3.[151] Unlike hydroxamates, *ortho*-aminoanilides exhibit slow-on/slow-off kinetics *via* a two-step binding mechanism, initially stabilized by an intramolecular hydrogen bond, followed by rearrangement involving zinc coordination and interaction with active site residues. This mechanism results in tight-binding properties.[160,161] Additionally, phenyl linkers, as used in tucidinostat, contribute to HDAC class I selectivity through π-π stacking with phenylalanine residues in the catalytic channel.[137] While avoiding hydroxamate-associated toxicity, tucidinostat can still cause hematologic side effects such as thrombocytopenia.[139]

In addition, numerous HDAC inhibitors are currently undergoing clinical investigation for a wide range of neoplastic and non-neoplastic indications. The phase two clinical candidate ricolinostat (see Fig. 6D) is applied orally for treatment of multiple myeloma (MM), as well as lymphomas and breast cancer. Similar to panobinostat, the treatment of MM in combination with a proteasome inhibitor appears to be promising, as both HDAC6 and the proteasome are involved in removing misfolded proteins and the combination of both inhibitors result in synergistic effects.[162] Another reason is to overcome resistance to proteasome inhibition by HDAC6 inhibitor treatment.[139] Ricolinostat is structurally similar to vorinostat, except for the cap group, which is responsible for its preferential inhibition of HDAC6. The X-ray structure of the HDAC6:ricolinostat complex revealed classic bidentate binding of the zinc ion by the hydroxamic acid, while the flexible linker enables two exclusive conformations for the cap group at the surface of the protein.[163]

1.3 Targeted Protein Degradation

Drug discovery is traditionally focused on small molecules. They target the active site or allosteric binding pockets of proteins to modulate the protein activity. Although this approach can be highly efficient, the number of drug targets, accessible by this mode of action, covers only a limited area of disease-related proteins. Especially considering the targets without enzymatic activity, including scaffolding proteins or transcription factors, the space of "undruggable" targets is substantial.[164,165] As these proteins can be also disease related, there is a tremendous need for new modalities in drug discovery, one of which is targeted protein degradation (TPD).[166] TPD takes advantage of the cellular degradation system, which is part of the physiological quality control mechanism. Incorrect folded proteins and proteins with high turnover rates get mainly degraded by the ubiquitin-proteasome system (UPS). First, they are recruited and polyubiquitinated by an E3 ligase system. Subsequently, this polyubiquitination signal is recognized by the proteasome, resulting in degradation of the target protein.[167]

1.3.1 The Ubiquitin-Proteasome System

TPD utilizes the cellular protein degradation abilities of the UPS. This system is based on the protein ubiquitin (Ub), composed of 76 amino acids and present in all eucaryotic cells.[168] A cascade of three ligases is necessary for the final Ub transfer (Fig. 8A). The ubiquitin-activating enzyme (E1) forms a thioester bond between its catalytic cysteine and the C-terminal carboxy group of Ub

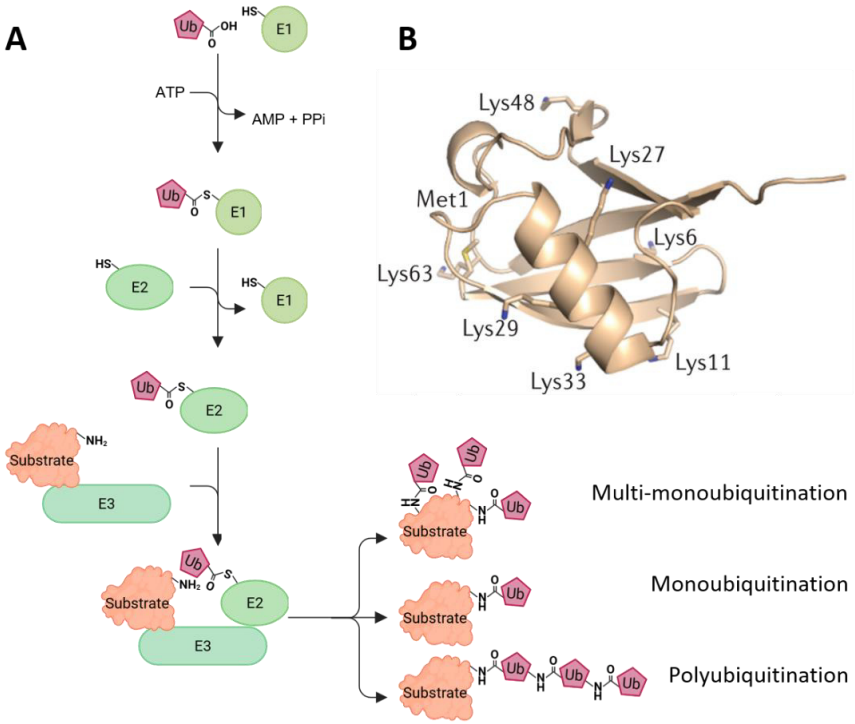

Figure 8. The E1-3 ligase cascade and ubiquitin. (A) The reactive cysteine of the ubiquitin-activating E1 ligase forms a thioester with the C-terminal carboxy group of ubiquitin (Ub) by hydrolyzing ATP. Subsequently, the Ub-loaded E1 transfers the Ub to a ubiquitin-conjugating E2 ligase, which gets recruited by a substrate protein loaded E3 ligase. This complex can form an isopeptide bond between the C-terminal carboxy group of Ub and an amino group of a substrate lysine residue. Monoubiquitination and multi-monoubiquitination or polyubiquitination are possible post-translational modifications. (B) Structure of ubiquitin (PDB: 1UBQ)[168] with labeled lysine and methionine residues for connecting further Ubs, resulting in polyubiquitin chains. Adapted from Buetow et al.[169] with the permission of Springer Nature (License number 501980533). Created with BioRender.com

recognizing the di-glycine motive of Ub, in an ATP and Mg^{2+} dependent-manner. Next, the E1 transfers the Ub to a ubiquitin-conjugating enzyme (E2) results in a thioester between the catalytic cysteine of the E2 and the C-terminal carboxy group of the substrate. Subsequently, the ubiquitin-loaded E2 and a target protein are recruited by an E3 ligase, facilitating the formation of an isopeptide bond between the C-terminal carboxy group of Ub and an ε-amino group of lysine residue or the N-terminal amino group of the target protein.[169] While the human genome encodes only two E1s, approximately 38 E2s, more than 600 E3s are identified, thus indicating the universal role of ubiquitination as well as the high substrate specificity of E3 ligases.[170,171] Lysine residues of targeted proteins can get monoubiquitinated and multi-monoubiquitinated by Ub loaded E3 ligases. Additionally, successive rounds of E3-catalyzed Ub transfers lead to polyubiquitination. Ubiquitin chains can be connected by one of seven lysine residues (K6, K11, K27, K29, K33, K48, and K63) or by the N-terminal methionine (Fig. 8B). They can be classified as homogeneous, mixed and branched, depending on the number and kind of connections occurring.[172] Homogeneous K48-linked polyubiquitin chains are arranged in a compact structure, while K63-linkage does not result in additional ubiquitin molecule interaction, leading to a rather open conformation.[173] This structural differences regulates the recognition and effect of the diverse PTMs by Ub. The most

abundant polyubiquitin chains are K48-linked and represent a common marker of proteasomal degradation.[174] Furthermore, K11-linkage is associated with degradation during mitosis, while K63-linkage results in lysosomal degradation of membrane proteins.[175,176] In addition, monoubiquitination as well as M1- and K63-linkage regulate nonproteolytic functions, including substrate´s activity, localization, or participation in cellular processes.[172]

Proteins marked with K48-linked polyubiquitin-chains, are recognized by the 26S proteasome, a barrel shaped multi-protein complex (Fig. 9). After the polyubiquitinated protein is recognized by the 26S proteasome, the ubiquitin chain is cut by proteasome bound deubiquitinases (DUBs) protecting Ub from degradation and recycling the Ub monomers. The target protein is degraded by the 26S proteasome complex, which comprises the 20S core particle with catalytic peptidase activity, bound to the 19S regulatory particle (RP).[177] The RP can be distinguished in two subcomplexes forming the base and the lid. To avoid non-specific degradation of cytosolic proteins, RP binds to one or both ends of the 20S proteasome (Fig. 9) and channels ubiquitinated proteins to the lumen of the barrel-shaped 20S proteasome. Furthermore, the base of the RP is equipped with ubiquitin-interacting proteins and exhibits a reverse chaperone function to unfold target proteins, thereby passing the target protein into the narrow pore of the 20S proteasome (Fig. 9A). The lid of the RP restricts access to the proteasome, where proteasome-associated DUBs reside. The 20S proteasome is composed of four heptameric rings, which comprise seven different α and β subunits, and is conserved from bacteria to mammals.[178–180] It exhibits three major peptidase activities: a chymotrypsin-like activity, cleaving after hydrophobic amino acids, a trypsin-like activity, cleaving after basic amino acids, and a caspase-like activity, cleaving after acidic amino acids. These protease activities are located in three different β subunits.[181,182] Peptide

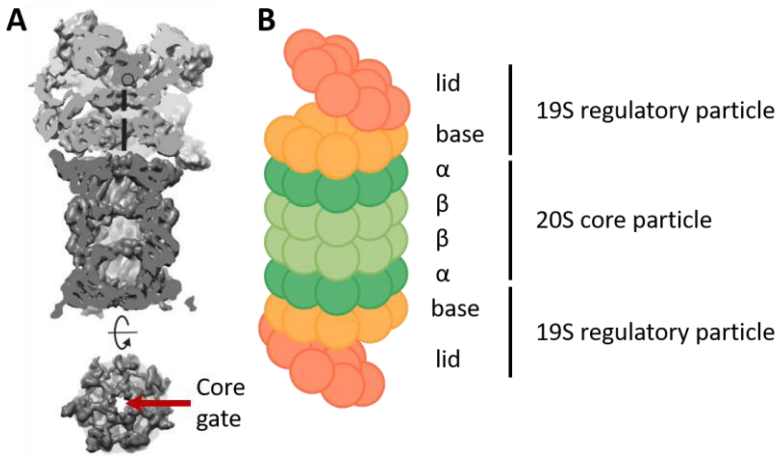

Figure 9. Structure of the proteasome. (A) Cryo-electron microscopy structure of the 20S core particle (dark gray) and the regulatory 19S regulatory particles (light gray). Bottom: Top-down view of the 20S core particle visualizes the small core gate and the lumen. (B) Schematic view of the 26S proteasome. Lid and base (red and orange) are part of the 19S cap regulatory particle, while α and β subunits assemble the 20S core particle. The peptidase activity is localized in β1, β2, and β5 subunit. Adapted from Bard et al.[186] and Nandi et al.[187] Created with BioRender.com

fragments of a size from three to 25 amino acids are products of this hydrolysis by the proteasome.[183] In addition to the constitutive proteasome, an immunoproteasome is described, characterized by the exchange of the three constitutive catalytic subunits to β1i, β2i, β5i. Its expression is induced by microbial infections and cytokines, including IFN-γ.[184] Through the exchange of the proteolytic domains, the immunoproteasome is specialized in antigen processing for presentation on major histocompatibility complex I molecules and immune response.[185]

1.3.2 E3 Ligases

E3 ligases play a pivotal role in TPD, as they are recruited by a majority of degraders to mark the protein of interest (POI) for proteasomal degradation. E3s recruit a Ub-loaded E2 and the target protein for ubiquitination and can be distinguished by their structure and ubiquitin transfer mechanism in really interesting new gene (RING)-type E3s, homologous to the E6AP carboxyl terminus (HECT)-type E3s, and RING-in between RING (RBR)-type E3s. While RING E3s act as a scaffolding domain for direct Ub transfer from the E2 to the target protein, HECT E3s form a Ub bound intermediate by transferring Ub from E2 to E3 before the target protein is ubiquitinated (Fig. 10 A, B and 11 D).[188] RBR E3s, including the E3 ligase parkin, function as a RING-HECT hybrid, as they encompass two RING domains connected by the in between RING (IBR) domain, but transfer Ub in a two-step mechanism. The RING1 recruits the Ub-loaded E2 and the Ub is transferred to a cysteine of RING2 before ubiquitination of the target occurs (Fig. 10 C and D).[189]

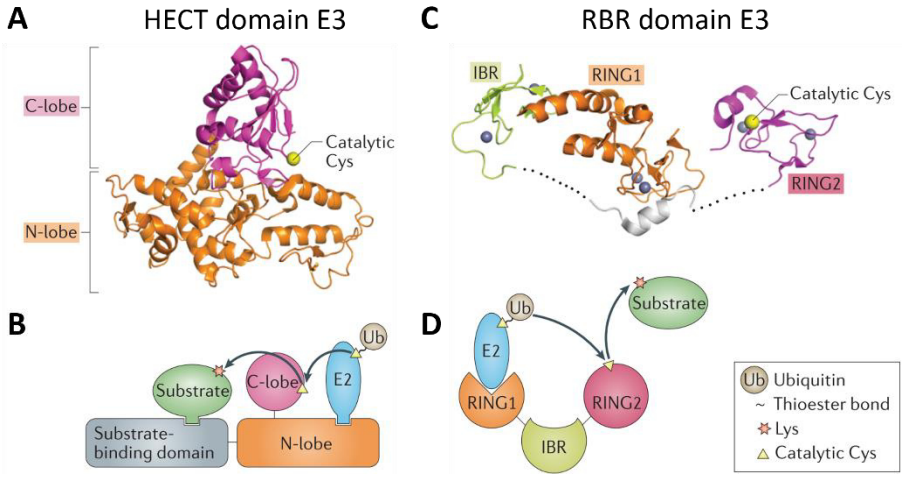

Figure 10. Structure and catalytic mechanism of HECT (homologous to the E6AP carboxyl terminus) and RBR (RING-in between RING) domain E3 ligases. (A) Crystal structure of the HECT domain from NEDD4L (PDB: 3JVZ). C-lobe with the catalytic cysteine in purple and N-lobe in orange. (B) Schematic catalytic mechanism of a HECT E3 ligase: The N-lobe recruits the Ub-loaded E2 ligase, which transfers the Ub to the catalytic cysteine of the C-lobe. From here, the Ub is fused to the lysine residue of the substrate, bound to the substrate-binding domain of the E3. (C) Crystal structure of the RBR domain of parkin (PDB: 5C23). RING1 (orange) and RING2 (purple), bearing the catalytic cysteine (yellow), are connected by the in between RING (IBR) domain and some unstructured regions (dashed lines). Stabilizing zinc ions are shown in gray spheres. (D) Schematic catalytic mechanism of a RBR E3 ligase: RING1 recruits the Ub-loaded E2 ligase, similar to RING E3s. However, the Ub is first transferred to the reactive cysteine of the RING2 domain, like in HECT E3s, before Ub is fused to the lysine of a substrate protein. Adapted from Buetow et al.[169] with the permission of Springer Nature (License number 501980533).

RING-type E3s are by far the largest E3 ligase family. The RING domain acts as a scaffolding protein and positions the ubiquitin-loaded E2 for ubiquitin transfer to the target protein.[190] There are different E2 ligases responsible for the first attachment of ubiquitin and elongation of polyubiquitin chains, exhibiting special linkage-preferences, as they need to recognize different target topologies.[191] In addition, the chain elongation requires not only a fast Ub transfer but also recognition of the distal Ub on the growing chain.[192,193] However, the RING domain is the most essential part of RING E3s to recruit Ub-loaded E2s and facilitate Ub-transfer. Two zinc ions coordinated by the RING-fingers, composed of cysteine and histidine residues, cause a rigid globular structure for protein-protein interaction (PPI).[194] RING E3s are a highly diverse group, while the E3 ligase casitas B-lineage lymphoma (CBL) is active as monomers, cIAP2 functions in homodimers, and suppressor breast cancer 1 (BRCA1) gains ubiquitin ligase activity by forming heterodimers with BRCD1 (Fig. 11 A-C). Furthermore, RING E3s appear in cullin-RING ligases (CRL), which are multi-protein complexes, comprising a central cullin protein (Cul1-3, 4A/B, 5, or 7) C-terminal bound to a RING box protein (RBX) 1 or 2 and N-terminal bound to a substrate recruiter (Fig. 11 E). With more than 300 different substrate receptors, CRLs are highly versatile in protein ubiquitination.[195]

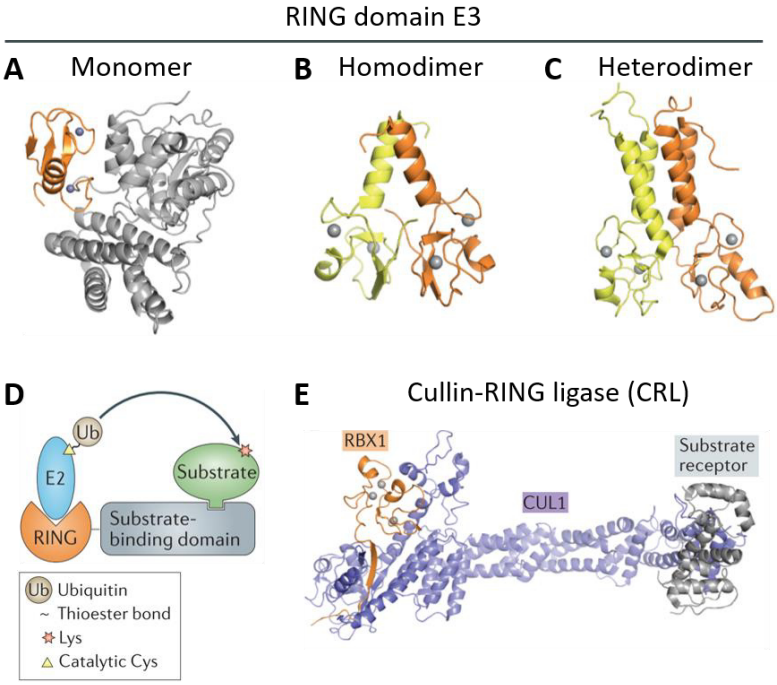

Figure 11. Structure and catalytic mechanism of RING (really interesting new gene) E3 ligases. (A) Crystal structure of the RING E3 monomer CBL (PDB: 1FBV). The RING domain is indicated in orange and the substrate-binding domain in gray. (B) Crystal structure of the RING E3 homodimer cIAP (PDB: 3EB5). One RING monomer is indicated in orange, the other in yellow. (C) Nuclear magnetic resonance structure of the RING E3 heterodimer BRCA1 (orange) and BARD1 (yellow). (D) Schematic catalytic mechanism of a RING E3 ligase: The RING domain enables Ub-loaded E2 ligase binding, and the substrate is recruited by the substrate-binding domain of the E3 ligase. The Ub transfer is carried out directly by the E2 ligase and no intermediate transfer to the E3 ligase is needed. (E) Crystal structure of a cullin-RING ligase (CRL). The RING box protein 1 (RBX1) is indicated in orange, cullin protein 1 in blue, and the substrate receptor in gray. Stabilizing zinc ions are shown in gray spheres. Adapted from Buetow et al.[169] with the permission of Springer Nature (License number 501980533).

Neural precursor cell expressed developmentally downregulated protein 8 (NEDD8) represents an essential PTM to activate CRLs, which is called neddylation. This ubiquitin-like protein is transferred by a NEDD8-activating enzyme (NAE)-E2 to the C-terminal domain of cullin and converts the binding partner RBX1 into an open conformation. It enables tethering RBX1 on a β-strand, bridging the distance to the target protein and freeing the RING domain for Ub transfer.[196,197] To prevent CRLs of neddylation, the NAE inhibitor MLN4924 was developed and leads to accumulation of ubiquitinated proteins in combination with anticancer effects.[198]

These high number of CRL´s substrate receptors enable recognition of an enormous variety of degrons, specific degradation signals within the protein structure. PTMs of degrons are key factors in timing protein-E3 ligase interaction, including HIF-1α. Under hypoxic conditions, HIF-1α forms a heterodimeric transcription factor for adaptation to low oxygen levels. Upon normoxic conditions, a HIF-1α-specific prolyl hydroxylase utilizes molecular oxygen for hydroxylation of proline (P564) of HIF-1α, generating the oxygen-dependent degron.[199] This degron is recognized by the E3 ligase VHL, connected by elongin B and C to Cul2 and RBX1.[200] VHL is associated with the von Hippel-Lindau syndrome, first described by von Hippel in 1911 and characterized by the development of multiple vascular tumors caused by mutations of *VHL* gene, disabling the assembly of $CRL2^{VHL}$ complex. Therefore *VHL* gene is considered an tumor suppressor gene.[201]

Similar to VHL, feminization-1 homolog b (FEM1B) is incorporated into a Cul2 E3 complex and is considered a tumor suppressor gene. Feminization-1 (FEM1) was found to regulate the sex determination pathway of nematodes by acting as an E3 ligase.[201] Likewise, its homolog b marks the oncoprotein Gli1 for proteasomal degradation in humans and FEM1B single nucleotide polymorphism is associated with polycystic ovary syndrome.[202,203]

$CRL4^{CRBN}$ represents another well-known E3 ligase complex. Consisting of cereblon (CRBN) connected by DNA damage-binding protein 1 (DDB1) to Cul4 and RBX1, it was identified as the driver of teratogen effects of the anti-insomnia drug thalidomide. It is recognized by CRBN and binds transcription factors to the E3 ligase. Subsequent polyubiquitination and degradation of the transcription factors results in the teratogen and immunomodulatory effects.[204] Thalidomide and derivatives are further introduced in chapter “1.3.4 Modalities for Target Protein Degradation – PROTACs & Beyond”. Cause of the neo-substrate binding is the structural similarity of thalidomide to the C-terminal cyclic imide degron recognized by CRBN (Fig. 12). This PTM originates from glutamine or asparagine and can occur by spontaneously cyclization, considered as protein damage, or is generated by specific enzymes.[205]

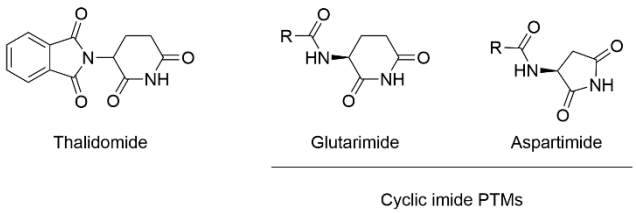

Figure 12. Thalidomide and the cyclic imide post-translational modifications (PTMs) glutarimide and aspartimide.

As CRBN binds to DDB1, it is considered as a DDB1-CUL4 associated factor (DCAF). There are more than 90 DCAFs known, categorized according to whether they contain WDR. The WDR facilitates ligand discovery as there are known binders of WDR, while targeting WDR-free DCAFs (e.g. CRBN and DCAF15-17) is more challenging and needs first-in-class ligands. DCAF11 belongs to the WDR containing and is mainly localized in the nucleus.[206,207]

Beside these CRL there are two homo-/heterodimer RING ligases frequently used in TPD. As mentioned earlier, inhibitor of apoptosis protein (IAP) E3s are involved in DNA repair, further they regulate apoptosis and innate immune response by regulation of nuclear factor "kappa-light-chain-enhancer" of activated B-cells signaling.[208] They were first described in baculoviral genome and protect cells from cell-death stimuli, thus are important for cancer cells, neuronal cells and for the efficient replication of many viruses. They contain one to three N-terminal baculovirus IAP repeats (BIR) domain and a C-terminal RING domain.[209] The BIR domain consist of approximately 70 residues and is responsible for binding the substrate groove of caspase.[210] However, only X chromosome-linked IAP (XIAP) directly inhibits caspases-3, -7, -9 and possess the highest anti-apoptotic activity, while cellular IAP1 and 2 (cIAP1/2) regulate caspase 8 indirect by tumor necrosis factor receptor signaling.[211,212] In addition, cIAP1 and 2 are able of ubiquitination of caspase-3 and -7 upon binding, resulting in the proteasomal degradation of the marked proteins.[213] As IAPs form dimers, this E3 ligase activity leads to autoubiquitination and degradation of them.[214] Further, the methyl-ester of the approved drug bestatin was found to interact with BIR3 of cIAP1 and promotes auto-ubiquitination of cIAP1.[215]

Similar to IAP, mouse double minute 2 (MDM2) is a RING-type E3 ubiquitin ligase that functions in dimers. MDM2 is closely linked to the tumor suppressor p53 as it is part of an autoregulatory feedback loop: p53 activates the transcription of MDM2, which in turn downregulates p53 activity.[216] MDM2 negatively regulates p53 through three mechanisms: it binds to the transactivation domain of p53, promotes its nuclear export, and facilitates its degradation by acting as an E3 ligase. As a result, p53 levels remain low under physiological conditions.[217] However, in response to DNA damage, the MDM2-binding domain of p53 becomes phosphorylated, preventing MDM2 interaction. This leads to p53 stabilization and activation,

thereby promoting DNA repair and cell cycle arrest.[218] In addition to targeting p53, MDM2 also undergoes autoubiquitination, allowing it to autoregulate its own protein levels.[219] As previously noted, p53 is frequently inactivated or downregulated in cancer. Accordingly, its negative regulator MDM2 is often amplified in various malignancies. Interestingly, mutations in p53 and amplification of MDM2 rarely occur simultaneously. For example, in soft tissue tumors, MDM2 amplification is favored over p53 mutation.[220] Due their critical in tumor biology, the p53–MDM2 interaction has become an important target for cancer drug development. The interaction is facilitated by a hydrophobic pocket of MDM2 for binding p53. Nutlins have been reported as potent PPI inhibitors by mimicking the p53 interaction and occupying this hydrophobic pocket.[221]

1.3.3 Mode of Action and Advantages of Targeted Protein Degradation

The key advantage of degraders, including proteolysis targeting chimeras (PROTACs), is their catalytic mode of action, which results in unique properties of degraders compared to occupancy-driven inhibitors. Degraders induce proximity between the POI and the E3 ligase, the catalytic complex, which is responsible for polyubiquitination. In case of CRL, representing the largest group of E3 ligases (see 1.3.2 E3 Ligases), a ubiquitin-loaded E2 is bound to the RING domain of the E3. This enables the polyubiquitination of the POI and subsequent degradation by the 26S proteasome (Fig. 13).[222] After dissociation of the ternary complex, composed of POI, degrader, and E3 ligase, the PROTAC can recruit the next POI for polyubiquitination. This, enables a catalytic mode of action of the degrader.[223]

Based on this mode of action, degraders possess promising advantages compared to occupancy-driven inhibitors, including prolonged pharmacological effects, subsequent potential longer dose intervals, and dose reduction. As adverse effects by off-target inhibition are also dose dependent, a decrease in side effects is expected due to dose reduction.[224] Further POI-independent adverse effects are presumed, because of the E3 ligase recruitment. However, as the E3 ligase is only transiently utilized, the physiological substrate degradation is probably not effected.[223] By degrading the POI, degrader enable to target proteins considered undruggable before, including transcription factors and other proteins that lack a catalytic function.[225] Another feature of the catalytic mode of action is the ability to overcome POI overexpression or amplification, which is a common escape strategy of cancer cells against occupancy-driven inhibitor treatment.[226] Moreover, PROTACs can bypass cancer cell resistance caused mutated ligand binding sites, as even weak binders are able to from stable ternary complex leading to degradation of the POI.[227] This is due to complex-supporting PPI of the POI and the E3 ligase, resulting in positive cooperativity.

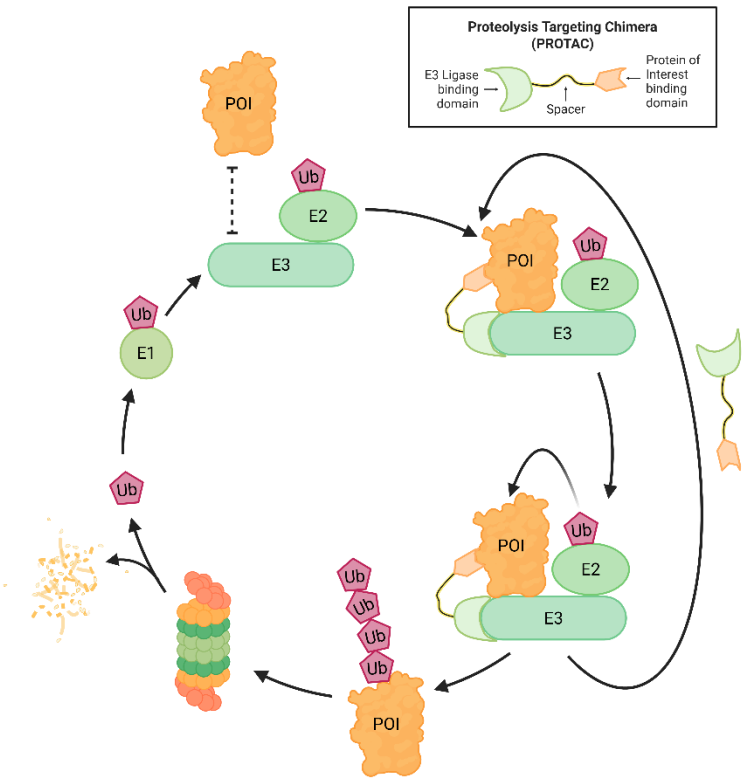

Figure 13. Mode of action of proteolysis targeting chimeras (PROTACs). Under physiological conditions, the protein of interest (POI) is not recognized by the E3 ligase. The PROTAC induces proximity between the POI and the E3 ligase, by bearing ligands for both proteins. As the E3 ligase recruited a ubiquitin (Ub) loaded E2 ligase, it enables the transfer of Ub to the POI. After multiple cycles of Ub-transfer, the POI is polyubiquitinated and recognized by the proteasome, leading to degradation of the POI and recycling of Ub. An E1 ligase activates the Ub by transfer to the E2, which is recruited by the E3. Together with the PROTAC, the E3 ligase complex is able to mark the next POI for proteasomal degradation. Remarkable is the catalytic mode of action of PROTACs. After the POI is ubiquitinated, the PROTAC molecule dissociates and can recruit the next POI for ubiquitination. Adapted from Li et al.[222] *Created with BioRender.com*

Furthermore, the additional PPI and cooperativity drives degradation specificity, as it is dependent of the recruited isoforms.[228] Thereby, a promiscuous POI ligand can enable selective degradation, if incorporated into a PROTAC.[229] However, non-cooperative ternary complexes can be sufficient in POI ubiquitination as well.[230] Moreover, the accessibility of free lysine residues of the POI and geometry of the ternary complex are additional crucial requirement for successful Ub-transfer. Therefore, the lysine residues facing the Ub-loaded E2 ligase are more accessible for ubiquitination, while those at the opposite side are less likely to be modified. However, a stabile ternary complex can be insufficient for target ubiquitination, if the POI is oriented away from the Ub-loaded E2.[231] These factors are influenced by the organization and interactions of the subunits of the ubiquitinating complex. Achieving flexibility to bridge the space between free lysine of the POI and C-terminus of ubiquitin can be beneficial.[232] This flexibility is also required for elongation of the Ub-chain.[192]

1.3.4 Modalities for Target Protein Degradation – PROTACs & Beyond

The first discovery of a small molecule reprogramming the function of an E3 ligase was the indoleacetic acid named auxin (Fig. 14). The phytohormone targets the E3 ligase complex consisting of Skp1/2, Cul1 and FBP complex (SCF) and transport inhibitor response 1 (TIR1), which leads to the recognition and degradation of a transcription repressor family. By removing the transcription repressors, auxin-response factors can bind to the auxin-response elements causing the expression of downstream genes, promoting cell growth. SCF^{TIR1} consists of a Cul1 scaffold connecting the RBX1 with SCF bound to the F-box TIR1.[233] Auxin binds to the substrate receptor TIR1, adding a hydrophobic patch to TIR1 and enables the binding of transcription repressors and subsequent polyubiquitination by SCF^{TIR1}. As the transcription repressors stick to TIR1 after the addition of auxin, this effect is considered as molecular glue (MG) degrader mechanism and is used for further molecules exhibiting a similar mode of action.[234] One of which can be found in human cells upon human papilloma virus (HPV) infection. HPV type 16 and 18 induce the expression of the viral protein E6, which recruits the human E3 ligase E3A to p53, leading to polyubiquitination and degradation of p53. This mechanism plays an essential role in HPV-induced carcinogenesis.[235]

The term molecular glue was first used by Schreiber in 1992,[236] describing the ability of cyclosporine A and FK506 to physically connect calcineurin to cyclophilin or FK506-binding protein 12 (FKBP12), respectively (Fig. 14). Under physiological conditions, binding of calcineurin to cyclophilin or FKBP12 was not observed, but by the addition of cyclosporin A or FK506 they

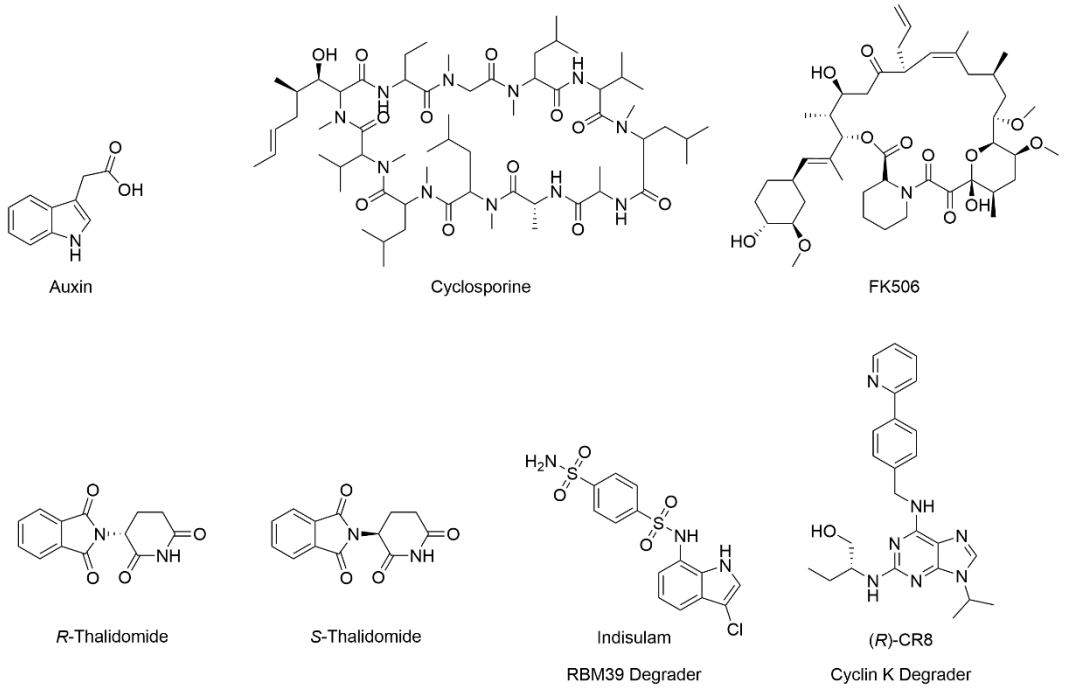

Figure 14. Examples for molecular glues and molecular glue degraders.

were glued together.[236] However, further studies indicated that in most cases molecular glues join proteins, which possess slight basal interaction.[237] MG degraders can be distinguished in natural degraders like the already introduced auxin and the viral protein E6, in contrast to synthetic compounds exhibiting MG degrader properties, including thalidomide and derivatives.

The anti-insomnia drug thalidomide was first authorized in Germany in October 1957 and partially sold without prescription, as it was found to be safe in rodents. In the early 1960s, an increasing number of children were born with hypoplastic limb defects and a correlation with thalidomide therapy during pregnancy lead to the withdrawal of the drug from commercial sales in 1961. In this time, thalidomide was responsible for more than 10,000 cases of affected embryos, while 20-36 days after fertilization was identified as the most sensitive period for development of malformations under the use of thalidomide.[238] The *S*-enantiomer is associated with the teratogenic effects, while the *R*-enantiomer represents the eutomer (Fig. 14).[239] However, thalidomide is hydrolysed fast and is rapidly racemized *in vivo*, so administering the eutomer is not an applicable strategy.[240] The observation of anti-inflammatory, anti-angiogenetic, and anti-myeloma effects led to the market reentry of thalidomide and development of derivatives classified as immunomodulatory imide drugs (IMiDs), including lenalidomide.[241] Despite the huge research effort, it took till 2010 to identify CRBN and $CRL4^{CRBN}$ as the molecular target of thalidomide, responsible for the teratogenicity.[204] IMiDs bound to CRBN induce recognition and polyubiquitination of the transcription factors Ikaros (IKZF1) and Aiolos (IKZF3) by $CRL4^{CRBN}$. Subsequent degradation of the transcription factors, responsible for immune cell differentiation lead to the anti-neoplastic effects.[242] Continuous research was able to identify even more neo-substrates of $CRL4^{CRBN}$ upon IMiD-treatment, including casein kinase 1α (CK1α), G1 to S phase transition 1 (GSPT1), and Sal-like protein 4 (SALL4), whereas the last one is mainly responsible for the teratogenicity in form of limb deformations.[243–245]

In analogy to IMiDs, the MG degrader properties of aryl sulfonamides, such as indisulam, were identified retrospectively (Fig. 14). By hijacking $CRL4^{DCAF15}$, indisulam induces degradation of the splicing factor RNA binding motif protein 39 (RBM39). RBM39 degradation causes aberrant pre-mRNA splicing resulting in cytotoxicity in hematopoietic and lymphoid cancer cells, especially under high DCAF15 expression. Interestingly, indisulam only exhibits binding affinity to the complex of DCAF15 and RBM39, not to the single proteins, indicating that high affinity ligands are not needed for effective MG degradation.[246] Despite their serendipitous identification, MG degraders encompasses advantages like non-saturable kinetics (hook effect, see 1.3.4.1 Proteolysis Targeting Chimeras (PROTACs)), more drug-like properties, and in case of thalidomide and derivatives, the existence of already approved drugs.[247] In recent years, drug discovery for MG

degraders has changed to more intentional screening methods. One approach is to investigate cytotoxicity data of small molecules and correlate them with E3 ligase expression levels. By this data-mining process, Słabicki *et al*. identified a correlation between the cytotoxicity of **(*R*)-CR8** (Fig. 14), a CDK inhibitor, and mRNA levels of DDB1, the CUL4 adaptor protein, bypassing the utilization of a substrate receptor. Further proteomics studies, knockout resistance screens, and crystal structures confirmed the recruitment of CDK12 to the DDB1-CUL4-RBX1 complex. As CDK12 binds cyclin K, bridging the gap to the Ub-loaded E2, cyclin K gets ubiquitinated and degraded.[248] Mayor-Ruiz *et al*. developed a phenotypic screening by inactivating the NEDD8-transferring E2 ligase ubiquitin conjugating enzyme E2 M (UBE2M) leading to CRL dependent degrader resistance. By comparison of $UBE2M^{WT}$ and $UBE2M^{inactive}$ cells, they identified different MG degraders, through screening over 2,000 small molecules. Further knockout resistance screens and proteomics studies were applied for E3 ligase and POI identification.[249]

Recent examples in development of degraders led to the closing of the gap between monovalent MG degraders and bifunctional PROTACs. The Nomura group reported two covalent handles, which can be fused to multiple POI ligands for the recruitment of RING finger protein (RNF) 126 or DCAF16, respectively. The ribociclib-based degrader **EST1060** and the **JQ1**-based degrader **ML 1-50** (Fig. 15) induced substantial degradation of CDK4 or bromodomain containing protein 4 (BRD4), respectively. Further, the concept could be expanded to additional targets, including the androgen receptor (AR) and bruton tyrosine kinase (BTK). Despite calling the compounds MG degraders, the authors state, the degraders can be considered as spacer-less or mini-PROTACs, as they are composed of a distinct E3 ligase recruiter and a POI ligand.[250,251]

As TPD is an innovative and modern field of research with ongoing development and new concepts, there are multiple modalities beyond MG degraders, PROTACs, and modalities in between. This includes heterobifunctional molecules targeting non-UPS dependent pathways, like autophagy-targeting chimeras (AUTACs), autophagosome-tethering compounds (ATTECs), lysosome-targeting chimeras (LYTACs) and antibody-based PROTACs (AbTACs). Similar to

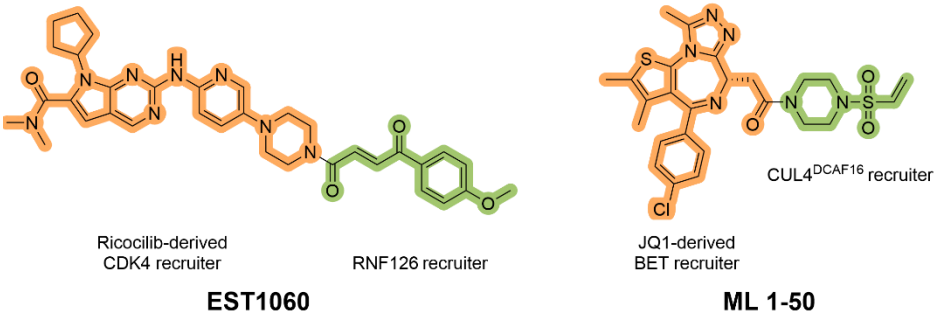

Figure 15. MG degraders, also considered as spacer-less or mini-PROTACs. The POI ligand is highlighted in orange and the E3 ligase recruiter in green.

PROTACs, AUTACs, and ATTECs target degradation of intracellular POIs. As *S*-guanylation leads to autophagy, AUTACs connect a guanine derivative to a POI recruiter (**AUTAC2**, Fig. 16), leading to successful degradation of FKBP12 and other proteins by exchanging the POI ligand. In addition, as autophagy is responsible for organelle and disease-related debris, AUTACs targeting mitochondria are able to remove fragmented mitochondria.[252] Similarly, Autophagy-targeting chimeras (AUTOTACs) target the same degradation mechanism, but with a ligand for the autophagy receptor p62. By activating p62, they lead to assembly of the autophagosome and degradation of the associated POI.[253] Comparable, ATTECs tether proteins directly to the autophagosome by recruiting 1B-light chain 3 (LC3), as part of the autophagosome membrane. Li *et al*. first discovered a ligand to degrade the mutant huntingtin protein by this mechanism, while further studies fused the LC3 ligand to a POI recruiter, creating heterobifunctional molecules like **10f**, which successfully

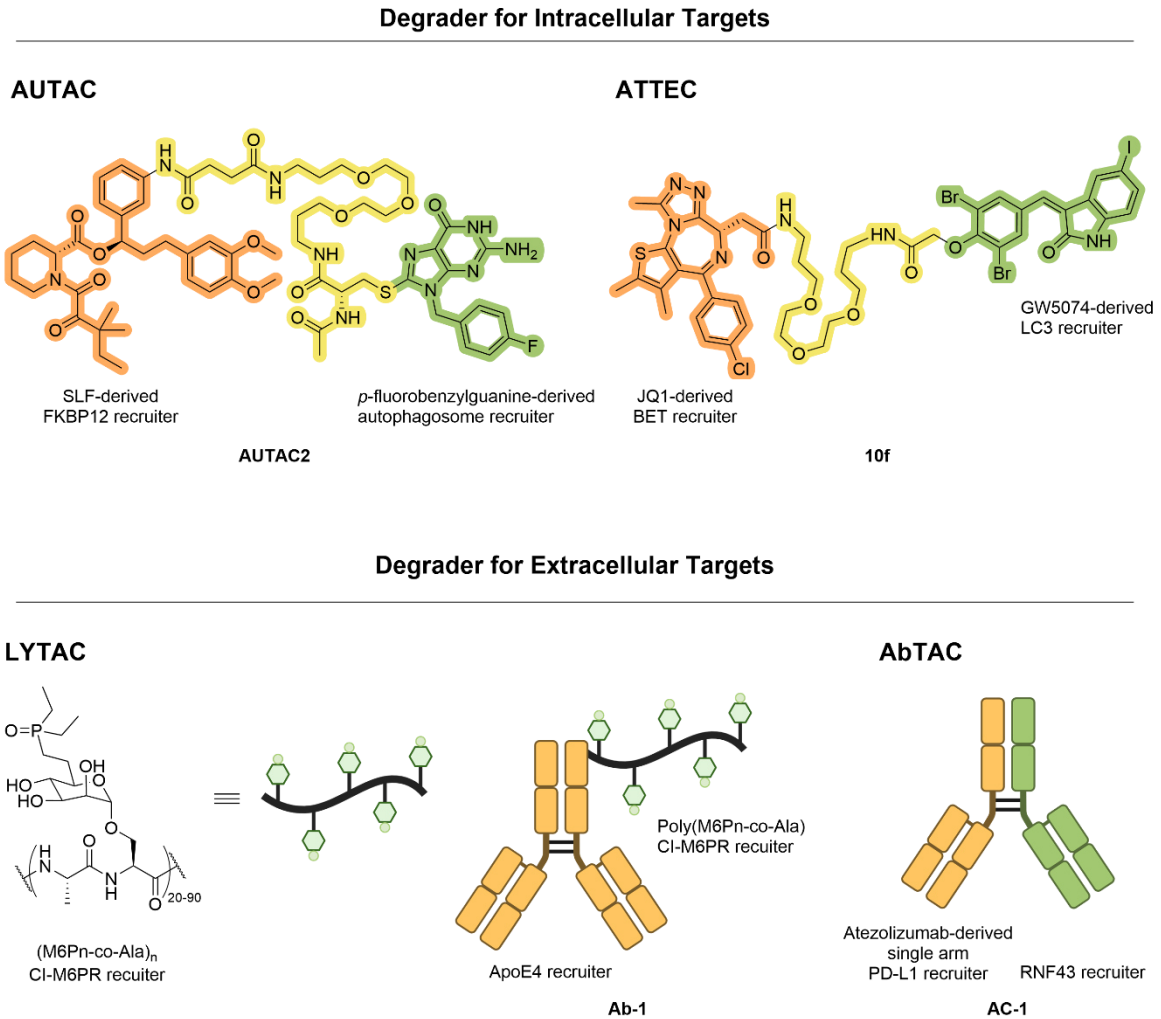

*Figure 16. Alternative degrader strategies for intra- and extracellular targets, each comprising a protein-of-interest ligand (POI, orange) and a degradation machinery recruiter (green), sometimes linked by a spacer (yellow). The autophagy-targeting chimera (AUTAC) **AUTAC2** contains SLF for FKBP12 binding joined via a spacer to p-fluorobenzylguanine for autophagosome recruitment. The autophagosome-tethering compound (ATTEC) **10f** links the BRD4 binder **JQ1** to the LC3 recruiter GW5074. Extracellular protein degraders often include antibodies: the lysosome-targeting chimera (LYTAC) **Ab-1** pairs an anti-ApoE4 antibody with an (M6Pn-co-Ala)$_n$ copolymer for CI-M6PR recruitment, while the antibody-based PROTAC (AbTAC) **AC-1** is a bispecific antibody combining atezolizumab for PD-L1 binding with an RNF43-recruiting arm to induce internalization and degradation.* Created with BioRender.com

degraded BRD4.[254,255] It should be noted, that the uses of the terms AUTAC, AUTOTAC, and ATTEC are not perfectly separated and can be used to describe identical compounds.[256] In contrast to this cytoplasmic POI recruitment, LYTACs and AbTACs trigger extracellular processes. After initial feasibility studies, the first LYTAC (**Ab-1**, Fig. 16) was composed of a monoclonal antibody (mAb) directed to the extracellular apolipoprotein E4 (ApoE4), related to Alzheimer´s disease. The mAb is conjugated to multiple serine-*O*-mannose-6-phosphonate (M6Pn) alanine copolymers (M6Pn-co-Ala)$_n$, which is recognized by the cation-independent mannose-6-phosphate receptor (CI-M6PR), a lysosome-targeting receptor. By internalization and shuttling to the lysosome, cellular uptake of ApoE4 was successful. Apart from extracellular targets, also transmembrane POIs were degraded by LYTACs, including epidermal growth factor receptor (EGFR).[257] AbTACs are also antibody-based, however, they are entirely recombinant bispecific antibodies. One antibody arm is directed against the POI and the other arm is directed against membrane-bound E3 ligase RNF43. Incorporating one arm of the programmed death-ligand 1 (PD-L1) binding mAb atezolizumab, Cotton *et al*. were able to degrade PD-L1 in a lysosomal-dependent manner with **AC-1** (Fig. 16).[258]

The promising opportunities of TPD will lead to the development of further modalities and techniques for targeted degradation. However, the next subchapters are focused on the modalities most relevant for this work.

1.3.4.1 Proteolysis Targeting Chimeras (PROTACs)

Proteolysis targeting chimeras are the most common modality in TPD with more than 6,000 PROTACs reported according to the PROTAC-DB 3.0.[259] These bifunctional molecules are composed of three parts: the POI ligand, binding the protein that is supposed to be degraded, an E3 ligase recruiter, enabling ubiquitination, and a spacer, connecting the two ligands and facilitating the optimal distance and geometry for the ternary complex (Fig. 13).[260]

Sakamoto *et al*. introduced the first PROTAC, which utilized a phospho-degron recognized by SCF$^{\beta\text{-TrCP1}}$ and comprised a phosphorylated decapeptide derived from Inhibitor of NF-κB α (IκBα).[261,262] By fusing the phospho-degron of IκBα to the methionine aminopeptidase-2 (MetAP-2) inhibitor ovalicin they developed **PROTAC-1** (Fig. 17), which successfully induced ubiquitination and degradation of MetAP-2. However, the use of the phosphorylated decapeptide limited cell permeability of **PROTAC-1**. In 2004, the first cell permeable PROTAC was introduced by combining a cell-penetration peptide sequence with the degron of HIF-1α. It contains a central proline, which is hydroxylated under normoxic conditions leading to VHL recruitment (**PROTAC-4**, Fig. 17). This enabled the degradation of FKBP12 or the androgen receptor in a cellular environment.[263] These

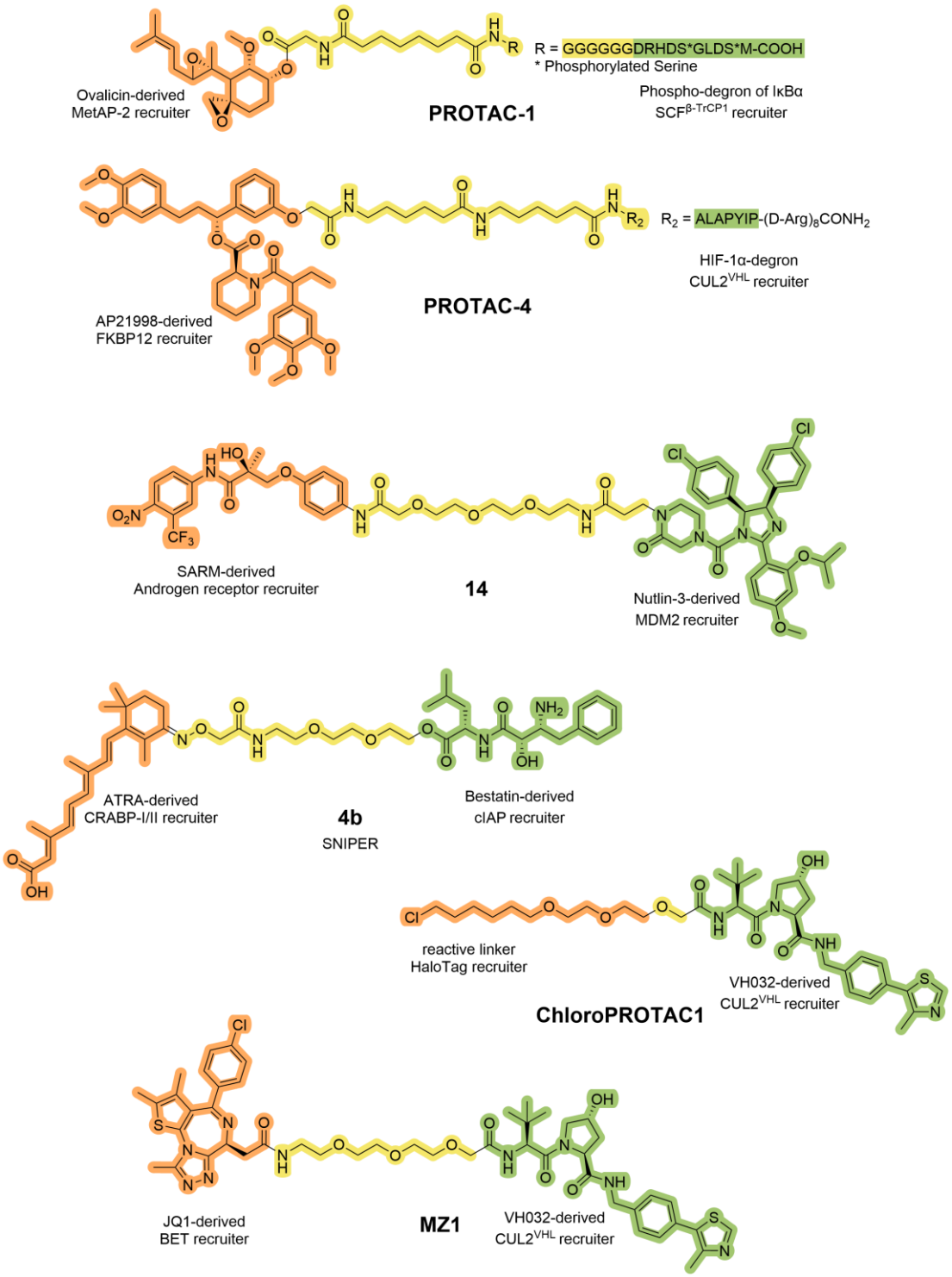

Figure 17. The first examples of PROTACs, introducing the E3 ligases for TPD or representing first non-peptide based PROTACs. The POI ligand is marked in orange, spacer in yellow and E3 ligase recruiter in green.

first generation of PROTACs successfully proved the feasibility of targeted protein degradation by heterobifunctional molecules, but only yielded low-micromolar activity due to the peptide substructure and limited cell permeability. In addition, peptide-based drug candidates also come with the risk of immunogenicity.[167]

The first non-peptide PROTAC was reported in 2008 that degrades the androgen receptor by recruitment of MDM2 with a nutlin-3 derivative (**14**, Fig. 17), thereby improving cell permeability and introducing the third E3 ligase for TPD.[264] However, it exhibited still low-micromolar activity. In the following years, a novel E3 ligase was introduced to TPD by Itoh *et al*. reporting PROTAC **4b**, which degraded cellular retinol- and retinoic acid-binding protein I and II (CRABP-I and II) in a sub-micromolar range by recruitment of cIAP1 using a bestatin-derived structure (Fig. 17).[265] As MDM2 and IAPs promote tumorigenesis by degradation of p53 and inhibition of apoptosis, respectively, they are often overexpressed in cancer cells, enabling cancer-specific POI degradation by degraders. Further, the utilization for TPD can lead to stabilization of the physiological substrate and yields additional antiproliferative efficiency.[266,267] PROTACs recruiting IAPs are also called specific and nongenetic IAP-dependent protein erasers (SNIPERs).[268] However, utilization of IAPs and MDM2 is limited due to autoubiquitination (see 1.3.2 E3 Ligases & Ligands).

Due to the limitations of the peptide-based VHL ligand, a small-molecule recruiter was developed in parallel, bearing the central hydroxy-proline. Fragment-based screens and docking studies led to the first non-peptide VHL ligand and further optimization yielded **VH032** with nanomolar binding activity.[269,270] **VH032** and its derivatives were used for the development of the first small-molecule VHL-recruiting PROTACs (**ChloroPROTAC1**, Fig. 17). The reactive chloroalkyl ligand enabled covalent binding to the haloalkane dehalogenase tag (HaloTag)-enhanced green fluorescent protein (EGFP) fusion-protein.[271] The HaloTag system utilizes a modified bacterial haloalkane dehalogenase and an electrophilic ligand.[272] While this system offers high specificity and flexibility by the irreversible covalent ligand and the possibility to fuse the HaloTag to any protein of choice, ChloroPROTACs can be only considered tool-compounds, which lose the ability of catalytic POI turnover, due to irreversible binding of the POI. More drug-like properties were gained by **MZ1**, utilizing again **VH032** but degrading BRD2, 3 and 4 by integration of the selective BET family recruiter **JQ1**. Similar to previous work, HIF-1α is not stabilized by hijacking VHL preventing undesired effects upon physiological substrate stabilization.[273]

However, in parallel CRBN was discovered as the target of IMiDs that results in the degradation of neosubstrates, including IKZF1 and 3.[242] This discovery led to the development of **dBET1** and **ARV-825** targeting CRBN with thalidomide and pomalidomide (Fig. 18). Both integrate **JQ1** as POI ligand, achieving BRD4 degradation, but differ in spacer design and length. Interestingly, **ARV-825** proved to be superior to conventional BRD4 inhibitors in terms of duration and exhibiting half maximal degradation concentration (DC_{50}) in the picomolar range. Further, Winter *et al*. accomplished *in vivo* degradation and expanded the portfolio of degradable proteins by CRBN to other targets such as FKBP12.[274,275]

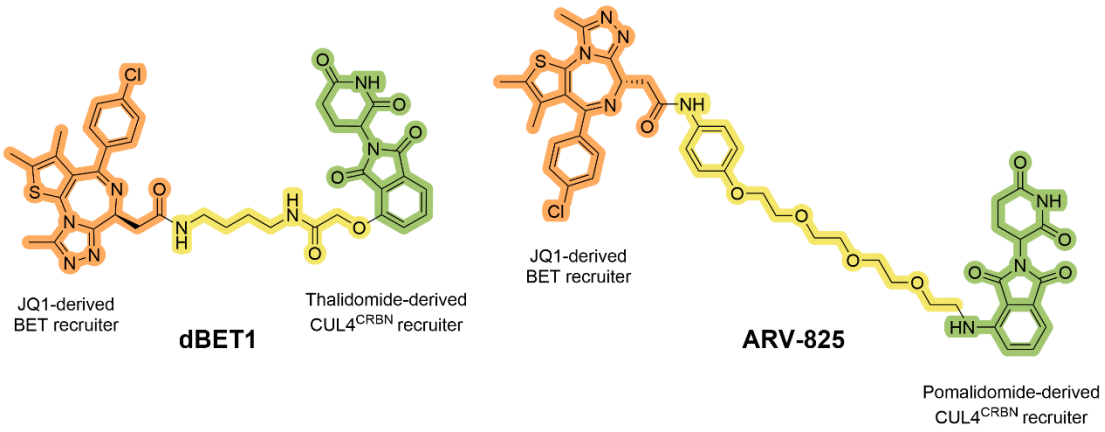

Figure 18. First CUL4^{CRBN} recruiting PROTACs. The POI ligand is marked in orange, spacer in yellow, and E3 ligase recruiter in green.

The spacer design for the mentioned PROTACs was rather simple, typically composed of polyethylene glycol (PEG) or alkyl chains. In recent times, spacer design has been recognized as a pivotal step in degrader development, to achieve a highly active ternary complex by enforcing suitable geometry and drug-like properties. Spacer length, composition, rigidity, and attachment point have to be optimized for every POI/E3 ligase pair separately. As ternary complex prediction remains a complex challenge, there are currently only limited application strategies for spacer development than trial and error.[276] Despite this, some experiences were gained in spacer optimization. There is a sweet-spot in spacer length that is considered optimal.[277] However, the range of optimal length could be rather wide, as in some cases only a minimal length is required upon which positive cooperativity supports the ternary complex.[228] Even short spacers can achieve stable E3-POI complexes and probably lead to more selective degradation, due to distinct interactions of E3 and POI.[278] Furthermore, a longer spacer, particularly alkyl-based, can also be associated with decreased solubility and absorption.[279] To handle this issue, spacer composition can be changed from alkyl to PEG-based, increasing water solubility with the risk of reduced cell permeability.[280] The composition can also affect the rigidity of the spacer, by incorporation of ethynyl or cyclic groups, including saturated heterocycles like piperazine and piperidine, or triazole and other aromatic groups or spiro-cyclic moieties (Fig. 19). Especially if the optimal length is

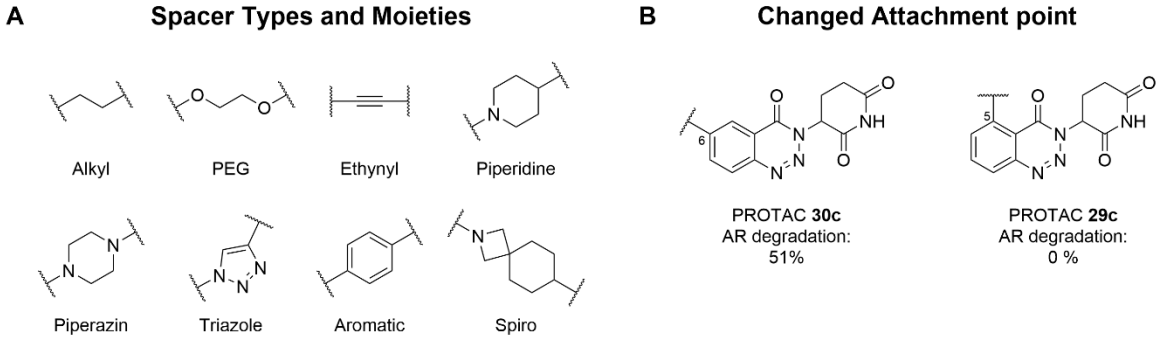

Figure 19. (A) Different types of spacers incorporated into PROTACs. (B) Effect of changed attachment points on androgen receptor (AR) degradation potency.

known, rigidification can be beneficial.[277] However, the majority of spacers is still alkyl-based, followed by PEG-based spacers.[280] In addition, more rigid spacers can also decrease degradation potency, probably due to less stable ternary complexes or reachable lysine residues for ubiquitination.[231,278,281] As the ternary complex is a highly dynamic construct, the sweet-spot between rigidification and flexibility has to be determined empirically. Besides the spacer composition and structure, the attachment points at the POI and E3 recruiters are also crucial. For instance, changing spacer attachment at the $CUL4^{CRBN}$ recruiter from position 6 to 5, the degradation potency of PROTAC **29c** is reduced from 51% (PROTAC **30c**) to 0% (Fig. 19).[281]

As the research field of TPD and PROTACs is still young and rapidly evolving, there are no approved PROTACs on the market yet, however, multiple are under clinical development. The first PROTAC entering the clinics was bavdegalutamide/**ARV-110**, recruiting CRBN by a fluoro-thalidomide ligand connected by a rigid piperazine-piperidine-spacer to the androgen receptor ligand (Fig. 20). It proved to degrade wild type and abiraterone or enzalutamide associated mutant AR. First disclosed preclinical data showed superiority of the oral administered PROTAC against occupancy driven inhibitors.[282] The most advanced PROTAC in clinical development is vepdegestrant/**ARV-471** (Fig. 20). Recently, the developing companies submitted a new drug application to the FDA for vepdegestrant, which is therefore estimated to be the first approved PROTAC.[283] This oral bioavailable estrogen receptor degrader targets both wild type and mutant ER. In the recent phase III clinical trial, it was tested in ER positive and human EGFR2 negative advanced breast cancer patients in monotherapy as well as in combination treatment with the CDK4/6 inhibitor palbociclib.[284] Apart from these two PROTACs developed by Arvinas, there are multiple others clinical trials for PROTACs from different companies, targeting also other tumor targets, including BTK, EGFR, B-cell lymphoma protein 6 and Kirsten rat sarcoma virus (KRAS).[285]

Furthermore, multiple innovative approaches have been developed to improve PROTACs in toxicity and physicochemical properties. [286–289]

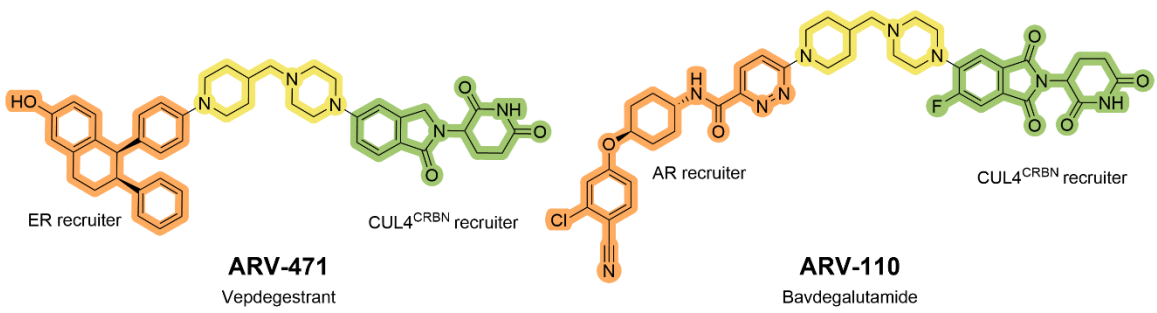

Figure 20. Vepdegestrant is the PROTAC in the most advanced clinical phase, while bavdegalutamide was the first PROTAC entering clinical trial.

1.3.4.2. Hydrophobic Tagging

An emerging alternative for PROTACs and MG degraders in TPD is hydrophobic tagging. The POI is destabilized or mimics destabilized proteins by the hydrophobic-tagged (HyT) degrader, resulting in recruitment of the cellular quality control machinery (Fig. 21).[290] Under physiological conditions, hydrophobic residues are mainly localized in the inner core of the protein, as they aggregate spontaneously in a hydrophobic collapse after biosynthesis, forming the secondary and ternary structure of the protein.[291] An incorrectly folded protein displays hydrophobic residues at its surface, which is recognized by chaperones, including the HSP70 member binding immunoglobulin protein (BiP).[292] Chaperones bind to these hydrophobic areas to prevent aggregation and support refolding of proteins, as aggregates are highly toxic for cells. In case of increased stress conditions or if refolding failed, the misfolded protein will be degraded by the UPS or the autophagy-lysosome system.[293] As mentioned before, the major cellular machinery disposing misfolded proteins is the UPS. The C-terminus of HSP70 interacting protein (CHIP) represents an E3 ligase, binding to the C-terminal domain of HSP70, HSC70, or HSP90 and transfers ubiquitin to the bound client proteins leading to proteasomal degradation of misfolded proteins. In addition, CHIP regulates elevated chaperone levels after recovery of stress conditions, by transferring ubiquitin to the chaperones itself.[294,295] HyT degraders mimic the hydrophobic residues at the surface of

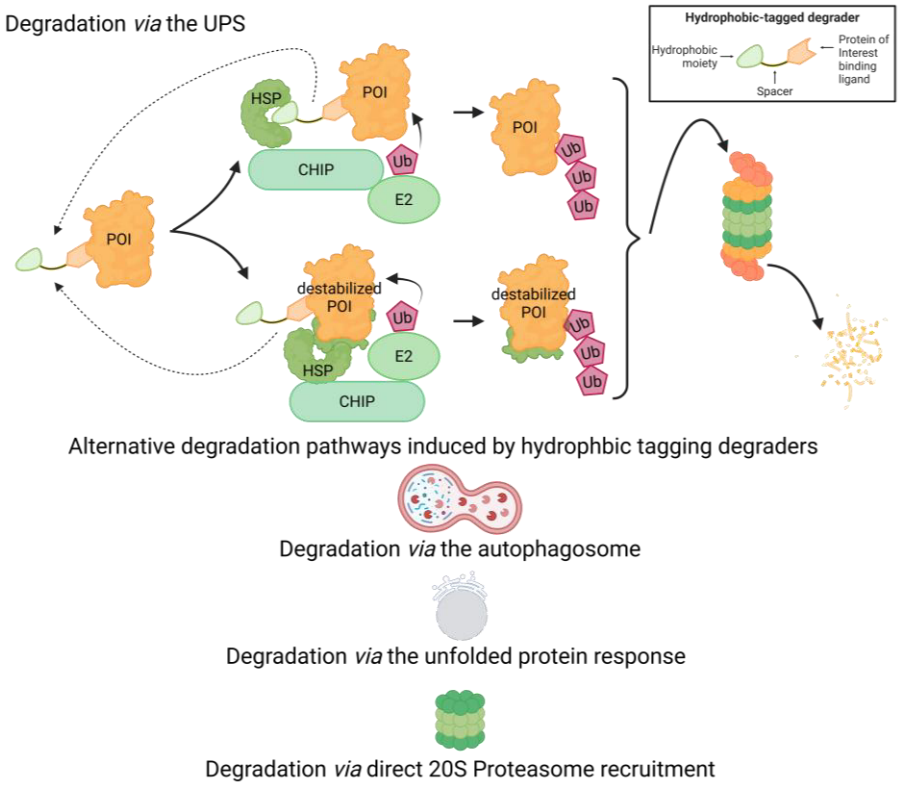

Figure 21. Degradation mechanism of HyT degraders. The most common mechanism is assumed to recruit heat shock proteins (HSP) by the HyT degrader or by the destabilized protein of interest (POI). These are recognized by E3 ligases like CHIP transfering ubiquitin (Ub) to the POI and lead to degradation of it. Alternative routes for degradation of the POI include pathways via the autophagosome, unfolded proteins response, or direct 20S proteasome recruitment. Created with BioRender.com

misfolded proteins, triggering the recognition of chaperones and refolding fails, thereby leading to proteasomal degradation (Fig. 21). However, as the exact mechanism of hydrophobic tag induced degradation is still not fully elucidated, there are further pathways proposed to be at least partially responsible for degradation. Autophagosome is also proposed to be involved as well as unfolded protein response (UPR) activated by endoplasmic reticulum stress, or ubiquitin independent proteasomal degradation by direct targeting of the 20S proteasome (Fig. 21).[296]

In 2011, Neklesa *et al*. disclosed the first HyT degraders.[297] By utilizing the HaloTag system, which was also used for the ChloroPROTACs, proteasomal degradation of HaloTag-EGFP fusion proteins was induced. The HyT degraders are composed of the covalent HaloTag ligand connected by a long triazol-containing PEG spacer to different hydrophobic moieties (Fig. 22). **HyT13** containing an adamantyl moiety was chosen for further *in vivo* studies, because of successful degradation, high stability, and cell permeability. By fusing the HaloTag to the known tumor target Harvey rat sarcoma virus mutant G12V ($HRAS^{G12V}$) it was confirmed that **HyT13** treatment can reduce $HRAS^{G12V}$-HaloTag levels *in vitro* and tumor growth *in vivo*.[297] Only one year later Long et *al*. published *tert*-butyl carbamate-protected arginine (Boc_3Arg) as a hydrophobic moiety do generate HyT degraders. They connected the covalent glutathione-S-transferase-α1 (GST-α1) recruiter ethacrynic acid to Boc_3Arg by an alkyl spacer to generate compound **EA-Boc_3Arg** (Fig. 22). The degrader was able to degrade GST-α1 in a time- and concentration-dependent manner. They also introduced the first non-covalent HyT degrader **TMP-Boc_3Arg** (Fig. 22), based on the approved drug trimethoprim, for successful *Escherichia coli* dihydrofolate reductase (eDHFR) degradation.[298] Subsequent studies revealed that the Boc3Arg moiety did not induced ubiquitination or destabilization of the POI. Instead the 20S proteasome is sufficient for degradation of the POI as Boc_3Arg is directly interacting and activating the proteasome core particle.[299] Further adamantyl-based HyT degraders were developed for multiple targets, including human EGFR3, AR, Polo-like-Kinase 1, or MDM2.[300–303] The hydrophobic tagging technique was further expanded to peptide-based degraders that target the tau protein, which is involved in Alzheimer´s disease.[304]

Development of the CDK4/6 targeting HyT degrader **LPM3770277** (Fig. 22) revealed a further degradation mechanism. Besides proteasomal degradation, lysosomal-mediated autophagy was identified as a degradation mechanism.[305] Similarly, assessment of degradation mechanism of HyT degraders **MS1943** and **3a** (Fig. 22), targeting enhancer of zeste homolog 2 (EZH2) and poly(ADP-ribose) polymerase (PARP) for degradation, respectively, revealed unexpected mechanisms of degradation. Treatment of both degraders result in upregulation of ER stress and UPR marker proteins, indicating the participation of degradation mechanism of HyT degraders.[306,307]

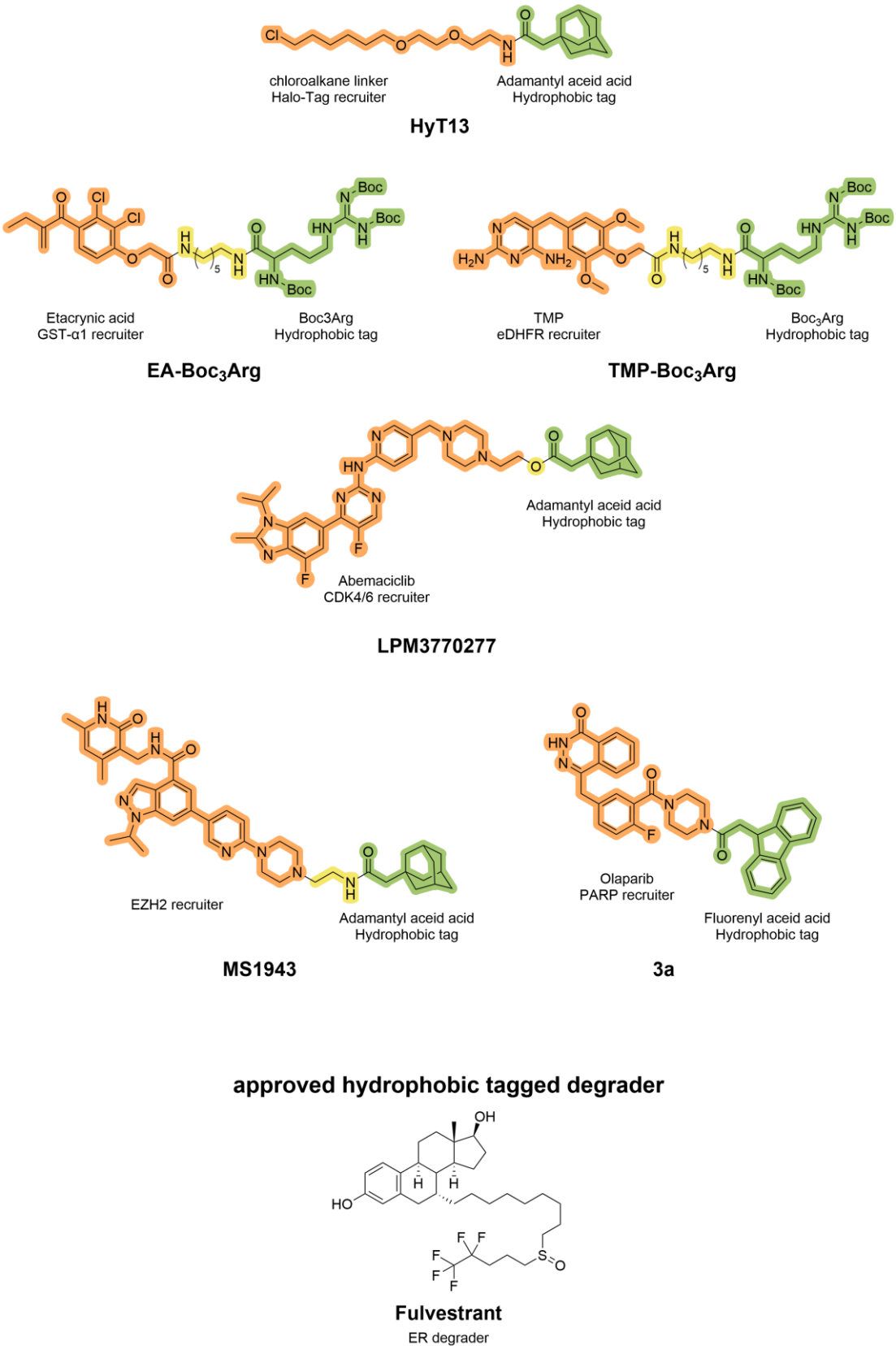

Figure 22. HyT degraders. The POI ligand is marked in orange, spacer in yellow, and the hydrophobic tag in green.

Additionally, a variety of hydrophobic tags were employed for TPD, like carboranes, norbornene, menthoxyacetyl, β-naphthoflavone, and D-ring-contracted artemisinin (Fig. 23).[308–312]

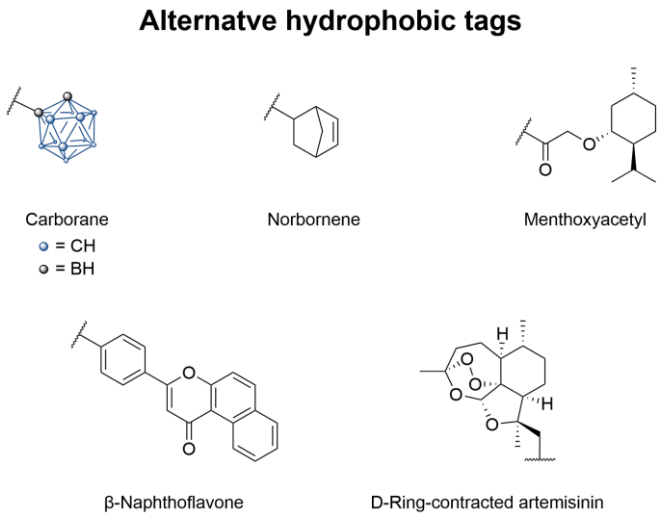

Figure 23. Alternative hydrophobic tags used for HyT degrader in TPD.

Although HyT degraders exhibit degradation potency commonly in the low micromolar to higher nanomolar range, they own specific advantages over PROTACs. The hydrophobic moiety of HyT degraders is smaller and easier to synthesize than E3 ligase ligands of PROTACs, which facilitates the design and synthesis of HyT degraders.[313] Direct comparison of the structurally related PROTAC **ND1-YL2** and HyT degrader, **YL2-HyT6** revealed higher cellular uptake and metabolic stability of the HyT degrader.[314] Furthermore, the conversion of an IAP-recruiting PROTAC into a HyT degrader, bearing an adamantyl moiety, reduced the molecular weight, number of hydrogen bond donors/acceptors and topological polar surface area. These more drug-like properties are accompanied by increased blood-brain barrier penetration.[315] Moreover, drug-like properties enabled oral administration of HyT degraders, while the corresponding PROTACs were applied intravenously.[311,316] This advanced drug-likeness is supported by the utilization of a different mechanism for degradation compared to PROTACs. The latter relies on ternary complex formation and specific molecular machinery, while HyT degradation is based on a not yet fully understood, but more versatile mechanism. Therefore, HyT degraders represent an alternative degradation strategy in case of ineffective PROTACs.[296]

HyT degraders are possibly more common than they are currently known. One *a posteriori* identified HyT degrader is the intramuscular administered estrogen receptor antagonist fulvestrant (Faslodex) approved for treatment of hormone receptor-positive metastatic breast cancer in post-menopausal women (Fig. 22).[317] The selective estrogen receptor degrader (SERD) relocates helix 12 upon binding to the ER. This structural change results in an increased hydrophobic surface of the nuclear receptor, leading to its destabilization and degradation.[318] Recent developments led to the approval of the oral bioavailable SERD elacestrant.[319]

1.3.5 HDAC Degraders

As TPD offers promising advantages over occupancy driven inhibitors it appears to be especially interesting for HDACs. Market authorized HDAC inhibitors have issues in HDAC selectivity and targeting the corepressor complexes associated with HDAC1-3. Both issues could be addressed by HDAC degraders through gain of selectivity and collateral degradation.[320]

The first histone deacetylase PROTAC was reported in 2018 and targeted the NAD^+-dependent SIRT2. A Cu(I)-catalyzed cycloaddition was used to connect a SIRT2 selective ligand with the spacer, fused to thalidomide for $CUL4^{CRBN}$ recruitment.[321] The first zinc-dependent HDAC PROTAC was the crebinostat-derived degrader **9c**, utilizing pomalidomide for CRBN recruitment and a PEG spacer (Fig. 24). As crebinostat is a non-selective inhibitor, cell-based assays confirmed inhibition of multiple HDAC-isoforms by **9c**, intriguingly, it selectively degrades HDAC6 with other isoforms

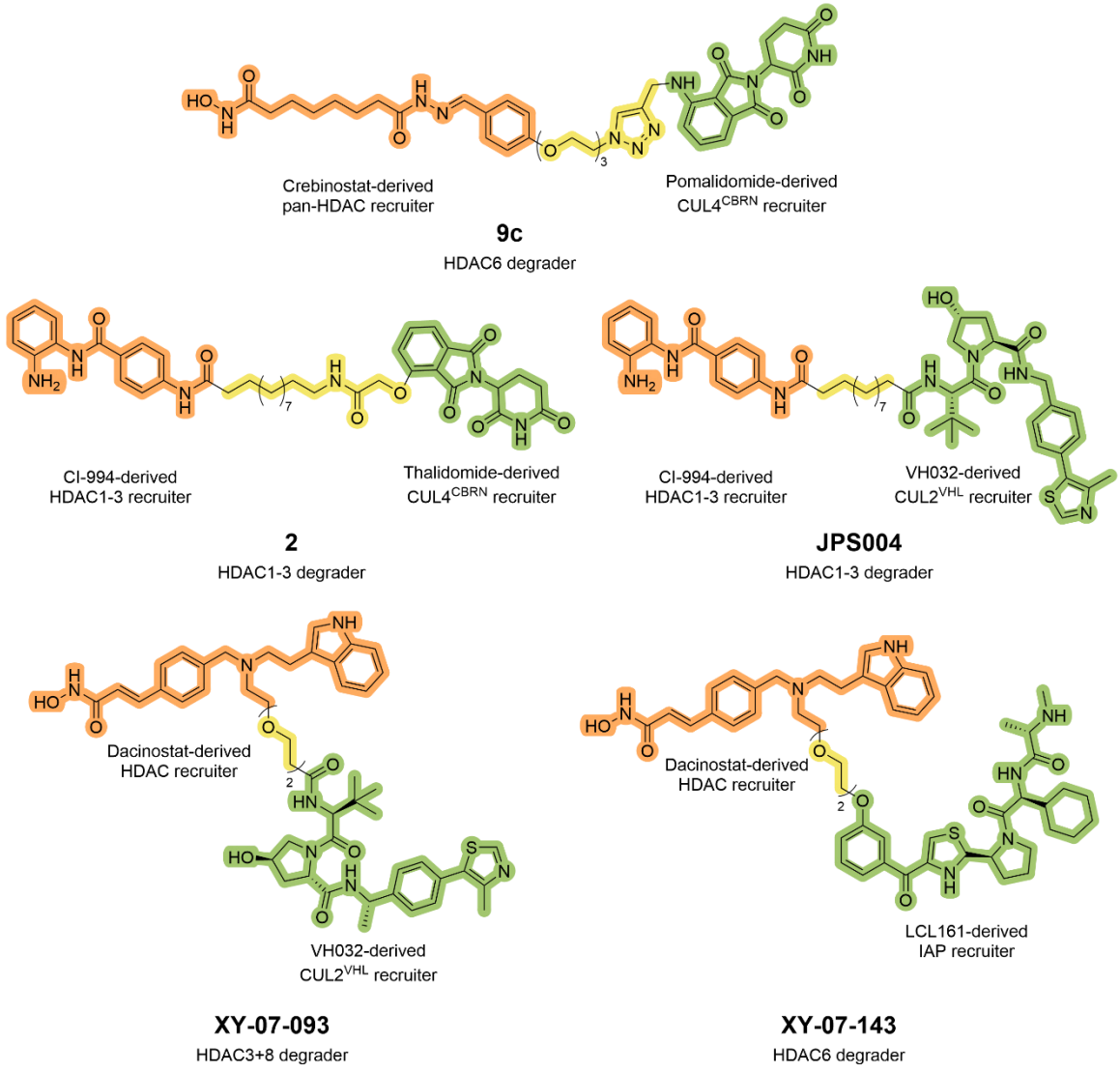

Figure 24. First-in-class HDAC PROTACs and degradation selectivity changes by switching E3 ligases. The POI ligand is marked in orange, spacer in yellow and E3 ligase recruiter in green.

been untouched.[322] In contrast, incorporation of an HDAC1-3 selective benzamide inhibitor into a $CUL4^{CRBN}$-recruiting PROTAC did not result in changed degradation selectivity. Instead, the HDAC1-3 selective inhibitor CI-994-based PROTAC **2** resulted in degradation of HDAC1-3. Similar PROTAC **JPS004** (Fig. 24), representing the first $CUL2^{VHL}$-recuiting HDAC-PROTAC, degraded HDAC1-3 but with increased potency.[323] However, Cao *et al*. reported in the same year CI-994-based $CUL4^{CRBN}$-recruiting PROTACs with shorter spacers, which resulted in preferential HDAC3 degradation over HDAC1-2.[324] The unexpected gain of selectivity by PROTACs incorporating promiscuous HDAC ligands was confirmed by a systematic screen of multiple HDAC PROTACs. Dacinostat was chosen as a non-selective HDAC inhibitor, and the new E3 ligase IAP was introduced for HDAC degradation. By changing the recruited E3 ligase from the $CUL2^{VHL}$-recruiting PROTAC **XY-07-093** to the IAP-recruiting PROTAC **XY-07-143** (Fig. 24), Xiong *et al*. induced a switch in degradation selectivity from HDAC3 and 8 to HDAC6, respectively, highlighting the impact of the chosen E3 ligase for degradation selectivity. Furthermore, they confirmed degradation potency and selectivity to be cell line dependent, similar to spacer length and attachment points (see 1.3.4.1 Proteolysis Targeting Chimeras).[325] As class I HDACs appear to be part of multi-protein complexes, the phenomenon of collateral degradation could be observed for other complex members. Neighboring proteins of the targeted HDAC isoform could be degraded by the PROTAC in combination with the targeted HDAC isoform. In case of HDAC3 degraders, this could result in SMRT/NCoR complex members, or MIER1-3 components in case of HDAC1-2. Intriguingly, PROTACs degrading MIER1-3 components were not able to degrade HDAC1-2.[325,326]

Today, more than 100 HDAC-PROTACs have been reported, with divergent HDAC ligands connected by a variety of spacers to recruiters of one of the three introduced E3 ligases.[259,327] Similar to the development in HDAC inhibitors, researchers are aiming to develop isoform selective degraders. As introduced earlier, CI-994 was used for the development of class I selective PROTACs and further optimization of **JPS004** resulted in identification of **JPS014** and **JPS016** (Fig. 25). These PROTACs differ to **JPS004** by the incorporation of oxygen atoms at both ends of the spacer and exhibit submicromolar DC_{50} values for HDAC1-2, while a hook effect occurs for HDAC3 degradation. This could be circumvented by changes in the $CUL2^{VHL}$ ligand and spacer attachment, leading to **JPS036** which exhibited a maximal degradation (D_{max}) of 77% for HDAC3 compared to HDAC1-2 D_{max} of 18-41%, thereby showed potent and preferential HDAC3 degradation (Fig. 25).[328] Xiao *et al*. used the HDAC inhibitor SR-3558 for PROTAC design, bearing a *n*-propyl-hydrazide as an alternative HDAC1-3 selective ZBG. $CUL4^{CRBN}$ and $CUL2^{VHL}$-recruiting PROTACs bearing PEG or alkyl spacers were evaluated and **XZ9002** exhibited potent HDAC3 degradation (DC_{50} = 4 nM) with HDAC1, 2, and 6 being unaffected (Fig. 25).[329]

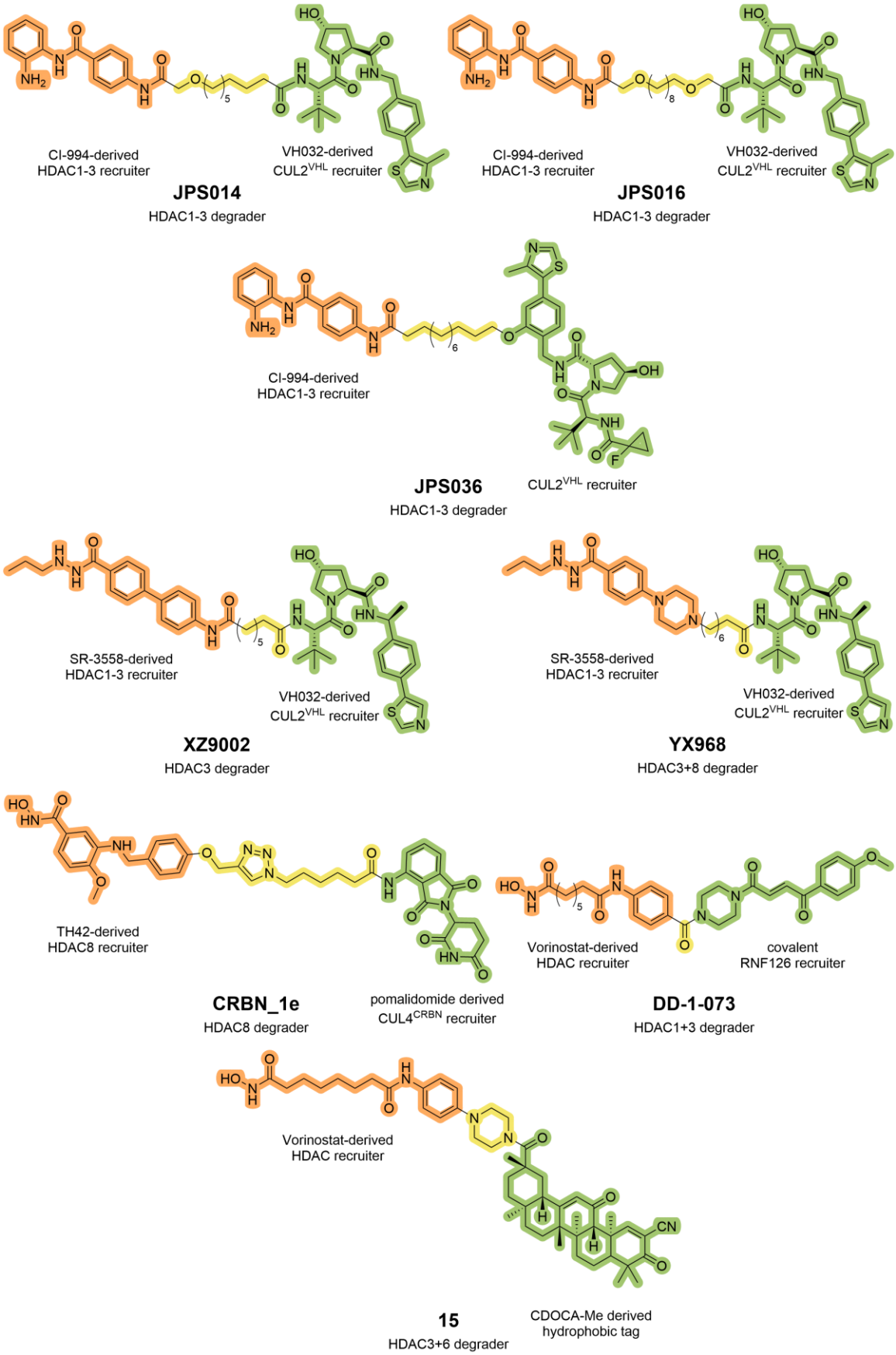

Figure 25. HDAC class I selective degraders. The POI ligand is marked in orange, spacer in yellow, and E3 ligase recruiter in green.

Further optimization of the HDAC ligand led to **YX968**, which achieved a single-digit nanomolar DC_{50} value for HDAC3 (Fig. 25). Surprisingly, HDAC8 was degraded with similar potency, along with collateral degradation of NCoR components.[326] Among others, Darwish *et al*. developed selective HDAC8 degrading PROTACs based on an inhibitor selective for HDAC8. Despite maintaining strong HDAC8 inhibition, $CUL2^{VHL}$-based PROTACs and adamantyl-based HyT degraders did not result in HDAC8 degradation. Only $CUL4^{CRBN}$-recruiting PROTACs achieved moderate HDAC8 degradation, including **CRBN_1e** (Fig. 25).[330] In addition, unconventional HDAC degraders, including the MG degrader or spacer-less PROTAC **DD-1-073** successfully induced HDAC1 and 3 degradation over HDAC2 and 6, by directly connecting an RNF126 recruiter to a vorinostat-like scaffold (Fig. 25).[250] Similarly, compound **15** targeted HDAC3 and 6 (Fig. 25), although designed as a multitarget drug combining the antitumor effects of 18β-glycyrrhetinic acid analogue methyl 2-cyano-3,11-dioxo-18β-olean-1,12-dien-30-oate (CDOCA-Me) with vorinostat. Compound **15** was able to reduce protein levels of HDAC 3 and 6, though mechanistic proof of degradation was not performed.[331]

Only few PROTACs were successfully developed for selective HDAC class IIa degradation. The trifluoromethyl-1,2,4-oxadiazole (TFMO) moiety, a class IIa-selective ZBG, was used in all class IIa degrader-studies currently published. PROTAC **11** exhibitted potent and selective HDAC4 degradation, while PROTAC **B4** showed potent and selective HDAC7 degradation (Fig. 26).[332–334]

HDAC class IIb targeting degraders, particularly targeting HDAC6, are probably most frequently reported among the zinc-dependent HDACs.[320] To obtain HDAC6 selectivity by design, the selective HDAC6 inhibitor nexturastat A was incorporated in various PROTACs. Wu *et al.* reported $CUL4^{CRBN}$-recruiting PROTACs with triazol-containing spacers. After optimizing spacer attachment and length, PROTAC **12d** exhibited a single-digit nanomolar DC_{50} value for HDAC6 as well as neo-substrate degradation due to the partial structure of pomalidomide, while sparing other HDAC isoforms (Fig. 26).[335] Sinatra *et al.* accelerated compound library preparation by establishing solid-phase parallel synthesis for PROTAC assembly.[336] The resulting most potent vorinostat-based degrader **A6** selectively degraded HDAC6 at a nanomolar DC_{50} level, confirming PROTAC-based selective HDAC6 degradation with promiscuous ligands and $CUL4^{CRBN}$ recruitment (Fig. 26).[337] The Hansen group further elaborated alternative ZBGs. Keuler, König, and Bückreiß *et al.* reported the first non-hydroxamate HDAC6-selective PROTAC utilizing the difluoromethyl-1,3,4-oxadiazole (DFMO) ZBG in the HDAC ligand. Both $CUL4^{CBRN}$ and $CUL2^{VHL}$-recruiting PROTACs showed significant HDAC6 degradation, while the pomalidomide-based PROTAC **1** exhibited the most potent degradation (Fig. 26).[338] Further improved DC_{50} values of HDAC6 was achieved by the ethyl-hydrazide-based $CUL4^{CRBN}$-recruiting PROTACs (**17c**) reported by Stopper and Honin *et al.*, while other HDAC isoform levels were unaffected (Fig. 26). However, $CUL2^{VHL}$-recruiting PROTACs,

showed no effect on HDAC6 levels.[339] Most recently Zhai *et al.* reported the first-in-class selective HDAC6 and 10 degrading PROTACs. Based on tubastatin A as a ligand and a CUL4^{CRBN} recruiter, the PROTAC **AP1** degraded HDAC6 and 10 with nanomolar DC_{50} values (Fig. 26).[340]

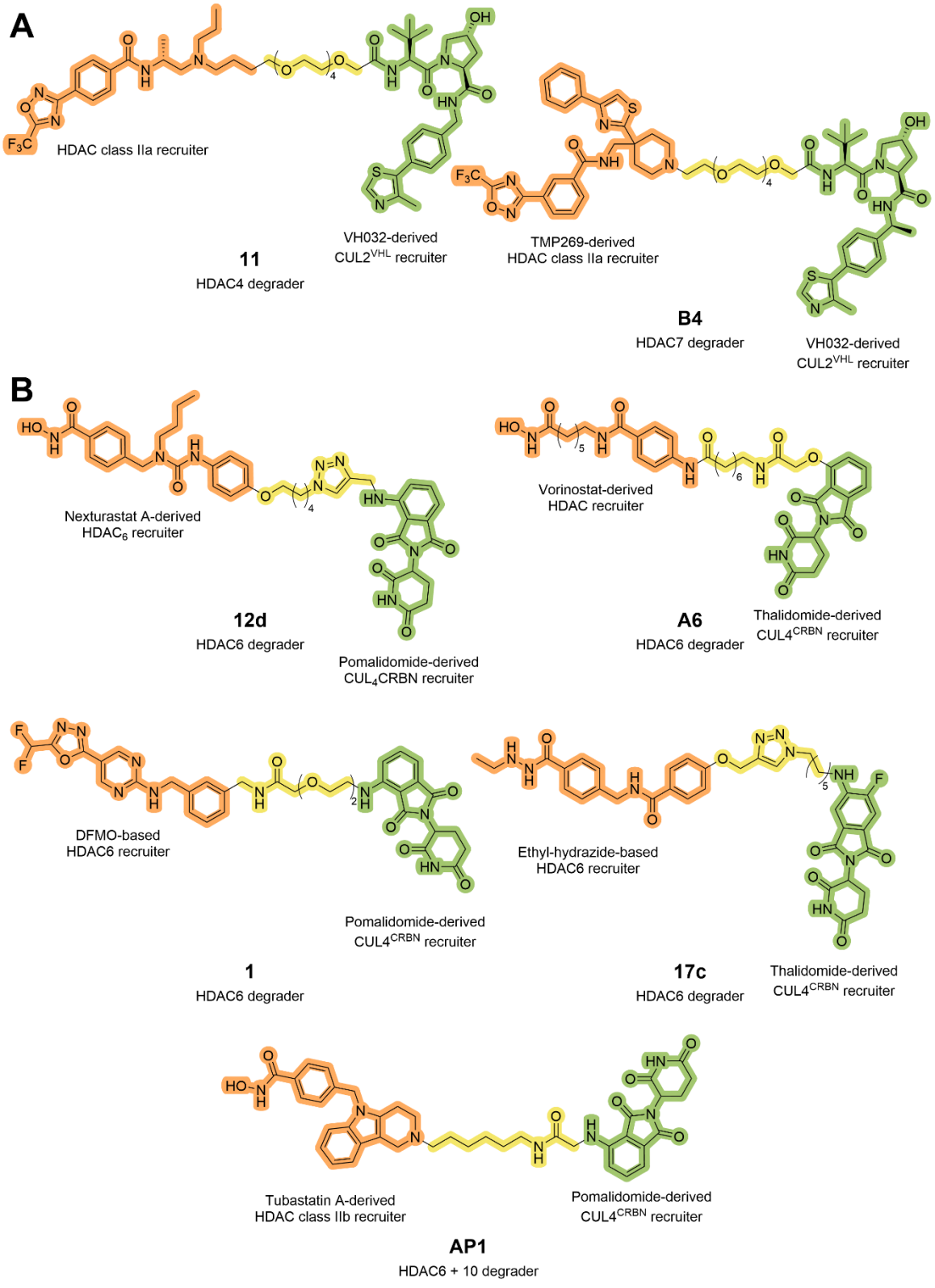

Figure 26. HDAC class II selective degraders. (A) HDAC class IIa selective PROTACs. (B) HDAC class IIb selective PROTACs. The POI ligand is marked in orange, spacer in yellow, and E3 ligase recruiter in green.

1.4 Scope of Thesis

Epigenetic modulators, like HDACs, play a crucial role in gene regulation and therefore impact a variety of physiological and pathophysiological mechanisms. They represent important targets for both cancerous and non-neoplastic diseases. This already led to the approval of six HDAC inhibitors by various national and international regulatory authorities. While these drugs have demonstrated therapeutic value, their limited isoform selectivity and associated toxicity highlights the need for the development of new drug modalities.[71,140,141] By the event-driven pharmacology, targeted protein degradation represents an alternative to occupancy-driven inhibitors, bearing the potential for increased isoform selectivity, extended duration of drug effects, reduced side effects, and the ability to overcome drug resistance. Recently, this led to the development of multiple HDAC degraders. However, it is important to note that degraders are susceptible to the development of resistance.[285] Moreover, the majority of HDAC degraders rely on one of the most commonly utilized E3 ligases in TPD, namely CRBN, VHL, and IAP.[341] To fully harness the potential of PROTACs and to provide alternatives in case of PROTAC resistance, there is a need to establish new E3 ligases for targeted degradation of HDACs. As certain E3 ligases are tissue or tumor enriched, their utilization would enable more specific PROTAC-therapies with reduced side effects.[342,343] Furthermore, the engagement of understudied E3 ligases can help to target new tumor entities, because of diverse and cell line-dependent degrader-sensitivity patterns.[344] Moreover, the E3 ligase ligands for CBRN and VHL come with certain limitations, as thalidomide and derivatives are associated with teratogenicity and stability issues, while VHL ligands are challenging by their molecular size and topological polar surface area.[224] The objective of this thesis is to develop and explore alternative HDAC degraders that are not based on the commonly utilized E3 ligases, with the aim of expanding the repertoire of E3 ligases available for HDAC degradation. Furthermore, this strategy may provide the opportunity to vary or increase the selectivity of the degraded HDAC isoform.

Chapter 2 covers the exploration of the E3 ligase FEM1B for the degradation of HDAC. The design of proteolysis targeting chimeras will be based on a previously published covalent ligand of FEM1B and the approved HDAC inhibitor vorinostat.[345] Solid-phase parallel synthesis will be utilized for the preparation of a set of PROTACs, differing in type and length of the spacer.[336,337] The aim of this study is to examine the impact of FEM1B on the degradation of different HDAC isoforms. First, the most efficacious compounds will be identified based on HDAC1 and 6 degradation in the multiple myeloma cell line MM.1S. The degradation capabilities of the selected PROTACs will be further characterized by the determination of DC_{50} and D_{max} values, as well as examination of the

inhibition of representative HDAC isoforms and confirmation of cellular target engagement. To further investigate the impact of FEM1B recruitment for HDAC degradation, the degradation selectivity for HDAC isoforms will be assessed, and proteasomal degradation will be confirmed. Subsequent analysis will include determination of degradation and antiproliferative effects in additional cancer cell lines. Furthermore, the anticancer effects in MM.1S cells will be evaluated in more detail. Finally, a global proteomics screen will be performed to determine the degradation selectivity beyond the selected HDAC isoforms.

Chapter 3 aims to employ the understudied DCAF11 as a suitable E3 ligase for HDAC degradation. The literature known vorinostat-based HDAC6 degrading PROTAC **A6** will be used as a template to design a set of PROTACs utilizing a previously published covalent DCAF11 warhead.[337,346] Solid-phase synthesis protocols will be employed for the synthesis of the target compounds. An initial degradation screening of HDAC1 and 6 in combination with a viability assay in MM.1S cells will be utilized for hit selection.[336,337] HDAC inhibition assays, analysis of histone H3 and α-tubulin hyperacetylation, and degradation studies using a negative control will be employed to confirm PROTAC target engagement and elucidate their mode of action. Potential anticancer effects in MM.1S cells will be confirmed by additional assays and further cancer cell lines will be used to determine the antiproliferative efficacy of selected DCAF11-recuitung PROTACs.

Chapter 4 focuses on the hydrophobic tagging approach, an alternative degradation method.[290] The aim of this study is to establish this technique as an additional opportunity for targeted degradation of HDACs. Therefore, a series of HDAC inhibitors with varying linker and cap types will be combined with a set of hydrophobic tags with and without the incorporation of spacers. The resin-based solid-phase synthesis approach will be used to prepare the hydrophobic-tagged HDAC inhibitors.[336,337] The antiproliferative activity in MM.1S cells will serve as main indicator for hit selection. Furthermore, the evaluation of HDAC isoform and cellular HDAC inhibition, in combination with identification of hyperacetylation of HDAC target proteins will be performed to confirm target engagement by the hydrophobic-tagged HDAC inhibitors. The degradation efficiency will be determined for the nuclear located isoforms HDAC1 and HDAC2, as well as for the cytosolic HDAC6. The proteasomal degradation will be confirmed by co-treatment with a proteasome inhibitor and the anticancer effects will be further assessed by determining the induction of apoptosis.

2 Development of the First-in-Class FEM1B-Recruiting Histone Deacetylase Degraders

Felix Feller, Irina Honin, Martina Miranda, Heiko Weber, Svenja Henze, Maria Hanl, and Finn K. Hansen

J. Med. Chem. **2025**, *68* (2), 1824–1843. https://doi.org/10.1021/acs.jmedchem.4c02569.

Please refer to Appendix I for the full text of the publication and the supplementary information.

2.1 Publication Summary

Targeted protein degradation is an emerging and rapidly expanding research field due to its unique mode of action. The most common modalities are PROTACs and MG degraders, which induce proximity between an E3 ubiquitin ligase and a POI, triggering polyubiquitination and proteasomal degradation.[222,260] This approach offers potential advantages such as prolonged pharmacological effects, improved selectivity, reduced off-target effects, the ability to overcome drug resistance, and the potential to utilize promiscuous warheads.[223,226,229]

Numerous PROTACs have been developed against a variety of targets, including HDACs.[327] These epigenetic modulators participate in multiple cellular processes, including chromatin remodeling by removing acetyl residues from histones and other proteins. Of the four HDAC classes, three share a zinc-dependent catalytic mechanism. Class I HDACs are primarily located in the nucleus and frequently overexpressed in human cancer, which often correlates with poor prognosis.[22,71] Thus, several HDAC inhibitors have been approved for cancer treatment and HDAC-targeting PROTACs have been developed.[110,111]

Although the human genome encodes over 600 E3 ligases, only three have been successfully applied for HDAC degradation.[171,327] Nevertheless, alternative E3 ligases offer opportunities for tissue or tumor selectivity, to provide options in case of PROTAC resistance, and to avoid limitations of established E3 ligase recruiters.[224,344] Recently, ligands for understudied E3 ligases have been developed, often bearing electrophilic warheads for covalent engagement.[345–349] Thereby, the corresponding PROTAC forms a covalent bond to a specific cysteine of the E3 ligase. This enables the covalent PROTAC-E3 ligase complex to recruit a POI, forming a pseudo-binary complex, for ubiquitin transfer and subsequent degradation of the POI.[350]

To expand the number of E3 ligases for targeted HDAC degradation and to profit from the pseudo-binary mechanism, the electrophilic ligand **EN106** was selected to target FEM1B.[345] A set of twelve

PROTACs was designed, derived from **EN106** and a non-selective vorinostat-like HDAC warhead, to achieve broad HDAC engagement. Both moieties were linked *via* spacers of varying length and rigidity (**1a-k**). A spacer-less variant (**2**) was included as well. All PROTACs were prepared by solid-phase synthesis, for rapid library generation, following our previously established protocols.[336,337] After modifying the 2-chlorotrityl chloride (2-CTC) resin, PROTACs were assembled from the HDAC warhead *via* the spacer to the FEM1B ligand by iterative amide coupling reactions. After cleavage, the PROTACs were purified by preparative high-performance liquid chromatography (HPLC) to a purity of > 95% with total yields of 9 – 45% over five to seven steps.

An initial antiproliferative screening in the multiple myeloma cell line MM.1S revealed single-digit micromolar half maximal effective concentration (EC_{50}) values, except for the C3 alkyl and PEG-based spacer-bearing PROTACs. Furthermore, a degradation screen for HDAC1 and 6 showed no significant changes in HDAC6 levels, while HDAC1 was strongly degraded by several compounds, particularly by those with shorter spacers. Based on the superior HDAC1 degradation and antiproliferative effects, PROTACs **1a**, **1g**, and **1j** were selected for further evaluation.

Comprehensive profiling of HDAC1 identified **1g** as the most effective degrader (D_{max} = 85.2%; DC_{50} = 257 nM). Furthermore, Target engagement was confirmed by *in vitro* enzyme inhibition assays and hyperacetylation studies of HDAC substrates. Both experiments revealed HDAC1, 2, and 6 engagement, with nanomolar IC_{50} values for HDAC1, 2, and 6 and hyperacetylation of histone H3 and α-tubulin, indicating reduced class I and HDAC6 activity. The determination of protein levels of class I isoforms, along with representatives of class IIa and IIb isoforms, after the treatment with the respective PROTAC showed significant HDAC1-3 degradation, while HDAC4, 6, and 8 remained unaffected. Compared to the selective HDAC6 degrader **A6**,[337] which shows structural similarity to **1j** but employs a different E3 ligase recruiter for CRBN-binding, this emphasizes the substantial impact of recruiting FEM1B for HDAC degradation.

Next, a non-degrading control (**1g-nc**) lacking the electrophilic warhead at the FEM1B ligand was designed and synthesized. **1g-nc** demonstrated no significant degradation of HDAC1, confirming covalent FEM1B engagement as essential for HDAC1 degradation. Further, co-treatments with **1g** and a proteasome inhibitor or vorinostat verified that HDAC1 degradation relies on proteasome activity and HDAC recruitment. Moreover, HDAC1 degradation induced by **1g** was confirmed in other cancer cell lines, which was accompanied by antiproliferative activity. However, these effects were less pronounced in the tested solid cancer cell lines, compared to MM.1S. Further, the antiproliferative effects in MM.1S cells were investigated by cell cycle analysis and annexin V/propidium iodide (PI) staining, confirming that all FEM1B-recruiting PROTACs induced cell cycle

arrest and apoptosis. In addition, long term effects on the replicative potential was investigated by a clonogenic growth assay and confirmed significant reduction in the number of colonies after treatment with **1a**, **1g**, and **1j**.

Finally, a global proteomics screen provided results for a less biased view on degradation selectivity of **1g**. In addition to HDAC1 and 2, it revealed significant degradation of proteins which are members of multi-protein complexes containing HDAC1, 2, or 3. This phenomenon is known as collateral degradation or bystander effect.[164,325]

In conclusion, this study successfully established FEM1B as a new E3 ligase for HDAC degradation. The glycine spacer-bearing PROTAC **1g** showed the most effective HDAC1-3 degradation and the strongest antiproliferative effects in different cancer cell lines. Compared to the structural similar CRBN-recruiting PROTAC **A6**, the FEM1B-recruiting PROTACs degraded HDAC1-3 instead of HDAC6, despite being based on the same non-selective vorinostat-like HDAC warhead. The selectivity switch induced by changing the recruited E3 ligase from CRBN to FEM1B for HDAC degradation highlights the impact of the chosen E3 ligase.

2.2 Author Contributions

Felix Feller: Study plan, compound design, synthesis (except of **1g-nc**), analytical characterization (except of **1g-nc**), CellTiter-Glo® cell viability assays, Simple Western™ immunoassays, immunoblot assays (except of HDAC3 and 8), HDAC enzyme inhibition assays, cell cycle assays, data analysis, writing – original draft.

Irina Honin: Clonogenic growth assays, CellTiter-Glo® cell viability assays of the non-degrading control **1g-nc** in MM.1 S cells.

Martina Miranda: Synthesis and analytical characterization of the non-degrading control **1g-nc**.

Heiko Weber: MTT cell viability assays.

Svenja Henze: Immunoblot assays for HDAC3 and 8.

Maria Hanl: Annexin V/PI assays.

Finn K. Hansen: Conceptualization, formal analysis, funding acquisition, project administration, resources, supervision, writing – review & editing.

3 Replacing a Cereblon Ligand by a DDB1 and CUL4 Associated Factor 11 (DCAF11) Recruiter Converts a Selective Histone Deacetylase 6 PROTAC into a Pan-Degrader

Felix Feller, Heiko Weber, Martina Miranda, Irina Honin, Maria Hanl, and Finn K. Hansen

ChemMedChem **2025**, *20* (10), e202500035. https://doi.org/10.1002/cmdc.202500035.

Please refer to Appendix II for the full text of the publication and the supplementary information.

3.1 Publication Summary

Cancer is a multi-factorial disease which can be treated not only on the genetic but also on the epigenetic level.[19] Therefore, epigenetic regulators, including HDACs, have emerged as promising anti-tumor targets. This is especially true, given that the up-regulation of multiple HDAC isoforms is associated with poor prognosis in cancer therapy, whereas the application of HDAC inhibitors can lead to reduced angiogenesis, cell migration, proliferation, and drug resistance. These effects are further supported by apoptosis induction and cell differentiation upon HDAC inhibitor treatment.[68,111,351] By hydrolyzing the amide bond of acetylated lysine residues of histones, HDACs restore the positive charge, leading to a more compact chromatin.[43] However, the three zinc dependent classes of HDACs also engage multiple non-histone targets.[71]

Besides the development of HDAC inhibitors, TPD represents a promising alternative for HDAC drug discovery. MG degraders or PROTACs have been designed and synthesized to hijack a suitable E3 ligase and bring it in close proximity to the POI, leading to its degradation through polyubiquitination and recognition by the proteasome.[172,352] TPD comes with several potential advantages over occupancy-driven inhibitors, due to its event-driven pharmacology, such as extended pharmacological effects, dose reduction, and overcoming drug resistance.[223,226]

Since the first PROTACs for zinc-dependent HDACs were disclosed in 2018, over 100 degraders have been reported, utilizing a broad variety of HDAC ligands.[327] However, only CRBN, VHL and IAP have been successfully employed thus far.[259] Expanding the number of E3 ligases for HDAC degradation is a substantial need, as there are over 600 ligases encoded in the human genome and targeting different E3 ligases offers unique benefits, including tissue or tumor specific activity.[164,171] For example, targeting DCAF11 appears promising because this could potentially stabilize the physiological substrate, the tumor suppressor p21.[353,354]

The PROTAC design was based on the previously published HDAC6 degrader **A6**.[337] As it bears a vorinostat-like HDAC ligand, it can potentially recruit a variety of HDAC isoforms and enables to study the effect of the recruited E3 ligase on HDAC degradation selectivity profile. For recruiting DCAF11, a previously reported electrophilic covalent ligand was selected.[346] The chosen warhead enables a pseudo-binary complex formation of the covalent PROTAC-E3 ligase complex, which only has to recruit the next POI for polyubiquitination.[350]

A set of ten spacers with varying rigidity and length was selected to connect POI and E3 ligase ligand (**1a-j**), with addition of the spacer-less compound **2**. The PROTACs were synthesized using a 2-CTC resin-based solid-phase approach to fully leverage the advantages of parallel synthesis.[336,337] The DCAF11 ligand was introduced by an on resin Ugi four-component reaction (U-4CR) to finalize the resin-bound PROTACs. After cleavage and purification by preparative HPLC, the eleven PROTACs of the set were afforded in total yields of 10 – 57% over five to seven steps.

To evaluate the degradation capabilities of the synthesized PROTACs, HDAC1 and 6 levels were determined after treatment of the multiple myeloma cell line MM.1S with the respective PROTAC. While the cyclic spacer-based PROTACs showed no significant effects on HDAC1, PEG spacer-based PROTACs resulted in up to 51% degradation of HDAC1. Moreover, the alkyl spacer-based PROTACs unveiled unexpected results: while **1h** with the C5 alkyl spacer exhibited no significant HDAC1 degradation, both longer and shorter spacers achieved significant degradation, with the spacer-less PROTAC **2** and the C11 spacer-bearing PROTAC **1j** being the most efficient HDAC1 degrader. In addition, **1j** and **2** were capable of inducing significant HDAC6 degradation. A cell viability assay demonstrated that the best degraders also exhibited the highest antiproliferative activity (**1j**: EC_{50} = 2.8 µM and **2**: EC_{50} = 1.5 µM), while the HDAC6-selective predecessor PROTAC **A6** showed no effect. This divergence could not be traced back to the DCAF11 ligand, as its contribution to cytotoxicity was found to be not significant compared to vorinostat.

Notably, i*n vitro* enzyme assays confirmed comparable HDAC1, 2, 4, and 6 inhibition for PROTAC **2** and **A6**, while **1j** exhibited higher IC_{50} values for all tested isoforms. HDAC inhibition was confirmed in a cellular setup by studying hyperacetylation of cellular HDAC substrates. The observed hyeracetylation of α-tubulin confirmed the HDAC6 inhibition trend from the enzyme assay, while hyperacetylation of histone H3 indicated a stronger HDAC class I inhibition for **1j** in comparison to **2** and **A6**.

For investigation in the degradation selectivity profile of the DCAF11-recruiting PROTACs, HDAC1 and 2, 4, and 6 were chosen as representatives of the classes I, IIa, and IIb, respectively. Both **1j** and **2** exhibited significant degradation of all tested isoforms. However, **2** degraded HDAC1 most

effectively (74%) compared to moderate HDAC2 (51%), HDAC4 (40%), and HDAC6 (26%) degradation. PROTAC **1j** was also most efficient in HDAC1 degradation (90%), but substantially more effective in HDAC2, 4, and 6 degradation (71 – 76%) compared to PROTAC **2**. Furthermore, a non-degrading control was designed and synthesized based on **1j**, lacking the chloroacetamide handle (**1j-nc**). Treatment of MM.1S cells with **1j-nc** resulted in unchanged HDAC1 levels, suggesting degradation dependency on DCAF11 and the covalent handle.

Next, the antiproliferative effects on MM.1S cells were studied in more detail. Both DCAF11-recruiting PROTACs induced cell cycle arrest and apoptosis. Similarly, pronounced antiproliferative effects could be observed in two additional solid cancer cell lines and a clonogenic growth assay revealed significant reduction in the number of colonies after treatment with **1j** and **2**, while **A6** and **1j-nc** did not result in any significant clonogenic effects.

In summary, the most effective degrader of this study (**1j**) showed significant degradation of all tested HDAC isoforms with a D_{max} of 90% for HDAC1. Further, HDAC degradation induced by **1j** and the spacer-less PROTAC **2** was accompanied by substantial antiproliferative effects in different cancer cell lines. In contrast to the HDAC6 selective, CRBN-recruiting PROTAC **A6**, the results highlight DCAF11 as an alternative E3 ligase applicable for pan-HDAC degradation.

3.2 Author Contributions

Felix Feller: Study plan, compound design, synthesis (except of **1j-nc**), analytical characterization (except of **1j-nc**), CellTiter-Glo® cell viability assays (except of **1g-nc**), Simple Western™ immunoassays, cellular HDAC inhibition assays, aqueous stability assays, immunoblot assays, HDAC enzyme inhibition assays, cell cycle assays, data analysis, writing – original draft.

Heiko Weber: MTT cell viability assays.

Martina Miranda: Synthesis and analytical characterization of the non-degrading control **1j-nc**.

Irina Honin: Clonogenic growth assays, CellTiter-Glo® cell viability assays of the non-degrading control **1j-nc** in MM.1 S cells.

Maria Hanl: Annexin V/PI assays.

Finn K. Hansen: Conceptualization, formal analysis, funding acquisition, project administration, resources, supervision, writing – review & editing.

4 Targeted Protein Degradation of Histone Deacetylases by Hydrophobically Tagged Inhibitors

Felix Feller and Finn K. Hansen

ACS Med. Chem. Lett. **2023**, *14* (12), 1863–1868.

https://doi.org/10.1021/acsmedchemlett.3c00468.

Please refer to Appendix III for the full text of the publication and the supplementary information.

4.1 Publication Summary

TPD has emerged as a powerful concept in drug discovery, offering the potential to eliminate disease-specific proteins rather than transiently inhibiting their activity. PROTACs and MG degraders are the most widely explored modalities, inducing proximity between the POI and an E3 ligase. While these approaches can yield potent and selective degraders, they also face notable challenges: PROTACs are limited by their large molecular size, while rational design of MG degraders is difficult. Furthermore, both are restricted by narrow structure-activity-relationships, possible teratogenicity, and the development of drug resistance.[224,344] Therefore, hydrophobic tagging represents an alternative technique in TPD. The hydrophobic tag is fused to a POI ligand, thereby forming the HyT degrader which mimics a destabilized protein upon binding or directly destabilizes the POI. This is recognized by the cellular repair machinery for refolding, including chaperones. In the presence of the HyT degrader, refolding fails which leads to the degradation of the POI.[290,313]

To investigate whether hydrophobic tagging is applicable for HDAC degradation, two series of hydrophobic-tagged HDAC inhibitors were designed and synthesized. The first set was composed out of a vorinostat-like HDAC inhibitor connected directly or by alkyl-spacers of different length to the hydrophobic tag (**1a-b**, **2a-f**). 2-(Adamantan-1-yl)acetic acid or 2-(9*H*-fluoren-9-yl)acetic acid were utilized as hydrophobic tags. For the second set, a C6 alkyl and a benzyl HDAC linker in combination with two different cap groups were incorporated. The hydrophobic tag was adopted as previously established by Neklesa *et al*. and fused by a Huisgen copper(I)-catalyzed azide-alkyne cycloaddition to the HDAC inhibitor (**3a-d**).[297] To evaluate if the triazole is sufficiently solvent exposed and does not impair HDAC binding, a docking study was performed. The docking indicated suitable solvent exposure of the triazole to function as an exit vector, as well as a binding mode of the ligand−triazole conjugate similar to vorinostat.

Previously established solid-phase synthesis protocols were applied for fast and modular preparation of the HyT degraders.[336,337] The adamantyl (**1a**, **2a-c**) and fluorenyl (**2b**, **2d-f**) tagged HDAC inhibitors of the first set were synthesized by subsequent amide couplings. Similarly, the HDAC inhibitor-scaffold of the second set of HyT degraders was synthesized this way. However, the hydrophobic tag was functionalized as an azide, following a known procedure, and coupled by a Cu(I)-catalyzed Huisgen 1,3-dipolar cycloaddition to the resin-bound HDAC inhibitor.[355] After cleavage and purification by preparative HPLC, this afforded HyT degraders **3a-d** in a yield of 37 – 89% over four steps. Similarly, the first set was cleaved and purified by preparative HPLC to provide the target compounds in yields ranging from 4 to 46% over five to seven steps.

For the biological evaluation of the HyT degraders, a phenotypic cell viability screen was performed, to identify the most cytotoxic compounds. The HyT degraders **1a**, **2a**, **2d**, and **3a** exhibited the best antiproliferative activity (EC_{50} = 3.97 – 11.6 µM), while other compounds showed no effect. These four compounds were selected for further investigations, starting with a cellular HDAC inhibition assay and enzyme inhibition assays for HDAC1, 2, and 6. The best performing HyT degrader **2d** exhibited cellular HDAC inhibition as well as HDAC1 and 2 enzyme inhibition compared to vorinostat. Interestingly, all tested HyT degrader outperformed vorinostat regarding HDAC6 inhibition.

To confirm the applicability of hydrophobic tagging for HDAC degradation, HDAC1, 2, and 6 levels were determined after treatment of MM.1S cells with the selected HyT degrader for 24 h. All compounds under investigation exhibited significant HDAC1 degradation, while **1a** and **2a** additionally reduced HDAC2 levels to some extent. Notably, HDAC6 levels remained unaffected by all degraders, despite high HDAC6 inhibition capabilities. Hence, to investigate cellular target engagement, the hyperacetylation of cellular HDAC substrates were evaluated. Cellular HDAC6 engagement was confirmed for all assessed HyT degraders by hyperacetylation of α-tubulin. Similarly, hyperacetylation of histone H3 confirmed HDAC class I engagement which was most prominent for **1a**. Additionally, HDAC4 inhibition and degradation was examined as an example for class IIa HDACs. None of the HyT degraders showed inhibition or degradation of HDAC4.

Remarkably, all HyT degraders under investigation showed HDAC6 inhibition and cellular target engagement but no HDAC6 degradation. Therefore, it was hypothesized that, by binding the wide CD2 pocket of HDAC6, the hydrophobic tag is not recognizable for the cellular quality control and HDAC6 is therefore not degraded.[47]

Moreover, to study the degradation mechanism of HDAC targeting HyT degraders, a co-treatment of **1a** and a proteasome inhibitor was performed. This resulted in a significant reduction of HDAC1

degradation by **1a** proving proteasomal dependency. However, some HDAC1 reduction remained, indicating additional degradation mechanisms. Finally, the antiproliferative effects of **1a**, **2a**, **2d**, and **3a** were investigated in more detail. All HyT degraders induced apoptosis and increased caspase 3 and 7 activity, except for **2d**.

Taken together, hydrophobic tagging has proven applicable for targeted HDAC degradation, especially for class I HDACs. The most potent HyT degrader **1a** achieved 47% degradation of HDAC1, induced apoptosis, and exhibited antiproliferative activity.

4.2 Author Contributions

Felix Feller: Study plan, compound design, synthesis, analytical characterization, MTT cell viability assays, cellular HDAC inhibition assays, HDAC enzyme inhibition assays, immunoblot assays, annexin V/PI assays, Caspase-Glo® 3/7 assays, data analysis, writing – original draft.

Finn K. Hansen: Conceptualization, formal analysis, funding acquisition, project administration, resources, supervision, docking study, writing – review & editing.

5 Summary

By estimation of the world health organization's cancer research agency, the global cancer burden will increase by 62% to over 27 million new cases by the year of 2040.[2] This trend indicates an urgent need for substantial investment in cancer-related drug discovery addressing this escalating numbers. Cancer is characterized by multiple aberrancies, the so called hallmarks of cancer, which provide various drug targets, including epigenetic regulators such as HDACs.[6] By removing acetyl residues from lysine side chains of histones, they affect DNA condensation and subsequent gene expression.[71] That way, HDACs are involved in several key cellular processes including differentiation, proliferation, and cell migration. Further, they contribute to carcinogenesis and cancer progression by promoting angiogenesis, chemoresistance as well as cancer cell survival rather than apoptosis.[68,111,351] Furthermore, HDACS are also frequently overexpressed in cancer and associated with poor survival.[110,111] Thus, they are promising targets in cancer therapy and have been extensively studied, which led to the approval of several HDAC inhibitors.[139]

Since TPD holds promising advantages over occupancy driven inhibitors, the development of HDAC degraders has recently become a prominent topic in drug discovery.[327] The two most common modalities, PROTACs and MG degraders, induce proximity between the POI and an E3 ligase for proteasomal degradation of the POI. Unlike inhibitors, degraders act in a catalytic mode of action and enable the removal of the respective target protein. This mechanism has the potential to result in numerous advantages, including targeting proteins considered undruggable before, prolonged pharmacological effects, reduced side effect, overcoming of drug resistance, and selectivity enhancement of non-selective POI ligands.[164,226]

Although the human genome encodes over 600 E3 ligases, only the well-studied E3 ligases CRBN, VHL, and IAP have been successfully harnessed for PROTAC-based HDAC degradation.[171,259] Expanding the use of understudied E3 ligases offers additional opportunities, such as tissue or tumor selective degradation and provide alternatives in case of PROTAC resistance development.[224,344] Additionally, the natural substrates of the E3 ligase can be stabilized by usage for TPD, which can be beneficial in case of MDM2 – p53 or DCAF11 – p21.[353,356] Besides, established E3 ligase ligands like IMiDs are associated with teratogenicity and stability issues, while VHL ligands are problematic in terms of their molecular size and topological polar surface area.[224] Thus, the development of ligands for understudied E3 ligases is a recent development in TPD.[345–349] Several of these ligands incorporate electrophilic warheads, such as chloroacetamide

groups, enabling covalent engagement of specific cysteine residues on the E3 ligase. When incorporated into a PROTAC, this enables a pseudo-binary complex instead of a ternary complex. The covalently bound PROTAC-E3 ligase complex only needs to recruit the next POI for polyubiquitination and subsequent degradation.[350]

The first project (chapter 2) investigated PROTACs engaging the understudied E3 ligase FEM1B for targeted HDAC degradation and compared them with the previously published CRBN-recruiting PROTAC **A6** (Fig. 27).[337] A vorinostat-like POI ligand was selected to target a broad range of different HDAC isoforms. For FEM1B recruitment, the electrophilic ligand **EN106** was chosen and incorporated with slight modifications.[345] Both moieties were connected by a variety of spacers, ranging from short cyclic spacers to PEG or alkyl spacers of different lengths. Additionally, a spacer-less PROTAC was designed. The resulting set of twelve PROTACs was prepared by an efficient and parallel solid-phase synthesis approach.[336,337] Starting with modifying the 2-CTC resin, the PROTACs were build up from the hydroxamic acid moiety of the HDAC ligand. The FEM1B ligand was synthesized according to literature before attachment to the resin bound precursor.[345] After cleavage and purification by preparative HPLC all compounds were afforded in a purity of > 95% and yields of 9 – 45% over 5 – 7 steps.

Initial antiproliferative screening in multiple myeloma cells revealed that most FEM1B-recruiting PROTACs exhibited single-digit micromolar EC_{50} values. Subsequent degradation profiling for HDAC1 and HDAC6 demonstrated that HDAC6 remained largely unaffected, whereas HDAC1 was significantly degraded by several compounds, particularly by those with short spacers and the C7 alkyl spacer-bearing **1j**. Based on pronounced HDAC1 degradation and notable antiproliferative activity, compounds **1a**, **1g**, and **1j** were chosen for a detailed characterization.

PROTAC **1g** was identified as the most potent degrader (D_{max} = 85.2%; DC_{50} = 257 nM). To confirm target engagement, *in vitro* enzyme inhibition assays and cellular hyperacetylation analysis of certain cellular HDAC substrates were performed. All PROTACs under study demonstrated nanomolar IC_{50} values for HDAC1, HDAC2, and HDAC6 and caused increased acetylation levels of histone H3 and α-tubulin, thereby proving the PROTAC-mediated suppression of class I HDACs and HDAC6 activity. To assess the degradation selectivity of FEM1B-recruiting PROTACs, HDAC levels of class I isoforms and representative class IIa and IIb isoforms were determined after the treatment with **1a**, **1g**, and **1j**. All three compounds induced significant degradation of HDAC1–3, while HDAC4, HDAC6, and HDAC8 remained unaffected. Compared to the HDAC6 selective PROTAC **A6**, structurally similar to **1j** but bearing a thalidomide derivative for CRBN recruitment, the results underscore the critical influence of FEM1B recruitment on degradation selectivity.[337]

Additionally, a non-degrading control (**1g-nc**), lacking the electrophilic FEM1B-binding motif, was synthesized to validate the degradation mechanism. Notably, **1g-nc** exhibited no detectable HDAC degradation. Further, the degradation mechanism of PROTAC **1g** was verified by rescue experiments through co-treatment with a proteasome inhibitor or vorinostat. HDAC1 degradation and antiproliferative effects induced by **1g** were also confirmed in three additional cancer cell lines, including solid cancer cell models and additional cell cycle analysis. Furthermore, annexin V/PI staining indicated cell cycle arrest and apoptosis induction by the FEM1B-recruiting degraders. Moreover, long-term effects were assessed *via* clonogenic growth assays, revealing significant reductions in colony formation upon treatment with **1a**, **1g**, and **1j**.

Finally, a global proteomic profiling provided an unbiased view of **1g** degradation-activity confirming HDAC1 and HDAC2 degradation. Additionally, collateral degradation of proteins associated with HDAC-containing multi-protein complexes was shown. This effect was previously described as the bystander effect in other degraders studies.[164,325]

In summary, FEM1B was successfully identified as a novel E3 ligase suitable for HDAC-targeted PROTACs. Among the tested compounds, the glycine spacer-bearing PROTAC **1g** (hereafter dubbed **FF2049**) achieved the most efficient HDAC1-3 degradation and anticancer effects. Importantly, FEM1B recruitment induced a selectivity shift compared to the CRBN-based degrader **A6**. It favors degradation of HDAC1-3 rather than HDAC6, despite employing the same vorinostat-derived non-selective HDAC ligand.

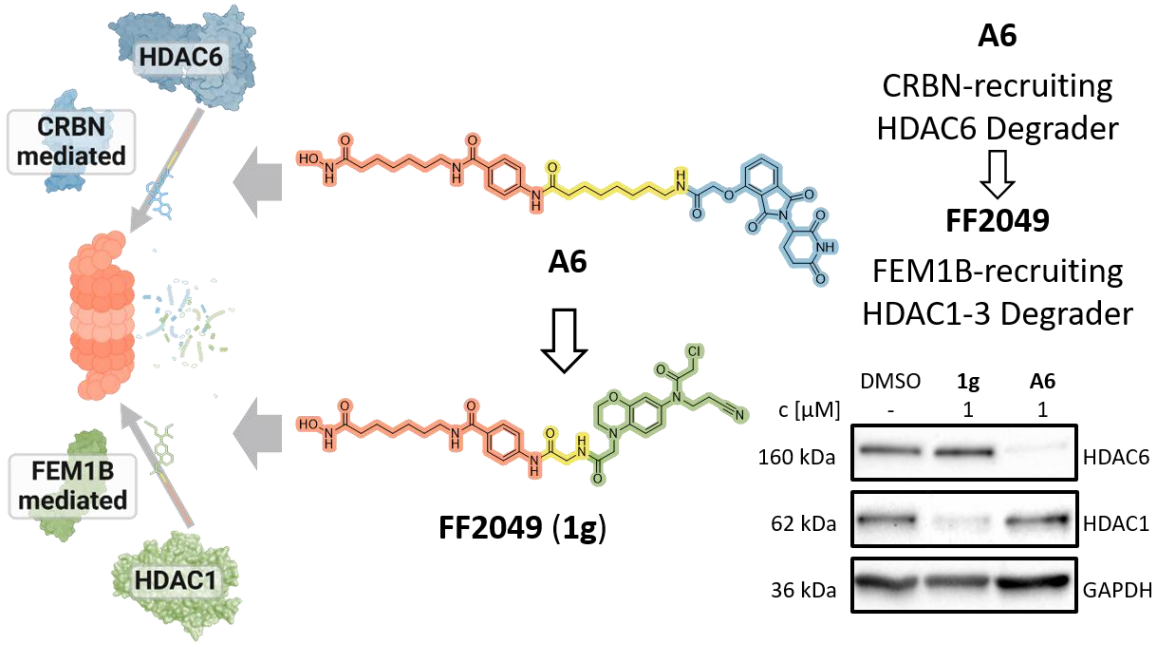

*Figure 27. FEM1B-recruting PROTAC **FF2049** (**1g**) and its effects in comparison to CRBN-recruiting PROTAC **A6.** Immunoblot results highlight the impact of the chosen E3 ligase for degradation selectivity. For more detailed information, see chapter 2.* Created with BioRender.com

Similarly, the second project (chapter 3) studied the feasibility of DCAF11 recruitment for HDAC degradation and its effect on different HDAC isoforms, in comparison to the CRBN-recruiting PROTAC **A6** (Fig. 28).[337] The E3 ligase DCAF11 is responsible for degrading the tumor suppressor p21. Therefore, targeting DCAF11 could stabilize p21 with potential benefits.[353,354]

The PROTAC design was based on the previously reported HDAC6-selective degrader **A6**, which employs a vorinostat-like POI ligand to enable engagement of multiple HDAC isoforms.[337] For DCAF11 recruitment, an electrophilic ligand derived from the U-4CR was selected.[346] Electrophilic warheads enable formation of a covalent PROTAC-E3 ligase complex that requires only POI recruitment to initiate its polyubiquitination and degradation.[350]

A series of ten PROTACs (**1a-1j**) with spacers of varying length and rigidity as well as a spacer-less compound (**2**), was synthesized *via* solid-phase synthesis.[336,337] The U-4CR was optimized to be performed on solid-phase. Accordingly, the desired PROTACs were prepared entirely on solid-phase to benefit from efficient parallel synthesis. Following cleavage and purification by preparative HPLC, all PROTACs were afforded in a purity of > 95% and in yields of 10 – 57% over five to seven steps.

For biological evaluation, HDAC1 and HDAC6 levels were evaluated after treating MM.1S cells with the respective PROTAC. Cyclic spacer-containing PROTACs displayed no significant HDAC1 degradation, whereas PEG spacer-bearing compounds achieved significant activity up to 51% degradation (**1e**) after treatment with 10 µM for 24 h. Interestingly, alkyl spacer-based PROTACs produced very heterogeneous results: while C5 spacer-bearing **1h** was inactive, both shorter (**2**) and longer spacers (**1j**) led to effective HDAC1 degradation up to 71%. Notably, only **1j** and **2** also reduced HDAC6 levels. Consistent with these findings, **1j** (EC_{50} = 2.8 µM) and **2** (EC_{50} = 1.5 µM) exhibited the strongest antiproliferative activity in MM.1S cells, whereas the parent CRBN-recruiting PROTAC **A6** was inactive. The DCAF11 ligand itself was not found to be responsible for antiproliferative activity of **1j** and **2**, since it did not contribute significantly to cytotoxicity of vorinostat.

Investigation of target engagement using *in vitro* HDAC inhibition assays revealed comparable HDAC1, 2, 4, and 6 inhibition by **2** and **A6**, while **1j** showed weaker activity. Determination of cellular hyperacetylation of histone H3 and α-tubulin confirmed HDAC1, 2, and 6 inhibition on a cellular level, albeit to different extents. Furthermore, degradation selectivity profiling demonstrated that both **1j** and **2** degraded HDAC1, 2, 4, and 6 with **1j** being more potent (HDAC1 D_{max} = 90%, HDAC2, 4, and 6 D_{max} = 71 –76%). PROTAC **2** was most active for HDAC1 (D_{max} = 74%) while degradation for HDAC2, 4, and 6 was only moderate. To confirm DCAF11-dependent

degradation, a non-degrading control lacking the covalent handle (**1j-nc**) was prepared, which was shown not to reduce HDAC1 levels.

Further investigation of the antiproliferative effects in MM.1S cells indicated cell cycle arrest and apoptosis induction by both **1j** and **2**. Additionally, antiproliferative effects were observed in two solid cancer cell lines, and a colony formation assay revealed reduced clonogenicity upon treatment with the DCAF11-recruiting PROTACs. These effects were either not observed for **A6** and **1j-nc** or only to a lesser extent.

In summary, this study established DCAF11 as a new E3 ligase for pan-HDAC degradation. The most active degrader **1j** (here after dubbed **FF2039**) achieved up to 90% HDAC1 degradation, as well as over 70% degradation for representative HDACs of class IIa and IIb, which was accompanied by strong anticancer effects. Compared to the parent PROTAC **A6**, which shares the same non-selective HDAC recruiter, switching from CRBN to DCAF11 shifted the degradation profile from HDAC6 selective degradation to pan-HDAC degradation.

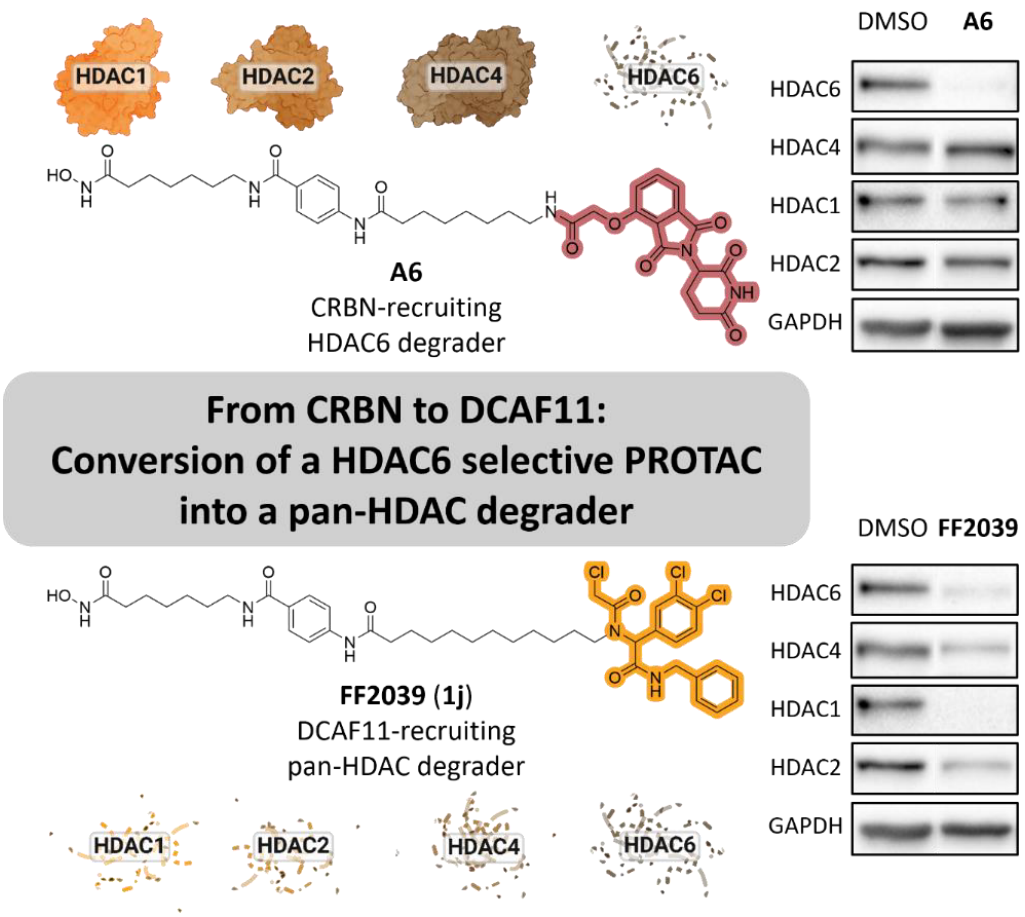

*Figure 28. DCAF11-recruting PROTAC **FF2039** (**1j**) and its degradation profile in comparison to CRBN-recruiting PROTAC **A6**, underscoring the importance of the selected E3 ligase for degradation selectivity. For more detailed information, see chapter 3.* Created with BioRender.com

In the third project (chapter 4), the alternative degradation methodology of hydrophobic tagging was assessed for targeted HDAC degradation (Fig. 29). While PROTACs and MG degraders have produced potent compounds, limitations persist: PROTACs suffer from high molecular weight and pharmacokinetic challenges, MG degraders are difficult to design rationally, and both face narrow structure–activity relationships, potential teratogenicity, and drug resistance.[224,344] Consequently, hydrophobic tagging has emerged as an alternative TPD approach. HyT degraders fuse a hydrophobic tag to a POI ligand, mimicking misfolded proteins and promoting degradation *via* the protein quality control machinery. When refolding fails, chaperone-mediated recognition leads to proteasomal elimination of the POI.[290,313]

To explore the applicability of hydrophobic tagging for HDAC degradation, two HyT degrader series were synthesized. The first set contained vorinostat-like HDAC inhibitors linked directly (**1a-b**) or through alkyl spacers of varying length (**2a-f**) to either 2-(adamantan-1-yl)acetic acid or 2-(9*H*-fluoren-9-yl)acetic acid as the hydrophobic tags. The second set varied the HDAC ligand and utilized a hydrophobic tag moiety that was previously established by Neklesa et *al*.[297] Benzyl or C6 alkyl HDAC linkers were combined with two distinct cap groups and azide-functionalized hydrophobic tags were coupled *via* a Huisgen copper(I)-catalyzed azide-alkyne cycloadditions (**3a-d**). Docking studies confirmed that the triazole linkage preserved the HDAC binding mode and assured an adequate solvent exposure for the hydrophobic tag.

Again, solid-phase synthesis based on the previously published protocols enabled efficient preparation of all compounds.[336,337] The first series (**1a**, **2a-f**) was obtained by sequential amide couplings (yields 4 – 46%, over five to seven steps), whereas the second set involved a Cu(I)-catalyzed Huisgen 1,3-dipolar cycloaddition on solid-phase as the final step on-resin (yields 37 – 89%, over four steps). After cleavage and preparative HPLC purification, the compounds were evaluated for biological activity in a purity of > 95%.

Phenotypic screening in MM.1S cells identified **1a**, **2a**, **2d**, and **3a** as the most potent antiproliferative agents (EC_{50} = 3.97 – 11.6 µM). Enzyme and cellular HDAC assays confirmed HDAC1 and HDAC2 inhibition, in the case of **2d** comparable to vorinostat, while all selected HyT degraders displayed superior HDAC6 inhibition. However, degradation profiling revealed a different pattern: all compounds significantly reduced HDAC1 levels after 24 h, with minor HDAC2 degradation by **1a** and **2a**, but showed no detectable HDAC6 degradation. Therefore, cellular target engagement was investigated by determination of hyperacetylated HDAC target proteins. The results indicated that all tested HyT degraders engage class I HDACs as well as HDAC6. Given this unexpected discrepancy between the apparent cellular HDAC6 engagement and the absence

of corresponding HDAC6 degradation, it was hypothesized that the hydrophobic tag cannot be efficiently be recognized within the large CD2 pocket of HDAC6.[47]

Mechanistic investigation demonstrated partial rescue of HDAC1 degradation upon co-treatment with a proteasome inhibitor. This indicates a proteasome-dependent degradation mechanism but also suggesting additional pathways. Additionally, further studies of the antiproliferative effects revealed caspase 3/7 activation and apoptosis induction by the HyT degraders.

In conclusion, hydrophobic tagging is feasible for HDAC degradation, particularly for class I isoforms. The most active compound **1a** achieved 47% of HDAC1 degradation, induced apoptosis, and exhibited notable antiproliferative activity. However, robust HDAC6 inhibition could not be transferred into degradation. This shows isoform-specific limitations of the hydrophobic tagging technology and supports the hypothesis that degradation efficacy depends on the structural accessibility of the hydrophobic tag. Besides that, the incomplete rescue by proteasome inhibition underscores the complexity of HyT-mediated degradation mechanisms.

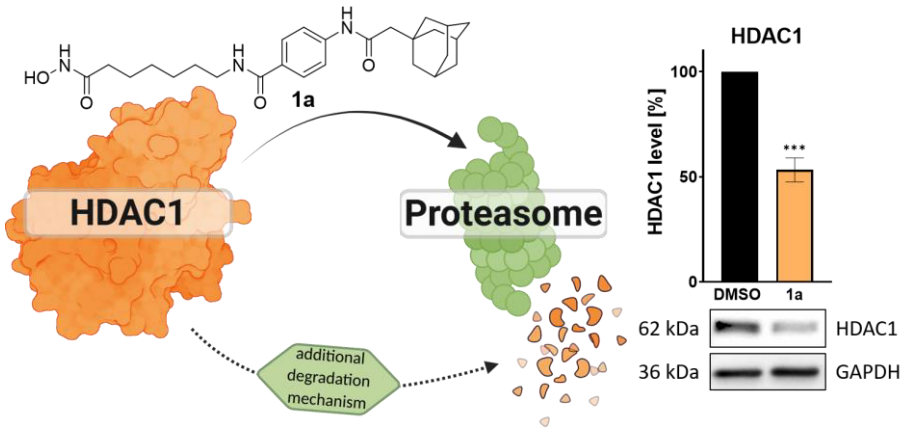

*Figure 29. Schematic presentation of degradation mechanism of HyT degrader **1a**, which showcased hydrophobic tagging for targeted HDAC degradation. For more detailed information, see chapter 4.* Created with BioRender.com

In summary, these three projects expanded the methodology of targeted HDAC degradation: They revealed the potential of FEM1B and DCAF11 for PROTAC-based HDAC degradation, as well as the feasibility of HDAC degradation *via* hydrophobic tagging. Further, the results of this thesis show that HDAC degradation profiles can be fine-tuned by selecting a suitable E3 ligase and degradation methodology, emphasizing the untapped potential of other understudied E3 ligases and alternative degradation methods.

6 References

(1) Ferlay J, Ervik M, Lam F, Laversanne M, Colombet M, Mery L, Piñeros M, Znaor A, Soerjomataram I, Bray F (2024). Global Cancer Observatory: Cancer Today. Lyon, France: International Agency for Research on Cancer. Available from: https://gco.iarc.who.int/today, accessed [18.09.2024].

(2) Hulvat, M. C. Cancer Incidence and Trends. *Surg. Clin. North Am.* **2020**, *100* (3), 469–481. https://doi.org/10.1016/j.suc.2020.01.002.

(3) Hanahan, D.; Weinberg, R. A. The Hallmarks of Cancer. *Cell* **2000**, *100* (1), 57–70. https://doi.org/10.1016/S0092-8674(00)81683-9.

(4) Hahn, W. C.; Counter, C. M.; Lundberg, A. S.; Beijersbergen, R. L.; Brooks, M. W.; Weinberg, R. A. Creation of Human Tumour Cells with Defined Genetic Elements. *Nature* **1999**, *400* (6743), 464–468. https://doi.org/10.1038/22780.

(5) Hanahan, D.; Weinberg, R. A. Hallmarks of Cancer: The Next Generation. *Cell* **2011**, *144* (5), 646–674. https://doi.org/10.1016/j.cell.2011.02.013.

(6) Hanahan, D. Hallmarks of Cancer: New Dimensions. *Cancer Discov.* **2022**, *12* (1), 31–46. https://doi.org/10.1158/2159-8290.CD-21-1059.

(7) Witsch, E.; Sela, M.; Yarden, Y. Roles for Growth Factors in Cancer Progression. *Physiology* **2010**, *25* (2), 85–101. https://doi.org/10.1152/physiol.00045.2009.

(8) Sherr, C. J.; McCormick, F. The RB and P53 Pathways in Cancer. *Cancer Cell* **2002**, *2* (2), 103–112. https://doi.org/10.1016/S1535-6108(02)00102-2.

(9) Adams, J. M.; Cory, S. The Bcl-2 Apoptotic Switch in Cancer Development and Therapy. *Oncogene* **2007**, *26* (9), 1324–1337. https://doi.org/10.1038/sj.onc.1210220.

(10) Blasco, M. A. Telomeres and Human Disease: Ageing, Cancer and Beyond. *Nat. Rev. Genet.* **2005**, *6* (8), 611–622. https://doi.org/10.1038/nrg1656.

(11) Bergers, G.; Benjamin, L. E. Tumorigenesis and the Angiogenic Switch. *Nat. Rev. Cancer* **2003**, *3* (6), 401–410. https://doi.org/10.1038/nrc1093.

(12) Cavallaro, U.; Christofori, G. Cell Adhesion and Signalling by Cadherins and Ig-CAMs in Cancer. *Nat. Rev. Cancer* **2004**, *4* (2), 118–132. https://doi.org/10.1038/nrc1276.

(13) Talmadge, J. E.; Fidler, I. J. AACR Centennial Series: The Biology of Cancer Metastasis: Historical Perspective. *Cancer Res.* **2010**, *70* (14), 5649–5669. https://doi.org/10.1158/0008-5472.CAN-10-1040.

(14) Negrini, S.; Gorgoulis, V. G.; Halazonetis, T. D. Genomic Instability an Evolving Hallmark of Cancer. *Nat. Rev. Mol. Cell Biol.* **2010**, *11* (3), 220–228. https://doi.org/10.1038/nrm2858.

(15) Waddington, C. H. The Epigenotype. *Int. J. Epidemiol.* **2012**, *41* (1), 10–13. https://doi.org/10.1093/ije/dyr184.

(16) Wu, C. -t.; Morris, J. R. Genes, Genetics, and Epigenetics: A Correspondence. *Science.* **2001**, *293* (5532), 1103–1105. https://doi.org/10.1126/science.293.5532.1103.

(17) Razin, A.; Riggs, A. D. DNA Methylation and Gene Function. *Science.* **1980**, *210* (4470), 604–610. https://doi.org/10.1126/science.6254144.

(18) Allis, C. D.; Jenuwein, T. The Molecular Hallmarks of Epigenetic Control. *Nat. Rev. Genet.* **2016**, *17* (8), 487–500. https://doi.org/10.1038/nrg.2016.59.

(19) Cutter, A. R.; Hayes, J. J. A Brief Review of Nucleosome Structure. *FEBS Lett.* **2015**, *589*, 2914–2922. https://doi.org/10.1016/j.febslet.2015.05.016.

(20) Zhou, B. R.; Jiang, J.; Feng, H.; Ghirlando, R.; Xiao, T. S.; Bai, Y. Structural Mechanisms of Nucleosome Recognition by Linker Histones. *Mol. Cell* **2015**, *59* (4), 628–638. https://doi.org/10.1016/j.molcel.2015.06.025.

(21) Fyodorov, D. V.; Zhou, B. R.; Skoultchi, A. I.; Bai, Y. Emerging Roles of Linker Histones in Regulating Chromatin Structure and Function. *Nat. Rev. Mol. Cell Biol.* **2018**, *19* (3), 192–206. https://doi.org/10.1038/nrm.2017.94.

(22) Bates, S. E. Epigenetic Therapies for Cancer. *N. Engl. J. Med.* **2020**, *383* (7), 650–663. https://doi.org/10.1056/NEJMra1805035.

(23) Cheung, P.; Tanner, K. G.; Cheung, W. L.; Sassone-Corsi, P.; Denu, J. M.; Allis, C. D. Synergistic Coupling of Histone H3 Phosphorylation and Acetylation in Response to Epidermal Growth Factor Stimulation. *Mol. Cell* **2000**, *5* (6), 905–915. https://doi.org/10.1016/S1097-2765(00)80256-7.

(24) Caron, C.; Boyault, C.; Khochbin, S. Regulatory Cross-Talk between Lysine Acetylation and Ubiquitination: Role in the Control of Protein Stability. *BioEssays* **2005**, *27* (4), 408–415. https://doi.org/10.1002/bies.20210.

(25) Tamaru, H.; Selker, E. U. A Histone H3 Methyltransferase Controls DNA Methylation in Neurospora Crassa. *Nature* **2001**, *414* (6861), 277–283. https://doi.org/10.1038/35104508.

(26) Tsai, W.-W.; Wang, Z.; Yiu, T. T.; Akdemir, K. C.; Xia, W.; Winter, S.; Tsai, C.-Y.; Shi, X.; Schwarzer, D.; Plunkett, W.; Aronow, B.; Gozani, O.; Fischle, W.; Hung, M.-C.; Patel, D. J.; Barton, M. C. TRIM24 Links a Non-Canonical Histone Signature to Breast Cancer. *Nature* **2010**, *468* (7326), 927–932. https://doi.org/10.1038/nature09542.

(27) Görisch, S. M.; Wachsmuth, M.; Tóth, K. F.; Lichter, P.; Rippe, K. Histone Acetylation Increases Chromatin Accessibility. *J. Cell Sci.* **2005**, *118* (24), 5825–5834. https://doi.org/10.1242/jcs.02689.

(28) Roth, S. Y.; Denu, J. M.; Allis, C. D. Histone Acetyltransferases. *Annu. Rev. Biochem.* **2001**, *70* (1), 81–120. https://doi.org/10.1146/annurev.biochem.70.1.81.

(29) Wang, L.; Tang, Y.; Cole, P. A.; Marmorstein, R. Structure and Chemistry of the P300/CBP and Rtt109 Histone Acetyltransferases: Implications for Histone Acetyltransferase Evolution and Function. *Curr. Opin. Struct. Biol.* **2008**, *18* (6), 741–747. https://doi.org/10.1016/j.sbi.2008.09.004.

(30) Ogryzko, V. V.; Schiltz, R. L.; Russanova, V.; Howard, B. H.; Nakatani, Y. The Transcriptional Coactivators P300 and CBP Are Histone Acetyltransferases. *Cell* **1996**, *87* (5), 953–959. https://doi.org/10.1016/S0092-8674(00)82001-2.

(31) Owen, D. J. The Structural Basis for the Recognition of Acetylated Histone H4 by the Bromodomain of Histone Acetyltransferase Gcn5p. *EMBO J.* **2000**, *19* (22), 6141–6149. https://doi.org/10.1093/emboj/19.22.6141.

(32) Tamkun, J. W.; Deuring, R.; Scott, M. P.; Kissinger, M.; Pattatucci, A. M.; Kaufman, T. C.; Kennison, J. A. Brahma: A Regulator of Drosophila Homeotic Genes Structurally Related to the Yeast Transcriptional Activator SNF2SWI2. *Cell* **1992**, *68* (3), 561–572. https://doi.org/10.1016/0092-8674(92)90191-E.

(33) Muller, S.; Filippakopoulos, P.; Knapp, S. Bromodomains as Therapeutic Targets. *Expert Rev. Mol. Med.* **2011**, *13* (9), e29. https://doi.org/10.1017/s1462399411001992.

(34) Li, G.; Tian, Y.; Zhu, W. G. The Roles of Histone Deacetylases and Their Inhibitors in Cancer Therapy. *Front. Cell Dev. Biol.* **2020**, *8* (9), 1–34. https://doi.org/10.3389/fcell.2020.576946.

(35) Allfrey, V. G.; Faulkner, R.; Mirsky, A. E. ACETYLATION AND METHYLATION OF HISTONES AND THEIR POSSIBLE ROLE IN THE REGULATION OF RNA SYNTHESIS. *Proc. Natl. Acad. Sci.* **1964**, *51* (5), 786–794. https://doi.org/10.1073/pnas.51.5.786.

(36) Inoue, A.; Fujimoto, D. Enzymatic Deacetylation of Histone. *Biochem. Biophys. Res. Commun.* **1969**, *36* (1), 146–150. https://doi.org/10.1016/0006-291X(69)90661-5.

(37) Taunton, J.; Hassig, C. A.; Schreiber, S. L. A Mammalian Histone Deacetylase Related to the Yeast Transcriptional Regulator Rpd3p. *Science.* **1996**, *272* (5260), 408–411. https://doi.org/10.1126/science.272.5260.408.

(38) Park, S.-Y.; Kim, J.-S. A Short Guide to Histone Deacetylases Including Recent Progress on Class II Enzymes. *Exp. Mol. Med.* **2020**, *52* (2), 204–212. https://doi.org/10.1038/s12276-020-0382-4.

(39) Dowling, D. P.; Di Costanzo, L.; Gennadios, H. A.; Christianson, D. W. Evolution of the Arginase Fold and Functional Diversity. *Cell. Mol. Life Sci.* **2008**, *65* (13), 2039–2055. https://doi.org/10.1007/s00018-008-7554-z.

(40) Finnin, M. S.; Donigian, J. R.; Cohen, A.; Richon, V. M.; Rifkind, R. A.; Marks, P. A.; Breslow, R.; Pavletich, N. P. Structures of a Histone Deacetylase Homologue Bound to the TSA and SAHA Inhibitors. *Nature* **1999**, *401* (6749), 188–193. https://doi.org/10.1038/43710.

(41) Somoza, J. R.; Skene, R. J.; Katz, B. A.; Mol, C.; Ho, J. D.; Jennings, A. J.; Luong, C.; Arvai, A.; Buggy, J. J.; Chi, E.; Tang, J.; Sang, B.-C.; Verner, E.; Wynands, R.; Leahy, E. M.; Dougan, D. R.; Snell, G.; Navre, M.; Knuth, M. W.; Swanson, R. V.; McRee, D. E.; Tari, L. W. Structural Snapshots of Human HDAC8 Provide Insights into the Class I Histone Deacetylases. *Structure* **2004**, *12* (7), 1325–1334. https://doi.org/10.1016/j.str.2004.04.012.

(42) Micelli, C.; Rastelli, G. Histone Deacetylases: Structural Determinants of Inhibitor Selectivity. *Drug Discov. Today* **2015**, *20* (6), 718–735. https://doi.org/10.1016/j.drudis.2015.01.007.

(43) Porter, N. J.; Christianson, D. W. Structure, Mechanism, and Inhibition of the Zinc-Dependent Histone Deacetylases. *Curr. Opin. Struct. Biol.* **2019**, *59*, 9–18. https://doi.org/10.1016/j.sbi.2019.01.004.

(44) Gantt, S. M. L.; Decroos, C.; Lee, M. S.; Gullett, L. E.; Bowman, C. M.; Christianson, D. W.; Fierke, C. A. General Base–General Acid Catalysis in Human Histone Deacetylase 8. *Biochemistry* **2016**, *55* (5), 820–832. https://doi.org/10.1021/acs.biochem.5b01327.

(45) Wu, R.; Wang, S.; Zhou, N.; Cao, Z.; Zhang, Y. A Proton-Shuttle Reaction Mechanism for Histone Deacetylase 8 and the Catalytic Role of Metal Ions. *J. Am. Chem. Soc.* **2010**, *132* (27), 9471–9479. https://doi.org/10.1021/ja103932d.

(46) Dowling, D. P.; Gantt, S. L.; Gattis, S. G.; Fierke, C. A.; Christianson, D. W. Structural Studies of Human Histone Deacetylase 8 and Its Site-Specific Variants Complexed with Substrate and Inhibitors. *Biochemistry* **2008**, *47* (51), 13554–13563. https://doi.org/10.1021/bi801610c.

(47) Hai, Y.; Christianson, D. W. Histone Deacetylase 6 Structure and Molecular Basis of Catalysis and Inhibition. *Nat. Chem. Biol.* **2016**, *12* (9), 741–747. https://doi.org/10.1038/nchembio.2134.

(48) Yang, X. J.; Seto, E. The Rpd3/Hda1 Family of Lysine Deacetylases: From Bacteria and Yeast to Mice and Men. *Nat. Rev. Mol. Cell Biol.* **2008**, *9* (3), 206–218. https://doi.org/10.1038/nrm2346.

(49) McKinsey, T. A.; Zhang, C.; Lu, J.; Olson, E. N. Signal-Dependent Nuclear Export of a Histone Deacetylase Regulates Muscle Differentiation. *Nature* **2000**, *408* (6808), 106–111. https://doi.org/10.1038/35040593.

(50) McKinsey, T. A.; Zhang, C. L.; Olson, E. N. MEF2: A Calcium-Dependent Regulator of Cell Division, Differentiation and Death. *Trends Biochem. Sci.* **2002**, *27* (1), 40–47. https://doi.org/10.1016/S0968-0004(01)02031-X.

(51) Seto, E.; Yoshida, M. Erasers of Histone Acetylation: The Histone Deacetylase Enzymes. *Cold Spring Harb. Perspect. Biol.* **2014**, *6* (4), a018713. https://doi.org/10.1101/cshperspect.a018713.

(52) Whitehead, L.; Dobler, M. R.; Radetich, B.; Zhu, Y.; Atadja, P. W.; Claiborne, T.; Grob, J. E.; McRiner, A.; Pancost, M. R.; Patnaik, A.; Shao, W.; Shultz, M.; Tichkule, R.; Tommasi, R. A.; Vash, B.; Wang, P.; Stams, T. Human HDAC Isoform Selectivity Achieved via Exploitation of the Acetate Release Channel with Structurally Unique Small Molecule Inhibitors. *Bioorg. Med. Chem.* **2011**, *19* (15), 4626–4634. https://doi.org/10.1016/j.bmc.2011.06.030.

(53) Methot, J. L.; Chakravarty, P. K.; Chenard, M.; Close, J.; Cruz, J. C.; Dahlberg, W. K.; Fleming, J.; Hamblett, C. L.; Hamill, J. E.; Harrington, P.; Harsch, A.; Heidebrecht, R.; Hughes, B.; Jung, J.; Kenific, C. M.; Kral, A. M.; Meinke, P. T.; Middleton, R. E.; Ozerova, N.; Sloman, D. L.; Stanton, M. G.; Szewczak, A. A.; Tyagarajan, S.; Witter, D. J.; Paul Secrist, J.; Miller, T. A.

Exploration of the Internal Cavity of Histone Deacetylase (HDAC) with Selective HDAC1/HDAC2 Inhibitors (SHI-1:2). *Bioorg. Med. Chem. Lett.* **2008**, *18* (3), 973–978. https://doi.org/10.1016/j.bmcl.2007.12.031.

(54) Ropero, S.; Esteller, M. The Role of Histone Deacetylases (HDACs) in Human Cancer. *Mol. Oncol.* **2007**, *1* (1), 19–25. https://doi.org/10.1016/j.molonc.2007.01.001.

(55) Millard, C. J.; Watson, P. J.; Fairall, L.; Schwabe, J. W. R. Targeting Class I Histone Deacetylases in a "Complex" Environment. *Trends Pharmacol. Sci.* **2017**, *38* (4), 363–377. https://doi.org/10.1016/j.tips.2016.12.006.

(56) Jones, P. L.; Veenstra, G. J. C.; Wade, P. A.; Vermaak, D.; Kass, S. U.; Landsberger, N.; Strouboulis, J.; Wolffe, A. P. Methylated DNA and MeCP2 Recruit Histone Deacetylase to Repress Transcription. *Nat. Genet.* **1998**, *19* (2), 187–191. https://doi.org/10.1038/561.

(57) Robertson, K. D.; Ait-Si-Ali, S.; Yokochi, T.; Wade, P. A.; Jones, P. L.; Wolffe, A. P. DNMT1 Forms a Complex with Rb, E2F1 and HDAC1 and Represses Transcription from E2F-Responsive Promoters. *Nat. Genet.* **2000**, *25* (3), 338–342. https://doi.org/10.1038/77124.

(58) Zhang, Y.; LeRoy, G.; Seelig, H.-P.; Lane, W. S.; Reinberg, D. The Dermatomyositis-Specific Autoantigen Mi2 is a Component of a Complex Containing Histone Deacetylase and Nucleosome Remodeling Activities. *Cell* **1998**, *95* (2), 279–289. https://doi.org/10.1016/S0092-8674(00)81758-4.

(59) You, A.; Tong, J. K.; Grozinger, C. M.; Schreiber, S. L. CoREST Is an Integral Component of the CoREST- Human Histone Deacetylase Complex. *Proc. Natl. Acad. Sci. U. S. A.* **2001**, *98* (4), 1454–1458. https://doi.org/10.1073/pnas.98.4.1454.

(60) Ding, Z.; Gillespie, L. L.; Paterno, G. D. Human MI-ER1 Alpha and Beta Function as Transcriptional Repressors by Recruitment of Histone Deacetylase 1 to Their Conserved ELM2 Domain. *Mol. Cell. Biol.* **2003**, *23* (1), 250–258. https://doi.org/10.1128/MCB.23.1.250-258.2003.

(61) Millard, C. J.; Watson, P. J.; Celardo, I.; Gordiyenko, Y.; Cowley, S. M.; Robinson, C. V.; Fairall, L.; Schwabe, J. W. R. Class I HDACs Share a Common Mechanism of Regulation by Inositol Phosphates. *Mol. Cell* **2013**, *51* (1), 57–67. https://doi.org/10.1016/j.molcel.2013.05.020.

(62) Guenther, M. G.; Lane, W. S.; Fischle, W.; Verdin, E.; Lazar, M. A.; Shiekhattar, R. A Core SMRT Corepressor Complex Containing HDAC3 and TBL1, a WD40-Repeat Protein Linked

to Deafness. *Genes Dev.* **2000**, *14* (9), 1048–1057. https://doi.org/10.1101/gad.14.9.1048.

(63) Ito, A.; Kawaguchi, Y.; Lai, C. H.; Kovacs, J. J.; Higashimoto, Y.; Appella, E.; Yao, T. P. MDM2-HDAC1-Mediated Deacetylation of P53 Is Required for Its Degradation. *EMBO J.* **2002**, *21* (22), 6236–6245. https://doi.org/10.1093/emboj/cdf616.

(64) Martínez-Balbás, M. A.; Bauer, U.-M.; Nielsen, S. J.; Brehm, A.; Kouzarides, T. Regulation of E2F1 Activity by Acetylation. *EMBO J.* **2000**, *19* (4), 662–671. https://doi.org/10.1093/emboj/19.4.662.

(65) Nalawansha, D. A.; Pflum, M. K. H. LSD1 Substrate Binding and Gene Expression Are Affected by HDAC1-Mediated Deacetylation. *ACS Chem. Biol.* **2017**, *12* (1), 254–264. https://doi.org/10.1021/acschembio.6b00776.

(66) Wilson, B. J.; Tremblay, A. M.; Deblois, G.; Sylvain-Drolet, G.; Giguère, V. An Acetylation Switch Modulates the Transcriptional Activity of Estrogen-Related Receptor α. *Mol. Endocrinol.* **2010**, *24* (7), 1349–1358. https://doi.org/10.1210/me.2009-0441.

(67) Deardorff, M. A.; Bando, M.; Nakato, R.; Watrin, E.; Itoh, T.; Minamino, M.; Saitoh, K.; Komata, M.; Katou, Y.; Clark, D.; Cole, K. E.; De Baere, E.; Decroos, C.; Di Donato, N.; Ernst, S.; Francey, L. J.; Gyftodimou, Y.; Hirashima, K.; Hullings, M.; Ishikawa, Y.; Jaulin, C.; Kaur, M.; Kiyono, T.; Lombardi, P. M.; Magnaghi-Jaulin, L.; Mortier, G. R.; Nozaki, N.; Petersen, M. B.; Seimiya, H.; Siu, V. M.; Suzuki, Y.; Takagaki, K.; Wilde, J. J.; Willems, P. J.; Prigent, C.; Gillessen-Kaesbach, G.; Christianson, D. W.; Kaiser, F. J.; Jackson, L. G.; Hirota, T.; Krantz, I. D.; Shirahige, K. HDAC8 Mutations in Cornelia de Lange Syndrome Affect the Cohesin Acetylation Cycle. *Nature* **2012**, *489* (7415), 313–317. https://doi.org/10.1038/nature11316.

(68) Witt, O.; Deubzer, H. E.; Milde, T.; Oehme, I. HDAC Family: What Are the Cancer Relevant Targets? *Cancer Lett.* **2009**, *277* (1), 8–21. https://doi.org/10.1016/j.canlet.2008.08.016.

(69) Lahm, A.; Paolini, C.; Pallaoro, M.; Nardi, M. C.; Jones, P.; Neddermann, P.; Sambucini, S.; Bottomley, M. J.; Lo Surdo, P.; Carfí, A.; Koch, U.; De Francesco, R.; Steinkühler, C.; Gallinari, P. Unraveling the Hidden Catalytic Activity of Vertebrate Class IIa Histone Deacetylases. *Proc. Natl. Acad. Sci. U. S. A.* **2007**, *104* (44), 17335–17340. https://doi.org/10.1073/pnas.0706487104.

(70) Fischle, W.; Dequiedt, F.; Hendzel, M. J.; Guenther, M. G.; Lazar, M. A.; Voelter, W.; Verdin, E. Enzymatic Activity Associated with Class II HDACs Is Dependent on a Multiprotein

Complex Containing HDAC3 and SMRT/N-CoR. *Mol. Cell* **2002**, *9* (1), 45–57. https://doi.org/10.1016/S1097-2765(01)00429-4.

(71) Ho, T. C. S.; Chan, A. H. Y.; Ganesan, A. Thirty Years of HDAC Inhibitors: 2020 Insight and Hindsight. *J. Med. Chem.* **2020**, *63* (21), 12460–12484. https://doi.org/10.1021/acs.jmedchem.0c00830.

(72) Tong, J. J. Identification of HDAC10, a Novel Class II Human Histone Deacetylase Containing a Leucine-Rich Domain. *Nucleic Acids Res.* **2002**, *30* (5), 1114–1123. https://doi.org/10.1093/nar/30.5.1114.

(73) Kaluza, D.; Kroll, J.; Gesierich, S.; Yao, T. P.; Boon, R. A.; Hergenreider, E.; Tjwa, M.; Rössig, L.; Seto, E.; Augustin, H. G.; Zeiher, A. M.; Dimmeler, S.; Urbich, C. Class IIb HDAC6 Regulates Endothelial Cell Migration and Angiogenesis by Deacetylation of Cortactin. *EMBO J.* **2011**, *30* (20), 4142–4156. https://doi.org/10.1038/emboj.2011.298.

(74) Kovacs, J. J.; Murphy, P. J. M.; Gaillard, S.; Zhao, X.; Wu, J.-T.; Nicchitta, C. V.; Yoshida, M.; Toft, D. O.; Pratt, W. B.; Yao, T.-P. HDAC6 Regulates Hsp90 Acetylation and Chaperone-Dependent Activation of Glucocorticoid Receptor. *Mol. Cell* **2005**, *18* (5), 601–607. https://doi.org/10.1016/j.molcel.2005.04.021.

(75) Subramanian, C.; Jarzembowski, J. A.; Opipari, A. W.; Castle, V. P.; Kwok, R. P. S. HDAC6 Deacetylates Ku70 and Regulates Ku70-Bax Binding in Neuroblastoma. *Neoplasia* **2011**, *13* (8), 726–734. https://doi.org/10.1593/neo.11558.

(76) Cohen, H. Y.; Lavu, S.; Bitterman, K. J.; Hekking, B.; Imahiyerobo, T. A.; Miller, C.; Frye, R.; Ploegh, H.; Kessler, B. M.; Sinclair, D. A. Acetylation of the C Terminus of Ku70 by CBP and PCAF Controls Bax-Mediated Apoptosis. *Mol. Cell* **2004**, *13* (5), 627–638. https://doi.org/10.1016/S1097-2765(04)00094-2.

(77) Gao, L.; Cueto, M. A.; Asselbergs, F.; Atadja, P. Cloning and Functional Characterization of HDAC11, a Novel Member of the Human Histone Deacetylase Family. *J. Biol. Chem.* **2002**, *277* (28), 25748–25755. https://doi.org/10.1074/jbc.M111871200.

(78) Kutil, Z.; Novakova, Z.; Meleshin, M.; Mikesova, J.; Schutkowski, M.; Barinka, C. Histone Deacetylase 11 Is a Fatty-Acid Deacylase. *ACS Chem. Biol.* **2018**, *13* (3), 685–693. https://doi.org/10.1021/acschembio.7b00942.

(79) Cao, J.; Sun, L.; Aramsangtienchai, P.; Spiegelman, N. A.; Zhang, X.; Huang, W.; Seto, E.; Lin, H. HDAC11 Regulates Type I Interferon Signaling through Defatty-Acylation of SHMT2.

Proc. Natl. Acad. Sci. **2019**, *116* (12), 5487–5492. https://doi.org/10.1073/pnas.1815365116.

(80) Vidal, M.; Gaber, R. F. RPD3 Encodes a Second Factor Required To Achieve Maximum Positive and Negative Transcriptional States in Saccharomyces Cerevisiae. *Mol. Cell. Biol.* **1991**, *11* (12), 6317–6327. https://doi.org/10.1128/mcb.11.12.6317-6327.1991.

(81) Yang, W.-M.; Yao, Y.-L.; Sun, J.-M.; Davie, J. R.; Seto, E. Isolation and Characterization of CDNAs Corresponding to an Additional Member of the Human Histone Deacetylase Gene Family. *J. Biol. Chem.* **1997**, *272* (44), 28001–28007. https://doi.org/10.1074/jbc.272.44.28001.

(82) Wang, Z.; Zang, C.; Cui, K.; Schones, D. E.; Barski, A.; Peng, W.; Zhao, K. Genome-Wide Mapping of HATs and HDACs Reveals Distinct Functions in Active and Inactive Genes. *Cell* **2009**, *138* (5), 1019–1031. https://doi.org/10.1016/j.cell.2009.06.049.

(83) Bhaskara, S.; Chyla, B. J.; Amann, J. M.; Knutson, S. K.; Cortez, D.; Sun, Z.-W.; Hiebert, S. W. Deletion of Histone Deacetylase 3 Reveals Critical Roles in S Phase Progression and DNA Damage Control. *Mol. Cell* **2008**, *30* (1), 61–72. https://doi.org/10.1016/j.molcel.2008.02.030.

(84) Labonte, M. J.; Wilson, P. M.; Fazzone, W.; Groshen, S.; Lenz, H. J.; Ladner, R. D. DNA Microarray Profiling of Genes Differentially Regulated by the Histone Deacetylase Inhibitors Vorinostat and LBH589 in Colon Cancer Cell Lines. *BMC Med. Genomics* **2009**, *2*, 1–20. https://doi.org/10.1186/1755-8794-2-67.

(85) Kurdistani, S. K.; Robyr, D.; Tavazoie, S.; Grunstein, M. Genome-Wide Binding Map of the Histone Deacetylase Rpd3 in Yeast. *Nat. Genet.* **2002**, *31* (3), 248–254. https://doi.org/10.1038/ng907.

(86) Ali, I.; Ruiz, D. G.; Ni, Z.; Johnson, J. R.; Zhang, H.; Li, P.-C.; Khalid, M. M.; Conrad, R. J.; Guo, X.; Min, J.; Greenblatt, J.; Jacobson, M.; Krogan, N. J.; Ott, M. Crosstalk between RNA Pol II C-Terminal Domain Acetylation and Phosphorylation via RPRD Proteins. *Mol. Cell* **2019**, *74* (6), 1164-1174.e4. https://doi.org/10.1016/j.molcel.2019.04.008.

(87) Li, Y.; Peng, L.; Seto, E. Histone Deacetylase 10 Regulates the Cell Cycle G2/M Phase Transition via a Novel Let-7–HMGA2–Cyclin A2 Pathway. *Mol. Cell. Biol.* **2015**, *35* (20), 3547–3565. https://doi.org/10.1128/MCB.00400-15.

(88) Tian, Y.; Wong, V. W. S.; Wong, G. L. H.; Yang, W.; Sun, H.; Shen, J.; Tong, J. H. M.; Go, M.

Y. Y.; Cheung, Y. S.; Lai, P. B. S.; Zhou, M.; Xu, G.; Huang, T. H. M.; Yu, J.; To, K. F.; Cheng, A. S. L.; Chan, H. L. Y. Histone Deacetylase HDAC8 Promotes Insulin Resistance and β-Catenin Activation in NAFLD-Associated Hepatocellular Carcinoma. *Cancer Res.* **2015**, *75* (22), 4803–4816. https://doi.org/10.1158/0008-5472.CAN-14-3786.

(89) Richon, V. M.; Sandhoff, T. W.; Rifkind, R. A.; Marks, P. A. Histone Deacetylase Inhibitor Selectively Induces P21WAF1 Expression and Gene-Associated Histone Acetylation. *Proc. Natl. Acad. Sci. U. S. A.* **2000**, *97* (18), 10014–10019. https://doi.org/10.1073/pnas.180316197.

(90) Park, I.; Kwon, M.; Paik, S.; Kim, H.; Lee, H.; Choi, E.; Lee, H. HDAC2/3 Binding and Deacetylation of BubR1 Initiates Spindle Assembly Checkpoint Silencing. *FEBS J.* **2017**, *284* (23), 4035–4050. https://doi.org/10.1111/febs.14286.

(91) Enoch, T.; Norbury, C. Cellular Responses to DNA Damage: Cell-Cycle Checkpoints, Apoptosis and the Roles of P53 and ATM. *Trends Biochem. Sci.* **1995**, *20* (10), 426–430. https://doi.org/10.1016/S0968-0004(00)89093-3.

(92) Juan, L.-J.; Shia, W.-J.; Chen, M.-H.; Yang, W.-M.; Seto, E.; Lin, Y.-S.; Wu, C.-W. Histone Deacetylases Specifically Down-Regulate P53-Dependent Gene Activation. *J. Biol. Chem.* **2000**, *275* (27), 20436–20443. https://doi.org/10.1074/jbc.M000202200.

(93) Yun, T.; Yu, K.; Yang, S.; Cui, Y.; Wang, Z.; Ren, H.; Chen, S.; Li, L.; Liu, X.; Fang, M.; Jiang, X. Acetylation of P53 Protein at Lysine 120 Up-Regulates Apaf-1 Protein and Sensitizes the Mitochondrial Apoptotic Pathway. *J. Biol. Chem.* **2016**, *291* (14), 7386–7395. https://doi.org/10.1074/jbc.M115.706341.

(94) Yang, Y.; Zhao, Y.; Liao, W.; Yang, J.; Wu, L.; Zheng, Z.; Yu, Y.; Zhou, W.; Li, L.; Feng, J.; Wang, H.; Zhu, W.-G. Acetylation of FoxO1 Activates Bim Expression to Induce Apoptosis in Response to Histone Deacetylase Inhibitor Depsipeptide Treatment. *Neoplasia* **2009**, *11* (4), 313-IN1. https://doi.org/10.1593/neo.81358.

(95) Sun, Q. Y.; Ding, L. W.; Johnson, K.; Zhou, S.; Tyner, J. W.; Yang, H.; Doan, N. B.; Said, J. W.; Xiao, J. F.; Loh, X. Y.; Ran, X. Bin; Venkatachalam, N.; Lao, Z.; Chen, Y.; Xu, L.; Fan, L. F.; Chien, W.; Lin, D. C.; Koeffler, H. P. SOX7 Regulates MAPK/ERK-BIM Mediated Apoptosis in Cancer Cells. *Oncogene* **2019**, *38* (34), 6196–6210. https://doi.org/10.1038/s41388-019-0865-8.

(96) Nebbioso, A.; Carafa, V.; Conte, M.; Tambaro, F. P.; Abbondanza, C.; Martens, J.; Nees, M.;

Benedetti, R.; Pallavicini, I.; Minucci, S.; Garcia-Manero, G.; Iovino, F.; Lania, G.; Ingenito, C.; Belsito Petrizzi, V.; Stunnenberg, H. G.; Altucci, L. C-Myc Modulation and Acetylation Is a Key HDAC Inhibitor Target in Cancer. *Clin. Cancer Res.* **2017**, *23* (10), 2542–2555. https://doi.org/10.1158/1078-0432.CCR-15-2388.

(97) Jackson, S. P.; Bartek, J. The DNA-Damage Response in Human Biology and Disease. *Nature* **2009**, *461* (7267), 1071–1078. https://doi.org/10.1038/nature08467.

(98) Huertas, P. DNA Resection in Eukaryotes: Deciding How to Fix the Break. *Nat. Struct. Mol. Biol.* **2010**, *17* (1), 11–16. https://doi.org/10.1038/nsmb.1710.

(99) Miller, K. M.; Tjeertes, J. V.; Coates, J.; Legube, G.; Polo, S. E.; Britton, S.; Jackson, S. P. Human HDAC1 and HDAC2 Function in the DNA-Damage Response to Promote DNA Nonhomologous End-Joining. *Nat. Struct. Mol. Biol.* **2010**, *17* (9), 1144–1151. https://doi.org/10.1038/nsmb.1899.

(100) Miller, K. M.; Maas, N. L.; Toczyski, D. P. Taking It off: Regulation of H3 K56 Acetylation by Hst3 and Hst4. *Cell Cycle* **2006**, *5* (22), 2561–2565. https://doi.org/10.4161/cc.5.22.3501.

(101) Kopito, R. R. Aggresomes, Inclusion Bodies and Protein Aggregation. *Trends Cell Biol.* **2000**, *10* (12), 524–530. https://doi.org/10.1016/S0962-8924(00)01852-3.

(102) Nicholson, J.; Jevons, S. J.; Groselj, B.; Ellermann, S.; Konietzny, R.; Kerr, M.; Kessler, B. M.; Kiltie, A. E. E3 Ligase CIAP2 Mediates Downregulation of MRE11 and Radiosensitization in Response to HDAC Inhibition in Bladder Cancer. *Cancer Res.* **2017**, *77* (11), 3027–3039. https://doi.org/10.1158/0008-5472.CAN-16-3232.

(103) Kim, M. S.; Kwon, H. J.; Lee, Y. M.; Baek, J. H.; Jang, J.-E.; Lee, S.-W.; Moon, E.-J.; Kim, H.-S.; Lee, S.-K.; Chung, H. Y.; Kim, C. W.; Kim, K.-W. Histone Deacetylases Induce Angiogenesis by Negative Regulation of Tumor Suppressor Genes. *Nat. Med.* **2001**, *7* (4), 437–443. https://doi.org/10.1038/86507.

(104) Zhang, M.; Xiang, S.; Joo, H.-Y.; Wang, L.; Williams, K. A.; Liu, W.; Hu, C.; Tong, D.; Haakenson, J.; Wang, C.; Zhang, S.; Pavlovicz, R. E.; Jones, A.; Schmidt, K. H.; Tang, J.; Dong, H.; Shan, B.; Fang, B.; Radhakrishnan, R.; Glazer, P. M.; Matthias, P.; Koomen, J.; Seto, E.; Bepler, G.; Nicosia, S. V.; Chen, J.; Li, C.; Gu, L.; Li, G.-M.; Bai, W.; Wang, H.; Zhang, X. HDAC6 Deacetylates and Ubiquitinates MSH2 to Maintain Proper Levels of MutSα. *Mol. Cell* **2014**, *55* (1), 31–46. https://doi.org/10.1016/j.molcel.2014.04.028.

(105) Kawaguchi, Y.; Kovacs, J. J.; McLaurin, A.; Vance, J. M.; Ito, A.; Yao, T.-P. The Deacetylase

HDAC6 Regulates Aggresome Formation and Cell Viability in Response to Misfolded Protein Stress. *Cell* **2003**, *115* (6), 727–738. https://doi.org/10.1016/S0092-8674(03)00939-5.

(106) Lee, J. Y.; Koga, H.; Kawaguchi, Y.; Tang, W.; Wong, E.; Gao, Y. S.; Pandey, U. B.; Kaushik, S.; Tresse, E.; Lu, J.; Taylor, J. P.; Cuervo, A. M.; Yao, T. P. HDAC6 Controls Autophagosome Maturation Essential for Ubiquitin-Selective Quality-Control Autophagy. *EMBO J.* **2010**, *29* (5), 969–980. https://doi.org/10.1038/emboj.2009.405.

(107) Oehme, I.; Linke, J.-P.; Böck, B. C.; Milde, T.; Lodrini, M.; Hartenstein, B.; Wiegand, I.; Eckert, C.; Roth, W.; Kool, M.; Kaden, S.; Gröne, H.-J.; Schulte, J. H.; Lindner, S.; Hamacher-Brady, A.; Brady, N. R.; Deubzer, H. E.; Witt, O. Histone Deacetylase 10 Promotes Autophagy-Mediated Cell Survival. *Proc. Natl. Acad. Sci.* **2013**, *110* (28), E2592-E2601. https://doi.org/10.1073/pnas.1300113110.

(108) Özdağ, H.; Teschendorff, A. E.; Ahmed, A. A.; Hyland, S. J.; Blenkiron, C.; Bobrow, L.; Veerakumarasivam, A.; Burtt, G.; Subkhankulova, T.; Arends, M. J.; Collins, V. P.; Bowtell, D.; Kouzarides, T.; Brenton, J. D.; Caldas, C. Differential Expression of Selected Histone Modifier Genes in Human Solid Cancers. *BMC Genomics* **2006**, *7* (1), 90. https://doi.org/10.1186/1471-2164-7-90.

(109) Park, B. L.; Kim, Y. J.; Cheong, H. S.; Lee, S. O.; Han, C. S.; Yoon, J.-H.; Park, J. H.; Chang, H. S.; Park, C.-S.; Lee, H.-S.; Shin, H. D. HDAC10 Promoter Polymorphism Associated with Development of HCC among Chronic HBV Patients. *Biochem. Biophys. Res. Commun.* **2007**, *363* (3), 776–781. https://doi.org/10.1016/j.bbrc.2007.09.026.

(110) Li, Y.; Seto, E. HDACs and HDAC Inhibitors in Cancer Development and Therapy. *Cold Spring Harb. Perspect. Med.* **2016**, *6* (10), 1–34. https://doi.org/10.1101/cshperspect.a026831.

(111) Mithraprabhu, S.; Kalff, A.; Chow, A.; Khong, T.; Spencer, A. Dysregulated Class I Histone Deacetylases Are Indicators of Poor Prognosis in Multiple Myeloma. *Epigenetics* **2014**, *9* (11), 1511–1520. https://doi.org/10.4161/15592294.2014.983367.

(112) Poyet, C.; Jentsch, B.; Hermanns, T.; Schweckendiek, D.; Seifert, H.-H.; Schmidtpeter, M.; Sulser, T.; Moch, H.; Wild, P. J.; Kristiansen, G. Expression of Histone Deacetylases 1, 2 and 3 in Urothelial Bladder Cancer. *BMC Clin. Pathol.* **2014**, *14* (1), 10. https://doi.org/10.1186/1472-6890-14-10.

(113) Oehme, I.; Deubzer, H. E.; Wegener, D.; Pickert, D.; Linke, J. P.; Hero, B.; Kopp-Schneider, A.; Westermann, F.; Ulrich, S. M.; Von Deimling, A.; Fischer, M.; Witt, O. Histone

Deacetylase 8 in Neuroblastoma Tumorigenesis. *Clin. Cancer Res.* **2009**, *15* (1), 91–99. https://doi.org/10.1158/1078-0432.CCR-08-0684.

(114) Milde, T.; Oehme, I.; Korshunov, A.; Kopp-Schneider, A.; Remke, M.; Northcott, P.; Deubzer, H. E.; Lodrini, M.; Taylor, M. D.; von Deimling, A.; Pfister, S.; Witt, O. HDAC5 and HDAC9 in Medulloblastoma: Novel Markers for Risk Stratification and Role in Tumor Cell Growth. *Clin. Cancer Res.* **2010**, *16* (12), 3240–3252. https://doi.org/10.1158/1078-0432.CCR-10-0395.

(115) Davidson, N. E. Combined Endocrine Therapy for Breast Cancer - New Life for an Old Idea? *J. Natl. Cancer Inst.* **2000**, *92* (11), 859–860. https://doi.org/10.1093/jnci/92.11.859.

(116) Kawai, H.; Li, H.; Avraham, S.; Jiang, S.; Avraham, H. K. Overexpression of Histone Deacetylase HDAC1 Modulates Breast Cancer Progression by Negative Regulation of Estrogen Receptor α. *Int. J. Cancer* **2003**, *107* (3), 353–358. https://doi.org/10.1002/ijc.11403.

(117) Yang, X.; Ferguson, A. T.; Nass, S. J.; Phillips, D. L.; Butash, K. A.; Wang, S. M.; Herman, J. G.; Davidson, N. E. Transcriptional Activation of Estrogen Receptor α in Human Breast Cancer Cells by Histone Deacetylase Inhibition. *Cancer Res.* **2000**, *60* (24), 6890–6894.

(118) Liu, T.; Tee, A. E. L.; Porro, A.; Smith, S. A.; Dwarte, T.; Liu, P. Y.; Iraci, N.; Sekyere, E.; Haber, M.; Norris, M. D.; Diolaiti, D.; Della Valle, G.; Perini, G.; Marshall, G. M. Activation of Tissue Transglutaminase Transcription by Histone Deacetylase Inhibition as a Therapeutic Approach for Myc Oncogenesis. *Proc. Natl. Acad. Sci.* **2007**, *104* (47), 18682–18687. https://doi.org/10.1073/pnas.0705524104.

(119) Keshelava, N.; Davicioni, E.; Wan, Z.; Ji, L.; Sposto, R.; Triche, T. J.; Reynolds, C. P. Histone Deacetylase 1 Gene Expression and Sensitization of Multidrug-Resistant Neuroblastoma Cell Lines to Cytotoxic Agents by Depsipeptide. *JNCI J. Natl. Cancer Inst.* **2007**, *99* (14), 1107–1119. https://doi.org/10.1093/jnci/djm044.

(120) Huang, B. H.; Laban, M.; Leung, C. H. W.; Lee, L.; Lee, C. K.; Salto-Tellez, M.; Raju, G. C.; Hooi, S. C. Inhibition of Histone Deacetylase 2 Increases Apoptosis and P21Cip1/WAF1 Expression, Independent of Histone Deacetylase 1. *Cell Death Differ.* **2005**, *12* (4), 395–404. https://doi.org/10.1038/sj.cdd.4401567.

(121) Atsumi, A.; Tomita, A.; Kiyoi, H.; Naoe, T. Histone Deacetylase 3 (HDAC3) Is Recruited to Target Promoters by PML-RARα as a Component of the N-CoR Co-Repressor Complex to

Repress Transcription in Vivo. *Biochem. Biophys. Res. Commun.* **2006**, *345* (4), 1471–1480. https://doi.org/10.1016/j.bbrc.2006.05.047.

(122) Qian, D. Z.; Kachhap, S. K.; Collis, S. J.; Verheul, H. M. W.; Carducci, M. A.; Atadja, P.; Pili, R. Class II Histone Deacetylases Are Associated with VHL-Independent Regulation of Hypoxia-Inducible Factor 1α. *Cancer Res.* **2006**, *66* (17), 8814–8821. https://doi.org/10.1158/0008-5472.CAN-05-4598.

(123) Mottet, D.; Bellahcène, A.; Pirotte, S.; Waltregny, D.; Deroanne, C.; Lamour, V.; Lidereau, R.; Castronovo, V. Histone Deacetylase 7 Silencing Alters Endothelial Cell Migration, a Key Step in Angiogenesis. *Circ. Res.* **2007**, *101* (12), 1237–1246. https://doi.org/10.1161/CIRCRESAHA.107.149377.

(124) Haggarty, S. J.; Koeller, K. M.; Wong, J. C.; Grozinger, C. M.; Schreiber, S. L. Domain-Selective Small-Molecule Inhibitor of Histone Deacetylase 6 (HDAC6)-Mediated Tubulin Deacetylation. *Proc. Natl. Acad. Sci.* **2003**, *100* (8), 4389–4394. https://doi.org/10.1073/pnas.0430973100.

(125) Park, J.-H.; Kim, S.-H.; Choi, M.-C.; Lee, J.; Oh, D.-Y.; Im, S.-A.; Bang, Y.-J.; Kim, T.-Y. Class II Histone Deacetylases Play Pivotal Roles in Heat Shock Protein 90-Mediated Proteasomal Degradation of Vascular Endothelial Growth Factor Receptors. *Biochem. Biophys. Res. Commun.* **2008**, *368* (2), 318–322. https://doi.org/10.1016/j.bbrc.2008.01.056.

(126) Liu, Y.; Tong, X.; Hu, W.; Chen, D. HDAC11: A Novel Target for Improved Cancer Therapy. *Biomed. Pharmacother.* **2023**, *166*, 115418. https://doi.org/10.1016/j.biopha.2023.115418.

(127) Shukla, S.; Tekwani, B. L. Histone Deacetylases Inhibitors in Neurodegenerative Diseases, Neuroprotection and Neuronal Differentiation. *Front. Pharmacol.* **2020**, *11* (4), 1–20. https://doi.org/10.3389/fphar.2020.00537.

(128) Chuang, D.-M.; Leng, Y.; Marinova, Z.; Kim, H.-J.; Chiu, C.-T. Multiple Roles of HDAC Inhibition in Neurodegenerative Conditions. *Trends Neurosci.* **2009**, *32* (11), 591–601. https://doi.org/10.1016/j.tins.2009.06.002.

(129) Arrowsmith, C. H.; Bountra, C.; Fish, P. V.; Lee, K.; Schapira, M. Epigenetic Protein Families: A New Frontier for Drug Discovery. *Nat. Rev. Drug Discov.* **2012**, *11* (5), 384–400. https://doi.org/10.1038/nrd3674.

(130) Zhang, S. Y.; Zhang, L. Y.; Wen, R.; Yang, N.; Zhang, T. N. Histone Deacetylases and Their

Inhibitors in Inflammatory Diseases. *Biomed. Pharmacother.* **2024**, *179* (8), 117295. https://doi.org/10.1016/j.biopha.2024.117295.

(131) Bode, K. A.; Schroder, K.; Hume, D. A.; Ravasi, T.; Heeg, K.; Sweet, M. J.; Dalpke, A. H. Histone Deacetylase Inhibitors Decrease Toll-like Receptor-mediated Activation of Proinflammatory Gene Expression by Impairing Transcription Factor Recruitment. *Immunology* **2007**, *122* (4), 596–606. https://doi.org/10.1111/j.1365-2567.2007.02678.x.

(132) Roger, T.; Lugrin, J.; Le Roy, D.; Goy, G.; Mombelli, M.; Koessler, T.; Ding, X. C.; Chanson, A.-L.; Reymond, M. K.; Miconnet, I.; Schrenzel, J.; François, P.; Calandra, T. Histone Deacetylase Inhibitors Impair Innate Immune Responses to Toll-like Receptor Agonists and to Infection. *Blood* **2011**, *117* (4), 1205–1217. https://doi.org/10.1182/blood-2010-05-284711.

(133) Gunst, J. D.; Pahus, M. H.; Rosás-Umbert, M.; Lu, I.-N.; Benfield, T.; Nielsen, H.; Johansen, I. S.; Mohey, R.; Østergaard, L.; Klastrup, V.; Khan, M.; Schleimann, M. H.; Olesen, R.; Støvring, H.; Denton, P. W.; Kinloch, N. N.; Copertino, D. C.; Ward, A. R.; Alberto, W. D. C.; Nielsen, S. D.; Puertas, M. C.; Ramos, V.; Reeves, J. D.; Petropoulos, C. J.; Martinez-Picado, J.; Brumme, Z. L.; Jones, R. B.; Fox, J.; Tolstrup, M.; Nussenzweig, M. C.; Caskey, M.; Fidler, S.; Søgaard, O. S. Early Intervention with 3BNC117 and Romidepsin at Antiretroviral Treatment Initiation in People with HIV-1: A Phase 1b/2a, Randomized Trial. *Nat. Med.* **2022**, *28* (11), 2424–2435. https://doi.org/10.1038/s41591-022-02023-7.

(134) Husain, M.; Cheung, C.-Y. Histone Deacetylase 6 Inhibits Influenza A Virus Release by Downregulating the Trafficking of Viral Components to the Plasma Membrane via Its Substrate, Acetylated Microtubules. *J. Virol.* **2014**, *88* (19), 11229–11239. https://doi.org/10.1128/JVI.00727-14.

(135) Saiz, M. L.; DeDiego, M. L.; López-García, D.; Corte-Iglesias, V.; Baragaño Raneros, A.; Astola, I.; Asensi, V.; López-Larrea, C.; Suarez-Alvarez, B. Epigenetic Targeting of the ACE2 and NRP1 Viral Receptors Limits SARS-CoV-2 Infectivity. *Clin. Epigenetics* **2021**, *13* (1), 187. https://doi.org/10.1186/s13148-021-01168-5.

(136) Jung, M.; Hoffmann, K.; Brosch, G.; Loidl, P. Analogues of Trichostatin a and Trapoxin B as Histone Deacetylase Inhibitors. *Bioorg. Med. Chem. Lett.* **1997**, *7* (13), 1655–1658. https://doi.org/10.1016/S0960-894X(97)00284-9.

(137) Abdallah, D. I.; de Araujo, E. D.; Patel, N. H.; Hasan, L. S.; Moriggl, R.; Krämer, O. H.; Gunning, P. T. Medicinal Chemistry Advances in Targeting Class I Histone Deacetylases.

Explor. Target. Anti-tumor Ther. **2023**, *4* (4), 757–779. https://doi.org/10.37349/etat.2023.00166.

(138) Melesina, J.; Simoben, C. V; Praetorius, L.; Bülbül, E. F.; Robaa, D.; Sippl, W. Strategies To Design Selective Histone Deacetylase Inhibitors. *ChemMedChem* **2021**, *16* (9), 1336–1359. https://doi.org/10.1002/cmdc.202000934.

(139) Bondarev, A. D.; Attwood, M. M.; Jonsson, J.; Chubarev, V. N.; Tarasov, V. V.; Schiöth, H. B. Recent Developments of HDAC Inhibitors: Emerging Indications and Novel Molecules. *Br. J. Clin. Pharmacol.* **2021**, *87* (12), 4577–4597. https://doi.org/10.1111/bcp.14889.

(140) Mullard, A. FDA Approves an HDAC Inhibitor for Duchenne Muscular Dystrophy. *Nat. Rev. Drug Discov.* **2024**, *23* (5), 329–329. https://doi.org/10.1038/d41573-024-00066-8.

(141) Rai, S.; Kim, W. S.; Ando, K.; Choi, I.; Izutsu, K.; Tsukamoto, N.; Yokoyama, M.; Tsukasaki, K.; Kuroda, J.; Ando, J.; Hidaka, M.; Koh, Y.; Shibayama, H.; Uchida, T.; Yang, D. H.; Ishitsuka, K.; Ishizawa, K.; Kim, J. S.; Lee, H. G.; Minami, H.; Eom, H. S.; Kurosawa, M.; Lee, J. H.; Lee, J. S.; Lee, W. S.; Nagai, H.; Shindo, T.; Yoon, D. H.; Yoshida, S.; Gillings, M.; Onogi, H.; Tobinai, K. Oral HDAC Inhibitor Tucidinostat in Patients with Relapsed or Refractory Peripheral T-Cell Lymphoma: Phase IIb Results. *Haematologica* **2022**, *108* (3), 811–821. https://doi.org/10.3324/haematol.2022.280996.

(142) Suo, J.; Zhu, K.; Zhuang, C.; Zhong, X.; Bravaccini, S.; Maltoni, R.; Bertucci, F.; Zheng, H.; Luo, T. Efficacy and Safety of Tucidinostat in Patients with Advanced Hormone Receptor-Positive Human Epidermal Growth Factor Receptor 2-Negative Breast Cancer: Real-World Insights. *Ann. Transl. Med.* **2023**, *11* (12), 409–409. https://doi.org/10.21037/atm-23-1913.

(143) Hristov, A. C.; Tejasvi, T.; Wilcox, R. A. Mycosis Fungoides and Sézary Syndrome: 2019 Update on Diagnosis, Risk-stratification, and Management. *Am. J. Hematol.* **2019**, *94* (9), 1027–1041. https://doi.org/10.1002/ajh.25577.

(144) Moskowitz, A. J.; Lunning, M. A.; Horwitz, S. M. How I Treat the Peripheral T-Cell Lymphomas. *Blood* **2014**, *123* (17), 2636–2644. https://doi.org/10.1182/blood-2013-12-516245.

(145) Robak, P.; Drozdz, I.; Szemraj, J.; Robak, T. Drug Resistance in Multiple Myeloma. *Cancer Treat. Rev.* **2018**, *70* (9), 199–208. https://doi.org/10.1016/j.ctrv.2018.09.001.

(146) Bhatia, S.; Krieger, V.; Groll, M.; Osko, J. D.; Reßing, N.; Ahlert, H.; Borkhardt, A.; Kurz, T.;

Christianson, D. W.; Hauer, J.; Hansen, F. K. Discovery of the First-in-Class Dual Histone Deacetylase–Proteasome Inhibitor. *J. Med. Chem.* **2018**, *61* (22), 10299–10309. https://doi.org/10.1021/acs.jmedchem.8b01487.

(147) Mercuri, E.; Bönnemann, C. G.; Muntoni, F. Muscular Dystrophies. *Lancet* **2019**, *394* (10213), 2025–2038. https://doi.org/10.1016/S0140-6736(19)32910-1.

(148) Marek, L.; Hamacher, A.; Hansen, F. K.; Kuna, K.; Gohlke, H.; Kassack, M. U.; Kurz, T. Histone Deacetylase (HDAC) Inhibitors with a Novel Connecting Unit Linker Region Reveal a Selectivity Profile for HDAC4 and HDAC5 with Improved Activity against Chemoresistant Cancer Cells. *J. Med. Chem.* **2013**, *56* (2), 427–436. https://doi.org/10.1021/jm301254q.

(149) Agarwal, R.; Pattarawat, P.; Duff, M. R.; Wang, H. C. R.; Baudry, J.; Smith, J. C. Structure-Based Identification of Novel Histone Deacetylase 4 (HDAC4) Inhibitors. *Pharmaceuticals* **2024**, *17* (7), 1–13. https://doi.org/10.3390/ph17070867.

(150) Fass, D. M.; Shah, R.; Ghosh, B.; Hennig, K.; Norton, S.; Zhao, W.-N.; Reis, S. A.; Klein, P. S.; Mazitschek, R.; Maglathlin, R. L.; Lewis, T. A.; Haggarty, S. J. Short-Chain HDAC Inhibitors Differentially Affect Vertebrate Development and Neuronal Chromatin. *ACS Med. Chem. Lett.* **2011**, *2* (1), 39–42. https://doi.org/10.1021/ml1001954.

(151) Lauffer, B. E. L.; Mintzer, R.; Fong, R.; Mukund, S.; Tam, C.; Zilberleyb, I.; Flicke, B.; Ritscher, A.; Fedorowicz, G.; Vallero, R.; Ortwine, D. F.; Gunzner, J.; Modrusan, Z.; Neumann, L.; Koth, C. M.; Lupardus, P. J.; Kaminker, J. S.; Heise, C. E.; Steiner, P. Histone Deacetylase (HDAC) Inhibitor Kinetic Rate Constants Correlate with Cellular Histone Acetylation but Not Transcription and Cell Viability. *J. Biol. Chem.* **2013**, *288* (37), 26926–26943. https://doi.org/10.1074/jbc.M113.490706.

(152) Shen, S.; Kozikowski, A. P. Why Hydroxamates May Not Be the Best Histone Deacetylase Inhibitors—What Some May Have Forgotten or Would Rather Forget? *ChemMedChem* **2016**, *11* (1), 15–21. https://doi.org/10.1002/cmdc.201500486.

(153) Hoshino, Y.; Okuno, M.; Kawamura, E.; Honda, K.; Inoue, S. Base-Mediated Rearrangement of Free Aromatic Hydroxamic Acids (ArCO–NHOH) to Anilines. *Chem. Commun.* **2009**, No. 17, 2281. https://doi.org/10.1039/b822806j.

(154) Lee, M. S.; Isobe, M. Metabolic Activation of the Potent Mutagen, 2-Naphthohydroxamic Acid, in Salmonella Typhimurium TA98. *Cancer Res.* **1990**, *50* (14), 4300–4307.

(155) Mercuri, E.; Vilchez, J. J.; Boespflug-Tanguy, O.; Zaidman, C. M.; Mah, J. K.; Goemans, N.;

Müller-Felber, W.; Niks, E. H.; Schara-Schmidt, U.; Bertini, E.; Comi, G. P.; Mathews, K. D.; Servais, L.; Vandenborne, K.; Johannsen, J.; Messina, S.; Spinty, S.; McAdam, L.; Selby, K.; Byrne, B.; Laverty, C. G.; Carroll, K.; Zardi, G.; Cazzaniga, S.; Coceani, N.; Bettica, P.; McDonald, C. M.; Acsadi, G.; Baranello, G.; Blaschek, A.; Brandsema, J.; Brogna, C.; Bruno, C.; Connolly, A.; de Groot, I.; De Waele, L.; Finanger, E.; Finkel, R.; Gidaro, T.; Guglieri, M.; Harper, A.; Lopez Lobato, M.; Madruga Garrido, M.; Magri, F.; Manousakis, G.; Masson, R.; Monduy, M.; Muelas Gomez, N.; Munell, F.; Nascimento, A.; Nevo, Y.; Pereon, Y.; Phan, H.; Sansone, V.; Scoto, M.; Vucinic, D.; Willis, T. Safety and Efficacy of Givinostat in Boys with Duchenne Muscular Dystrophy (EPIDYS): A Multicentre, Randomised, Double-Blind, Placebo-Controlled, Phase 3 Trial. *Lancet Neurol.* **2024**, *23* (4), 393–403. https://doi.org/10.1016/S1474-4422(24)00036-X.

(156) Nakajima, H.; Kim, Y. B.; Terano, H.; Yoshida, M.; Horinouchi, S. FR901228, a Potent Antitumor Antibiotic, Is a Novel Histone Deacetylase Inhibitor. *Exp. Cell Res.* **1998**, *241* (1), 126–133. https://doi.org/10.1006/excr.1998.4027.

(157) Kim, B.; Ratnayake, R.; Lee, H.; Shi, G.; Zeller, S. L.; Li, C.; Luesch, H.; Hong, J. Synthesis and Biological Evaluation of Largazole Zinc-Binding Group Analogs. *Bioorganic Med. Chem.* **2017**, *25* (12), 3077–3086. https://doi.org/10.1016/j.bmc.2017.03.071.

(158) Vickers, C. J.; Olsen, C. A.; Leman, L. J.; Ghadiri, M. R. Discovery of HDAC Inhibitors That Lack an Active Site Zn^{2+}-Binding Functional Group. *ACS Med. Chem. Lett.* **2012**, *3* (6), 505–508. https://doi.org/10.1021/ml300081u.

(159) Marson, C. M.; Matthews, C. J.; Yiannaki, E.; Atkinson, S. J.; Soden, P. E.; Shukla, L.; Lamadema, N.; Thomas, N. S. B. Discovery of Potent, Isoform-Selective Inhibitors of Histone Deacetylase Containing Chiral Heterocyclic Capping Groups and a N-(2-Aminophenyl)Benzamide Binding Unit. *J. Med. Chem.* **2013**, *56* (15), 6156–6174. https://doi.org/10.1021/jm400634n.

(160) Bressi, J. C.; Jennings, A. J.; Skene, R.; Wu, Y.; Melkus, R.; Jong, R. De; O'Connell, S.; Grimshaw, C. E.; Navre, M.; Gangloff, A. R. Exploration of the HDAC2 Foot Pocket: Synthesis and SAR of Substituted N-(2-Aminophenyl)Benzamides. *Bioorg. Med. Chem. Lett.* **2010**, *20* (10), 3142–3145. https://doi.org/10.1016/j.bmcl.2010.03.091.

(161) Schäker-Hübner, L.; Haschemi, R.; Büch, T.; Kraft, F. B.; Brumme, B.; Schöler, A.; Jenke, R.; Meiler, J.; Aigner, A.; Bendas, G.; Hansen, F. K. Balancing Histone Deacetylase (HDAC) Inhibition and Drug-likeness: Biological and Physicochemical Evaluation of Class I Selective

HDAC Inhibitors. *ChemMedChem* **2022**, *17* (9), e202100755. https://doi.org/10.1002/cmdc.202100755.

(162) Hideshima, T.; Richardson, P. G.; Anderson, K. C. Mechanism of Action of Proteasome Inhibitors and Deacetylase Inhibitors and the Biological Basis of Synergy in Multiple Myeloma. *Mol. Cancer Ther.* **2011**, *10* (11), 2034–2042. https://doi.org/10.1158/1535-7163.MCT-11-0433.

(163) Porter, N. J.; Mahendran, A.; Breslow, R.; Christianson, D. W. Unusual Zinc-Binding Mode of HDAC6-Selective Hydroxamate Inhibitors. *Proc. Natl. Acad. Sci.* **2017**, *114* (51), 13459–13464. https://doi.org/10.1073/pnas.1718823114.

(164) Békés, M.; Langley, D. R.; Crews, C. M. PROTAC Targeted Protein Degraders: The Past Is Prologue. *Nat. Rev. Drug Discov.* **2022**, *21* (3), 181–200. https://doi.org/10.1038/s41573-021-00371-6.

(165) Hopkins, A. L.; Groom, C. R. The Druggable Genome. *Nat. Rev. Drug Discov.* **2002**, *1* (9), 727–730. https://doi.org/10.1038/nrd892.

(166) Valeur, E.; Guéret, S. M.; Adihou, H.; Gopalakrishnan, R.; Lemurell, M.; Waldmann, H.; Grossmann, T. N.; Plowright, A. T. New Modalities for Challenging Targets in Drug Discovery. *Angew. Chemie Int. Ed.* **2017**, *56* (35), 10294–10323. https://doi.org/10.1002/anie.201611914.

(167) Pettersson, M.; Crews, C. M. PROteolysis TArgeting Chimeras (PROTACs) — Past, Present and Future. *Drug Discov. Today Technol.* **2019**, *31*, 15–27. https://doi.org/10.1016/j.ddtec.2019.01.002.

(168) Vijay-kumar, S.; Bugg, C. E.; Cook, W. J. Structure of Ubiquitin Refined at 1.8 Å Resolution. *J. Mol. Biol.* **1987**, *194* (3), 531–544. https://doi.org/10.1016/0022-2836(87)90679-6.

(169) Buetow, L.; Huang, D. T. Structural Insights into the Catalysis and Regulation of E3 Ubiquitin Ligases. *Nat. Rev. Mol. Cell Biol.* **2016**, *17* (10), 626–642. https://doi.org/10.1038/nrm.2016.91.

(170) Ye, Y.; Rape, M. Building Ubiquitin Chains: E2 Enzymes at Work. *Nat. Rev. Mol. Cell Biol.* **2009**, *10* (11), 755–764. https://doi.org/10.1038/nrm2780.

(171) Li, W.; Bengtson, M. H.; Ulbrich, A.; Matsuda, A.; Reddy, V. A.; Orth, A.; Chanda, S. K.; Batalov, S.; Joazeiro, C. A. P. Genome-Wide and Functional Annotation of Human E3 Ubiquitin Ligases Identifies MULAN, a Mitochondrial E3 That Regulates the Organelle's

Dynamics and Signaling. *PLoS One* **2008**, *3* (1), e1487. https://doi.org/10.1371/journal.pone.0001487.

(172) Komander, D.; Rape, M. The Ubiquitin Code. *Annu. Rev. Biochem.* **2012**, *81* (1), 203–229. https://doi.org/10.1146/annurev-biochem-060310-170328.

(173) Tenno, T.; Fujiwara, K.; Tochio, H.; Iwai, K.; Morita, E. H.; Hayashi, H.; Murata, S.; Hiroaki, H.; Sato, M.; Tanaka, K.; Shirakawa, M. Structural Basis for Distinct Roles of Lys63- and Lys48-linked Polyubiquitin Chains. *Genes to Cells* **2004**, *9* (10), 865–875. https://doi.org/10.1111/j.1365-2443.2004.00780.x.

(174) Peng, J.; Schwartz, D.; Elias, J. E.; Thoreen, C. C.; Cheng, D.; Marsischky, G.; Roelofs, J.; Finley, D.; Gygi, S. P. A Proteomics Approach to Understanding Protein Ubiquitination. *Nat. Biotechnol.* **2003**, *21* (8), 921–926. https://doi.org/10.1038/nbt849.

(175) Jin, L.; Williamson, A.; Banerjee, S.; Philipp, I.; Rape, M. Mechanism of Ubiquitin-Chain Formation by the Human Anaphase-Promoting Complex. *Cell* **2008**, *133* (4), 653–665. https://doi.org/10.1016/j.cell.2008.04.012.

(176) Mukhopadhyay, D.; Riezman, H. Proteasome-Independent Functions of Ubiquitin in Endocytosis and Signaling. *Science.* **2007**, *315* (5809), 201–205. https://doi.org/10.1126/science.1127085.

(177) Finley, D. Recognition and Processing of Ubiquitin-Protein Conjugates by the Proteasome. *Annu. Rev. Biochem.* **2009**, *78* (1), 477–513. https://doi.org/10.1146/annurev.biochem.78.081507.101607.

(178) Glickman, M. H.; Rubin, D. M.; Fried, V. A.; Finley, D. The Regulatory Particle of the Saccharomyces Cerevisiae Proteasome. *Mol. Cell. Biol.* **1998**, *18* (6), 3149–3162. https://doi.org/10.1128/MCB.18.6.3149.

(179) Voges, D.; Zwickl, P.; Baumeister, W. The 26S Proteasome: A Molecular Machine Designed for Controlled Proteolysis. *Annu. Rev. Biochem.* **1999**, *68* (1), 1015–1068. https://doi.org/10.1146/annurev.biochem.68.1.1015.

(180) Pickart, C. M.; Cohen, R. E. Proteasomes and Their Kin: Proteases in the Machine Age. *Nat. Rev. Mol. Cell Biol.* **2004**, *5* (3), 177–187. https://doi.org/10.1038/nrm1336.

(181) Heinemeyer, W.; Fischer, M.; Krimmer, T.; Stachon, U.; Wolf, D. H. The Active Sites of the Eukaryotic 20 S Proteasome and Their Involvement in Subunit Precursor Processing. *J. Biol. Chem.* **1997**, *272* (40), 25200–25209. https://doi.org/10.1074/jbc.272.40.25200.

(182) Groll, M.; Heinemeyer, W.; Jäger, S.; Ullrich, T.; Bochtler, M.; Wolf, D. H.; Huber, R. The Catalytic Sites of 20S Proteasomes and Their Role in Subunit Maturation: A Mutational and Crystallographic Study. *Proc. Natl. Acad. Sci.* **1999**, *96* (20), 10976–10983. https://doi.org/10.1073/pnas.96.20.10976.

(183) Kisselev, A. F.; Akopian, T. N.; Woo, K. M.; Goldberg, A. L. The Sizes of Peptides Generated from Protein by Mammalian 26 and 20 S Proteasomes. Implications for Understanding the Degradative Mechanism and Antigen Presentation. *J. Biol. Chem.* **1999**, *274* (6), 3363–3371. https://doi.org/10.1074/jbc.274.6.3363.

(184) Griffin, T. A.; Nandi, D.; Cruz, M.; Fehling, H. J.; Kaer, L. Van; Monaco, J. J.; Colbert, R. A. Immunoproteasome Assembly: Cooperative Incorporation of Interferon γ (IFN-γ)–Inducible Subunits. *J. Exp. Med.* **1998**, *187* (1), 97–104. https://doi.org/10.1084/jem.187.1.97.

(185) Murata, S.; Takahama, Y.; Kasahara, M.; Tanaka, K. The Immunoproteasome and Thymoproteasome: Functions, Evolution and Human Disease. *Nat. Immunol.* **2018**, *19* (9), 923–931. https://doi.org/10.1038/s41590-018-0186-z.

(186) Bard, J. A. M.; Goodall, E. A.; Greene, E. R.; Jonsson, E.; Dong, K. C.; Martin, A. Structure and Function of the 26S Proteasome. *Annu. Rev. Biochem.* **2018**, *87* (1), 697–724. https://doi.org/10.1146/annurev-biochem-062917-011931.

(187) Nandi, D.; Tahiliani, P.; Kumar, A.; Chandu, D. The Ubiquitin-Proteasome System. *J. Biosci.* **2006**, *31* (1), 137–155. https://doi.org/10.1007/BF02705243.

(188) Zheng, N.; Shabek, N. Ubiquitin Ligases: Structure, Function, and Regulation. *Annu. Rev. Biochem.* **2017**, *86* (1), 129–157. https://doi.org/10.1146/annurev-biochem-060815-014922.

(189) Smit, J. J.; Sixma, T. K. RBR E3-ligases at Work. *EMBO Rep.* **2014**, *15* (2), 142–154. https://doi.org/10.1002/embr.201338166.

(190) Zheng, N.; Wang, P.; Jeffrey, P. D.; Pavletich, N. P. Structure of a C-Cbl–UbcH7 Complex. *Cell* **2000**, *102* (4), 533–539. https://doi.org/10.1016/S0092-8674(00)00057-X.

(191) Christensen, D. E.; Brzovic, P. S.; Klevit, R. E. E2–BRCA1 RING Interactions Dictate Synthesis of Mono- or Specific Polyubiquitin Chain Linkages. *Nat. Struct. Mol. Biol.* **2007**, *14* (10), 941–948. https://doi.org/10.1038/nsmb1295.

(192) Wu, K.; Kovacev, J.; Pan, Z.-Q. Priming and Extending: A UbcH5/Cdc34 E2 Handoff

Mechanism for Polyubiquitination on a SCF Substrate. *Mol. Cell* **2010**, *37* (6), 784–796. https://doi.org/10.1016/j.molcel.2010.02.025.

(193) Brown, N. G.; VanderLinden, R.; Watson, E. R.; Weissmann, F.; Ordureau, A.; Wu, K.-P.; Zhang, W.; Yu, S.; Mercredi, P. Y.; Harrison, J. S.; Davidson, I. F.; Qiao, R.; Lu, Y.; Dube, P.; Brunner, M. R.; Grace, C. R. R.; Miller, D. J.; Haselbach, D.; Jarvis, M. A.; Yamaguchi, M.; Yanishevski, D.; Petzold, G.; Sidhu, S. S.; Kuhlman, B.; Kirschner, M. W.; Harper, J. W.; Peters, J.-M.; Stark, H.; Schulman, B. A. Dual RING E3 Architectures Regulate Multiubiquitination and Ubiquitin Chain Elongation by APC/C. *Cell* **2016**, *165* (6), 1440–1453. https://doi.org/10.1016/j.cell.2016.05.037.

(194) Deshaies, R. J.; Joazeiro, C. A. P. RING Domain E3 Ubiquitin Ligases. *Annu. Rev. Biochem.* **2009**, *78* (1), 399–434. https://doi.org/10.1146/annurev.biochem.78.101807.093809.

(195) Metzger, M. B.; Pruneda, J. N.; Klevit, R. E.; Weissman, A. M. RING-Type E3 Ligases: Master Manipulators of E2 Ubiquitin-Conjugating Enzymes and Ubiquitination. *Biochim. Biophys. Acta - Mol. Cell Res.* **2014**, *1843* (1), 47–60. https://doi.org/10.1016/j.bbamcr.2013.05.026.

(196) Duda, D. M.; Borg, L. A.; Scott, D. C.; Hunt, H. W.; Hammel, M.; Schulman, B. A. Structural Insights into NEDD8 Activation of Cullin-RING Ligases: Conformational Control of Conjugation. *Cell* **2008**, *134* (6), 995–1006. https://doi.org/10.1016/j.cell.2008.07.022.

(197) Lydeard, J. R.; Schulman, B. A.; Harper, J. W. Building and Remodelling Cullin-RING E3 Ubiquitin Ligases. *EMBO Rep.* **2013**, *14* (12), 1050–1061. https://doi.org/10.1038/embor.2013.173.

(198) Soucy, T. A.; Smith, P. G.; Milhollen, M. A.; Berger, A. J.; Gavin, J. M.; Adhikari, S.; Brownell, J. E.; Burke, K. E.; Cardin, D. P.; Critchley, S.; Cullis, C. A.; Doucette, A.; Garnsey, J. J.; Gaulin, J. L.; Gershman, R. E.; Lublinsky, A. R.; McDonald, A.; Mizutani, H.; Narayanan, U.; Olhava, E. J.; Peluso, S.; Rezaei, M.; Sintchak, M. D.; Talreja, T.; Thomas, M. P.; Traore, T.; Vyskocil, S.; Weatherhead, G. S.; Yu, J.; Zhang, J.; Dick, L. R.; Claiborne, C. F.; Rolfe, M.; Bolen, J. B.; Langston, S. P. An Inhibitor of NEDD8-Activating Enzyme as a New Approach to Treat Cancer. *Nature* **2009**, *458* (7239), 732–736. https://doi.org/10.1038/nature07884.

(199) Jaakkola, P.; Mole, D. R.; Tian, Y.-M.; Wilson, M. I.; Gielbert, J.; Gaskell, S. J.; Kriegsheim, A. von; Hebestreit, H. F.; Mukherji, M.; Schofield, C. J.; Maxwell, P. H.; Pugh, ‡ Christopher W.; Ratcliffe, ‡ Peter J. Targeting of HIF-α to the von Hippel-Lindau Ubiquitylation Complex by O2 -Regulated Prolyl Hydroxylation. *Science.* **2001**, *292* (5516), 468–472. https://doi.org/10.1126/science.1059796.

(200) Kamura, T.; Maenaka, K.; Kotoshiba, S.; Matsumoto, M.; Kohda, D.; Conaway, R. C.; Conaway, J. W.; Nakayama, K. I. VHL-Box and SOCS-Box Domains Determine Binding Specificity for Cul2-Rbx1 and Cul5-Rbx2 Modules of Ubiquitin Ligases. *Genes Dev.* **2004**, *18* (24), 3055–3065. https://doi.org/10.1101/gad.1252404.

(201) Cai, W.; Yang, H. The Structure and Regulation of Cullin 2 Based E3 Ubiquitin Ligases and Their Biological Functions. *Cell Div.* **2016**, *11* (1), 7. https://doi.org/10.1186/s13008-016-0020-7.

(202) Gilder, A. S.; Chen, Y. Bin; Jackson, R. J.; Jiang, J.; Maher, J. F. Fem1b Promotes Ubiquitylation and Suppresses Transcriptional Activity of Gli1. *Biochem. Biophys. Res. Commun.* **2013**, *440* (3), 431–436. https://doi.org/10.1016/j.bbrc.2013.09.090.

(203) Goodarzi, M. O.; Maher, J. F.; Cui, J.; Guo, X.; Taylor, K. D.; Azziz, R. FEM1A and FEM1B: Novel Candidate Genes for Polycystic Ovary Syndrome. *Hum. Reprod.* **2008**, *23* (12), 2842–2849. https://doi.org/10.1093/humrep/den324.

(204) Ito, T.; Ando, H.; Suzuki, T.; Ogura, T.; Hotta, K.; Imamura, Y.; Yamaguchi, Y.; Handa, H. Identification of a Primary Target of Thalidomide Teratogenicity. *Science.* **2010**, *327* (5971), 1345–1350. https://doi.org/10.1126/science.1177319.

(205) Ichikawa, S.; Flaxman, H. A.; Xu, W.; Vallavoju, N.; Lloyd, H. C.; Wang, B.; Shen, D.; Pratt, M. R.; Woo, C. M. The E3 Ligase Adapter Cereblon Targets the C-Terminal Cyclic Imide Degron. *Nature.* **2022**, *610*, 775–782. https://doi.org/10.1038/s41586-022-05333-5.

(206) Miao, Q.; Kadam, V. D.; Mukherjee, A.; Tan, Z.; Teng, M. Unlocking DCAFs To Catalyze Degrader Development: An Arena for Innovative Approaches. *J. Med. Chem.* **2023**, *66* (19), 13369–13383. https://doi.org/10.1021/acs.jmedchem.3c01209.

(207) Thul, P. J.; Åkesson, L.; Wiking, M.; Mahdessian, D.; Geladaki, A.; Ait Blal, H.; Alm, T.; Asplund, A.; Björk, L.; Breckels, L. M.; Bäckström, A.; Danielsson, F.; Fagerberg, L.; Fall, J.; Gatto, L.; Gnann, C.; Hober, S.; Hjelmare, M.; Johansson, F.; Lee, S.; Lindskog, C.; Mulder, J.; Mulvey, C. M.; Nilsson, P.; Oksvold, P.; Rockberg, J.; Schutten, R.; Schwenk, J. M.; Sivertsson, Å.; Sjöstedt, E.; Skogs, M.; Stadler, C.; Sullivan, D. P.; Tegel, H.; Winsnes, C.; Zhang, C.; Zwahlen, M.; Mardinoglu, A.; Pontén, F.; von Feilitzen, K.; Lilley, K. S.; Uhlén, M.; Lundberg, E. A Subcellular Map of the Human Proteome. *Science.* **2017**, *356* (6340), eaal3321. https://doi.org/10.1126/science.aal3321.

(208) Hu, S.; Yang, X. Cellular Inhibitor of Apoptosis 1 and 2 Are Ubiquitin Ligases for the

Apoptosis Inducer Smac/DIABLO. *J. Biol. Chem.* **2003**, *278* (12), 10055–10060. https://doi.org/10.1074/jbc.M207197200.

(209) Fulda, S.; Vucic, D. Targeting IAP Proteins for Therapeutic Intervention in Cancer. *Nat. Rev. Drug Discov.* **2012**, *11* (2), 109–124. https://doi.org/10.1038/nrd3627.

(210) Huang, Y.; Park, Y. C.; Rich, R. L.; Segal, D.; Myszka, D. G.; Wu, H. Structural Basis of Caspase Inhibition by XIAP. *Cell* **2001**, *104* (5), 781–790. https://doi.org/10.1016/S0092-8674(01)00273-2.

(211) Eckelman, B. P.; Salvesen, G. S.; Scott, F. L. Human Inhibitor of Apoptosis Proteins: Why XIAP Is the Black Sheep of the Family. *EMBO Rep.* **2006**, *7* (10), 988–994. https://doi.org/10.1038/sj.embor.7400795.

(212) Rothe, M.; Pan, M.; Henzel, W. J.; Ayres, T. M.; V. Goeddel, D. The TNFR2-TRAF Signaling Complex Contains Two Novel Proteins Related to Baculoviral Inhibitor of Apoptosis Proteins. *Cell* **1995**, *83* (7), 1243–1252. https://doi.org/10.1016/0092-8674(95)90149-3.

(213) Choi, Y. E.; Butterworth, M.; Malladi, S.; Duckett, C. S.; Cohen, G. M.; Bratton, S. B. The E3 Ubiquitin Ligase CIAP1 Binds and Ubiquitinates Caspase-3 and -7 via Unique Mechanisms at Distinct Steps in Their Processing. *J. Biol. Chem.* **2009**, *284* (19), 12772–12782. https://doi.org/10.1074/jbc.M807550200.

(214) Yang, Y.; Fang, S.; Jensen, J. P.; Weissman, A. M.; Ashwell, J. D. Ubiquitin Protein Ligase Activity of IAPs and Their Degradation in Proteasomes in Response to Apoptotic Stimuli. *Science.* **2000**, *288* (5467), 874–877. https://doi.org/10.1126/science.288.5467.874.

(215) Sekine, K.; Takubo, K.; Kikuchi, R.; Nishimoto, M.; Kitagawa, M.; Abe, F.; Nishikawa, K.; Tsuruo, T.; Naito, M. Small Molecules Destabilize CIAP1 by Activating Auto-Ubiquitylation. *J. Biol. Chem.* **2008**, *283* (14), 8961–8968. https://doi.org/10.1074/jbc.M709525200.

(216) Wu, X.; Bayle, J. H.; Olson, D.; Levine, A. J. The P53-Mdm-2 Autoregulatory Feedback Loop. *Genes Dev.* **1993**, *7* (7a), 1126–1132. https://doi.org/10.1101/gad.7.7a.1126.

(217) Michael, D.; Oren, M. The P53–Mdm2 Module and the Ubiquitin System. *Semin. Cancer Biol.* **2003**, *13* (1), 49–58. https://doi.org/10.1016/S1044-579X(02)00099-8.

(218) Craig, A. L.; Burch, L.; Vojtesek, B.; Mikutowska, J.; Thompson, A.; Hupp, T. R. Novel Phosphorylation Sites of Human Tumour Suppressor Protein P53 at Ser20 and Thr18 That Disrupt the Binding of Mdm2 (Mouse Double Minute 2) Protein Are Modified in Human Cancers. *Biochem. J.* **1999**, *342* (1), 133. https://doi.org/10.1042/0264-6021:3420133.

(219) Fang, S.; Jensen, J. P.; Ludwig, R. L.; Vousden, K. H.; Weissman, A. M. Mdm2 Is a RING Finger-Dependent Ubiquitin Protein Ligase for Itself and P53. *J. Biol. Chem.* **2000**, *275* (12), 8945–8951. https://doi.org/10.1074/jbc.275.12.8945.

(220) Momand, J.; Jung, D.; Wilczynski, S.; Niland, J. The MDM2 Gene Amplification Database. *Nucleic Acids Res.* **1998**, *26* (15), 3453–3459. https://doi.org/10.1093/nar/26.15.3453.

(221) Vassilev, L. T.; Vu, B. T.; Graves, B.; Carvajal, D.; Podlaski, F.; Filipovic, Z.; Kong, N.; Kammlott, U.; Lukacs, C.; Klein, C.; Fotouhi, N.; Liu, E. A. In Vivo Activation of the P53 Pathway by Small-Molecule Antagonists of MDM2. *Science.* **2004**, *303* (5659), 844–848. https://doi.org/10.1126/science.1092472.

(222) Li, K.; Crews, C. M. PROTACs: Past, Present and Future. *Chem. Soc. Rev.* **2022**, *51* (12), 5214–5236. https://doi.org/10.1039/D2CS00193D.

(223) Bondeson, D. P.; Mares, A.; Smith, I. E. D.; Ko, E.; Campos, S.; Miah, A. H.; Mulholland, K. E.; Routly, N.; Buckley, D. L.; Gustafson, J. L.; Zinn, N.; Grandi, P.; Shimamura, S.; Bergamini, G.; Faelth-Savitski, M.; Bantscheff, M.; Cox, C.; Gordon, D. A.; Willard, R. R.; Flanagan, J. J.; Casillas, L. N.; Votta, B. J.; Den Besten, W.; Famm, K.; Kruidenier, L.; Carter, P. S.; Harling, J. D.; Churcher, I.; Crews, C. M. Catalytic in Vivo Protein Knockdown by Small-Molecule PROTACs. *Nat. Chem. Biol.* **2015**, *11* (8), 611–617. https://doi.org/10.1038/nchembio.1858.

(224) Hughes, S. J.; Testa, A.; Thompson, N.; Churcher, I. The Rise and Rise of Protein Degradation: Opportunities and Challenges Ahead. *Drug Discov. Today* **2021**, *26* (12), 2889–2897. https://doi.org/10.1016/j.drudis.2021.08.006.

(225) Krone, M. W.; Crews, C. M. Next Steps for Targeted Protein Degradation. *Cell Chem. Biol.* **2025**, *32* (2), 219–226. https://doi.org/10.1016/j.chembiol.2024.10.004.

(226) Salami, J.; Alabi, S.; Willard, R. R.; Vitale, N. J.; Wang, J.; Dong, H.; Jin, M.; McDonnell, D. P.; Crew, A. P.; Neklesa, T. K.; Crews, C. M. Androgen Receptor Degradation by the Proteolysis-Targeting Chimera ARCC-4 Outperforms Enzalutamide in Cellular Models of Prostate Cancer Drug Resistance. *Commun. Biol.* **2018**, *1* (1), 1–9. https://doi.org/10.1038/s42003-018-0105-8.

(227) Buhimschi, A. D.; Armstrong, H. A.; Toure, M.; Jaime-Figueroa, S.; Chen, T. L.; Lehman, A. M.; Woyach, J. A.; Johnson, A. J.; Byrd, J. C.; Crews, C. M. Targeting the C481S Ibrutinib-Resistance Mutation in Bruton's Tyrosine Kinase Using PROTAC-Mediated Degradation.

Biochemistry **2018**, *57* (26), 3564–3575. https://doi.org/10.1021/acs.biochem.8b00391.

(228) Gadd, M. S.; Testa, A.; Lucas, X.; Chan, K.-H.; Chen, W.; Lamont, D. J.; Zengerle, M.; Ciulli, A. Structural Basis of PROTAC Cooperative Recognition for Selective Protein Degradation. *Nat. Chem. Biol.* **2017**, *13* (5), 514–521. https://doi.org/10.1038/nchembio.2329.

(229) Alabi, S.; Jaime-Figueroa, S.; Yao, Z.; Gao, Y.; Hines, J.; Samarasinghe, K. T. G.; Vogt, L.; Rosen, N.; Crews, C. M. Mutant-Selective Degradation by BRAF-Targeting PROTACs. *Nat. Commun.* **2021**, *12* (1), 920. https://doi.org/10.1038/s41467-021-21159-7.

(230) Zorba, A.; Nguyen, C.; Xu, Y.; Starr, J.; Borzilleri, K.; Smith, J.; Zhu, H.; Farley, K. A.; Ding, W. D.; Schiemer, J.; Feng, X.; Chang, J. S.; Uccello, D. P.; Young, J. A.; Garcia-Irrizary, C. N.; Czabaniuk, L.; Schuff, B.; Oliver, R.; Montgomery, J.; Hayward, M. M.; Coe, J.; Chen, J.; Niosi, M.; Luthra, S.; Shah, J. C.; El-Kattan, A.; Qiu, X.; West, G. M.; Noe, M. C.; Shanmugasundaram, V.; Gilbert, A. M.; Brown, M. F.; Calabrese, M. F. Delineating the Role of Cooperativity in the Design of Potent PROTACs for BTK. *Proc. Natl. Acad. Sci. U. S. A.* **2018**, *115* (31), E7285–E7292. https://doi.org/10.1073/pnas.1803662115.

(231) Crowe, C.; Nakasone, M. A.; Chandler, S.; Craigon, C.; Sathe, G.; Tatham, M. H.; Makukhin, N.; Hay, R. T.; Ciulli, A. Mechanism of Degrader-Targeted Protein Ubiquitinability. *Sci. Adv.* **2024**, *10* (41), 2024.02.05.578957. https://doi.org/10.1126/sciadv.ado6492.

(232) Baek, K.; Krist, D. T.; Prabu, J. R.; Hill, S.; Klügel, M.; Neumaier, L. M.; von Gronau, S.; Kleiger, G.; Schulman, B. A. NEDD8 Nucleates a Multivalent Cullin–RING–UBE2D Ubiquitin Ligation Assembly. *Nature* **2020**, *578* (7795), 461–466. https://doi.org/10.1038/s41586-020-2000-y.

(233) Gray, W. M.; Kepinski, S.; Rouse, D.; Leyser, O.; Estelle, M. Auxin Regulates SCFTIR1-Dependent Degradation of AUX/IAA Proteins. *Nature* **2001**, *414* (6861), 271–276. https://doi.org/10.1038/35104500.

(234) Tan, X.; Calderon-Villalobos, L. I. A.; Sharon, M.; Zheng, C.; Robinson, C. V.; Estelle, M.; Zheng, N. Mechanism of Auxin Perception by the TIR1 Ubiquitin Ligase. *Nature* **2007**, *446* (7136), 640–645. https://doi.org/10.1038/nature05731.

(235) Lou, Z.; Wang, S. E3 Ubiquitin Ligases and Human Papillomavirus-Induced Carcinogenesis. *J. Int. Med. Res.* **2014**, *42* (2), 247–260. https://doi.org/10.1177/0300060513506655.

(236) Schreiber, S. L. Immunophilin-Sensitive Protein Phosphatase Action in Cell Signaling Pathways. *Cell* **1992**, *70* (3), 365–368. https://doi.org/10.1016/0092-8674(92)90158-9.

(237) Cao, S.; Kang, S.; Mao, H.; Yao, J.; Gu, L.; Zheng, N. Defining Molecular Glues with a Dual-Nanobody Cannabidiol Sensor. *Nat. Commun.* **2022**, *13* (1), 815. https://doi.org/10.1038/s41467-022-28507-1.

(238) Miller, M. T.; Strömland, K. Teratogen Update: Thalidomide: A Review, with a Focus on Ocular Findings and New Potential Uses. *Teratology* **1999**, *60* (5), 306–321. https://doi.org/10.1002/(SICI)1096-9926(199911)60:5<306::AID-TERA11>3.0.CO;2-Y.

(239) Blaschke, G.; Kraft, H. P.; Fickentscher, K.; Köhler, F. [Chromatographic separation of racemic thalidomide and teratogenic activity of its enantiomers (author's transl)]. *Arzneimittelforschung.* **1979**, *29* (10), 1640–1642.

(240) Eriksson, T.; Björkman, S.; Roth, B.; Fyge, Å.; Höuglund, P. Stereospecific Determination, Chiral Inversion in Vitro and Pharmacokinetics in Humans of the Enantiomers of Thalidomide. *Chirality* **1995**, *7* (1), 44–52. https://doi.org/10.1002/chir.530070109.

(241) Bartlett, J. B.; Dredge, K.; Dalgleish, A. G. The Evolution of Thalidomide and Its IMiD Derivatives as Anticancer Agents. *Nat. Rev. Cancer* **2004**, *4* (4), 314–322. https://doi.org/10.1038/nrc1323.

(242) Krönke, J.; Udeshi, N. D.; Narla, A.; Grauman, P.; Hurst, S. N.; McConkey, M.; Svinkina, T.; Heckl, D.; Comer, E.; Li, X.; Ciarlo, C.; Hartman, E.; Munshi, N.; Schenone, M.; Schreiber, S. L.; Carr, S. A.; Ebert, B. L. Lenalidomide Causes Selective Degradation of IKZF1 and IKZF3 in Multiple Myeloma Cells. *Science.* **2014**, *343* (6168), 301–305. https://doi.org/10.1126/science.1244851.

(243) Krönke, J.; Fink, E. C.; Hollenbach, P. W.; MacBeth, K. J.; Hurst, S. N.; Udeshi, N. D.; Chamberlain, P. P.; Mani, D. R.; Man, H. W.; Gandhi, A. K.; Svinkina, T.; Schneider, R. K.; McConkey, M.; Järås, M.; Griffiths, E.; Wetzler, M.; Bullinger, L.; Cathers, B. E.; Carr, S. A.; Chopra, R.; Ebert, B. L. Lenalidomide Induces Ubiquitination and Degradation of CK1α in Del(5q) MDS. *Nature* **2015**, *523* (7559), 183–188. https://doi.org/10.1038/nature14610.

(244) Matyskiela, M. E.; Lu, G.; Ito, T.; Pagarigan, B.; Lu, C. C.; Miller, K.; Fang, W.; Wang, N. Y.; Nguyen, D.; Houston, J.; Carmel, G.; Tran, T.; Riley, M.; Nosaka, L.; Lander, G. C.; Gaidarova, S.; Xu, S.; Ruchelman, A. L.; Handa, H.; Carmichael, J.; Daniel, T. O.; Cathers, B. E.; Lopez-Girona, A.; Chamberlain, P. P. A Novel Cereblon Modulator Recruits GSPT1 to the CRL4 CRBN Ubiquitin Ligase. *Nature* **2016**, *535* (7611), 252–257. https://doi.org/10.1038/nature18611.

(245) Donovan, K. A.; An, J.; Nowak, R. P.; Yuan, J. C.; Fink, E. C.; Berry, B. C.; Ebert, B. L.; Fischer, E. S. Thalidomide Promotes Degradation of SALL4, a Transcription Factor Implicated in Duane Radial Ray Syndrome. *Elife* **2018**, *7*, 1–25. https://doi.org/10.7554/eLife.38430.

(246) Han, T.; Goralski, M.; Gaskill, N.; Capota, E.; Kim, J.; Ting, T. C.; Xie, Y.; Williams, N. S.; Nijhawan, D. Anticancer Sulfonamides Target Splicing by Inducing RBM39 Degradation via Recruitment to DCAF15. *Science.* **2017**, *356* (6336), eaal3755. https://doi.org/10.1126/science.aal3755.

(247) Domostegui, A.; Nieto-Barrado, L.; Perez-Lopez, C.; Mayor-Ruiz, C. Chasing Molecular Glue Degraders: Screening Approaches. *Chem. Soc. Rev.* **2022**, *51* (13), 5498–5517. https://doi.org/10.1039/d2cs00197g.

(248) Słabicki, M.; Kozicka, Z.; Petzold, G.; Li, Y.-D.; Manojkumar, M.; Bunker, R. D.; Donovan, K. A.; Sievers, Q. L.; Koeppel, J.; Suchyta, D.; Sperling, A. S.; Fink, E. C.; Gasser, J. A.; Wang, L. R.; Corsello, S. M.; Sellar, R. S.; Jan, M.; Gillingham, D.; Scholl, C.; Fröhling, S.; Golub, T. R.; Fischer, E. S.; Thomä, N. H.; Ebert, B. L. The CDK Inhibitor CR8 Acts as a Molecular Glue Degrader That Depletes Cyclin K. *Nature* **2020**, *585* (7824), 293–297. https://doi.org/10.1038/s41586-020-2374-x.

(249) Mayor-Ruiz, C.; Bauer, S.; Brand, M.; Kozicka, Z.; Siklos, M.; Imrichova, H.; Kaltheuner, I. H.; Hahn, E.; Seiler, K.; Koren, A.; Petzold, G.; Fellner, M.; Bock, C.; Müller, A. C.; Zuber, J.; Geyer, M.; Thomä, N. H.; Kubicek, S.; Winter, G. E. Rational Discovery of Molecular Glue Degraders via Scalable Chemical Profiling. *Nat. Chem. Biol.* **2020**, *16* (11), 1199–1207. https://doi.org/10.1038/s41589-020-0594-x.

(250) Toriki, E. S.; Papatzimas, J. W.; Nishikawa, K.; Dovala, D.; Frank, A. O.; Hesse, M. J.; Dankova, D.; Song, J.-G.; Bruce-Smythe, M.; Struble, H.; Garcia, F. J.; Brittain, S. M.; Kile, A. C.; McGregor, L. M.; McKenna, J. M.; Tallarico, J. A.; Schirle, M.; Nomura, D. K. Rational Chemical Design of Molecular Glue Degraders. *ACS Cent. Sci.* **2023**, *9* (5), 915–926. https://doi.org/10.1021/acscentsci.2c01317.

(251) Lim, M.; Cong, T. Do; Orr, L. M.; Toriki, E. S.; Kile, A. C.; Papatzimas, J. W.; Lee, E.; Lin, Y.; Nomura, D. K. DCAF16-Based Covalent Handle for the Rational Design of Monovalent Degraders. *ACS Cent. Sci.* **2024**, *10* (7), 1318–1331. https://doi.org/10.1021/acscentsci.4c00286.

(252) Takahashi, D.; Moriyama, J.; Nakamura, T.; Miki, E.; Takahashi, E.; Sato, A.; Akaike, T.; Itto-Nakama, K.; Arimoto, H. AUTACs: Cargo-Specific Degraders Using Selective Autophagy.

Mol. Cell **2019**, *76* (5), 797-810.e10. https://doi.org/10.1016/j.molcel.2019.09.009.

(253) Ji, C. H.; Kim, H. Y.; Lee, M. J.; Heo, A. J.; Park, D. Y.; Lim, S.; Shin, S.; Yang, W. S.; Jung, C. A.; Kim, K. Y.; Jeong, E. H.; Park, S. H.; Bin Kim, S.; Lee, S. J.; Na, J. E.; Kang, J. I.; Chi, H. M.; Kim, H. T.; Kim, Y. K.; Kim, B. Y.; Kwon, Y. T. The AUTOTAC Chemical Biology Platform for Targeted Protein Degradation via the Autophagy-Lysosome System. *Nat. Commun.* **2022**, *13* (1), 1–14. https://doi.org/10.1038/s41467-022-28520-4.

(254) Li, Z.; Wang, C.; Wang, Z.; Zhu, C.; Li, J.; Sha, T.; Ma, L.; Gao, C.; Yang, Y.; Sun, Y.; Wang, J.; Sun, X.; Lu, C.; Difiglia, M.; Mei, Y.; Ding, C.; Luo, S.; Dang, Y.; Ding, Y.; Fei, Y.; Lu, B. Allele-Selective Lowering of Mutant HTT Protein by HTT–LC3 Linker Compounds. *Nature* **2019**, *575* (7781), 203–209. https://doi.org/10.1038/s41586-019-1722-1.

(255) Pei, J.; Pan, X.; Wang, A.; Shuai, W.; Bu, F.; Tang, P.; Zhang, S.; Zhang, Y.; Wang, G.; Ouyang, L. Developing Potent LC3-Targeting AUTAC Tools for Protein Degradation with Selective Autophagy. *Chem. Commun.* **2021**, *57* (97), 13194–13197. https://doi.org/10.1039/d1cc04661f.

(256) Ding, Y.; Xing, D.; Fei, Y.; Luo, S.; Lu, B. Perspectives of Autophagy-Tethering Compounds (ATTECs) in Drug Discovery. *Med. Plus* **2024**, *1* (1), 100004. https://doi.org/10.1016/j.medp.2023.100004.

(257) Banik, S. M.; Pedram, K.; Wisnovsky, S.; Ahn, G.; Riley, N. M.; Bertozzi, C. R. Lysosome-Targeting Chimaeras for Degradation of Extracellular Proteins. *Nature* **2020**, *584* (7820), 291–297. https://doi.org/10.1038/s41586-020-2545-9.

(258) Cotton, A. D.; Nguyen, D. P.; Gramespacher, J. A.; Seiple, I. B.; Wells, J. A. Development of Antibody-Based PROTACs for the Degradation of the Cell-Surface Immune Checkpoint Protein PD-L1. *J. Am. Chem. Soc.* **2021**, *143* (2), 593–598. https://doi.org/10.1021/jacs.0c10008.

(259) Ge, J.; Li, S.; Weng, G.; Wang, H.; Fang, M.; Sun, H.; Deng, Y.; Hsieh, C.-Y.; Li, D.; Hou, T. PROTAC-DB 3.0: An Updated Database of PROTACs with Extended Pharmacokinetic Parameters. *Nucleic Acids Res.* **2025**, *53* (D1), D1510–D1515. https://doi.org/10.1093/nar/gkae768.

(260) Bond, M. J.; Crews, C. M. Proteolysis Targeting Chimeras (PROTACs) Come of Age: Entering the Third Decade of Targeted Protein Degradation. *RSC Chem. Biol.* **2021**, *2* (3), 725–742. https://doi.org/10.1039/d1cb00011j.

(261) Sakamoto, K. M.; Kim, K. B.; Kumagai, A.; Mercurio, F.; Crews, C. M.; Deshaies, R. J. Protacs: Chimeric Molecules That Target Proteins to the Skp1-Cullin-F Box Complex for Ubiquitination and Degradation. *Proc. Natl. Acad. Sci. U. S. A.* **2001**, *98* (15), 8554–8559. https://doi.org/10.1073/pnas.141230798.

(262) Yaron, A.; Hatzubai, A.; Davis, M.; Lavon, I.; Amit, S.; Manning, A. M.; Andersen, J. S.; Mann, M.; Mercurio, F.; Ben-Neriah, Y. Identification of the Receptor Component of the IκBα–Ubiquitin Ligase. *Nature* **1998**, *396* (6711), 590–594. https://doi.org/10.1038/25159.

(263) Schneekloth, J. S.; Fonseca, F. N.; Koldobskiy, M.; Mandal, A.; Deshaies, R.; Sakamoto, K.; Crews, C. M. Chemical Genetic Control of Protein Levels: Selective in Vivo Targeted Degradation. *J. Am. Chem. Soc.* **2004**, *126* (12), 3748–3754. https://doi.org/10.1021/ja039025z.

(264) Schneekloth, A. R.; Pucheault, M.; Tae, H. S.; Crews, C. M. Targeted Intracellular Protein Degradation Induced by a Small Molecule: En Route to Chemical Proteomics. *Bioorg. Med. Chem. Lett.* **2008**, *18* (22), 5904–5908. https://doi.org/10.1016/j.bmcl.2008.07.114.

(265) Itoh, Y.; Ishikawa, M.; Naito, M.; Hashimoto, Y. Protein Knockdown Using Methyl Bestatin−Ligand Hybrid Molecules: Design and Synthesis of Inducers of Ubiquitination-Mediated Degradation of Cellular Retinoic Acid-Binding Proteins. *J. Am. Chem. Soc.* **2010**, *132* (16), 5820–5826. https://doi.org/10.1021/ja100691p.

(266) Anifowose, A.; Agbowuro, A. A.; Yang, X.; Wang, B. Anticancer Strategies by Upregulating P53 through Inhibition of Its Ubiquitination by MDM2. *Med. Chem. Res.* **2020**, *29* (7), 1105–1121. https://doi.org/10.1007/s00044-020-02574-9.

(267) Wang, C.; Zhang, Y.; Shi, L.; Yang, S.; Chang, J.; Zhong, Y.; Li, Q.; Xing, D. Recent Advances in IAP-Based PROTACs (SNIPERs) as Potential Therapeutic Agents. *J. Enzyme Inhib. Med. Chem.* **2022**, *37* (1), 1437–1453. https://doi.org/10.1080/14756366.2022.2074414.

(268) Okuhira, K.; Demizu, Y.; Hattori, T.; Ohoka, N.; Shibata, N.; Nishimaki-Mogami, T.; Okuda, H.; Kurihara, M.; Naito, M. Development of Hybrid Small Molecules That Induce Degradation of Estrogen Receptor-alpha and Necrotic Cell Death in Breast Cancer Cells. *Cancer Sci.* **2013**, *104* (11), 1492–1498. https://doi.org/10.1111/cas.12272.

(269) Buckley, D. L.; Van Molle, I.; Gareiss, P. C.; Tae, H. S.; Michel, J.; Noblin, D. J.; Jorgensen, W. L.; Ciulli, A.; Crews, C. M. Targeting the von Hippel–Lindau E3 Ubiquitin Ligase Using Small Molecules To Disrupt the VHL/HIF-1α Interaction. *J. Am. Chem. Soc.* **2012**, *134* (10), 4465–

4468. https://doi.org/10.1021/ja209924v.

(270) Galdeano, C.; Gadd, M. S.; Soares, P.; Scaffidi, S.; Van Molle, I.; Birced, I.; Hewitt, S.; Dias, D. M.; Ciulli, A. Structure-Guided Design and Optimization of Small Molecules Targeting the Protein–Protein Interaction between the von Hippel–Lindau (VHL) E3 Ubiquitin Ligase and the Hypoxia Inducible Factor (HIF) Alpha Subunit with in Vitro Nanomolar Affinities. *J. Med. Chem.* **2014**, *57* (20), 8657–8663. https://doi.org/10.1021/jm5011258.

(271) Buckley, D. L.; Raina, K.; Darricarrere, N.; Hines, J.; Gustafson, J. L.; Smith, I. E.; Miah, A. H.; Harling, J. D.; Crews, C. M. HaloPROTACS: Use of Small Molecule PROTACs to Induce Degradation of HaloTag Fusion Proteins. *ACS Chem. Biol.* **2015**, *10* (8), 1831–1837. https://doi.org/10.1021/acschembio.5b00442.

(272) Los, G. V; Encell, L. P.; McDougall, M. G.; Hartzell, D. D.; Karassina, N.; Zimprich, C.; Wood, M. G.; Learish, R.; Ohana, R. F.; Urh, M.; Simpson, D.; Mendez, J.; Zimmerman, K.; Otto, P.; Vidugiris, G.; Zhu, J.; Darzins, A.; Klaubert, D. H.; Bulleit, R. F.; Wood, K. V. HaloTag: A Novel Protein Labeling Technology for Cell Imaging and Protein Analysis. *ACS Chem. Biol.* **2008**, *3* (6), 373–382. https://doi.org/10.1021/cb800025k.

(273) Zengerle, M.; Chan, K.-H.; Ciulli, A. Selective Small Molecule Induced Degradation of the BET Bromodomain Protein BRD4. *ACS Chem. Biol.* **2015**, *10* (8), 1770–1777. https://doi.org/10.1021/acschembio.5b00216.

(274) Winter, G. E.; Buckley, D. L.; Paulk, J.; Roberts, J. M.; Souza, A.; Dhe-Paganon, S.; Bradner, J. E. Phthalimide Conjugation as a Strategy for in Vivo Target Protein Degradation. *Science.* **2015**, *348* (6241), 1376–1381. https://doi.org/10.1126/science.aab1433.

(275) Lu, J.; Qian, Y.; Altieri, M.; Dong, H.; Wang, J.; Raina, K.; Hines, J.; Winkler, J. D.; Crew, A. P.; Coleman, K.; Crews, C. M. Hijacking the E3 Ubiquitin Ligase Cereblon to Efficiently Target BRD4. *Chem. Biol.* **2015**, *22* (6), 755–763. https://doi.org/10.1016/j.chembiol.2015.05.009.

(276) Troup, R. I.; Fallan, C.; Baud, M. G. J. Current Strategies for the Design of PROTAC Linkers: A Critical Review. *Explor. Target. Anti-tumor Ther.* **2020**, *1* (5), 273–312. https://doi.org/10.37349/etat.2020.00018.

(277) Qin, C.; Hu, Y.; Zhou, B.; Fernandez-Salas, E.; Yang, C. Y.; Liu, L.; McEachern, D.; Przybranowski, S.; Wang, M.; Stuckey, J.; Meagher, J.; Bai, L.; Chen, Z.; Lin, M.; Yang, J.; Ziazadeh, D. N.; Xu, F.; Hu, J.; Xiang, W.; Huang, L.; Li, S.; Wen, B.; Sun, D.; Wang, S. Discovery of QCA570 as an Exceptionally Potent and Efficacious Proteolysis Targeting

Chimera (PROTAC) Degrader of the Bromodomain and Extra-Terminal (BET) Proteins Capable of Inducing Complete and Durable Tumor Regression. *J. Med. Chem.* **2018**, *61* (15), 6685–6704. https://doi.org/10.1021/acs.jmedchem.8b00506.

(278) Nowak, R. P.; Deangelo, S. L.; Buckley, D.; He, Z.; Donovan, K. A.; An, J.; Safaee, N.; Jedrychowski, M. P.; Ponthier, C. M.; Ishoey, M.; Zhang, T.; Mancias, J. D.; Gray, N. S.; Bradner, J. E.; Fischer, E. S. Plasticity in Binding Confers Selectivity in Ligand-Induced Protein Degradation Article. *Nat. Chem. Biol.* **2018**, *14* (7), 706–714. https://doi.org/10.1038/s41589-018-0055-y.

(279) Gleeson, M. P. Generation of a Set of Simple, Interpretable ADMET Rules of Thumb. *J. Med. Chem.* **2008**, *51* (4), 817–834. https://doi.org/10.1021/jm701122q.

(280) Dong, Y.; Ma, T.; Xu, T.; Feng, Z.; Li, Y.; Song, L.; Yao, X.; Ashby, C. R.; Hao, G. F. Characteristic Roadmap of Linker Governs the Rational Design of PROTACs. *Acta Pharm. Sin. B* **2024**, *14* (10), 4266–4295. https://doi.org/10.1016/j.apsb.2024.04.007.

(281) Takwale, A. D.; Jo, S.-H.; Jeon, Y. U.; Kim, H. S.; Shin, C. H.; Lee, H. K.; Ahn, S.; Lee, C. O.; Du Ha, J.; Kim, J.-H.; Hwang, J. Y. Design and Characterization of Cereblon-Mediated Androgen Receptor Proteolysis-Targeting Chimeras. *Eur. J. Med. Chem.* **2020**, *208*, 112769. https://doi.org/10.1016/j.ejmech.2020.112769.

(282) Snyder, L. B.; Neklesa, T. K.; Willard, R. R.; Gordon, D. A.; Pizzano, J.; Vitale, N.; Robling, K.; Dorso, M. A.; Moghrabi, W.; Landrette, S.; Gedrich, R.; Lee, S. H.; Taylor, I. C. A.; Houston, J. G. Preclinical Evaluation of Bavdegalutamide (ARV-110), a Novel PROteolysis TArgeting Chimera Androgen Receptor Degrader. *Mol. Cancer Ther.* **2025**, *24* (4), 511–522. https://doi.org/10.1158/1535-7163.MCT-23-0655.

(283) Ma, Z.; Zhou, J. NDA Submission of Vepdegestrant (ARV-471) to U.S. FDA: The Beginning of a New Era of PROTAC Degraders. *J. Med. Chem.* **2025**, *68* (14), 14129–14136. https://doi.org/10.1021/acs.jmedchem.5c01818.

(284) Hamilton, E. P.; Ma, C.; De Laurentiis, M.; Iwata, H.; Hurvitz, S. A.; Wander, S. A.; Danso, M.; Lu, D. R.; Perkins Smith, J.; Liu, Y.; Tran, L.; Anderson, S.; Campone, M. VERITAC-2: A Phase III Study of Vepdegestrant, a PROTAC ER Degrader, versus Fulvestrant in ER+/HER2- Advanced Breast Cancer. *Futur. Oncol.* **2024**, *20* (32), 2447–2455. https://doi.org/10.1080/14796694.2024.2377530.

(285) Hinterndorfer, M.; Spiteri, V. A.; Ciulli, A.; Winter, G. E. Targeted Protein Degradation for

Cancer Therapy. *Nat. Rev. Cancer* **2025**, *21* (10), 638–654. https://doi.org/10.1038/s41568-025-00817-8.

(286) Hong, K. B.; An, H. Degrader–Antibody Conjugates: Emerging New Modality. *J. Med. Chem.* **2023**, *66* (1), 140–148. https://doi.org/10.1021/acs.jmedchem.2c01791.

(287) Reynders, M.; Matsuura, B. S.; Bérouti, M.; Simoneschi, D.; Marzio, A.; Pagano, M.; Trauner, D. PHOTACs Enable Optical Control of Protein Degradation. *Sci. Adv.* **2020**, *6* (8), 315–329. https://doi.org/10.1126/sciadv.aay5064.

(288) Lebraud, H.; Wright, D. J.; Johnson, C. N.; Heightman, T. D. Protein Degradation by In-Cell Self-Assembly of Proteolysis Targeting Chimeras. *ACS Cent. Sci.* **2016**, *2* (12), 927–934. https://doi.org/10.1021/acscentsci.6b00280.

(289) Edmondson, S. D.; Yang, B.; Fallan, C. Proteolysis Targeting Chimeras (PROTACs) in 'beyond Rule-of-Five' Chemical Space: Recent Progress and Future Challenges. *Bioorg. Med. Chem. Lett.* **2019**, *29* (13), 1555–1564. https://doi.org/10.1016/j.bmcl.2019.04.030.

(290) Neklesa, T. K.; Crews, C. M. Greasy Tags for Protein Removal. *Nature* **2012**, *487* (7407), 308–309. https://doi.org/10.1038/487308a.

(291) Agashe, V. R.; Shastry, M. C. R.; Udgaonkar, J. B. Initial Hydrophobic Collapse in the Folding of Barstar. *Nature* **1995**, *377* (6551), 754–757. https://doi.org/10.1038/377754a0.

(292) Blond-Elguindi, S.; Cwirla, S. E.; Dower, W. J.; Lipshutz, R. J.; Sprang, S. R.; Sambrook, J. F.; Gething, M. J. H. Affinity Panning of a Library of Peptides Displayed on Bacteriophages Reveals the Binding Specificity of BiP. *Cell* **1993**, *75* (4), 717–728. https://doi.org/10.1016/0092-8674(93)90492-9.

(293) Kubota, H. Quality Control Against Misfolded Proteins in the Cytosol: A Network for Cell Survival. *J. Biochem.* **2009**, *146* (5), 609–616. https://doi.org/10.1093/jb/mvp139.

(294) Connell, P.; Ballinger, C. A.; Jiang, J.; Wu, Y.; Thompson, L. J.; Höhfeld, J.; Patterson, C. The Co-Chaperone CHIP Regulates Protein Triage Decisions Mediated by Heat-Shock Proteins. *Nat. Cell Biol.* **2001**, *3* (1), 93–96. https://doi.org/10.1038/35050618.

(295) Zhang, H.; Amick, J.; Chakravarti, R.; Santarriaga, S.; Schlanger, S.; McGlone, C.; Dare, M.; Nix, J. C.; Scaglione, K. M.; Stuehr, D. J.; Misra, S.; Page, R. C. A Bipartite Interaction between Hsp70 and CHIP Regulates Ubiquitination of Chaperoned Client Proteins. *Structure* **2015**, *23* (3), 472–482. https://doi.org/10.1016/j.str.2015.01.003.

(296) He, Q.; Zhao, X.; Wu, D.; Jia, S.; Liu, C.; Cheng, Z.; Huang, F.; Chen, Y.; Lu, T.; Lu, S. Hydrophobic Tag-Based Protein Degradation: Development, Opportunity and Challenge. *Eur. J. Med. Chem.* **2023**, *260* (8), 115741. https://doi.org/10.1016/j.ejmech.2023.115741.

(297) Neklesa, T. K.; Tae, H. S.; Schneekloth, A. R.; Stulberg, M. J.; Corson, T. W.; Sundberg, T. B.; Raina, K.; Holley, S. A.; Crews, C. M. Small-Molecule Hydrophobic Tagging–Induced Degradation of HaloTag Fusion Proteins. *Nat. Chem. Biol.* **2011**, *7* (8), 538–543. https://doi.org/10.1038/nchembio.597.

(298) Long, M. J. C.; Gollapalli, D. R.; Hedstrom, L. Inhibitor Mediated Protein Degradation. *Chem. Biol.* **2012**, *19* (5), 629–637. https://doi.org/10.1016/j.chembiol.2012.04.008.

(299) Shi, Y.; Long, M. J. C.; Rosenberg, M. M.; Li, S.; Kobjack, A.; Lessans, P.; Coffey, R. T.; Hedstrom, L. Boc 3 Arg-Linked Ligands Induce Degradation by Localizing Target Proteins to the 20S Proteasome. *ACS Chem. Biol.* **2016**, *11* (12), 3328–3337. https://doi.org/10.1021/acschembio.6b00656.

(300) Xie, T.; Lim, S. M.; Westover, K. D.; Dodge, M. E.; Ercan, D.; Ficarro, S. B.; Udayakumar, D.; Gurbani, D.; Tae, H. S.; Steven, M.; Sim, T.; Marto, J. A.; Jänne, P. A.; Crews, C. M.; Gray, N. S. Pharmacological Targeting of the Pseudokinase Her3. **2014**, *10* (12), 1006–1012. https://doi.org/10.1038/nchembio.1658.Pharmacological.

(301) Gustafson, J. L.; Neklesa, T. K.; Cox, C. S.; Roth, A. G.; Buckley, D. L.; Tae, H. S.; Sundberg, T. B.; Stagg, D. B.; Hines, J.; McDonnell, D. P.; Norris, J. D.; Crews, C. M. Small-Molecule-Mediated Degradation of the Androgen Receptor through Hydrophobic Tagging. *Angew. Chemie Int. Ed.* **2015**, *54* (33), 9659–9662. https://doi.org/10.1002/anie.201503720.

(302) Rubner, S.; Scharow, A.; Schubert, S.; Berg, T. Selective Degradation of Polo-like Kinase 1 by a Hydrophobically Tagged Inhibitor of the Polo-Box Domain. *Angew. Chemie - Int. Ed.* **2018**, *57* (52), 17043–17047. https://doi.org/10.1002/anie.201809640.

(303) Nietzold, F.; Rubner, S.; Berg, T. The Hydrophobically-Tagged MDM2-P53 Interaction Inhibitor Nutlin-3a-HT Is More Potent against Tumor Cells than Nutlin-3a. *Chem. Commun.* **2019**, *55* (95), 14351–14354. https://doi.org/10.1039/c9cc07795b.

(304) Gao, N.; Chu, T.-T.; Li, Q.-Q.; Lim, Y.-J.; Qiu, T.; Ma, M.-R.; Hu, Z.-W.; Yang, X.-F.; Chen, Y.-X.; Zhao, Y.-F.; Li, Y.-M. Hydrophobic Tagging-Mediated Degradation of Alzheimer's Disease Related Tau. *RSC Adv.* **2017**, *7* (64), 40362–40366. https://doi.org/10.1039/C7RA05347A.

(305) Qiu, J.; Bai, X.; Zhang, W.; Ma, M.; Wang, W.; Liang, Y.; Wang, H.; Tian, J.; Yu, P.

LPM3770277, a Potent Novel CDK4/6 Degrader, Exerts Antitumor Effect Against Triple-Negative Breast Cancer. *Front. Pharmacol.* **2022**, *13* (4), 1–11. https://doi.org/10.3389/fphar.2022.853993.

(306) Ma, A.; Stratikopoulos, E.; Park, K.-S.; Wei, J.; Martin, T. C.; Yang, X.; Schwarz, M.; Leshchenko, V.; Rialdi, A.; Dale, B.; Lagana, A.; Guccione, E.; Parekh, S.; Parsons, R.; Jin, J. Discovery of a First-in-Class EZH2 Selective Degrader. *Nat. Chem. Biol.* **2020**, *16* (2), 214–222. https://doi.org/10.1038/s41589-019-0421-4.

(307) Go, A.; Jang, J. W.; Lee, W.; Ha, J. Du; Kim, H. J.; Nam, H. J. Augmentation of the Antitumor Effects of PARP Inhibitors in Triple-Negative Breast Cancer via Degradation by Hydrophobic Tagging Modulation. *Eur. J. Med. Chem.* **2020**, *204*, 112635. https://doi.org/10.1016/j.ejmech.2020.112635.

(308) Asawa, Y.; Nishida, K.; Kawai, K.; Domae, K.; Ban, H. S.; Kitazaki, A.; Asami, H.; Kohno, J. Y.; Okada, S.; Tokuma, H.; Sakano, D.; Kume, S.; Tanaka, M.; Nakamura, H. Carborane as an Alternative Efficient Hydrophobic Tag for Protein Degradation. *Bioconjug. Chem.* **2021**, *32* (11), 2377–2385. https://doi.org/10.1021/acs.bioconjchem.1c00431.

(309) Shoda, T.; Ohoka, N.; Tsuji, G.; Fujisato, T.; Inoue, H.; Demizu, Y.; Naito, M.; Kurihara, M. Targeted Protein Degradation by Chimeric Compounds Using Hydrophobic E3 Ligands and Adamantane Moiety. *Pharmaceuticals* **2020**, *13* (3), 1–13. https://doi.org/10.3390/ph13030034.

(310) Li, J.; Liu, T.; Song, Y.; Wang, M.; Liu, L.; Zhu, H.; Li, Q.; Lin, J.; Jiang, H.; Chen, K.; Zhao, K.; Wang, M.; Zhou, H.; Lin, H.; Luo, C. Discovery of Small-Molecule Degraders of the CDK9-Cyclin T1 Complex for Targeting Transcriptional Addiction in Prostate Cancer. *J. Med. Chem.* **2022**, *65* (16), 11034–11057. https://doi.org/10.1021/acs.jmedchem.2c00257.

(311) Xie, S.; Zhan, F.; Zhu, J.; Sun, Y.; Zhu, H.; Liu, J.; Chen, J.; Zhu, Z.; Yang, D.-H.; Chen, Z.-S.; Yao, H.; Xu, J.; Xu, S. Discovery of Norbornene as a Novel Hydrophobic Tag Applied in Protein Degradation. *Angew. Chemie Int. Ed.* **2023**, *62* (13), 1–12. https://doi.org/10.1002/anie.202217246.

(312) Qing, L.; Yu, Q.; Wang, C.; Lu, X.; Yang, Y.; Chen, X.; Li, X.; Min, J.; Pan, W.; He, H.; Zhong, H.; Zhang, S. Discovery of D-Ring-Contracted Artemisinin as a Potent Hydrophobic Tag for Targeted Protein Degradation. *J. Med. Chem.* **2025**, *68* (2), 1619–1631. https://doi.org/10.1021/acs.jmedchem.4c02269.

(313) Xie, S.; Zhu, J.; Li, J.; Zhan, F.; Yao, H.; Xu, J.; Xu, S. Small-Molecule Hydrophobic Tagging: A Promising Strategy of Druglike Technology for Targeted Protein Degradation. *J. Med. Chem.* **2023**, *66* (16), 10917–10933. https://doi.org/10.1021/acs.jmedchem.3c00736.

(314) Choi, S. R.; Wang, H. M.; Shin, M. H.; Lim, H.-S. Hydrophobic Tagging-Mediated Degradation of Transcription Coactivator SRC-1. *Int. J. Mol. Sci.* **2021**, *22* (12), 6407. https://doi.org/10.3390/ijms22126407.

(315) Hirai, K.; Yamashita, H.; Tomoshige, S.; Mishima, Y.; Niwa, T.; Ohgane, K.; Ishii, M.; Kanamitsu, K.; Ikemi, Y.; Nakagawa, S.; Taguchi, H.; Sato, S.; Hashimoto, Y.; Ishikawa, M. Conversion of a PROTAC Mutant Huntingtin Degrader into Small-Molecule Hydrophobic Tags Focusing on Drug-like Properties. *ACS Med. Chem. Lett.* **2022**, *13* (3), 396–402. https://doi.org/10.1021/acsmedchemlett.1c00500.

(316) Xie, S.; Sun, Y.; Liu, Y.; Li, X.; Li, X.; Zhong, W.; Zhan, F.; Zhu, J.; Yao, H.; Yang, D.-H.; Chen, Z.-S.; Xu, J.; Xu, S. Development of Alectinib-Based PROTACs as Novel Potent Degraders of Anaplastic Lymphoma Kinase (ALK). *J. Med. Chem.* **2021**, *64* (13), 9120–9140. https://doi.org/10.1021/acs.jmedchem.1c00270.

(317) Croxtall, J. D.; McKeage, K. Fulvestrant. *Drugs* **2011**, *71* (3), 363–380. https://doi.org/10.2165/11204810-000000000-00000.

(318) Wu, Y. L.; Yang, X.; Ren, Z.; McDonnell, D. P.; Norris, J. D.; Willson, T. M.; Greene, G. L. Structural Basis for an Unexpected Mode of SERM-Mediated ER Antagonism. *Mol. Cell* **2005**, *18* (4), 413–424. https://doi.org/10.1016/j.molcel.2005.04.014.

(319) Hoy, S. M. Elacestrant: First Approval. *Drugs* **2023**, *83* (6), 555–561. https://doi.org/10.1007/s40265-023-01861-0.

(320) Patel, U.; Smalley, J. P.; Hodgkinson, J. T. PROTAC Chemical Probes for Histone Deacetylase Enzymes. *RSC Chem. Biol.* **2023**, *4* (9), 623–634. https://doi.org/10.1039/d3cb00105a.

(321) Schiedel, M.; Herp, D.; Hammelmann, S.; Swyter, S.; Lehotzky, A.; Robaa, D.; Oláh, J.; Ovádi, J.; Sippl, W.; Jung, M. Chemically Induced Degradation of Sirtuin 2 (Sirt2) by a Proteolysis Targeting Chimera (PROTAC) Based on Sirtuin Rearranging Ligands (SirReals). *J. Med. Chem.* **2018**, *61* (2), 482–491. https://doi.org/10.1021/acs.jmedchem.6b01872.

(322) Yang, K.; Song, Y.; Xie, H.; Wu, H.; Wu, Y.-T.; Leisten, E. D.; Tang, W. Development of the First Small Molecule Histone Deacetylase 6 (HDAC6) Degraders. *Bioorg. Med. Chem. Lett.* **2018**, *28* (14), 2493–2497. https://doi.org/10.1016/j.bmcl.2018.05.057.

(323) Smalley, J. P.; Adams, G. E.; Millard, C. J.; Song, Y.; Norris, J. K. S.; Schwabe, J. W. R.; Cowley, S. M.; Hodgkinson, J. T. PROTAC-Mediated Degradation of Class I Histone Deacetylase Enzymes in Corepressor Complexes. *Chem. Commun.* **2020**, *56* (32), 4476–4479. https://doi.org/10.1039/d0cc01485k.

(324) Cao, F.; de Weerd, S.; Chen, D.; Zwinderman, M. R. H.; van der Wouden, P. E.; Dekker, F. J. Induced Protein Degradation of Histone Deacetylases 3 (HDAC3) by Proteolysis Targeting Chimera (PROTAC). *Eur. J. Med. Chem.* **2020**, *208, 112800*. https://doi.org/10.1016/j.ejmech.2020.112800.

(325) Xiong, Y.; Donovan, K. A.; Eleuteri, N. A.; Kirmani, N.; Yue, H.; Razov, A.; Krupnick, N. M.; Nowak, R. P.; Fischer, E. S. Chemo-Proteomics Exploration of HDAC Degradability by Small Molecule Degraders. *Cell Chem. Biol.* **2021**, *28* (10), 1514–1527.e4. https://doi.org/10.1016/j.chembiol.2021.07.002.

(326) Xiao, Y.; Hale, S.; Awasthee, N.; Meng, C.; Zhang, X.; Liu, Y.; Ding, H.; Huo, Z.; Lv, D.; Zhang, W.; He, M.; Zheng, G.; Liao, D. HDAC3 and HDAC8 PROTAC Dual Degrader Reveals Roles of Histone Acetylation in Gene Regulation. *Cell Chem. Biol.* **2023**, *30* (11), 1421-1435.e12. https://doi.org/10.1016/j.chembiol.2023.07.010.

(327) Fischer, F.; Alves Avelar, L. A.; Murray, L.; Kurz, T. Designing HDAC-PROTACs: Lessons Learned so Far. *Future Med. Chem.* **2022**, *14* (3), 143–166. https://doi.org/10.4155/fmc-2021-0206.

(328) Smalley, J. P.; Baker, I. M.; Pytel, W. A.; Lin, L.-Y.; Bowman, K. J.; Schwabe, J. W. R.; Cowley, S. M.; Hodgkinson, J. T. Optimization of Class I Histone Deacetylase PROTACs Reveals That HDAC1/2 Degradation Is Critical to Induce Apoptosis and Cell Arrest in Cancer Cells. *J. Med. Chem.* **2022**, *65* (7), 5642–5659. https://doi.org/10.1021/acs.jmedchem.1c02179.

(329) Xiao, Y.; Wang, J.; Zhao, L. Y.; Chen, X.; Zheng, G.; Zhang, X.; Liao, D. Discovery of Histone Deacetylase 3 (HDAC3)-Specific PROTACs. *Chem. Commun.* **2020**, *56* (68), 9866–9869. https://doi.org/10.1039/D0CC03243C.

(330) Darwish, S.; Ghazy, E.; Heimburg, T.; Herp, D.; Zeyen, P.; Salem-Altintas, R.; Ridinger, J.; Robaa, D.; Schmidtkunz, K.; Erdmann, F.; Schmidt, M.; Romier, C.; Jung, M.; Oehme, I.; Sippl, W. Design, Synthesis and Biological Characterization of Histone Deacetylase 8 (HDAC8) Proteolysis Targeting Chimeras (PROTACs) with Anti-Neuroblastoma Activity. *Int. J. Mol. Sci.* **2022**, *23* (14), 7535. https://doi.org/10.3390/ijms23147535.

(331) Huang, M.; Xie, X.; Gong, P.; Wei, Y.; Du, H.; Xu, Y.; Xu, Q.; Jing, Y.; Zhao, L. A 18β-Glycyrrhetinic Acid Conjugate with Vorinostat Degrades HDAC3 and HDAC6 with Improved Antitumor Effects. *Eur. J. Med. Chem.* **2020**, *188*, 111991. https://doi.org/10.1016/j.ejmech.2019.111991.

(332) Macabuag, N.; Esmieu, W.; Breccia, P.; Jarvis, R.; Blackaby, W.; Lazari, O.; Urbonas, L.; Eznarriaga, M.; Williams, R.; Strijbosch, A.; Van de Bospoort, R.; Matthews, K.; Clissold, C.; Ladduwahetty, T.; Vater, H.; Heaphy, P.; Stafford, D. G.; Wang, H.-J.; Mangette, J. E.; McAllister, G.; Beaumont, V.; Vogt, T. F.; Wilkinson, H. A.; Doherty, E. M.; Dominguez, C. Developing HDAC4-Selective Protein Degraders to Investigate the Role of HDAC4 in Huntington's Disease Pathology. *J. Med. Chem.* **2022**, *65* (18), 12445–12459. https://doi.org/10.1021/acs.jmedchem.2c01149.

(333) Kadier, K.; Niu, T.; Ding, B.; Chen, B.; Qi, X.; Chen, D.; Cheng, X.; Fang, Y.; Zhou, J.; Zhao, W.; Liu, Z.; Yuan, Y.; Zhou, Z.; Dong, X.; Yang, B.; He, Q.; Cao, J.; Jiang, L.; Zhu, C. PROTAC-Mediated HDAC7 Protein Degradation Unveils Its Deacetylase-Independent Proinflammatory Function in Macrophages. *Adv. Sci.* **2024**, *2309459*, 1–18. https://doi.org/10.1002/advs.202309459.

(334) Jin, Y.; Qi, X.; Yu, X.; Cheng, X.; Chen, B.; Wu, M.; Zhang, J.; Yin, H.; Lu, Y.; Zhou, Y.; Pang, A.; Lin, Y.; Jiang, L.; Shi, Q.; Geng, S.; Zhou, Y.; Yao, X.; Li, L.; Duan, H.; Che, J.; Cao, J.; He, Q.; Dong, X. Discovery of a Potential Hematologic Malignancies Therapy: Selective and Potent HDAC7 PROTAC Degrader Targeting Non-Enzymatic Function. *Acta Pharm. Sin. B* **2025**, *15* (3), 1659–1679. https://doi.org/10.1016/j.apsb.2025.01.021.

(335) Wu, H.; Yang, K.; Zhang, Z.; Leisten, E. D.; Li, Z.; Xie, H.; Liu, J.; Smith, K. A.; Novakova, Z.; Barinka, C.; Tang, W. Development of Multifunctional Histone Deacetylase 6 Degraders with Potent Antimyeloma Activity. *J. Med. Chem.* **2019**, *62* (15), 7042–7057. https://doi.org/10.1021/acs.jmedchem.9b00516.

(336) Sinatra, L.; Bandolik, J. J.; Roatsch, M.; Sönnichsen, M.; Schoeder, C. T.; Hamacher, A.; Schöler, A.; Borkhardt, A.; Meiler, J.; Bhatia, S.; Kassack, M. U.; Hansen, F. K. Hydroxamic Acids Immobilized on Resins (HAIRs): Synthesis of Dual-Targeting HDAC Inhibitors and HDAC Degraders (PROTACs). *Angew. Chemie Int. Ed.* **2020**, *59* (50), 22494–22499. https://doi.org/10.1002/anie.202006725.

(337) Sinatra, L.; Yang, J.; Schliehe-Diecks, J.; Dienstbier, N.; Vogt, M.; Gebing, P.; Bachmann, L. M.; Sönnichsen, M.; Lenz, T.; Stühler, K.; Schöler, A.; Borkhardt, A.; Bhatia, S.; Hansen, F. K.

Solid-Phase Synthesis of Cereblon-Recruiting Selective Histone Deacetylase 6 Degraders (HDAC6 PROTACs) with Antileukemic Activity. *J. Med. Chem.* **2022**, *65* (24), 16860–16878. https://doi.org/10.1021/acs.jmedchem.2c01659.

(338) Keuler, T.; König, B.; Bückreiß, N.; Kraft, F. B.; König, P.; Schäker-Hübner, L.; Steinebach, C.; Bendas, G.; Gütschow, M.; Hansen, F. K. Development of the First Non-Hydroxamate Selective HDAC6 Degraders. *Chem. Commun.* **2022**, *58* (79), 11087–11090. https://doi.org/10.1039/D2CC03712B.

(339) Stopper, D.; Honin, I.; Feller, F.; Hansen, F. K. Development of Ethyl-Hydrazide-Based Selective Histone Deacetylase 6 (HDAC6) PROTACs. *ACS Med. Chem. Lett.* **2025**, *16* (3), 487–495. https://doi.org/10.1021/acsmedchemlett.5c00033.

(340) Zhai, S.; Honin, I.; Schäker-Hübner, L.; Hanl, M.; Jacobi, L.; Dressler, F.; Pieńkowska, D. E.; König, P.; Gerhartz, J.; Voget, R.; Bendas, G.; Gütschow, M.; Meissner, F.; Burckhardt, B. B.; Nowak, R. P.; Steinebach, C.; Hansen, F. K. Development and Characterization of the First Selective Class IIb Histone Deacetylase Degraders. *J. Med. Chem.* **2025**, *68* (13), 13793–13821. https://doi.org/10.1021/acs.jmedchem.5c00674.

(341) Chen, S.; Zheng, Y.; Liang, B.; Yin, Y.; Yao, J.; Wang, Q.; Liu, Y.; Neamati, N. The Application of PROTAC in HDAC. *Eur. J. Med. Chem.* **2023**, *260* (5), 115746. https://doi.org/10.1016/j.ejmech.2023.115746.

(342) Liu, L.; Damerell, D. R.; Koukouflis, L.; Tong, Y.; Marsden, B. D.; Schapira, M. UbiHub: A Data Hub for the Explorers of Ubiquitination Pathways. *Bioinformatics* **2019**, *35* (16), 2882–2884. https://doi.org/10.1093/bioinformatics/bty1067.

(343) He, Y.; Zhang, X.; Chang, J.; Kim, H.-N.; Zhang, P.; Wang, Y.; Khan, S.; Liu, X.; Zhang, X.; Lv, D.; Song, L.; Li, W.; Thummuri, D.; Yuan, Y.; Wiegand, J. S.; Ortiz, Y. T.; Budamagunta, V.; Elisseeff, J. H.; Campisi, J.; Almeida, M.; Zheng, G.; Zhou, D. Using Proteolysis-Targeting Chimera Technology to Reduce Navitoclax Platelet Toxicity and Improve Its Senolytic Activity. *Nat. Commun.* **2020**, *11* (1), 1996. https://doi.org/10.1038/s41467-020-15838-0.

(344) Ottis, P.; Palladino, C.; Thienger, P.; Britschgi, A.; Heichinger, C.; Berrera, M.; Julien-Laferriere, A.; Roudnicky, F.; Kam-Thong, T.; Bischoff, J. R.; Martoglio, B.; Pettazzoni, P. Cellular Resistance Mechanisms to Targeted Protein Degradation Converge Toward Impairment of the Engaged Ubiquitin Transfer Pathway. *ACS Chem. Biol.* **2019**, *14*, 2215−2223. https://doi.org/10.1021/acschembio.9b00525.

(345) Henning, N. J.; Manford, A. G.; Spradlin, J. N.; Brittain, S. M.; Zhang, E.; McKenna, J. M.; Tallarico, J. A.; Schirle, M.; Rape, M.; Nomura, D. K. Discovery of a Covalent FEM1B Recruiter for Targeted Protein Degradation Applications. *J. Am. Chem. Soc.* **2022**, *144* (2), 701–708. https://doi.org/10.1021/jacs.1c03980.

(346) Zhang, X.; Luukkonen, L. M.; Eissler, C. L.; Crowley, V. M.; Yamashita, Y.; Schafroth, M. A.; Kikuchi, S.; Weinstein, D. S.; Symons, K. T.; Nordin, B. E.; Rodriguez, J. L.; Wucherpfennig, T. G.; Bauer, L. G.; Dix, M. M.; Stamos, D.; Kinsella, T. M.; Simon, G. M.; Baltgalvis, K. A.; Cravatt, B. F. DCAF11 Supports Targeted Protein Degradation by Electrophilic Proteolysis-Targeting Chimeras. *J. Am. Chem. Soc.* **2021**, *143* (13), 5141–5149. https://doi.org/10.1021/jacs.1c00990.

(347) Ward, C. C.; Kleinman, J. I.; Brittain, S. M.; Lee, P. S.; Chung, C. Y. S.; Kim, K.; Petri, Y.; Thomas, J. R.; Tallarico, J. A.; McKenna, J. M.; Schirle, M.; Nomura, D. K. Covalent Ligand Screening Uncovers a RNF4 E3 Ligase Recruiter for Targeted Protein Degradation Applications. *ACS Chem. Biol.* **2019**, *14* (11), 2430–2440. https://doi.org/10.1021/acschembio.8b01083.

(348) Luo, M.; Spradlin, J. N.; Boike, L.; Tong, B.; Brittain, S. M.; McKenna, J. M.; Tallarico, J. A.; Schirle, M.; Maimone, T. J.; Nomura, D. K. Chemoproteomics-Enabled Discovery of Covalent RNF114-Based Degraders That Mimic Natural Product Function. *Cell Chem. Biol.* **2021**, *28* (4), 559-566.e15. https://doi.org/10.1016/j.chembiol.2021.01.005.

(349) Zhang, X.; Crowley, V. M.; Wucherpfennig, T. G.; Dix, M. M.; Cravatt, B. F. Electrophilic PROTACs That Degrade Nuclear Proteins by Engaging DCAF16. *Nat. Chem. Biol.* **2019**, *15* (7), 737–746. https://doi.org/10.1038/s41589-019-0279-5.

(350) Kiely-Collins, H.; Winter, G. E.; Bernardes, G. J. L. The Role of Reversible and Irreversible Covalent Chemistry in Targeted Protein Degradation. *Cell Chem. Biol.* **2021**, *28* (7), 952–968. https://doi.org/10.1016/j.chembiol.2021.03.005.

(351) Krieger, V.; Hamacher, A.; Cao, F.; Stenzel, K.; Gertzen, C. G. W.; Schäker-Hübner, L.; Kurz, T.; Gohlke, H.; Dekker, F. J.; Kassack, M. U.; Hansen, F. K. Synthesis of Peptoid-Based Class I-Selective Histone Deacetylase Inhibitors with Chemosensitizing Properties. *J. Med. Chem.* **2019**, *62* (24), 11260–11279. https://doi.org/10.1021/acs.jmedchem.9b01489.

(352) Schapira, M.; Calabrese, M. F.; Bullock, A. N.; Crews, C. M. Targeted Protein Degradation: Expanding the Toolbox. *Nat. Rev. Drug Discov.* **2019**, *18* (12), 949–963. https://doi.org/10.1038/s41573-019-0047-y.

(353) Chen, Z.; Wang, K.; Hou, C.; Jiang, K.; Chen, B.; Chen, J.; Lao, L.; Qian, L.; Zhong, G.; Liu, Z.; Zhang, C.; Shen, H. CRL4BDCAF11 E3 Ligase Targets P21 for Degradation to Control Cell Cycle Progression in Human Osteosarcoma Cells. *Sci. Rep.* **2017**, *7* (1), 1175. https://doi.org/10.1038/s41598-017-01344-9.

(354) Hines, J.; Lartigue, S.; Dong, H.; Qian, Y.; Crews, C. M. MDM2-Recruiting PROTAC Offers Superior, Synergistic Antiproliferative Activity via Simultaneous Degradation of BRD4 and Stabilization of P53. *Cancer Res.* **2019**, *79* (1), 251–262. https://doi.org/10.1158/0008-5472.CAN-18-2918.

(355) Rubner, S.; Schubert, S.; Berg, T. Poloxin-2HT+: Changing the Hydrophobic Tag of Poloxin-2HT Increases Plk1 Degradation and Apoptosis Induction in Tumor Cells. *Org. Biomol. Chem.* **2019**, *17* (12), 3113–3117. https://doi.org/10.1039/c9ob00080a.

(356) Hines, J.; Lartigue, S.; Dong, H.; Qian, Y.; Crews, C. M. MDM2-Recruiting PROTAC Offers Superior, Synergistic Antiproliferative Activity via Simultaneous Degradation of BRD4 and Stabilization of P53. *Cancer Res.* **2019**, *79* (1), 251–262. https://doi.org/10.1158/0008-5472.CAN-18-2918.

7 Appendix

7.1 Appendix I. Publication 1. Development of the First-in-Class FEM1B-Recruiting Histone Deacetylase Degraders

The following pages include the full text and supplementary information of the article "Development of the First-in-Class FEM1B-Recruiting Histone Deacetylase Degraders", as it was published in the Journal of Medicinal Chemistry by the American Chemical Society.

Felix Feller, Irina Honin, Martina Miranda, Heiko Weber, Svenja Henze, Maria Hanl, and Finn K. Hansen.

Development of the First-in-Class FEM1B-Recruiting Histone Deacetylase Degraders. *J. Med. Chem.* **2025**, *68*, 1824–1843. https://doi.org/10.1021/acs.jmedchem.4c02569.

Journal of Medicinal Chemistry

pubs.acs.org/jmc

Article

Development of the First-in-Class FEM1B-Recruiting Histone Deacetylase Degraders

Felix Feller, Irina Honin, Martina Miranda, Heiko Weber, Svenja Henze, Maria Hanl, and Finn K. Hansen*

Cite This: J. Med. Chem. 2025, 68, 1824−1843

Read Online

ACCESS | Metrics & More | Article Recommendations | Supporting Information

ABSTRACT: Targeted protein degradation (TPD) represents a promising alternative to conventional occupancy-driven protein inhibition. Despite the existence of more than 600 E3 ligases in the human proteome, so far only a few have been utilized for TPD of histone deacetylases (HDACs), which represent important epigenetic anticancer drug targets. In this study, we disclose the first-in-class Fem-1 homologue B (FEM1B)-recruiting HDAC degraders. A set of 12 proteolysis targeting chimeras (PROTACs) was synthesized using a solid-phase supported parallel synthesis approach utilizing a covalent FEM1B ligand as an E3 ligase warhead. The evaluation of the HDAC degradation efficiency revealed substantial HDAC1 degradation by the top-performing degrader **FF2049** (**1g**: D_{max} = 85%; DC_{50} = 257 nM). Unlike our previously published cereblon-recruiting selective HDAC6 degrader, **A6**, which uses the same HDAC ligand, the FEM1B-based PROTACs achieved selective HDAC1−3 degradation. This unexpected change in the HDAC isoform degradation profile was accompanied by significant enhancement of the antiproliferative properties.

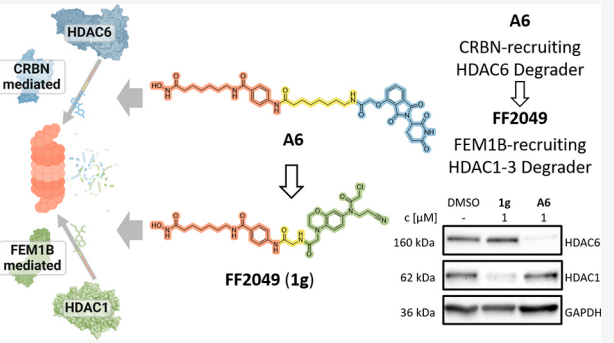

INTRODUCTION

In recent years, targeted protein degradation (TPD) has gained increasing interest due to its potential to overcome limitations of conventional protein inhibition. TPD encompasses two main modalities: molecular glues and proteolysis targeting chimeras (PROTACs). However, the distinction between these approaches is increasingly blurred.[1] Monovalent molecular glues are often identified serendipitously, whereas the discovery and design of the heterobivalent PROTACs tend to follow a more rational approach.[2] The latter consist of a protein of interest (POI) ligand and an E3 ligase recruiter, connected by a suitable spacer. This structure enables PROTACs to induce proximity between the POI and an E3 ligase, which is accompanied by an ubiquitin-loaded E2 ligase (Figure 1, middle).[3] For Cullin RING ligases (CRLs), representing the major class of E3 ligase complexes, the E2 ligase transfers ubiquitin to the bound substrate/POI, typically leading to polyubiquitination and subsequent degradation via the ubiquitin-proteasome system (UPS).[4,5]

The key advantage of PROTACs is their catalytic mode of action.[6] This translates into promising properties like prolonged pharmacological effects and dose reduction of administered PROTACs compared to a classical inhibitor. These benefits potentially elongate treatment intervals and reduce side effects. In addition, PROTACs can also overcome cancer cell resistances to occupancy-driven inhibitors. For example, target amplification or overexpression can effectively be addressed by PROTACs.[7] Moreover, PROTACs can bypass drug target alterations since they do not rely on tight-binding POI ligands. Even weak binding ligands can sufficiently form a productive ternary complex, supported by stabilizing protein−protein interactions (PPIs).[7,8] These PPIs depend on the respective E3 and recruited POI and can enhance selectivity of promiscuous POI ligands when incorporated into a PROTAC.[9]

Recently, this approach has been applied to the targeted degradation of histone deacetylases (HDACs).[10−13] HDACs are key components of the epigenetic machinery, with their primary function to hydrolyze acetylated lysine residues on histones. This restores the positive charge on the amine, leading to a more compact chromatin structure. In addition to histones, there are multiple other HDAC substrates, depending on the isoform and some HDACs are part of multiprotein complexes. The enzyme family is divided into four zinc-dependent classes consisting of 11 isoforms: class I (HDAC1−3 and 8), class IIa (HDAC4, 5, 7 and 9), class IIb (HDAC6 and 10), and class IV (HDAC11).[14,15]

Received: October 23, 2024
Revised: November 25, 2024
Accepted: December 30, 2024
Published: January 13, 2025

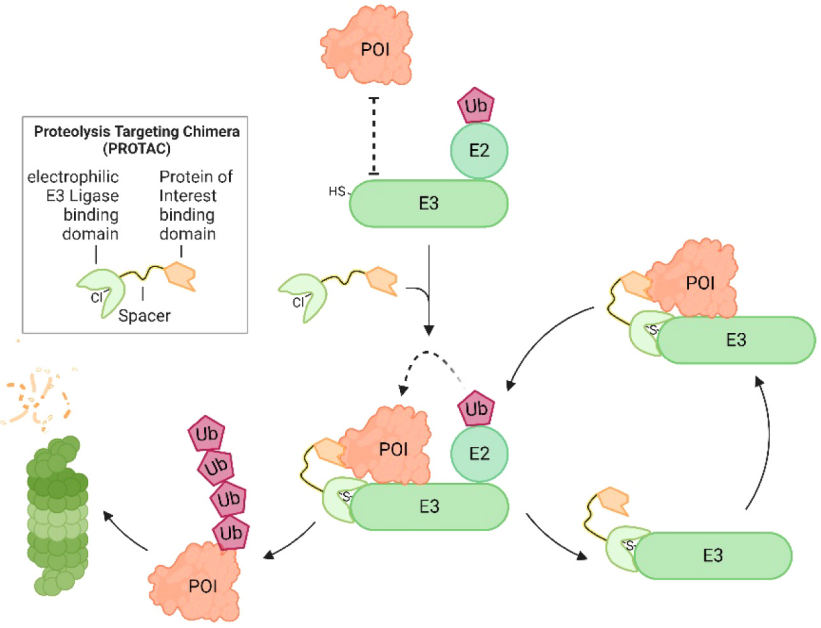

Figure 1. Mode of action of PROTACs covalently targeting the E3 ligase. Top: under physiological conditions, POI and E3 ligase are not in contact. Adding the electrophilic PROTAC induces proximity between POI and E3 ligase, which is accompanied by an ubiquitin-loaded E2. This complex (middle) facilitates polyubiquitination and proteasomal degradation of the POI (bottom left). By binding the E3 ligase covalently, PROTAC and E3 form a pseudobinary complex capable of recruiting the next POI (cycle on the right).

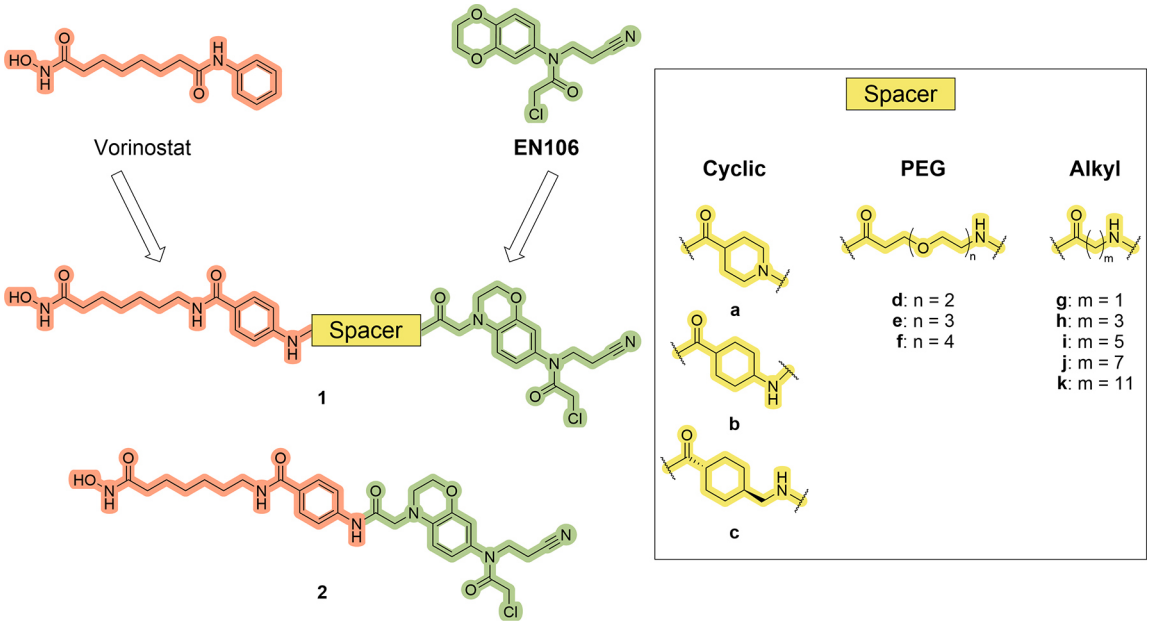

Figure 2. Design of FEM1B-recruiting HDAC degraders. The PROTAC design is inspired by vorinostat as POI ligand (orange) and by **EN106** as FEM1B recruiter (green).[36] Eleven different PROTACs were designed, incorporating a variety of spacers (yellow, **1a**–**k**), and a spacer-less variant (**2**).

HDACs are compelling targets in oncology, as their overexpression is associated with poor prognosis in diseases such as multiple myeloma, adenocarcinoma of the lung, and acute myeloid leukemia.[16−18] Furthermore, HDAC inhibition disrupts the cell cycle, reduces DNA-damage response, and impairs metastasis, angiogenesis, and proliferation.[19] Additionally, HDAC inhibition can enhance apoptosis and cell differentiation, and increase chemosensitization of tumor cells.[20,21] Currently, there are five HDAC inhibitors (HDACi) approved by the U.S. Food and Drug Administration (FDA) or European Medicines Agency: vorinostat, romidepsin, belinostat, and panobinostat for the treatment of T-cell lymphoma or multiple myeloma as well as givinostat for treatment of Duchenne muscular dystrophy.[14,22] In addition, the National Medical Products Administration of China has approved the class I selective HDACi tucidinostat (formerly known as chidamide) for the treatment of hormone receptor positive breast cancer and peripheral T-cell lymphoma.[23,24]

Although the human genome encodes for more than 600 E3 ligases,[25] only a few are predominately used in PROTAC development. For HDAC degradation, this is further limited to cereblon (CRBN), Von Hippel-Lindau (VHL), and cellular

https://doi.org/10.1021/acs.jmedchem.4c02569
J. Med. Chem. 2025, 68, 1824−1843

Scheme 1. Solid-Phase Synthesis of FEM1B-Recruiting HDAC PROTACs[a]

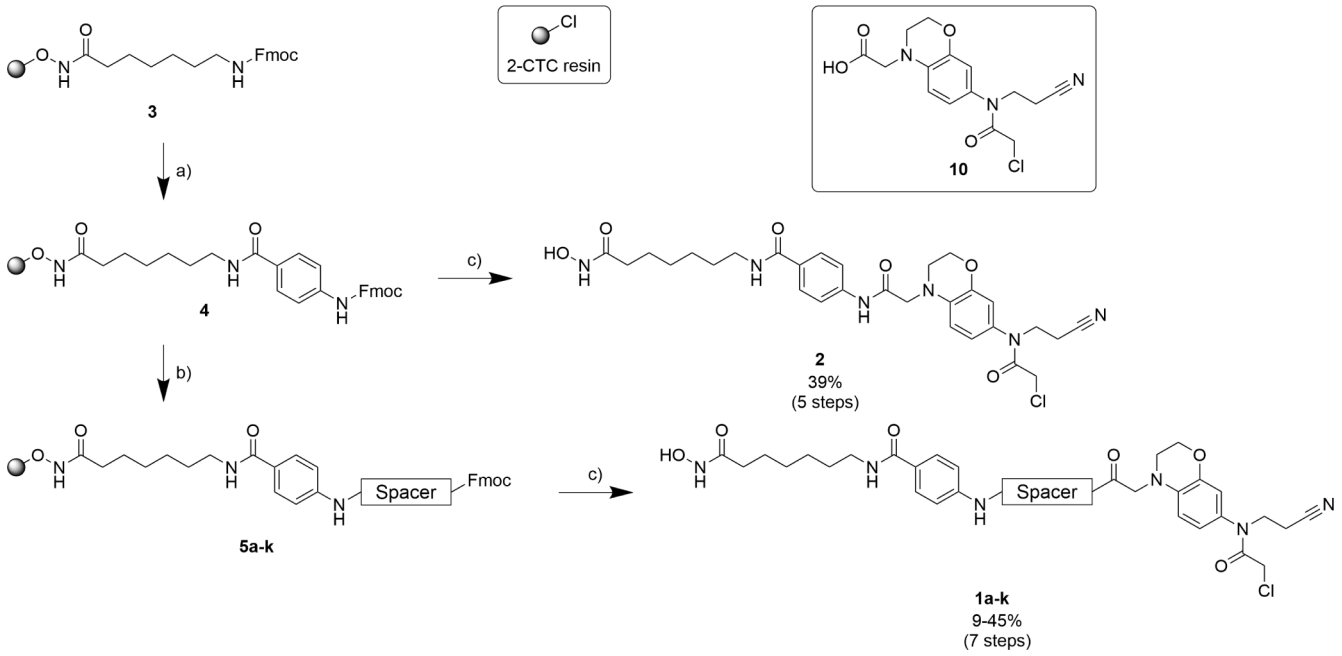

[a]Reagents and conditions: a) (i) 20% piperidine, DMF, rt, 2 × 5 min, (ii) Fmoc-4-aminobenzoic acid, HATU, HOBt·H_2O, DIPEA, DMF, rt, 18 h; b) (i) 20% piperidine, DMF, rt, 2 × 5 min, (ii) Fmoc-NH-spacer-COOH, HATU, HOBt·H_2O, DIPEA, DMF, rt, 18 h; c) (i) 20% piperidine, DMF, rt, 2 × 5 min, (ii) FEM1B ligand (**10**), HATU, HOBt·H_2O, DIPEA, DMF, rt, 18 h, (iii) 5% TFA, 5% triisopropylsilane, CH_2Cl_2, rt, 1 h.

inhibitor of apoptosis proteins (cIAP).[26] To fully harness the potential of PROTACs, the range of utilized E3 ligases needs to be expanded. As expression levels and activity of certain E3 ligases are tissue- or cell-type dependent, identifying and using new E3 ligases could enable the development of tissue specific PROTACs with reduced side effects. Likewise, targeting tumor-enriched or tumor-essential E3 ligases presents a promising opportunity to expand the range of E3 ligases employed, further enhancing the therapeutic potential of PROTACs in oncology.[27] In addition, the most commonly used ligands for CRBN and VHL have certain limitations: thalidomide and derivatives are associated with teratogenicity and stability concerns, while VHL ligands tend to increase molecular weight and total polar surface area, which can create challenges for oral bioavailability and application.[28] Furthermore, expanding the utilization of alternative E3 ligases can help to overcome cancer resistance against degraders. In fact, resistance mechanisms against PROTACs arise primarily at the CRL, but rarely at the POI, as they heavily rely on a multiprotein complex for successful degradation.[29,30] Studies have shown that PROTACs can restore POI degradation in PROTAC-resistant cells by changing the recruited E3 ligase from CRBN to VHL.[31] This highlights the importance of expanding the repertoire of E3 ligases used in TPD.

Expanding the range of ligandable E3 ligases for use in PROTACs is a recent development in TPD. For example, E3 ligases such as Ring Finger Protein 4 (RNF4),[32] Ring Finger Protein 114 (RNF114),[33] DDB1- and CUL4-associated factor 11 (DCAF11),[34] DDB1- and CUL4-associated factor 16 (DCAF16),[35] and Fem-1 homologue B (FEM1B)[36] were successfully hijacked for TPD in recent years. All mentioned E3 ligases were targeted by covalent ligands, typically containing electrophilic groups (primarily chloroacetic acid residues), which engage specific cysteine residues of the E3 ligase. Subsequently, the ternary complex transitions into a pseudobinary complex in which the covalently bound PROTAC-E3 ligase complex only needs to recruit the next POI for polyubiquitination (Figure 1, right).[37]

The FEM1B ligand **EN106** (Figure 2) was discovered by the Nomura group[36] through a competitive fluorescence polarization assay. Subsequent liquid-chromatography-tandem mass spectrometry experiments confirmed that **EN106** forms adducts exclusively with C186, a residue located in a region that is critical for FEM1Bs substrate recognition. This ligand was then transformed into PROTACs capable of targeting and degrading bromodomain-containing protein 4 (BRD4) or Abelson murine leukemia viral oncogene homologue and fusion protein (c-ABL/BCR-ABL).[36] The aim of this study is to functionalize the FEM1B ligand **EN106** for targeted degradation of HDACs, thereby expanding the range of E3 ligases employed for HDAC degradation. To this end, a set of 12 PROTACs was synthesized using the FDA-approved, unselective HDAC inhibitor vorinostat as a template for the POI ligand,[14] with the goal of targeting a broad spectrum of HDACs. The synthesis of the FEM1B-recruiting degraders was realized on solid-phase, to benefit from the typically good yields and the parallel synthesis approach of solid-phase synthesis. All synthesized compounds were subsequently examined for their degradation efficacy and cytotoxicity. A detailed biological investigation of the most active compounds uncovered notable changes in the HDAC degradation selectivity profile and led to the identification of the PROTAC **1g**, which demonstrated substantial antiproliferative properties.

RESULTS AND DISCUSSION

Design and Synthesis of FEM1B-Recruiting HDAC PROTACs. To investigate whether FEM1B recruitment can induce targeted degradation of HDACs, we designed a set of 12 target compounds (Figure 2). Most of these compounds follow the conventional PROTAC structure, consisting of three

https://doi.org/10.1021/acs.jmedchem.4c02569
J. Med. Chem. 2025, 68, 1824−1843

components: a HDAC ligand, a FEM1B recruiter, and a connecting spacer. We chose the previously published covalent E3 ligase ligand of Nomura and coworkers[36] (**10**, Schemes 1 and S1) to hijack FEM1B and to induce proteasomal degradation of HDACs. The POI ligand was inspired by the unselective HDAC inhibitor vorinostat, in order to engage a broad spectrum of HDAC isoforms. The exit vector of the POI and E3 ligase ligands have been already established,[36,38] but for the PROTAC spacers, we incorporated a variety of different types to cover a broad range of length, rigidity, and polarity. For the design of our PROTACs, we included three short and rigid cyclic spacers (**1a−c**), three longer and flexible polyethylene glycol (PEG) spacers (**1d−f**), and alkyl spacers of varying lengths in combination with high flexibility (**1g−k**). In addition, a spacer-less compound (**2**) was designed to minimize the distance between the HDAC and FEM1B ligand (Figure 2).

The desired PROTACs were prepared by solid-phase synthesis to enable a rapid generation of a degrader library. To this end, we followed our previously published protocol[38,39] starting from a 2-chlorotrityl chloride resin (2-CTC resin, Scheme 1). In detail, the resin was first modified by the reaction with *N*-hydroxyphthalimide. The phthaloyl group was subsequently deprotected by treatment with hydrazine hydrate to release the immobilized hydroxylamine as a precursor of the zinc-binding group (not shown). Next, the linker of the HDAC ligand was added by the attachment of Fmoc-protected 7-aminoheptanoic acid using HATU and HOBt as reagents for the amide coupling reaction. This provided the preloaded resin **3**[39] with a loading of 0.62−0.68 mmol/g, serving as key building block for the subsequent parallel synthesis. After Fmoc-deprotection of the resin-bound precursor, Fmoc-protected *para*-aminobenzoic acid was added as the HDACi cap group by another amide coupling reaction. This sequence yielded the resin-bound, Fmoc-protected HDAC ligand **4**. To generate the library of 12 PROTACs, the FEM1B ligand **10** was synthesized according to literature known protocols, with slight modification (Scheme S1).[36] In the first step, the FEM1B ligand was attached to the resin bound HDAC ligand **4** by Fmoc deprotection and amide coupling reaction. After cleavage from the resin by treatment with 5% TFA and 5% triisopropylsilane in dichloromethane, the spacer-less PROTAC **2** was generated in a yield of 39% over 5 steps and a purity of >95% after purification by preparative HPLC. The 11 spacer-containing PROTACs were synthesized in a similar manner, with the additional step of coupling the respective Fmoc-protected spacer (**5a−k**) before attaching the FEM1B ligand **10**. After cleavage and purification by preparative HPLC, the spacer-containing PROTACs (**1a−k**) were obtained with yields ranging from 9% to 45% over 7 steps.

FEM1B-Recruiting PROTACs Show HDAC1 Degradation and Antiproliferative Activity. All PROTACs were first tested for their antiproliferative activity against the human multiple myeloma cell line MM.1S using a cell viability assay (Figure 3A). The published selective HDAC6 PROTAC **A6**[11] was included as a control (Figure 3B), which recruits CRBN with a thalidomide-based ligand. **A6** is analogous to **1j**, only differing in the E3 ligase ligand. With the exception of the three PEG spacer-bearing PROTACs (**1d−f**) and the γ-aminobutyric acid derivative **1h**, all compounds showed single-digit micromolar half maximal effective concentration (EC_{50}) values against MM.1S. Notably, **1g**, **1j** and **1k** outperformed ricolinostat, a HDAC6 preferential inhibitor currently in clinical development.[19] In contrast, **A6** did not show antiproliferative effects against the multiple myeloma cell line.

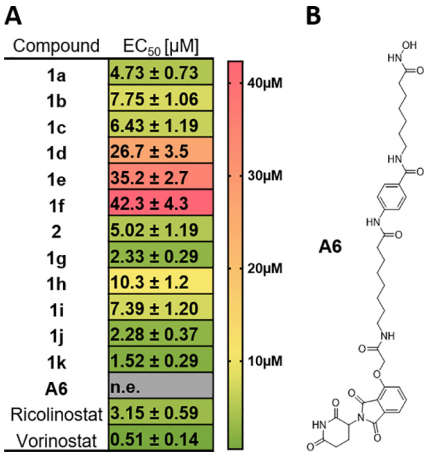

Figure 3. Antiproliferative activity of FEM1B-recruiting HDAC PROTACs in MM.1S cells. (A) MM.1S cells were treated with the indicated compounds in increasing concentration for 72 h followed by a CellTiter-Glo cell viability assay. Mean ± standard deviation of $n = 3$ biological replicates, each performed in duplicates; n.e.: no effect (≤25% effect up to 50 μM). (B) Structure of the CRBN-recruiting HDAC6 PROTAC **A6**.[11]

Building on the promising antiproliferative activity of our degraders, we performed an initial degradation screen at 1 μM (Figure 4). HDAC1 and 6 were investigated due to their

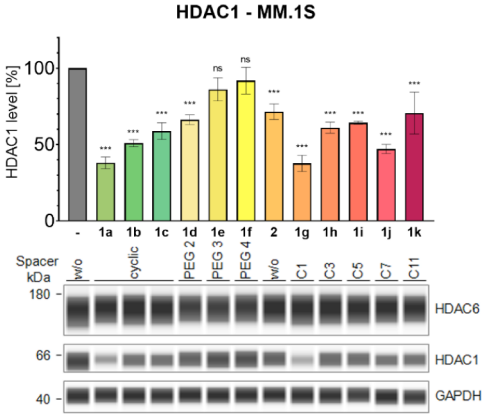

Figure 4. Initial degradation screen of HDAC1 and 6 by Simple Western immunoassay analysis of MM.1S cell lysates. MM.1S cells were treated with the indicated compounds (1 μM) or vehicle (DMSO) for 24 h. Top: Quantification of HDAC1 levels, presented as mean ± standard deviation of $n = 3$ biological replicates; Significance compared to vehicle: ns = $p \geq 0.05$; *** = $p \leq 0.001$. Bottom: Representative images from a total of $n = 3$ biological replicates, labeled with spacer type; w/o: without spacer.

contrasting cellular location and their representation of two well-studied classes I and IIb.[14] Automated Simple Western immunoassays revealed that HDAC6 levels remained largely unaffected by the treatment with the PROTACs. In contrast, HDAC1 levels showed significant degradation in the case of most compounds, particularly those with shorter spacers, except for **1j**. The most prominent effect was observed for **1g**, **1a**, and **1j** with 62.3, 61.9, and 52.8% degradation of HDAC1 at 1 μM. These three degraders were selected for further investigations.

Degradation Potency, Target Engagement, and Selective HDAC1−3 Degradation of 1a, 1g, and 1j. To further characterize the degradation profile of the three initial

https://doi.org/10.1021/acs.jmedchem.4c02569
J. Med. Chem. 2025, 68, 1824−1843

hits, we determined the maximal degradation (D_{max}) and half-maximal degradation concentration (DC_{50}) of **1a**, **1g**, and **1j** for HDAC1 (Figure 5). To this end, MM.1S cells were treated with

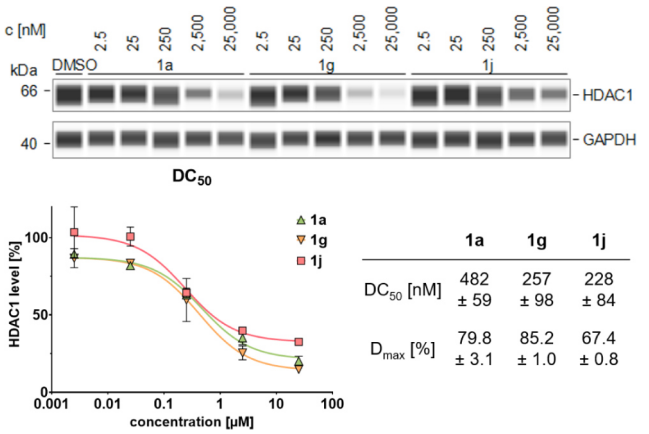

	1a	1g	1j
DC_{50} [nM]	482 ± 59	257 ± 98	228 ± 84
D_{max} [%]	79.8 ± 3.1	85.2 ± 1.0	67.4 ± 0.8

Figure 5. DC_{50} and D_{max} determination for HDAC1 by Simple Western immunoassay analysis of MM.1S cell lysates. MM.1S cells treated with the indicated compounds or vehicle (DMSO) in increasing concentrations for 24 h. Top: Representative images from a total of n = 3 biological replicates. Bottom: Quantification of HDAC1 levels (DC_{50} and D_{max}), presented as mean ± standard deviation of n = 3 biological replicates.

the indicated compounds in increasing concentrations for 24 h. The most effective HDAC1 degrader from the initial screen, **1g**, demonstrated an excellent D_{max} of 85.2% and low DC_{50} of 257 nM. **1a** exhibited a slightly lower D_{max} in combination with a less favorable DC_{50}, while **1j** displayed a comparable DC_{50} combined with a lower D_{max} compared to **1g**. In addition, the degradation mediated by **1g** was not only concentration dependent, but also time dependent (Figure S1).

Interestingly, all hits induced HDAC1 degradation without affecting HDAC6 levels, despite being equipped with an unselective HDAC recruiter. This raises the questions of whether target binding is altered by the incorporation of the vorinostat-like ligand into the FEM1B-engaging PROTACs and which other HDAC isoforms might be degraded. To clarify the first question, we conducted *in vitro* HDAC enzyme inhibition assays, which are summarized in Table 1. The assays revealed that the lowest half maximal inhibitory concentration (IC_{50}) values were observed for HDAC6 inhibition with IC_{50} values ranging from 0.004 to 0.009 μM, while the IC_{50} values for HDAC1 and 2 inhibition ranged from 0.070 to 0.094 μM and 0.143 to 0.196 μM, respectively. All FEM1B-recruiting PROTACs outperformed the control inhibitors vorinostat and ricolinostat in inhibiting HDAC1, 2, and 6, while for all compounds under study the inhibition of HDAC4 was weak.

The target engagement was orthogonally validated in a cellular environment by analyzing MM.1S cell lysates by immunoblot analysis to assess the hyperacetylation of HDAC target proteins after PROTAC treatment. The hyperacetylation of histone H3 indicates HDAC class I inhibition/degradation, while α-tubulin hyperacetylation was used as an indicator of reduced HDAC6 activity. The results, depicted in Figure 6,

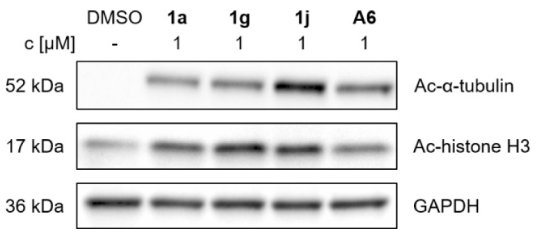

Figure 6. Cellular target engagement by **1a**, **1g**, **1j**, and **A6**. Immunoblot analysis of acetylated α-tubulin and histone H3 in MM.1S cell lysates after treatment with the indicated compounds (1 μM) or vehicle (DMSO) for 24 h. Representative images from a total of n = 3 biological replicates.

confirmed strong target engagement of the compounds in the cellular environment. In good agreement with the enzymatic data, the three FEM1B-recruiting PROTACs showed higher activity against class I HDACs, and **1j** additionally against HDAC6, than the CRBN recruiting PROTAC **A6**.

Since all selected PROTACs demonstrated engagement of multiple HDAC isoforms, the degradation profile was investigated in more detail. Immunoblot analysis was conducted to examine degradation of all HDAC isoforms from class I (HDAC1, 2, 3 and 8) and representative isoforms for class IIa (HDAC4) and IIb (HDAC6). Remarkably, the FEM1B-based PROTACs induced strong and selective degradation of HDAC1−3 while all other investigated isoforms remained unaffected (Figure 7). This degradation pattern stands in pronounced contrast to our previously published CRBN-based PROTAC **A6**, which selectively degraded HDAC6. These findings confirm that FEM1B recruitment is not only suitable for HDAC degradation, but also offers selectivity for HDAC1−3. For instance, comparing **A6** and **1j**—both of which share the same HDAC ligand and spacer but differ in the E3 ligase warhead—revealed a switch in selectivity from HDAC6 degradation to HDAC1−3 degradation. This highlights the potential for fine-tuning PROTAC selectivity by altering the recruited E3 ligase.

Degradation Confirmation, Rescue Experiments, and Cross-Cell Line HDAC Degradation. To confirm that

Table 1. HDAC Isoform Inhibition by FEM1B-Recruiting PROTACs

			IC_{50} [μM][a]			
Compound	Spacer structure	E3 ligase	HDAC1	HDAC2	HDAC4	HDAC6
1a	cyclic	FEM1B	0.094 ± 0.006	0.196 ± 0.011	8.60 ± 0.33	0.006 ± 0.001
1g	C1	FEM1B	0.074 ± 0.003	0.156 ± 0.004	13.3 ± 1.0	0.009 ± 0.001
1j	C7	FEM1B	0.070 ± 0.005	0.143 ± 0.002	3.62 ± 0.43	0.004 ± 0.001
A6	C7	CRBN	0.125 ± 0.009	0.274 ± 0.036	5.26 ± 0.50	0.009 ± 0.004
Vorinostat	-	-	0.094 ± 0.010	0.215 ± 0.028	n.e.	0.046 ± 0.005
Ricolinostat	-	-	0.160 ± 0.005	0.361 ± 0.036	7.22 ± 0.39	0.018 ± 0.002

[a]Mean ± standard deviation of at least two independent experiments, each performed in duplicates. n.e.: no effect (≤30% inhibition up to 10 μM).

https://doi.org/10.1021/acs.jmedchem.4c02569
J. Med. Chem. 2025, 68, 1824−1843

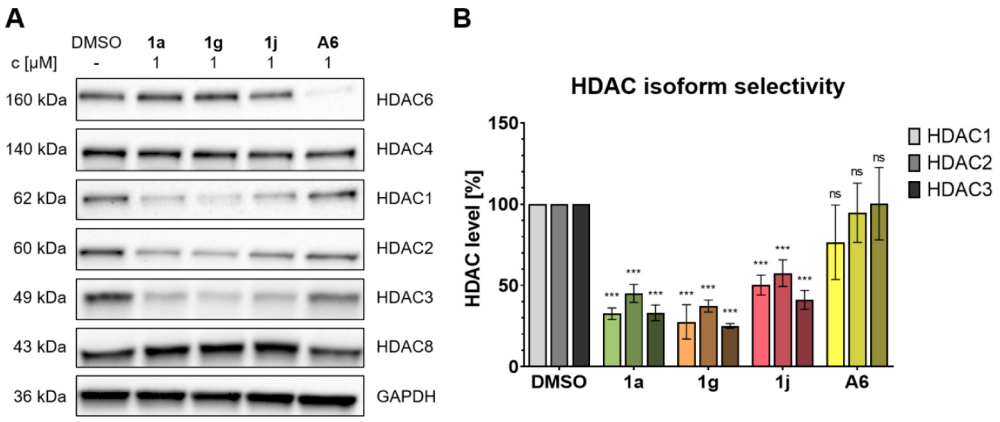

Figure 7. HDAC isoform degradation selectivity of the selected PROTACs. MM.1S cells were treated with the indicated compounds (1 μM) or vehicle (DMSO) for 24 h. HDAC1−4, HDAC6, and HDAC8 levels were analyzed by immunoblotting. (A) Representative images from a total of $n = 3$ biological replicates. (B) Quantification of HDAC1, 2, and 3 levels, presented as mean ± standard deviation of $n = 3$ biological replicates; significance compared to vehicle: ns = $p \geq 0.05$; *** = $p \leq 0.001$.

Scheme 2. Synthesis of the Nondegrading Control 1g-nc[a]

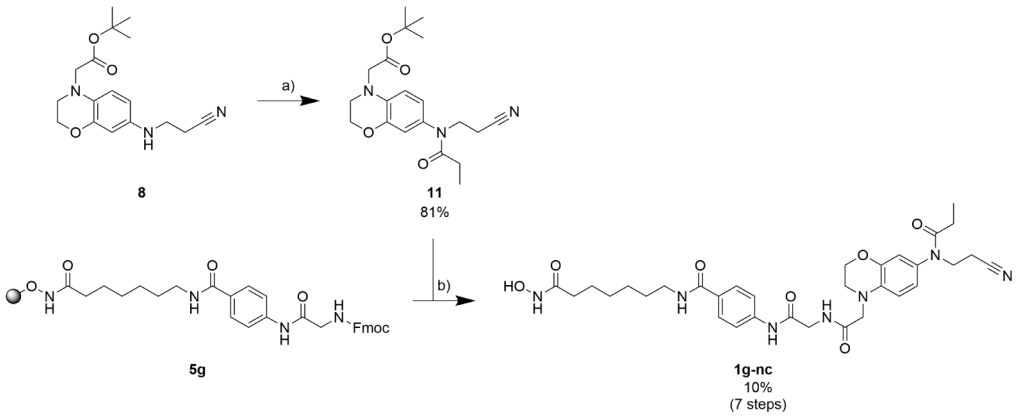

[a]Reagents and conditions: a) Triethylamine, propionyl chloride, CH_2Cl_2, 0 °C to rt, 4 h; b) (i) **11**, TFA/CH_2Cl_2 (1/3 v/v), rt, 2 h; (ii) **5g**, 20% piperidine, DMF, rt, 2 × 5 min; (iii) **5g**-NH_2, **11**-COOH, HATU, HOBt·H_2O, DIPEA, DMF, rt, 18 h; (iv) 5% TFA, 5% triisopropylsilane, CH_2Cl_2, rt, 1 h.

degradation is FEM1B dependent, we synthesized a nondegrading control of **1g**, which was the most active PROTAC. The nondegrading control **1g-nc** was designed to lack the electrophilic warhead and instead bears a propionyl moiety, which is known to abolish binding to FEM1B.[36] This was realized by treating **8** with propionyl chloride to yield the corresponding tertiary amide, deprotection of the *tert*-butyl ester, and the subsequent amide coupling with the solid-phase bound precursor **5g** (Scheme 2). After cleavage from the resin, the nondegrading control **1g-nc** was generated in a purity of >95% after purification by preparative HPLC.

In addition, we performed rescue experiments by pretreatment with an excess of vorinostat and studied whether the degradation is neddylation-dependent. Treating MM.1S cells with the nondegrading control led to no degradation, thereby confirming the requirement of FEM1B binding for degradation (Figure 8). A similar result was gained by cotreatment of **1g** and vorinostat. The latter displaces the PROTAC from the binding pocket of HDAC1, disrupting ternary complex formation, and prohibits degradation of HDAC1. Suppressing the activity of E3 ligases by the neddylation inhibitor MLN4924 also rescued HDAC1 from degradation by **1g**. All taken together, these data

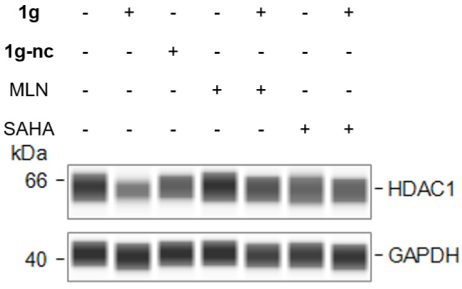

Figure 8. Compound **1g** induces degradation *via* binding to FEM1B and HDAC1 in neddylation-dependent manner. HDAC1 levels were determined by Simple Western immunoassay analysis of MM.1S cell lysates. MM.1S cells were incubated with **1g** (1 μM), **1g-nc** (1 μM), MLN4924 (MLN, 10 μM), vorinostat (SAHA, 10 μM) or the indicated cotreatment for 6 h. For cotreatments, the incubation with MLN4924 and vorinostat started 30 min before the addition of **1g**. Representative image from a total of $n = 3$ biological replicates.

demonstrate that the observed HDAC degradation occurs *via* ternary complex formation and the UPS.

The multiple myeloma cell line MM.1S is a widely used cancer model for evaluating degraders,[10,40−42] but we wanted to explore whether the FEM1B-recruiting degraders could also reduce

https://doi.org/10.1021/acs.jmedchem.4c02569
J. Med. Chem. 2025, 68, 1824−1843

HDAC1 levels in other cancer entities. To this end, we analyzed HDAC1 degradation by our best degrader **1g** in three additional cell lines: the acute monocytic leukemia cell line MV4−11, the mamma carcinoma cell line MDA-MB-231, and the glioblastoma cell line U-87MG. The results are summarized in Figure 9.

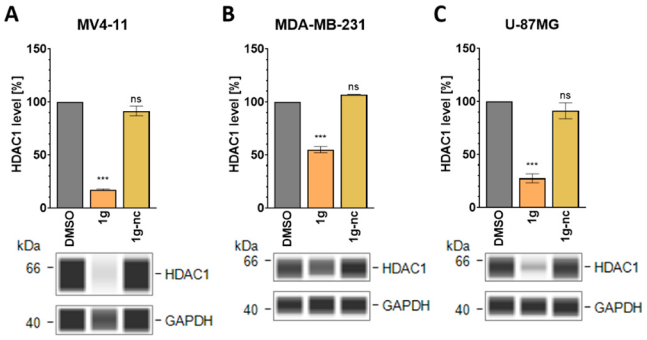

Figure 9. Cell line dependent degradation of HDAC1 by FEM1B-recruiting PROTACs. Simple Western immunoassay analysis of MV4−11 (A), MDA-MB-231 (B), or U-87MG (C) cell lysates. The cells were incubated with the indicated compound (10 μM) or vehicle (DMSO) for 24 h. Top: Quantification of HDAC1 levels, presented as mean ± standard deviation and representative images of $n = 2$ biological replicates; Significance compared to vehicle: ns = $p \geq 0.05$ and *** = $p \leq 0.001$; bottom: representative images from a total of $n = 2$ biological replicates.

PROTAC **1g** induced significant HDAC1 degradation in MV4−11 cells as well as in the two solid tumor cell lines MDA-MB-231 and U-87MG. The most pronounced HDAC1 degradation was observed in MV4−11 (87%), followed by the degradation in U-87MG cells (75%), while the HDAC1 degradation in MDA-MB-231 was the weakest (53%). In contrast, the nondegrading control **1g-nc** did not affect HDAC1 levels in any cell line, indicating that the observed effects for **1g** were caused by ternary complex formation and FEM1B recruitment.

Antiproliferative Activity of 1a, 1g, and 1j Originates from Cell Cycle Arrest and Induction of Apoptosis. To determine whether the degradation resulted in antiproliferative activity, viability assays were conducted (Table 2). The two hematological cancer cell lines MM.1S and MV4−11 exhibited similar results: The antiproliferative activity increased from **1a** to **1j**, whereas the nondegrading control showed no or only minimal toxicity. The antiproliferative effects against MV4−11 cells was for all compounds more pronounced than against MM.1S. In contrast, the results in the solid tumor cell lines were notably weaker, particularly in U-87MG cells, and the potency ranking of the PROTACs changed. Importantly, the non-degrading control **1g-nc** again showed no effects, reinforcing the assumption that the observed antiproliferative effects were related to ternary complex formation and subsequent HDAC degradation. When compared to the included controls, all FEM1B-recruiting PROTACs were significantly more effective than the CRBN-based **A6**. Notably, **1j** even outperformed the clinical candidate ricolinostat in the hematological cell lines MM.1S and MV4−11, demonstrating its superior activity in these models.

For a more detailed picture of the cellular effects of the FEM1B-recruiting PROTACs, we studied the impact of **1a**, **1g**, and **1j** on the different stages of the cell cycle (Figure 10A,B). The different phases of the cell cycle were analyzed after staining with propidium iodide (PI) to quantify DNA content. The three FEM1B-recruiting PROTACs showed a significant reduction in S phase in combination with an increase in sub G1 phase, indicating cell cycle arrest and induction of apoptosis. In comparison, both the nondegrading control **1g-nc** as well as the CRBN recruiting PROTAC **A6** produced no significant changes. These results were confirmed by the measurement of apoptosis induction by annexin V/PI staining (Figure 10C,D). The FEM1B-recruiting PROTACs **1a**, **1g**, and **1j** induced a significant increase in early and late apoptotic cells, while the nondegrading control **1g-nc** and CBRN recruiting **A6** caused no significant changes.

Clonogenic Growth Assay. The results of short-term cell viability assays were complemented by a clonogenic growth assay, which was used to assess the long-term effects on replicative potential of MDA-MB-231 cells. The clonogenic growth was determined by counting the number of colonies after 48 h of treatment with the respective compounds or vehicle, followed by 9 days of growth. All three PROTACs (**1a**, **1g**, **1j**) showed reduced clonogenic growth, similar to the effects observed with the HDACi vorinostat and ricolinostat (Figure 11). In contrast, the CRBN-recruiting degrader **A6** showed no reduction in clonogenic growth. While FEM1B-recruiting PROTACs initially appeared less effective than HDAC inhibitors in short-term metabolic activity assays (Table 2), their long-term efficacy was demonstrated through a significant reduction in clonogenic growth. In good agreement with the previous assays, the nondegrading control **1g-nc** exhibited no significant antiproliferative effects in the clonogenic growth assay.

Quantitative Proteomics and Collateral Degradation. To analyze the selectivity profile of the best degrader **1g** in more detail, a global quantitative proteomics screen was conducted in MM.1S cells after 6 h treatment with **1g** (0.5 μM). The analysis

Table 2. Antiproliferative Activity of FEM1B-Recruiting HDAC PROTACs Against Different Hematological and Solid Cancer Cell Lines

Compound	EC_{50} [μM][a]			
	MM.1S	MV4−11	MDA-MB-231	U-87MG
1a	4.73 ± 0.73	1.14 ± 0.37	8.68 ± 2.17	66.0 ± 9.2
1g	2.33 ± 0.29	0.958 ± 0.140	26.5 ± 3.1	37.4 ± 11.5
1j	2.28 ± 0.37	0.358 ± 0.068	23.3 ± 3.3	49.7 ± 7.2
1g-nc	n.e.	14.1 ± 3.2	n.e.	n.e.
A6	n.e.	17.5 ± 1.4	n.e.	n.e.
Ricolinostat	3.15 ± 0.59	0.713 ± 0.116	6.09 ± 2.99	7.59 ± 1.14
Vorinostat	0.501 ± 0.135	0.166 ± 0.029	2.39 ± 0.22	3.59 ± 0.76

[a]Mean ± standard deviation of at least three independent experiments. n.e.: no effect (≤25% effect up to 50 μM).

https://doi.org/10.1021/acs.jmedchem.4c02569
J. Med. Chem. 2025, 68, 1824−1843

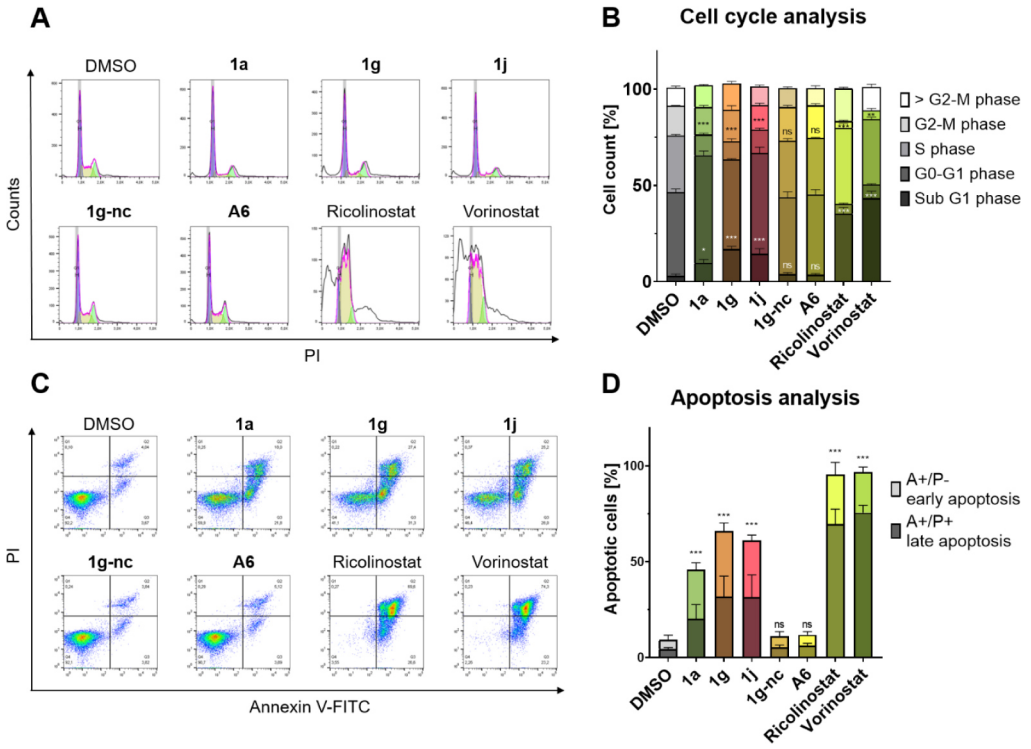

Figure 10. Cell cycle and apoptosis induction analysis by flow cytometry. MM.1S cells were treated with the respective compound (10 μM) or vehicle (DMSO) for 48 h. (A) Representative data of cell cycle analysis of MM.1S cells after PI staining. (B) Quantification of cell cycle analysis, presented as mean ± standard deviation of $n = 3$ biological replicates, each performed in duplicates. (C) Representative data of apoptosis induction analysis of MM.1S cells after annexin V-FITC/PI staining. (D) Quantification of apoptosis induction analysis, presented as mean ± standard deviation of $n = 3$ biological replicates, each performed in triplicates. Significance of apoptosis analysis is regarding the combined quantities of early and late apoptosis. In the case of (B) and (D), significance of quantification is compared to vehicle: ns = $p \geq 0.05$; * = $p \leq 0.05$; ** = $p \leq 0.01$ and *** = $p \leq 0.001$.

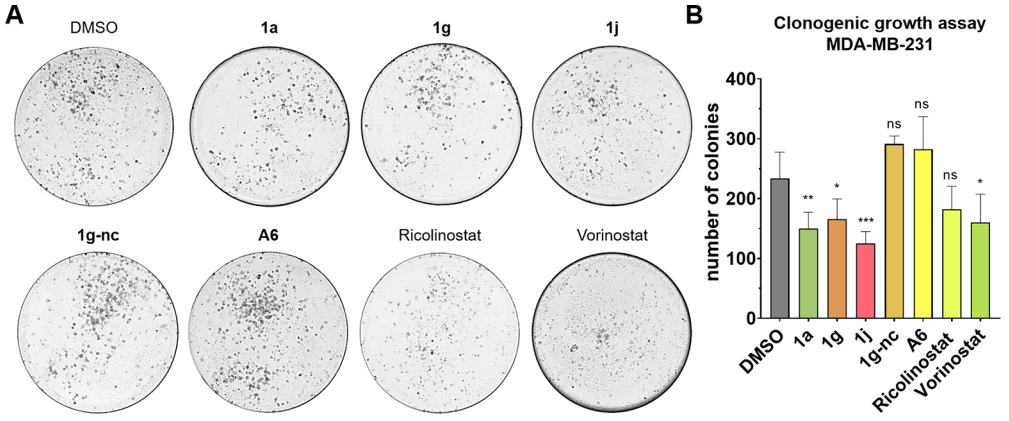

Figure 11. Clonogenic growth assay of FEM1B-recruiting PROTACs. MDA-MB-231 cells were treated with the respective compound (10 μM) or vehicle (DMSO) for 48 h. (A) Representative images of two biological replicates after 9 days of growth and crystal violet staining. (B) Quantification of counted colonies, presented as mean ± standard deviation of pooled data of two biological replicates, each performed in triplicates. Significance of quantification compared to vehicle: ns = $p \geq 0.05$; * = $p \leq 0.05$; ** = $p \leq 0.01$ and *** = $p \leq 0.001$.

was performed using diaPASEF-based mass spectrometry and more than 5700 proteins could be identified.[43] As presented in Figure 12, the results indicated moderate but significant HDAC1 and 2 degradation by **1g**. Interestingly, KDM1A (LSD1), RCOR1, RCOR3, SIN3A, NCOR1, and MIER1 showed an even more pronounced degradation. All mentioned proteins represent family members of multisubunit complexes (CoREST, SMRT/NCoR, SIN3, and MIER) which contain HDAC1/2 or 3.[44,45] The phenomenon of degraded proteins within multisubunit complexes that contain the POI can be explained by E3 ligase recruitment and ternary complex formation. This process not only leads to the polyubiquitination of the POI but also of other members within the entire complex. This so-called collateral degradation (or bystander effect) has been previously observed for other degraders and can occur to neighboring members within multiprotein complexes containing the POI.[27,41]

CONCLUSION

In this study, we have designed and synthesized the first-in-class FEM1B-recruiting HDAC degrading PROTACs. The prepared compounds feature varying spacers, which led to differences in

https://doi.org/10.1021/acs.jmedchem.4c02569
J. Med. Chem. 2025, 68, 1824−1843

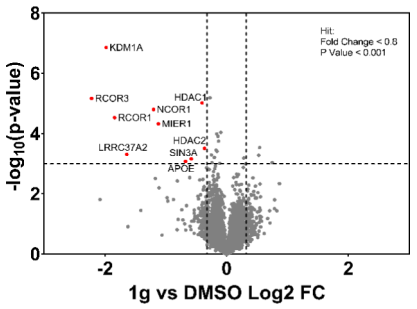

Figure 12. diaPASEF quantitative proteomics for the FEM1B-recruiting degrader **1g**. MM.1S cells were treated with **1g** (0.5 μM) for 6 h. Scatter plot of log2 fold change in **1g** treated cells compared to vehicle (DMSO) versus -log10 of the p-value. Proteins with <0.8-fold change and >0.001 p-value compared to vehicle treatment are considered to be significant (red). Presented as mean of n = 2 independent experiment.

both antiproliferative activity and degradation efficacy of HDAC1 in multiple myeloma cell line MM.1S. The best degrader **1g** (hereafter dubbed **FF2049**), containing a short glycine spacer, caused time- and concentration-dependent degradation of HDAC1 with a DC_{50} value of 257 nM and a D_{max} of 85%. Furthermore, the examined PROTACs showed fascinating selectivity profiles: they effectively degraded the class I members HDAC1, 2 and 3, while showing no degradation of HDAC8, the remaining member of class I. Although vorinostat is known to be an unselective HDACi,[46] and the HDAC ligand used in these PROTACs is based on vorinostat, no degradation of the class IIa and IIb representatives HDAC4 and 6 was observed. The HDAC1−3 selectivity appears to be driven entirely by the recruitment of FEM1B. The selectivity switch induced by the FEM1B recruiter becomes even more apparent when compared to our previously published PROTAC **A6**. Like the FEM1B-recruiting PROTACs **1a**−**k** and **2**, **A6** uses the same vorinostat-like POI ligand, but instead of recruiting FEM1B, **A6** contains a thalidomide derivate to recruit CRBN, resulting in selective degradation of HDAC6.

As degradation can be very cell line specific, we confirmed that HDAC1 degradation is not restricted to MM.1S cells but also occurs in MV4−11, MDA-MB-231 and U-87MG cells. These results suggest that FEM1B-based TPD could be extended to other cancer entities. Furthermore, we demonstrated that HDAC degradation translates into antiproliferative activity, even in the triple negative breast cancer cell line MDA-MB-231.[47] This short-term antiproliferative activity was further validated by analysis of the log-term efficacy, as seen in clonogenic growth assays with MDA-MB-231 cells. Additionally, the cytotoxicity in MM.1S was shown to result from cell cycle arrest and the induction of apoptosis. Finally, through a global proteomics screen, we were able to show that treatment of MM.1S cells with **FF2049** resulted in collateral degradation of neighboring proteins within HDAC1−3-containing multiprotein complexes. These results highlight the broader impact of the FEM1B-recruiting HDAC PROTACs on cellular protein networks.

Taken together, by employing FEM1B for HDAC degradation via **FF2049** and comparing it to our previously published HDAC6-selective PROTAC **A6**, we were able to highlight the impact of the chosen E3 ligase on the selectivity profile. This illustrates how switching E3 ligases can drastically alter the degradation pattern of PROTACs, even when utilizing the same HDAC ligand.

EXPERIMENTAL SECTION

Chemistry. *General Remarks.* Chemicals were purchased from ABCR, Acros Organics, BLDpharm, Carl Roth, Fisher Scientific, Fluorochem, Sigma-Aldrich, Tokyo Chemical Industry, and VWR Chemicals. Fmoc protection was performed according to our previously published protocol.[39] Technical grade solvents were distilled prior to use. For all HPLC purposes, acetonitrile in HPLC-grade quality (HiPerSolv CHROMANORM, VWR) was used. Water was purified with a PURELAB flex (ELGA VEOLIA). Thin layer chromatography was carried out with precoated silica gel (60 F_{254}) aluminum sheets from Merck. Detection was performed with UV light at 254 and 360 nm. Acros Organics silica gel 60 (70−230 mesh) was taken for preparative column chromatography. Uncorrected melting points were measured on a Gallenkamp Melting Point Device (MPD350.BM3.5).

High Performance Liquid Chromatography (HPLC). A Thermo Fisher Scientific UltiMateTM 3000 UHPLC system with a Nucleodur 100-5 C18 (250 × 4.6 mm, Macherey Nagel) with a flow rate of 1 mL/min and a temperature of 25 °C or a 100-5 C18 (100 × 3 mm, Macherey Nagel) with a flow rate of 0.5 mL/min and a temperature of 25 °C with an appropriate gradient were used. For preparative purposes a AZURA Prep. 500/1000 gradient system with a Nucleodur 110−5 C18 HTec (150 × 32 mm, Macherey Nagel) column with 20 mL/min was used. Detection was implemented by UV absorption measurement at a wavelength of λ = 220 nm and λ = 250 nm. Bidest. H_2O (A) and MeCN (B) were used as eluents with an addition of 0.1% TFA for eluent A. The purity of all final compounds was 95% or higher. Purity was determined via HPLC with the Nucleodur 100-5 C18 (250 × 4.6 mm, Macherey Nagel) at 250 nm. The following gradients were applied: A (95% A and 5% B for 5 min, to 5% A and 95% B in 5 min, 5% A and 95% B for 12 min), B (95% A and 5% B for 5 min, to 5% A and 95% B in 10 min, 5% A and 95% B for 12 min).

Mass Spectrometry. Low resolution electrospray ionization mass spectra (LRMS) were acquired with an Advion expression compact mass spectrometer coupled with an automated Advion TLC plate reader Plate Express (Advion, Ithaca, NY, USA). ESI-MS (LCMS) analyses were carried out on an API 2000 mass spectrometer coupled with an Agilent HPLC HP 1100 using an EC50/2 Nucleodur C18 Gravity 3 μm column or on an Agilent Infinity Lab LC/MSD-system coupled with an Agilent HPLC 1260 Infinity II using an EC50/2 Nucleodur C18 Gravity 3 μm column. The purity of synthesized compounds was determined by HPLC-DAD. HR-ESI-MS spectra were recorded on a Bruker micrOTOF-Q mass spectrometer coupled with a HPLC Dionex UltiMate 3000 or a LTQ Orbitrap XL.

Nuclear Magnet Resonance (NMR) Spectroscopy. NMR spectra were recorded on a Bruker Avance III 600 (600 MHz ^{1}H NMR, 151 MHz ^{13}C NMR). Chemical shifts are given in parts per million (ppm) referring to the signal center using the solvent peaks for reference, DMSO-d_6 (2.49/39.7) or $CDCl_3$ (7.26/77.16). The multiplicity of each signal is reported as singlet (s), doublet (d), triplet (t), multiplet (m) or combinations thereof. Multiplicities and coupling constants are reported as measured and might disagree with the expected values.

General Procedure A (Amide Coupling on Resin). This procedure was performed as previously published.[38,39] This reaction was performed in a scale of 0.21−3.72 mmol. The

https://doi.org/10.1021/acs.jmedchem.4c02569
J. Med. Chem. 2025, 68, 1824−1843

preloaded resin **3** (loading: 0.618−0.681 mmol/g, prepared according to our previously published protocol[38,39] was swelled in DMF for 1 h. After deprotection of the Fmoc group by treatment with the deprotection solution (20% piperidine in DMF) two times for 5 min, the resin was washed with DMF (4 × 5 mL), MeOH (4 × 5 mL) and DMF (4 × 5 mL). In parallel, the respective Fmoc protected acid (2.00 equiv), HATU (2.00 equiv), HOBt·H_2O (2.00 equiv), and DIPEA (3.00 eq−4.00 eq) were dissolved in DMF and stirred for 5 min. This solution was added to the resin and the amide coupling was performed for 18 h. Subsequently, the resin was washed with DMF (5 × 5 mL) and CH_2Cl_2 (10 × 5 mL) and the completion of the reaction was confirmed via TNBS test, conducted according to manufacturer's protocol, and by HPLC analysis after test cleavage. The modified resin was dried *in vacuo*.

General Procedure B (Cleavage from Resin). This procedure was performed as previously published.[38,39] For confirmation of completion of the reaction, dried resin (2−3 mg) was shaken with the cleavage solution (CH_2Cl_2/TFA, 95/5 *v*/*v*; 100 μL/mg) for 1 h at room temperature. After filtration, the solution was adjusted to 1 mL with MeCN and analyzed by HPLC.

The large scale cleavage for purification of the final compounds, was carried out in the same way using CH_2Cl_2/TFA/TIPS, 90/5/5 (*v*/*v*/*v*), but after 1 h of incubation the cleavage solution was removed under reduced pressure and the crude product was dissolved in DMSO/acetone (15/85 *v*/*v*) for purification by preparative HPLC.

*1-(2-{7-[2-Chloro-N-(2-cyanoethyl)acetamido]-2,3-dihydro-4H-benzo[b][1,4]oxazin-4-yl}acetyl)-N-(4-{[7-(hydroxyamino)-7-oxoheptyl]carbamoyl}phenyl)piperidine-4-carboxamide·TFA (**1a**).* Fmoc-protected 4-aminobenzoic acid (1.38 g, 3.72 mmol, 2.00 equiv) was coupled to **3** (2.73 g, 1.86 mmol, 1.00 equiv) according to **general procedure A** using HATU (1.41 g, 3.72 mmol, 2.00 equiv), HOBt·H_2O (0.57 g, 3.72 mmol, 2.00 equiv), and DIPEA (971 μL, 5.58 mmol, 3.00 equiv) dissolved in DMF (4.67 mL). The second coupling cycle was performed according to **general procedure A** using the resin bound precursor **4** (300 mg, 0.17 mmol, 1.00 equiv), Fmoc-protected isonipecotic acid (120 mg, 0.34 mmol, 2.00 equiv), HATU (130 mg, 0.34 mmol, 2.00 equiv), HOBt·H_2O (52 mg, 0.34 mmol, 2.00 equiv), and DIPEA (89 μL, 0.51 mmol, 3.00 equiv) dissolved in DMF (0.4 mL). The final coupling step was also performed according to **general procedure A** using the resin bound precursor **5a** (160 mg, 0.08 mmol, 1.00 equiv) and the TFA salt of **10** (76 mg, 0.17 mmol, 2.00 equiv), HATU (64 mg, 0.17 mmol, 2.00 equiv), HOBt·H_2O (26 mg, 0.17 mmol, 2.00 equiv), and DIPEA (59 μL, 0.34 mmol, 4.00 equiv) dissolved in DMF (0.4 mL). Cleavage was performed according to **general procedure B** and purification by preparative HPLC afforded the TFA salt of **1a** as an amorphous pale violet powder (22 mg, 27 μmol). Yield 32% (over 7 steps from **3**); **^{1}H NMR** (600 MHz, DMSO-d_6) δ = 10.31 (s, 1H), 10.13 (s, 1H), 8.28 (t, *J* = 5.6 Hz, 1H), 7.79 (d, *J* = 8.4 Hz, 2H), 7.66 (d, *J* = 8.4 Hz, 2H), 6.79−6.69 (m, 2H), 6.56 (d, *J* = 8.4 Hz, 1H), 4.40−4.18 (m, 5H), 4.01 (s, 2H), 3.94 (d, *J* = 13.3 Hz, 1H), 3.80 (t, *J* = 6.7 Hz, 2H), 3.45−3.37 (m, 2H), 3.26−3.18 (m, 2H), 3.11 (t, *J* = 12.7 Hz, 1H), 2.71−2.59 (m, 4H), 1.94 (t, *J* = 7.4 Hz, 2H), 1.85 (t, *J* = 15.0 Hz, 2H), 1.75−1.65 (m, 1H), 1.54−1.44 (m, 5H), 1.33−1.22 (m, 4H), C−N*H*−OH signal could not be detected due to solvent exchange; **^{13}C NMR** (151 MHz, DMSO-d_6) δ = 173.2, 169.1, 166.4, 166.0, 165.5, 158.1 (q, ^2J = 35.4 Hz, TFA), 143.4, 141.6, 136.0, 129.1, 128.5, 127.9, 120.7, 118.8, 118.2, 115.0, 111.7, 64.2, 50.8, 46.8, 45.0, 43.6, 42.6, 42.3, 40.8, 40.1, 32.2, 29.1, 28.6, 28.3, 28.1, 26.2, 25.1, 15.7. **HRMS (ESI)** *m*/*z* [M + H]$^+$ calcd for $C_{35}H_{44}ClN_7O_7$ 710.3064, found 710.3036; **HPLC** (gradient B), t_R = 13.23 min, 99.1% purity.

*4-[4-(2-{7-[2-Chloro-N-(2-cyanoethyl)acetamido]-2,3-dihydro-4H-benzo[b][1,4]oxazin-4-yl}acetamido)cyclohexane-1-carboxamido]-N-[7-(hydroxyamino)-7-oxoheptyl]-benzamide·TFA (**1b**).* Fmoc-protected 4-aminobenzoic acid (0.96 g, 2.60 mmol, 2.00 equiv) was coupled to **3** (2.11 g, 1.30 mmol, 1.00 equiv) according to **general procedure A** using HATU (0.99 g, 2.60 mmol, 2.00 equiv), HOBt·H_2O (0.40 g, 2.60 mmol, 2.00 equiv), and DIPEA (680 μL, 3.90 mmol, 3.00 equiv) dissolved in DMF (3.3 mL). The second coupling cycle was performed according to **general procedure A** using the resin bound precursor **4** (305 mg, 0.20 mmol, 1.00 equiv), Fmoc-protected 4-aminocyclohexane-1-carboxylic acid (142 mg, 0.39 mmol, 2.00 equiv), HATU (148 mg, 0.39 mmol, 2.00 equiv), HOBt·H_2O (60 mg, 0.39 mmol, 2.00 equiv), and DIPEA (102 μL, 0.58 mmol, 3.00 equiv) dissolved in DMF (0.6 mL). The final coupling step was also performed according to **general procedure A** using the resin bound precursor **5b** (151 mg, 0.09 mmol, 1.00 equiv) and the TFA salt of **10** (80 mg, 0.18 mmol, 2.00 equiv), HATU (67 mg, 0.18 mmol, 2.00 equiv), HOBt·H_2O (27 mg, 0.18 mmol, 2.00 equiv), and DIPEA (63 μL, 0.35 mmol, 4.00 equiv) dissolved in DMF (0.3 mL). Cleavage was performed according to **general procedure B** and purification by preparative HPLC afforded the TFA salt of **1b** as an amorphous pale yellow powder (7 mg, 8 μmol). Yield 9% (over 7 steps from **3**); **^{1}H NMR** (600 MHz, DMSO-d_6) δ = 10.30 (s, 1H), 10.00 (s, 1H), 8.27 (t, *J* = 5.7 Hz, 1H), 7.97*/7.92 (d/d, *J* = 7.3, 8.0 Hz, 1H), 7.79−7.76 (m, 2H), 7.68−7.63 (m, 2H), 6.78−6.73 (m, 2H), 6.61−6.54 (m, 1H), 4.25−4.20 (m, 2H), 4.00 (d, *J* = 5.2 Hz, 2H), 3.96 (s, 1H), 3.88 (s, 2H), 3.82−3.76 (m, 2H), 3.49−3.46 (m, 2H), 3.25−3.19 (m, 2H), 2.71−2.64 (m, 2H), 1.94 (t, *J* = 7.4 Hz, 2H), 1.90−1.76 (m, 4H), 1.74−1.68 (m, 1H), 1.65−1.60 (m, 1H), 1.56−1.44 (m, 6H), 1.32−1.23 (m, 5H), C−N*H*−OH signal could not be detected due to solvent exchange; due to two conformers of the cyclohexane spacer signals can occur as two distinct sets of signals. (*) correspond to peaks assigned to the minor conformational isomer; **^{13}C NMR** (151 MHz, DMSO-d_6) δ = 174.2, 174.1, 169.1, 168.3, 167.9, 166.0, 165.5, 158.2 (q, ^2J = 34.3 Hz, TFA), 143.6, 143.6, 141.8, 141.7, 135.8, 135.7, 129.0, 128.9, 128.9, 128.8, 127.9, 120.7, 118.8, 118.7, 118.1, 115.2, 115.1, 111.8, 111.6, 64.2, 64.2, 53.5, 53.0, 47.5, 47.5, 47.2, 45.0, 45.0, 44.0, 42.3, 42.3, 40.1, 32.2, 31.5, 29.1, 28.8, 28.3, 28.0, 26.2, 25.1, 24.4, 15.7, 15.7. **HRMS (ESI)** *m*/*z* [M + H]$^+$ calcd for $C_{36}H_{46}ClN_7O_7$ 724.3220, found 724.3208; **HPLC** (gradient B), t_R = 13.27 min, 98.7% purity.

*4-{(1r,4r)-4-[(2-{7-[2-Chloro-N-(2-cyanoethyl)acetamido]-2,3-dihydro-4H-benzo[b][1,4]oxazin-4-yl}acetamido)-methyl]cyclohexane-1-carboxamido}-N-[7-(hydroxyamino)-7-oxoheptyl]benzamide·TFA (**1c**).* Fmoc protected 4-aminobenzoic acid (1.38 g, 3.72 mmol, 2.00 equiv) was coupled to **3** (2.73 g, 1.86 mmol, 1.00 equiv) according to **general procedure A** using HATU (1.41 g, 3.72 mmol, 2.00 equiv), HOBt·H_2O (0.57 g, 3.72 mmol, 2.00 equiv), and DIPEA (971 μL, 5.58 mmol, 3.00 equiv) dissolved in DMF (4.67 mL). The second coupling cycle was performed according to **general procedure A** using the resin bound precursor **4** (303 mg, 0.19 mmol, 1.00 equiv), trans-4-(Fmoc-aminomethyl)cyclohexanecarboxylic acid (147 mg, 0.39 mmol, 2.00 equiv), HATU (147 mg, 0.39 mmol, 2.00 equiv), HOBt·H_2O (59 mg, 0.39 mmol, 2.00 equiv), and DIPEA (101 μL, 0.58 mmol, 3.00 equiv) dissolved in DMF

https://doi.org/10.1021/acs.jmedchem.4c02569
J. Med. Chem. 2025, 68, 1824−1843

(0.5 mL). The final coupling step was also performed according to **general procedure A** using the resin bound precursor **5c** (152 mg, 0.09 mmol, 1.00 equiv) and the TFA salt of **10** (80 mg, 0.18 mmol, 2.00 equiv), HATU (67 mg, 0.18 mmol, 2.00 equiv), HOBt·H_2O (27 mg, 0.18 mmol, 2.00 equiv), and DIPEA (63 μL, 0.35 mmol, 4.00 equiv) dissolved in DMF (0.3 mL). Cleavage was performed according to **general procedure B** and purification by preparative HPLC afforded the TFA salt of **1c** as an amorphous pale yellow powder (19 mg, 23 μmol). Yield 26% (over 7 steps from **3**); **^{1}H NMR** (600 MHz, DMSO-d_6) δ = 10.31 (s, 1H), 9.98 (s, 1H), 8.26 (t, J = 5.6 Hz, 1H), 8.00 (t, J = 5.9 Hz, 1H), 7.77 (d, J = 8.5 Hz, 2H), 7.64 (d, J = 8.8 Hz, 2H), 6.79−6.75 (m, 2H), 6.54 (d, J = 8.2 Hz, 1H), 4.25 (t, J = 4.4 Hz, 2H), 3.99 (s, 2H), 3.90 (s, 2H), 3.79 (t, J = 6.6 Hz, 2H), 3.47 (t, J = 4.4 Hz, 2H), 3.24−3.18 (m, 2H), 2.96 (t, J = 6.3 Hz, 2H), 2.67 (t, J = 6.6 Hz, 2H), 2.27 (tt, J = 12.1, 3.6 Hz, 1H), 1.94 (t, J = 7.4 Hz, 2H), 1.88−1.81 (m, 2H), 1.78−1.73 (m, 2H), 1.52−1.46 (m, 4H), 1.43−1.34 (m, 3H), 1.32−1.21 (m, 4H), 0.96−0.87 (m, 2H), C−N*H*−OH signal could not be detected due to solvent exchange; **^{13}C NMR** (151 MHz, DMSO-d_6) δ = 174.5, 169.1, 168.8, 166.0, 165.5, 158.2 (q, ^2J = 36.7 Hz, TFA), 143.7, 141.8, 135.7, 129.1, 128.9, 127.8, 120.7, 118.7, 118.1, 115.4 (q, ^1J = 291.0 Hz), 115.2, 111.7, 64.2, 53.6, 47.5, 45.0, 44.9, 44.6, 42.2, 40.1, 37.0, 32.2, 29.5, 29.1, 28.6, 28.3, 26.2, 25.1, 15.7. **HRMS (ESI)** m/z [M + H]$^+$ calcd for $C_{37}H_{48}ClN_7O_7$ 738.3377, found 738.3374; **HPLC** (gradient B), t_R = 13.37 min, 97.3% purity.

*4-(3-{2-[2-(2-{7-[2-Chloro-N-(2-cyanoethyl)acetamido]-2,3-dihydro-4H-benzo[b][1,4]oxazin-4-yl}acetamido)-ethoxy]ethoxy}propanamido)-N-[7-(hydroxyamino)-7-oxoheptyl]benzamide·TFA (**1d**).* Fmoc-protected 4-aminobenzoic acid (0.96 g, 2.60 mmol, 2.00 equiv) was coupled to **3** (2.11 g, 1.30 mmol, 1.00 equiv) according to **general procedure A** using HATU (0.99 g, 2.60 mmol, 2.00 equiv), HOBt·H_2O (0.40 g, 2.60 mmol, 2.00 equiv), and DIPEA (680 μL, 3.90 mmol, 3.00 equiv) dissolved in DMF (3.3 mL). The second coupling cycle was performed according to **general procedure A** using the resin bound precursor **4** (300 mg, 0.17 mmol, 1.00 equiv), Fmoc-NH-PEG2-acid (136 mg, 0.34 mmol, 2.00 equiv), HATU (130 mg, 0.34 mmol, 2.00 equiv), HOBt·H_2O (52 mg, 0.34 mmol, 2.00 equiv), and DIPEA (89 μL, 0.51 mmol, 3.00 equiv) dissolved in DMF (0.4 mL). The final coupling step was also performed according to **general procedure A** using the resin bound precursor **5d** (166 mg, 0.08 mmol, 1.00 equiv) and the TFA salt of **10** (75 mg, 0.17 mmol, 2.00 equiv), HATU (63 mg, 0.17 mmol, 2.00 equiv), HOBt·H_2O (25 mg, 0.17 mmol, 2.00 equiv), and DIPEA (57 μL, 0.33 mmol, 4.00 equiv) dissolved in DMF (0.3 mL). Cleavage was performed according to **general procedure B** and purification by preparative HPLC afforded the TFA salt of **1d** as an amorphous pale violet powder (27 mg, 31 μmol). Yield 38% (over 7 steps from **3**); **^{1}H NMR** (600 MHz, DMSO-d_6) δ = 10.31 (s, 1H), 10.12 (s, 1H), 8.28 (t, J = 5.6 Hz, 1H), 8.03 (t, J = 5.8 Hz, 1H), 7.78 (d, J = 8.8 Hz, 2H), 7.64 (d, J = 8.8 Hz, 2H), 6.79−6.72 (m, 2H), 6.52 (d, J = 8.4 Hz, 1H), 4.25−4.20 (m, 2H), 3.99 (s, 2H), 3.88 (s, 2H), 3.79 (t, J = 6.6 Hz, 2H), 3.70 (t, J = 6.2 Hz, 2H), 3.54−3.46 (m, 4H), 3.44 (t, J = 4.5 Hz, 2H), 3.40 (t, J = 5.9 Hz, 2H), 3.25−3.18 (m, 4H), 2.67 (t, J = 6.6 Hz, 2H), 2.57 (t, J = 6.3 Hz, 2H), 1.94 (t, J = 7.4 Hz, 2H), 1.53−1.45 (m, 4H), 1.33−1.21 (m, 4H), C−N*H*−OH signal could not be detected due to solvent exchange; **^{13}C NMR** (151 MHz, DMSO-d_6) δ = 169.5, 169.1, 169.0, 166.0, 165.5, 158.1 (q, ^2J = 36.1 Hz, TFA), 143.7, 141.5, 135.7, 129.1, 127.9, 122.9, 120.8, 118.8, 118.1, 115.2, 111.8, 69.6, 69.5, 68.9, 66.5, 64.2, 53.6, 47.5, 45.0, 42.3, 40.1, 38.4, 37.2, 32.2, 29.1, 28.3, 26.2, 25.1, 15.7. **HRMS (ESI)** m/z [M + H]$^+$ calcd for $C_{36}H_{48}ClN_7O_9$ 758.3275, found 758.3279; **HPLC** (gradient B), t_R = 12.90 min, 97.3% purity.

*4-(1-{7-[2-Chloro-N-(2-cyanoethyl)acetamido]-2,3-dihydro-4H-benzo[b][1,4]oxazin-4-yl}-2-oxo-6,9,12-trioxa-3-azapentadecan-15-amido)-N-[7-(hydroxyamino)-7-oxoheptyl]-benzamide·TFA (**1e**).* Fmoc-protected 4-aminobenzoic acid (0.96 g, 2.60 mmol, 2.00 equiv) was coupled to **3** (2.11 g, 1.30 mmol, 1.00 equiv) according to **general procedure A** using HATU (0.99 g, 2.60 mmol, 2.00 equiv), HOBt·H_2O (0.40 g, 2.60 mmol, 2.00 equiv), and DIPEA (680 μL, 3.90 mmol, 3.00 equiv) dissolved in DMF (3.3 mL). The second coupling cycle was performed according to **general procedure A** using the resin bound precursor **4** (300 mg, 0.17 mmol, 1.00 equiv), Fmoc-NH-PEG3-acid (151 mg, 0.34 mmol, 2.00 equiv), HATU (130 mg, 0.34 mmol, 2.00 equiv), HOBt·H_2O (52 mg, 0.34 mmol, 2.00 equiv), and DIPEA (89 μL, 0.51 mmol, 3.00 equiv) dissolved in DMF (0.4 mL). The final coupling step was also performed according to **general procedure A** using the resin bound precursor **5e** (163 mg, 0.08 mmol, 1.00 equiv) and the TFA salt of **10** (72 mg, 0.16 mmol, 2.00 equiv), HATU (61 mg, 0.16 mmol, 2.00 equiv), HOBt·H_2O (24 mg, 0.16 mmol, 2.00 equiv), and DIPEA (56 μL, 0.32 mmol, 4.00 equiv) dissolved in DMF (0.4 mL). Cleavage was performed according to **general procedure B** and purification by preparative HPLC afforded the TFA salt of **1e** as an amorphous pale violet powder (24 mg, 26 μmol). Yield 32% (over 7 steps from **3**); **^{1}H NMR** (600 MHz, DMSO-d_6) δ = 10.31 (s, 1H), 10.11 (s, 1H), 8.28 (t, J = 5.6 Hz, 1H), 8.03 (t, J = 5.7 Hz, 1H), 7.78 (d, J = 8.7 Hz, 2H), 7.64 (d, J = 8.6 Hz, 2H), 6.79−6.73 (m, 2H), 6.53 (d, J = 8.4 Hz, 1H), 4.25−4.21 (m, 2H), 3.99 (s, 2H), 3.88 (s, 2H), 3.79 (t, J = 6.7 Hz, 2H), 3.70 (t, J = 6.2 Hz, 2H), 3.53−3.47 (m, 6H), 3.47−3.43 (m, 4H), 3.39 (t, J = 5.9 Hz, 2H), 3.25−3.18 (m, 4H), 2.67 (t, J = 6.6 Hz, 2H), 2.57 (t, J = 6.2 Hz, 2H), 1.94 (t, J = 7.4 Hz, 2H), 1.53−1.45 (m, 4H), 1.33−1.22 (m, 4H), C−N*H*−OH signal could not be detected due to solvent exchange; **^{13}C NMR** (151 MHz, DMSO-d_6) δ = 169.5, 169.1, 169.0, 166.0, 165.5, 158.2 (q, ^2J = 36.5 Hz, TFA), 143.7, 141.5, 135.7, 129.1, 129.1, 127.9, 120.8, 118.8, 118.1, 115.2, 111.8, 66.5, 64.2, 53.6, 47.5, 45.0, 42.3, 40.1, 38.4, 37.2, 32.2, 29.1, 28.3, 26.2, 25.1, 15.7. **HRMS (ESI)** m/z [M + H]$^+$ calcd $C_{38}H_{52}ClN_7O_{10}$ for 802.3537, found 802.3550; **HPLC** (gradient B), t_R = 12.95 min, 99.1% purity.

*4-(1-{7-[2-Chloro-N-(2-cyanoethyl)acetamido]-2,3-dihydro-4H-benzo[b][1,4]oxazin-4-yl}-2-oxo-6,9,12,15-tetraoxa-3-azaoctadecan-18-amido)-N-[7-(hydroxyamino)-7-oxoheptyl]benzamide·TFA (**1f**).* Fmoc-protected 4-aminobenzoic acid (0.96 g, 2.60 mmol, 2.00 equiv) was coupled to **3** (2.11 g, 1.30 mmol, 1.00 equiv) according to **general procedure A** using HATU (0.99 g, 2.60 mmol, 2.00 equiv), HOBt·H_2O (0.40 g, 2.60 mmol, 2.00 equiv), and DIPEA (680 μL, 3.90 mmol, 3.00 equiv) dissolved in DMF (3.3 mL). The second coupling cycle was performed according to **general procedure A** using the resin bound precursor **4** (300 mg, 0.17 mmol, 1.00 equiv), Fmoc-NH-PEG4-acid (166 mg, 0.34 mmol, 2.00 equiv), HATU (130 mg, 0.34 mmol, 2.00 equiv), HOBt·H_2O (52 mg, 0.34 mmol, 2.00 equiv), and DIPEA (89 μL, 0.51 mmol, 3.00 equiv) dissolved in DMF (0.4 mL). The final coupling step was also performed according to **general procedure A** using the resin bound precursor **5f** (167 mg, 0.08 mmol, 1.00 equiv) and the TFA salt of **10** (70 mg, 0.16 mmol, 2.00 equiv), HATU (59 mg, 0.16 mmol, 2.00 equiv), HOBt·H_2O (24 mg, 0.16 mmol, 2.00 equiv), and DIPEA (54 μL, 0.31 mmol, 4.00 equiv) dissolved in

https://doi.org/10.1021/acs.jmedchem.4c02569
J. Med. Chem. 2025, 68, 1824−1843

DMF (0.4 mL). Cleavage was performed according to **general procedure B** and purification by preparative HPLC afforded the TFA salt of **1f** as an amorphous violet powder (24 mg, 25 μmol). Yield 32% (over 7 steps from **3**); **^{1}H NMR** (600 MHz, DMSO-d_6) δ = 10.31 (s, 1H), 10.11 (s, 1H), 8.28 (t, J = 5.6 Hz, 1H), 8.04 (t, J = 5.7 Hz, 1H), 7.78 (d, J = 8.7 Hz, 2H), 7.64 (d, J = 8.7 Hz, 2H), 6.79−6.72 (m, 2H), 6.53 (d, J = 8.5 Hz, 1H), 4.26−4.21 (m, 2H), 3.99 (s, 2H), 3.89 (s, 2H), 3.79 (t, J = 6.6 Hz, 2H), 3.70 (t, J = 6.2 Hz, 2H), 3.52−3.46 (m, 12H), 3.44 (t, J = 4.5 Hz, 2H), 3.40 (t, J = 5.9 Hz, 2H), 3.25−3.18 (m, 4H), 2.67 (t, J = 6.6 Hz, 2H), 2.57 (t, J = 6.2 Hz, 2H), 1.94 (t, J = 7.4 Hz, 2H), 1.53−1.45 (m, 4H), 1.32−1.21 (m, 4H), C−N*H*−OH signal could not be detected due to solvent exchange; **^{13}C NMR** (151 MHz, DMSO-d_6) δ = 169.5, 169.1, 169.0, 166.0, 165.5, 158.1 (q, ^2J = 36.3 Hz, TFA), 143.7, 141.5, 135.7, 129.1, 129.1, 127.9, 120.8, 118.8, 118.1, 115.2, 111.8, 69.7, 69.7, 69.7, 69.7, 69.7, 69.6, 68.9, 66.5, 64.2, 53.6, 47.5, 45.0, 42.3, 40.1, 38.4, 37.2, 32.2, 29.1, 28.3, 26.2, 25.1, 15.7. **HRMS (ESI)** m/z $[M + H]^+$ calcd for $C_{40}H_{56}ClN_7O_{11}$ 846.3799, found 846.3797; **HPLC** (gradient B), t_R = 12.98 min, 99.5% purity.

*4-[2-(2-{7-[2-Chloro-N-(2-cyanoethyl)acetamido]-2,3-dihydro-4H-benzo[b][1,4]oxazin-4-yl}acetamido)acetamido]-N-[7-(hydroxyamino)-7-oxoheptyl]benzamide (**1g**).* Fmoc-protected 4-aminobenzoic acid (1.38 g, 3.72 mmol, 2.00 equiv) was coupled to **3** (2.73 g, 1.86 mmol, 1.00 equiv) according to **general procedure A** using HATU (1.41 g, 3.72 mmol, 2.00 equiv), HOBt·H_2O (0.57 g, 3.72 mmol, 2.00 equiv), and DIPEA (971 μL, 5.58 mmol, 3.00 equiv) dissolved in DMF (4.67 mL). The second coupling cycle was performed according to **general procedure A** using the resin bound precursor **4** (308 mg, 0.21 mmol, 1.00 equiv), Fmoc-Gly-OH (130 mg, 0.43 mmol, 2.00 equiv), HATU (163 mg, 0.43 mmol, 2.00 equiv), HOBt·H_2O (66 mg, 0.43 mmol, 2.00 equiv), and DIPEA (112 μL, 0.64 mmol, 3.00 equiv) dissolved in DMF (0.5 mL). The final coupling step was also performed according to **general procedure A** using the resin bound precursor **5g** (169 mg, 0.10 mmol, 1.00 equiv) and the TFA salt of **10** (92 mg, 0.20 mmol, 2.00 equiv), HATU (78 mg, 0.20 mmol, 2.00 equiv), HOBt·H_2O (31 mg, 0.20 mmol, 2.00 equiv), and DIPEA (71 μL, 0.41 mmol, 4.00 equiv) dissolved in DMF (0.4 mL). Cleavage was performed according to **general procedure B** and purification by preparative HPLC afforded **1g** as an amorphous pale violet powder (29 mg, 45 μmol). Yield 45% (over 7 steps from **3**); **^{1}H NMR** (600 MHz, DMSO-d_6) δ = 10.31 (s, 1H), 10.17 (s, 1H), 8.63 (s, 1H), 8.34 (t, J = 5.8 Hz, 1H), 8.29 (t, J = 5.6 Hz, 1H), 7.79 (d, J = 8.7 Hz, 2H), 7.63 (d, J = 8.8 Hz, 2H), 6.80−6.76 (m, 2H), 6.64 (d, J = 9.2 Hz, 1H), 4.28−4.24 (m, 2H), 4.00 (d, J = 5.3 Hz, 4H), 3.94 (d, J = 5.7 Hz, 2H), 3.79 (t, J = 6.7 Hz, 2H), 3.48 (t, J = 4.4 Hz, 2H), 3.25−3.18 (m, 2H), 2.67 (t, J = 6.6 Hz, 2H), 1.94 (t, J = 7.4 Hz, 2H), 1.54−1.45 (m, 4H), 1.33−1.22 (m, 4H); **^{13}C NMR** (151 MHz, DMSO-d_6) δ = 169.6, 169.1, 167.8, 166.0, 165.5, 143.7, 141.2, 135.6, 129.3, 129.2, 128.0, 120.8, 118.8, 118.2, 115.2, 112.1, 64.2, 53.6, 47.5, 45.0, 42.6, 42.3, 40.1, 32.2, 29.1, 28.3, 26.2, 25.1, 15.7. **HRMS (ESI)** m/z $[M + H]^+$ calcd for $C_{31}H_{38}ClN_7O_7$ 656.2594, found 656.2586; **HPLC** (gradient B), t_R = 12.88 min, 97.6% purity.

*4-[4-(2-{7-[2-Chloro-N-(2-cyanoethyl)acetamido]-2,3-dihydro-4H-benzo[b][1,4]oxazin-4-yl}acetamido)-butanamido]-N-[7-(hydroxyamino)-7-oxoheptyl]-benzamide·TFA (**1h**).* Fmoc-protected 4-aminobenzoic acid (1.38 g, 3.72 mmol, 2.00 equiv) was coupled to **3** (2.73 g, 1.86 mmol, 1.00 equiv) according to **general procedure A** using HATU (1.41 g, 3.72 mmol, 2.00 equiv), HOBt·H_2O (0.57 g, 3.72 mmol, 2.00 equiv), and DIPEA (971 μL, 5.58 mmol, 3.00 equiv) dissolved in DMF (4.67 mL). The second coupling cycle was performed according to **general procedure A** using the resin bound precursor **4** (308 mg, 0.21 mmol, 1.00 equiv), Fmoc-GABA−OH (142 mg, 0.42 mmol, 2.00 equiv), HATU (159 mg, 0.42 mmol, 2.00 equiv), HOBt·H_2O (64 mg, 0.42 mmol, 2.00 equiv), and DIPEA (109 μL, 0.63 mmol, 3.00 equiv) dissolved in DMF (0.5 mL). The final coupling step was also performed according to **general procedure A** using the resin bound precursor **5h** (163 mg, 0.10 mmol, 1.00 equiv) and the TFA salt of **10** (88 mg, 0.19 mmol, 2.00 equiv), HATU (74 mg, 0.19 mmol, 2.00 equiv), HOBt·H_2O (30 mg, 0.19 mmol, 2.00 equiv), and DIPEA (68 μL, 0.39 mmol, 4.00 equiv) dissolved in DMF (0.3 mL). Cleavage was performed according to **general procedure B** and purification by preparative HPLC afforded the TFA salt of **1h** as an amorphous pale violet powder (32 mg, 40 μmol). Yield 42% (over 7 steps from **3**); **^{1}H NMR** (600 MHz, DMSO-d_6) δ = 10.31 (s, 1H), 10.07 (s, 1H), 8.27 (t, J = 5.6 Hz, 1H), 8.06 (t, J = 5.8 Hz, 1H), 7.77 (d, J = 8.7 Hz, 2H), 7.64 (d, J = 8.6 Hz, 2H), 6.80−6.70 (m, 2H), 6.53 (d, J = 8.5 Hz, 1H), 4.27−4.22 (m, 2H), 3.98 (s, 2H), 3.87 (s, 2H), 3.77 (t, J = 6.6 Hz, 2H), 3.44 (t, J = 4.5 Hz, 2H), 3.24−3.18 (m, 2H), 3.17−3.11 (m, 2H), 2.66 (t, J = 6.6 Hz, 2H), 2.33 (t, J = 7.4 Hz, 2H), 1.94 (t, J = 7.4 Hz, 2H), 1.77−1.70 (m, 2H), 1.53−1.45 (m, 4H), 1.32−1.22 (m, 4H), C−N*H*−OH signal could not be detected due to solvent exchange; **^{13}C NMR** (151 MHz, DMSO-d_6) δ = 171.2, 169.1, 168.9, 166.0, 165.5, 158.0 (q, ^2J = 33.9 Hz, TFA), 143.7, 141.6, 135.7, 129.1, 129.0, 127.9, 120.8, 118.7, 118.1, 115.2, 111.8, 64.1, 53.8, 47.5, 45.0, 42.3, 40.1, 38.1, 33.8, 32.2, 29.1, 28.3, 26.2, 25.1, 25.0, 15.7. **HRMS (ESI)** m/z $[M + H]^+$ calcd for $C_{33}H_{42}ClN_7O_7$ 684.2907, found 684.2900; **HPLC** (gradient B), t_R = 12.92 min, 99.3% purity.

*4-[6-(2-{7-[2-Chloro-N-(2-cyanoethyl)acetamido]-2,3-dihydro-4H-benzo[b][1,4]oxazin-4-yl}acetamido)-hexanamido]-N-[7-(hydroxyamino)-7-oxoheptyl]benzamide (**1i**).* Fmoc-protected 4-aminobenzoic acid (1.38 g, 3.72 mmol, 2.00 equiv) was coupled to **3** (2.73 g, 1.86 mmol, 1.00 equiv) according to **general procedure A** using HATU (1.41 g, 3.72 mmol, 2.00 equiv), HOBt·H_2O (0.57 g, 3.72 mmol, 2.00 equiv), and DIPEA (971 μL, 5.58 mmol, 3.00 equiv) dissolved in DMF (4.67 mL). The second coupling cycle was performed according to **general procedure A** using the resin bound precursor **4** (302 mg, 0.21 mmol, 1.00 equiv), Fmoc-protected 6-aminohexanoic acid (148 mg, 0.41 mmol, 2.00 equiv), HATU (156 mg, 0.41 mmol, 2.00 equiv), HOBt·H_2O (63 mg, 0.41 mmol, 2.00 equiv), and DIPEA (107 μL, 0.62 mmol, 3.00 equiv) dissolved in DMF (0.5 mL). The final coupling step was also performed according to **general procedure A** using the resin bound precursor **5i** (156 mg, 0.09 mmol, 1.00 equiv) and the TFA salt of **10** (83 mg, 0.19 mmol, 2.00 equiv), HATU (70 mg, 0.19 mmol, 2.00 equiv), HOBt·H_2O (28 mg, 0.19 mmol, 2.00 equiv), and DIPEA (64 μL, 0.37 mmol, 4.00 equiv) dissolved in DMF (0.3 mL). Cleavage was performed according to **general procedure B** and purification by preparative HPLC afforded **1i** as an amorphous pale violet powder (28 mg, 40 μmol). Yield 44% (over 7 steps from **3**); **^{1}H NMR** (600 MHz, DMSO-d_6) δ = 10.31 (s, 1H), 10.04 (s, 1H), 8.27 (t, J = 5.6 Hz, 1H), 7.98 (t, J = 5.8 Hz, 1H), 7.77 (d, J = 8.8 Hz, 2H), 7.64 (d, J = 8.8 Hz, 2H), 6.79−6.72 (m, 2H), 6.52 (d, J = 8.4 Hz, 1H), 4.25−4.21 (m, 2H), 3.99 (s, 2H), 3.86 (s, 2H), 3.78 (t, J = 6.6 Hz, 2H), 3.43−3.42 (m, 2H), 3.24−3.18 (m, 2H), 3.11−3.05 (m, 2H), 2.66 (t, J = 6.7 Hz, 2H), 2.31 (t, J = 7.4 Hz, 2H), 1.93 (t, J = 7.4 Hz, 2H), 1.62−1.54 (m, 2H), 1.53−1.39 (m, 6H), 1.32−1.22 (m, 6H), C−N*H*−OH signal

https://doi.org/10.1021/acs.jmedchem.4c02569
J. Med. Chem. 2025, 68, 1824−1843

could not be detected due to solvent exchange; **^{13}C NMR** (151 MHz, DMSO-d_6) δ = 171.5, 169.1, 168.7, 166.0, 165.6, 143.7, 141.7, 135.7, 129.1, 129.0, 127.9, 120.8, 118.8, 118.1, 115.2, 111.7, 64.2, 53.7, 47.5, 45.0, 42.3, 40.1, 38.3, 36.4, 32.2, 29.1, 28.9, 28.3, 26.2, 26.0, 25.1, 24.7, 15.7. **HRMS (ESI)** m/z [M + H]$^+$ calcd for $C_{35}H_{46}ClN_7O_7$ 712.3220, found 712.3212; **HPLC** (gradient B), t_R = 13.21 min, 97.0% purity.

*4-[8-(2-{7-[2-Chloro-N-(2-cyanoethyl)acetamido]-2,3-dihydro-4H-benzo[b][1,4]oxazin-4-yl}acetamido)-octanamido]-N-[7-(hydroxyamino)-7-oxoheptyl]-benzamide·TFA (**1j**).* Fmoc-protected 4-aminobenzoic acid (1.01 g, 2.73 mmol, 2.00 equiv) was coupled to **3** (1.99 g, 1.37 mmol, 1.00 equiv) according to **general procedure A** using HATU (1.04 g, 2.73 mmol, 2.00 equiv), HOBt·H_2O (0.42 g, 2.73 mmol, 2.00 equiv), and DIPEA (714 μL, 4.10 mmol, 3.00 equiv) dissolved in DMF (3.42 mL). The second coupling cycle was performed according to **general procedure A** using the resin bound precursor **4** (1.55 g, 0.95 mmol, 1.00 equiv), Fmoc-protected 8-aminooctanoic acid (0.73 g, 1.91 mmol, 2.00 equiv), HATU (0.73 g, 2.91 mmol, 2.00 equiv), HOBt·H_2O (0.29 g, 1.91 mmol, 2.00 equiv), and DIPEA (498 μL, 2.86 mmol, 3.00 equiv) dissolved in DMF (2.4 mL). The final coupling step was also performed according to **general procedure A** using the resin bound precursor **5j** (150 mg, 0.09 mmol, 1.00 equiv) and the TFA salt of **10** (79 mg, 0.17 mmol, 2.00 equiv), HATU (66 mg, 0.18 mmol, 2.00 equiv), HOBt·H_2O (27 mg, 0.18 mmol, 2.00 equiv), and DIPEA (61 μL, 0.35 mmol, 4.00 equiv) dissolved in DMF (0.3 mL). Cleavage was performed according to **general procedure B** and purification by preparative HPLC afforded the TFA salt of **1j** as an amorphous white powder (24 mg, 29 μmol). Yield 37% (over 7 steps from **3**); **^{1}H NMR** (600 MHz, DMSO-d_6) δ = 10.31 (s, 1H), 10.03 (s, 1H), 8.26 (t, J = 5.6 Hz, 1H), 7.96 (t, J = 5.8 Hz, 1H), 7.77 (d, J = 8.5 Hz, 2H), 7.64 (d, J = 8.5 Hz, 2H), 6.79−6.73 (m, 2H), 6.52 (d, J = 8.4 Hz, 1H), 4.24 (t, J = 4.3 Hz, 2H), 3.99 (s, 2H), 3.86 (s, 2H), 3.79 (t, J = 6.6 Hz, 2H), 3.45 (t, J = 4.4 Hz, 2H), 3.25−3.18 (m, 2H), 3.10−3.04 (m, 2H), 2.67 (t, J = 6.6 Hz, 2H), 2.31 (t, J = 7.4 Hz, 2H), 1.94 (t, J = 7.4 Hz, 2H), 1.62−1.55 (m, 2H), 1.52−1.46 (m, 4H), 1.43−1.37 (m, 2H), 1.33−1.21 (m, 10H), C−N*H*−OH signal could not be detected due to solvent exchange; **^{13}C NMR** (151 MHz, DMSO-d_6) δ = 171.7, 169.3, 168.8, 166.2, 165.7, 158.3 (q, ^2J = 36.2 Hz, TFA), 143.9, 141.9, 135.9, 129.2, 129.1, 128.1, 120.9, 118.9, 118.2, 115.4, 111.9, 64.3, 53.9, 47.7, 45.2, 42.4, 40.2, 38.5, 36.6, 32.4, 29.2, 29.2, 28.8, 28.6, 28.5, 26.4, 26.4, 25.2, 25.1, 15.9. **HRMS (ESI)** m/z [M + H]$^+$ calcd for $C_{37}H_{50}ClN_7O_7$ 740.3533, found 740.3519; **HPLC** (gradient A), t_R = 11.23 min, 98.8% purity.

*4-[12-(2-{7-[2-Chloro-N-(2-cyanoethyl)acetamido]-2,3-dihydro-4H-benzo[b][1,4]oxazin-4-yl}acetamido)-dodecanamido]-N-[7-(hydroxyamino)-7-oxoheptyl]-benzamide (**1k**).* Fmoc-protected 4-aminobenzoic acid (1.38 g, 3.72 mmol, 2.00 equiv) was coupled to **3** (2.73 g, 1.86 mmol, 1.00 equiv) according to **general procedure A** using HATU (1.41 g, 3.72 mmol, 2.00 equiv), HOBt·H_2O (0.57 g, 3.72 mmol, 2.00 equiv), and DIPEA (971 μL, 5.58 mmol, 3.00 equiv) dissolved in DMF (4.67 mL). The second coupling cycle was performed according to **general procedure A** using the resin bound precursor **4** (304 mg, 0.21 mmol, 1.00 equiv), Fmoc-protected 12-aminododecanoic acid (186 mg, 0.41 mmol, 2.00 equiv), HATU (156 mg, 0.41 mmol, 2.00 equiv), HOBt·H_2O (63 mg, 0.41 mmol, 2.00 equiv), and DIPEA (107 μL, 0.62 mmol, 3.00 equiv) dissolved in DMF (0.5 mL). The final coupling step was also performed according to **general procedure A** using the resin bound precursor **5k** (167 mg, 0.09 mmol, 1.00 equiv) and the TFA salt of **10** (84 mg, 0.19 mmol, 2.00 equiv), HATU (71 mg, 0.19 mmol, 2.00 equiv), HOBt·H_2O (29 mg, 0.19 mmol, 2.00 equiv), and DIPEA (65 μL, 0.37 mmol, 4.00 equiv) dissolved in DMF (0.4 mL). Cleavage was performed according to **general procedure B** and purification by preparative HPLC afforded **1k** as an amorphous white powder (25 mg, 31 μmol). Yield 34% (over 7 steps from **3**); **^{1}H NMR** (600 MHz, DMSO-d_6) δ = 10.31 (s, 1H), 10.03 (s, 1H), 8.63 (s, 1H), 8.27 (t, J = 5.6 Hz, 1H), 7.95 (t, J = 5.7 Hz, 1H), 7.77 (d, J = 8.8 Hz, 2H), 7.64 (d, J = 8.8 Hz, 2H), 6.79−6.72 (m, 2H), 6.51 (d, J = 8.5 Hz, 1H), 4.26−4.22 (m, 2H), 3.99 (s, 2H), 3.86 (s, 2H), 3.79 (t, J = 6.7 Hz, 2H), 3.45 (t, J = 4.4 Hz, 2H), 3.25−3.18 (m, 2H), 3.09−3.02 (m, 2H), 2.67 (t, J = 6.6 Hz, 2H), 2.31 (t, J = 7.4 Hz, 2H), 1.94 (t, J = 7.4 Hz, 2H), 1.62−1.54 (m, 2H), 1.53−1.45 (m, 4H), 1.42−1.34 (m, 2H), 1.32−1.19 (m, 18H); **^{13}C NMR** (151 MHz, DMSO-d_6) δ = 171.6, 169.1, 168.6, 166.0, 165.6, 143.7, 141.7, 135.7, 129.1, 128.9, 127.9, 120.7, 118.7, 118.1, 115.2, 111.7, 64.2, 53.8, 47.5, 45.0, 42.3, 40.1, 38.4, 36.4, 32.2, 29.1, 29.1, 29.0, 28.9, 28.8, 28.7, 28.7, 28.3, 26.3, 26.2, 25.1, 25.0, 15.7. **HRMS (ESI)** m/z [M + H]$^+$ calcd for $C_{41}H_{58}ClN_7O_7$ 796.4159, found 796.4159; **HPLC** (gradient B), t_R = 14.98 min, 98.9% purity.

*4-[2-(2-{7-[N-(2-Cyanoethyl)propionamido]-2,3-dihydro-4H-benzo[b][1,4]oxazin-4-yl}acetamido)acetamido]-N-[7-(hydroxyamino)-7-oxoheptyl]benzamide·TFA (**1g-nc**).* Fmoc-protected 4-aminobenzoic acid (1.38 g, 3.72 mmol, 2.00 equiv) was coupled to **3** (2.73 g, 1.86 mmol, 1.00 equiv) according to **general procedure A** using HATU (1.41 g, 3.72 mmol, 2.00 equiv), HOBt·H_2O (0.57 g, 3.72 mmol, 2.00 equiv), and DIPEA (971 μL, 5.58 mmol, 3.00 equiv) dissolved in DMF (4.67 mL). The second coupling cycle was performed according to **general procedure A** using the resin bound precursor **4** (308 mg, 0.21 mmol, 1.00 equiv), Fmoc-Gly-OH (130 mg, 0.43 mmol, 2.00 equiv), HATU (163 mg, 0.43 mmol, 2.00 equiv), HOBt·H_2O (66 mg, 0.43 mmol, 2.00 equiv), and DIPEA (112 μL, 0.64 mmol, 3.00 equiv) dissolved in DMF (0.5 mL). For the next coupling step, **11** was deprotected by stirring in TFA/CH_2Cl_2 (7.5 mL, 1/3 v/v) for 2 h, concentrated under reduce pressure and used without further purification. The final coupling step was also performed according to **general procedure A** using the resin bound precursor **5g** (167 mg, 0.09 mmol, 1.00 equiv) and the TFA salt of the deprotected **11** (100 mg, 0.24 mmol, 2.00 equiv), HATU (92 mg, 0.24 mmol, 2.00 equiv), HOBt·H_2O (37 mg, 0.24 mmol, 2.00 equiv), and DIPEA (84 μL, 0.48 mmol, 4.00 equiv) dissolved in DMF (0.4 mL). Cleavage was performed according to **general procedure B** and purification by preparative HPLC afforded the TFA salt of **1g-nc** as an amorphous white powder (7 mg, 12 μmol). Yield 10% (over 7 steps from **3**); **^{1}H NMR** (600 MHz, DMSO-d_6) δ = 10.31 (s, 1H), 10.16 (s, 1H), 8.34 (t, J = 5.9 Hz, 1H), 8.29 (t, J = 5.6 Hz, 1H), 7.79 (d, J = 8.2 Hz, 2H), 7.63 (d, J = 8.3 Hz, 2H), 6.74−6.56 (m, 3H), 4.26 (t, J = 4.4 Hz, 2H), 3.99−3.91 (m, 4H), 3.75 (t, J = 6.7 Hz, 2H), 3.47−3.46 (m, 2H), 3.25−3.19 (m, 2H), 2.65 (t, J = 6.6 Hz, 2H), 2.02−1.96 (m, 2H), 1.94 (t, J = 7.4 Hz, 2H), 1.53−1.46 (m, 4H), 1.32−1.23 (m, 4H), 0.89 (t, J = 7.5 Hz, 3H), C−N*H*−OH signal could not be detected due to solvent exchange; **^{13}C NMR** (151 MHz, DMSO-d_6) δ = 173.2, 169.7, 169.1, 167.8, 165.5, 158.0 (q, ^2J = 35.4 Hz, TFA), 143.7, 141.2, 135.1, 131.0, 129.3, 120.8, 119.0, 118.2, 115.3, 112.2, 64.2, 53.7, 47.5, 44.2, 42.6, 40.1, 32.2, 29.1, 28.3, 26.8, 26.2, 25.1, 15.9, 9.4. **HRMS (ESI)** m/z [M + H]$^+$ calcd for $C_{32}H_{41}N_7O_7$

https://doi.org/10.1021/acs.jmedchem.4c02569
J. Med. Chem. 2025, 68, 1824−1843

636.3140, found 636.3136; **HPLC** (gradient B), t_R = 12.16 min, 97.1% purity.

*4-(2-{7-[2-Chloro-N-(2-cyanoethyl)acetamido]-2,3-dihydro-4H-benzo[b][1,4]oxazin-4-yl}acetamido)-N-[7-(hydroxyamino)-7-oxoheptyl]benzamide·TFA (**2**).* Fmoc protected 4-aminobenzoic acid (1.38 g, 3.72 mmol, 2.00 equiv) was coupled to **3** (2.73 g, 1.86 mmol, 1.00 equiv) according to **general procedure A** using HATU (1.41 g, 3.72 mmol, 2.00 equiv), HOBt·H_2O (0.57 g, 3.72 mmol, 2.00 equiv), and DIPEA (971 μL, 5.58 mmol, 3.00 equiv) dissolved in DMF (4.67 mL). The final coupling step was also performed according to **general procedure A** using the resin bound precursor **4** (144 mg, 0.09 mmol, 1.00 equiv) and the TFA salt of **10** (83 mg, 0.18 mmol, 2.00 equiv), HATU (70 mg, 0.18 mmol, 2.00 equiv), HOBt·H_2O (28 mg, 0.18 mmol, 2.00 equiv), and DIPEA (64 μL, 0.37 mmol, 4.00 equiv) dissolved in DMF (0.4 mL). Cleavage was performed according to **general procedure B** and purification by preparative HPLC afforded the TFA salt of **2** as an amorphous pale brown powder (26 mg, 36 μmol). Yield 39% (over 5 steps from **3**); **^{1}H NMR** (600 MHz, DMSO-d_6) δ = 10.31 (s, 1H), 10.27 (s, 1H), 8.30 (t, J = 5.6 Hz, 1H), 7.80 (d, J = 8.3 Hz, 2H), 7.66 (d, J = 8.3 Hz, 2H), 6.79 (s, 1H), 6.78−6.74 (m, 1H), 6.64 (d, J = 8.5 Hz, 1H), 4.26 (t, J = 4.4 Hz, 2H), 4.19 (s, 2H), 4.00 (s, 2H), 3.79 (t, J = 6.7 Hz, 2H), 3.53 (t, J = 4.4 Hz, 2H), 3.25−3.18 (m, 2H), 2.67 (t, J = 6.6 Hz, 2H), 1.93 (t, J = 7.4 Hz, 2H), 1.53−1.43 (m, 4H), 1.33−1.22 (m, 4H), C−N*H*−OH signal could not be detected due to solvent exchange; **^{13}C NMR** (151 MHz, DMSO-d_6) δ = 169.1, 168.3, 166.0, 165.4, 158.0 (q, ^2J = 35.6 Hz, TFA), 143.6, 141.1, 135.6, 129.3, 129.1, 128.0, 120.9, 118.8, 118.3, 115.3, 111.6, 64.2, 53.5, 47.4, 45.0, 42.3, 40.1, 32.2, 29.0, 28.3, 26.2, 25.1, 15.7. **HRMS (ESI)** m/z [M + H]$^+$ calcd for $C_{29}H_{35}ClN_6O_6$ 599.2379, found 599.2377; **HPLC** (gradient B), t_R = 13.33 min, 97.3% purity.

*tert-Butyl 2-(7-nitro-2,3-dihydro-4H-benzo[b][1,4]oxazin-4-yl)acetate (**6**).* Commercially available 7-Nitro-3,4-dihydro-2*H*-benzo[*b*][1,4]oxazine (1.00 g, 5.38 mmol, 1.00 equiv) was dissolved in DMF (20 mL) and cooled to 0 °C. NaH (237 mg, 5.92 mmol, 1.0 eq, 60% in mineral oil) was added in small portions and stirred for 30 min. Next, *tert*-butyl bromoatecate (803 μL, 5.38 mmol, 1.00 equiv) was added dropwise and the cooling was removed. The solution was stirred for 2 h at room temperature, before it was cooled again to 0 °C and water (60 mL) was added. The suspension was filtered to afford **6** as a yellow solid (1.47 g, 5.00 mmol). Yield: 93%; mp. 110−112 °C; Rf = 0.78 (cyclohexane/EtOAc, 1/1, *v*/*v*); **^{1}H NMR** (600 MHz, $CDCl_3$) δ = 7.77 (dd, J = 9.0, 2.6 Hz, 1H), 7.68 (d, J = 2.7 Hz, 1H), 6.45 (d, J = 9.0 Hz, 1H), 4.28 (t, J = 4.5 Hz, 2H), 3.99 (s, 2H), 3.57 (t, J = 4.6 Hz, 2H), 1.44 (s, 9H); **NMR** (151 MHz, $CDCl_3$) δ = 168.2, 142.8, 140.8, 138.6, 119.0, 112.4, 109.6, 83.0, 64.1, 53.3, 48.3, 28.2. **LRMS (ESI)** m/z [M + H]$^+$ calcd for $C_{14}H_{18}N_2O_5$ 295.1, found 295.0.

*tert-Butyl 2-(7-nitro-2,3-dihydro-4H-benzo[b][1,4]oxazin-4-yl)acetate (**7**).* Compound **6** (1.35 g, 4.59 mmol, 1.00 equiv) was dissolved in EtOH/H_2O (30 mL, 3/1 *v*/*v*). NH_4Cl (1.49 g, 27.6 mmol, 6.00 equiv) was added and the solution was heated to 60 °C. After the addition of Fe powder (1.30 g, 23.0 mmol, 5.00 equiv), the mixture was heated to 80 °C and stirred for 18 h. The reaction mixture was filtered through Celite, saturated sodium carbonate solution (10 mL) was added and extracted with EtOAc (3 × 30 mL). The combined organic phases were washed with brine, dried over Na_2SO_4, and concentrated under reduced pressure to afford 7 as a brown oil (1.03 g, 3.90 mmol). Yield: 85%; Rf = 0.64 (CH_2CL_2/MeOH 95/5 *v*/*v*); **^{1}H NMR** (600 MHz, $CDCl_3$) δ = 6.37 (d, J = 8.4 Hz, 1H), 6.25 (d, J = 2.5 Hz, 1H), 6.21 (dd, J = 8.5, 2.6 Hz, 1H), 4.27−4.22 (m, 2H), 3.81 (s, 2H), 3.49−3.08 (m, 4H), 1.41 (s, 9H); **NMR** (151 MHz, $CDCl_3$) δ = 170.2, 145.2, 138.5, 127.7, 113.2, 108.9, 105.0, 81.7, 65.3, 54.0, 48.4, 28.2. **LRMS (ESI)** m/z [M + H]$^+$ calcd for $C_{14}H_{20}N_2O_3$ 264.1, found 264.7.

*tert-Butyl 2-{7-[(2-cyanoethyl)amino]-2,3-dihydro-4H-benzo[b][1,4]oxazin-4-yl}acetate (**8**).* The aniline **7** (1.00 g, 3.78 mmol, 1.00 equiv) was dissolved in acrylonitrile (15 mL) and basic alumina (0.78 g, 7.57 mmol, 2.00 equiv) was added. The reaction mixture was stirred for 18 h at 80 °C. Subsequently, EtOAc (20 mL) was added and the mixture was filtered through Celite. Water (20 mL) was added to the filtrate and extracted with EtOAc (3 × 30 mL). The combined organic phases were washed with brine, dried over Na_2SO_4, and concentrated under reduced pressure. Purification by silica gel column chromatography provided **8** as a brown oil (1.06 g, 3.34 mmol). Yield: 88%; Rf = 0.58 (cyclohexane/EtOAc, 1/1, *v*/*v*); **^{1}H NMR** (600 MHz, $CDCl_3$) δ = 6.53−6.06 (m, 3H), 4.26 (t, J = 4.5 Hz, 2H), 3.97−3.71 (m, 2H), 3.60−3.02 (m, 5H), 2.58 (t, J = 6.5 Hz, 2H), 1.42 (s, 9H); **NMR** (151 MHz, $CDCl_3$) δ = 170.0, 145.4, 138.8, 127.9, 118.5, 113.4, 107.5, 103.2, 81.8, 65.3, 53.9, 48.4, 41.1, 28.2, 18.2. **LRMS (ESI)** m/z [M + H]$^+$ calcd for $C_{17}H_{23}N_3O_3$ 318.2, found 318.0.

*tert-Butyl 2-{7-[2-chloro-N-(2-cyanoethyl)acetamido]-2,3-dihydro-4H-benzo[b][1,4]oxazin-4-yl] acetate (**9**).* Compound **8** (925 mg, 2.91 mmol, 1.00 equiv) was dissolved in CH_2Cl_2 (15 mL) and the solution was cooled to 0 °C. Triethylamine (1.22 mL, 8.74 mmol, 3.00 equiv) and chloroacetyl chloride (351 μL, 4.37 mmol, 1.50 equiv) were added dropwise. The cooling was removed and the solution was stirred for 45 min at room temperature. Water (20 mL) was added and the mixture was extracted with CH_2Cl_2 (3 × 30 mL). The combined organic phases were washed with brine, dried over Na_2SO_4, and concentrated under reduced pressure. Purification by silica gel column chromatography yielded **9** as a brown oil (976 mg, 2.48 mmol). Yield: 85%; Rf = 0.44 (cyclohexane/EtOAc, 1/1, *v*/*v*); **^{1}H NMR** (600 MHz, $CDCl_3$) δ = (dd, J = 8.5, 2.5 Hz, 1H), 6.66 (d, J = 2.5 Hz, 1H), 6.48 (d, J = 8.5 Hz, 1H), 4.30−4.26 (m, 2H), 3.93−3.87 (m, 6H), 3.51−3.48 (m, 2H), 2.66 (t, J = 7.0 Hz, 2H), 1.43 (s, 9H); **NMR** (151 MHz, $CDCl_3$) δ = 169.0, 167.3, 144.6, 135.6, 129.8, 120.9, 117.7, 115.6, 111.9, 82.4, 64.7, 53.1, 47.9, 46.1, 42.0, 28.2, 16.3. **LCMS (ESI)** (90% H_2O + 2 mM NH_4OAc to 100% MeCN in 10 min, then 100% MeCN for 5 min, DAD 220−600 nm), t_R = 6.56 min, m/z [M + H]$^+$ calcd for $C_{19}H_{24}ClN_3O_4$ 394.2, found 394.1.

*2-{7-[2-Chloro-N-(2-cyanoethyl)acetamido]-2,3-dihydro-4H-benzo[b][1,4]oxazin-4-yl}acetic acid·TFA (**10**).* For *tert*-butyl deprotection, compound **9** (1.57 g, 3.94 mmol, 1.00 equiv) was dissolved in CH_2Cl_2 (60 mL) and cooled to 0 °C. TFA (20 mL) was added dropwise and the solution was stirred at room temperature, after cooling was removed. After 2 h, the solvent was removed under reduced pressure and to provide the TFA salt of **10** as a brown oil (1.64 g, 3.62 mmol), which was used without further purification. Yield: 92%; **^{1}H NMR** (600 MHz, $CDCl_3$) δ = 6.70 (d, J = 8.4 Hz, 1H), 6.67 (s, 1H), 6.52 (d, J = 8.5 Hz, 1H), 4.34−4.27 (m, 2H), 4.07 (s, 2H), 3.92−3.87 (m, 4H), 3.51 (t, J = 4.5 Hz, 2H), 2.66 (t, J = 6.9 Hz, 2H); **NMR** (151 MHz, $CDCl_3$) δ = 173.8, 167.7, 144.7, 135.4, 130.0, 121.0, 117.7, 115.7, 112.0, 64.7, 52.0, 47.8, 46.2, 42.0, 16.3. **LCMS (ESI)** (90% H_2O + 2 mM NH_4OAc to 100% MeCN in 10 min,

https://doi.org/10.1021/acs.jmedchem.4c02569
J. Med. Chem. 2025, 68, 1824−1843

then 100% MeCN for 5 min, DAD 220−600 nm), tR = 0.93 min, m/z $[M + H]^+$ calcd for $C_{15}H_{16}ClN_3O_4$ 338.1, found 338.0.

tert-Butyl 2-{7-[N-(2-cyanoethyl)propionamido]-2,3-dihydro-4H-benzo[b][1,4]oxazin-4-yl}acetate (11). Compound **8** (175 mg, 0.55 mmol, 1.00 equiv) was dissolved in CH_2Cl_2 (2.8 mL) and the solution was cooled to 0 °C. Triethylamine (231 μL, 1.65 mmol, 3.00 equiv) and propionyl chloride (73 μL, 0.83 mmol, 1.50 equiv) were added dropwise and the mixture stirred for 3.5 h. Next, water (5 mL) was added and the mixture was extracted with CH_2Cl_2 (3 × 5 mL). The combined organic phases were washed with brine and concentrated under reduced pressure. Purification by silica gel column chromatography (cyclohexane/EtOAc, 1/1 v/v) provided **11** as an amber oil (167 mg, 0.48 mmol). Yield 81%; R_f = 0.36 (cyclohexane/EtOAc, 1/1 v/v); **^{1}H NMR** (600 MHz, DMSO-d_6) δ = 6.70−6.66 (m, 2H), 6.57 (d, J = 8.2 Hz, 1H), 4.21 (t, J = 4.4 Hz, 2H), 4.07 (s, 2H), 3.76 (t, J = 6.7 Hz, 2H), 3.43 (t, J = 4.4 Hz, 2H), 2.65 (t, J = 6.7 Hz, 2H), 2.03−1.95 (m, 2H), 1.37 (s, 9H), 0.89 (t, J = 7.4 Hz, 3H); **^{13}C NMR** (151 MHz, DMSO-d_6) δ = 173.1, 169.1, 143.6, 134.7, 130.9, 120.8, 118.9, 115.4, 111.8, 80.9, 64.3, 52.1, 46.9, 44.2, 27.7, 26.7, 15.9, 9.4. **LRMS (ESI)** m/z $[M + H]^+$ calcd for $C_{20}H_{27}N_3O_4$ 374.2, found 374.1.

Cell Culture. The human multiple myeloma cell line MM.1S (CRL-2974) was obtained from American Type Culture Collection (ATCC, Manassas, VA, USA) and the human acute monocytic leukemia cell line MV4−11 (ACC 102) was obtained from DSMZ (Leibniz Institute DSMZ-German Collection of Microorganisms and Cell Cultures GmbH, Hannover, Germany). MM.1S and MV4−11 cells were cultivated in RPMI 1640 medium (Catalog#21875-034, Gibco, ThermoFisher Scientific Inc., Waltham, MA, USA) supplemented with 10% FBS (PAN Biotech GmbH; Aidenbach, Germany), 100 IU/mL penicillin and 0.1 mg/mL streptomycin (PAN Biotech GmbH). The medium for the MM.1S cells contained additionally 1 mM sodium pyruvate (ThermoFisher Scientific Inc.). The human breast cancer cell line MDA-MB-231 (HTB-26) and the human malignant glioma cell line U-87MG were cultivated in DMEM medium (Catalog#41966-029, Gibco, ThermoFisher Scientific Inc.) supplemented with 10% FBS (PAN Biotech GmbH), 100 IU/mL penicillin and 0.1 mg/mL streptomycin (PAN Biotech GmbH). All cells were cultured at 37 °C in a 5% CO_2 atmosphere. Incubation times, as part of assay protocols, were performed under these conditions as well. The semiadherent MM.1S were detached mechanically by using a cell scraper and the adhered MDA-MB-132 were trypsinased by trypsin/EDTA (0.05%/0.02% in DPBS, PAN Biotech GmbH) whereas the U-87MG were detached by EDTA (0.46 g/L in DPBS, Catalog# P04-36500).

Simple Western Immunoassay. For the cell lysates, MM.1S (0.5 × 10^6 cells/mL), MV4−11 (1 × 10^6 cells/mL), MDA-MB-231 (0.18 × 10^6 cells/mL) or U-87MG (0.18 × 10^6 cells/mL) cells were seeded and incubated with the indicated concentration of compound or vehicle (DMSO) for the given time. The adherent cells were cultured for 24 h under cell culture conditions for attachment before treatment. Cell lysis was performed with Cell Extraction Buffer (10 mM Tris, pH 7.4, 100 mM NaCl, 1 mM EDTA, 1 mM EGTA, 1 mM NaF, 20 mM $Na_4P_2O_7$, 2 mM Na_3VO_4, 1% Triton× −100, 10% glycerol, 0.1% SDS, 0.5% deoxycholate; Catalog# FNN0011, Thermo Fisher Scientific Inc., Waltham, MA, USA) with addition of Halt Protease Inhibitor Cocktail (100×) (Catalog# 78429, Life Technologies GmbH, Carlsbad, CA, USA) and phenylmethanesulfonyl fluoride (Catalog# 10837091001, Sigma-Aldrich, St. Louis, MO, USA) according to manufacturer's instructions. Protein content was determined by Pierce BCA Protein Assay Kit (Catalog# 23225, Thermo Fisher Scientific Inc.) according to manufacturer's guidelines. Cell lysates were diluted to a final concentration of 1 mg/mL and denatured according to manufacturer's guidelines. Anti-HDAC1 (Catalog# 5356S, Cell Signaling Technology, Denver, MA, USA), anti-HDAC6 (Catalog#7558S, Cell Signaling Technology) and anti-GAPDH (Catalog# 2118S, Cell Signaling Technology) antibodies were used in a dilution from 1:50−1:1250. The 12−230 kDa Fluorescence Separation 8 × 25 Capillary Cartridges (Catalog# SM-FL004-1, Protein Simple, Bio-Techne, Minneapolis, MN, USA) were used for separation and the Anti-Mouse Detection Module (Catalog# DM-002, Protein Simple) was used for detection with addition of 20x Anti-Rabbit HRP Conjugate (Catalog# 043-426, Protein Simple) according to manufacturer's instructions. The assay was performed with the Jess Simple Western System (catalog# 004-650, Protein Simple), according to manufacturer's settings. Evaluation and quantification was performed with the compass software (6.2.0, Protein Simple). GAPDH intensity was used as loading control. GraphPad Prism (GraphPad Software, San Diego, CA, USA) was used for normalization, statistical analysis, and bar graph creation. Significance testing was performed with a one-way analysis of variance (ANOVA). Half maximal degradation concentration (DC_{50}) was determined by plotting dose response curves and nonlinear regression. Dunnett's posthoc test was employed to obtain significance levels of each mean compared to a reference mean value.

CellTiter-Glo Cell Viability Assay. For the cell viability assay the automated pipetting robot system ASSIST PLUS (Model# 4505, Integra Biosciences, Bibertal, Germany) was used. MM.1S (2.5 × 10^3 cells/well) or MV4−11 (4 × 10^3 cells/well) were seeded in white 384-well plates (Greiner Bio-One, Kremsmuenster, Austria, #781080). The cells were incubated with the respective compounds in increasing concentrations. For this purpose, the dilution series were prepared in 200-fold concentration in DMSO and further diluted to 10-fold concentration in medium. The final DMSO concentration was 0.5%. The toxicity of compounds was determined after 72 h using the CellTiter-Glo 2.0 Cell Viability Assay (Promega, Madison, WI, USA, #G9242) according to the manufacturer's protocol. Subsequently, the luminescence was measured using a Tecan Spark (Tecan Group AG, Maennedorf, Swiss) and the half maximal effective concentration (EC_{50}) was determined by plotting dose response curves and nonlinear regression with GraphPad Prism (GraphPad Software, San Diego, CA, USA).

Immunoblot. The cell lysis was performed as descripted in Simple Western Immunoassay. Samples were denatured by Laemmli 2× Concentrate (Catalog# S3401-10VL, Sigma-Aldrich) for 5 min at 95 °C, and Precision Plus Protein Unstained Standard was used as molecular weight marker (Catalog# 1610363, Bio-Rad, Hercules, CA, USA). SDS-PAGE was performed with 10 or 12% Mini-PROTEAN TGX Stain-Free Gel (Catalog# 458035, Bio-Rad) at 200 V for 50 min (Catalog# 458035, Bio-Rad). Afterward, proteins were transferred with the Trans-Blot Turbo Transfer System (Catalog# 1704150, Bio-Rad) to Immobilon-FL PVDF membranes (Catalog# IPFL00005, Millipore Merck, Burlington, MA, USA) at 1.0 A for 30 min. After detection of the total protein by the ChemiDoc XRS+ System (Catalog# 1708265, Bio-Rad), the membranes were treated with 5% milk-powder solution for 1 h at room temperature under slight agitation. Subsequently, the

https://doi.org/10.1021/acs.jmedchem.4c02569
J. Med. Chem. 2025, 68, 1824−1843

membranes were treated with anti-HDAC1 (Catalog# 5356S, Cell Signaling Technology), anti-HDAC2 (Catalog# sc-9959, Santa Cruz Biotechnology, Dallas, TX, USA), anti-HDAC3 (Catalog# 85057S, Cell Signaling Technology), anti-HDAC4 (Catalog#7628S, Cell Signaling Technology), anti-HDAC6 (Catalog#7558S, Cell Signaling Technology), anti-HDAC8-(Catalog#66042S, Cell Signaling Technology), antiacetyl-histone H3 (Lys9/Lys14) (Catalog# 9677S, Cell Signaling Technology), antiacetyl-α-tubulin (Catalog#5335, Cell Signaling Technology) or anti-GAPDH (Catalog# 2118S, Cell Signaling Technology) antibody solutions in 1:1000−1:8000 dilutions at 4 °C, overnight. Treatment with HRP-conjugated secondary antimouse (Catalog# 1030−05, SouthernBiotech, Birminham, AL, USA) and antirabbit (Catalog# 4030-05, SouthernBiotech) antibody solution was performed for 1.5 h, and membranes were developed with clarity western ECL substrate (Catalog# 1705061, Bio-Rad). The ChemiDoc XRS+ System was used for detection and Image Lab Software 6.1 (Bio-Rad) for quantification. The total protein intensity was used as a loading control. GraphPad Prism (GraphPad Software) was used for normalization, statistical analysis, and bar graph creation. Significance testing was performed with a one-way analysis of variance (ANOVA). Dunnett's posthoc test was employed to obtain significance levels of each mean compared to a reference mean value.

HDAC Enzyme Inhibition Assay. *In vitro* inhibitory activities against HDAC1, 2 and HDAC6 were measured using a previously published protocol.[48] *In vitro* inhibitory activities against HDAC4 were measured using a previously published protocol with slight modifications.[49] For test compounds and controls, serial dilutions of the respective DMSO stock solution in DMSO were prepared, and 1.0 μL/well of this serial dilution were transferred into OptiPlate-96 black microplates (PerkinElmer, Waltham, MN, USA). A volume of 4 μL/well assay buffer (50 mM Tris−HCl, pH 8.0, 137 mM NaCl, 2.7 mM KCl, 1.0 mM $MgCl_2 \cdot 6H_2O$, 0.1 mg/mL BSA) was added. In the case of HDAC1, 2 and HDAC6, a volume of 35 μL/well of the fluorogenic substrate ZMAL (Z- Lys(Ac)-AMC,[50] 21.43 μM in assay buffer) and 10 μL/well enzyme solution were added. In the case of HDAC4, 35 μL/well of the fluorogenic substrate Boc-Lys(Tfa)-AMC (42.86 μM in assay buffer, Catalog# 4060676, Bachem, Budendorf, Swiss) were added, followed by 10 μL/well of enzyme solution. Human recombinant HDAC1 (Catalog# 50051, BPS Bioscience, San Diego, CA, USA), HDAC2 (Catalog# 50052, BPS Bioscience), HDAC4 (Catalog# 50004, BPS Bioscience), or HDAC6 (Catalog# 50006, BPS Bioscience) were used. The total assay volume of 50 μL (max. 2% DMSO) was incubated at 37 °C for 90 min. Subsequently, 50 μL/well of trypsin (0.4 mg/mL) in trypsin buffer (50 mM Tris−HCl, pH 8.0, 100 mM NaCl) was added, followed by additional 30 min of incubation at 37 °C. Fluorescence (excitation λ = 355 nm, emission λ = 460 nm) was measured using a FLUOstar OPTIMA microplate reader (BMG labtech, Ortenburg, Germany). The half maximal inhibitory concentration (IC_{50}) was determined by plotting dose response curves and nonlinear regression with GraphPad Prism (GraphPad Software).

MTT Cell Viability Assay. U-87MG cells (3×10^3 cells/well) or MDA-MB-231 cells (5×10^3 cells/well) respectively were seeded in 96-well flat-bottomed plates. After 24 h the cells were incubated with the stock solutions of the respective compounds dissolved in DMSO (highest DMSO concentration, 0.5%) to reach the final concentrations as indicated. Controls received DPBS or DMSO. Following a 71 h incubation period 20 μL of a freshly prepared 5 mg/mL MTT (3-(4,5-dimethylthiazol-2-yl)-2,5-diphenyltetrazolium bromide, AppliChem GmbH, Darmstadt, Germany) solution were added into each well. The supernatant was discarded after 1 h incubation at 37 °C and the precipitated formazan was dissolved in 200 μL DMSO/well. Absorption was measured at 570 nm with background subtraction at 690 nm using a photometric microplate reader (Thermo Scientific Multiskan EX, Thermo Fisher Scientific). Data was further subtracted by the DMSO control and normalized on DPBS. The half-maximal effective concentration (EC_{50}) was determined by plotting dose response curves and nonlinear regression with GraphPad Prism (GraphPad Software).

Cell Cycle Analysis. MM.1S cells (3×10^3 cells/mL) were seeded in 12 well plates (Starlab GmbH, Hamburg, Germany) and incubated with the indicated concentration of compound or vehicle (DMSO) for 48 h under cell culture conditions. Subsequently, the cells were washed with DPBS (Catalog# P04-36500, PAN Biotech), resuspended in 1 mL EtOH/DPBS (7/3 v/v), and fixed for 30 min at 4 °C. The samples were rehydrated with DPBS and treated with 5 μg/mL RNase (Catalog# EN0531, ThermoFisher Scientific Inc.) for 15 min at room temperature. The staining was performed with 3 μM propidium iodide (in DPBS) for 15 min at room temperature and analyzed by flow cytometry (Guava easyCyteTM, Luminex, Austin, TX, USA). The data was analyzed by FlowJo v10.5.3 Software (BD Life Sciences, Franklin Lakes, NJ, USA), using the Watson Pragmatic algorithm.[51] GraphPad Prism (GraphPad Software) was used for normalization, statistical analysis, and bar graph creation. Significance testing was performed with a one-way analysis of variance (ANOVA). Dunnett's posthoc test was employed to obtain significance levels of each mean compared to a reference mean value.

Annexin V/PI Assay. To determine apoptosis, MM1.S cells (0.5×10^6 cells/mL) were seeded in sterile 24-well plates (CytoOne, Hamburg, Germany) and incubated for 48 h at 37 °C and 5% CO_2 under humidified air with 10 μM of the respective compounds or vehicle control (DMSO). Final DMSO concentration was 0.1%. After 48 h, cells were washed with ice-cold DPBS, diluted in 100 μL staining buffer (HEPES 0.01 M, NaCl 0.14 M, $CaCl_2 \times 2\ H_2O$ 2.5 mM) and transferred to a 96 well plate. Staining was performed with 5 μL FITC Annexin V (Catalog#640945, Biolegend, San Diego, CA, USA) and 10 μL of propidium iodide (Catalog#421301, Biolegend) per well. Fluorescence was measured by flow cytometry (Guava easyCyteTM, Luminex, Austin, Texas). GraphPad Prism (GraphPad Software) was used for normalization, statistical analysis, and bar graph creation. Significance testing was performed with a one-way analysis of variance (ANOVA). Dunnett's posthoc test was employed to obtain significance levels of each mean compared to a reference mean value.

Clonogenic Growth Assay. Five $\times 10^5$ MDA-MB-231 cells were seeded into T25 cell culture flasks and stimulated with 10 μM of respective compounds or vehicle (0.7% DMSO) for 48 h. Subsequently, cells were harvested and plated in 6-well plates at a density of 750 cells per well in triplicates. The cell culture medium was changed after 5 days. Nine days after plating, the colonies were carefully washed with 500 μL DPBS and stained with 500 μL crystal violet solution (0.5% in Methanol). After 30 min of incubation at room temperature, the wells were gently rinsed with deionized water. After counting the formed colonies, GraphPad Prism (GraphPad Software) was used for bar graph

https://doi.org/10.1021/acs.jmedchem.4c02569
J. Med. Chem. 2025, 68, 1824−1843

creation. Significance testing was performed with a one-way analysis of variance (ANOVA). Dunnett's post-hoc test was employed to obtain significance levels of each mean compared to a reference mean value.

Proteomics Screen. *Sample Preparation LFQ Quantitative Mass Spectrometry.* Cells were lysed by addition of lysis buffer (8 M Urea, 50 mM NaCl, 50 mM 4-(2-hydroxyethyl)-1-piperazineethanesulfonic acid (EPPS) pH 8.5, Protease and Phosphatase inhibitors) and homogenization by bead beating (BioSpec) for three repeats of 30 at 2400 strokes/min. Bradford assay was used to determine the final protein concentration in the clarified cell lysate. Fifty micrograms of protein for each sample was reduced, alkylated and precipitated using methanol/chloroform as previously described[52] and the resulting washed precipitated protein was allowed to air-dry. Precipitated protein was resuspended in 4 M urea, 50 mM HEPES pH 7.4, followed by dilution to 1 M urea with the addition of 200 mM EPPS, pH 8. Proteins were digested with the addition of LysC (1:50; enzyme:protein) and trypsin (1:50; enzyme:protein) for 12 h at 37 °C. Sample digests were acidified with formic acid to a pH of 2−3 before desalting using C18 solid phase extraction plates (SOLA, Thermo Fisher Scientific). Desalted peptides were dried in a vacuum-centrifuged and reconstituted in 0.1% formic acid for liquid chromatography−mass spectrometry analysis.

Data were collected using a TimsTOF HT (Bruker Daltonics, Bremen, Germany) coupled to a nano-Elute LC pump (Bruker Daltonics, Bremen, Germany) via a CaptiveSpray nano-electrospray source. Peptides were separated on a reversed-phase C18 column (25 cm × 75 μm ID, 1.6 μM, IonOpticks, Australia) containing an integrated captive spray emitter. Peptides were separated using a 50 min gradient of 2−30% buffer (acetonitrile in 0.1% formic acid) with a flow rate of 250 nL/min and column temperature maintained at 50 °C.

The TIMS elution voltages were calibrated linearly with three points (Agilent ESI-L Tuning Mix Ions; 622, 922, 1,222 m/z) to determine the reduced ion mobility coefficients ($1/K_0$). To perform diaPASEF, we used py_diAID,[53] a python package, to assess the precursor distribution in the m/z-ion mobility plane to generate a diaPASEF acquisition scheme with variable window isolation widths that are aligned to the precursor density in m/z. Data was acquired using 20 cycles with three mobility window scans each (creating 60 windows) covering the diagonal scan line for doubly and triply charged precursors, with singly charged precursors able to be excluded by their position in the m/z-ion mobility plane. These precursor isolation windows were defined between 350−1250 m/z and $1/k_0$ of 0.6−1.45 V × s/cm^2.

LC-MS Data Analysis. The diaPASEF raw file processing and controlling peptide and protein level false discovery rates, assembling proteins from peptides, and protein quantification from peptides were performed using library free analysis in DIA-NN 1.8.[54] Library free mode performs an *in silico* digestion of a given protein sequence database alongside deep learning-based predictions to extract the DIA precursor data into a collection of MS2 spectra. The search results are then used to generate a spectral library which is then employed for the targeted analysis of the DIA data searched against a Swissprot human database (January 2021). Database search criteria largely followed the default settings for directDIA including: tryptic with two missed cleavages, carbamidomethylation of cysteine, and oxidation of methionine and precursor Q-value (FDR) cutoff of 0.01. Precursor quantification strategy was set to Robust LC (high accuracy) with RT-dependent cross run normalization. Proteins with low sum of abundance (<2,000 × no. of treatments) were excluded from further analysis and resulting data was filtered to only include proteins that had a minimum of 3 counts in at least 4 replicates of each independent comparison of treatment sample to the DMSO control. Protein abundances were scaled using in-house scripts in the R framework (R Development Core Team, 2014) and proteins with missing values were imputed by random selection from a Gaussian distribution either with a mean of the nonmissing values for that treatment group or with a mean equal to the median of the background (in cases when all values for a treatment group are missing). Significant changes comparing the relative protein abundance of these treatment to DMSO control comparisons were assessed by moderated t test as implemented in the limma package within the R framework.[55] GraphPad Prism (GraphPad Software) was used for dot plot creation.

■ ASSOCIATED CONTENT

Supporting Information

The Supporting Information is available free of charge at https://pubs.acs.org/doi/10.1021/acs.jmedchem.4c02569.

Supplementary Figures and Schemes, ^{1}H NMR, ^{13}C NMR, and HPLC data (PDF)

Molecular strings formula (CSV)

■ AUTHOR INFORMATION

Corresponding Author

Finn K. Hansen − *Department of Pharmaceutical and Cell Biological Chemistry, Pharmaceutical Institute, University of Bonn institution, Bonn 53121, Germany;* orcid.org/0000-0001-9765-5975; Email: finn.hansen@uni-bonn.de

Authors

Felix Feller − *Department of Pharmaceutical and Cell Biological Chemistry, Pharmaceutical Institute, University of Bonn institution, Bonn 53121, Germany;* orcid.org/0009-0007-1820-772X

Irina Honin − *Department of Pharmaceutical and Cell Biological Chemistry, Pharmaceutical Institute, University of Bonn institution, Bonn 53121, Germany*

Martina Miranda − *Department of Pharmaceutical and Cell Biological Chemistry, Pharmaceutical Institute, University of Bonn institution, Bonn 53121, Germany*

Heiko Weber − *Department of Pharmaceutical and Cell Biological Chemistry, Pharmaceutical Institute, University of Bonn institution, Bonn 53121, Germany*

Svenja Henze − *Department of Pharmaceutical and Cell Biological Chemistry, Pharmaceutical Institute, University of Bonn institution, Bonn 53121, Germany*

Maria Hanl − *Department of Pharmaceutical and Cell Biological Chemistry, Pharmaceutical Institute, University of Bonn institution, Bonn 53121, Germany*

Complete contact information is available at: https://pubs.acs.org/10.1021/acs.jmedchem.4c02569

Author Contributions

The manuscript was written through contributions of all authors. All authors have given approval to the final version of the manuscript.

Funding

Funding by the Deutsche Forschungsgemeinschaft (DFG, German Research Foundation)−GRK2873 (494832089) is gratefully acknowledged.

Notes

Global proteomics data will be publicly available at the Fischer Lab's Proteomics database: https://proteomics.fischerlab.org:wp-esf_579/580−FF2049

The authors declare no competing financial interest.

■ ACKNOWLEDGMENTS

We thank Katherine A. Donovan, Eric S. Fischer and the Fischer Lab Degradation Proteomics Initiative for collection of the global proteomics data supported by NIH CA214608 and CA218278. Marlene Scherer is gratefully acknowledged for experimental support. The TOC graphic and Figure 1 were created with BioRender.

■ ABBREVIATIONS

2-CTC resin, 2-Chlorotrityl resin; APOE, Apolipoprotein E; BCR-ABL, Breakpoint cluster region protein − Abelson murine leukemia viral oncogene homologue fusions protein; BRD4, Bromodomain-containing protein 4; c-ABL, Abelson murine leukemia viral oncogene homologue; cIAP, Cellular inhibitor of apoptosis protein; CoREST, Co-repressor of REST; CRBN, Cereblon; CRL, Cullin RING ligase; CUL2, Cullin-2; DC_{50}, Half-maximal degradation concentration; DCAF11, DDB1- and CUL4-associated factor 11; DCAF16, DDB1- and CUL4-associated factor 16; diaPASEF, Data-independent acquisition of parallel accumulation-serial fragmentation; DIPEA, *N,N*-Diisopropylethylamine; D_{max}, Maximal degradation; DMF, Dimethylformamide; DMSO, Dimethyl sulfoxide; DNA, Deoxyribonucleic acid; EC_{50}, Half maximal effective concentration; FDA, U.S. Food and Drug Administration; FEM1B, Fem-1 homologue B; FITC, Fluorescein isothiocyanate; GAPDH, Glyceraldehyde 3-phosphate dehydrogenase; HATU, Hexafluorophosphate azabenzotriazole tetramethyl uronium; HDAC, histone deacetylase; HDACi, histone deacetylase inhibitor; HOBt, Hydroxybenzotriazole; HPLC, High-performance liquid chromatography; IC_{50}, Half maximal inhibitory concentration; KDM1A, Lysine (K)-specific demethylase 1A; LRRC37A2, Leucine-rich repeat-containing protein 37A2; LSD1, Lysine-specific histone demethylase 1; MDA-MB-231, M.D. Anderson-Metastatic Breast-231, human breast cancer cell line; MIER, mesoderm induction early response; MIER1, mesoderm induction early response protein 1; MLN, MLN4924, neddylation inhibitor; MM.1S, Multiple myeloma steroid sensitive cell line; MV4−11, acute monocytic leukemia cell line; NCoR, Nuclear receptor corepressor; NCOR1, nuclear receptor corepressor 1; PEG, polyethylene glycol; PI, propidium iodide; POI, protein of interest; PPI, protein−protein interaction; PROTAC, proteolysis targeting chimera; RCOR1 and 3, REST corepressor 1 and 3; RNF4, Ring Finger Protein 4; RNF114, Ring Finger Protein 114; rt, room temperature; SAHA, suberoylanilide hydroxamic acid, or vorinostat; SIN3, switch-independent 3; SIN3A, SIN3 homologue A; SMRT, silencing mediator for retinoid and thyroid hormone receptor; TFA, trifluoracetic acid; TPD, targeted protein degradation; U-87MG, Uppsala 87 Malignant Glioma cell line; UBE2G1, ubiquitin-conjugating enzyme E2 G1; UPS, ubiquitin-proteasome system; VHL, Von Hippel-Lindau

■ REFERENCES

(1) Bond, M. J.; Crews, C. M. Proteolysis Targeting Chimeras (PROTACs) Come of Age: Entering the Third Decade of Targeted Protein Degradation. *RSC Chem. Biol.* **2021**, *2* (3), 725−742.

(2) Li, K.; Crews, C. M. PROTACs: Past, Present and Future. *Chem. Soc. Rev.* **2022**, *51* (12), 5214−5236.

(3) Burslem, G. M.; Crews, C. M. Proteolysis-Targeting Chimeras as Therapeutics and Tools for Biological Discovery. *Cell* **2020**, *181* (1), 102−114.

(4) Zheng, N.; Shabek, N. Ubiquitin Ligases: Structure, Function, and Regulation. *Annu. Rev. Biochem.* **2017**, *86* (1), 129−157.

(5) Komander, D.; Rape, M. The Ubiquitin Code. *Annu. Rev. Biochem.* **2012**, *81* (1), 203−229.

(6) Bondeson, D. P.; Mares, A.; Smith, I. E. D.; Ko, E.; Campos, S.; Miah, A. H.; Mulholland, K. E.; Routly, N.; Buckley, D. L.; Gustafson, J. L.; Zinn, N.; Grandi, P.; Shimamura, S.; Bergamini, G.; Faelth-Savitski, M.; Bantscheff, M.; Cox, C.; Gordon, D. A.; Willard, R. R.; Flanagan, J. J.; Casillas, L. N.; Votta, B. J.; Den Besten, W.; Famm, K.; Kruidenier, L.; Carter, P. S.; Harling, J. D.; Churcher, I.; Crews, C. M. Catalytic in Vivo Protein Knockdown by Small-Molecule PROTACs. *Nat. Chem. Biol.* **2015**, *11* (8), 611−617.

(7) Salami, J.; Alabi, S.; Willard, R. R.; Vitale, N. J.; Wang, J.; Dong, H.; Jin, M.; McDonnell, D. P.; Crew, A. P.; Neklesa, T. K.; et al. Androgen Receptor Degradation by the Proteolysis-Targeting Chimera ARCC-4 Outperforms Enzalutamide in Cellular Models of Prostate Cancer Drug Resistance. *Commun. Biol.* **2018**, *1* (1), 100.

(8) Alabi, S. B.; Crews, C. M. Major Advances in Targeted Protein Degradation: PROTACs, LYTACs, and MADTACs. *J. Biol. Chem.* **2021**, *296*, 100647.

(9) Alabi, S.; Jaime-Figueroa, S.; Yao, Z.; Gao, Y.; Hines, J.; Samarasinghe, K. T. G.; Vogt, L.; Rosen, N.; Crews, C. M. Mutant-Selective Degradation by BRAF-Targeting PROTACs. *Nat. Commun.* **2021**, *12* (1), 920.

(10) Yang, K.; Song, Y.; Xie, H.; Wu, H.; Wu, Y.-T.; Leisten, E. D.; Tang, W. Development of the First Small Molecule Histone Deacetylase 6 (HDAC6) Degraders. *Bioorg. Med. Chem. Lett.* **2018**, *28* (14), 2493−2497.

(11) Sinatra, L.; Yang, J.; Schliehe-Diecks, J.; Dienstbier, N.; Vogt, M.; Gebing, P.; Bachmann, L. M.; Sönnichsen, M.; Lenz, T.; Stühler, K.; Schöler, A.; Borkhardt, A.; Bhatia, S.; Hansen, F. K. Solid-Phase Synthesis of Cereblon-Recruiting Selective Histone Deacetylase 6 Degraders (HDAC6 PROTACs) with Antileukemic Activity. *J. Med. Chem.* **2022**, *65* (24), 16860−16878.

(12) Keuler, T.; König, B.; Bückreiß, N.; Kraft, F. B.; König, P.; Schäker-Hübner, L.; Steinebach, C.; Bendas, G.; Gütschow, M.; Hansen, F. K. Development of the First Non-Hydroxamate Selective HDAC6 Degraders. *Chem. Commun.* **2022**, *58* (79), 11087−11090.

(13) Smalley, J. P.; Baker, I. M.; Pytel, W. A.; Lin, L.-Y.; Bowman, K. J.; Schwabe, J. W. R.; Cowley, S. M.; Hodgkinson, J. T. Optimization of Class I Histone Deacetylase PROTACs Reveals That HDAC1/2 Degradation Is Critical to Induce Apoptosis and Cell Arrest in Cancer Cells. *J. Med. Chem.* **2022**, *65* (7), 5642−5659.

(14) Ho, T. C. S.; Chan, A. H. Y.; Ganesan, A. Thirty Years of HDAC Inhibitors: 2020 Insight and Hindsight. *J. Med. Chem.* **2020**, *63* (21), 12460−12484.

(15) Bates, S. E. Epigenetic Therapies for Cancer. *N. Engl. J. Med.* **2020**, *383* (7), 650−663.

(16) Mithraprabhu, S.; Kalff, A.; Chow, A.; Khong, T.; Spencer, A. Dysregulated Class I Histone Deacetylases Are Indicators of Poor Prognosis in Multiple Myeloma. *Epigenetics* **2014**, *9* (11), 1511−1520.

(17) Minamiya, Y.; Ono, T.; Saito, H.; Takahashi, N.; Ito, M.; Motoyama, S.; Ogawa, J. Strong Expression of HDAC3 Correlates with a Poor Prognosis in Patients with Adenocarcinoma of the Lung. *Tumour Biol.* **2010**, *31* (5), 533−539.

(18) Bradbury, C. A.; Khanim, F. L.; Hayden, R.; Bunce, C. M.; White, D. A.; Drayson, M. T.; Craddock, C.; Turner, B. M. Histone Deacetylases in Acute Myeloid Leukaemia Show a Distinctive Pattern of Expression That Changes Selectively in Response to Deacetylase Inhibitors. *Leukemia* **2005**, *19* (10), 1751−1759.

(19) Li, Y.; Seto, E. HDACs and HDAC Inhibitors in Cancer Development and Therapy. *Cold Spring Harb. Perspect. Med.* **2016**, *6* (10), 1−34.

https://doi.org/10.1021/acs.jmedchem.4c02569
J. Med. Chem. 2025, 68, 1824−1843

(20) Witt, O.; Deubzer, H. E.; Milde, T.; Oehme, I. HDAC Family: What Are the Cancer Relevant Targets? *Cancer Lett.* **2009**, *277* (1), 8−21.
(21) Krieger, V.; Hamacher, A.; Cao, F.; Stenzel, K.; Gertzen, C. G. W.; Schäker-Hübner, L.; Kurz, T.; Gohlke, H.; Dekker, F. J.; Kassack, M. U.; Hansen, F. K. Synthesis of Peptoid-Based Class I-Selective Histone Deacetylase Inhibitors with Chemosensitizing Properties. *J. Med. Chem.* **2019**, *62* (24), 11260−11279.
(22) Mullard, A. FDA Approves an HDAC Inhibitor for Duchenne Muscular Dystrophy. *Nat. Rev. Drug Discovery* **2024**, *23* (5), 329.
(23) Rai, S.; Kim, W. S.; Ando, K.; Choi, I.; Izutsu, K.; Tsukamoto, N.; Yokoyama, M.; Tsukasaki, K.; Kuroda, J.; Ando, J.; Hidaka, M.; Koh, Y.; Shibayama, H.; Uchida, T.; Yang, D. H.; Ishitsuka, K.; Ishizawa, K.; Kim, J. S.; Lee, H. G.; Minami, H.; Eom, H. S.; Kurosawa, M.; Lee, J. H.; Lee, J. S.; Lee, W. S.; Nagai, H.; Shindo, T.; Yoon, D. H.; Yoshida, S.; Gillings, M.; Onogi, H.; Tobinai, K. Oral HDAC Inhibitor Tucidinostat in Patients with Relapsed or Refractory Peripheral T-Cell Lymphoma: Phase IIb Results. *Haematologica* **2023**, *108* (3), 811−821.
(24) Suo, J.; Zhu, K.; Zhuang, C.; Zhong, X.; Bravaccini, S.; Maltoni, R.; Bertucci, F.; Zheng, H.; Luo, T. Efficacy and Safety of Tucidinostat in Patients with Advanced Hormone Receptor-Positive Human Epidermal Growth Factor Receptor 2-Negative Breast Cancer: Real-World Insights. *Ann. Transl. Med.* **2023**, *11* (12), 409−409.
(25) Li, W.; Bengtson, M. H.; Ulbrich, A.; Matsuda, A.; Reddy, V. A.; Orth, A.; Chanda, S. K.; Batalov, S.; Joazeiro, C. A. P. Genome-Wide and Functional Annotation of Human E3 Ubiquitin Ligases Identifies MULAN, a Mitochondrial E3 That Regulates the Organelle's Dynamics and Signaling. *PLoS One* **2008**, *3* (1), No. e1487.
(26) Weng, G.; Cai, X.; Cao, D.; Du, H.; Shen, C.; Deng, Y.; He, Q.; Yang, B.; Li, D.; Hou, T. PROTAC-DB 2.0: An Updated Database of PROTACs. *Nucleic Acids Res.* **2023**, *51* (D1), D1367−D1372.
(27) Békés, M.; Langley, D. R.; Crews, C. M. PROTAC Targeted Protein Degraders: The Past Is Prologue. *Nat. Rev. Drug Discovery* **2022**, *21* (3), 181−200.
(28) Hughes, S. J.; Testa, A.; Thompson, N.; Churcher, I. The Rise and Rise of Protein Degradation: Opportunities and Challenges Ahead. *Drug Discovery Today* **2021**, *26* (12), 2889−2897.
(29) Ottis, P.; Palladino, C.; Thienger, P.; Britschgi, A.; Heichinger, C.; Berrera, M.; Julien-Laferriere, A.; Roudnicky, F.; Kam-Thong, T.; Bischoff, J. R.; et al. Cellular Resistance Mechanisms to Targeted Protein Degradation Converge Toward Impairment of the Engaged Ubiquitin Transfer Pathway. *ACS Chem. Biol.* **2019**, *14* (10), 2215−2223.
(30) Mayor-Ruiz, C.; Jaeger, M. G.; Bauer, S.; Brand, M.; Sin, C.; Hanzl, A.; Mueller, A. C.; Menche, J.; Winter, G. E. Plasticity of the Cullin-RING Ligase Repertoire Shapes Sensitivity to Ligand-Induced Protein Degradation. *Mol. Cell* **2019**, *75* (4), 849−858.E8.
(31) Zhang, L.; Riley-Gillis, B.; Vijay, P.; Shen, Y. Acquired Resistance to BET-PROTACs (Proteolysis-Targeting Chimeras) Caused by Genomic Alterations in Core Components of E3 Ligase Complexes. *Mol. Cancer Ther.* **2019**, *18* (7), 1302−1311.
(32) Ward, C. C.; Kleinman, J. I.; Brittain, S. M.; Lee, P. S.; Chung, C. Y. S.; Kim, K.; Petri, Y.; Thomas, J. R.; Tallarico, J. A.; McKenna, J. M.; Schirle, M.; Nomura, D. K. Covalent Ligand Screening Uncovers a RNF4 E3 Ligase Recruiter for Targeted Protein Degradation Applications. *ACS Chem. Biol.* **2019**, *14* (11), 2430−2440.
(33) Spradlin, J. N.; Hu, X.; Ward, C. C.; Brittain, S. M.; Jones, M. D.; Ou, L.; To, M.; Proudfoot, A.; Ornelas, E.; Woldegiorgis, M.; Olzmann, J. A.; Bussiere, D. E.; Thomas, J. R.; Tallarico, J. A.; McKenna, J. M.; Schirle, M.; Maimone, T. J.; Nomura, D. K. Harnessing the Anti-Cancer Natural Product Nimbolide for Targeted Protein Degradation. *Nat. Chem. Biol.* **2019**, *15* (7), 747−755.
(34) Zhang, X.; Luukkonen, L. M.; Eissler, C. L.; Crowley, V. M.; Yamashita, Y.; Schafroth, M. A.; Kikuchi, S.; Weinstein, D. S.; Symons, K. T.; Nordin, B. E.; Rodriguez, J. L.; Wucherpfennig, T. G.; Bauer, L. G.; Dix, M. M.; Stamos, D.; Kinsella, T. M.; Simon, G. M.; Baltgalvis, K. A.; Cravatt, B. F. DCAF11 Supports Targeted Protein Degradation by Electrophilic Proteolysis-Targeting Chimeras. *J. Am. Chem. Soc.* **2021**, *143* (13), 5141−5149.
(35) Zhang, X.; Crowley, V. M.; Wucherpfennig, T. G.; Dix, M. M.; Cravatt, B. F. Electrophilic PROTACs That Degrade Nuclear Proteins by Engaging DCAF16. *Nat. Chem. Biol.* **2019**, *15* (7), 737−746.
(36) Henning, N. J.; Manford, A. G.; Spradlin, J. N.; Brittain, S. M.; Zhang, E.; McKenna, J. M.; Tallarico, J. A.; Schirle, M.; Rape, M.; Nomura, D. K. Discovery of a Covalent FEM1B Recruiter for Targeted Protein Degradation Applications. *J. Am. Chem. Soc.* **2022**, *144* (2), 701−708.
(37) Kiely-Collins, H.; Winter, G. E.; Bernardes, G. J. L. The Role of Reversible and Irreversible Covalent Chemistry in Targeted Protein Degradation. *Cell Chem. Biol.* **2021**, *28* (7), 952−968.
(38) Feller, F.; Hansen, F. K. Targeted Protein Degradation of Histone Deacetylases by Hydrophobically Tagged Inhibitors. *ACS Med. Chem. Lett.* **2023**, *14* (12), 1863−1868.
(39) Sinatra, L.; Bandolik, J. J.; Roatsch, M.; Sönnichsen, M.; Schoeder, C. T.; Hamacher, A.; Schöler, A.; Borkhardt, A.; Meiler, J.; Bhatia, S.; Kassack, M. U.; Hansen, F. K. Hydroxamic Acids Immobilized on Resins (HAIRs): Synthesis of Dual-Targeting HDAC Inhibitors and HDAC Degraders (PROTACs). *Angew. Chem., Int. Ed.* **2020**, *59* (50), 22494−22499.
(40) Patel, U.; Smalley, J. P.; Hodgkinson, J. T. PROTAC Chemical Probes for Histone Deacetylase Enzymes. *RSC Chem. Biol.* **2023**, *4* (9), 623−634.
(41) Xiong, Y.; Donovan, K. A.; Eleuteri, N. A.; Kirmani, N.; Yue, H.; Razov, A.; Krupnick, N. M.; Nowak, R. P.; Fischer, E. S. Chemo-Proteomics Exploration of HDAC Degradability by Small Molecule Degraders. *Cell Chem. Biol.* **2021**, *28*, 1514−1527.e4.
(42) Yang, H.; Lv, W.; He, M.; Deng, H.; Li, H.; Wu, W.; Rao, Y. Plasticity in Designing PROTACs for Selective and Potent Degradation of HDAC6. *Chem. Commun.* **2019**, *55* (98), 14848−14851.
(43) Meier, F.; Brunner, A. D.; Frank, M.; Ha, A.; Bludau, I.; Voytik, E.; Kaspar-Schoenefeld, S.; Lubeck, M.; Raether, O.; Bache, N.; Aebersold, R.; Collins, B. C.; Röst, H. L.; Mann, M. DiaPASEF: Parallel Accumulation−Serial Fragmentation Combined with Data-Independent Acquisition. *Nat. Methods* **2020**, *17* (12), 1229−1236.
(44) Millard, C. J.; Watson, P. J.; Fairall, L.; Schwabe, J. W. R. Targeting Class I Histone Deacetylases in a "Complex" Environment. *Trends Pharmacol. Sci.* **2017**, *38* (4), 363−377.
(45) Wang, S.; Fairall, L.; Pham, T. K.; Ragan, T. J.; Vashi, D.; Collins, M. O.; Dominguez, C.; Schwabe, J. W. R. A Potential Histone-Chaperone Activity for the MIER1 Histone Deacetylase Complex. *Nucleic Acids Res.* **2023**, *51* (12), 6006−6019.
(46) Marks, P. A.; Breslow, R. Dimethyl Sulfoxide to Vorinostat: Development of This Histone Deacetylase Inhibitor as an Anticancer Drug. *Nat. Biotechnol.* **2007**, *25* (1), 84−90.
(47) Simu, S.; Marcovici, I.; Dobrescu, A.; Malita, D.; Dehelean, C. A.; Coricovac, D.; Olaru, F.; Draghici, G. A.; Navolan, D. Insights into the Behavior of Triple-Negative MDA-MB-231 Breast Carcinoma Cells Following the Treatment with 17β-Ethinylestradiol and Levonorgestrel. *Molecules* **2021**, *26* (9), 2776.
(48) Schäker-Hübner, L.; Warstat, R.; Ahlert, H.; Mishra, P.; Kraft, F. B.; Schliehe-Diecks, J.; Schöler, A.; Borkhardt, A.; Breit, B.; Bhatia, S.; Hügle, M.; Günther, S.; Hansen, F. K. 4-Acyl Pyrrole Capped HDAC Inhibitors: A New Scaffold for Hybrid Inhibitors of BET Proteins and Histone Deacetylases as Antileukemia Drug Leads. *J. Med. Chem.* **2021**, *64* (19), 14620−14646.
(49) Reßing, N.; Schliehe-Diecks, J.; Watson, P. R.; Sönnichsen, M.; Cragin, A. D.; Schöler, A.; Yang, J.; Schäker-Hübner, L.; Borkhardt, A.; Christianson, D. W.; Bhatia, S.; Hansen, F. K. Development of Fluorinated Peptoid-Based Histone Deacetylase (HDAC) Inhibitors for Therapy-Resistant Acute Leukemia. *J. Med. Chem.* **2022**, *65* (22), 15457−15472.
(50) Kraft, F. B.; Hanl, M.; Feller, F.; Schäker-Hübner, L.; Hansen, F. K. Photocaged Histone Deacetylase Inhibitors as Prodrugs in Targeted Cancer Therapy. *Pharmaceuticals* **2023**, *16* (3), 356.
(51) Watson, J. V.; Chambers, S. H.; Smith, P. J. A Pragmatic Approach to the Analysis of DNA Histograms with a Definable G1 Peak. *Cytometry* **1987**, *8* (1), 1−8.

https://doi.org/10.1021/acs.jmedchem.4c02569
J. Med. Chem. 2025, 68, 1824−1843

(52) Donovan, K. A.; An, J.; Nowak, R. P.; Yuan, J. C.; Fink, E. C.; Berry, B. C.; Ebert, B. L.; Fischer, E. S. Thalidomide Promotes Degradation of SALL4, a Transcription Factor Implicated in Duane Radial Ray Syndrome. *Elife* **2018**, *7*, No. e38430.
(53) Skowronek, P.; Thielert, M.; Voytik, E.; Tanzer, M. C.; Hansen, F. M.; Willems, S.; Karayel, O.; Brunner, A. D.; Meier, F.; Mann, M. Rapid and In-Depth Coverage of the (Phospho-) Proteome With Deep Libraries and Optimal Window Design for Dia-PASEF. *Mol. Cell. Proteomics* **2022**, *21* (9), 100279.
(54) Demichev, V.; Messner, C. B.; Vernardis, S. I.; Lilley, K. S.; Ralser, M. D.-N. DIA-NN: Neural networks and interference correction enable deep proteome coverage in high throughput. *Nat. Methods* **2020**, *17* (1), 41−44.
(55) Ritchie, M. E.; Phipson, B.; Wu, D.; Hu, Y.; Law, C. W.; Shi, W.; Smyth, G. K. Limma Powers Differential Expression Analyses for RNA-Sequencing and Microarray Studies. *Nucleic Acids Res.* **2015**, *43* (7), No. e47.

https://doi.org/10.1021/acs.jmedchem.4c02569
J. Med. Chem. 2025, 68, 1824−1843

Supplementary Information

Development of the First-in-Class FEM1B-Recruiting Histone Deacetylase Degraders

Felix Feller,[a] Irina Honin,[a] Martina Miranda,[a] Heiko Weber,[a] Svenja Henze,[a] Maria Hanl,[a]
Finn K. Hansen[a]*

[a]Department of Pharmaceutical and Cell Biological Chemistry, Pharmaceutical Institute, University of Bonn, An der Immenburg 4, 53121 Bonn, Germany.

*finn.hansen@uni-bonn.de

Table of contents

1. Supplementary Schemes and Figures

Scheme S1. Synthesis of FEM1B ligand according to literature known protocol[1] with slight modifications[a]

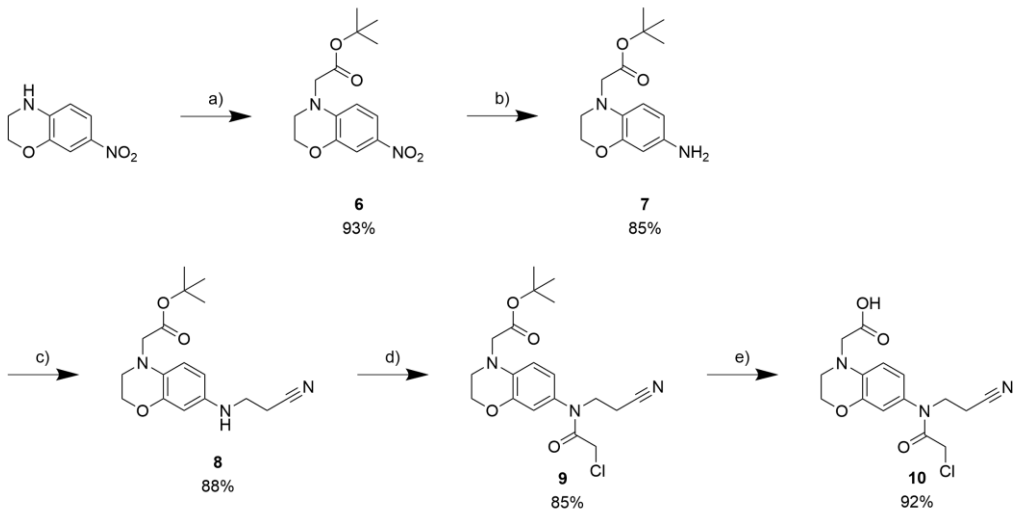

[a]*Reagents and conditions*: (a) *tert*-Butyl bromoacetate, NaH, DMF, 0 °C to rt, 2 h; (b) Fe, NH_4Cl, EtOH/H_2O (3/1 *v*/*v*), 80 °C, 20 h; (c) basic alumina, acrylonitrile, 80 °C, 20 h; (d) chloroacetyl chloride, triethylamine, CH_2Cl_2, 0 °C to rt, 30 min; (e) TFA, CH_2Cl_2, rt, 2 h.

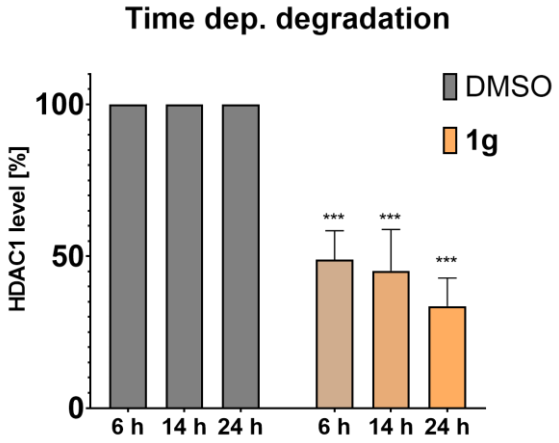

Figure S1. Time dependent degradation of HDAC1 by **1g**. Simple western™ immunoassay analysis of MM.1S cell lysates. MM.1S cells were treated for with **1g** (1 µM) or vehicle (DMSO) for the indicated incubation-time, presented as mean ± standard deviation of n = 3 biological replicates. Significance compared to vehicle: *** = p≤0.001.

2. NMR Data of compounds in biological testing

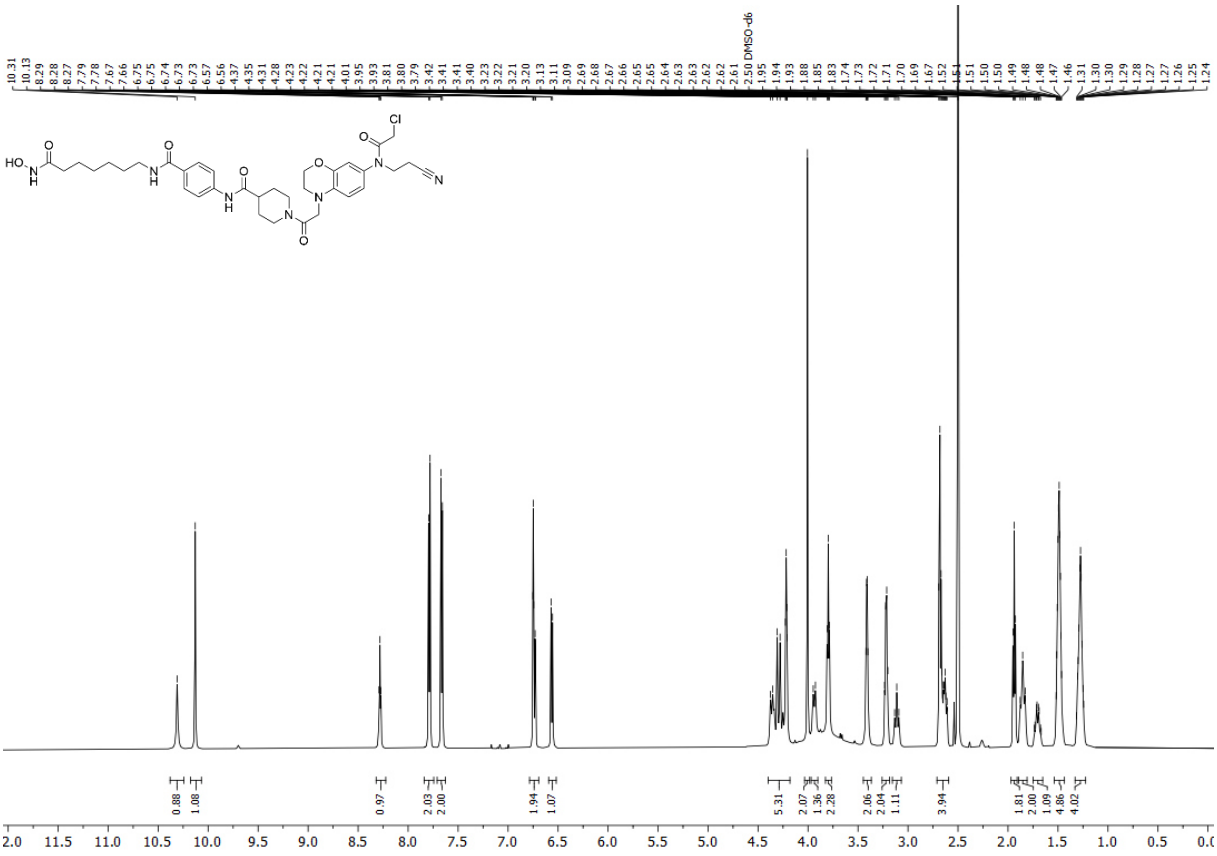

^{1}H NMR spectrum of **1a** (600 MHz, DMSO-d_6).

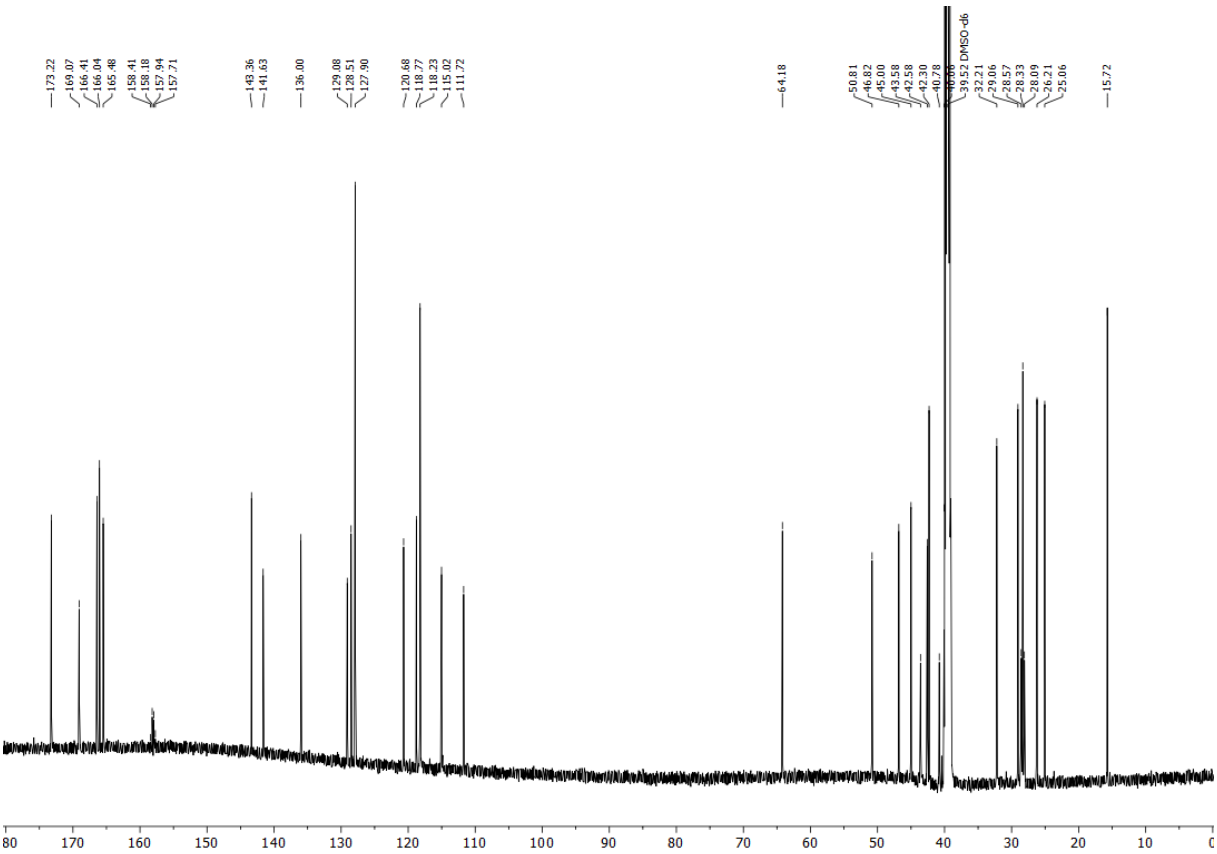

^{13}C NMR spectrum of **1a** (151 MHz, DMSO-d_6).

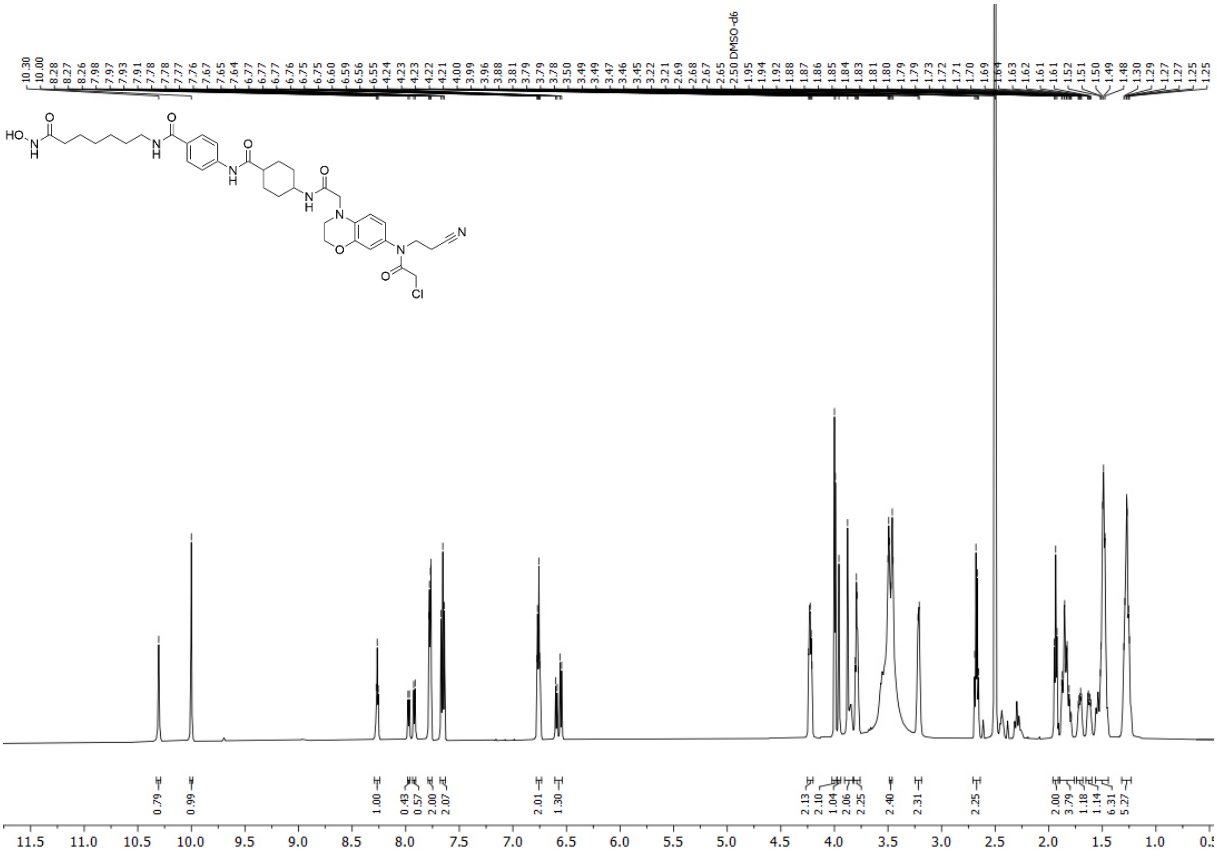

^{1}H NMR spectrum of **1b** (600 MHz, DMSO-d_6).

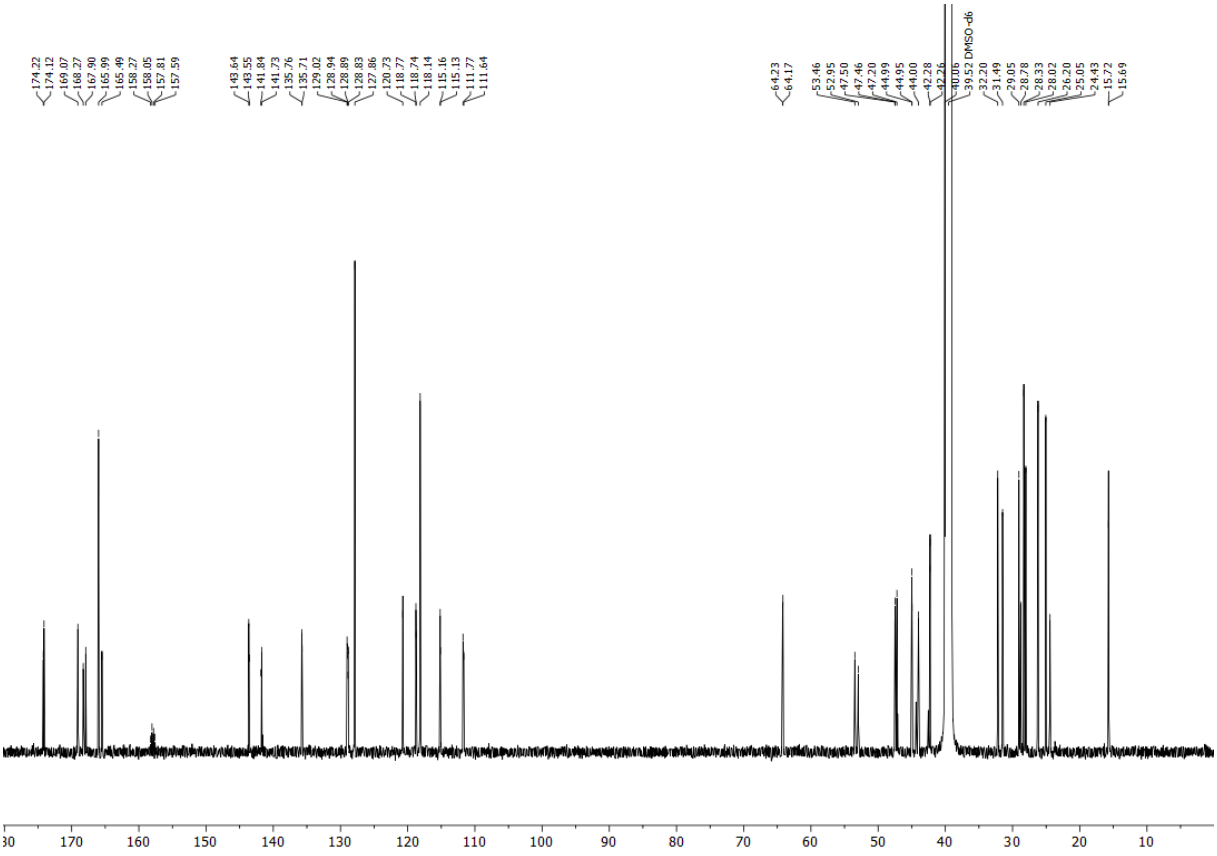

^{13}C NMR spectrum of **1b** (151 MHz, DMSO-d_6).

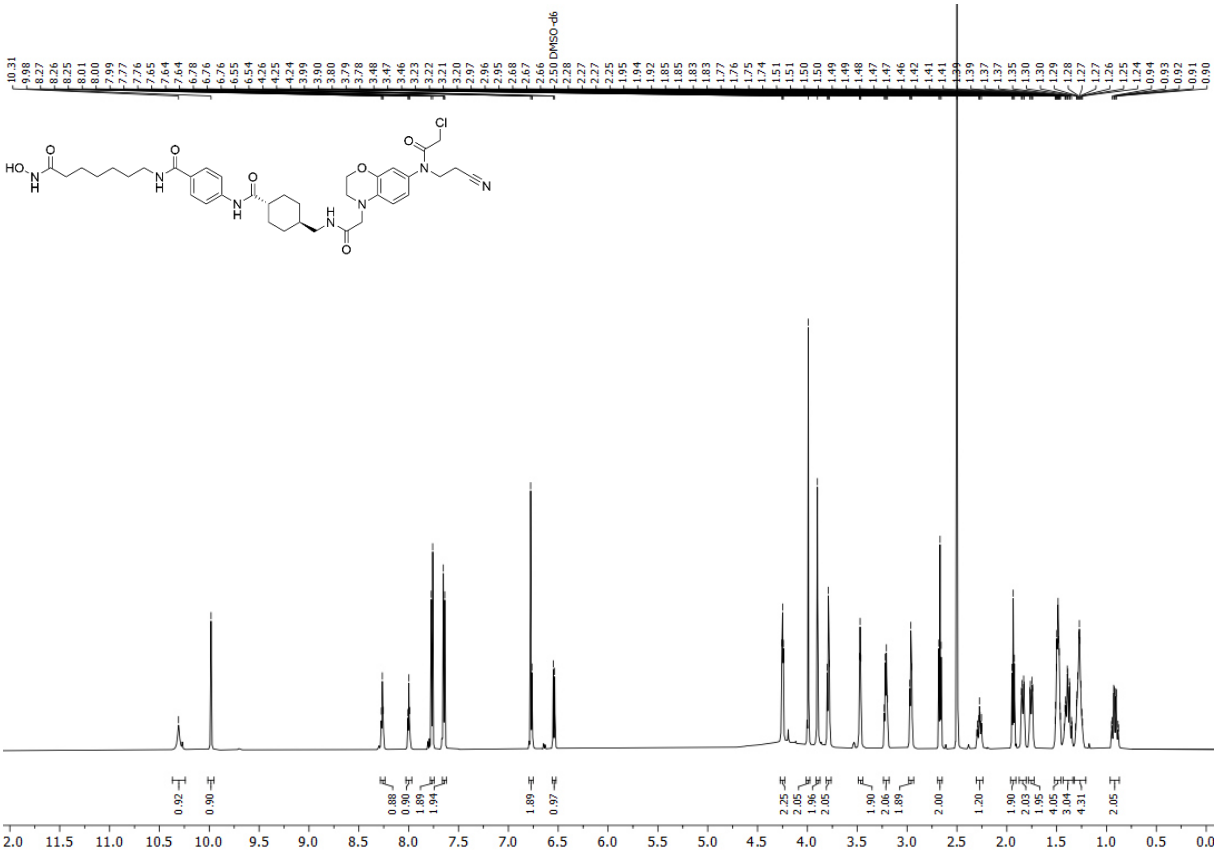

^{1}H NMR spectrum of **1c** (600 MHz, DMSO-d_6).

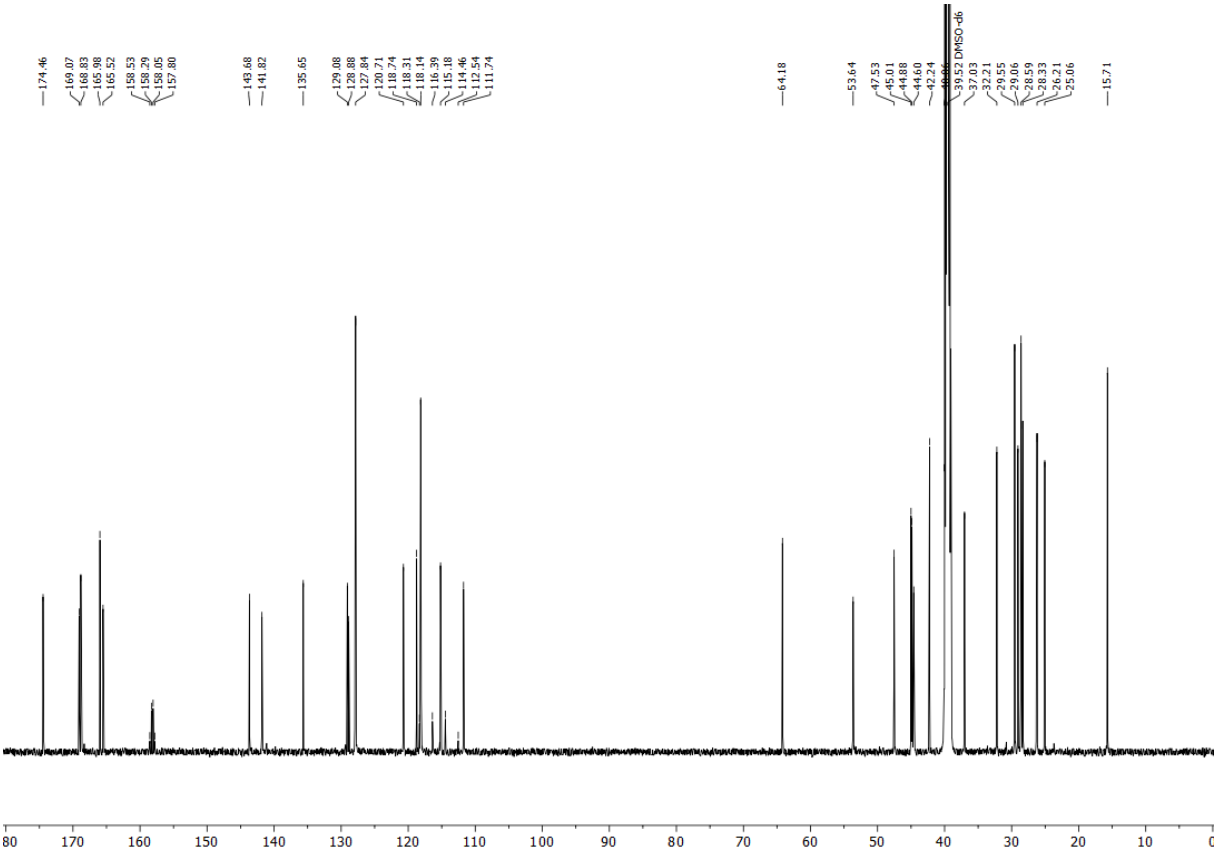

^{13}C NMR spectrum of **1c** (151 MHz, DMSO-d_6).

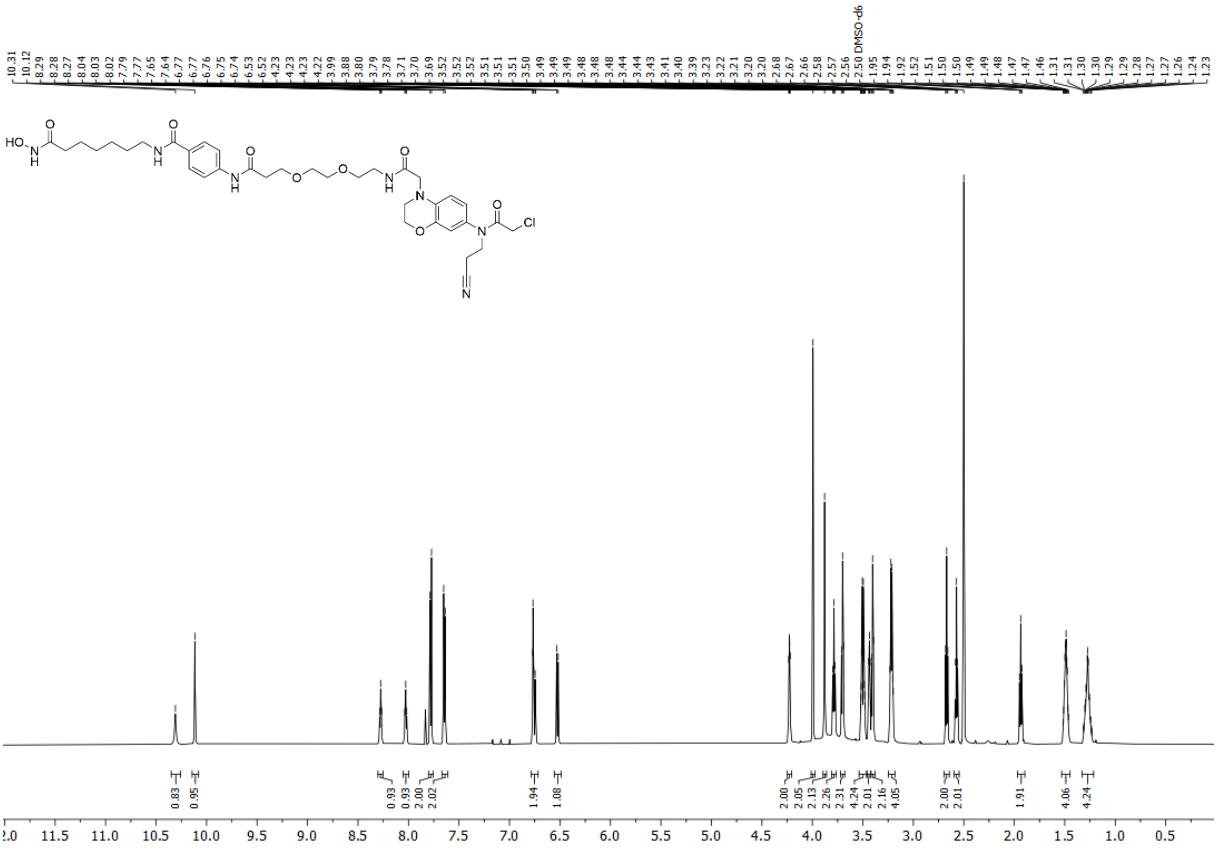

^{1}H NMR spectrum of **1d** (600 MHz, DMSO-d_6).

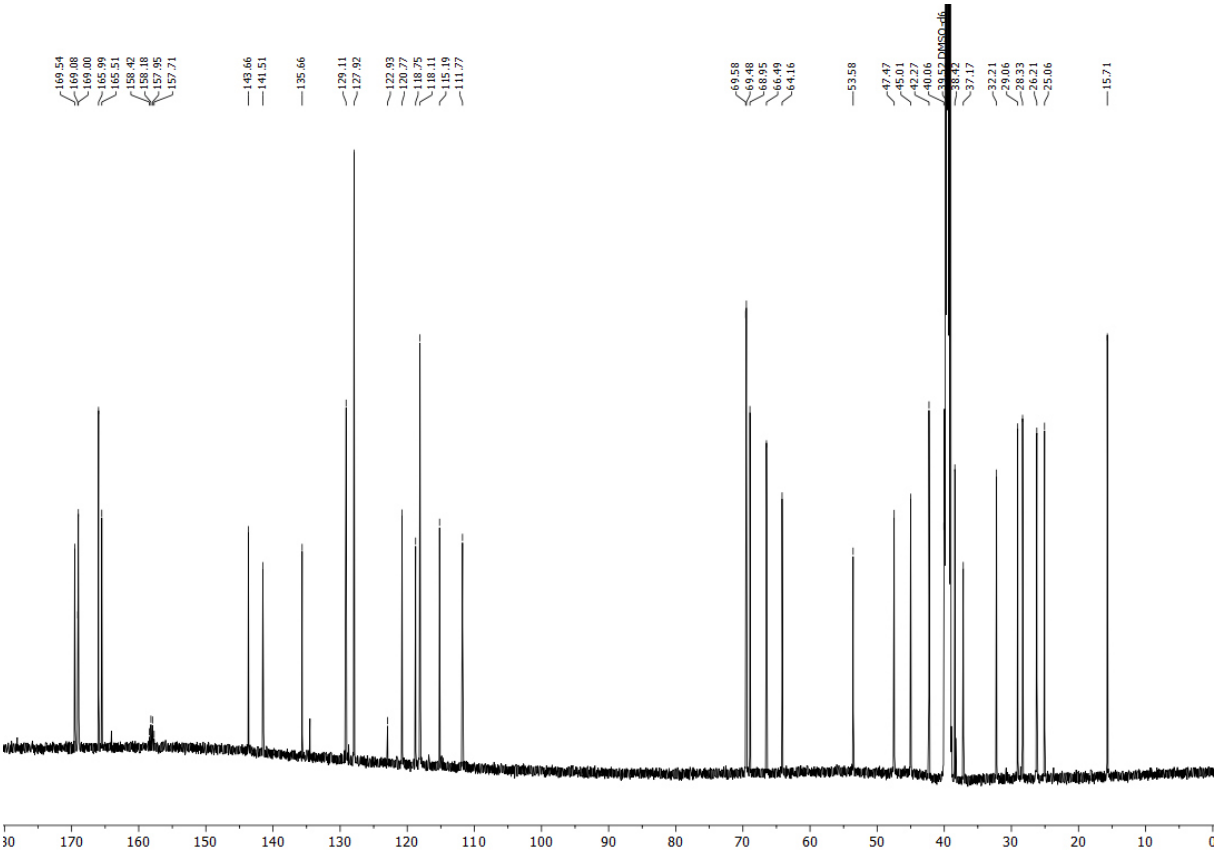

^{13}C NMR spectrum of **1d** (151 MHz, DMSO-d_6).

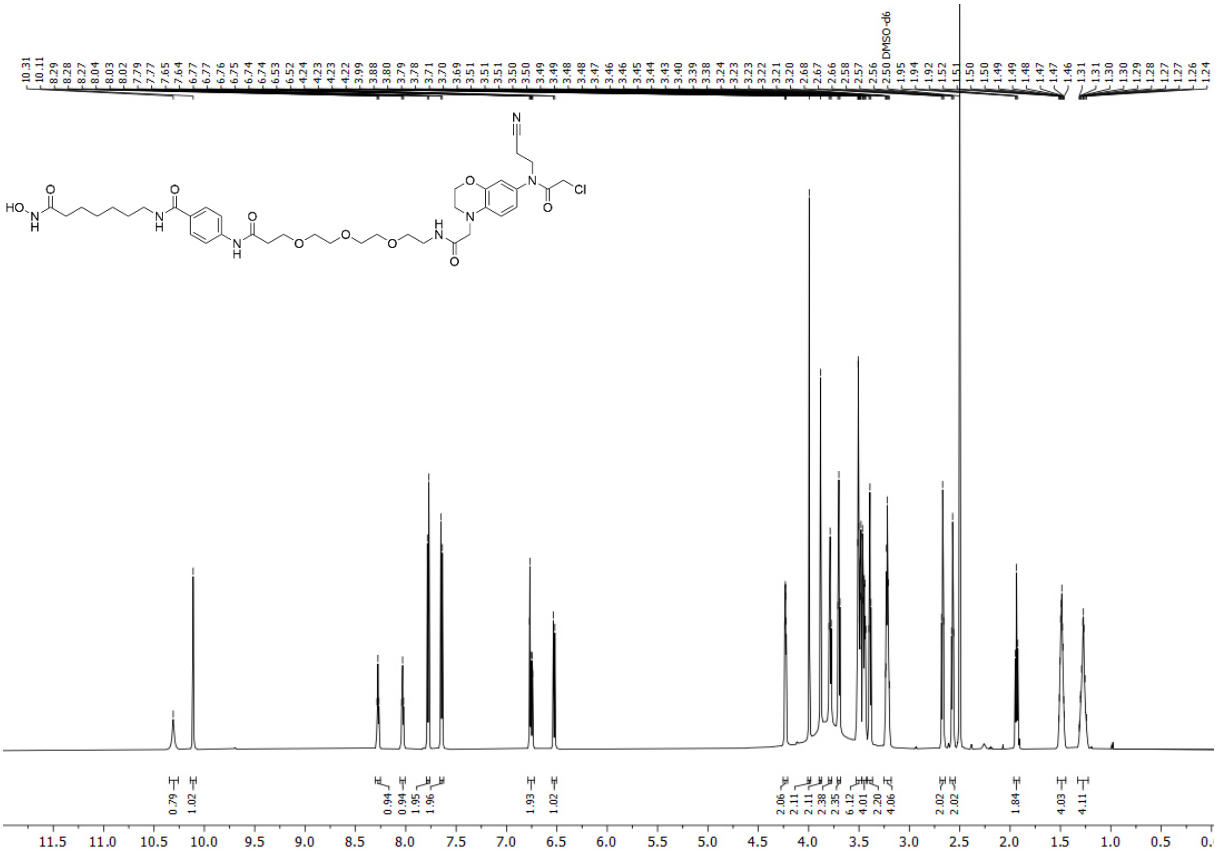

^{1}H NMR spectrum of **1e** (600 MHz, DMSO-d_6).

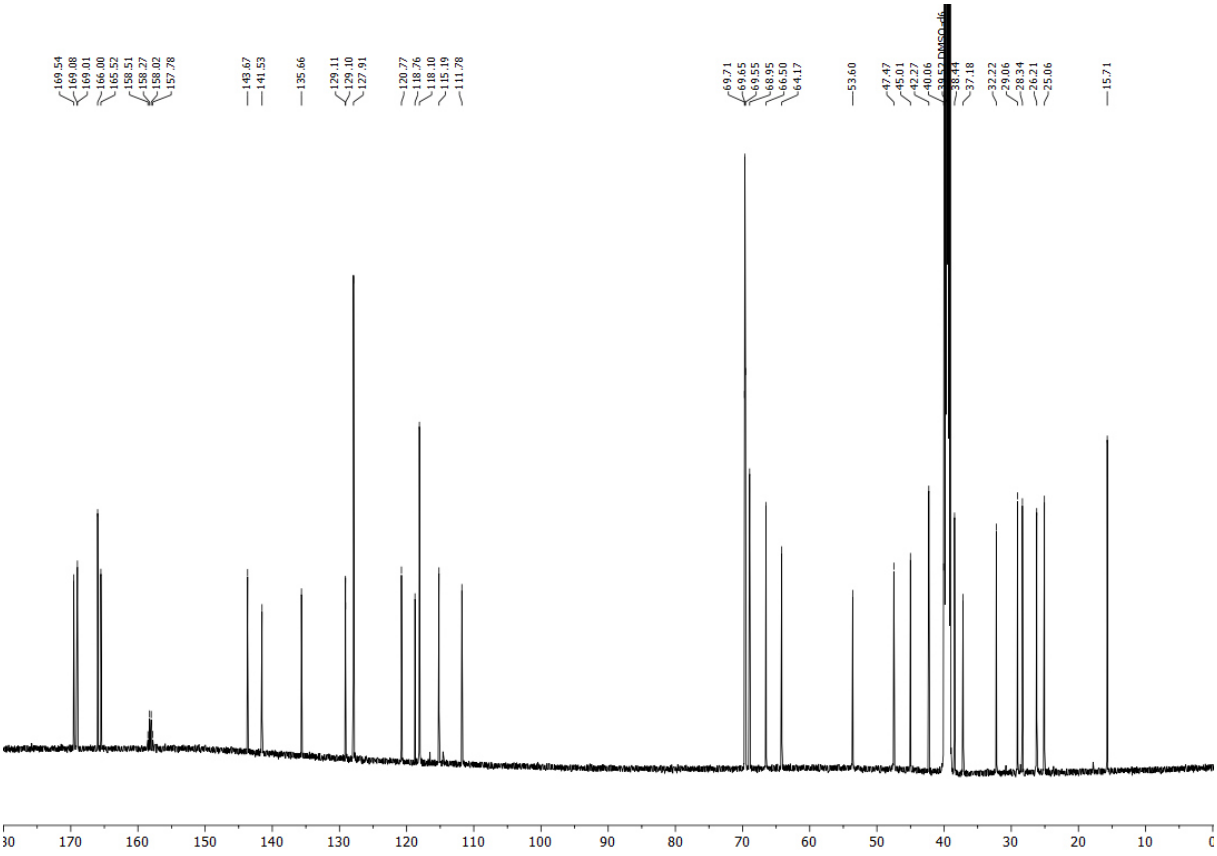

^{13}C NMR spectrum of **1e** (151 MHz, DMSO-d_6).

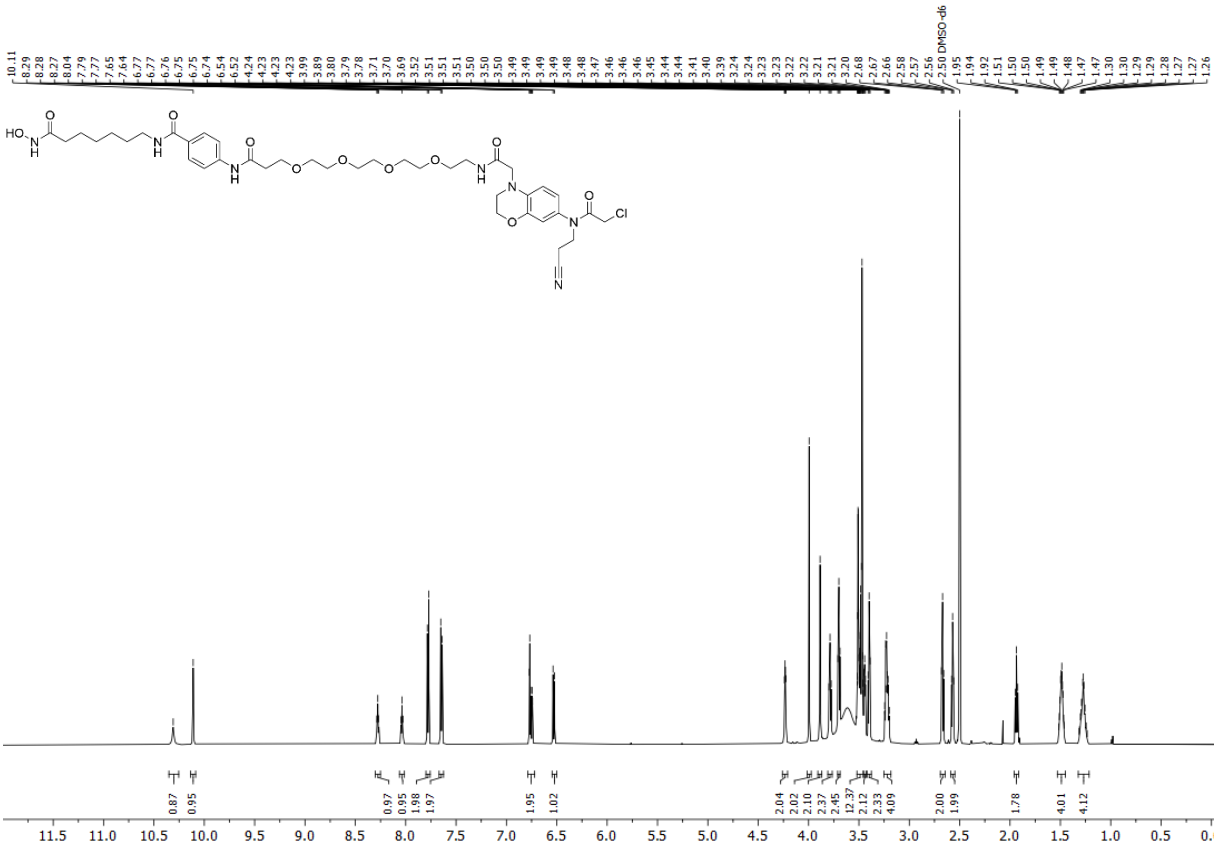

^{1}H NMR spectrum of **1f** (600 MHz, DMSO-d_6).

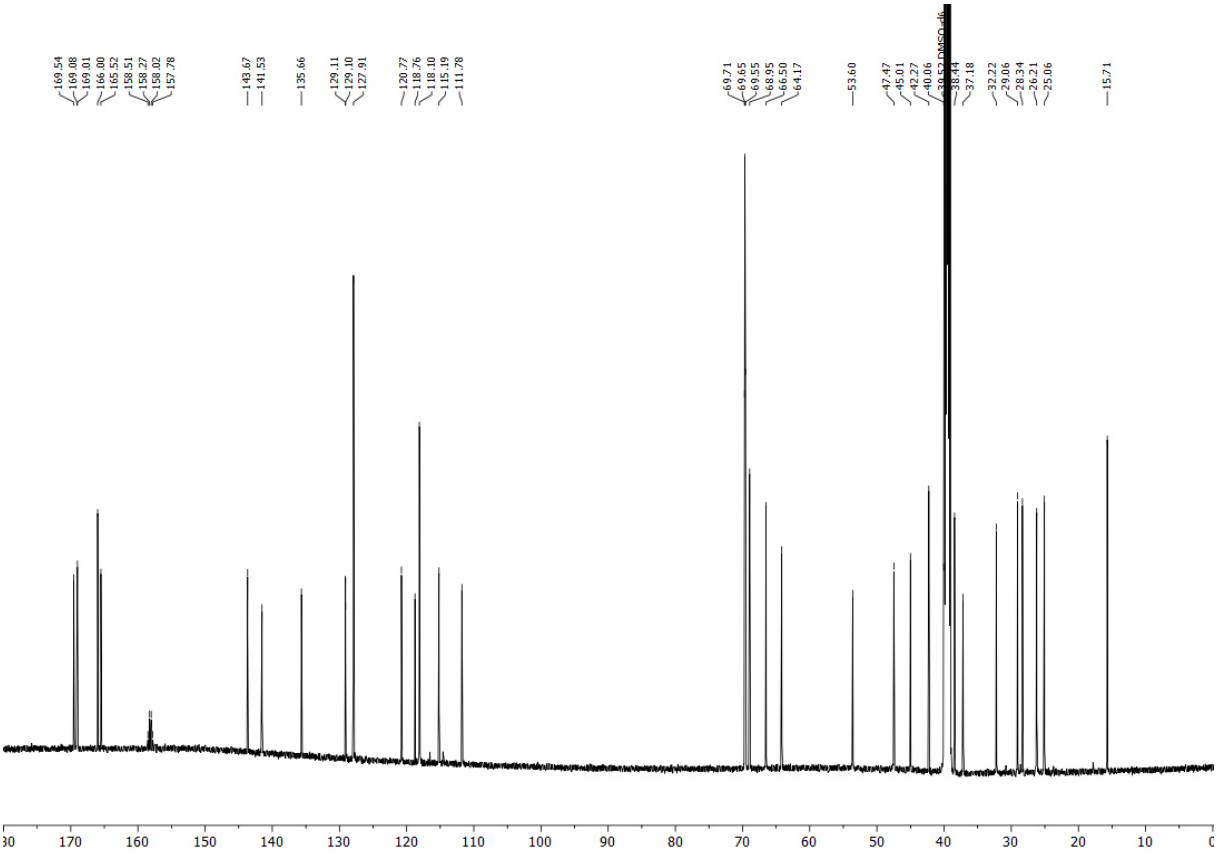

^{13}C NMR spectrum of **1f** (151 MHz, DMSO-d_6).

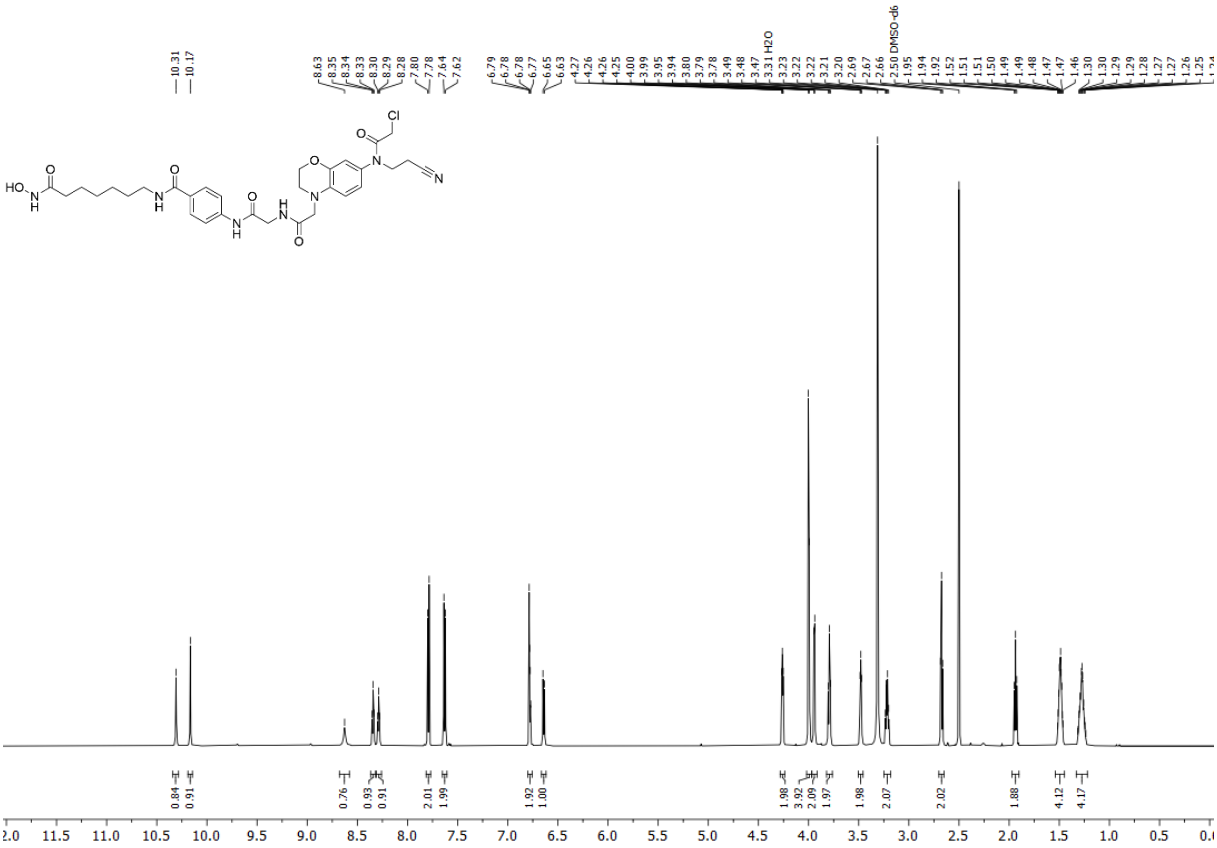

^{1}H NMR spectrum of **1g** (600 MHz, DMSO-d_6).

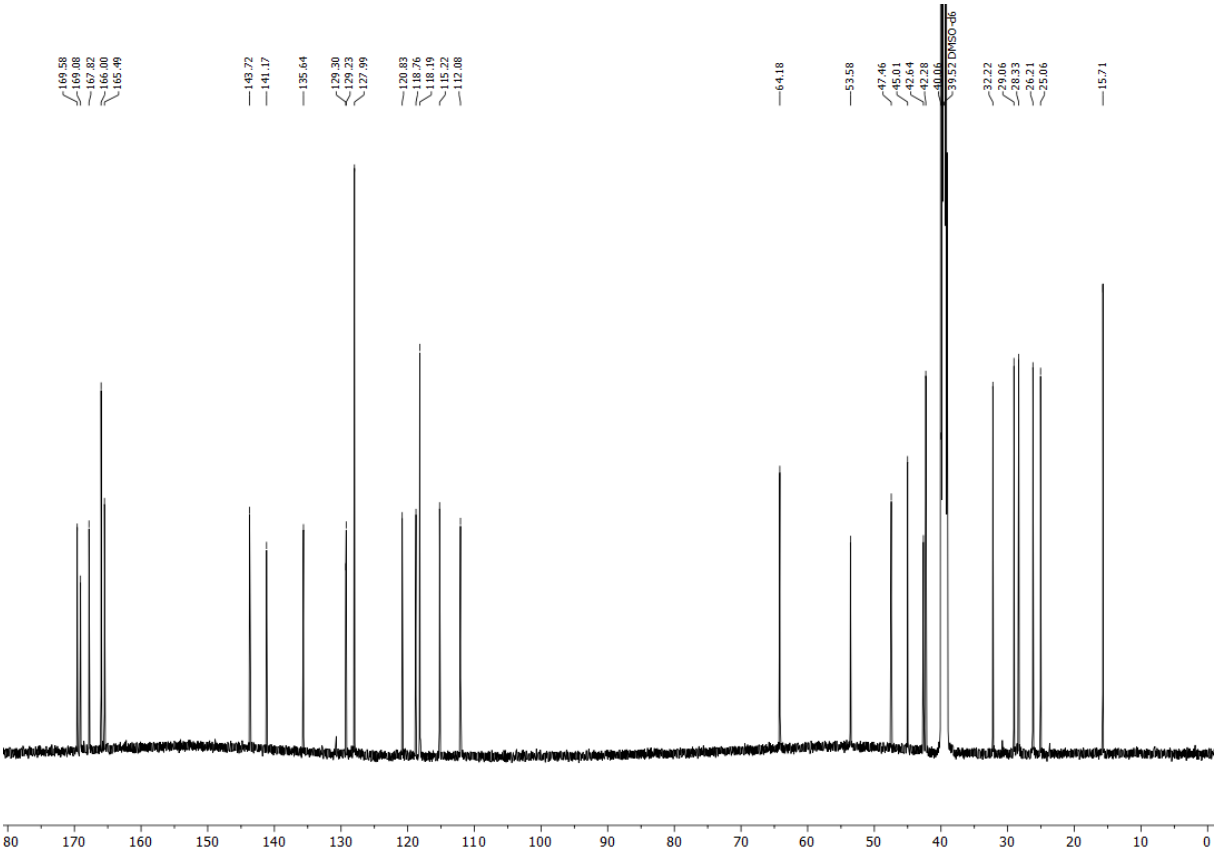

^{13}C NMR spectrum of **1g** (151 MHz, DMSO-d_6).

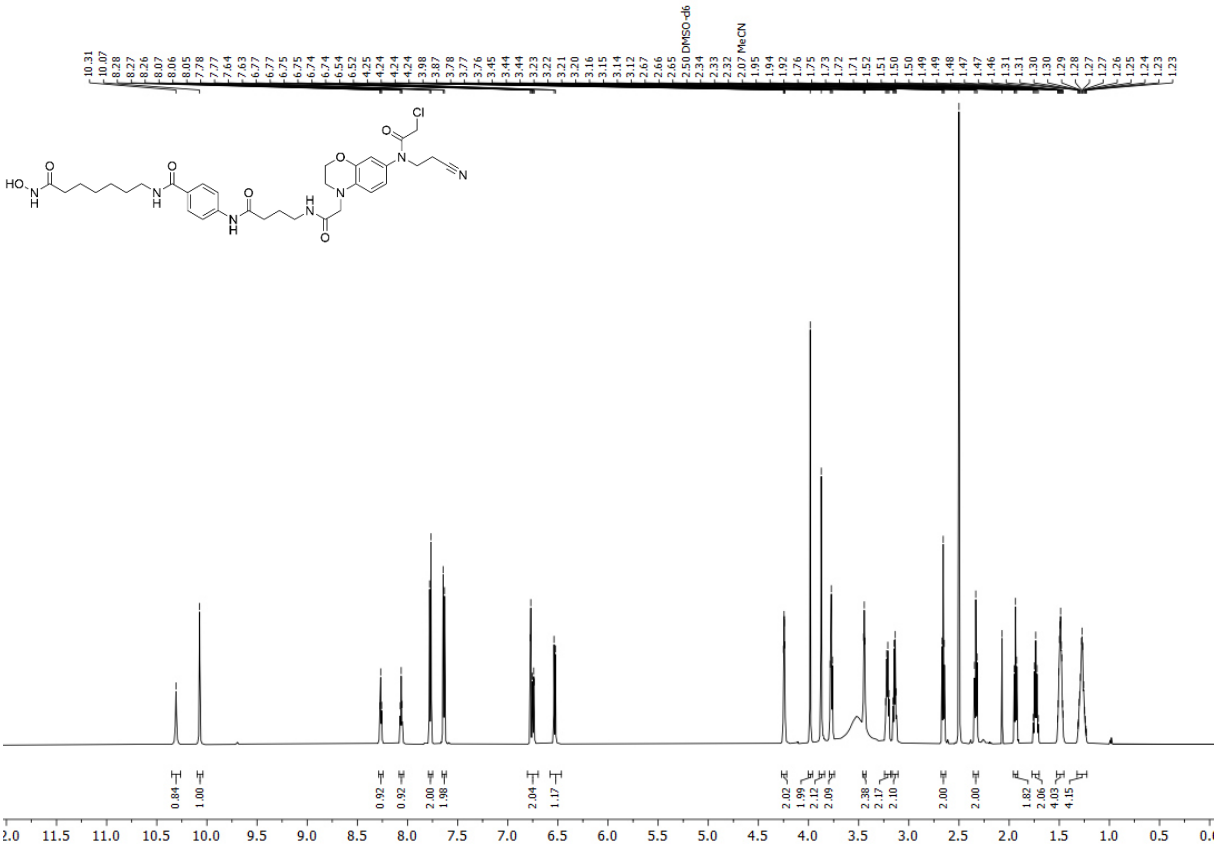

^{1}H NMR spectrum of **1h** (600 MHz, DMSO-d_6).

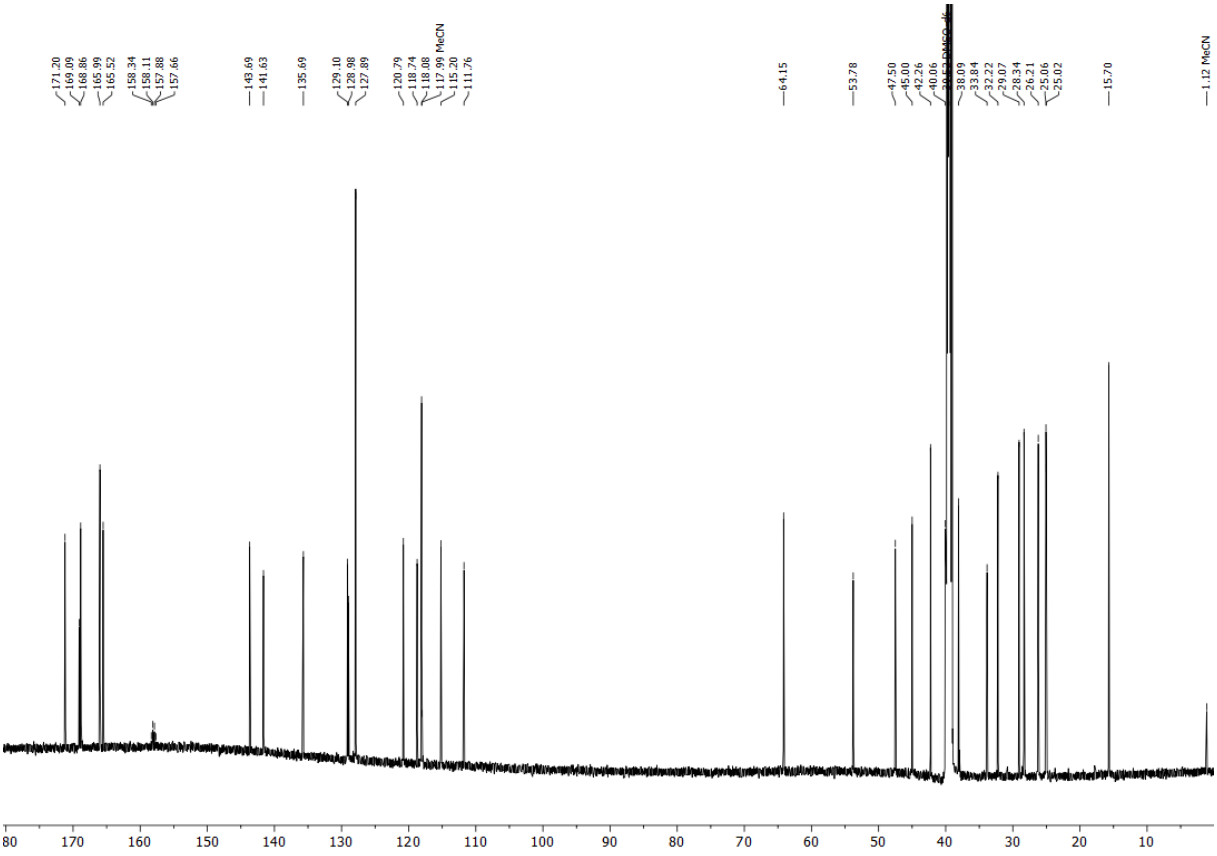

^{13}C NMR spectrum of **1h** (151 MHz, DMSO-d_6).

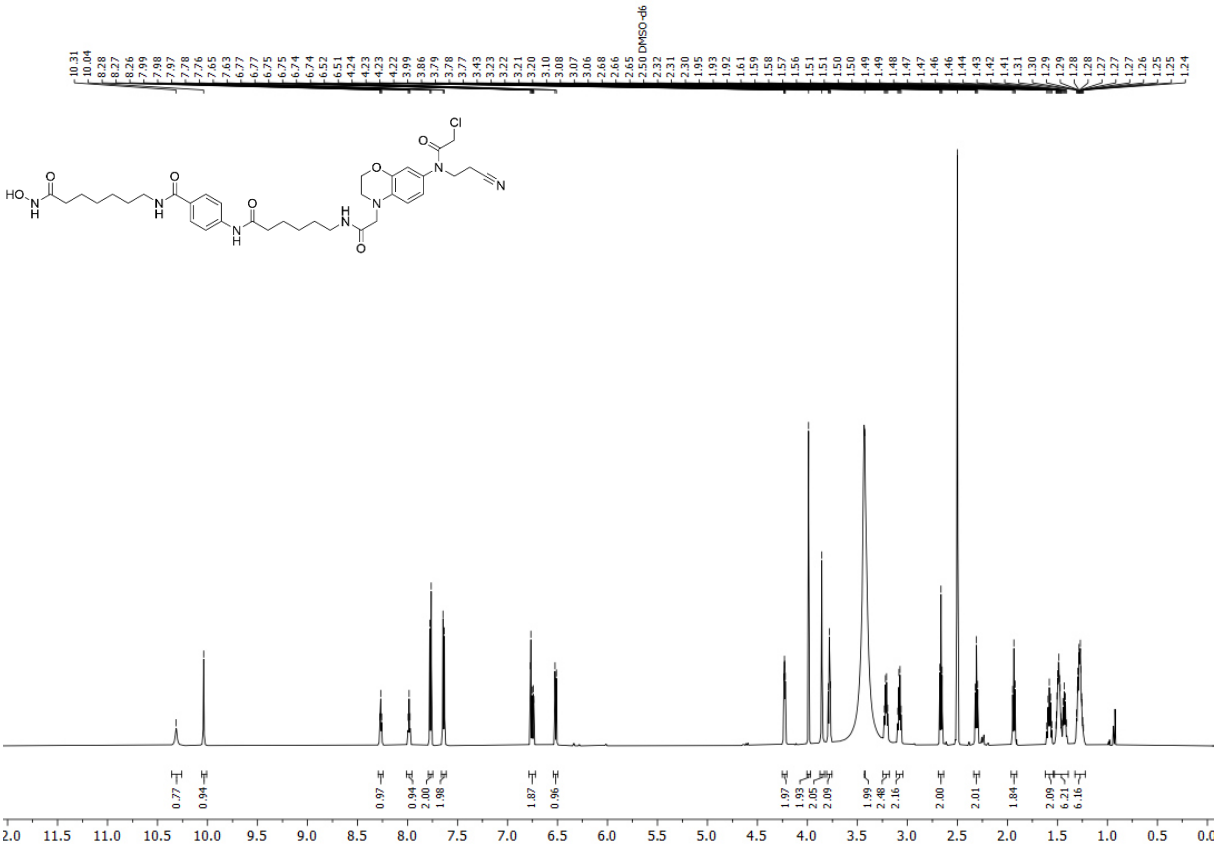

^{1}H NMR spectrum of **1i** (600 MHz, DMSO-d_6).

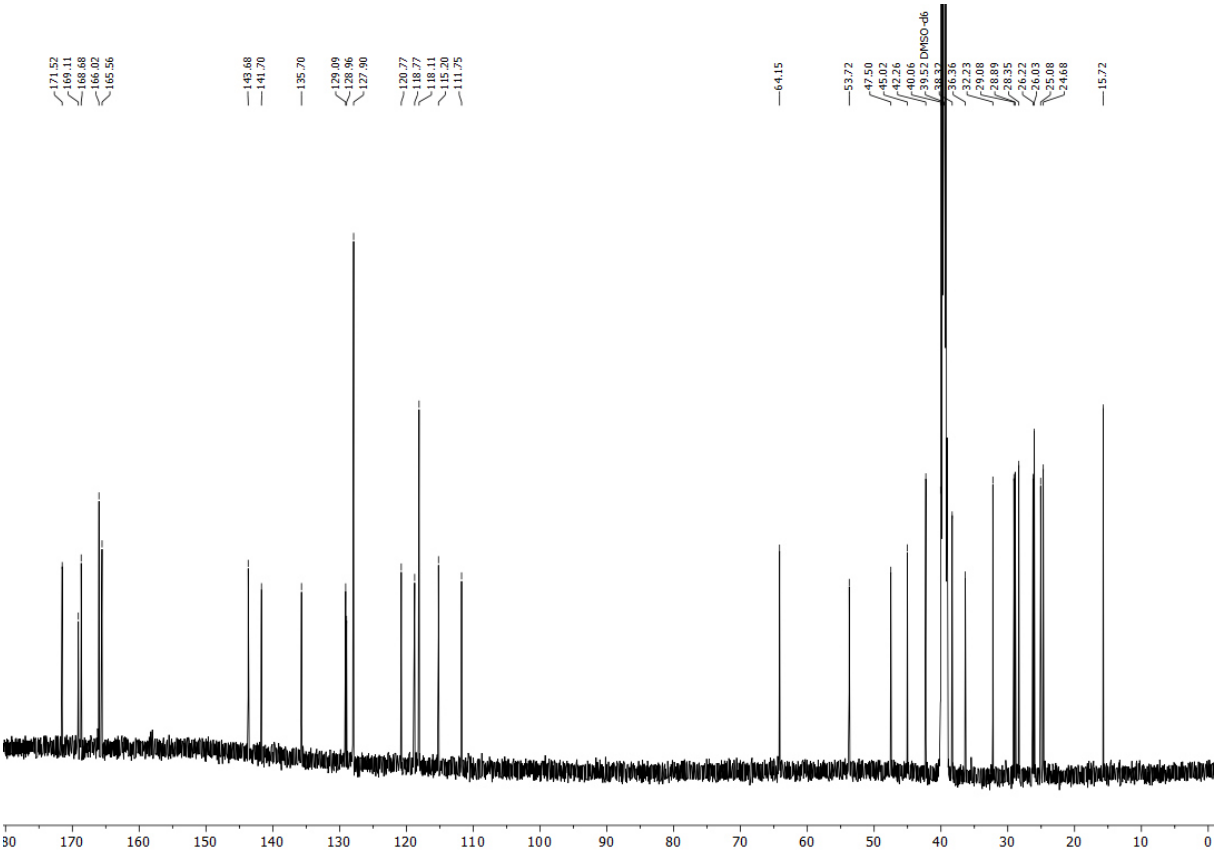

^{13}C NMR spectrum of **1i** (151 MHz, DMSO-d_6).

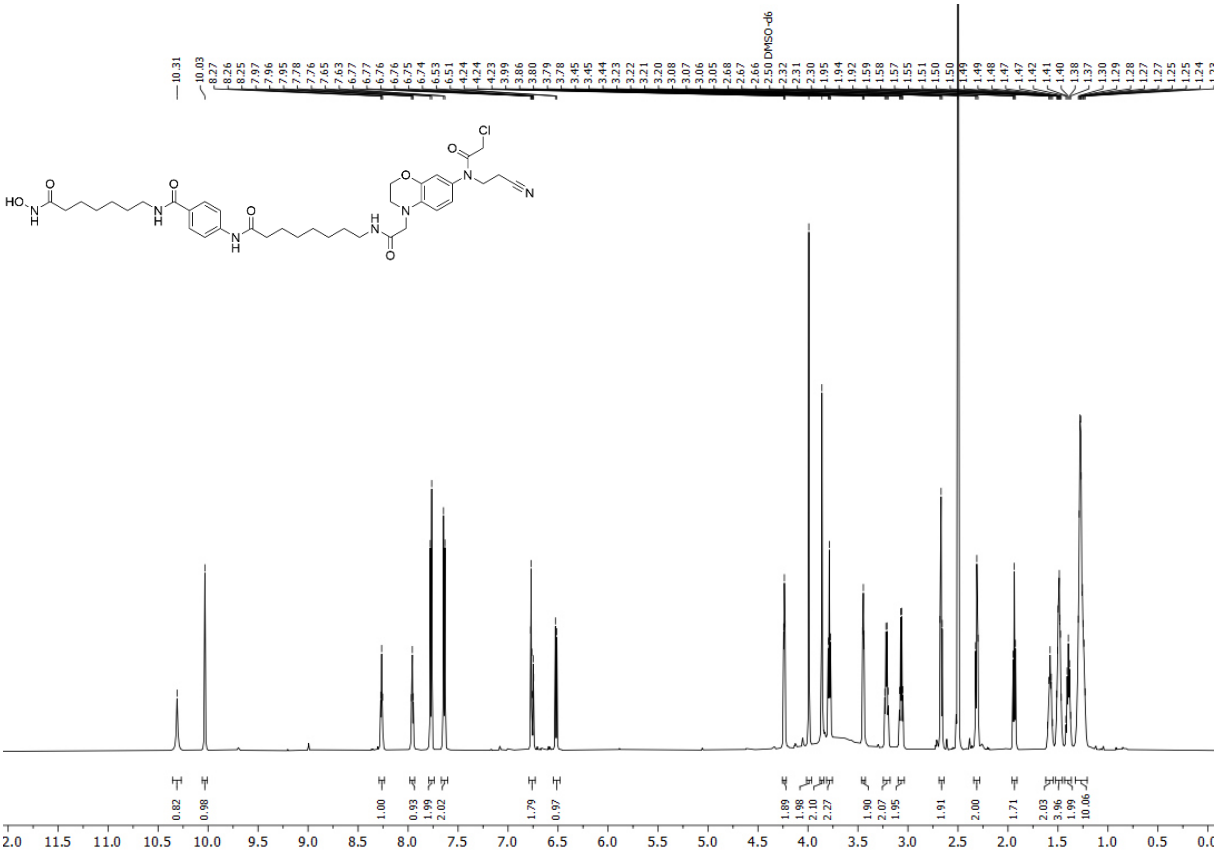

^{1}H NMR spectrum of **1j** (600 MHz, DMSO-d_6).

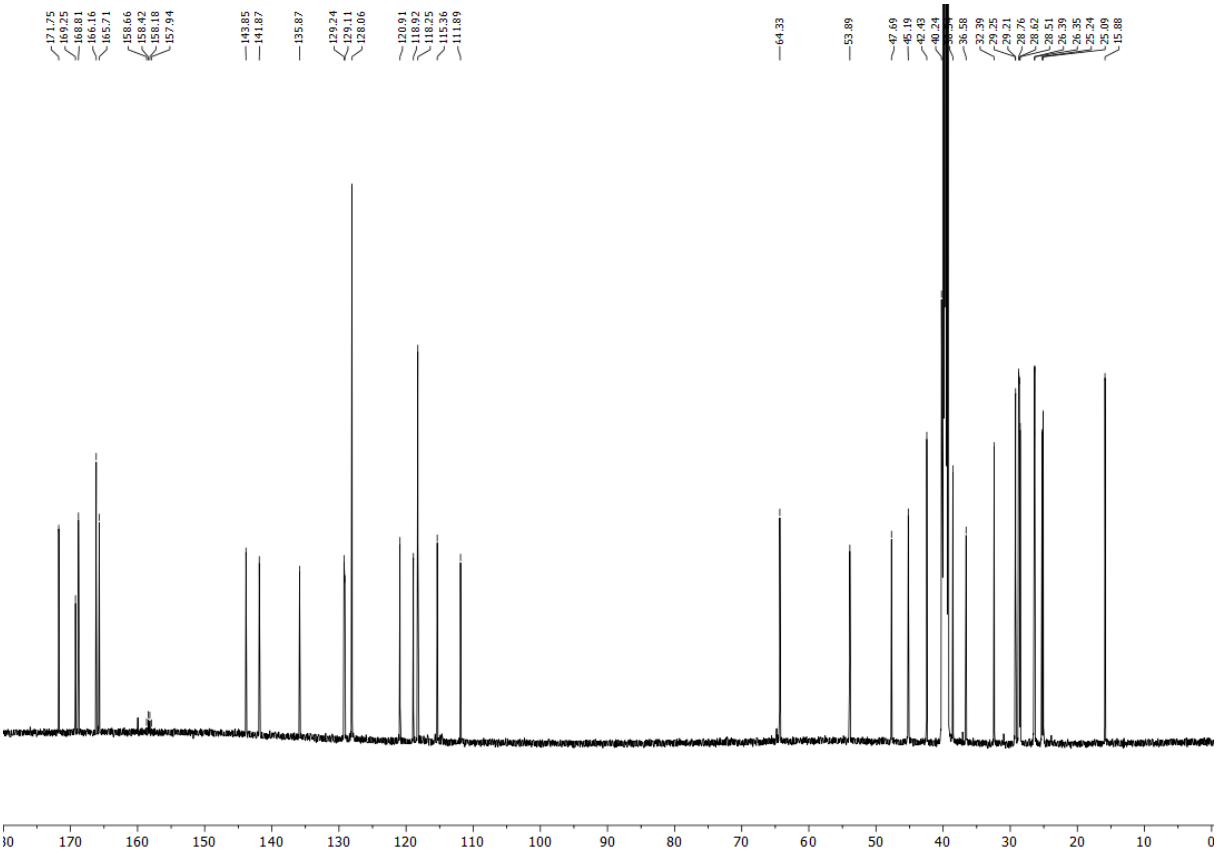

^{13}C NMR spectrum of **1j** (151 MHz, DMSO-d_6).

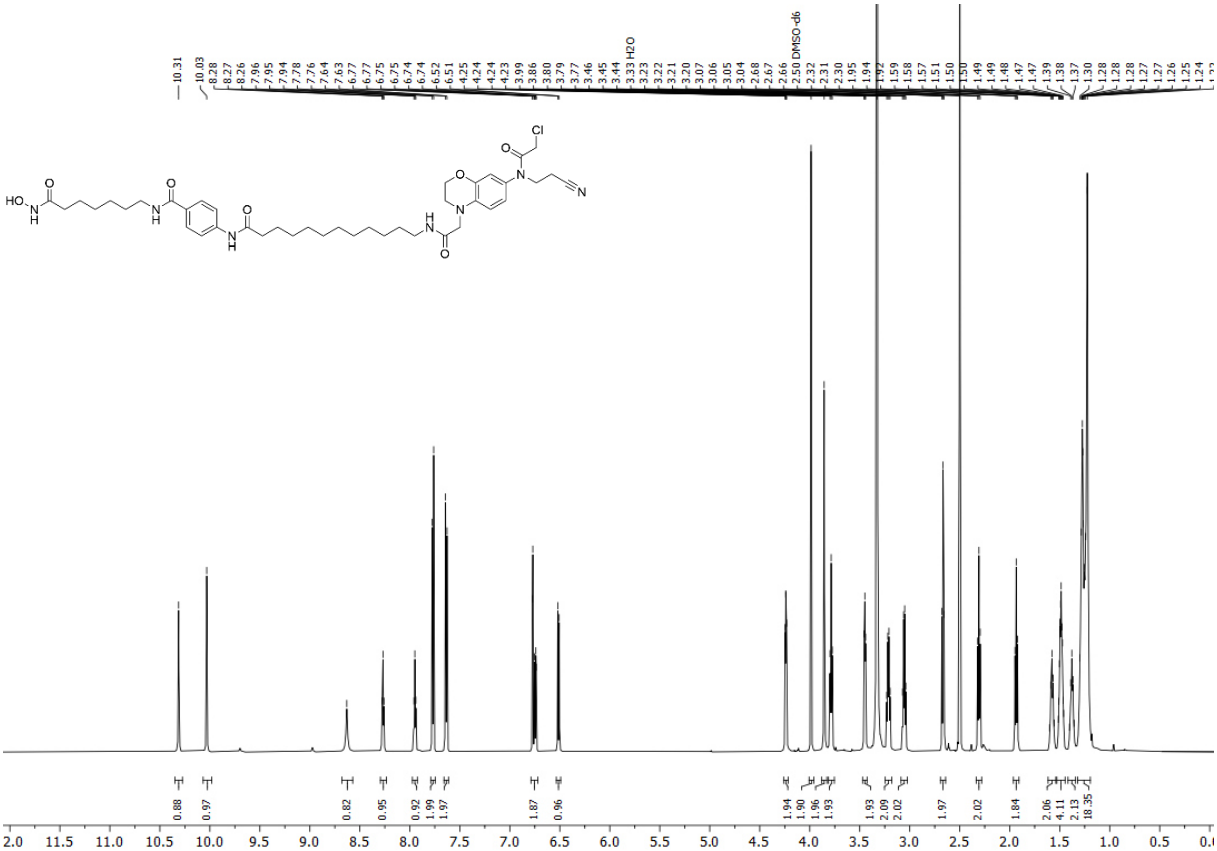

^{1}H NMR spectrum of **1k** (600 MHz, DMSO-d_6).

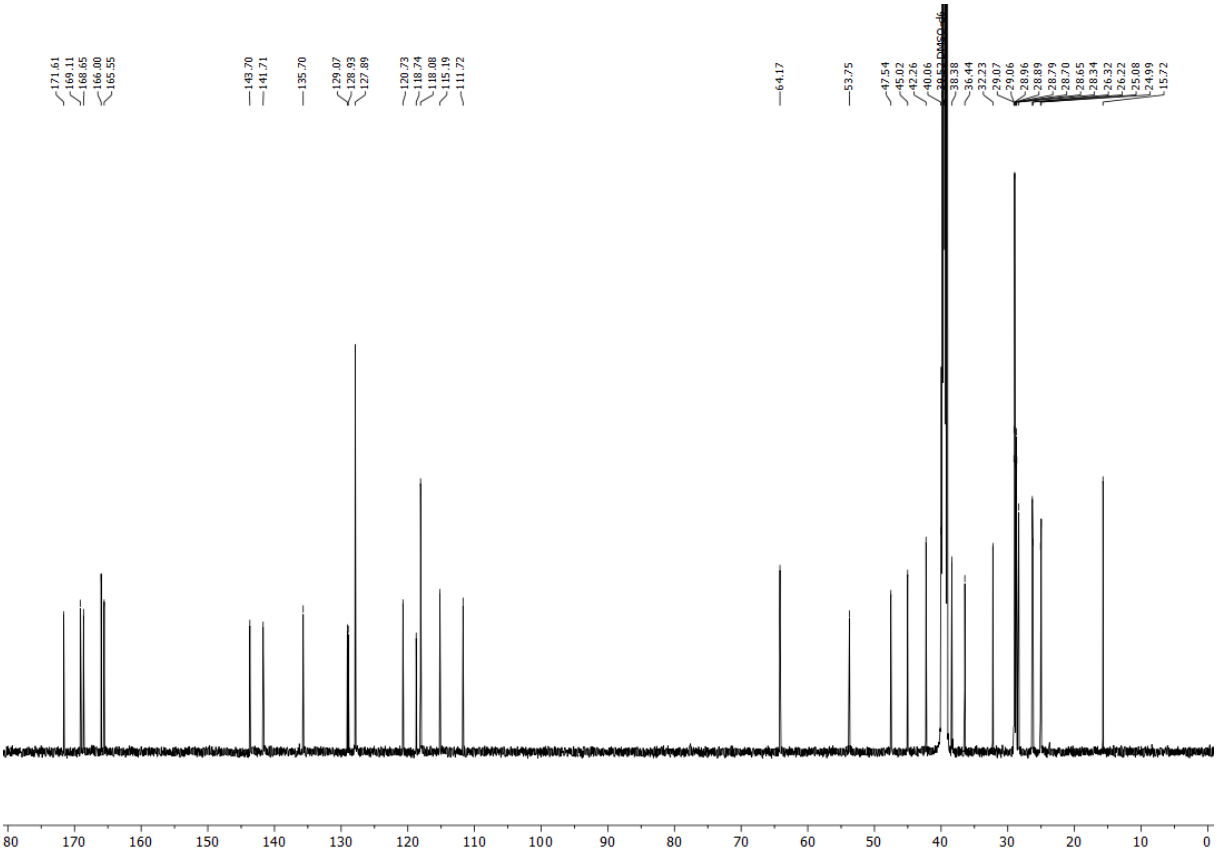

^{13}C NMR spectrum of **1k** (151 MHz, DMSO-d_6).

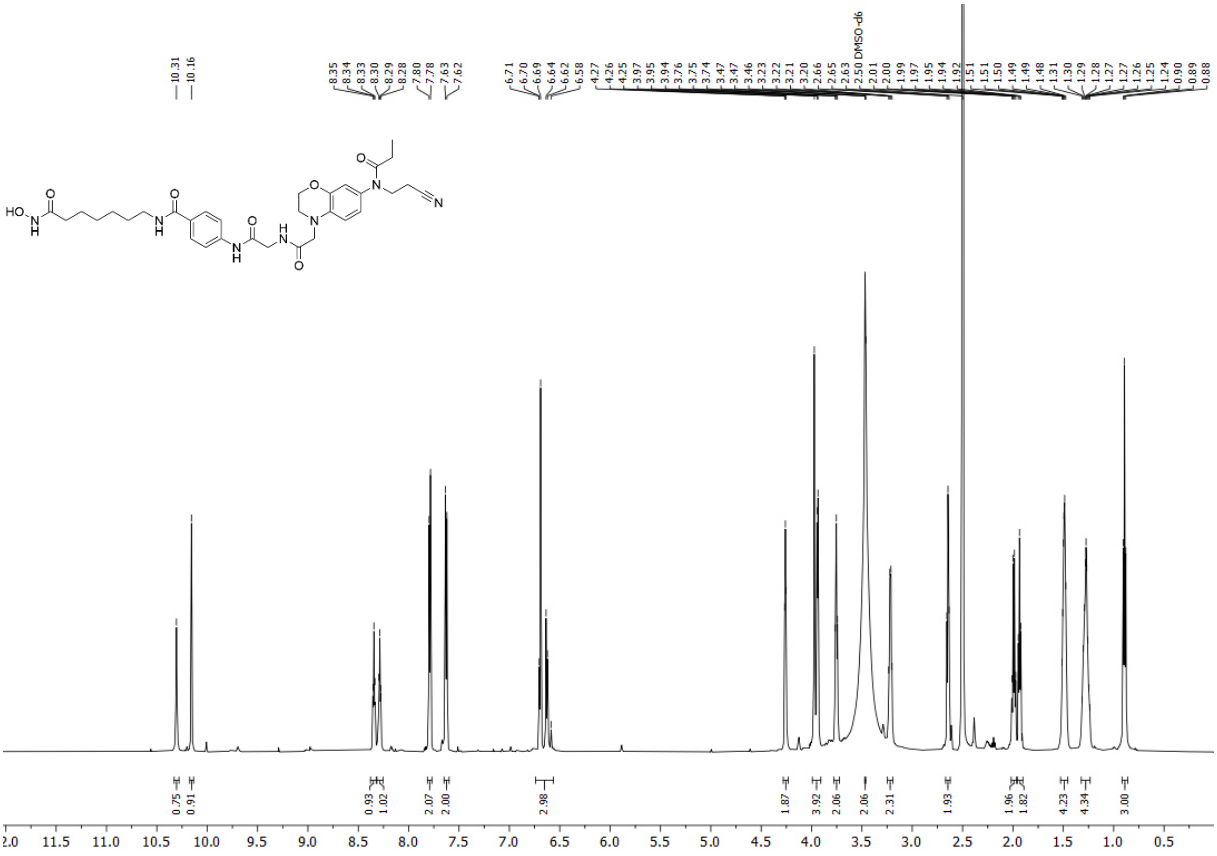

^{1}H NMR spectrum of **1g-nc** (600 MHz, DMSO-d_6).

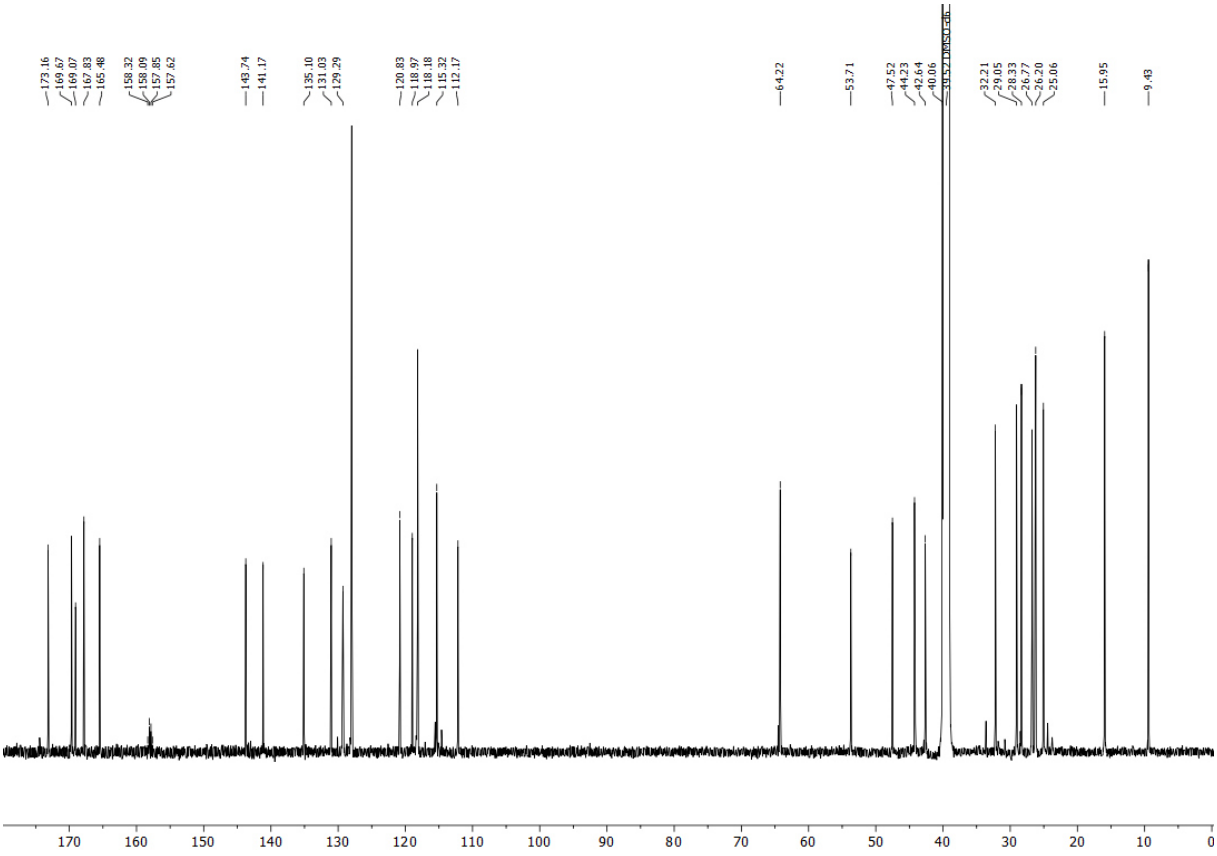

^{13}C NMR spectrum of **1g-nc** (151 MHz, DMSO-d_6).

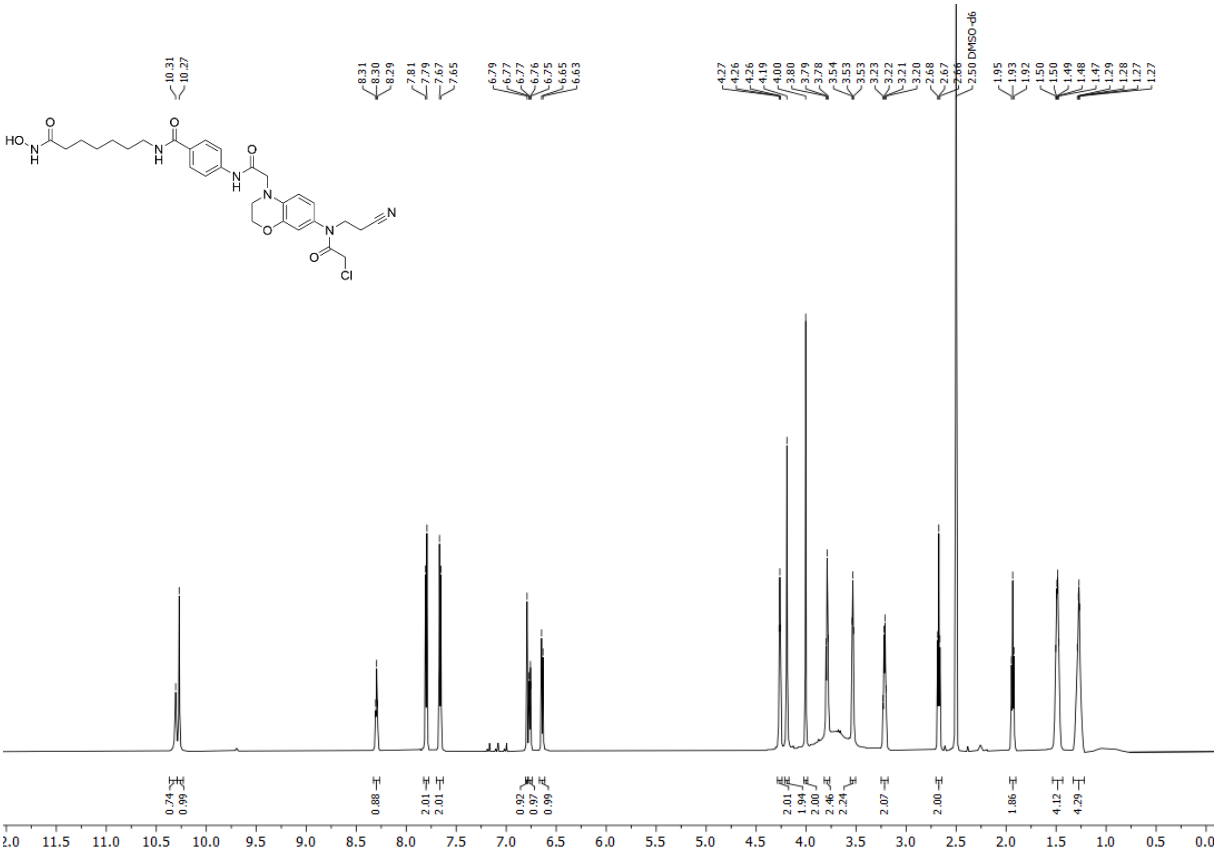

^{1}H NMR spectrum of **2** (600 MHz, DMSO-d_6).

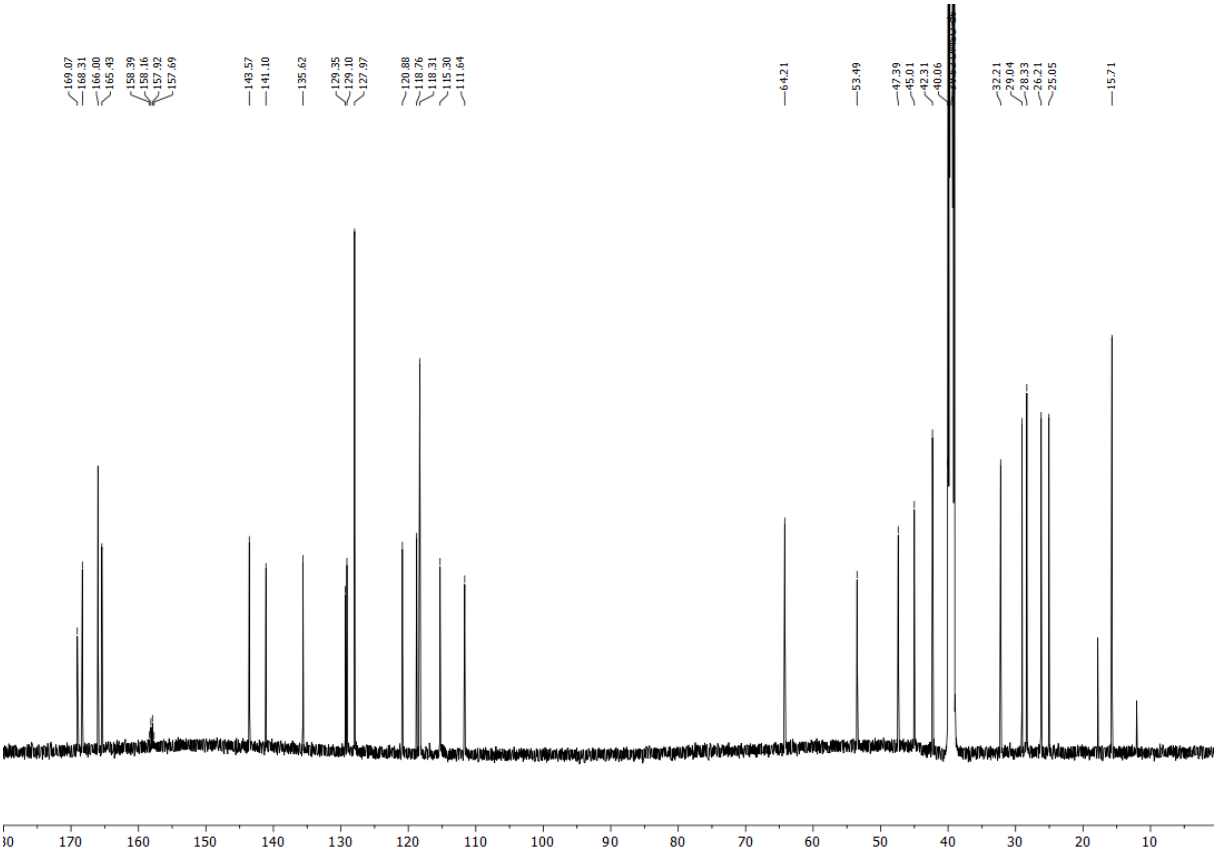

^{13}C NMR spectrum of **2** (151 MHz, DMSO-d_6).

3. HPLC chromatograms of compounds in biological testing

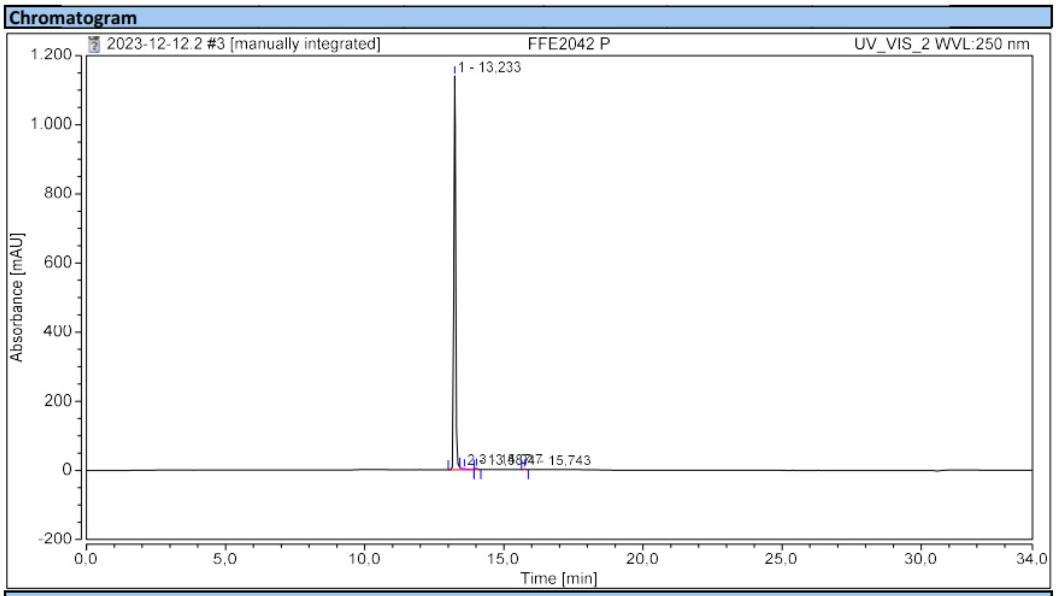

Integration Results

No.	Peak Name	Retention Time min	Area mAU*min	Height mAU	Relative Area %	Relative Height %	Amount n.a.
1		13,233	83,997	1139,744	99,05	99,41	n.a.
2		13,587	0,370	1,306	0,44	0,11	n.a.
3		14,017	0,344	4,313	0,41	0,38	n.a.
4		15,743	0,090	1,092	0,11	0,10	n.a.
Total:			**84,801**	**1146,454**	**100,00**	**100,00**	

HPLC chromatogram of **1a** (gradient B, purity: 99.1%).

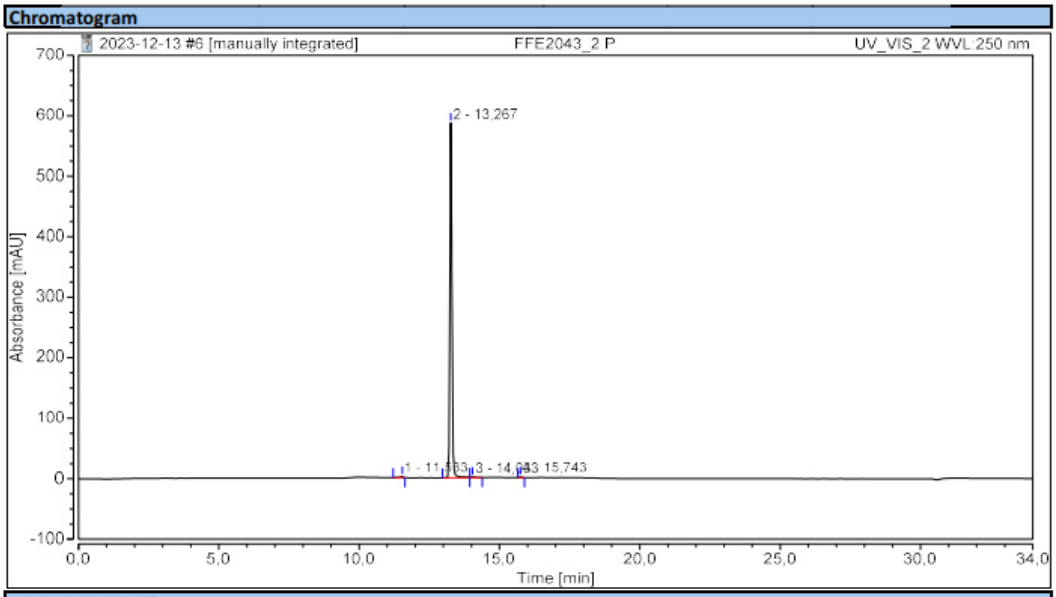

Integration Results

No.	Peak Name	Retention Time min	Area mAU*min	Height mAU	Relative Area %	Relative Height %	Amount n.a.
1		11,533	0,286	2,393	0,58	0,40	n.a.
2		13,267	49,038	586,870	98,74	99,13	n.a.
3		14,033	0,224	1,280	0,45	0,22	n.a.
4		15,743	0,115	1,451	0,23	0,25	n.a.
Total:			**49,663**	**591,995**	**100,00**	**100,00**	

HPLC chromatogram of **1b** (gradient B, purity: 98.7%).

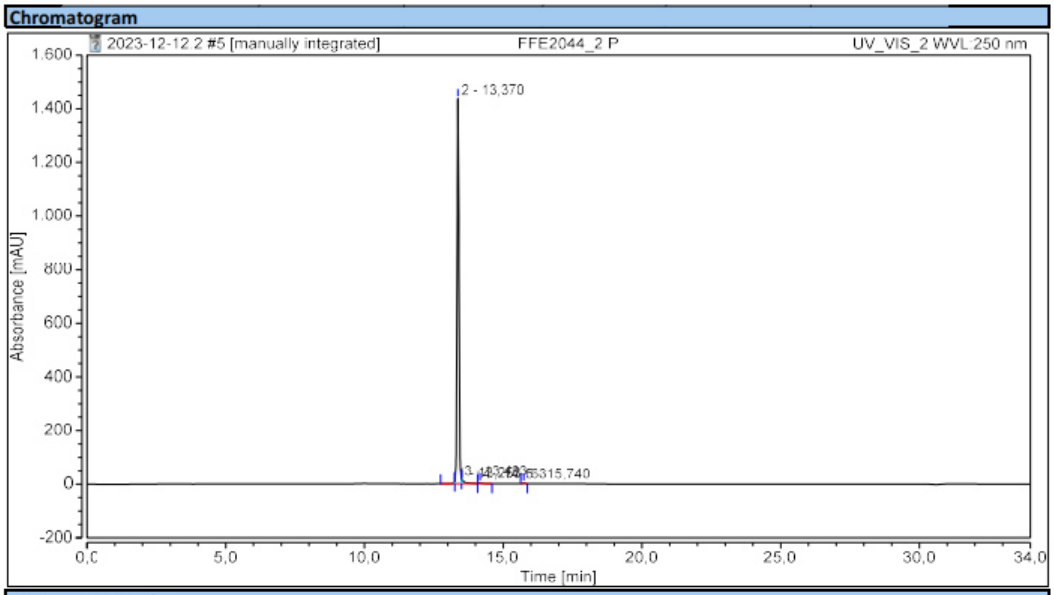

Integration Results

No.	Peak Name	Retention Time min	Area mAU*min	Height mAU	Relative Area %	Relative Height %	Amount n.a.
1		13,253	0,362	6,518	0,32	0,45	n.a.
2		13,370	109,044	1435,827	97,28	98,06	n.a.
3		13,493	2,103	15,729	1,88	1,07	n.a.
4		14,163	0,377	3,375	0,34	0,23	n.a.
5		15,740	0,209	2,766	0,19	0,19	n.a.
Total:			**112,096**	**1464,214**	**100,00**	**100,00**	

HPLC chromatogram of **1c** (gradient B, purity: 97.3%).

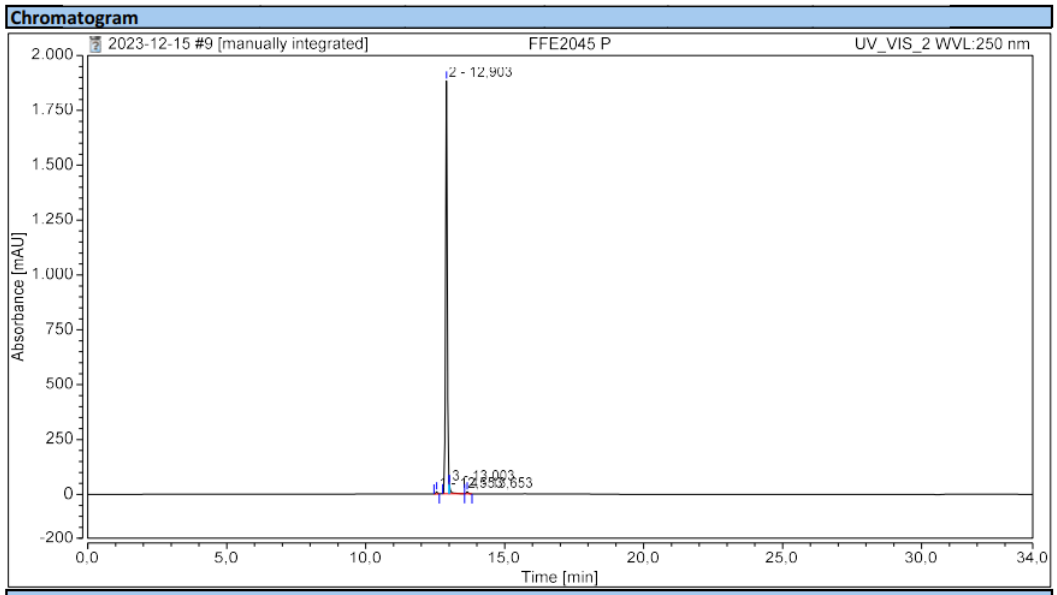

Integration Results

No.	Peak Name	Retention Time min	Area mAU*min	Height mAU	Relative Area %	Relative Height %	Amount n.a.
1		12,553	0,648	9,919	0,46	0,51	n.a.
2		12,903	136,688	1880,377	97,33	96,88	n.a.
3		13,003	2,393	41,252	1,70	2,13	n.a.
4		13,653	0,710	9,422	0,51	0,49	n.a.
Total:			**140,440**	**1940,971**	**100,00**	**100,00**	

HPLC chromatogram of **1d** (gradient B, purity: 97.3%).

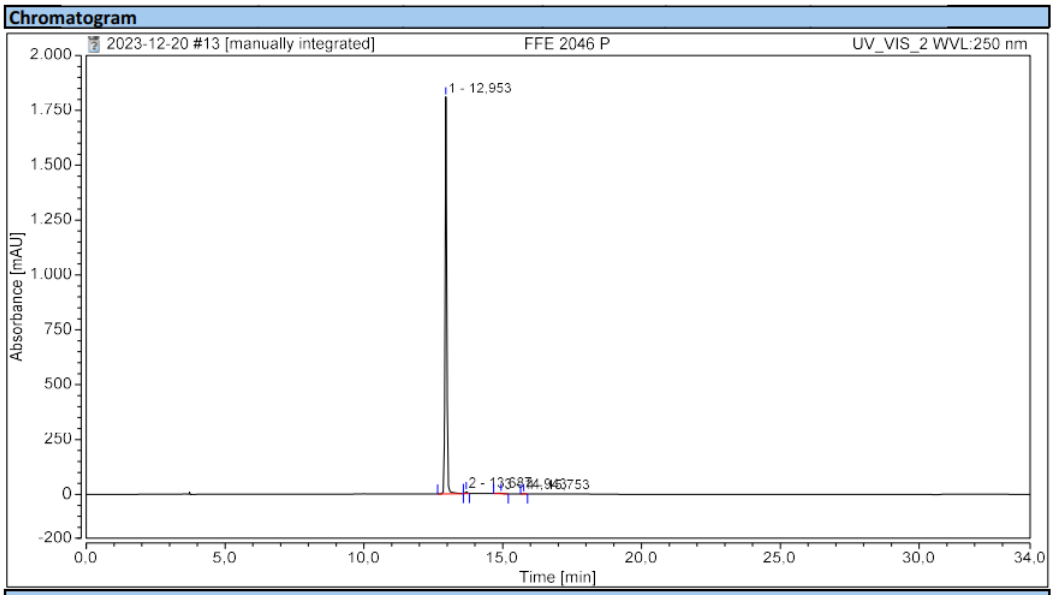

Integration Results

No.	Peak Name	Retention Time min	Area mAU*min	Height mAU	Relative Area %	Relative Height %	Amount n.a.
1		12,953	134,440	1809,154	99,06	99,30	n.a.
2		13,687	0,758	9,091	0,56	0,50	n.a.
3		14,943	0,397	2,250	0,29	0,12	n.a.
4		15,753	0,117	1,358	0,09	0,07	n.a.
Total:			**135,712**	**1821,853**	**100,00**	**100,00**	

HPLC chromatogram of **1e** (gradient B, purity: 99.1%).

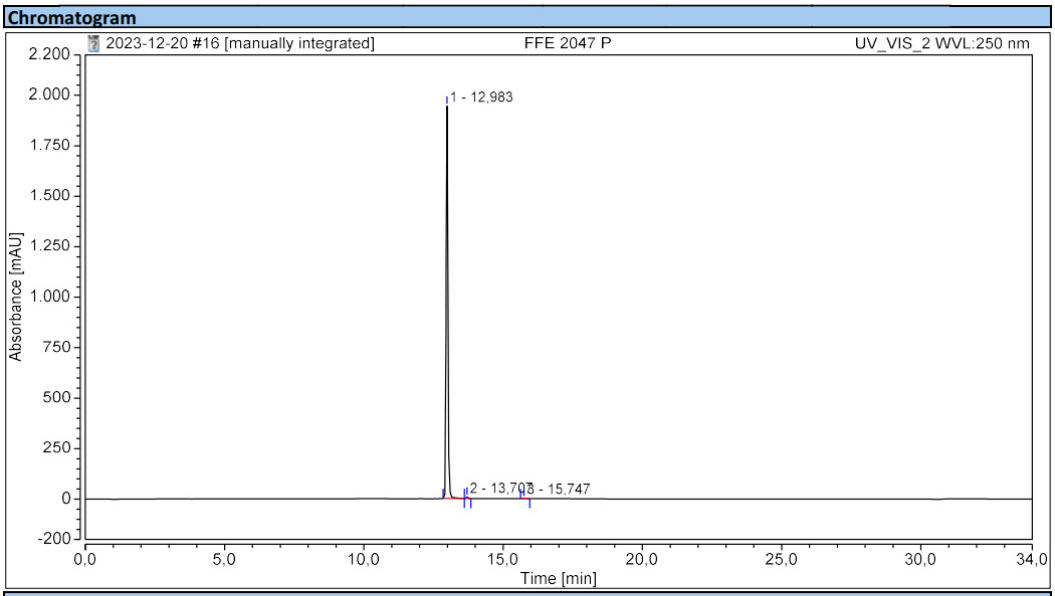

Integration Results

No.	Peak Name	Retention Time min	Area mAU*min	Height mAU	Relative Area %	Relative Height %	Amount n.a.
1		12,983	147,581	1942,855	99,50	99,54	n.a.
2		13,707	0,607	7,439	0,41	0,38	n.a.
3		15,747	0,139	1,525	0,09	0,08	n.a.
Total:			**148,327**	**1951,820**	**100,00**	**100,00**	

HPLC chromatogram of **1f** (gradient B, purity: 99.5%).

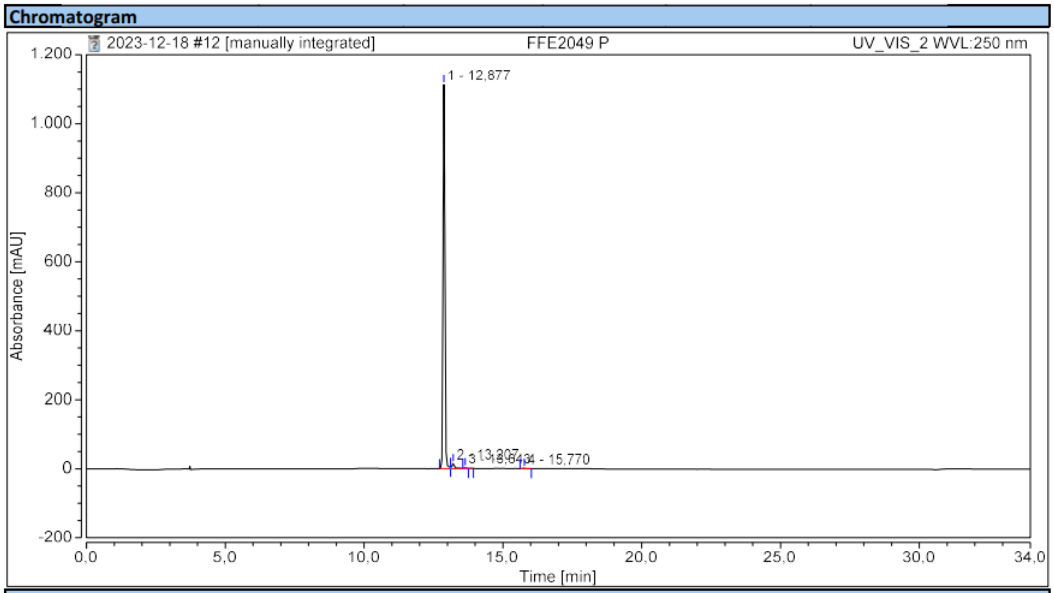

Integration Results

No.	Peak Name	Retention Time min	Area mAU*min	Height mAU	Relative Area %	Relative Height %	Amount n.a.
1		12,877	80,587	1113,081	97,59	98,47	n.a.
2		13,207	1,754	14,462	2,12	1,28	n.a.
3		13,643	0,132	1,837	0,16	0,16	n.a.
4		15,770	0,101	1,030	0,12	0,09	n.a.
Total:			**82,573**	**1130,410**	**100,00**	**100,00**	

HPLC chromatogram of **1g** (gradient B, purity: 97.6%).

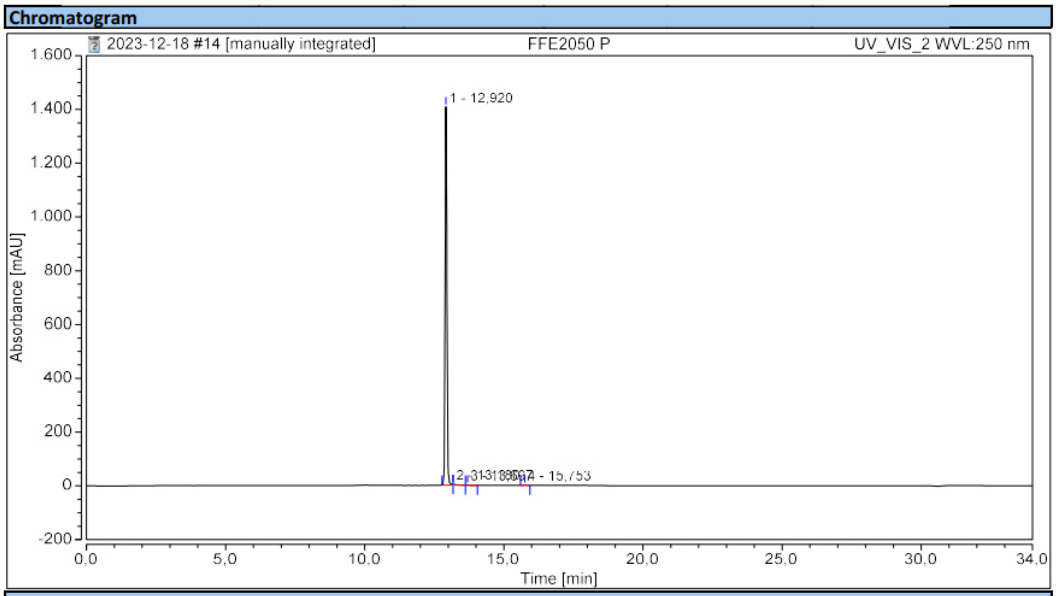

Integration Results

No.	Peak Name	Retention Time min	Area mAU*min	Height mAU	Relative Area %	Relative Height %	Amount n.a.
1		12,920	102,852	1407,184	99,25	99,56	n.a.
2		13,180	0,470	2,897	0,45	0,20	n.a.
3		13,697	0,160	1,839	0,15	0,13	n.a.
4		15,753	0,145	1,538	0,14	0,11	n.a.
Total:			**103,626**	**1413,459**	**100,00**	**100,00**	

HPLC chromatogram of **1h** (gradient B, purity: 99.3%).

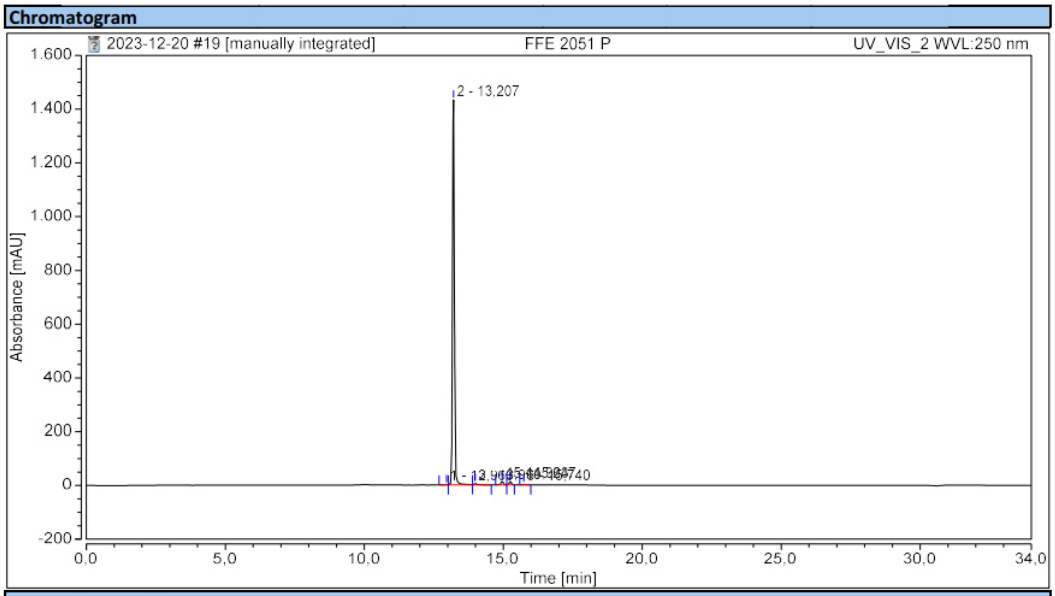

Integration Results

No.	Peak Name	Retention Time min	Area mAU*min	Height mAU	Relative Area %	Relative Height %	Amount n.a.
1		12,963	0,141	0,998	0,12	0,07	n.a.
2		13,207	110,220	1432,307	97,04	97,69	n.a.
3		13,990	0,575	5,031	0,51	0,34	n.a.
4		14,963	1,245	12,998	1,10	0,89	n.a.
5		15,247	1,204	12,668	1,06	0,86	n.a.
6		15,740	0,196	2,243	0,17	0,15	n.a.
Total:			**113,581**	**1466,244**	**100,00**	**100,00**	

HPLC chromatogram of **1i** (gradient B, purity: 97.0%).

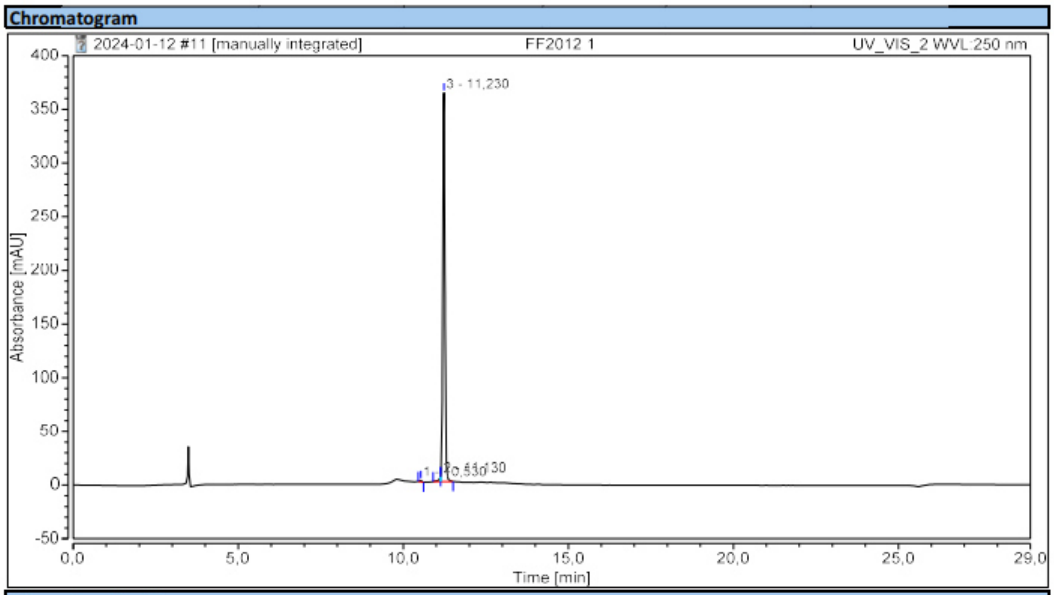

Integration Results

No.	Peak Name	Retention Time min	Area mAU*min	Height mAU	Relative Area %	Relative Height %	Amount n.a.
1		10,530	0,091	1,360	0,33	0,37	n.a.
2		11,130	0,243	4,442	0,89	1,21	n.a.
3		11,230	27,099	362,129	98,78	98,42	n.a.
Total:			**27,433**	**367,931**	**100,00**	**100,00**	

HPLC chromatogram of **1j** (gradient A, purity: 98.8%).

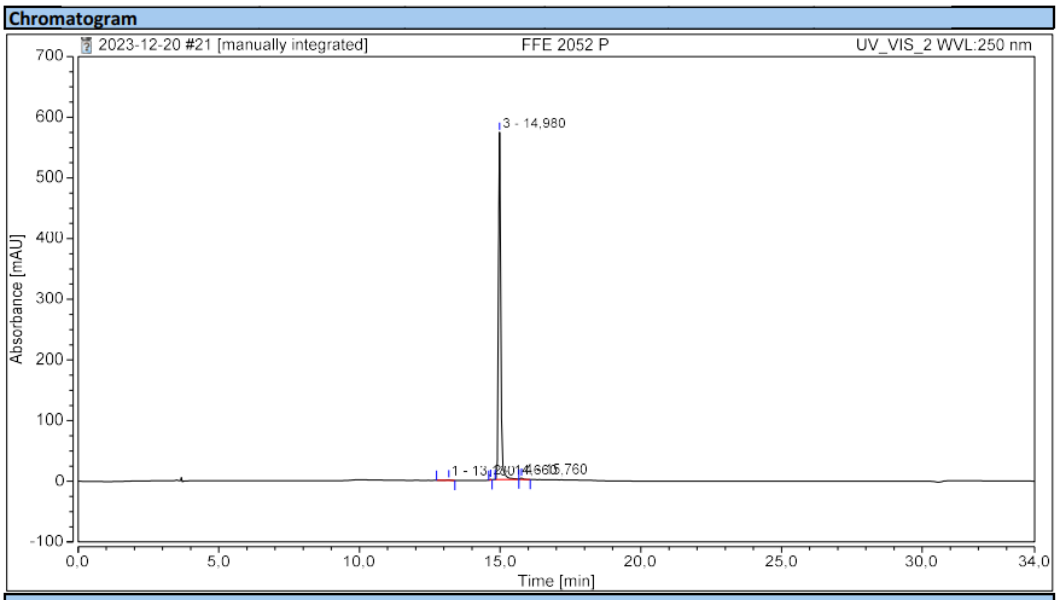

Integration Results

No.	Peak Name	Retention Time min	Area mAU*min	Height mAU	Relative Area %	Relative Height %	Amount n.a.
1		13,180	0,214	0,967	0,39	0,17	n.a.
2		14,660	0,076	1,289	0,14	0,22	n.a.
3		14,980	53,795	572,184	98,90	99,19	n.a.
4		15,760	0,310	2,400	0,57	0,42	n.a.
Total:			**54,396**	**576,841**	**100,00**	**100,00**	

HPLC chromatogram of **1k** (gradient B, purity: 98.9%).

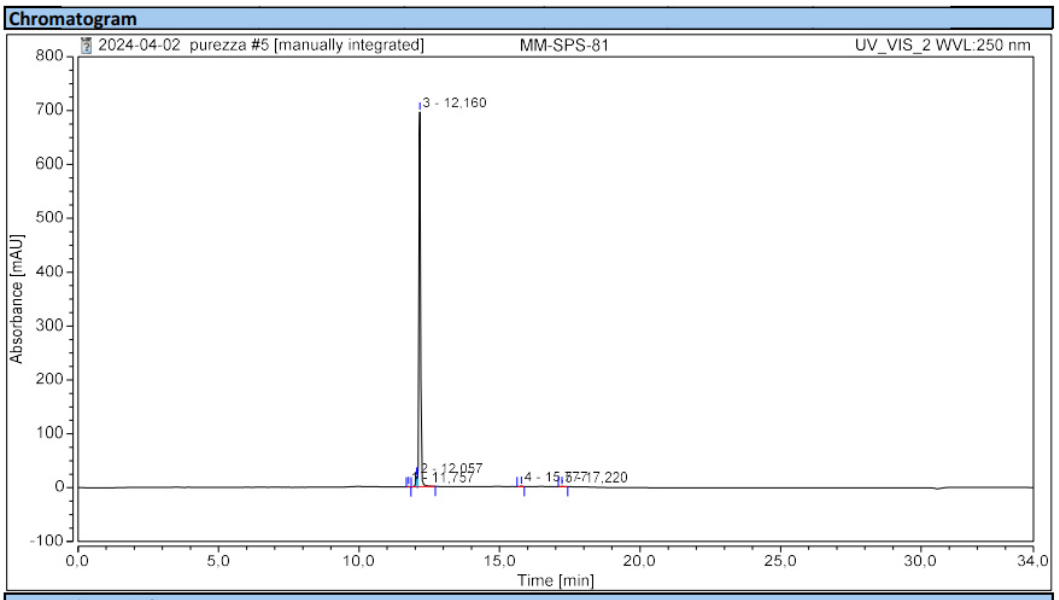

Integration Results

No.	Peak Name	Retention Time min	Area mAU*min	Height mAU	Relative Area %	Relative Height %	Amount n.a.
1		11,757	0,057	0,953	0,12	0,13	n.a.
2		12,057	1,144	18,029	2,46	2,52	n.a.
3		12,160	45,139	695,723	97,14	97,17	n.a.
4		15,777	0,070	0,841	0,15	0,12	n.a.
5		17,220	0,060	0,449	0,13	0,06	n.a.
Total:			**46,470**	**715,995**	**100,00**	**100,00**	

HPLC chromatogram of **1g-nc** (gradient B, purity: 97.1%).

Chromatogram

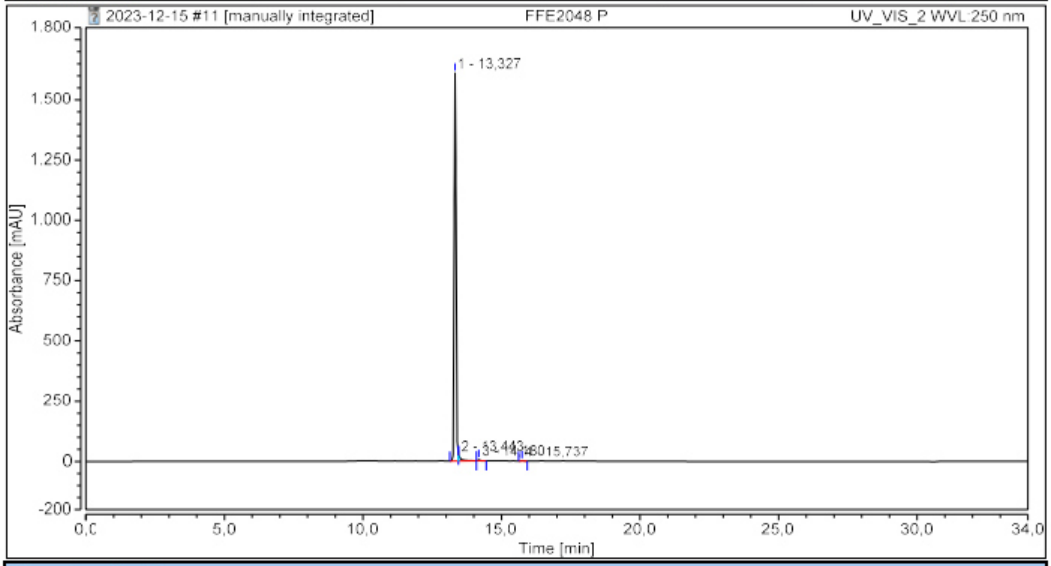

Integration Results

No.	Peak Name	Retention Time min	Area mAU*min	Height mAU	Relative Area %	Relative Height %	Amount n.a.
1		13,327	118,702	1610,163	97,27	98,13	n.a.
2		13,443	2,691	22,951	2,21	1,40	n.a.
3		14,180	0,512	6,039	0,42	0,37	n.a.
4		15,737	0,132	1,687	0,11	0,10	n.a.
Total:			**122,036**	**1640,840**	**100,00**	**100,00**	

HPLC chromatogram of **2** (gradient B, purity: 97.3%).

4. References

(1) Henning, N. J.; Manford, A. G.; Spradlin, J. N.; Brittain, S. M.; Zhang, E.; McKenna, J. M.; Tallarico, J. A.; Schirle, M.; Rape, M.; Nomura, D. K. Discovery of a Covalent FEM1B Recruiter for Targeted Protein Degradation Applications. *J. Am. Chem. Soc.* **2022**, *144* (2), 701–708. https://doi.org/10.1021/jacs.1c03980.

7.2 Appendix II. Publication 2. Replacing a Cereblon Ligand by a DDB1 and CUL4 Associated Factor 11 (DCAF11) Recruiter Converts a Selective Histone Deacetylase 6 PROTAC into a Pan- Degrader

The following pages include the full text and supplementary information of the article "Replacing a Cereblon Ligand by a DDB1 and CUL4 Associated Factor 11 (DCAF11) Recruiter Converts a Selective Histone Deacetylase 6 PROTAC into a Pan-Degrader", as it was published in ChemMedChem by Wiley-VCH GmbH.

Felix Feller, Heiko Weber, Martina Miranda, Irina Honin, Maria Hanl, and Finn K. Hansen.

Replacing a Cereblon Ligand by a DDB1 and CUL4 Associated Factor 11 (DCAF11) Recruiter Converts a Selective Histone Deacetylase 6 PROTAC into a Pan-Degrader. *ChemMedChem* **2025**, *20*, 1–33. https://doi.org/10.1002/cmdc.202500035.

ChemMedChem

Research Article
doi.org/10.1002/cmdc.202500035

Chemistry Europe
European Chemical Societies Publishing

www.chemmedchem.org

Replacing a Cereblon Ligand by a DDB1 and CUL4 Associated Factor 11 (DCAF11) Recruiter Converts a Selective Histone Deacetylase 6 PROTAC into a Pan-Degrader

Felix Feller,[a] Heiko Weber,[a] Martina Miranda,[a] Irina Honin,[a] Maria Hanl,[a] and Finn K. Hansen*[a]

Proteolysis-targeting chimeras (PROTACs) have recently gained popularity as targeted protein degradation (TPD) promises to overcome the limitations of occupancy-driven pharmacology. However, most degraders rely on a small number of E3 ligases. In this study, we present the first-in-class histone deacetylase (HDAC) PROTACs recruiting the DDB1- and CUL4- associated factor 11 (DCAF11). We established a synthesis route entirely on solid-phase to prepare a set of eleven degraders. The long and flexible spacer bearing **FF2039** (**1j**) showed significant HDAC1 and 6 degradation in combination with cytotoxicity against the multiple myeloma cell line MM.1S. Further investigations revealed that **1j** was also able to degrade HDAC isoforms of class I, IIa and IIb. Compared to our previously published cereblon-recruiting HDAC6 selective PROTAC **A6**, we succesfully transformed the selective degrader into a pan-HDAC degrader by switching the recruited E3 ligase. A detailed profiling of the anticancer properties of **1j** demonstrated its significant anti-proliferative activity against both hematological and solid cancer cell lines, driven by cell cycle arrest and apoptosis induction.

Introduction

Cancer is the cause of nearly 10 million deaths per year, making it one of humanity's most significant disease burdens, particularly in western societies.[1] It arises from a variety of factors, including genetic mutations and epigenetic alterations, the latter involving chromatin modifications without changes to the DNA sequence.[2] Chromatin remodeling, like ε-lysine acetylation of histones, is tightly regulated, as it is responsible for modulation of transcription, DNA repair, replication, and condensation.[3] To reverse the acetylation, histone deacetylases (HDACs) hydrolyze the amide bond, restoring the positive charge of the lysine and resulting in a more compact chromatin.[4]

HDACs can be distinguished into four classes: Class I (HDAC1-3 and 8), class IIa (HDAC4, 5, 7 and 9), class IIb (HDAC6 and 10), and class IV (HDAC11) are zinc-dependent deacylases. Depending on the isoform, they are primarily localized in the nucleus or in the cytoplasm and some contribute to multi-protein complexes. In addition, HDACs act on multiple substrates beyond histones and are involved in the hydrolysis of more than just acetyl groups.[5,6] The up-regulation and high expression of different HDAC isoforms are associated with poor prognosis in cancers such as multiple myeloma and acute myeloid leukemia.[7,8] Therefore, HDAC inhibition is a promising strategy for tumor therapy. Numerous studies have demonstrated that HDAC inhibitors (HDACi) reduce angiogenesis, cell migration, proliferation, and resistance to chemotherapy. Furthermore, inhibition of HDACs promotes apoptosis and enhances cell differentiation.[6,9] U.S. Food and Drug Administration (FDA) or European Medicines Agency (EMA) approved HDACi, such as vorinostat, belinostat, and romidepsin, for the treatment of T-cell lymphoma, panobinostat for the treatment of multiple myeloma, and givinostat for treating Duchenne muscular dystrophy.[10,11] In addition, the National Medical Product Administration of China approved tucidinostat for treating peripheral T-cell lymphoma and hormone receptor positive breast cancer.[12,13]

A promising alternative to conventional occupancy-driven inhibitors is targeted protein degradation (TPD) for example by molecular glues or proteolysis-targeting chimeras (PROTACs). In this approach, an E3 ligase is hijacked by a molecular glue or PROTAC to polyubiquitinate a protein of interest (POI), leading to its degradation. In Cullin RING E3 ligases, the largest group of E3 ligases, the E3 ligase complex works alongside an ubiquitin-loaded E2 enzyme, which transfers ubiquitin to the substrate or POI. This leads to subsequent degradation by the ubiquitin-proteasome system (UPS).[14,15] This catalytic mode of action provides significant advantages, such as extended pharmacological effects, doses reduction, and potentially minimizing adverse effects.[16,17] Importantly, degraders can overcome cancer resistance mechanisms, such as target amplification or overexpression, through their catalytic activity.[18] Additionally,

[a] F. Feller, H. Weber, M. Miranda, I. Honin, Dr. M. Hanl, Prof. Dr. F. K. Hansen
Department of Pharmaceutical and Cell Biological Chemistry
Pharmaceutical Institute
University of Bonn, An der Immenburg 4, 53121 Bonn, Germany
E-mail: finn.hansen@uni-bonn.de

Supporting information for this article is available on the WWW under https://doi.org/10.1002/cmdc.202500035

they can counteract resistance caused by altered ligand binding sites, as even weak binders can still enable efficient degradation.[19]

While molecular glues identification is often serendipitous, PROTACs can be designed more rationally. However, due to recent discoveries in degrader development it becomes more and more difficult to differentiate between molecular glues and PROTACs. This becomes particular evident in a series of linker-less PROTACs that combine a POI-warhead with a covalent handle for a specific E3 ligase. These compounds, termed monovalent molecular glues or linker-less PROTACs, challenge traditional classifications.[20,21]

PROTACs for targeted degradation of HDACs were introduced in 2018, and since then, over 100 HDAC PROTACs have been published.[22–26] Despite the use of many different HDAC ligands, only three E3 ligases have been employed according to PROTAC-DB 3.0: Cereblon (CRBN), Von Hippel-Lindau (VHL), and the inhibitor of apoptosis protein (IAP).[27] The first PROTAC for targeted degradation of an HDAC was the crebinostat-derived degrader **I** (Figure 1). It used pomalidomide for CRBN recruitment and despite PROTAC **I** contains a pan-HDAC ligand, only HDAC6 was degraded.[22] PROTAC **II** and **IV** are representatives of the first successful recruitment of VHL and IAP, respectively. PROTAC **III** contains a benzamide for targeting class I HDACs, and the switch to a CRBN recruiter shows similar degradation selectivity as **II**, but to a lesser extent.[28] The E3 ligase switch from **IV** to **V** yielded a different result: Both contain the pan-HDAC inhibitor dacinostat and a polyethylene glycol (PEG) spacer, but the IAP-recruiting **IV** resulted in HDAC6 degradation, while **V** degraded HDAC3 and 8 by VHL recruitment.[29] With

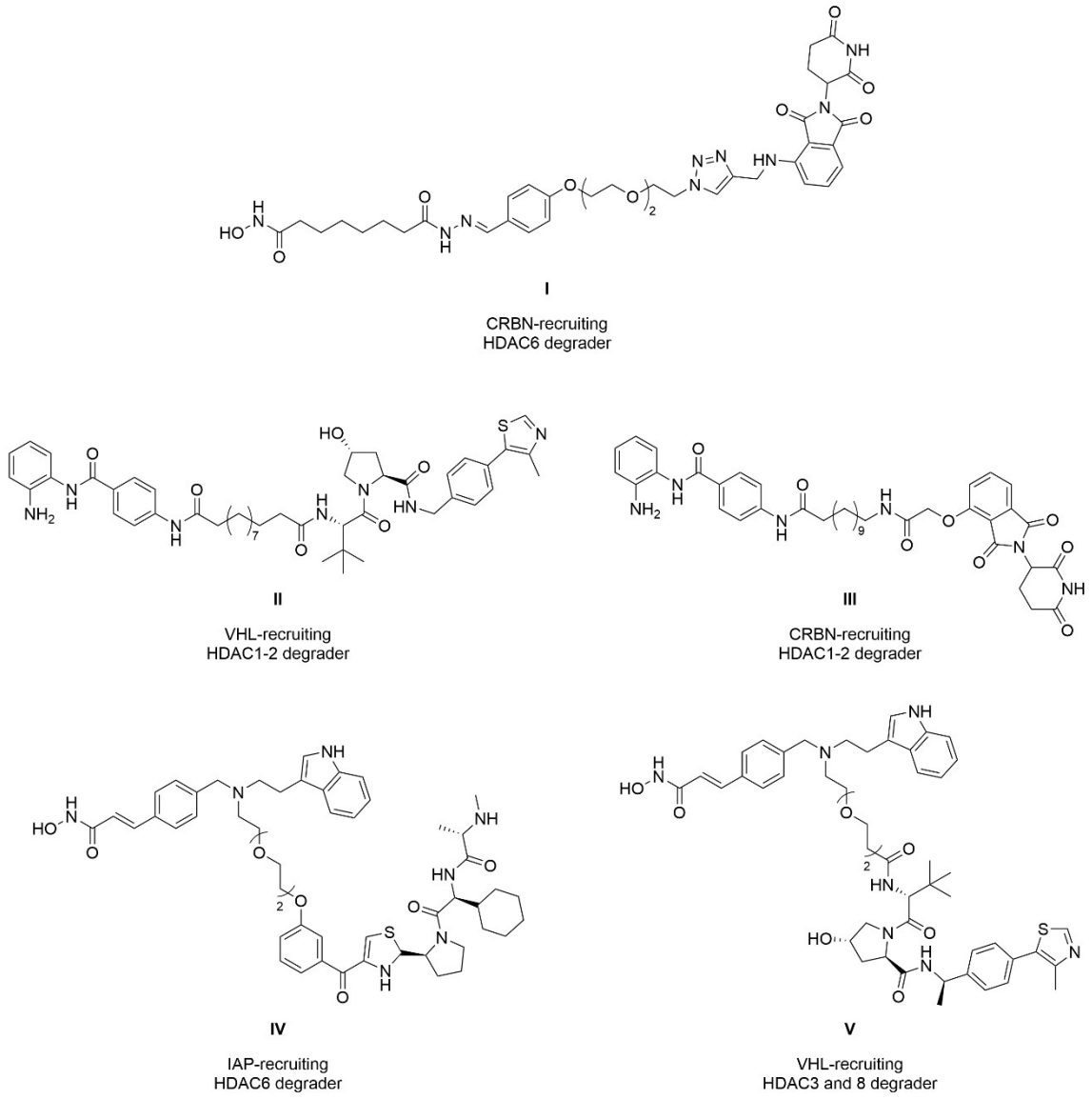

Figure 1. Comparison of HDAC PROTACs recruiting different E3 ligases. PROTAC **I**[22] was the first utilization of CRBN for HDAC degradation, while PROTAC **II**[28] represents the first VHL-based HDAC degrader. PROTAC **III**[28] showed similar degradation selectivity as PROTAC **II**, but to a lesser extent by switching back to a CRBN recruiter. The first successful utilization of IAP for targeted HDAC degradation was PROTAC **IV**[29] and changing the E3 ligase to VHL, represented by PROTAC **V**,[29] resulted in a switch of degraded isoforms.

more than 600 E3 ligases encoded in the human genome, there is a significant need to expand the number of utilized E3 ligases for HDAC degradation.[30] Furthermore, unlocking specific E3 ligases with dedicated tissue or cell-type specificity holds great potential for achieving degradation in the desired tissue. Likewise, targeting tumor- or disease-enriched E3 ligase could enable the development of more refined and selective degraders.[31,32] Expanding the use of new E3 ligases can also help to target new tumor entities; for example, it has been shown that the sensitivity pattern of tested tumor cell lines to PROTACs changes by switching from CRBN to VHL.[33] However, ligands for both E3 s come with some limitations, as thalidomide is associated with teratogenicity and stability issues, while the VHL ligands increase molecular weight and topological polar surface area, which can be challenging for oral bioavailability.[17] Using E3 ligases which degrade tumor suppressor-proteins can have additional anticancer effects. For example, mouse double minute 2 homolog (MDM2) recruitment for TPD leads to a stabilization of p53 and p21 is substrate of the E3 ligase DCAF11.[34,35]

Lately, the range of E3 ligases used in TPD has expanded. For example, ligands for Fem-1 homolog B (FEM1B),[36] Ring Finger Protein 4 (RNF4),[37] Ring Finger Protein 114 (RNF114),[38] DDB1- and CUL4-associated factor 11 (DCAF11),[39–43] and DDB1- and CUL4-associated factor 16 (DCAF16)[44] have been utilized in TPD strategies. These ligands share an electrophilic warhead to engage the E3 ligase, resulting in a pseudo-binary complex of E3 ligase, covalently bound PROTAC, and POI. This results in simpler kinetics, as the covalent construct of E3 ligase and PROTAC only needs to recruit a new POI molecule for polyubiquitination.[45]

In this work, we utilized the Ugi four component reaction (U-4CR)-derived DCAF11 ligand of Zhang et al.,[39] because of its promising degradation results and fast accessibility due to the U-4CR. Based on our previously published HDAC6 degrader **A6**, we started to design the DCAF11-recruiting PROTACs (Figure 2).[46] In our previous studies, we developed a highly modular approach for the solid-phase synthesis of PROTACs and extended this approach to the synthesis of hydrophobically tagged HDAC inhibitors.[46–48] Adapting the U-4CR to the solid-phase conditions allowed us to synthesize a set of eleven PROTACs entirely on resin. The subsequent biological evaluation revealed significant degradation of HDAC1, correlating with cytotoxic effects in the multiple myeloma cell line MM.1S.

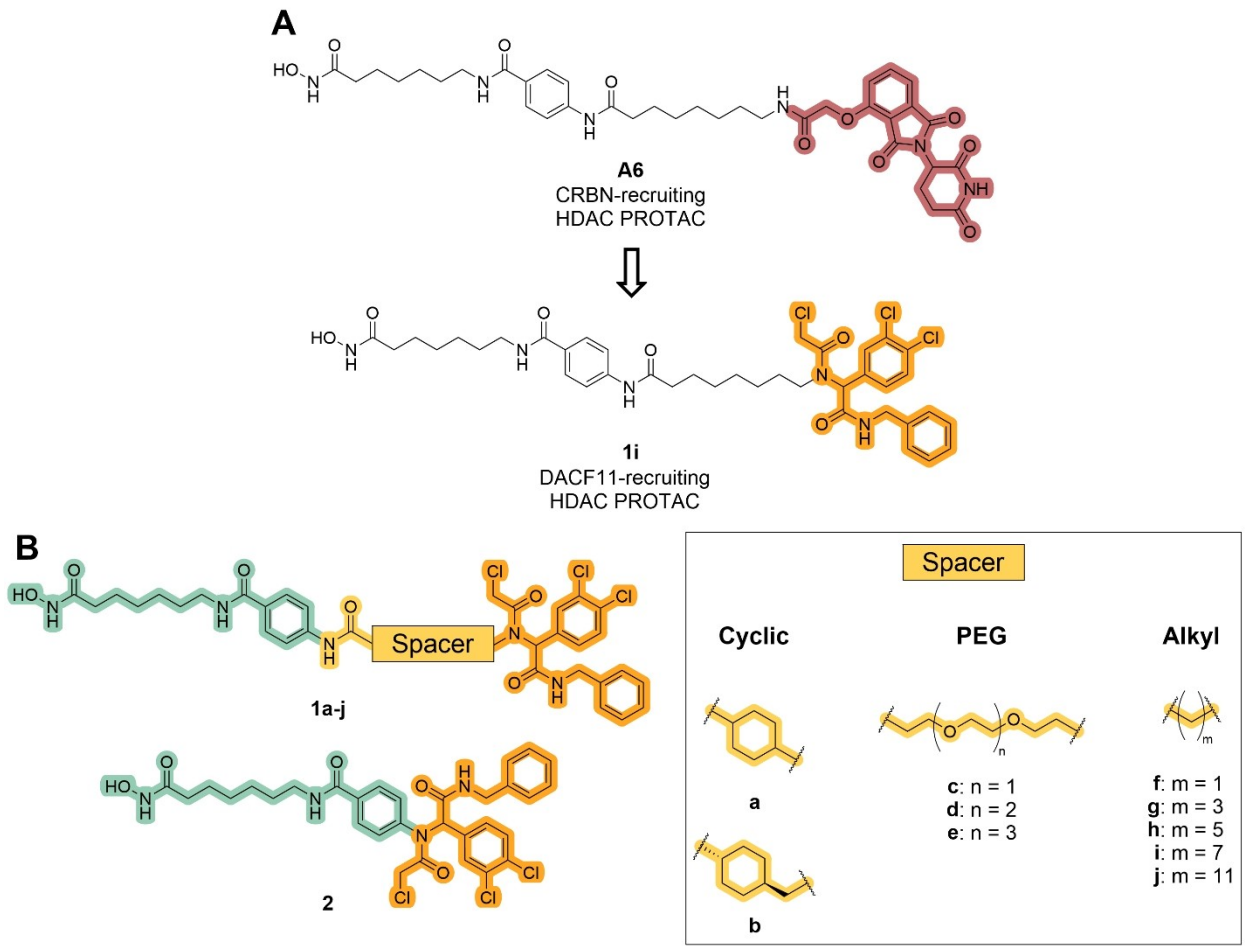

Figure 2. Design of DCAF11-recruiting HDAC PROTACs. (A) Switch from the CRBN-recruiting thalidomide-based E3 ligase ligand (red) of **A6** to the DCAF11-recruiting ligand (orange). (B) The DCAF11-based HDAC PROTACs (**1a-j**) consist of three parts: The vorinostat-like HDAC ligand (green) and the DCAF11 ligand (orange) are connected by a broad spectrum of spacers (yellow). The spacer-less compound **2** consist only of the HDAC and DCAF11 ligand.

Notably, further investigation of compounds **1j** and **2**, which share the POI ligand with **A6** but differ in linker length and E3 ligase ligand, revealed enhanced degradation capabilities and both compounds induced pan-HDAC degradation across all isoforms tested. This effect was accompanied by increased cell cycle arrest, apoptosis induction, and long-term antiproliferative activity.

Results and Discussion

Design and Synthesis of DCAF11-Recruiting HDAC PROTACs

The design of our PROTACs was based on the best degrader of our previous HDAC degrader study, **A6**,[46] which combines a vorinostat-like HDAC inhibitor and a thalidomide-based CRBN ligand, fused by a C7 aliphatic spacer (Figure 2A). Although vorinostat is a pan-HDAC inhibitor, **A6** specifically targeted HDAC6 for degradation. The aim of this study was to investigate how switching the E3 ligase affects the HDAC degradation selectivity profile.

To convert the CRBN-utilizing PROTAC into one that recruits DCAF11, we replaced the thalidomide-based ligand (red, **A6**) with a DCAF11 ligand (orange, **1i**, Figure 2A). We retained the vorinostat-like pan-HDACi ligand and C7 linker, to trace back any possible effects to the exchange of the E3 ligase recruiter. The initial PROTAC **1i**, which represents the direct DCAF11-recruiting analog of **A6**, was complemented by a set of nine degraders, bearing a broad range of different spacers to introduce diversity in regards to chain length, lipophilicity, and rigidity. In detail, two short and rigid cyclic spacers (**1a-b**, Figure 2B), three more flexible PEG spacers (**1c-e**), and some alkyl spacers ranging from C1-C11 (**1f-j**) were selected. As mentioned before, the line between PROTACs and molecular glues is becoming increasingly blurred,[20,49] we also designed a compound that can be considered as a spacer-less PROTAC (**2**). In total, we decided to synthesize eleven PROTACs to study the effect of DCAF11 recruitment on HDAC degradation. The synthesis of the DCAF11-recruiting PROTACs was completely carried out on solid support and is shown in Scheme 1. For resin modification, loading determination, and amide coupling reactions, our previously published protocols were used.[46–48] Specifically, the commercially available 2-chlorotrityl chloride (2-CTC) resin was modified with *N*-hydroxyphthalimide to immobilize the hydroxylamine as the precursor for the hydroxamic acid on the resin (not shown). The subsequent hydrazine monohydrate-mediated deprotection released the resin-bound hydroxylamine, enabling its coupling with Fmoc-7-aminoheptanoic acid, which was facilitated by HATU and HOBt. This step formed the zinc-binding group and linker of the resin-bound HDAC inhibitor **3**. After Fmoc-deprotection of the precursor, Fmoc-4-aminobenzoic acid was used to complete the HDACi **4**. The last step before the introduction of the DCAF11 ligand was the attachment of various spacers, which was performed in the same manner as previous couplings steps to produce **5a-j**. The precursors **4** and **5a-j** were then used to install the DCAF11 ligand by an on resin U-4CR. To this end, 3,4-dichlorobenzaldehyde, 2-chloroacetic acid, and benzyl isocyanide were used in the U-4CR. This synthetic approach enabled the introduction of the DCAF11 ligand in one final

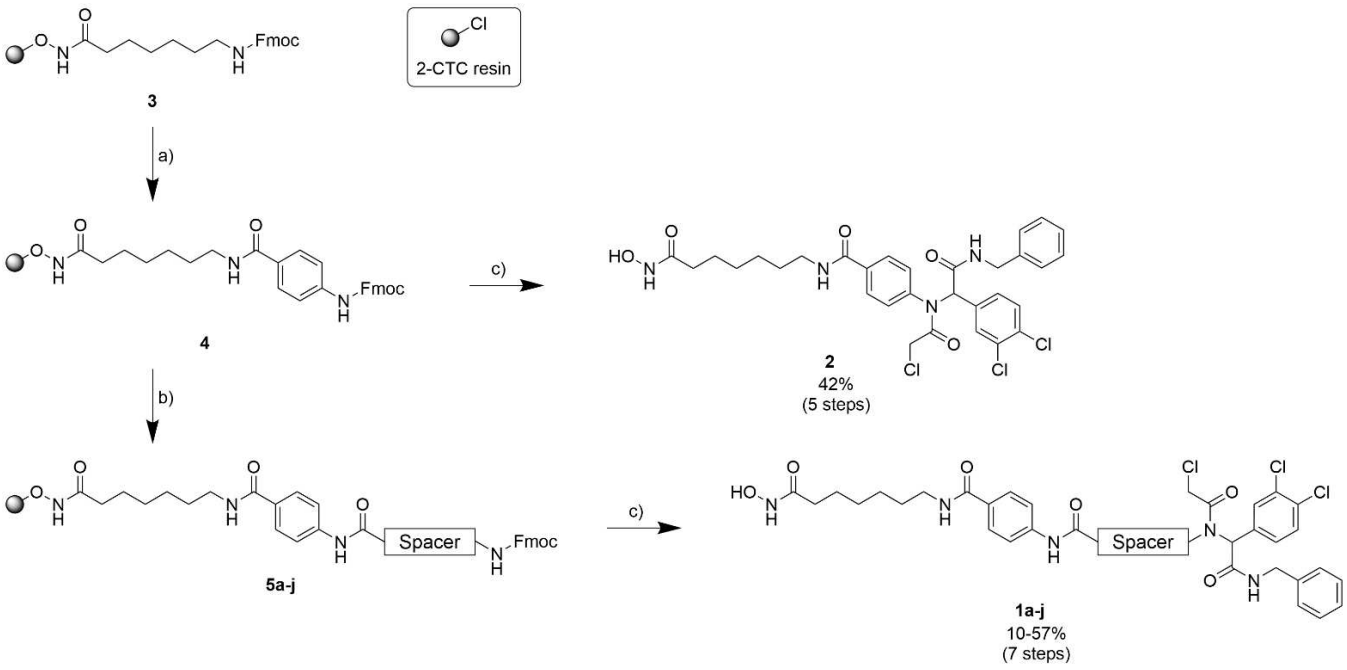

Scheme 1. Solid-phase synthesis of DCAF11-recruiting HDAC PROTACs. *Reagents and conditions*: a) (i) 20% Piperidine, DMF, rt, 2×5 min, (ii) Fmoc-4-aminobenzoic acid, HATU, HOBt·H_2O, DIPEA, DMF, rt, 18 h; b) (i) 20% piperidine, DMF, rt, 2×5 min, (ii) Fmoc-NH-spacer-COOH, HATU, HOBt·H_2O, DIPEA, DMF, rt, 18 h; c) (i) 20% piperidine, DMF, rt, 2×5 min, (ii) 3,4-dichlorobenzaldehyde, 2-chloroacetic acid, benzyl isocyanide, DMF/MeOH (1/1 *v/v*), rt, 72 h, (iii) 5% TFA, 5% triisopropylsilane, CH_2Cl_2, rt, 1 h.

step. Finally, all compounds were cleaved from the resin and purified by preparative HPLC to >95% purity.

Degradation and Antiproliferative Activity of DCAF11-Recruiting PROTACs

To investigate the HDAC degradation capability of the novel DCAF11-recruiting PROTACs, we treated the multiple myeloma cell line MM.1S with the compounds and performed automated Simple Western™ immunoassays. According to DepMap, MM.1S cells show similar baseline expression levels of DCAF11 and CRBN (5.02 and 4.9 (log2) transcription per million respectively).[50] We first examined the effects on HDAC1 and 6 protein levels, as they represent members of the most studied HDAC classes (I and IIb) and are mainly located in opposite cellular compartments (nucleus and cytoplasm). Figure 3 summarizes the analyzed HDAC1 and 6 levels: HDAC1 was not degraded by PROTACs bearing the cyclic spacers, but the longer and more polar PEG spacer-containing PROTACs showed a significant reduction of up to 51% (**1e**). The alkyl spacer-based compounds revealed some unexpected results: while the C5 spacer (compound **1h**) did not reduce HDAC1 levels, PROTACs with both shorter and longer spacers showed a trend toward significant HDAC1 degradation. Interestingly, also the spacer-less degrader **2** demonstrated significant HDAC1 degradation. The most pronounced reduction of HDAC1 levels was detected for spacer-less PROTAC **2** (55%) and the longest C11 spacer bearing PROTAC **1j** (71%). In addition, these two PROTACs were also capable of achieving significant reduction of HDAC6 protein levels, whereas all the other compounds showed no significant effects on HDAC6 protein abundance.

Encouraged by the promising reductions in HDAC1 and HDAC6 levels, we further investigated the phenotypic effects of our DCAF11-recruiting PROTACs on cancer cells. Accordingly, we performed a cell viability assay on multiple myeloma MM.1S cells after treatment with the indicated compounds. The results are presented in Figure 4. The rigid cyclic spacer-bearing PROTACs (**1a**, **1b**) demonstrated diminished antiproliferative activity, whereas the spacer-less (**2**: $EC_{50} = 1.5$ μM) and the longest alkyl spacer (**1j**: $EC_{50} = 2.8$ μM) yielded pronounced degradation of both HDAC1 and 6. In addition, **2** and **1j** displayed superior antiproliferative activity in MM.1S cells compared to ricolinostat, an HDACi currently under clinical investigation.[51] Furthermore, we investigated the contribution of the DCAF11 ligand to the antiproliferative activity of the PROTACs. To this end, we synthesized the *n*-propyl-substituted DCAF11 warhead **6** (see Scheme S1, Supporting Information) and tested a 1:1 combination of vorinostat and **6** in a cell viability assay. Since the EC_{50} of the combination treatment was similar to that of vorinostat alone, the DCAF11 ligand seems not to add significant cytotoxicity (Figure S1, Supporting Information). In contrast, the thalidomide-based PROTAC **A6** showed no effect on the viability of MM.1S cells, which is in line with the literature, where there was little to no effect by **A6** depending on the cell line.[46,52]

Notably, the antiproliferative activity of **2** and **1j** is reduce compared to the parent HDACi vorinostat by a factor of ~3 – 6, which is comparable to the previously published FEM1B-recruiting PROTACs sharing the same POI ligand.[52] To investigate this reduced antiproliferative activity in comparison to vorinostat, we tested cell permeability using a cellular HDAC inhibition assay in the presence and absence of IGEPAL as a permeabilization agent. Cellular permeability does not appear

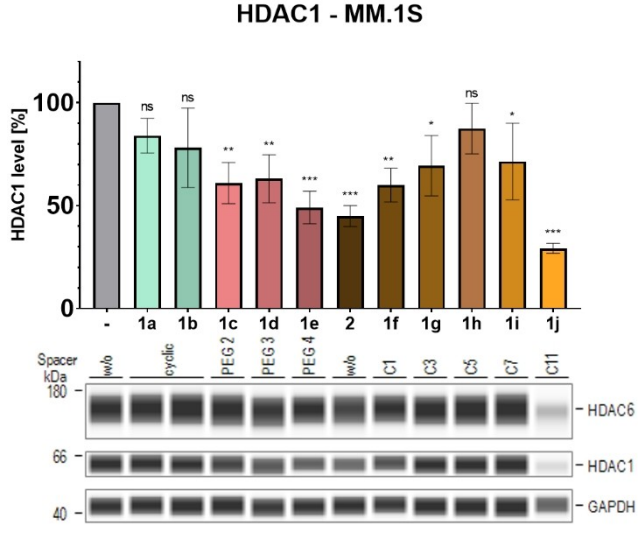

Figure 3. Initial degradation screening of HDAC1 and 6 by DCAF11-recruiting PROTACs by Simple Western™ immunoassay analysis of MM.1S cell lysates. MM.1S cells were treated with the indicated compound (10 μM) or vehicle (DMSO) for 24 h. Top: Quantification of HDAC1 levels, presented as mean ± standard deviation of n = 3 biological replicates; Significance compared to vehicle: ns = $p \geq 0.05$; * = $p \leq 0.05$, ** = $p \leq 0.01$, *** = $p \leq 0.001$. Bottom: Representative images from a total of n = 3 biological replicates, labeled with spacer type; w/o: without spacer.

Compound	EC_{50} [μM][a]
1a	34 ± 6
1b	18 ± 3
1c	6.2 ± 0.7
1d	6.9 ± 0.6
1e	7.3 ± 0.5
2	1.5 ± 0.1
1f	19 ± 3
1g	16 ± 2
1h	18 ± 7
1i	12 ± 2
1j	2.8 ± 0.1
A6	n.e.
Ricolinostat	3.0 ± 0.6
Vorinostat	0.51 ± 0.14

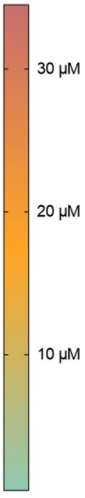

Figure 4. Antiproliferative activity of DCAF11-recruiting PROTACs. [a]Mean ± standard deviation of EC_{50} of three independent experiments, each in duplicates; n.e.: no effect (≤25% effect up to 50 μM). Antiproliferative activity of DCAF11-recruiting PROTACs in MM.1S cells after 72 h.

to be an issue for the PROTACs, as cellular HDAC inhibition is not dependent on the addition of IGEPAL (Figure S2, Supporting Information). Finally, aqueous stability was identified as a potential source of reduced antiproliferative activity. Vorinostat remained intact in DPBS buffer for 72 hours, whereas PROTAC **2** decomposed by 31% over the same period. During the first 24 hours, PROTAC **1j** showed similar stability to **2**. However, after 72 hours, **1j** showed a degradation profile that was comparable to that of **A6**, with a reduction in content of more than 90% (Figure S3, Supporting Information).

Target Engagement and HDAC Degradation Selectivity Profile of 2 and 1j

For further investigations, we selected the two most effective HDAC1 degraders from this set (**2** and **1j**), as they also demonstrated the highest antiproliferative activity. As target engagement is crucial for targeted protein degradation, we next investigated the HDAC inhibition efficiency of the PROTAC hits. To distinguish between their effects on the various isoforms, we evaluated the inhibitory activity on representative isoforms from different HDAC classes, namely HDAC1, 2, 4 and 6 (Table 1). Compound **2** demonstrated comparable inhibition results as **A6**. However, **1j**, the most potent degrader, exhibited comparatively weaker inhibition of all tested isoforms. The half-maximal inhibitory concentration (IC_{50}) is consistently ~4-8 times higher than that of **2**

Moreover, the capability to reduce the enzymatic activity of HDACs was confirmed by a cellular target engagement assay. MM.1S cells were treated with the PROTACs and the level of acetylated HDAC substrate proteins was subsequently determined. Class I HDACs deacetylate histone H3, and thus hyperacetylation of histone H3 indicates class I HDAC inhibition. Conversely, hyperacetylation of α-tubulin serves a marker of HDAC6 inhibition. Both hit compounds are capable of inhibiting class I and HDAC6 in a cellular environment, confirming effective target engagement in MM.1S cells (Figure 5). With regards to the HDAC6 inhibition, the trend of the enzyme inhibition data was thus confirmed. However, histone H3 hyperacetylation was more pronounced by **1j**, compared to **2** and **A6.**

In the next step, we investigated whether this target engagement translates into degradation of multiple HDAC isoforms. HDAC1, 2, 4, and 6 levels were determined by immunoblot analysis of MM.1S cell lysates and the CRBN-recruiting PROTAC **A6** was used as control. The immunoblot analysis confirmed the automated Simple Western™ immunoassay results, as **1j** showed most pronounced degradation of all tested HDAC isoforms (Figure 6). In detail, the strongest maximal degradation (D_{max}) was observed for HDAC1 (90%) by **1j**, while the degradation of HDAC2, 4, and 6 ranged from 71–76%. D_{max} of compound **2**, although slightly less efficient, was also the strongest for HDAC1 (74%) followed by HDAC2 (51%), while HDAC4 (40%) and HDAC6 (26%) were also degraded, but to a lesser extent (see Table S1, Supporting Information). In contrast, **A6** selectively degraded HDAC6 without significant effects on the other HDAC isoforms, as previously reported.[46] By utilizing DCAF11 instead of CRBN for HDAC degradation, **1j** and **2** are able to broaden the scope of degraded HDAC isoforms, degrading not only HDAC6 but also HDAC1, 2, 4, and 6. In addition, the degradation pattern of **1j** was further investigated by its time dependency. Treatment of MM.1S cells revealed significant degradation of HDAC1 and 6 after 6 h, which increased after 14 h and 24 h (Figure S4, Supporting Information).

Table 1. HDAC isoform inhibition by DCAF11-recruiting PROTACs.

Compound	E3 ligase	IC_{50} [μM][a]			
		HDAC1	HDAC2	HDAC4	HDAC6
2	DCAF11	0.159 ± 0.044	0.298 ± 0.011	3.26 ± 0.08	0.007 ± 0.001
1j	DCAF11	1.03 ± 0.04	2.15 ± 0.11	12.4 ± 1.5	0.053 ± 0.001
A6	CRBN	0.125 ± 0.009	0.274 ± 0.036	5.26 ± 0.50	0.009 ± 0.004
Vorinostat	-	0.094 ± 0.010	0.215 ± 0.028	n.e.	0.046 ± 0.005
Ricolinostat	-	0.156 ± 0.005	0.361 ± 0.036	7.22 ± 0.39	0.018 ± 0.002

[a]Mean ± standard deviation is shown of at least two independent experiments,each performed in duplicates. n.e.: no effect (≤30% inhibition up to 10 μM).

Cell Cycle Arrest and Apoptosis Induction of 2 and 1j

To gain a more comprehensive understanding of the cellular effects of **2** and **1j**, cell cycle and apoptosis induction was analyzed. After treating MM.1S cells with the indicated compounds or vehicle for 48 h, the cells were permeabilized, fixed, and stained with propidium iodide (PI) to quantify the DNA content by flow cytometry (Figure 7A, B). The treatment of both PROTACs (**2**, **1j**) resulted in an increase of the sub G1 phase, while the S phase was decreased. This indicates cell cycle arrest

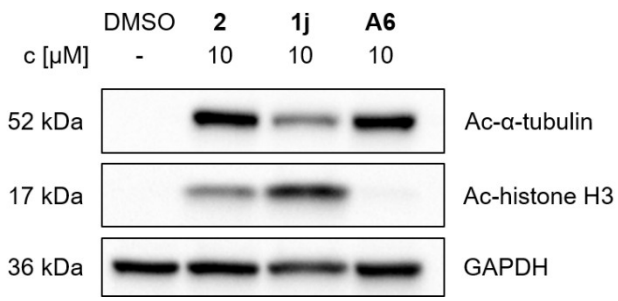

Figure 5. Cellular target engagement by **2**, **1j**, and **A6**. Immunoblot analysis of acetylated α-tubulin and histone H3 in MM.1S cell lysates. Cells were treated with the indicated compounds (10 μM) or vehicle (DMSO) for 24 h. Representative images from a total of n = 3 biological replicates.

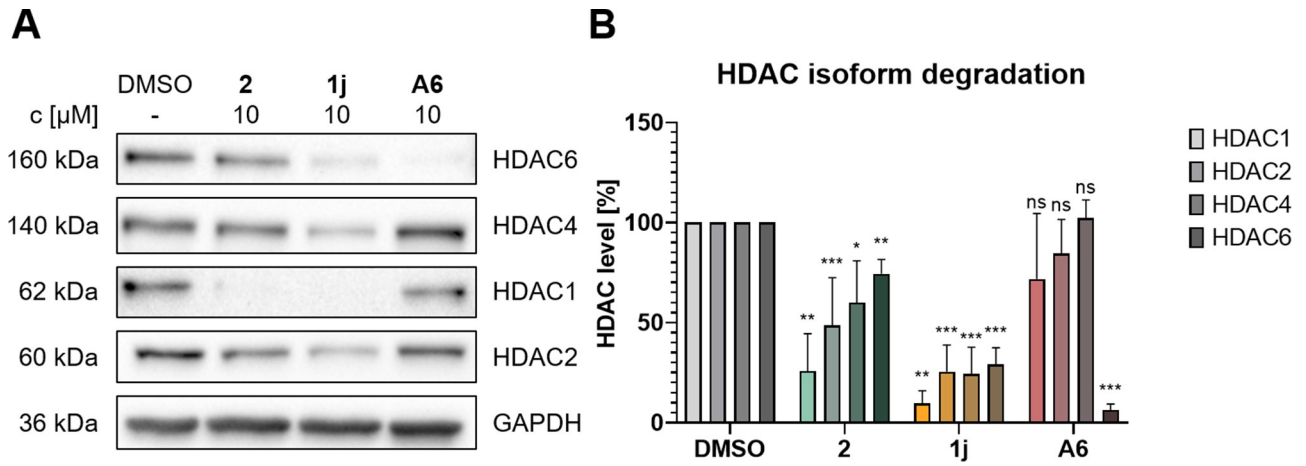

Figure 6. Examination of HDAC isoform degradation. MM.1S cells were treated with the indicated compounds (10 μM) or vehicle (DMSO) for 24 h. HDAC1, 2, 4, and 6 levels were analyzed by immunoblotting. (A) Representative images from a total of n = 3 biological replicates. (B) Quantification of HDAC1, 2, 4, and 6 presented as mean ± standard deviation of n = 3 biological replicates; significance compared to vehicle: ns = $p \geq 0.05$; * = $p \leq 0.05$; ** = $p \leq 0.01$; *** = $p \leq 0.001$.

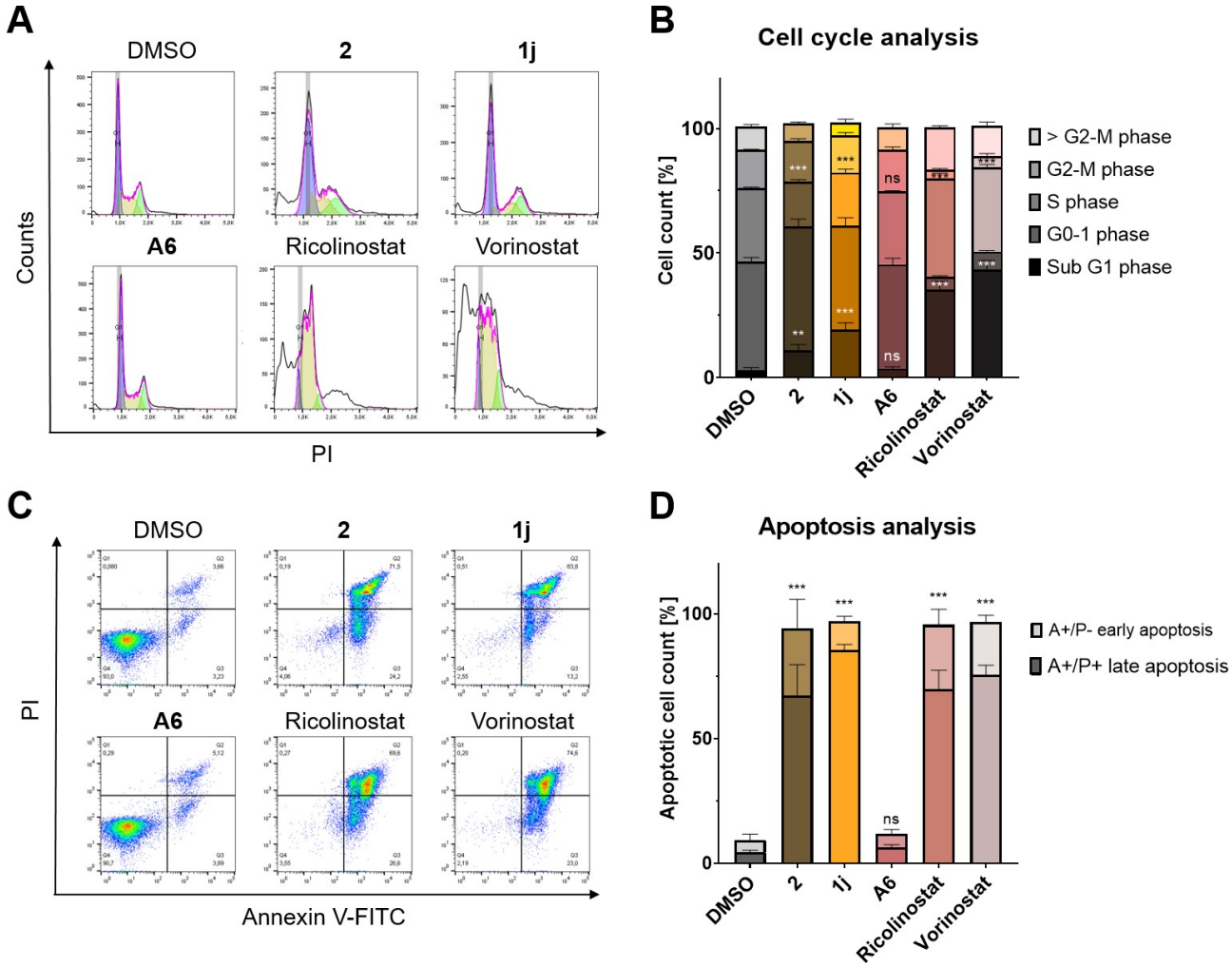

Figure 7. Cell cycle and apoptosis induction analysis by flow cytometry. MM.1S cells were treated with the respective compound (10 μM) or vehicle (DMSO) for 48 h. (A) Representative data of cell cycle analysis of MM.1S cells after PI staining. (B) Quantification of cell cycle analysis, presented as mean ± standard deviation of n = 3 biological replicates, each performed in duplicates. (C) Representative data of apoptosis induction analysis of MM.1S cells after annexin V-FITC/PI staining. (D) Quantification of apoptosis induction analysis, presented as mean ± standard deviation of n = 3 biological replicates, each performed in triplicates. Significance of apoptosis analysis is regarding the combined quantities of early and late apoptosis. In the case of (B) and (D), significance of quantification is compared to vehicle: ns = $p \geq 0.05$; ** = $p \leq 0.01$ and *** = $p \leq 0.001$.

and apoptosis induction. In contrast, the CRBN-recruiting PROTAC **A6** indicated no significant changes in cell cycle. However, the included HDACi ricolinostat and vorinostat both showed stronger effects on the different phases of the cell cycle. The apoptosis induction was additionally assessed by staining with FITC labeled annexin V and PI. Flow cytometry analysis with these two dyes enables the distinctions between early and late apoptotic cells besides unaffected cells (Figure 7C, D). This analysis revealed less differences between the DCAF11-recruiting PROTACs and the HDACi. All compounds significantly induced apoptosis, to a comparable extent. The only exception is **A6**, which stayed on the level of vehicle control. This proves that the antiproliferative activity of **2** and **1j** in MM.1S cells is based on the arrest of cell cycle and of induction of apoptosis.

Synthesis and Evaluation of the Non-Degrading Control 1j-nc

In the next step, we wanted to design and synthesize a non-degrading control for the most effective PROTAC **1j**. It is essential that the non-degrading control is as comparable to the PROTAC as possible, without binding to the E3 ligase. By the absence of degradation, the non-degrading control proves TPD, which requires the E3 ligase for the reduction of protein levels. In addition, it enables to distinguish between inhibitor and degrader effects. In case of **1j** the non-degrading control was designed by substituting the electrophilic warhead of the DCAF11 ligand. The replacement of 2-chloroacetic acid by propionic acid led to no successful U-4CR, because of reduced nucleophilicity of the propionic acid. We successfully obtained the U-4CR product bound on resin by switching to formic acid. After cleavage and purification, as described before, **1j-nc** was prepared in 38% yield over seven steps (Scheme 2).

The non-degrading control was then used to treat MM.1S cells in direct comparison to the related PROTAC **1j**. In comparison to **1j**, the non-degrading control **1j-nc** was not able to affect the protein levels of HDAC1 and 6 (Figure 8), proving that covalent binding to DCAF11 is crucial for degradation.

Cross Cell Line Activity of 2 and 1j

Encouraged by the positive results in the multiple myeloma cell line MM.1S, we wanted to expand the application of the DCAF11 PROTACs to other cancer models. The triple negative

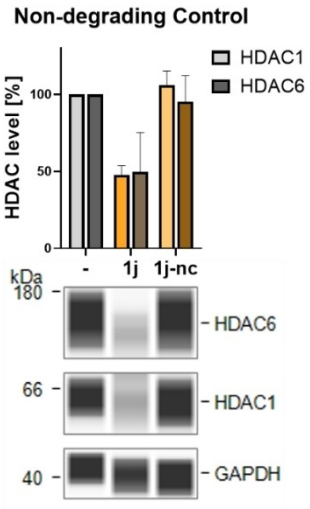

Figure 8. Evaluation of the effects of the non-degrading control **1j-nc** on HDAC protein levels. Simple Western™ immunoassay analysis of MM.1S cell lysates. MM.1S cells were incubated with **1j** (10 μM), **1j-nc** (10 μM), or vehicle (DMSO) for 14 h. Representative image from a total of n = 2 biological replicates.

breast cancer cell line MDA-MB-231 and the glioblastoma cell line U-87MG were selected as they depict aggressive and hard to treat solid tumors, in which HDACi showed first promising effects.[53,54] The phenotypic cell viability screening demonstrated that both PROTACs exhibited cytotoxicity against all tested cell lines (Table 2). However, the effect was diminished in the solid cancer cell lines, particularly for U-87MG, in comparison to the multiple myeloma cell line MM.1S. As anticipated, the non-degrading control **1j-nc** demonstrated no activity in MDA-MB-231, indicating that degradation is the underlying cause of cytotoxicity. However, **1j-nc** exhibited some impact on MM.1S and U-87MG, but consistently weaker compared to the PROTACs.

As **2** and **1j** led to reduced cytotoxicity in U-87MG cells, we analyzed HDAC1 and 6 degradation in this cell line. We chose the same treatment conditions as for MM.1S and the automated Simple Western™ immunoassay analysis confirmed significant degradation for HDAC1 by **2** and significant HDAC1 and 6 degradation by **1j** (Figure S5, Supporting Information). Nevertheless, the degradation was weaker in U-87MG cells compared to MM.1S which is in good agreement with data from the viability assays.

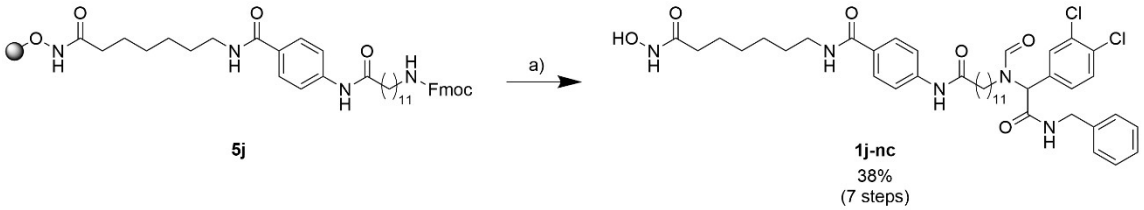

5j → **1j-nc** 38% (7 steps)

Scheme 2. Synthesis of the non-degrading control (**1j-nc**) based on **1**. *Reagents and conditions*: a) (i) 20% piperidine, DMF, rt, 2×5 min, (ii) 3,4-dichlorobenzaldehyde, formic acid, benzyl isocyanide, DMF/MeOH (1/1 *v*/*v*), rt, 72 h, (iii) 5% TFA, 5% triisopropylsilane, CH_2Cl_2, rt, 1 h.

Clonogenic Growth Inhibition by 2 and 1j

The short-term effects on cancer cell lines were supported by a clonogenic growth assay. Using this assay, we could study the long-term anticancer effects of DCAF11-recruiting HDAC PROTACs. The solid cancer cell line MDA-MB-231 was chosen for this investigation, because of the elevated effect on cell viability and the better growth pattern, compared to U-87MG. The triple negative breast cancer cells were incubated for 48 h with the respective compound, before they were isolated and grown for nine days. The resulting colonies were quantified and are depicted in Figure 9. Both **2** and **1j** resulted in a significant reduction of colonies. However, **1j** demonstrated a more pronounced reduction in clonogenic growth, which aligns with the enhanced HDAC degradation. The two HDACi, included as a control, demonstrated a trend to a reduction in colony count, albeit less pronounced and not significant. Notably, **2** and **1j** outperformed ricolinostat and vorinostat in the long-term clonogenic growth assays. In contrast, the thalidomide-based HDAC PROTAC **A6** did not result in a significant reduction in clonogenic growth.

Table 2. Antiproliferative activity of DCAF11 PROTACs against different tumor entities.

Compound	EC_{50} [μM][a]		
	MM.1S	MDA-MB-231	U-87MG
2	1.5 ± 0.1	8.8 ± 3.2	12 ± 3
1j	2.8 ± 0.1	28 ± 10	30 ± 5
1j-nc	8.6 ± 1.5	n.e.	43 ± 18
A6	n.e.	n.e.	n.e.
Ricolinostat	3.0 ± 0.6	6.1 ± 3.0	7.6 ± 1.1
Vorinostat	0.51 ± 0.14	2.4 ± 0.2	3.6 ± 0.8

[a]Mean ± standard deviation of at least three independent experiments. n.e.: no effect (≤25% effect up to 50 μM). Antiproliferative activity of respective compounds in different cancer cell lines after 72 h.

Conclusions

In summary, we present the first-in-class DCAF11-recruiting HDAC PROTACs. These novel compounds are derived from our previously reported HDAC PROTAC **A6** but feature a DCAF11 ligand in place of the CRBN ligand. The synthesis was performed entirely on solid-phase, which accelerated the synthesis and gave compounds **1a-j** and **2** in yields of up to 57% over seven steps. The subsequent evaluation of the PROTACs for HDAC degradation uncovered **2** and **1j** (hereafter dubbed **FF2039**) as the most effective HDAC1 degraders with additional HDAC6 degradation capabilities. Moreover, we demonstrated that HDAC degradation translates into antiproliferative activity against MM.1S cells, with cytotoxicity appearing to correlate with the degree of HDAC1 degradation. An *in vitro* enzyme inhibition assay revealed that **2** showed comparable inhibition to **A6** against HDAC1, 2, 4, and 6, whereas **FF2039** displayed reduced inhibition of all tested isoforms. In contrast, the cellular target engagement analysis showed a distinct inhibition of HDAC6 by both PROTACs and a stronger inhibition of class I HDACs by **2** and **FF2039** compared to **A6**. Both **2** and **FF2039** were able to significantly degrade HDACs of class I, IIa, and IIb, with **FF2039** emerging as the more efficient degrader. In detail, **FF2039** could achieve a pronounced degradation of all four tested isoforms (D_{max}: 71–90%), demonstrating robust pan-HDAC degradation activity. This demonstrates not only the

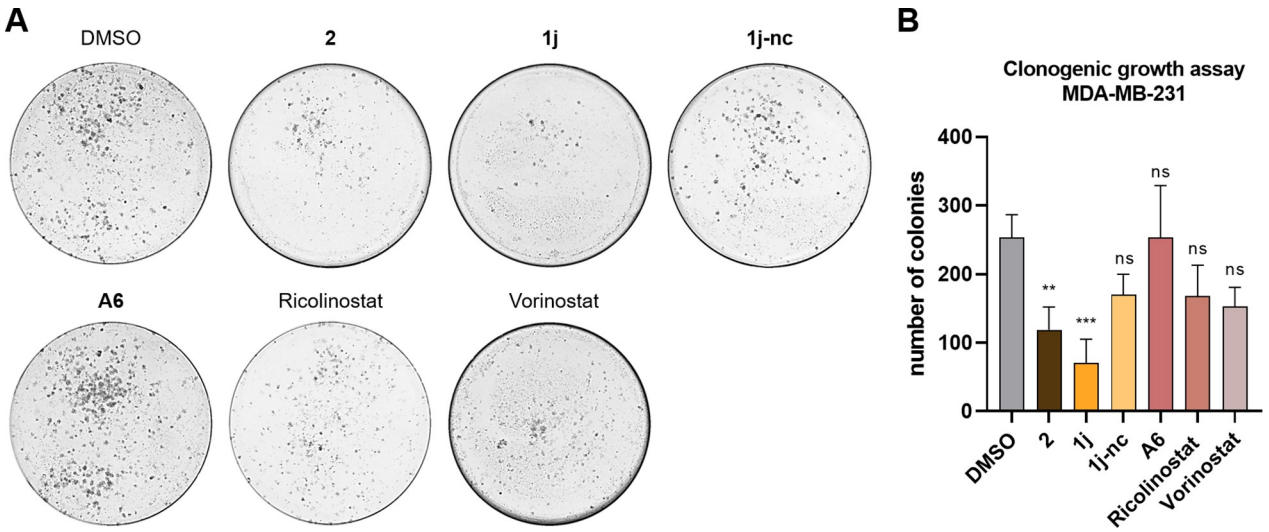

Figure 9. Clonogenic growth assay of DCAF11-recruiting PROTACs. MDA-MB-231 cells were treated with 10 μM of the respective compound or vehicle (DMSO) for 48 hours. (A) Representative images of crystal violet stained colonies after nine days of growth. (B) Quantification of counted colonies, presented as mean ± standard deviation of three biological replicates, each performed in triplicates. Significance of quantification compared to vehicle: ns = $p \geq 0.05$; ** = $p \leq 0.01$ and *** = $p \leq 0.001$.

successful incorporation of a DCAF11 recruiter for targeted HDAC degradation but also underscores the critical role of the chosen E3 ligase in governing degradation selectivity. Similar to the shift in degradation selectivity observed when PROTAC **IV** was transitioned to **V** by replacing IAP with VHL, we showed that substituting the CRBN ligand with a DCAF11 recruiter shifted selectivity from HDAC6-specific to pan-HDAC degradation.[29]

This change in the selectivity profile creates new opportunities to investigate and compare HDAC isoform-specific or general effects. Importantly, PROTACs affect not only the enzymatic but also the non-enzymatic functions of their targets. While HDAC6 selective degraders allow for a more detailed assessment of HDAC6 function in pathology and physiology, a pan-HDAC degrader may provide a more general picture of HDACs functions across different isoforms and may also reveal isoform synergies in terms of phenotypic effects such as anticancer activity. In addition, both approaches may have potential clinical applications. While pan-HDAC degraders could be developed to treat multiple cancers,[51] selective HDAC6 PROTACs, like selective HDAC6 inhibitors,[55] could be used in neurodegenerative diseases, inflammatory diseases, and some cancers. In the latter case, it would be important to replace the non-selective HDAC inhibitor warhead in **A6** with a selective HDAC6 inhibitor scaffold to avoid class I effects resulting from HDAC inhibition.

To verify that degradation is mediated via DCAF11 recruitment, we synthesized the non-degrading control **1j-nc** based on **FF2039**. No effects on HDAC1 and HDAC6 levels were observed with **1j-nc**, confirming the necessity of covalent binding to the E3 ligase for effective degradation. In addition, we could show that **2** and **FF2039** possess antiproliferative activity in the triple negative breast cancer cell line MDA-MB-231 and the glioblastoma cell line U-87MG. The non-degrading control showed no or less effects in all cell lines. Furthermore, for a deeper understanding of the anticancer properties, cell cycle and apoptosis induction were examined in MM.1S cells. Compound **2** and **FF2039** induced greater cell cycle arrest and apoptosis compared to the CBRN-recruiting **A6**. An investigation of the long-term effects on the solid tumor cell line MDA-MB-231 revealed that the DCAF11-recruiting degraders significantly reduced clonogenic growth, outperforming the HDACi vorinostat and ricolinostat, whereas **A6** showed no reduction.

Taken together, we developed the first DCAF11-based HDAC degraders and our most advanced degrader, **FF2039**, represents the first tool to achieve pan-HDAC degradation. This elucidates the effects of the selected E3 ligase for TPD.

Funding Sources

Funding by the Deutsche Forschungsgemeinschaft (DFG, German Research Foundation)–GRK2873 (494832089) is gratefully acknowledged. The new NMR console for the 500 MHz NMR spectrometer used in this research was funded by the Deutsche Forschungsgemeinschaft (DFG, German Research Foundation) under project number 507275896.

Acknowledgements

Marlene Scherer is gratefully acknowledged for experimental support. The graphical abstract was created with BioRender. Open Access funding enabled and organized by Projekt DEAL.

Conflict of Interests

The authors declare no conflict of interest.

Data Availability Statement

The data that support the findings of this study are available from the corresponding author upon reasonable request.

Keywords: DDB1- and CUL4-associated factor 11 (DCAF11) · Histone deacetylase (HDAC) · Proteolysis targeting chimeras (PROTACs) · Solid-phase synthesis · Targeted Protein Degradation (TPD)

[1] J. Ferlay, M. Ervik, F. Lam, M. Laversanne, M. Colombet, L. Mery, M. Piñeros, A. Znaor, I. Soerjomataram, F. Bray (**2024**). Global Cancer Observatory: Cancer Today. Lyon, France: International Agency for Research on Cancer. Available from: https://gco.iarc.who.int/today, accessed [18.09.2024].
[2] A. R. Cutter, J. J. Hayes, *FEBS Lett.* **2015**, *589*, 2914–2922.
[3] M. A. Dawson, T. Kouzarides, *Cell* **2012**, *150*, 12–27.
[4] N. J. Porter, D. W. Christianson, *Curr. Opin. Struct. Biol.* **2019**, *59*, 9–18.
[5] T. C. S. Ho, A. H. Y. Chan, A. Ganesan, *J. Med. Chem.* **2020**, *63*, 12460–12484.
[6] O. Witt, H. E. Deubzer, T. Milde, I. Oehme, *Cancer Lett.* **2009**, *277*, 8–21.
[7] S. Mithraprabhu, A. Kalff, A. Chow, T. Khong, A. Spencer, *Epigenetics* **2014**, *9*, 1511–1520.
[8] C. A. Bradbury, F. L. Khanim, R. Hayden, C. M. Bunce, D. A. White, M. T. Drayson, C. Craddock, B. M. Turner, *Leukemia* **2005**, *19*, 1751–1759.
[9] V. Krieger, A. Hamacher, F. Cao, K. Stenzel, C. G. W. Gertzen, L. Schäker-Hübner, T. Kurz, H. Gohlke, F. J. Dekker, M. U. Kassack, F. K. Hansen, *J. Med. Chem.* **2019**, *62*, 11260–11279.
[10] J. P. Smalley, S. M. Cowley, J. T. Hodgkinson, *Molecules* **2020**, *25*, 1–30.
[11] A. Mullard, *Nat. Rev. Drug Discov.* **2024**, *23*, 329–329.
[12] S. Rai, W. S. Kim, K. Ando, I. Choi, K. Izutsu, N. Tsukamoto, M. Yokoyama, K. Tsukasaki, J. Kuroda, J. Ando, M. Hidaka, Y. Koh, H. Shibayama, T. Uchida, D. H. Yang, K. Ishitsuka, K. Ishizawa, J. S. Kim, H. G. Lee, H. Minami, H. S. Eom, M. Kurosawa, J. H. Lee, J. S. Lee, W. S. Lee, H. Nagai, T. Shindo, D. H. Yoon, S. Yoshida, M. Gillings, H. Onogi, K. Tobinai, *Haematologica* **2022**, *108*, 811–821.
[13] J. Suo, K. Zhu, C. Zhuang, X. Zhong, S. Bravaccini, R. Maltoni, F. Bertucci, H. Zheng, T. Luo, *Ann. Transl. Med.* **2023**, *11*, 409–409.
[14] M. Schapira, M. F. Calabrese, A. N. Bullock, C. M. Crews, *Nat. Rev. Drug Discov.* **2019**, *18*, 949–963.
[15] D. Komander, M. Rape, *Annu. Rev. Biochem.* **2012**, *81*, 203–229.
[16] D. P. Bondeson, A. Mares, I. E. D. Smith, E. Ko, S. Campos, A. H. Miah, K. E. Mulholland, N. Routly, D. L. Buckley, J. L. Gustafson, N. Zinn, P. Grandi, S. Shimamura, G. Bergamini, M. Faelth-Savitski, M. Bantscheff, C. Cox, D. A. Gordon, R. R. Willard, J. J. Flanagan, L. N. Casillas, B. J. Votta, W. Den Besten, K. Famm, L. Kruidenier, P. S. Carter, J. D. Harling, I. Churcher, C. M. Crews, *Nat. Chem. Biol.* **2015**, *11*, 611–617.
[17] S. J. Hughes, A. Testa, N. Thompson, I. Churcher, *Drug Discov. Today* **2021**, *26*, 2889–2897.
[18] J. Salami, S. Alabi, R. R. Willard, N. J. Vitale, J. Wang, H. Dong, M. Jin, D. P. McDonnell, A. P. Crew, T. K. Neklesa, C. M. Crews, *Commun. Biol.* **2018**, *1*, 1–9.
[19] A. D. Buhimschi, H. A. Armstrong, M. Toure, S. Jaime-Figueroa, T. L. Chen, A. M. Lehman, J. A. Woyach, A. J. Johnson, J. C. Byrd, C. M. Crews, *Biochemistry* **2018**, *57*, 3564–3575.

[20] E. S. Toriki, J. W. Papatzimas, K. Nishikawa, D. Dovala, A. O. Frank, M. J. Hesse, D. Dankova, J.-G. Song, M. Bruce-Smythe, H. Struble, F. J. Garcia, S. M. Brittain, A. C. Kile, L. M. McGregor, J. M. McKenna, J. A. Tallarico, M. Schirle, D. K. Nomura, *ACS Cent. Sci.* **2023**, *9*, 915–926.
[21] M. Lim, T. Do Cong, L. M. Orr, E. S. Toriki, A. C. Kile, J. W. Papatzimas, E. Lee, Y. Lin, D. K. Nomura, *ACS Cent. Sci.* **2024**, *10*, 1318–1331.
[22] K. Yang, Y. Song, H. Xie, H. Wu, Y.-T. Wu, E. D. Leisten, W. Tang, *Bioorg. Med. Chem. Lett.* **2018**, *28*, 2493–2497.
[23] F. Fischer, L. A. Alves Avelar, L. Murray, T. Kurz, *Future Med. Chem.* **2022**, *14*, 143–166.
[24] U. Patel, J. P. Smalley, J. T. Hodgkinson, *RSC Chem. Biol.* **2023**, *4*, 623–634.
[25] S. Chen, Y. Zheng, B. Liang, Y. Yin, J. Yao, Q. Wang, Y. Liu, N. Neamati, *Eur. J. Med. Chem.* **2023**, *260*, 115746.
[26] Z. Huang, L. Zeng, B. Cheng, D. Li, *Eur. J. Med. Chem.* **2024**, *276*, 116696.
[27] J. Ge, S. Li, G. Weng, H. Wang, M. Fang, H. Sun, Y. Deng, C.-Y. Hsieh, D. Li, T. Hou, *Nucleic Acids Res.* **2024**, *2127*, 1–6.
[28] J. P. Smalley, G. E. Adams, C. J. Millard, Y. Song, J. K. S. Norris, J. W. R. Schwabe, S. M. Cowley, J. T. Hodgkinson, *Chem. Commun.* **2020**, *56*, 4476–4479.
[29] Y. Xiong, K. A. Donovan, N. A. Eleuteri, N. Kirmani, H. Yue, A. Razov, N. M. Krupnick, R. P. Nowak, E. S. Fischer, *Cell Chem. Biol.* **2021**, 1–14.
[30] W. Li, M. H. Bengtson, A. Ulbrich, A. Matsuda, V. A. Reddy, A. Orth, S. K. Chanda, S. Batalov, C. A. P. Joazeiro, *PLoS One* **2008**, *3*, e1487.
[31] L. Liu, D. R. Damerell, L. Koukouflis, Y. Tong, B. D. Marsden, M. Schapira, *Bioinformatics* **2019**, *35*, 2882–2884.
[32] Y. He, X. Zhang, J. Chang, H. N. Kim, P. Zhang, Y. Wang, S. Khan, X. Liu, X. Zhang, D. Lv, L. Song, W. Li, D. Thummuri, Y. Yuan, J. S. Wiegand, Y. T. Ortiz, V. Budamagunta, J. H. Elisseeff, J. Campisi, M. Almeida, G. Zheng, D. Zhou, *Nat. Commun.* **2020**, *11*, 1996.
[33] P. Ottis, C. Palladino, P. Thienger, A. Britschgi, C. Heichinger, M. Berrera, A. Julien-Laferriere, F. Roudnicky, T. Kam-Thong, J. R. Bischoff, B. Martoglio, P. Pettazzoni, *ACS Chem. Biol.* **2019**, *14*, 2215–2223.
[34] J. Hines, S. Lartigue, H. Dong, Y. Qian, C. M. Crews, *Cancer Res.* **2019**, *79*, 251–262.
[35] Z. Chen, K. Wang, C. Hou, K. Jiang, B. Chen, J. Chen, L. Lao, L. Qian, G. Zhong, Z. Liu, C. Zhang, H. Shen, *Sci. Rep.* **2017**, *7*, 1175.
[36] N. J. Henning, A. G. Manford, J. N. Spradlin, S. M. Brittain, E. Zhang, J. M. McKenna, J. A. Tallarico, M. Schirle, M. Rape, D. K. Nomura, *J. Am. Chem. Soc.* **2022**, *144*, 701–708.
[37] C. C. Ward, J. I. Kleinman, S. M. Brittain, P. S. Lee, C. Y. S. Chung, K. Kim, Y. Petri, J. R. Thomas, J. A. Tallarico, J. M. McKenna, M. Schirle, D. K. Nomura, *ACS Chem. Biol.* **2019**, *14*, 2430–2440.
[38] J. N. Spradlin, X. Hu, C. C. Ward, S. M. Brittain, M. D. Jones, L. Ou, M. To, A. Proudfoot, E. Ornelas, M. Woldegiorgis, J. A. Olzmann, D. E. Bussiere, J. R. Thomas, J. A. Tallarico, J. M. McKenna, M. Schirle, T. J. Maimone, D. K. Nomura, *Nat. Chem. Biol.* **2019**, *15*, 747–755.
[39] X. Zhang, L. M. Luukkonen, C. L. Eissler, V. M. Crowley, Y. Yamashita, M. A. Schafroth, S. Kikuchi, D. S. Weinstein, K. T. Symons, B. E. Nordin, J. L. Rodriguez, T. G. Wucherpfennig, L. G. Bauer, M. M. Dix, D. Stamos, T. M. Kinsella, G. M. Simon, K. A. Baltgalvis, B. F. Cravatt, *J. Am. Chem. Soc.* **2021**, *143*, 5141–5149.
[40] G. Xue, J. Xie, M. Hinterndorfer, M. Cigler, L. Dötsch, H. Imrichova, P. Lampe, X. Cheng, S. R. Adariani, G. E. Winter, H. Waldmann, *Nat. Commun.* **2023**, *14*, 7908.
[41] R. C. Sarott, I. You, Y. Der Li, S. T. Toenjes, K. A. Donovan, P. Seo, M. Ordonez, W. S. Byun, M. M. Hassan, F. Wachter, E. T. Chouchani, M. Słabicki, E. S. Fischer, B. L. Ebert, S. M. Hinshaw, N. S. Gray, *J. Am. Chem. Soc.* **2023**, *145*, 21937–21944.
[42] G. Tin, M. Cigler, M. Hinterndorfer, K. D. Dong, H. Imrichova, S. P. Gygi, G. E. Winter, *Bioorganic Med. Chem. Lett.* **2024**, *107*, 129779.
[43] Y. Wang, T. Wei, M. Zhao, A. Huang, F. Sun, L. Chen, R. Lin, Y. Xie, M. Zhang, S. Xu, Z. Sun, L. Hong, R. Wang, R. Tian, G. Li, *PLOS Biol.* **2024**, *22*, e3002550.
[44] X. Zhang, V. M. Crowley, T. G. Wucherpfennig, M. M. Dix, B. F. Cravatt, *Nat. Chem. Biol.* **2019**, *15*, 737–746.
[45] H. Kiely-Collins, G. E. Winter, G. J. L. Bernardes, *Cell Chem. Biol.* **2021**, *28*, 952–968.
[46] L. Sinatra, J. Yang, J. Schliehe-Diecks, N. Dienstbier, M. Vogt, P. Gebing, L. M. Bachmann, M. Sönnichsen, T. Lenz, K. Stühler, A. Schöler, A. Borkhardt, S. Bhatia, F. K. Hansen, *J. Med. Chem.* **2022**, *65*, 16860–16878.
[47] L. Sinatra, J. J. Bandolik, M. Roatsch, M. Sönnichsen, C. T. Schoeder, A. Hamacher, A. Schöler, A. Borkhardt, J. Meiler, S. Bhatia, M. U. Kassack, F. K. Hansen, *Angew. Chemie Int. Ed.* **2020**, *59*, 22494–22499.
[48] F. Feller, F. K. Hansen, *ACS Med. Chem. Lett.* **2023**, *14*, 1863–1868.
[49] M. J. Bond, C. M. Crews, *RSC Chem. Biol.* **2021**, *2*, 725–742.
[50] DepMap, Broad (**2023**). DepMap 23Q4 Public. Figshare+. Dataset. https://doi.org/10.25452/figshare.plus.24667905.v2, https://depmap.org/portal, accessed on the 30th of January 2025.
[51] Y. Li, E. Seto, *Cold Spring Harb. Perspect. Med.* **2016**, *6*, 1–34.
[52] F. Feller, I. Honin, M. Miranda, H. Weber, S. Henze, M. Hanl, F. K. Hansen, *J. Med. Chem.* **2025**, *68*, 1824–1843.
[53] S. A. Mehmood, K. K. Sahu, S. Sengupta, S. Partap, R. Karpoormath, B. Kumar, D. Kumar, *Med. Oncol.* **2023**, *40*, 201.
[54] M. J. Williams, W. G. B. Singleton, S. P. Lowis, K. Malik, K. M. Kurian, *Front. Oncol.* **2017**, *7:45*.
[55] Z. Huang, L. Li, B. Cheng, D. Li, *Biomed. Pharmacother.* **2024**, *178*, 117218.
[56] T. Ciossek, H. Julius, H. Wieland, T. Maier, T. Beckers, *Anal. Biochem.* **2008**, *372*, 72–81.
[57] C. Bonfils, A. Kalita, M. Dubay, L. L. Siu, M. A. Carducci, G. Reid, R. E. Martell, J. M. Besterman, Z. Li, *Clin. Cancer Res.* **2008**, *14*, 3441–3449.
[58] L. Schäker-Hübner, R. Warstat, H. Ahlert, P. Mishra, F. B. Kraft, J. Schliehe-Diecks, A. Schöler, A. Borkhardt, B. Breit, S. Bhatia, M. Hügle, S. Günther, F. K. Hansen, *J. Med. Chem.* **2021**, *64*, 14620–14646.
[59] N. Reßing, J. Schliehe-Diecks, P. R. Watson, M. Sönnichsen, A. D. Cragin, A. Schöler, J. Yang, L. Schäker-Hübner, A. Borkhardt, D. W. Christianson, S. Bhatia, F. K. Hansen, *J. Med. Chem.* **2022**, *65*, 15457–15472.
[60] F. B. Kraft, M. Hanl, F. Feller, L. Schäker-Hübner, F. K. Hansen, *Pharmaceuticals* **2023**, *16*, 356.
[61] J. V. Watson, S. H. Chambers, P. J. Smith, *Cytometry* **1987**, *8*, 1–8.

Manuscript received: January 14, 2025
Revised manuscript received: February 18, 2025
Accepted manuscript online: February 20, 2025
Version of record online: March 24, 2025

ChemMedChem

Supporting Information

Replacing a Cereblon Ligand by a DDB1 and CUL4 Associated Factor 11 (DCAF11) Recruiter Converts a Selective Histone Deacetylase 6 PROTAC into a Pan-Degrader

Felix Feller, Heiko Weber, Martina Miranda, Irina Honin, Maria Hanl, and Finn K. Hansen*

Supplementary Information

Replacing a Cereblon Ligand by a DDB1 and CUL4 Associated Factor 11 (DCAF11) Recruiter Converts a Selective Histone Deacetylase 6 PROTAC into a Pan-Degrader

Felix Feller,[a] Heiko Weber,[a] Martina Miranda,[a] Irina Honin,[a] Maria Hanl,[a] Finn K. Hansen[a]*

[a]Department of Pharmaceutical and Cell Biological Chemistry, Pharmaceutical Institute, University of Bonn, An der Immenburg 4, 53121 Bonn, Germany.

Table of contents

1. Supplementary Tables and Figures

A

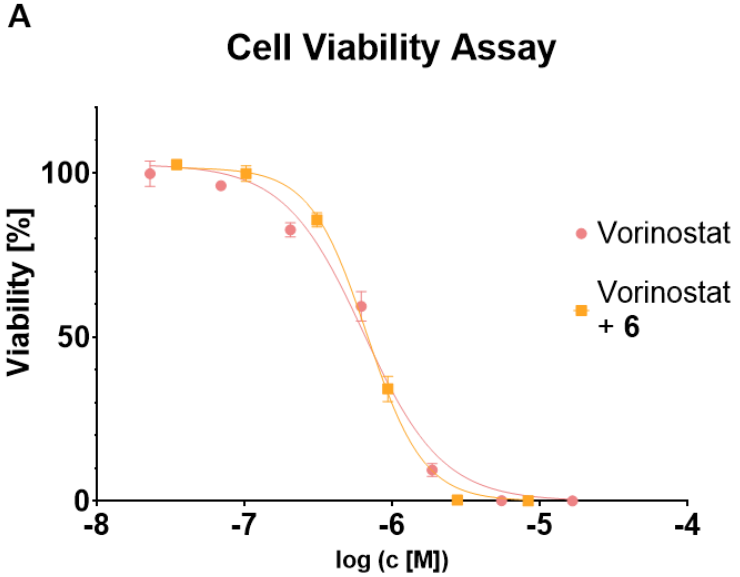

B

Compound	EC_{50} [µM] MM.1S
Vorinostat	0.59 ± 0.09
Vorinostat + **6**	0.73 ± 0.06

Figure S1. Antiproliferative activity of DCAF11-ligand **6** in combination (1:1) with vorinostat compared to the single treatment with vorinostat in MM.1S cells after 72 h. (A) Representative concentration response curves. (B) Mean ± standard deviation of EC_{50} determination of two independent experiments, each performed in duplicates.

A

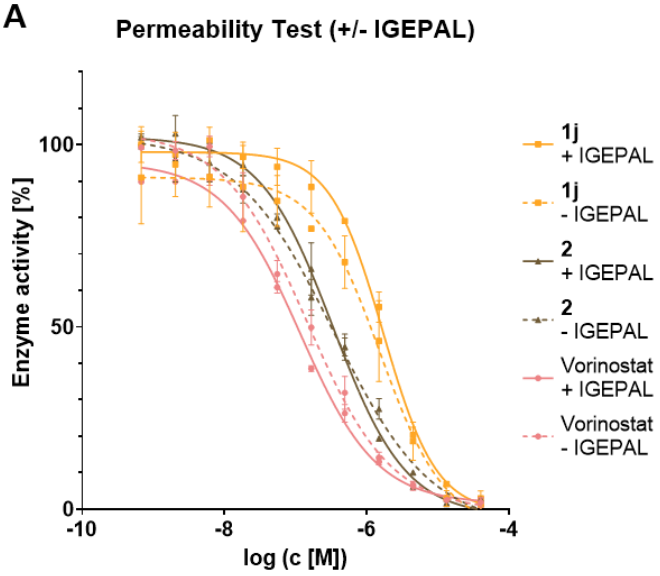

B

	IC_{50} + IGEPAL [µM]	IC_{50} - IGEPAL [µM]
1j	1.7 ± 0.1	1.7 ± 0.2
2	0.33 ± 0.01	0.41 ± 0.09
Vorinostat	0.13 ± 0.01	0.15 ± 0.01

Figure S2. Cell permeability test by a cellular HDAC inhibition assay performed in the presence and absence of the cell permeabilizing agent IGEPAL. MM.1S cells were treated with increasing concentrations of the respective compounds. (A) Representative concentration response curves. (B) Mean ± standard deviation of IC_{50} determination of two independent experiments, each performed in duplicates.

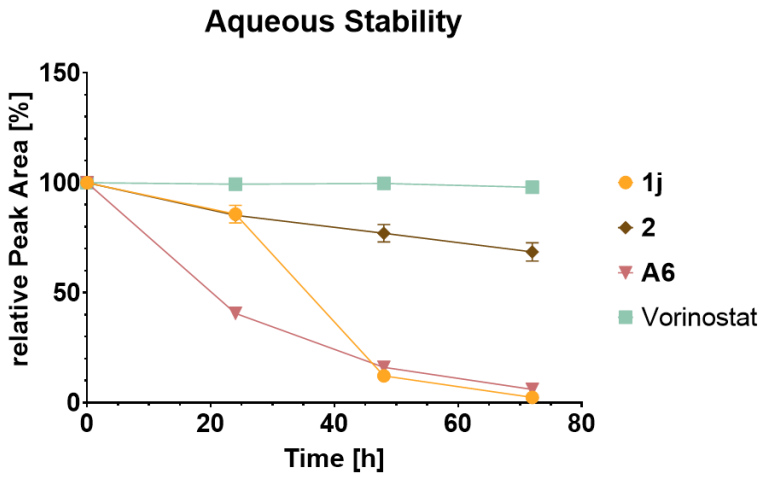

Figure S3. Aqueous stability of the DCAF11-recruting PROTACs (**1j** and **2**) compared to vorinostat and **A6**. Compounds were diluted in DPBS buffer (pH = 7.4; final DMSO concentration: 10%) and the remaining compound content was analyzed by HPLC. The peak area at 0 h was used for normalization. Mean ± standard deviation of n = 2 replicates.

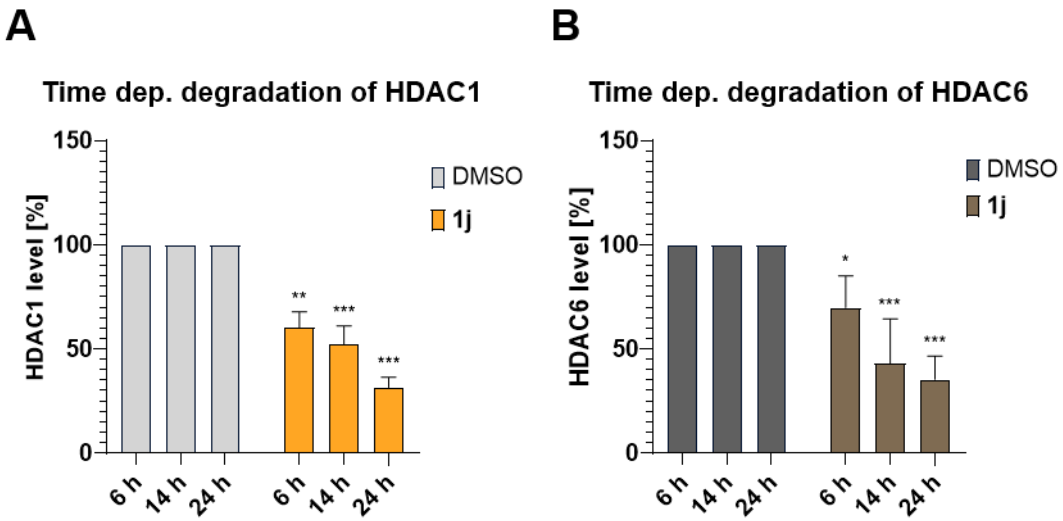

Figure S4. Analysis of time dependent degradation by **1j** of HDAC1 (A) and HDAC6 (B) by Simple Western™ immunoassay analysis of MM.1S cell lysates. MM.1S cells were treated with **1j** (10 µM) or vehicle (DMSO) for the indicated time period. Quantification of protein levels presented as mean ± standard deviation of n = 3 biological replicates. Significance compared to vehicle: * = p≤0.05, ** = p≤0.01, *** = p≤0.001.

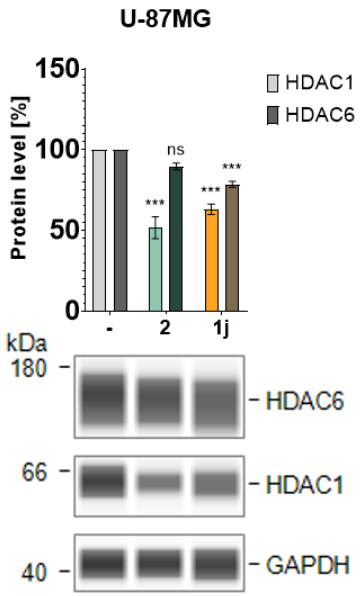

Figure S5. Analysis of HDAC1 and 6 degradation in U-87MG cells. Simple western immunoassay analysis of U-87MG cell lysates. The cells were treated with the indicated compound (10 µM) or vehicle (DMSO) for 24 h. Top: Quantification of HDAC levels, presented as mean ± standard deviation of n = 2 biological replicates; Significance compared to vehicle: ns = $p \geq 0.05$ and *** = $p \leq 0.001$. Bottom: Representative images of n = 2 biological replicates.

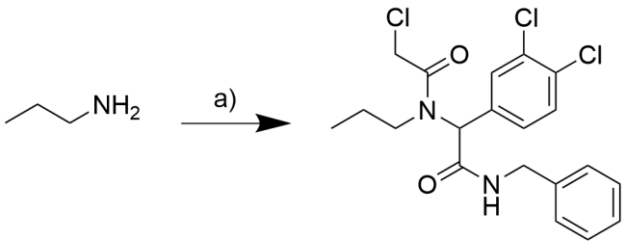

6

53%

Scheme S1. Synthesis of the DCAF11 ligand **6**. *Reaction conditions*: 3,4-dichlorobenzaldehyde, 2-chloroacetic acid, benzyl isocyanide, MeOH, rt, 72 h.

Table S1. Maximal degradation (D_{max}) of PROTAC **1j** and **2** of the respective HDAC isoforms.

	D_{max}[a]	
	1j	**2**
HDAC1	90 ± 6	74 ± 19
HDAC2	75 ± 13	51 ± 24
HDAC4	76 ± 13	40 ± 20
HDAC6	71 ± 8	26 ± 7

[a]MM.1S cells were treated with the indicated compounds (10 µM) or vehicle (DMSO) for 24 h. HDAC1, 2, 4, and 6 levels were analyzed by immunoblotting. The quantification of the D_{max} values is presented as mean ± standard deviation of n = 3 biological replicates.

2. Biological Experiments

No unexpected or unusually high safety hazards were encountered.

2.1. Cell Culture

The human multiple myeloma cell line MM.1S (CRL-2974) was obtained from American Type Culture Collection (ATCC, Manassas, VA, USA). The semi-adherent cells were cultivated in RPMI 1640 medium (Catalog#21875-034, Gibco, ThermoFisher Scientific Inc., Waltham, MA, USA) supplemented with 10% FBS (PAN Biotech GmbH; Aidenbach, Germany), 100 IU/mL penicillin, 0.1 mg/mL streptomycin (PAN Biotech GmbH) and 1 mM sodium pyruvate (ThermoFisher Scientific Inc.). The human breast cancer cell line MDA-MB-231 (HTB-26) and the human malignant glioma cell line U-87MG were cultivated in DMEM medium (Catalog#41966-029, Gibco, ThermoFisher Scientific Inc.) supplemented with 10% FBS (PAN Biotech GmbH), 100 IU/mL penicillin and 0.1 mg/mL streptomycin (PAN Biotech GmbH). All cells were cultured at 37 °C in a 5% CO_2 atmosphere. Incubation times, as part of assay protocols, were performed under these conditions as well. The semi-adherent MM.1S were detached mechanically by using a cell scraper and the adhered MDA-MB-132 were trypsinased by trypsin/EDTA (0.05%/0.02% in DPBS, PAN Biotech GmbH) whereas the U-87MG were detached by EDTA (0.46 g/L in DPBS, Catalog# P04-36500).

2.2. Simple Western™ Immunoassay

For the cell lysates, MM.1S (0.5×10^6 cells/mL) or U-87MG (0.18×10^6 cells/mL) cells were seeded and incubated with the indicated concentration of compound or vehicle (DMSO) for the given time. The adherent cells were cultured for 24 h under cell culture conditions for attachment before treatment. Cell lysis was performed with Cell Extraction Buffer (10 mM Tris, pH 7.4, 100 mM NaCl, 1 mM EDTA, 1 mM EGTA, 1 mM NaF, 20 mM $Na_4P_2O_7$, 2 mM Na_3VO_4, 1% Triton™ ×-100, 10% glycerol, 0.1% SDS, 0.5% deoxycholate; Catalog# FNN0011, Thermo Fisher Scientific Inc., Waltham, MA, USA) with addition of Halt Protease Inhibitor Cocktail (100×) (Catalog# 78429, Life Technologies GmbH, Carlsbad, CA, USA) and phenylmethanesulfonyl fluoride (Catalog# 10837091001, Sigma-Aldrich, St. Louis, MO, USA) according to manufacturer´s instructions. Protein content was determined by Pierce™ BCA Protein Assay Kit (Catalog# 23225, Thermo Fisher Scientific Inc.) according to manufacturer´s guidelines. Cell lysates were diluted to a final concentration of 1 mg/mL and denatured according to manufacturer's guidelines. Anti-HDAC1 (Catalog# 5356S, Cell Signaling Technology, Denver, MA, USA), anti-HDAC6 (Catalog#7558S, Cell Signaling Technology) and anti-GAPDH (Catalog# 2118S, Cell Signaling Technology) antibodies were used in a dilution from 1:50-1:1250. The 12-230 kDa Fluorescence Separation 8x25 Capillary Cartridges (Catalog# SM-FL004-1, Protein Simple, Bio-Techne, Minneapolis, MN, USA) were used for separation and the Anti-Mouse Detection Module (Catalog# DM-002, Protein Simple) was used for detection with addition of 20x Anti-Rabbit HRP

Conjugate (Catalog# 043-426, Protein Simple) according to manufacturer´s instructions. The assay was performed with the Jess Simple Western System (catalog# 004-650, Protein Simple), according to manufacturer´s settings. Evaluation and quantification was performed with the compass software (6.2.0, Protein Simple). GraphPad Prism (GraphPad Software, San Diego, CA, USA) was used for normalization, statistical analysis and bar graph creation. Significance testing was performed with a one-way analysis of variance (ANOVA). Dunnett's post-hoc test was employed to obtain significance levels of each mean compared to a reference mean value.

2.3. CellTiter-Glo® Cell Viability Assay

For the cell viability assay the automated pipetting robot system ASSIST PLUS (Model# 4505, Integra Biosciences, Bibertal, Germany) was used. MM.1S (2.5×10^3 cells/well) were seeded in white 384-well plates (Greiner Bio-One, Kremsmuenster, Austria, #781080). The cells were incubated with the respective compounds in increasing concentrations. For this purpose, the dilution series were prepared in 200-fold concentration in DMSO and further diluted to 10-fold concentration in medium. The final DMSO concentration was 0.5%. The toxicity of compounds was determined after 72 h using the CellTiter-Glo 2.0 Cell Viability Assay (Promega, Madison, WI, USA, #G9242) according to the manufacturer´s protocol. Subsequently, the luminescence was measured using a Tecan Spark (Tecan Group AG, Maennedorf, Swiss) and the half maximal effective concentration (EC_{50}) was determined by plotting dose response curves and nonlinear regression with GraphPad Prism (GraphPad Software, San Diego, CA, USA).

2.4. Cellular HDAC Inhibition Assay

The HDAC whole cell assay is based on the assay established by Ciossek et al.[1] and Bonfils et al.[2] with minor changes. MM.1S multiple myeloma cells were seeded in a concentration of 75×10^3 cells/well (total volume of 189 µL) in 96-well cell culture microplates (Catalog# 655086, Greiner Bio-One). The DMSO-stock solutions were used to perform a serial dilution in DMSO. Next, the cells were treated with 1 µL of the serial dilution (190 × concentrate) for 18 h. To investigate cell membrane penetration of the tested compounds, the substrate solution containing 3 mM Boc-Lys(ε-Ac)-AMC (Catalog# 233691-67-3, BLD pharma) was prepared with and without IGEPAL CA-630 (0.5%, Catalog# J61055, Alfa Aesar). 10 µL of the substrate solution was added and incubated for 3 h under cell culture conditions. The reaction was stopped with 100 µL of stop solution (50 mM Tris-HCl, 137 mM NaCl, 2.7 mM KCl, 1 mM $MgCl_2$, 1% IGEPAL CA-630, 10 µM Vorinostat, 2.0 mg/mL Trypsin) and incubated for 1.5 h under cell culture conditions. The fluorescence signal was measured by a FLUOstar OPTIMA microplate reader (BMG labtech, Ortenburg, Germany) at excitation of $\lambda = 355$ nm and emission of $\lambda = 460$ nm. All Compounds were tested in two independent experiments in duplicates and IC_{50} was determined by nonlinear regression with GraphPad Prim.

2.5. Aqueous Stability Assay

For stability testing in aqueous solution, a 10-fold concentrated DMSO solution of the respective compounds was diluted in DPBS to generate a 10 µM concentration (final DMSO content of 10%). Samples of the aqueous solutions were taken after 0, 24, 48, and 72 h at room temperature and the amounts of the parental compound and potential fragments were monitored by HPLC gradient A (see 3.1 General Information). The peak area of the 0 h sample was used for normalization. All compounds were tested in duplicates and GraphPad Prim was used for evaluation and data visualization.

2.6. Immunoblot

The cell lysis was performed as descripted in **3.2. Simple Western Immunoassay**. Samples were denatured by Laemmli 2× Concentrate (Catalog# S3401-10VL, Sigma-Aldrich) for 5 min at 95 °C, and Precision Plus Protein Unstained Standard was used as molecular weight marker (Catalog# 1610363, Bio-Rad, Hercules, CA, USA). SDS-PAGE was performed with 10 or 12% Mini-PROTEAN TGX Stain-Free Gel (Catalog# 458035, Bio-Rad) at 200 V for 50 min (Catalog# 458035, Bio-Rad). Afterwards, proteins were transferred with the Trans-Blot Turbo Transfer System (Catalog# 1704150, Bio-Rad) to Immobilon-FL PVDF membranes (Catalog# IPFL00005, Millipore Merck, Burlington, MA, USA) at 1.0 A for 30 min and treated with 5% milk-powder solution for 1 h at room temperature under slight agitation. Subsequently, the membranes were treated with anti-HDAC1 (Catalog# 5356S, Cell Signaling Technology), anti-HDAC2 (Catalog# sc-9959, Santa Cruz Biotechnology, Dallas, TX, USA), anti-HDAC4 (Catalog#7628S, Cell Signaling Technology), anti-HDAC6 (Catalog#7558S, Cell Signaling Technology), anti-acetyl-histone H3 (Catalog# 9677S, Cell Signaling Technology), anti-acetyl-α-tubulin (Catalog#5335, Cell Signaling Technology) or anti-GAPDH (Catalog# 2118S, Cell Signaling Technology) antibody solutions in 1:1000–1:8000 dilutions at 4 °C overnight. Treatment with HRP-conjugated secondary anti-mouse (Catalog# 1030-05, SouthernBiotech, Birminham, AL, USA) and anti-rabbit (Catalog# 4030-05, SouthernBiotech) antibody solution was performed for 1.5 h and membranes were developed with clarity western ECL substrate (Catalog# 1705061, Bio-Rad). The ChemiDoc XRS+ System (Catalog# 1708265, Bio-Rad) was used for detection and Image Lab Software 6.1 (Bio-Rad) for quantification. GraphPad Prism (GraphPad Software) was used for normalization, statistical analysis, and bar graph creation. Significance testing was performed with a one-way analysis of variance (ANOVA). Dunnett's post-hoc test was employed to obtain significance levels of each mean compared to a reference mean value.

2.7. HDAC Enzyme Inhibition Assay

In vitro inhibitory activities against HDAC1, 2, and 6 were measured using a previously published protocol.[3] *In vitro* inhibitory activities against HDAC4 were measured using a previously published protocol with slight modifications.[4] For test compounds and controls, serial dilutions of the respective DMSO stock solution in DMSO were prepared, and 1.0 µL/well of this serial dilution were transferred

into OptiPlate-96 black microplates (PerkinElmer, Waltham, MN, USA). A volume of 4 µL/well assay buffer (50 mM Tris−HCl, pH 8.0, 137 mM NaCl, 2.7 mM KCl, 1.0 mM MgCl2·6H2O, 0.1 mg/mL BSA) was added. In the case of HDAC1, 2, and 6, a volume of 35 µL/well of the fluorogenic substrate ZMAL (Z- Lys(Ac)-AMC,[5] 21.43 µM in assay buffer) and 10 µL/well enzyme solution were added. In the case of HDAC4, 35 µL/well of the fluorogenic substrate Boc-Lys(Tfa)-AMC (42.86 µM in assay buffer, Catalog# 4060676, Bachem, Budendorf, Swiss) were added, followed by 10 µL/well of enzyme solution. Human recombinant HDAC1 (Catalog# 50051, BPS Bioscience, San Diego, CA, USA), HDAC2 (Catalog# 50052, BPS Bioscience), HDAC4 (Catalog# 50004, BPS Bioscience), or HDAC6 (Catalog# 50006, BPS Bioscience) were used. The total assay volume of 50 µL (max. 2% DMSO) was incubated at 37 °C for 90 min. Subsequently, 50 µL/well of trypsin (0.4 mg/mL) in trypsin buffer (50 mM Tris−HCl, pH 8.0, 100 mM NaCl) was added, followed by additional 30 min of incubation at 37 °C. Fluorescence (excitation λ = 355 nm, emission λ = 460 nm) was measured using a FLUOstar OPTIMA microplate reader (BMG labtech, Ortenburg, Germany). The half maximal inhibitory concentration (IC_{50}) was determined by plotting dose response curves and nonlinear regression with GraphPad Prism (GraphPad Software).

2.8. MTT Cell Viability Assay

U-87MG cells (3×10^3 cells/well) or MDA-MB-231 cells (5×10^3 cells/well) were seeded in 96-well flat-bottomed plates. After 24 h the cells were incubated with the stock solutions of the respective compounds dissolved in DMSO (highest DMSO concentration, 0.5%) to reach the final concentrations as indicated. Controls received DPBS or DMSO. Following a 71 h incubation period 20 µl of a freshly prepared 5 mg/ml MTT (3-(4,5-dimethylthiazol-2-yl)-2,5-diphenyltetrazolium bromide, AppliChem GmbH, Darmstadt, Germany) solution were added into each well. The supernatant was discarded after 1 h incubation at 37 °C and the precipitated formazan was dissolved in 200 µl DMSO/well. Absorption was measured at 570 nm with background subtraction at 690 nm using a photometric microplate reader (Thermo Scientific Multiskan EX, Thermo Fisher Scientific). Data was further subtracted by the DMSO control and normalized on DPBS. The half-maximal effective concentration (EC_{50}) was determined by plotting dose response curves and nonlinear regression with GraphPad Prism (GraphPad Software).

2.9. Cell Cycle Analysis

MM.1S cells (3×10^3 cells/mL) were seeded in twelve well plates (Starlab GmbH, Hamburg, Germany) and incubated with the indicated concentration of compound or vehicle (DMSO) for 48 h under cell culture conditions. Subsequently, the cells were washed with DPBS (Catalog# P04-36500, PAN Biotech), resuspended in 1 mL EtOH/DPBS (7/3 *v*/*v*), and fixed for 30 min at 4 °C. The samples were rehydrated with DPBS and treated with 5 µg/mL RNAse (Catalog# EN0531, ThermoFisher Scientific Inc.) for 15 min at room temperature. The staining was performed with 3 µM propidium iodide (in DPBS) for 15 min at room temperature and analyzed by flow cytometry (Guava easyCyteTM, Luminex,

Austin, TX, USA). The data was analyzed by FlowJo v10.5.3 Software (BD Life Sciences, Franklin Lakes, NJ, USA), using the Watson Pragmatic algorithm.[6] GraphPad Prism (GraphPad Software) was used for normalization, statistical analysis, and bar graph creation. Significance testing was performed with a one-way analysis of variance (ANOVA). Dunnett's post-hoc test was employed to obtain significance levels of each mean compared to a reference mean value.

2.10. Annexin V/PI Assay

To determine apoptosis, MM1.S cells (0.5×10^6 cells/mL) were seeded in sterile 24-well plates (CytoOne, Hamburg, Germany) and incubated for 48 h at 37 °C and 5% CO_2 under humidified air with 10 µM of the respective compounds or vehicle control (DMSO). Final DMSO concentration was 0.1%. After 48 h, cells were washed with ice-cold DPBS, diluted in 100 µL staining buffer (HEPES 0.01 M, NaCl 0.14 M, $CaCl_2 \times 2\ H_2O$ 2.5 mM) and transferred to a 96 well plate. Staining was performed with 5 µL FITC Annexin V (Catalog#640945, Biolegend, San Diego, CA, USA) and 10 µL of propidium iodide (Catalog#421301, Biolegend) per well. Fluorescence was measured by flow cytometry (Guava® easyCyteTM, Luminex, Austin, Texas). GraphPad Prism (GraphPad Software) was used for normalization, statistical analysis, and bar graph creation. Significance testing was performed with a one-way analysis of variance (ANOVA). Dunnett's post-hoc test was employed to obtain significance levels of each mean compared to a reference mean value.

2.11. Clonogenic growth assay

5×10^5 MDA-MB-231 cells were seeded into T25 cell culture flasks and stimulated with 10 µM of respective compounds or vehicle (0.7% DMSO) for 48 hours. Subsequently, cells were harvested and plated in 6-well plates at a density of 750 cells per well in triplicates. The cell culture medium was changed after five days. Nine days after plating, the colonies were carefully washed with 500 µL DPBS and stained with 500 µL crystal violet solution (0.5% in methanol). After 30 minutes of incubation at room temperature, the wells were gently rinsed with deionized water. After counting the formed colonies, GraphPad Prism (GraphPad Software) was used for bar graph creation. Significance testing was performed with a one-way analysis of variance (ANOVA). Dunnett's post-hoc test was employed to obtain significance levels of each mean compared to a reference mean value.

3. Chemical Experiments

No unexpected or unusually high safety hazards were encountered.

3.1. General Information

Chemicals were purchased from ABCR, Acros Organics, BLDpharm, Carl Roth, Fisher Scientific, Fluorochem, Sigma Aldrich, Tokyo Chemical Industry, and VWR Chemicals. Fmoc protection was performed according to our previously published protocol.[7] Technical grade solvents were distilled prior to use. For all HPLC purposes, acetonitrile in HPLC-grade quality (HiPerSolv CHROMANORM, VWR) was used. Water was purified with a PURELAB flex® (ELGA VEOLIA). Acros Organics silica gel 60 (70–230 mesh) was taken for preparative column chromatography. Uncorrected melting points were measured on a Gallenkamp Melting Point Device (MPD350.BM3.5). A Thermo Fisher Scientific UltiMateTM 3000 UHPLC system with a Nucleodur 100-5 C18 (250 × 4.6 mm, Macherey Nagel) with a flow rate of 1 mL/min and a temperature of 25 °C or a 100-5 C18 (100 × 3 mm, Macherey Nagel) with a flow rate of 0.5 mL/min and a temperature of 25 °C with an appropriate gradient were used. For preparative purposes a AZURA Prep. 500/1000 gradient system with a Nucleodur 110-5 C18 HTec (150 × 32 mm, Macherey Nagel) column with 20 mL/min was used. Detection was implemented by UV absorption measurement at a wavelength of λ = 220 nm and λ = 250 nm. Bidest. H_2O (A) and MeCN (B) were used as eluents with an addition of 0.1% TFA for eluent A. The purity of all final compounds was 95% or higher. Purity was determined *via* HPLC with the Nucleodur 100-5 C18 (250 x 4.6 mm, Macherey Nagel) at 250 nm. The following gradients were applied: A (95% A and 5% B for 5 min, to 5% A and 95% B in 5 min, 5% A and 95% B for 12 min), B (95% A and 5% B for 5 min, to 5% A and 95% B in 10 min, 5% A and 95% B for 12 min). HR-ESI-MS spectra were recorded on a Bruker micrOTOF-Q mass spectrometer coupled with a HPLC Dionex UltiMate 3000 or a LTQ Orbitrap XL. NMR spectra were recorded on a Bruker Avance DRX 500 (500 MHz ^{1}H NMR, 126 MHz ^{13}C NMR) and a Bruker Avance III 600 (600 MHz ^{1}H NMR, 151 MHz ^{13}C NMR). Chemical shifts are given in parts per million (ppm) referring to the signal center using the solvent peaks for reference, DMSO-d_6 (2.49/39.7). The multiplicity of each signal is reported as singlet (s), doublet (d), triplet (t), multiplet (m) or combinations thereof. Multiplicities and coupling constants are reported as measured and might disagree with the expected values. Due to the well-known phenomenon of cis/trans-amide bond rotamers in peptoids,[8] ^{1}H and ^{13}C NMR signals can occur as two distinct sets of signals. ^{1}H NMR signals marked with an asterisk (*) correspond to peaks assigned to the minor rotamer conformation. Due to solvent exchange C-N*H*-OH signals are partly not detectable in ^{1}H NMR spectra.

3.2. General Procedures

General Procedure A (Amide coupling on resin)

This procedure was performed as previously published.[7,9] This reaction was performed in a scale of 0.21 – 3.72 mmol. The preloaded resin **3** (loading: 0.618 – 0.681 mmol/g, prepared according to our previously published protocol[7,9]) was swelled in DMF for 1 h. After deprotection of the Fmoc group by treatment with the deprotection solution (20% piperidine in DMF) two times for 5 min, the resin was washed with DMF (4 × 5 mL), MeOH (4 × 5 mL) and DMF (4 × 5 mL). In parallel, the respective Fmoc-protected acid (2.00 eq), HATU (2.00 eq), HOBt*H_2O (2.00 eq), and DIPEA (3.00 eq) were dissolved in DMF and stirred for 5 min. This solution was added to the resin and the amide coupling was performed for 18 h. Subsequently, the resin was washed with DMF (5 × 5 mL) and CH_2Cl_2 (10 × 5 mL) and the completion of the reaction was confirmed *via* TNBS test, conducted according to manufacturer´s protocol, and by HPLC analysis after test cleavage (**general procedure C**). The modified resin was dried *in vacuo*.

General Procedure B (Ugi four-component reaction on resin)

The Ugi four-component reaction on resin was performed in a scale of 0.08-0.12 mmol. The preloaded resin was swelled and deprotected as described in **general procedure A**. The resin was washed with DMF (4 × 5 mL), MeOH (4 × 5 mL) and DMF/MeOH (1/1 *v*/*v*, 4 × 5 mL). In parallel, 3,4-dichlorobenzaldehyde (4.00 eq.), 2-chloroacetic acid (4.00 eq.) and benzyl isocyanide (4.00 eq.) was dissolved in DMF/MeOH (1/1 *v*/*v*). The solution was added to the resin and the mixture was shaken for 72 h. Subsequently, the resin was washed with DMF (5 × 5 mL) and CH_2Cl_2 (10 × 5 mL) and the completion of the reaction was confirmed *via* TNBS test, conducted according to manufacturer´s protocol, and by HPLC analysis after test cleavage (**general procedure C**). The modified resin was dried *in vacuo*.

General Procedure C (cleavage from resin)

This procedure was performed as previously published.[7,9] For confirmation of completion of the reaction, dried resin (2-3 mg) was shaken with the cleavage solution (CH_2Cl_2/TFA, 95/5 *v*/*v*; 100 µL/mg) for 1 h at room temperature. After filtration, the solution was adjusted to 1 mL with MeCN and analyzed by HPLC.

The large scale cleavage for purification of the final compounds was carried out in the same way using CH_2Cl_2/TFA/TIPS, 90/5/5 (*v*/*v*/*v*), but after 1 h of incubation the cleavage solution was removed under reduced pressure and the crude product was dissolved in DMSO/acetone (15/85 *v*/*v*) for purification by preparative HPLC.

3.3. Preparation of Compounds

4-(4-{*N*-[2-(Benzylamino)-1-(3,4-dichlorophenyl)-2-oxoethyl]-2-chloroacetamido}cyclohexane-1-carboxamido)-*N*-[7-(hydroxyamino)-7-oxoheptyl]benzamide·TFA (1a)

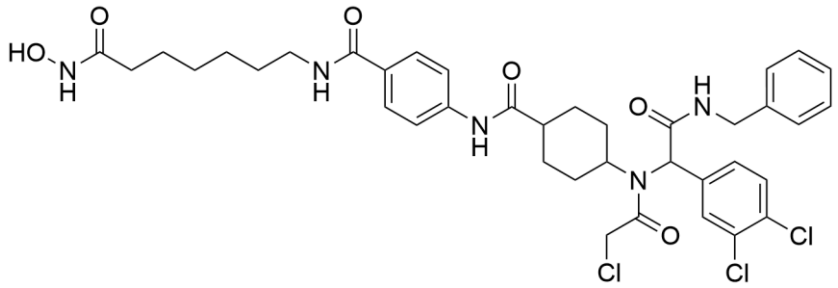

Fmoc-protected 4-aminobenzoic acid (0.96 g, 2.60 mmol, 2.00 eq) was coupled to **3** (2.11 g, 1.30 mmol, 1.00 eq) according to **general procedure A** using HATU (0.99 g, 2.60 mmol, 2.00 eq), HOBt*H_2O (0.40 g, 2.60 mmol, 2.00 eq), and DIPEA (680 µL, 3.90 mmol, 3.00 eq) dissolved in DMF (3.3 mL). The second coupling cycle was performed according to **general procedure A** using the resin bound precursor **4** (300 mg, 0.17 mmol, 1.00 eq), Fmoc-protected 4-aminocyclohexane-1-carboxylic acid (125 mg, 0.34 mmol, 2.00 eq), HATU (130 mg, 0.34 mmol, 2.00 eq), HOBt*H_2O (52 mg, 0.34 mmol, 2.00 eq), and DIPEA (89 µL, 0.51 mmol, 3.00 eq) dissolved in DMF (0.4 mL). Subsequently, the Ugi four-component reaction was performed according to **general procedure B** using the resin bound precursor **5a** (145 mg, 0.08 mmol, 1.00 eq), 3,4-dichlorobenzaldehyde (57 mg, 0.32 mmol, 4.00 eq), 2-chloroacetic acid (30 mg, 0.32 mmol, 4.00 eq), and benzyl isocyanide (45 µL, 0.32 mmol, 4.00 eq) in DMF/MeOH (1/1 *v*/*v*, 0.3 mL). Cleavage was performed according to **general procedure C** and purification by preparative HPLC afforded the TFA salt of **1a** as an amorphous white powder (20 mg, 22 µmol).

Yield 28%; **^{1}H NMR** (500 MHz, DMSO-d_6) δ = 10.31 (s, 1H), 10.03/9.93* (s/s, 1H), 8.30 – 8.22 (m, 1H), 7.82 – 7.47 (m, 7H), 7.46 – 7.15 (m, 6H), 5.19/4.99* (s/s, 1H), 4.82 – 4.61 (m, 1H), 4.48 – 4.21 (m, 3H), 3.87 – 3.73 (m, 2H), 3.25 – 3.17 (m, 2H), 2.73 – 2.55 (m, 1H), 2.33 – 2.21 (m, 1H), 2.12 – 1.77 (m, 6H), 1.58 – 1.37 (m, 6H), 1.33 – 1.22 (m, 4H); **^{13}C NMR** (126 MHz, DMSO-d_6) δ = 174.0, 169.1, 167.8, 167.6, 165.5, 158.1 (q, ^2J = 36.6 Hz, TFA), 141.7, 139.2, 138.5, 129.8, 128.9, 128.8, 128.6, 128.5, 128.0, 127.8, 127.8, 127.0, 126.5, 118.5, 60.1, 59.8, 57.3, 43.4, 42.7, 40.1, 32.2, 30.5, 29.0, 28.5, 28.3, 27.8, 27.0, 26.2, 25.0. **HRMS (ESI)** *m/z* $[M+H]^+$ calcd for $C_{38}H_{44}Cl_3N_5O_6$ 772.2430, found 772.2445; **HPLC** (gradient B), t_R = 15.50 min, 96.7% purity.

4-[(1*r*,4*r*)-4-({*N*-[2-(Benzylamino)-1-(3,4-dichlorophenyl)-2-oxoethyl]-2-chloroacetamido}methyl) cyclohexane-1-carboxamido]-*N*-[7-(hydroxyamino)-7-oxoheptyl]benzamide (1b)

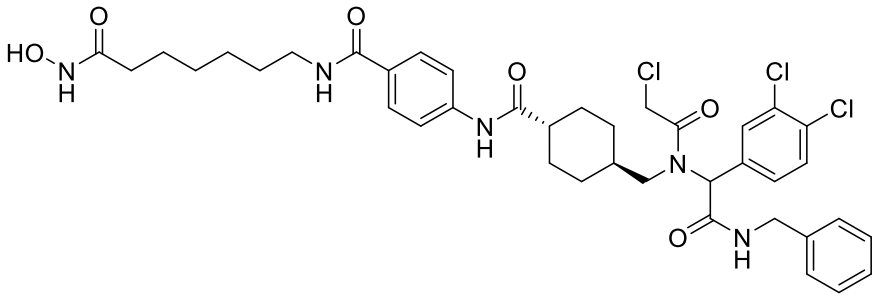

Fmoc-protected 4-aminobenzoic acid (0.96 g, 2.60 mmol, 2.00 eq) was coupled to **3** (2.11 g, 1.30 mmol, 1.00 eq) according to **general procedure A** using HATU (0.99 g, 2.60 mmol, 2.00 eq), HOBt*H_2O (0.40 g, 2.60 mmol, 2.00 eq), and DIPEA (680 µL, 3.90 mmol, 3.00 eq) dissolved in DMF (3.3 mL). The second coupling cycle was performed according to **general procedure A** using the resin bound precursor **4** (300 mg, 0.17 mmol, 1.00 eq), Fmoc-4-AMCHC-OH (129 mg, 0.34 mmol, 2.00 eq), HATU (130 mg, 0.34 mmol, 2.00 eq), HOBt*H_2O (52 mg, 0.34 mmol, 2.00 eq), and DIPEA (89 µL, 0.51 mmol, 3.00 eq) dissolved in DMF (0.4 mL). Subsequently, the Ugi four-component reaction was performed according to **general procedure B** using the resin bound precursor **5b** (142 mg, 0.08 mmol, 1.00 eq), 3,4-dichlorobenzaldehyde (57 mg, 0.32 mmol, 4.00 eq), 2-chloroacetic acid (30 mg, 0.32 mmol, 4.00 eq), and benzyl isocyanide (45 µL, 0.32 mmol, 4.00 eq) in DMF/MeOH (1/1 *v*/*v*, 0.3 mL). Cleavage was performed according to **general procedure C** and purification by preparative HPLC afforded **1b** as an amorphous white powder (6 mg, 8 µmol).

Yield 10%; **^{1}H NMR** (600 MHz, DMSO-d_6) δ = 10.30 (s, 1H), 9.98 (s, 1H), 8.85*/8.26 (s/t, *J* = 5.6 Hz, 1H), 7.76 (d, *J* = 8.6 Hz, 2H), 7.73 – 7.57 (m, 4H), 7.45 – 7.19 (m, 6H), 5.63*/5.52 (s/s, 1H), 4.53 – 4.25 (m, 4H), 3.32 – 3.14 (m, 4H), 2.28 – 2.11 (m, 2H), 1.93 (t, *J* = 7.4 Hz, 2H), 1.85 – 1.68 (m, 2H), 1.67 – 1.44 (m, 6H), 1.32 – 1.10 (m, 6H), 0.99 – 0.80 (m, 2H); **^{13}C NMR** (151 MHz, DMSO-d_6) δ = 174.3, 169.1, 167.8, 166.9, 165.5, 141.8, 139.2, 137.6, 131.6, 130.7, 130.6, 130.3, 130.0, 128.9, 128.2, 127.8, 127.1, 126.7, 118.1, 63.3, 53.5, 44.6, 42.7, 42.4, 40.1, 38.9, 36.3, 32.2, 29.1, 28.8, 28.6, 28.5, 28.3, 26.2, 25.1. **HRMS (ESI)** *m/z* $[M+H]^+$ calcd for $C_{39}H_{46}Cl_3N_5O_6$ 786.2586, found 786.2627; **HPLC** (gradient B), t_R = 15.54 min, 96.0% purity.

4-[5-(2-Chloroacetyl)-4-(3,4-dichlorophenyl)-3-oxo-1-phenyl-8,11-dioxa-2,5-diazatetradecan-14-amido]-*N*-[7-(hydroxyamino)-7-oxoheptyl]benzamide·TFA (1c)

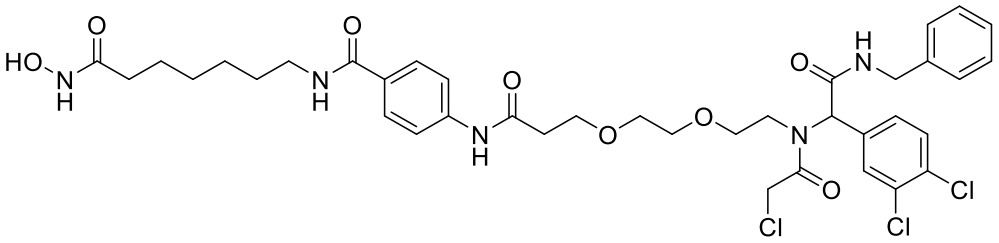

Fmoc-protected 4-aminobenzoic acid (0.96 g, 2.60 mmol, 2.00 eq) was coupled to **3** (2.11 g, 1.30 mmol, 1.00 eq) according to **general procedure A** using HATU (0.99 g, 2.60 mmol, 2.00 eq), HOBt*H_2O (0.40 g, 2.60 mmol, 2.00 eq), and DIPEA (680 µL, 3.90 mmol, 3.00 eq) dissolved in DMF (3.3 mL). The second coupling cycle was performed according to **general procedure A** using the resin bound precursor **4** (300 mg, 0.17 mmol, 1.00 eq), Fmoc-*N*-amido-PEG2-acid (136 mg, 0.34 mmol, 2.00 eq), HATU (130 mg, 0.34 mmol, 2.00 eq), HOBt*H_2O (52 mg, 0.34 mmol, 2.00 eq), and DIPEA (89 µL, 0.51 mmol, 3.00 eq) dissolved in DMF (0.4 mL). Subsequently, the Ugi four-component reaction was performed according to **general procedure B** using the resin bound precursor **5c** (163 mg, 0.08 mmol, 1.00 eq), 3,4-dichlorobenzaldehyde (58 mg, 0.32 mmol, 4.00 eq), 2-chloroacetic acid (31 mg, 0.32 mmol, 4.00 eq), and benzyl isocyanide (45 µL, 0.32 mmol, 4.00 eq) in DMF/MeOH (1/1 *v*/*v*, 0.4 mL). Cleavage was performed according to **general procedure C** and purification by preparative HPLC afforded the TFA salt of **1c** as an amorphous white powder (33 mg, 36 µmol).

Yield 44%; **^{1}H NMR** (600 MHz, DMSO-d_6) δ = 10.31 (s, 1H), 10.10 (s, 1H), 8.85*/8.53 (s/t, *J* = 6.0 Hz, 1H), 8.28 (t, *J* = 5.6 Hz, 1H), 7.78 (d, *J* = 8.5 Hz, 2H), 7.64 (d, *J* = 8.5 Hz, 2H), 7.62 (d, *J* = 8.4 Hz, 1H), 7.51 (s, 1H), 7.36 – 7.19 (m, 6H), 5.77/5.65* (s/s, 1H), 4.65 – 4.50 (m, 2H), 4.35 – 4.27 (m, 2H), 3.65 (t, *J* = 6.3 Hz, 2H), 3.58 – 3.51 (m, 2H), 3.44 – 3.39 (m, 2H), 3.35 – 3.17 (m, 6H), 2.56 (t, *J* = 6.2 Hz, 2H), 1.94 (t, *J* = 7.4 Hz, 2H), 1.53 – 1.45 (m, 4H), 1.32 – 1.22 (m, 4H); **^{13}C NMR** (151 MHz, DMSO-d_6) δ = 169.4, 169.1, 167.8, 167.3, 165.5, 158.2 (q, ^2J = 37.0 Hz, TFA), 141.5, 139.0, 137.3, 131.0, 130.8, 130.6, 130.4, 129.5, 129.1, 128.2, 127.9, 127.2, 126.8, 118.1, 114.5 (q, ^1J = 290.8 Hz, TFA), 69.7, 69.3, 68.7, 66.5, 61.7, 46.3, 42.8, 42.4, 40.1, 37.1, 32.2, 29.1, 28.3, 26.2, 25.1. **HRMS (ESI)** *m/z* $[M+H]^+$ calcd for $C_{38}H_{46}Cl_3N_5O_8$ 806.2485, found 806.2478; **HPLC** (gradient A), t_R = 12.08 min, 99.2% purity.

4-[5-(2-Chloroacetyl)-4-(3,4-dichlorophenyl)-3-oxo-1-phenyl-8,11,14-trioxa-2,5-diazaheptadecan-17-amido]-*N*-[7-(hydroxyamino)-7-oxoheptyl]benzamide·TFA (1d)

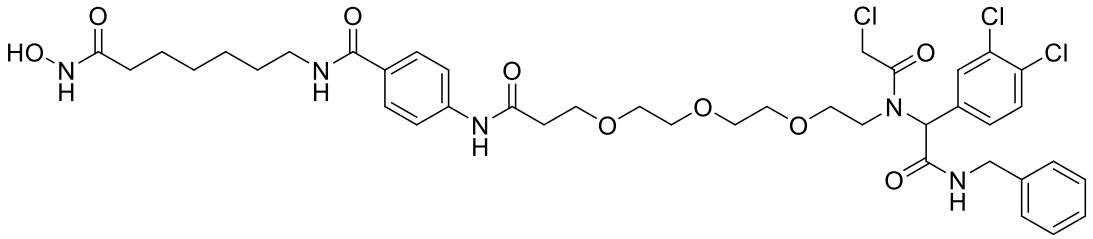

Fmoc-protected 4-aminobenzoic acid (0.96 g, 2.60 mmol, 2.00 eq) was coupled to **3** (2.11 g, 1.30 mmol, 1.00 eq) according to **general procedure A** using HATU (0.99 g, 2.60 mmol, 2.00 eq), HOBt*H_2O (0.40 g, 2.60 mmol, 2.00 eq), and DIPEA (680 µL, 3.90 mmol, 3.00 eq) dissolved in DMF (3.3 mL). The second coupling cycle was performed according to **general procedure A** using the resin bound precursor **4** (300 mg, 0.17 mmol, 1.00 eq), Fmoc-*N*-amido-PEG3-acid (151 mg, 0.34 mmol, 2.00 eq), HATU (130 mg, 0.34 mmol, 2.00 eq), HOBt*H_2O (52 mg, 0.34 mmol, 2.00 eq), and DIPEA (89 µL, 0.51 mmol, 3.00 eq) dissolved in DMF (0.4 mL). Subsequently, the Ugi four-component reaction was performed according to **general procedure B** using the resin bound precursor **5d** (170 mg, 0.08 mmol, 1.00 eq), 3,4-dichlorobenzaldehyde (60 mg, 0.33 mmol, 4.00 eq), 2-chloroacetic acid (32 mg, 0.33 mmol, 4.00 eq), and benzyl isocyanide (46 µL, 0.33 mmol, 4.00 eq) in DMF/MeOH (1/1 *v*/*v*, 0.4 mL). Cleavage was performed according to **general procedure C** and purification by preparative HPLC afforded the TFA salt of **1d** as an amorphous white powder (35 mg, 36 µmol).

Yield 43%; **^{1}H NMR** (500 MHz, DMSO-d_6) δ = 10.31 (s, 1H), 10.10 (s, 1H), 8.84*/8.51 (s/t, *J* = 6.0 Hz, 1H), 8.27 (t, *J* = 5.6 Hz, 1H), 7.78 (d, *J* = 8.7 Hz, 2H), 7.68 – 7.48 (m, 4H), 7.36 – 7.18 (m, 6H), 5.77/5.66* (s/s, 1H), 4.66 – 4.52 (m, 2H), 4.36 – 4.28 (m, 2H), 3.69 (t, *J* = 6.2 Hz, 2H), 3.62 – 3.12 (m, 14H), 2.57 (t, *J* = 6.3 Hz, 2H), 1.94 (t, *J* = 7.4 Hz, 2H), 1.55 – 1.44 (m, 4H), 1.34 – 1.21 (m, 4H); **^{13}C NMR** (126 MHz, DMSO-d_6) δ = 169.5, 169.1, 167.8, 167.3, 165.5, 158.2 (q, ^2J = 37.3 Hz, TFA), 141.5, 139.0, 137.3, 131.1, 130.8, 130.6, 130.4, 129.5, 129.1, 128.2, 127.9, 127.2, 126.8, 118.1, 115.2 (q, ^1J = 290.3 Hz, TFA), 69.7, 69.6, 69.6, 69.5, 68.6, 66.5, 61.7, 46.4, 42.8, 42.4, 40.1, 37.2, 32.2, 29.1, 28.3, 26.2, 25.1. **HRMS (ESI)** *m/z* $[M+H]^+$ calcd for $C_{40}H_{50}Cl_3N_5O_9$ 850.2747, found 850.2751; **HPLC** (gradient A), t_R = 12.09 min, 98.9% purity.

4-[5-(2-Chloroacetyl)-4-(3,4-dichlorophenyl)-3-oxo-1-phenyl-8,11,14,17-tetraoxa-2,5-diazaicosan-20-amido]-*N*-[7-(hydroxyamino)-7-oxoheptyl]benzamide (1e)

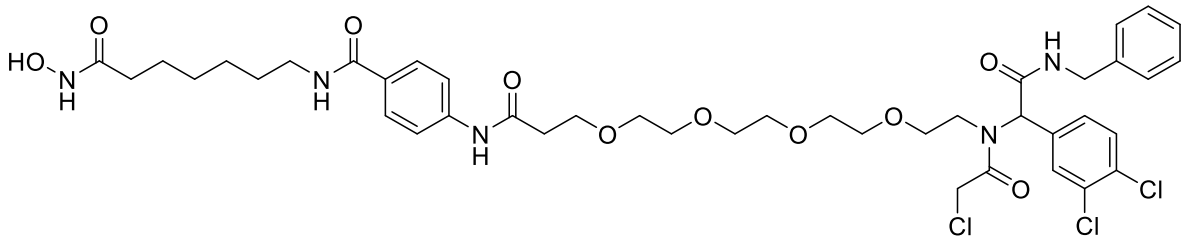

Fmoc-protected 4-aminobenzoic acid (0.96 g, 2.60 mmol, 2.00 eq) was coupled to **3** (2.11 g, 1.30 mmol, 1.00 eq) according to **general procedure A** using HATU (0.99 g, 2.60 mmol, 2.00 eq), HOBt*H_2O (0.40 g, 2.60 mmol, 2.00 eq), and DIPEA (680 µL, 3.90 mmol, 3.00 eq) dissolved in DMF (3.3 mL). The second coupling cycle was performed according to **general procedure A** using the resin bound precursor **4** (300 mg, 0.17 mmol, 1.00 eq), Fmoc-*N*-amido-PEG4-acid (166 mg, 0.34 mmol, 2.00 eq), HATU (130 mg, 0.34 mmol, 2.00 eq), HOBt*H_2O (52 mg, 0.34 mmol, 2.00 eq), and DIPEA (89 µL, 0.51 mmol, 3.00 eq) dissolved in DMF (0.4 mL). Subsequently, the Ugi four-component reaction was performed according to **general procedure B** using the resin bound precursor **5e** (184 mg, 0.09 mmol, 1.00 eq), 3,4-dichlorobenzaldehyde (61 mg, 0.34 mmol, 4.00 eq), 2-chloroacetic acid (32 mg, 0.34 mmol, 4.00 eq), and benzyl isocyanide (47 µL, 0.34 mmol, 4.00 eq) in DMF/MeOH (1/1 *v*/*v*, 0.4 mL). Cleavage was performed according to **general procedure C** and purification by preparative HPLC afforded **1e** as an amorphous white powder (43 mg, 48 µmol).

Yield 57%; **^{1}H NMR** (600 MHz, DMSO-d_6) δ = 10.31 (s, 1H), 10.11 (s, 1H), 8.63*/8.51 (s/t, *J* = 6.0 Hz, 1H), 8.28 (t, *J* = 5.6 Hz, 1H), 7.78 (d, *J* = 8.7 Hz, 2H), 7.67 – 7.49 (m, 4H), 7.36 – 7.19 (m, 6H), 5.77/5.65* (s/s, 1H), 4.65 – 4.54 (m, 2H), 4.38 – 4.27 (m, 2H), 3.70 (t, *J* = 6.2 Hz, 2H), 3.63 – 3.34 (m, 14H), 3.28 – 3.16 (m, 4H), 2.57 (t, *J* = 6.3 Hz, 2H), 1.94 (t, *J* = 7.4 Hz, 2H), 1.53 – 1.45 (m, 4H), 1.33 – 1.22 (m, 4H); **^{13}C NMR** (151 MHz, DMSO-d_6) δ = 169.5, 169.1, 167.8, 167.3, 165.5, 141.5, 139.0, 137.3, 131.1, 130.8, 130.6, 130.4, 129.5, 129.1, 128.2, 127.9, 127.2, 126.8, 118.1, 69.7, 69.7, 69.7, 69.6, 69.6, 69.5, 68.6, 66.5, 61.7, 46.4, 42.8, 42.4, 40.1, 37.2, 32.2, 29.1, 28.3, 26.2, 25.1. **HRMS (ESI)** *m/z* $[M+H]^+$ calcd for $C_{42}H_{54}Cl_3N_5O_{10}$ 894.3009, found 894.3009; **HPLC** (gradient A), t_R = 12.08 min, 97.9% purity.

4-(2-{*N*-[2-(Benzylamino)-1-(3,4-dichlorophenyl)-2-oxoethyl]-2-chloroacetamido}acetamido)-*N*-[7-(hydroxyamino)-7-oxoheptyl]benzamide (1f)

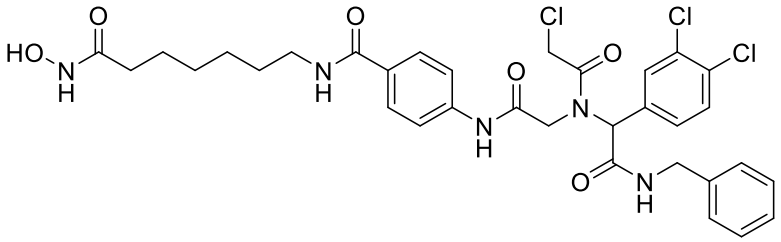

Fmoc-protected 4-aminobenzoic acid (1.38 g, 3.72 mmol, 2.00 eq) was coupled to **3** (2.73 g, 1.86 mmol, 1.00 eq) according to **general procedure A** using HATU (1.41 g, 3.72 mmol, 2.00 eq), HOBt*H_2O (0.57 g, 3.72 mmol, 2.00 eq), and DIPEA (971 µL, 5.58 mmol, 3.00 eq) dissolved in DMF (4.67 mL). The second coupling cycle was performed according to **general procedure A** using the resin bound precursor **4** (308 mg, 0.21 mmol, 1.00 eq), Fmoc-Gly-OH (130 mg, 0.43 mmol, 2.00 eq), HATU (163 mg, 0.43 mmol, 2.00 eq), HOBt*H_2O (66 mg, 0.43 mmol, 2.00 eq), and DIPEA (112 µL, 0.64 mmol, 3.00 eq) dissolved in DMF (0.5 mL). Subsequently, the Ugi four-component reaction was performed according to **general procedure B** using the resin bound precursor **5f** (160 mg, 0.10 mmol, 1.00 eq), 3,4-dichlorobenzaldehyde (74 mg, 0.41 mmol, 4.00 eq), 2-chloroacetic acid (39 mg, 0.41 mmol, 4.00 eq), and benzyl isocyanide (58 µL, 0.41 mmol, 4.00 eq) in DMF/MeOH (1/1 *v*/*v*, 0.4 mL). Cleavage was performed according to **general procedure C** and purification by preparative HPLC afforded **1f** as an amorphous white powder (24 mg, 35 µmol).

Yield 36%; **^{1}H NMR** (500 MHz, DMSO-d_6) δ = 10.30 (s, 1H), 10.11 (s, 1H), 9.17*/8.94 (s/t, *J* = 5.9 Hz, 1H), 8.28 (t, *J* = 5.6 Hz, 1H), 7.76 (d, *J* = 8.8 Hz, 2H), 7.54 (d, *J* = 8.3 Hz, 1H), 7.49 – 7.39 (m, 3H), 7.38 – 7.27 (m, 3H), 7.26 – 7.18 (m, 3H), 6.16/5.83* (s/s, 1H), 4.59 – 4.45 (m, 2H), 4.42 – 4.23 (m, 4H), 3.25 – 3.18 (m, 2H), 1.94 (t, *J* = 7.4 Hz, 2H), 1.53 – 1.44 (m, 4H), 1.33 – 1.22 (m, 4H); **^{13}C NMR** (126 MHz, DMSO-d_6) δ = 169.1, 168.0, 167.8, 167.1, 165.4, 140.7, 138.7, 136.1, 131.1, 131.0, 131.0, 130.4, 129.7, 129.4, 128.3, 127.8, 127.3, 126.9, 118.3, 59.6, 48.8, 42.8, 42.3, 40.1, 32.2, 29.0, 28.3, 26.2, 25.0. **HRMS (ESI)** *m/z* $[M+H]^+$ calcd for $C_{33}H_{36}Cl_3N_5O_6$ 704.1804, found 704.1769; **HPLC** (gradient A), t_R = 11.93 min, 97.9% purity.

4-(4-{*N*-[2-(Benzylamino)-1-(3,4-dichlorophenyl)-2-oxoethyl]-2-chloroacetamido}butanamido)-*N*-[7-(hydroxyamino)-7-oxoheptyl]benzamide (1g)

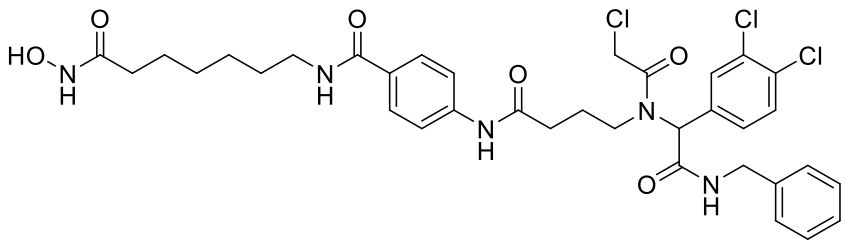

Fmoc-protected 4-aminobenzoic acid (1.38 g, 3.72 mmol, 2.00 eq) was coupled to **3** (2.73 g, 1.86 mmol, 1.00 eq) according to **general procedure A** using HATU (1.41 g, 3.72 mmol, 2.00 eq), HOBt*H_2O (0.57 g, 3.72 mmol, 2.00 eq), and DIPEA (971 µL, 5.58 mmol, 3.00 eq) dissolved in DMF (4.67 mL). The second coupling cycle was performed according to **general procedure A** using the resin bound precursor **4** (308 mg, 0.21 mmol, 1.00 eq), Fmoc-GABA-OH (142 mg, 0.42 mmol, 2.00 eq), HATU (159 mg, 0.42 mmol, 2.00 eq), HOBt*H_2O (64 mg, 0.42 mmol, 2.00 eq), and DIPEA (109 µL, 0.63 mmol, 3.00 eq) dissolved in DMF (0.5 mL). Subsequently, the Ugi four-component reaction was performed according to **general procedure B** using the resin bound precursor **5g** (163 mg, 0.10 mmol, 1.00 eq), 3,4-dichlorobenzaldehyde (74 mg, 0.41 mmol, 4.00 eq), 2-chloroacetic acid (39 mg, 0.41 mmol, 4.00 eq), and benzyl isocyanide (58 µL, 0.41 mmol, 4.00 eq) in DMF/MeOH (1/1 *v*/*v*, 0.4 mL). Cleavage was performed according to **general procedure C** and purification by preparative HPLC afforded **1g** as an amorphous white powder (39 mg, 53 µmol).

Yield 55%; **^{1}H NMR** (600 MHz, DMSO-d_6) δ = 10.31 (s, 1H), 10.01 (s, 1H), 8.84*/8.59 (s/t, *J* = 6.0 Hz, 1H), 8.28 (t, *J* = 5.7 Hz, 1H), 7.78 (d, *J* = 8.4 Hz, 2H), 7.64 – 7.49 (m, 4H), 7.35 – 7.19 (m, 6H), 5.83/5.67* (s/s, 1H), 4.61 – 4.44 (m, 2H), 4.41 – 4.25 (m, 2H), 3.41 – 3.30 (m, 2H), 3.25 – 3.19 (m, 2H), 2.21 (d, *J* = 7.0 Hz, 2H), 1.94 (t, *J* = 7.4 Hz, 2H), 1.82 – 1.36 (m, 6H), 1.33 – 1.22 (m, 4H); **^{13}C NMR** (151 MHz, DMSO-d_6) δ = 170.7, 169.1, 167.9, 166.8, 165.5, 141.5, 139.0, 137.1, 131.2, 131.0, 130.7, 130.5, 129.6, 129.0, 128.2, 127.9, 127.2, 126.8, 118.1, 61.2, 45.9, 42.4, 42.4, 40.1, 33.0, 32.2, 29.1, 28.3, 26.2, 25.1, 24.9. **HRMS (ESI)** *m/z* $[M+H]^+$ calcd for $C_{35}H_{40}Cl_3N_5O_6$ 732.2117, found 732.2094; **HPLC** (gradient A), t_R = 11.98 min, 98.7% purity.

4-(6-{*N*-[2-(Benzylamino)-1-(3,4-dichlorophenyl)-2-oxoethyl]-2-chloroacetamido}hexanamido)-*N*-[7-(hydroxyamino)-7-oxoheptyl]benzamide·TFA (1h)

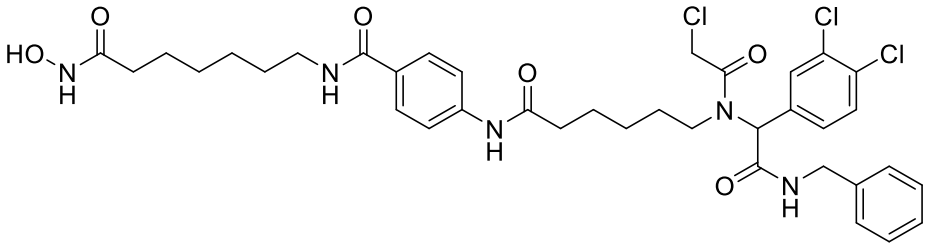

Fmoc-protected 4-aminobenzoic acid (1.38 g, 3.72 mmol, 2.00 eq) was coupled to **3** (2.73 g, 1.86 mmol, 1.00 eq) according to **general procedure A** using HATU (1.41 g, 3.72 mmol, 2.00 eq), HOBt*H_2O (0.57 g, 3.72 mmol, 2.00 eq), and DIPEA (971 µL, 5.58 mmol, 3.00 eq) dissolved in DMF (4.67 mL). The second coupling cycle was performed according to **general procedure A** using the resin bound precursor **4** (302 mg, 0.21 mmol, 1.00 eq), Fmoc-6-Ahx-OH (148 mg, 0.41 mmol, 2.00 eq), HATU (156 mg, 0.41 mmol, 2.00 eq), HOBt*H_2O (63 mg, 0.41 mmol, 2.00 eq), and DIPEA (107 µL,

0.62 mmol, 3.00 eq) dissolved in DMF (0.5 mL). Subsequently, the Ugi four-component reaction was performed according to **general procedure B** using the resin bound precursor **5h** (164 mg, 0.10 mmol, 1.00 eq), 3,4-dichlorobenzaldehyde (74 mg, 0.41 mmol, 4.00 eq), 2-chloroacetic acid (39 mg, 0.41 mmol, 4.00 eq), and benzyl isocyanide (58 µL, 0.41 mmol, 4.00 eq) in DMF/MeOH (1/1 *v*/*v*, 0.4 mL). Cleavage was performed according to **general procedure C** and purification by preparative HPLC afforded the TFA salt of **1h** as an amorphous white powder (38 mg, 44 µmol).

Yield 45%; **^{1}H NMR** (600 MHz, DMSO-d_6) δ = 10.31 (s, 1H), 10.01 (s, 1H), 8.86*/8.57 (s/t, *J* = 6.0 Hz, 1H), 8.27 (t, *J* = 5.6 Hz, 1H), 7.77 (d, *J* = 8.7 Hz, 2H), 7.68 – 7.61 (m, 3H), 7.52 (s, 1H), 7.37 – 7.16 (m, 6H), 5.81/5.65* (s/s, 1H), 4.55 – 4.24 (m, 4H), 3.31 (t, *J* = 7.4 Hz, 2H), 3.25 – 3.18 (m, 2H), 2.22 (t, *J* = 7.5 Hz, 2H), 1.94 (t, *J* = 7.4 Hz, 2H), 1.53 – 1.02 (m, 14H); **^{13}C NMR** (151 MHz, DMSO-d_6) δ = 171.4, 169.1, 167.9, 166.6, 165.5, 158.0 (q, ^2J = 34.4 Hz, TFA), 141.7, 139.1, 137.3, 131.1, 130.9, 130.7, 130.5, 129.6, 128.9, 128.2, 127.9, 127.2, 126.8, 118.1, 61.3, 46.5, 42.6, 42.4, 40.1, 36.3, 32.2, 29.1, 28.9, 28.3, 26.2, 25.8, 25.1, 24.5. **HRMS (ESI)** *m/z* $[M+H]^+$ calcd for $C_{37}H_{44}Cl_3N_5O_6$ 760.2430, found 760.2415; **HPLC** (gradient A), t_R = 12.15 min, 97.9% purity.

4-(8-{*N*-[2-(Benzylamino)-1-(3,4-dichlorophenyl)-2-oxoethyl]-2-chloroacetamido}octanamido)-*N*-[7-(hydroxyamino)-7-oxoheptyl]benzamide·TFA (1i)

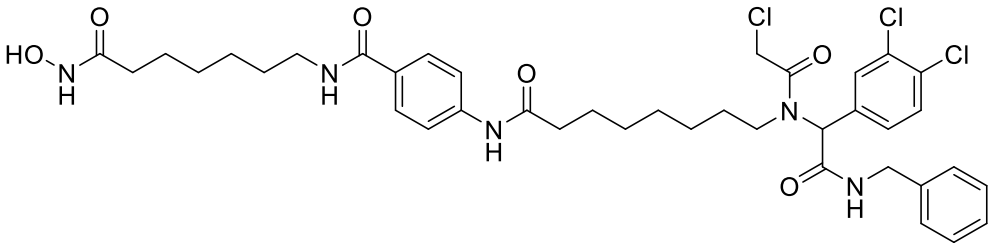

Fmoc-protected 4-aminobenzoic acid (1.01 g, 2.73 mmol, 2.00 eq) was coupled to **3** (1.99 g, 1.37 mmol, 1.00 eq) according to **general procedure A** using HATU (1.04 g, 2.73 mmol, 2.00 eq), HOBt*H_2O (0.42 g, 2.73 mmol, 2.00 eq), and DIPEA (714 µL, 4.10 mmol, 3.00 eq) dissolved in DMF (3.42 mL). The second coupling cycle was performed according to **general procedure A** using the resin bound precursor **4** (1.55 g, 0.95 mmol, 1.00 eq), Fmoc-8-Aoc-OH (0.73 g, 1.91 mmol, 2.00 eq), HATU (0.73 g, 2.91 mmol, 2.00 eq), HOBt*H_2O (0.29 g, 1.91 mmol, 2.00 eq), and DIPEA (498 µL, 2.86 mmol, 3.00 eq) dissolved in DMF (2.4 mL). Subsequently, the Ugi four-component reaction was performed according to **general procedure B** using the resin bound precursor **5i** (200 mg, 0.12 mmol, 1.00 eq), 3,4-dichlorobenzaldehyde (84 mg, 0.47 mmol, 4.00 eq), 2-chloroacetic acid (44 mg, 0.47 mmol, 4.00 eq), and benzyl isocyanide (65 µL, 0.47 mmol, 4.00 eq) in DMF/MeOH (1/1 *v*/*v*, 0.4 mL). Cleavage was performed according to **general procedure C** and purification by preparative HPLC afforded the TFA salt of **1i** as an amorphous white powder (39 mg, 47 µmol).

Yield 40%; **^{1}H NMR** (600 MHz, DMSO-d_6) δ = 10.32 (s, 1H), 10.03 (s, 1H), 8.85*/8.58 (s/t, *J* = 6.1 Hz, 1H), 8.27 (t, *J* = 5.6 Hz, 1H), 7.77 (d, *J* = 8.6 Hz, 2H), 7.64 (d, *J* = 8.5 Hz, 3H), 7.60 – 7.49 (m, 1H), 7.35 – 7.20 (m, 6H), 5.83/5.65* (s/s, 1H), 4.53 – 4.42 (m, 2H), 4.36 – 4.25 (m, 2H), 3.37 – 3.24 (m, 2H), 3.24 – 3.19 (m, 2H), 2.28 (t, *J* = 7.5 Hz, 2H), 1.94 (t, *J* = 7.4 Hz, 2H), 1.56 – 0.93 (m, 18H); **^{13}C NMR** (151 MHz, DMSO-d_6) δ = 171.5, 169.1, 167.9, 166.7, 165.5, 158.3 (q, ^2J = 37.8 Hz, TFA), 141.7, 139.1, 137.3, 131.2, 130.9, 130.7, 130.5, 129.7, 128.9, 128.2, 127.9, 127.2, 126.8, 118.1, 115.2 (q, ^1J = 289.7 Hz, TFA), 62.0, 61.2, 46.5, 42.5, 40.1, 36.4, 32.2, 29.1, 28.4, 28.3, 28.2, 26.2, 25.9, 25.5, 25.1, 24.8. **HRMS (ESI)** *m/z* $[M+H]^+$ calcd for $C_{39}H_{48}Cl_3N_5O_6$ 788.2743, found 788.2741; **HPLC** (gradient A), t_R = 12.45 min, 98.7% purity.

4-(12-{*N*-[2-(Benzylamino)-1-(3,4-dichlorophenyl)-2-oxoethyl]-2-chloroacetamido} dodecanamido)-*N*-[7-(hydroxyamino)-7-oxoheptyl]benzamide (1j)

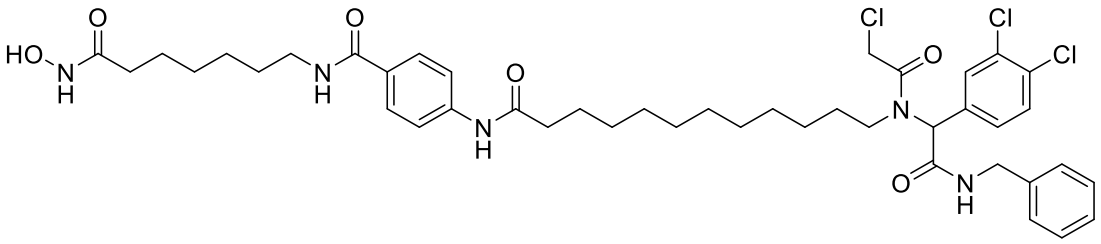

Fmoc-protected 4-aminobenzoic acid (1.38 g, 3.72 mmol, 2.00 eq) was coupled to **3** (2.73 g, 1.86 mmol, 1.00 eq) according to **general procedure A** using HATU (1.41 g, 3.72 mmol, 2.00 eq), HOBt*H_2O (0.57 g, 3.72 mmol, 2.00 eq), and DIPEA (971 µL, 5.58 mmol, 3.00 eq) dissolved in DMF (4.67 mL). The second coupling cycle was performed according to **general procedure A** using the resin bound precursor **4** (304 mg, 0.21 mmol, 1.00 eq), Fmoc-12-Ado-OH (186 mg, 0.41 mmol, 2.00 eq), HATU (156 mg, 0.41 mmol, 2.00 eq), HOBt*H_2O (63 mg, 0.41 mmol, 2.00 eq), and DIPEA (107 µL, 0.62 mmol, 3.00 eq) dissolved in DMF (0.5 mL). Subsequently, the Ugi four-component reaction was performed according to **general procedure B** using the resin bound precursor **5j** (170 mg, 0.10 mmol, 1.00 eq), 3,4-dichlorobenzaldehyde (74 mg, 0.41 mmol, 4.00 eq), 2-chloroacetic acid (39 mg, 0.41 mmol, 4.00 eq), and benzyl isocyanide (58 µL, 0.41 mmol, 4.00 eq) in DMF/MeOH (1/1 *v*/*v*, 0.4 mL). Cleavage was performed according to **general procedure C** and purification by preparative HPLC afforded **1j** as an amorphous white powder (34 mg, 40 µmol).

Yield 43%; **^{1}H NMR** (600 MHz, DMSO-d_6) δ = 10.31 (s, 1H), 10.03 (s, 1H), 8.83*/8.58 (s/t, *J* = 6.0 Hz, 1H), 8.27 (t, *J* = 5.7 Hz, 1H), 7.77 (d, *J* = 8.4 Hz, 2H), 7.69 – 7.61 (m, 3H), 7.59 – 7.49 (m, 1H), 7.35 – 7.19 (m, 6H), 5.84/5.65* (s/s, 1H), 4.54 – 4.40 (m, 2H), 4.38 – 4.25 (m, 2H), 3.25 – 3.18 (m, 2H), 2.31 (t, *J* = 7.4 Hz, 2H), 1.94 (t, *J* = 7.4 Hz, 2H), 1.66 – 0.64 (m, 28H); **^{13}C NMR** (151 MHz, DMSO-d_6) δ = 171.6, 169.1, 168.0, 166.7, 165.5, 141.7, 139.0, 137.3, 131.3, 130.9, 130.8, 130.5, 129.8, 128.9, 127.9, 127.2, 126.8, 118.1, 61.1, 46.4, 42.5, 42.4, 40.1, 36.4, 32.2, 29.1, 28.9, 28.8, 28.8, 28.7, 28.7,

28.6, 28.3, 28.2, 26.2, 25.9, 25.1, 25.0. **HRMS (ESI)** *m/z* $[M+H]^+$ calcd for $C_{43}H_{56}Cl_3N_5O_6$ 844.3369, found 844.3361; **HPLC** (gradient A), t_R = 13.61 min, 96.5% purity.

4-(12-{*N*-[2-(Benzylamino)-1-(3,4-dichlorophenyl)-2-oxoethyl]formamido}dodecanamido)-*N*-[7-(hydroxyamino)-7-oxoheptyl]benzamide (1j-nc)

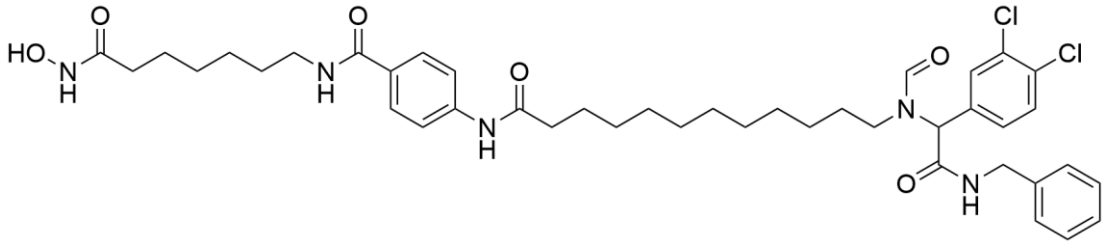

Fmoc-protected 4-aminobenzoic acid (1.38 g, 3.72 mmol, 2.00 eq) was coupled to **3** (2.73 g, 1.86 mmol, 1.00 eq) according to **general procedure A** using HATU (1.41 g, 3.72 mmol, 2.00 eq), HOBt*H_2O (0.57 g, 3.72 mmol, 2.00 eq), and DIPEA (971 µL, 5.58 mmol, 3.00 eq) dissolved in DMF (4.67 mL). The second coupling cycle was performed according to **general procedure A** using the resin bound precursor **4** (302 mg, 0.19 mmol, 1.00 eq), Fmoc-12-Ado-OH (174 mg, 0.39 mmol, 2.00 eq), HATU (147 mg, 0.39 mmol, 2.00 eq), HOBt*H_2O (59 mg, 0.39 mmol, 2.00 eq), and DIPEA (101 µL, 0.75 mmol, 3.00 eq) dissolved in DMF (0.5 mL). Subsequently, the Ugi four-component reaction was performed according to **general procedure B** with a slide modification, using the resin bound precursor **5j** (148 mg, 0.08 mmol, 1.00 eq), 3,4-dichlorobenzaldehyde (60 mg, 0.34 mmol, 4.00 eq), formic acid (13 µL, 0.34 mmol, 4.00 eq), and benzyl isocyanide (47 µL, 0.34 mmol, 4.00 eq) in DMF/MeOH (1/1 *v*/*v*, 0.3 mL). Cleavage was performed according to **general procedure C** and purification by preparative HPLC afforded **1j-nc** as an amorphous white powder (24 mg, 30 µmol).

Yield 38%; **^{1}H NMR** (600 MHz, DMSO-d_6) δ = 10.31 (s, 1H), 10.03 (s, 1H), 8.87/8.63* (t/t, *J* = 5.8/6.0 Hz, 1H), 8.27 (t, *J* = 5.7 Hz, 1H), 8.20*/8.10 (s/s, 1H), 7.77 (d, *J* = 8.5 Hz, 2H), 7.68 – 7.62 (m, 3H), 7.55 – 7.50 (m, 1H), 7.34 – 7.19 (m, 6H), 5.75*/5.38 (s/s, 1H), 4.38 – 4.28 (m, 2H), 3.31 – 3.18 (m, 4H), 2.31 (t, *J* = 7.4 Hz, 2H), 1.94 (t, *J* = 7.4 Hz, 2H), 1.62 – 1.55 (m, 2H), 1.52 – 1.45 (m, 4H), 1.32 – 0.97 (m, 20H); **^{13}C NMR** (151 MHz, DMSO-d_6) δ = 171.8, 169.3, 168.3, 168.0, 165.7, 163.9, 163.4, 141.9, 139.2, 138.9, 137.8, 137.5, 131.4, 131.2, 131.1, 131.1, 131.0, 130.9, 130.7, 130.6, 129.7, 129.1, 128.9, 128.5, 128.4, 128.1, 127.6, 127.4, 127.2, 127.0, 118.2, 62.4, 58.5, 46.2, 43.6, 42.8, 42.6, 40.2, 36.6, 32.4, 29.8, 29.2, 29.1, 29.0, 28.9, 28.9, 28.8, 28.7, 28.5, 27.3, 26.4, 26.4, 25.9, 25.2, 25.2f. **HRMS (ESI)** *m/z* $[M+H]^+$ calcd for $C_{42}H_{55}Cl_2N_5O_6$ 796.3602, found 796.3605; **HPLC** (gradient A), t_R = 13.43 min, 99.9% purity.

4-{*N*-[2-(Benzylamino)-1-(3,4-dichlorophenyl)-2-oxoethyl]-2-chloroacetamido}-*N*-[7-(hydroxyamino)-7-oxoheptyl]benzamide (2)

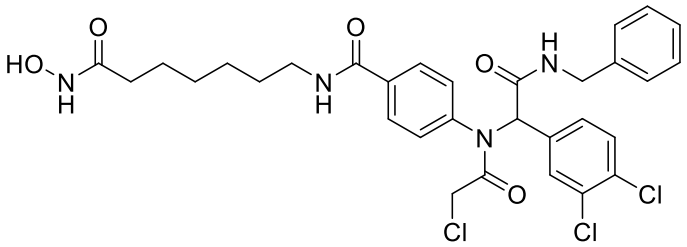

Fmoc-protected 4-aminobenzoic acid (1.38 g, 3.72 mmol, 2.00 eq) was coupled to **3** (2.73 g, 1.86 mmol, 1.00 eq) according to **general procedure A** using HATU (1.41 g, 3.72 mmol, 2.00 eq), HOBt*H_2O (0.57 g, 3.72 mmol, 2.00 eq), and DIPEA (971 µL, 5.58 mmol, 3.00 eq) dissolved in DMF (4.7 mL). Subsequently, the Ugi four-component reaction was performed according to **general procedure B** using the resin bound precursor **4** (143 mg, 0.10 mmol, 1.00 eq), 3,4-dichlorobenzaldehyde (66 mg, 0.37 mmol, 4.00 eq), 2-chloroacetic acid (35 mg, 0.37 mmol, 4.00 eq), and benzyl isocyanide (51 µL, 0.37 mmol, 4.00 eq) in DMF/MeOH (1/1 *v*/*v*, 0.3 mL). Cleavage was performed according to **general procedure C** and purification by preparative HPLC afforded **2** as an amorphous white powder (24 mg, 37 µmol).

Yield 42%; **^{1}H NMR** (500 MHz, DMSO-d_6) δ = 10.30 (s, 1H), 8.76 (t, *J* = 6.0 Hz, 1H), 8.42 (t, *J* = 5.6 Hz, 1H), 7.72 (d, *J* = 8.2 Hz, 2H), 7.46 – 7.18 (m, 9H), 7.09 – 7.01 (m, 1H), 6.08 (s, 1H), 4.40 – 4.26 (m, 2H), 4.02 – 3.91 (m, 2H), 3.24 – 3.17 (m, 2H), 1.93 (t, *J* = 7.4 Hz, 2H), 1.51 – 1.44 (m, 4H), 1.30 – 1.21 (m, 4H); **^{13}C NMR** (126 MHz, DMSO-d_6) δ = 169.1, 168.4, 165.4, 164.9, 140.4, 139.0, 135.3, 134.3, 132.2, 130.8, 130.5, 130.5, 130.4, 130.1, 128.2, 127.7, 127.1, 126.8, 63.3, 42.9, 42.4, 40.1, 32.2, 28.9, 28.3, 26.2, 25.0. **HRMS (ESI)** *m/z* $[M+H]^+$ calcd for $C_{31}H_{33}Cl_3N_4O_5$ 647.1589, found 647.1568; **HPLC** (gradient A), t_R = 12.07 min, 97.1% purity.

***N*-benzyl-2-(2-chloro-*N*-propylacetamido)-2-(3,4-dichlorophenyl)acetamide (6)**

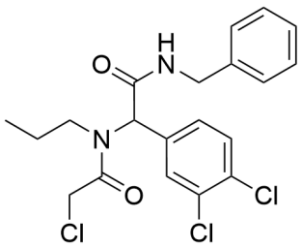

A round bottom flask was prepared with molecular sieve (100 mg; 4 Å) and dry MeOH (4 mL). n-Propylamine (157 µL, 1.89 mmol, 1.20 eq) and 3,4-dichlorobenzaldehyde (340 mg, 1.89 mmol, 1.20 eq) were added and stirred for 30 min at room temperature, before 2-chloroacetic acid (150 mg, 1.57 mmol, 1.00 eq) was added to the mixture. After additional 10 min, benzyl isocyanide (220 µL, 1.57 mmol, 1.00 eq) was added and the resulting solution was stirred for 72 h at room temperature. The

resulting precipitate was filtered, washed with MeOH (20 mL), dissolved in CH_2Cl_2 (20 mL) to remove the molecular sieve. The solvent was removed under reduced pressure and the resulting solid was dried *in vacuo*. DCAF11 ligand **6** was afforded as a with powder (358 mg, 0,837 mmol). Yield 53%; mp. 175 – 177 °C; Rf = 0.39 (cyclohexane/EtOAc, 2/1, *v*/*v*); **^{1}H NMR** (500 MHz, DMSO-d_6) δ = 8.55 (t, *J* = 5.9 Hz, 1H), 7.64 (d, *J* = 8.4 Hz, 1H), 7.53 (s, 1H), 7.37 – 7.19 (m, 6H), 5.81 (s, 1H), 4.56 – 4.23 (m, 4H), 3.30 – 3.24 (m, 2H), 1.52 – 0.79 (m, 2H), 0.68 – 0.55 (m, 3H); **^{13}C NMR** (126 MHz, DMSO-d_6) δ = 167.9, 166.7, 139.0, 137.4, 131.1, 130.8, 130.6, 130.4, 129.6, 128.2, 127.2, 126.8, 61.2, 48.2, 42.5, 42.4, 22.5, 10.8. **HRMS (ESI)** *m/z* $[M+Na]^+$ calcd for $C_{20}H_{21}Cl_3N_2O_2$ 449.0561, found 449.0537; **HPLC** (gradient A), t_R = 13.57 min, 99.0% purity.

3.4. NMR Data of compounds in biological testing

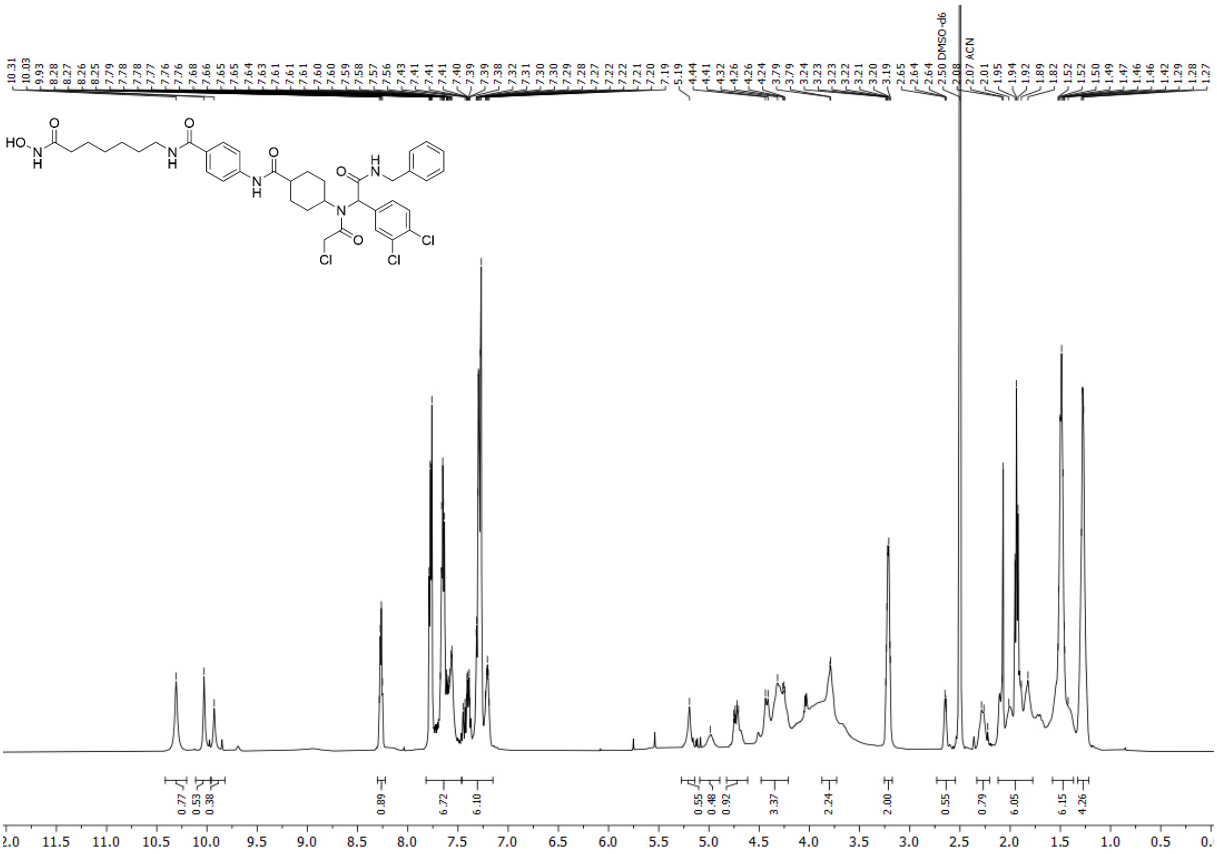

^{1}H NMR spectrum of **1a** (500 MHz, DMSO-d_6).

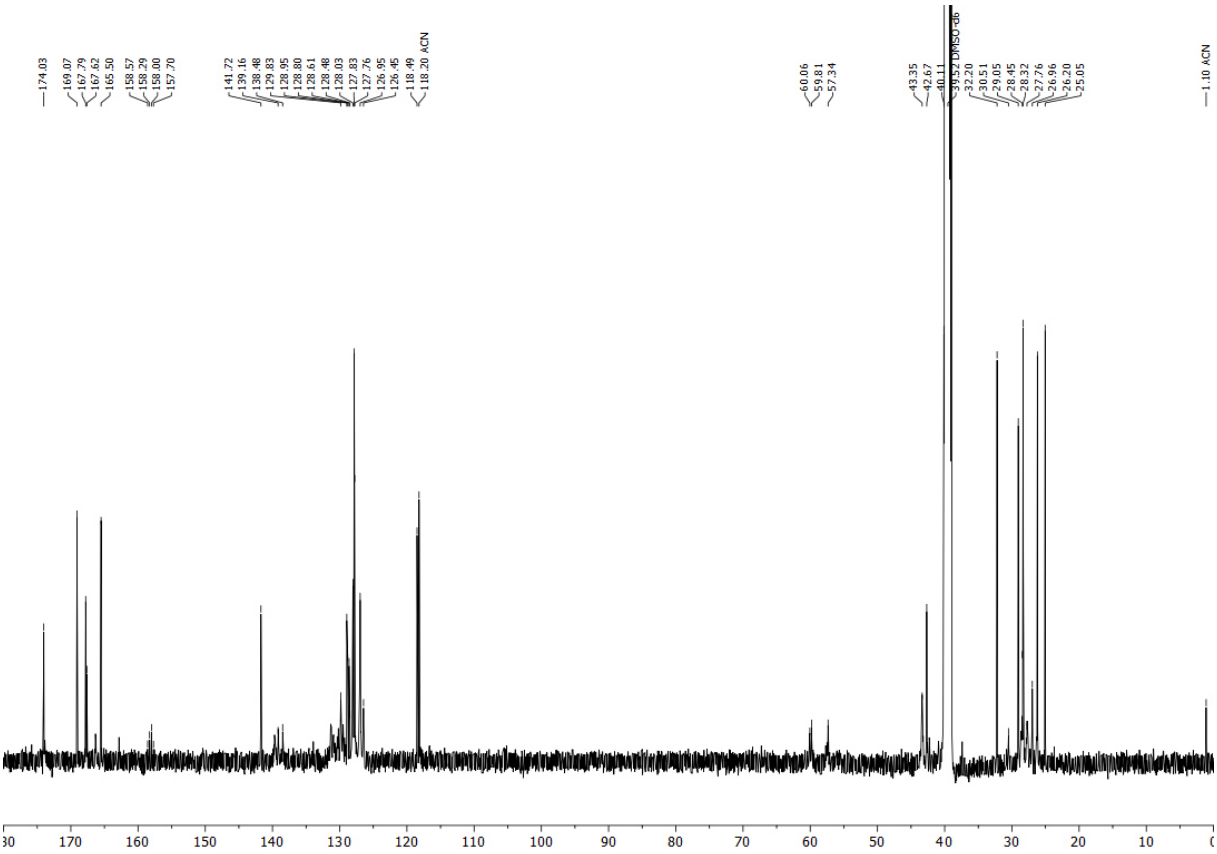

^{13}C NMR spectrum of **1a** (126 MHz, DMSO-d_6).

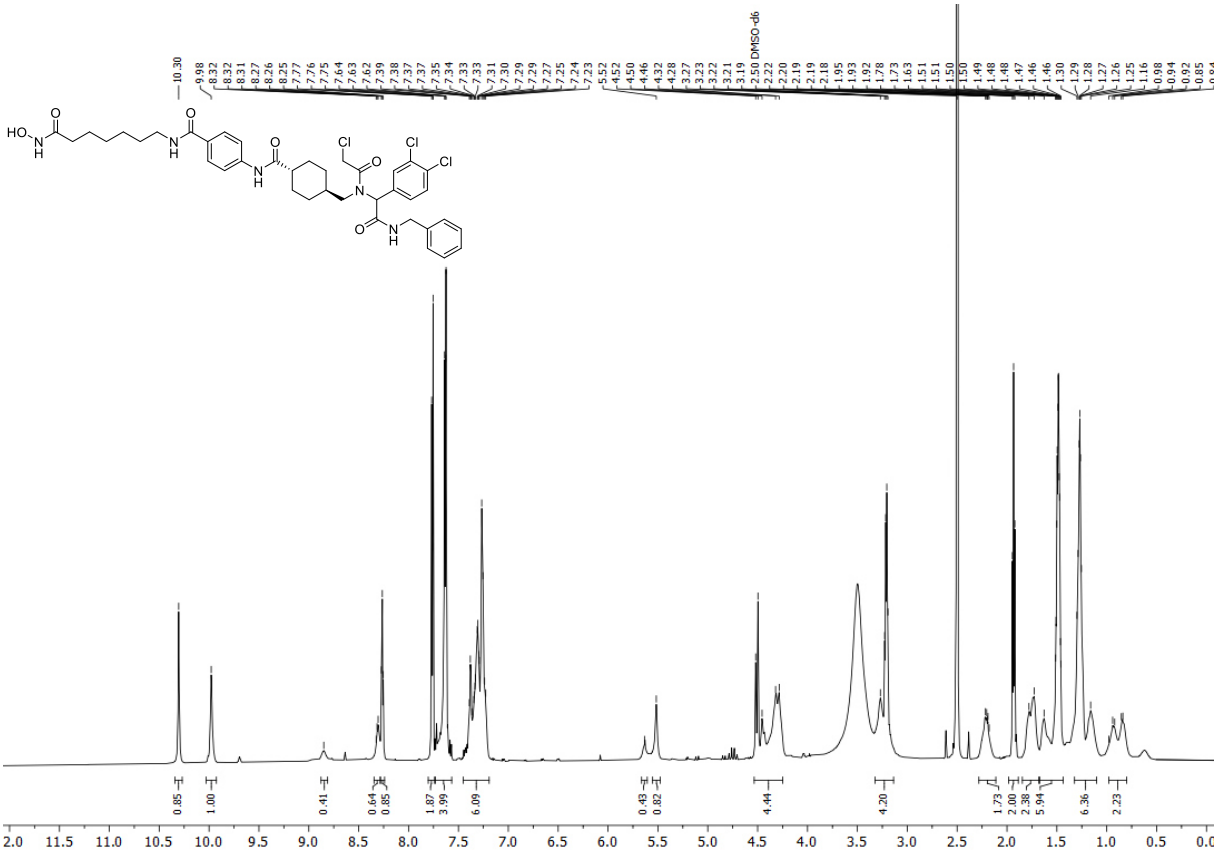

^{1}H NMR spectrum of **1b** (600 MHz, DMSO-d_6).

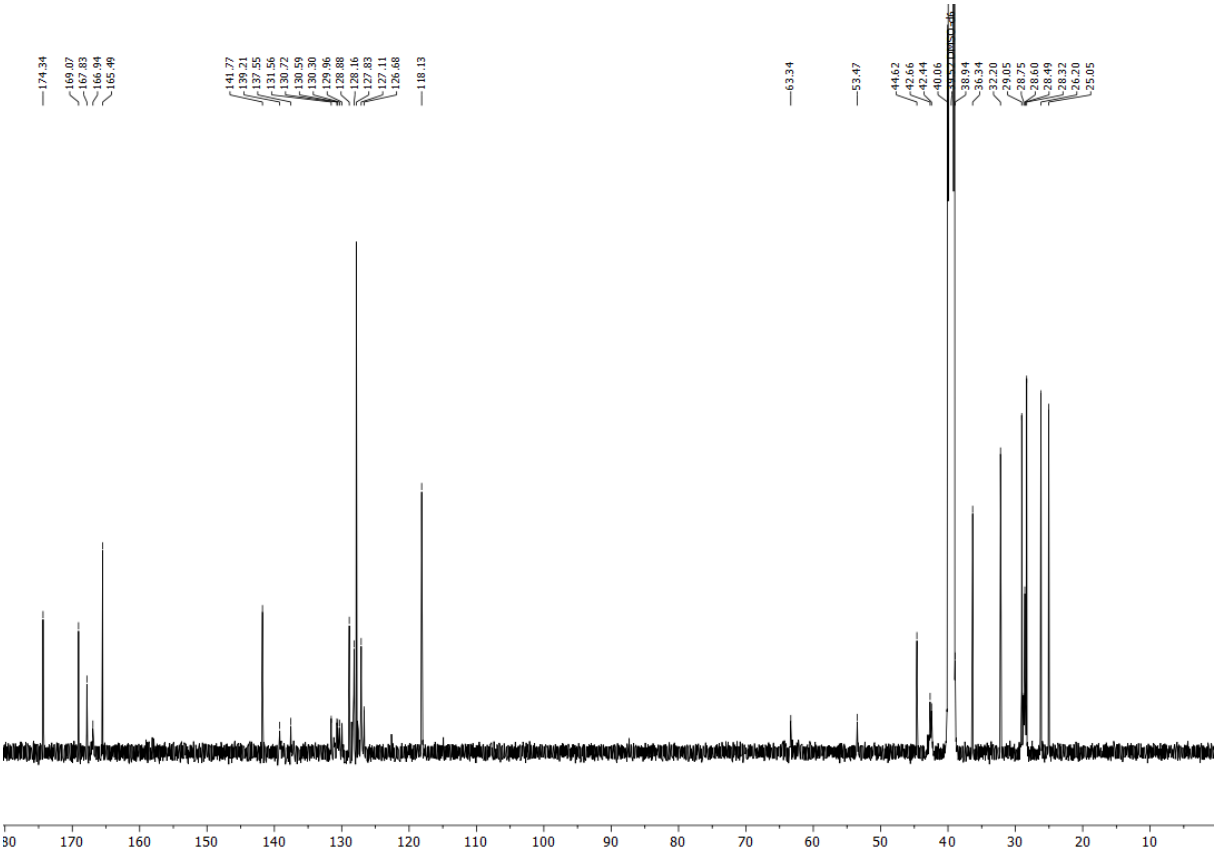

^{13}C NMR spectrum of **1b** (151 MHz, DMSO-d_6).

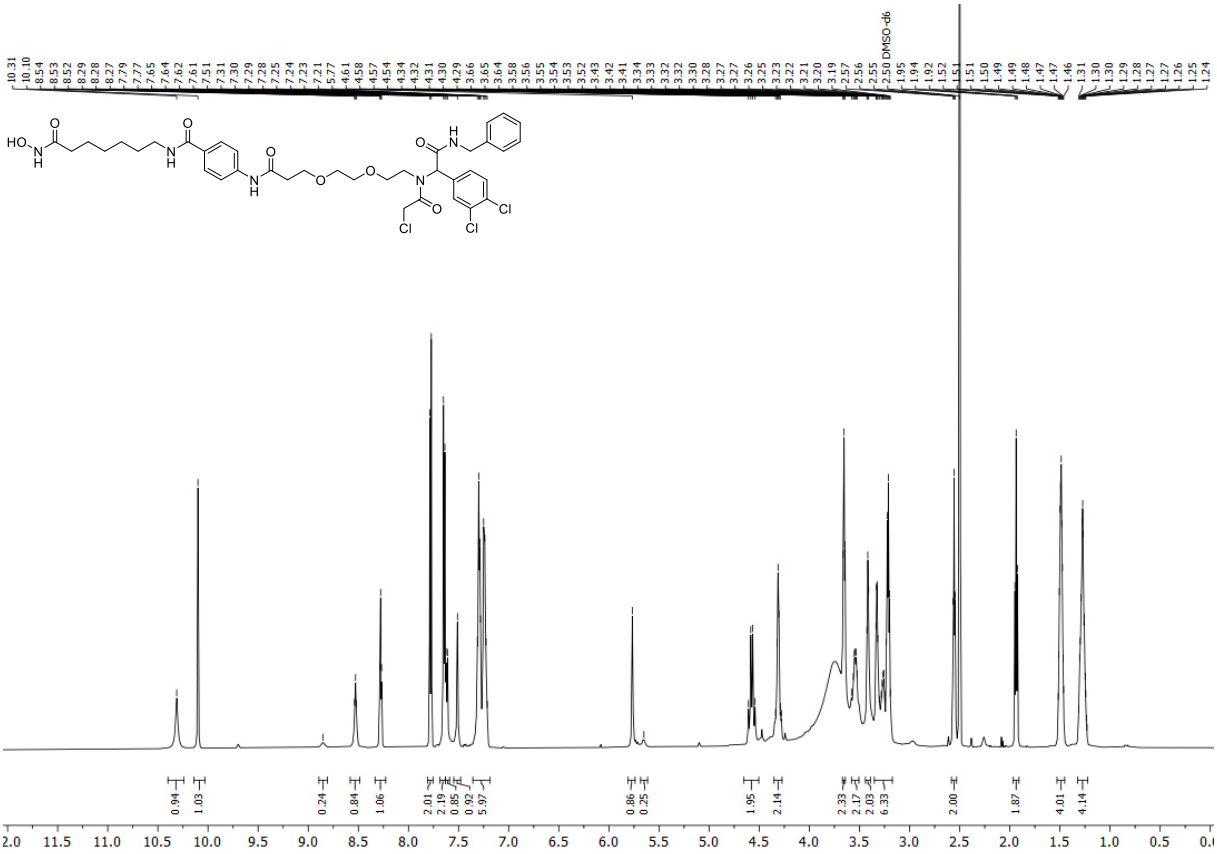

^{1}H NMR spectrum of **1c** (600 MHz, DMSO-d_6).

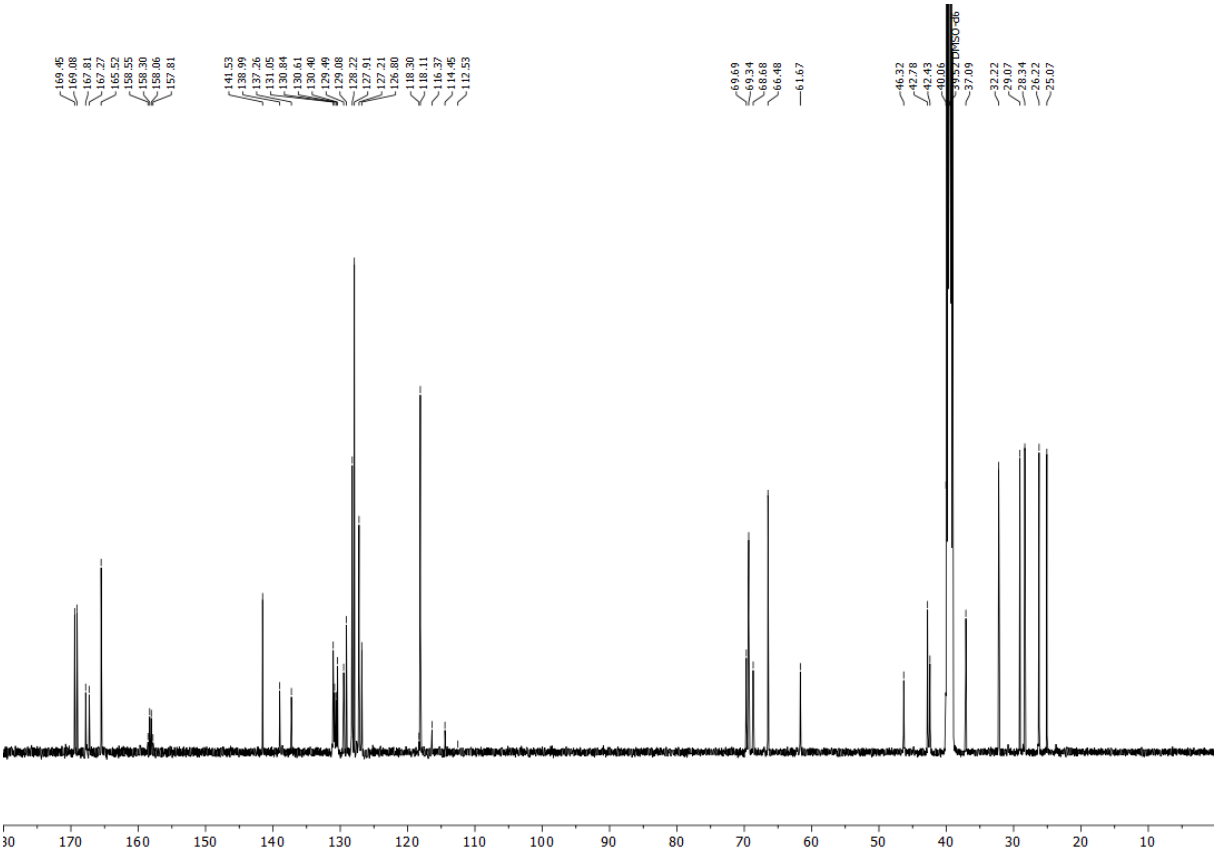

^{13}C NMR spectrum of **1c** (151 MHz, DMSO-d_6).

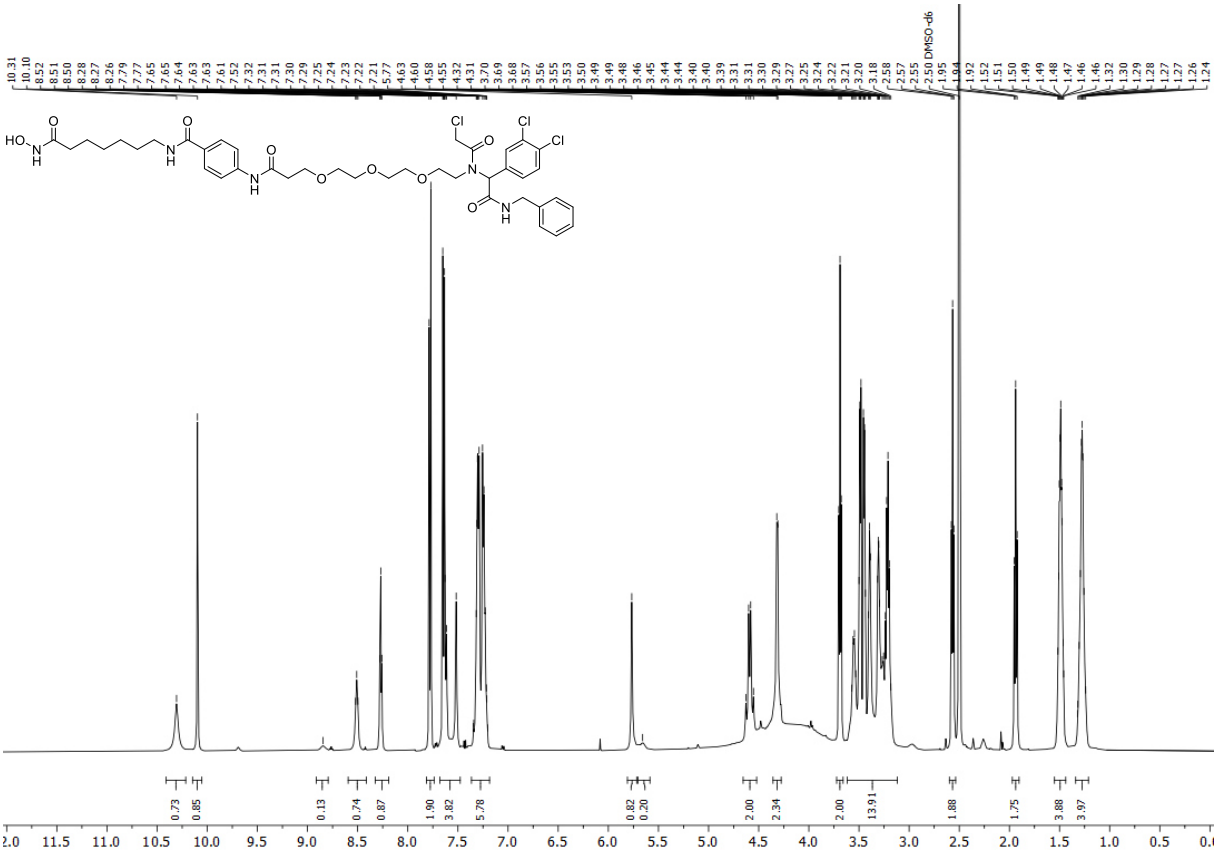

^{1}H NMR spectrum of **1d** (500 MHz, DMSO-d_6).

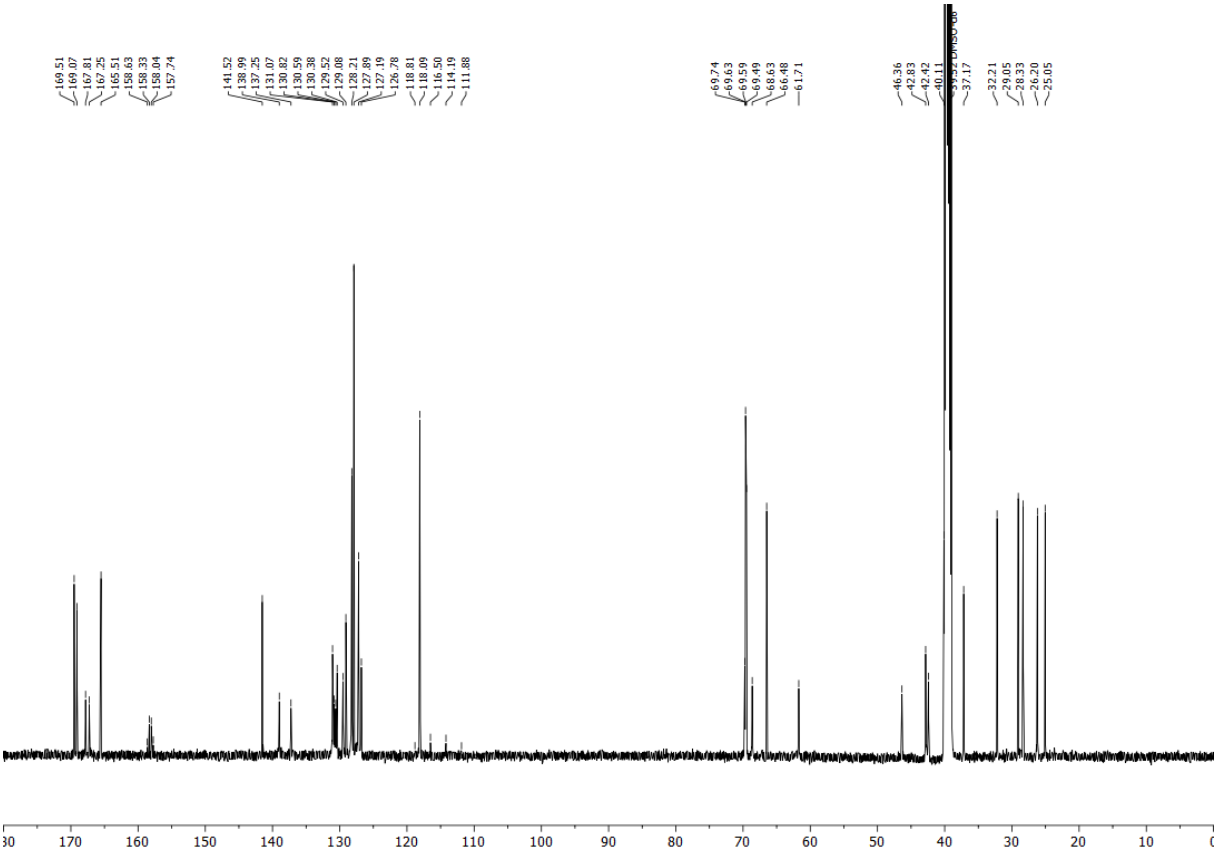

^{13}C NMR spectrum of **1d** (126 MHz, DMSO-d_6).

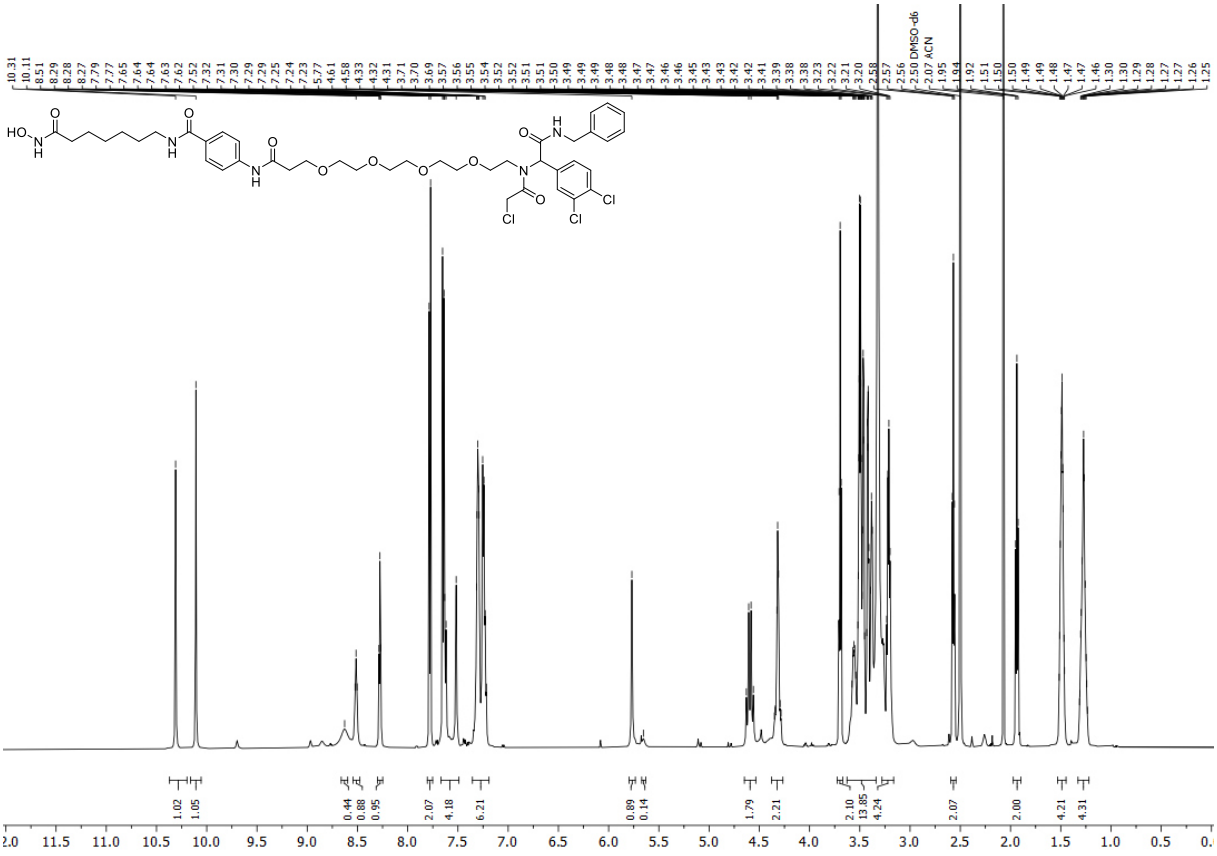

^{1}H NMR spectrum of **1e** (600 MHz, DMSO-d_6).

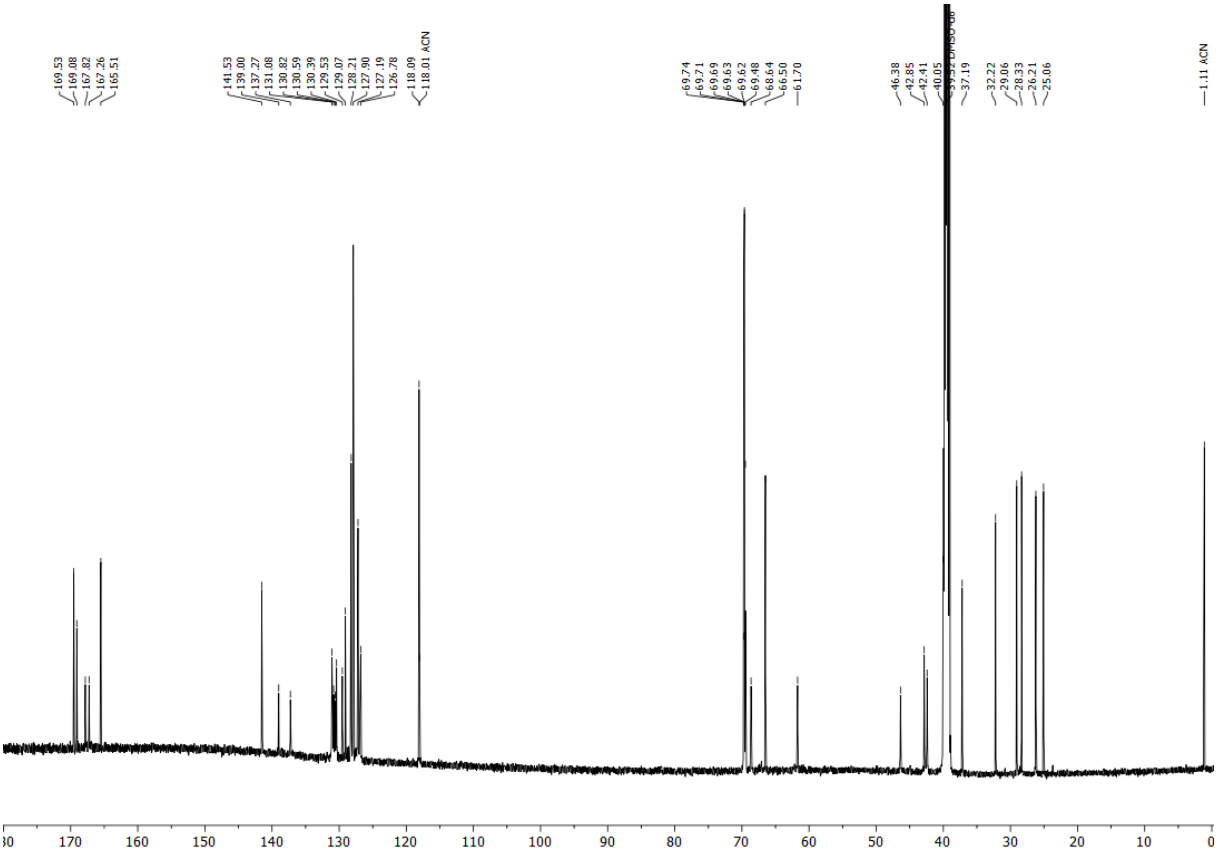

^{13}C NMR spectrum of **1e** (151 MHz, DMSO-d_6).

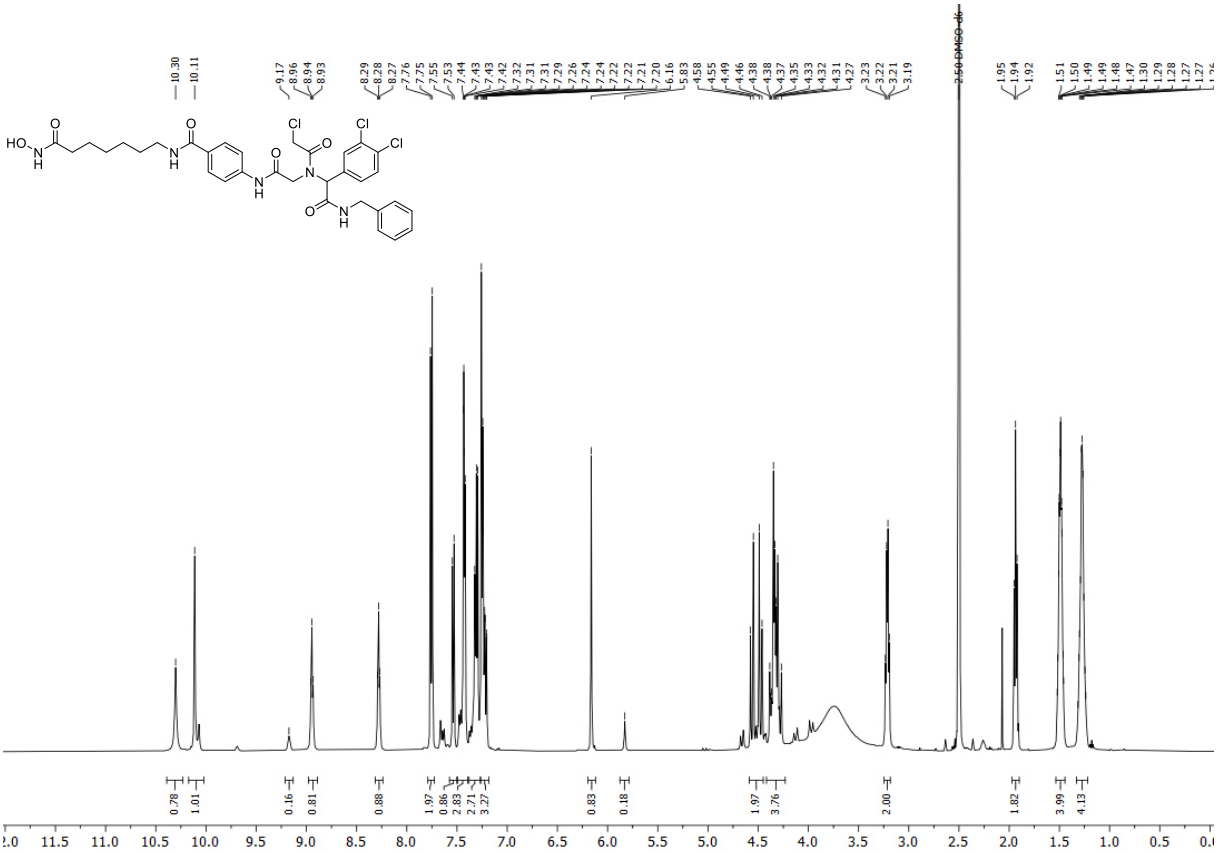

^{1}H NMR spectrum of **1f** (500 MHz, DMSO-d_6).

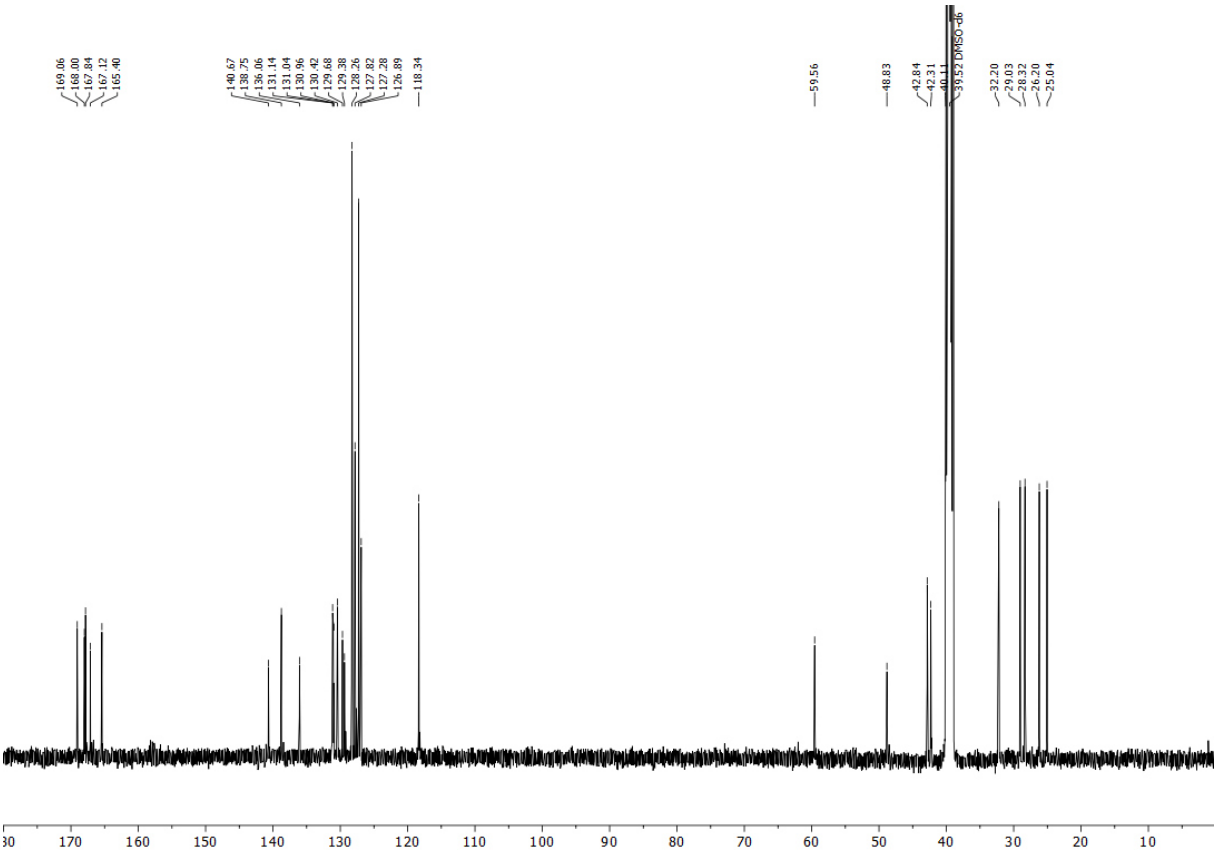

^{13}C NMR spectrum of **1f** (126 MHz, DMSO-d_6).

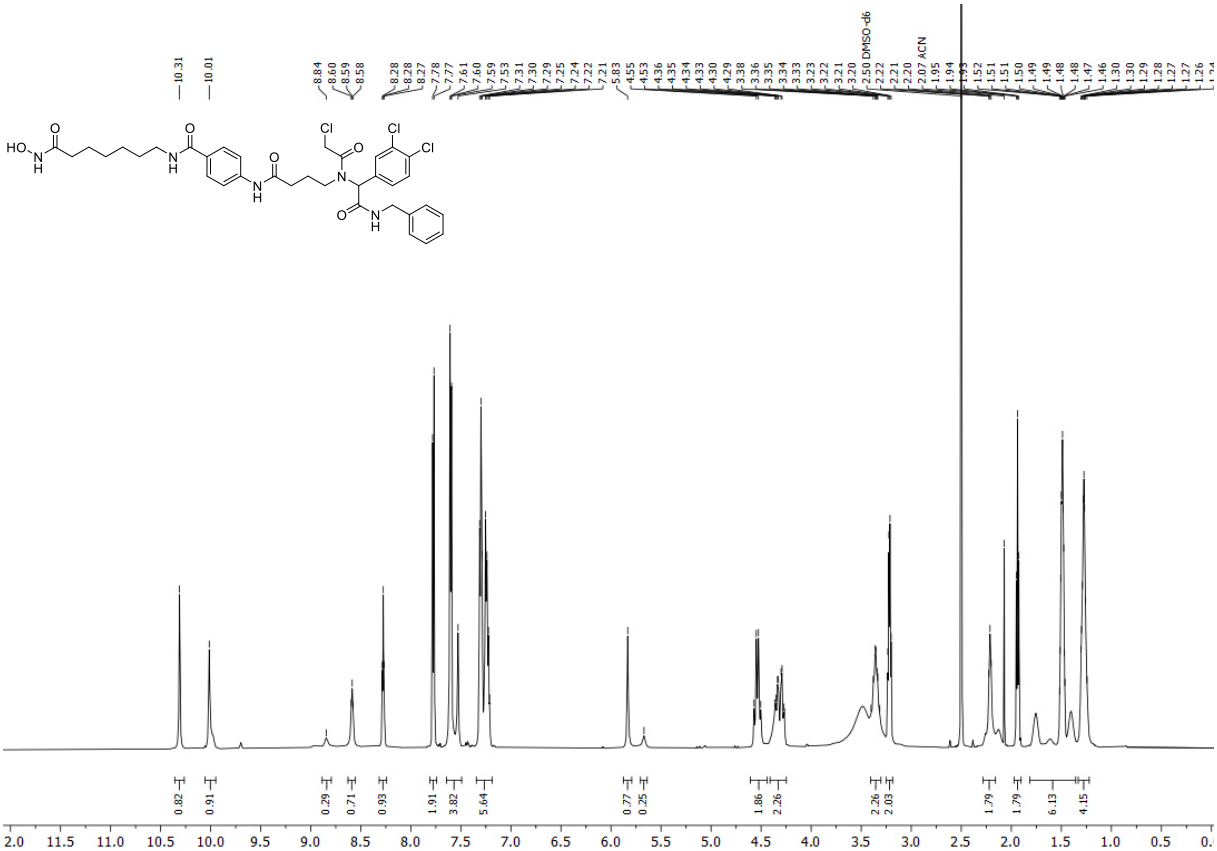

^{1}H NMR spectrum of **1g** (600 MHz, DMSO-d_6).

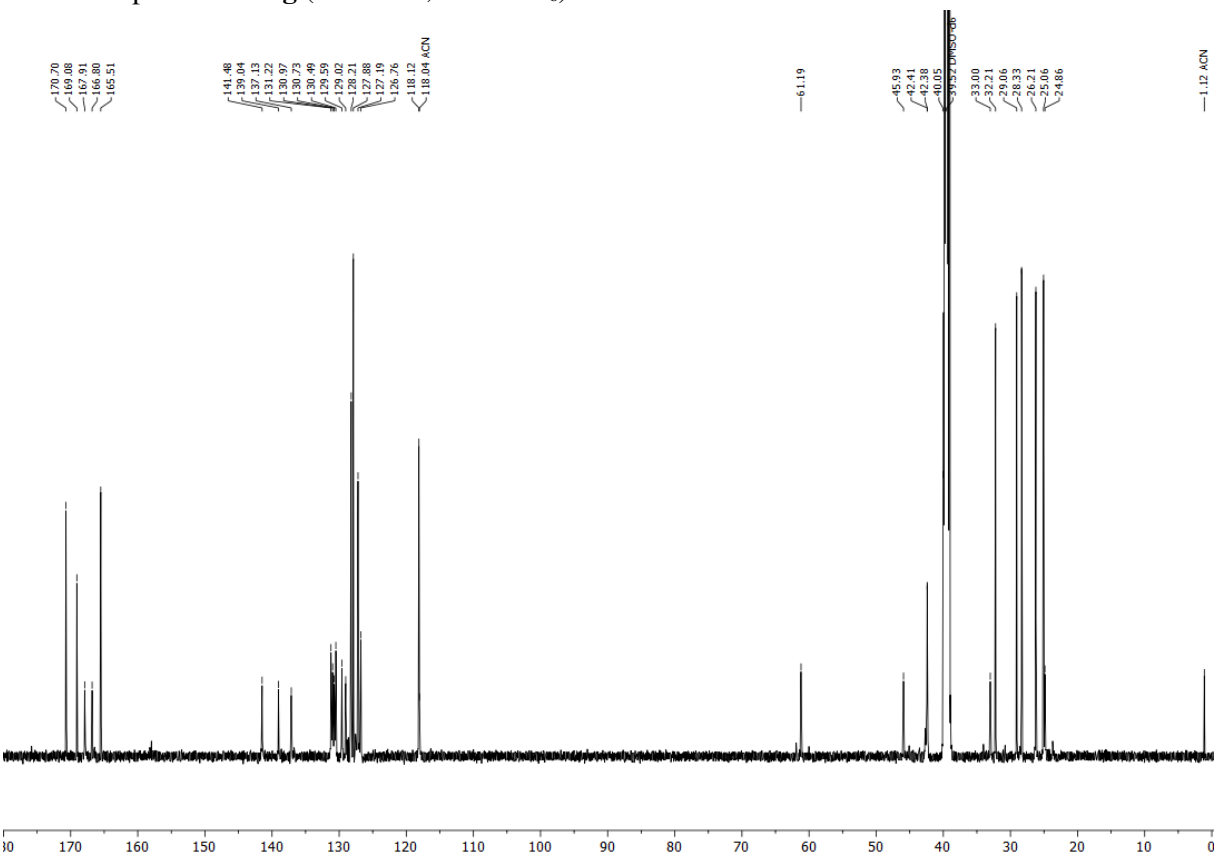

^{13}C NMR spectrum of **1g** (151 MHz, DMSO-d_6).

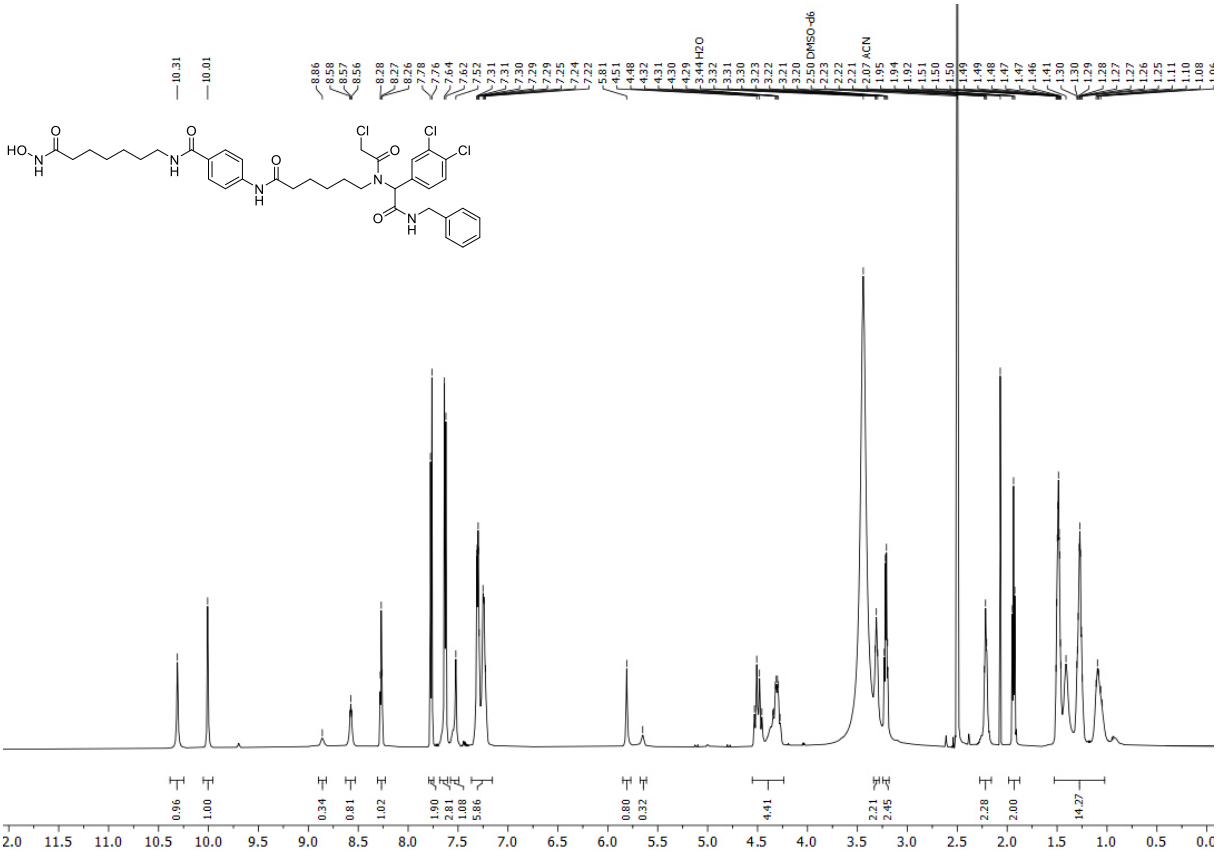

^{1}H NMR spectrum of **1h** (600 MHz, DMSO-d_6).

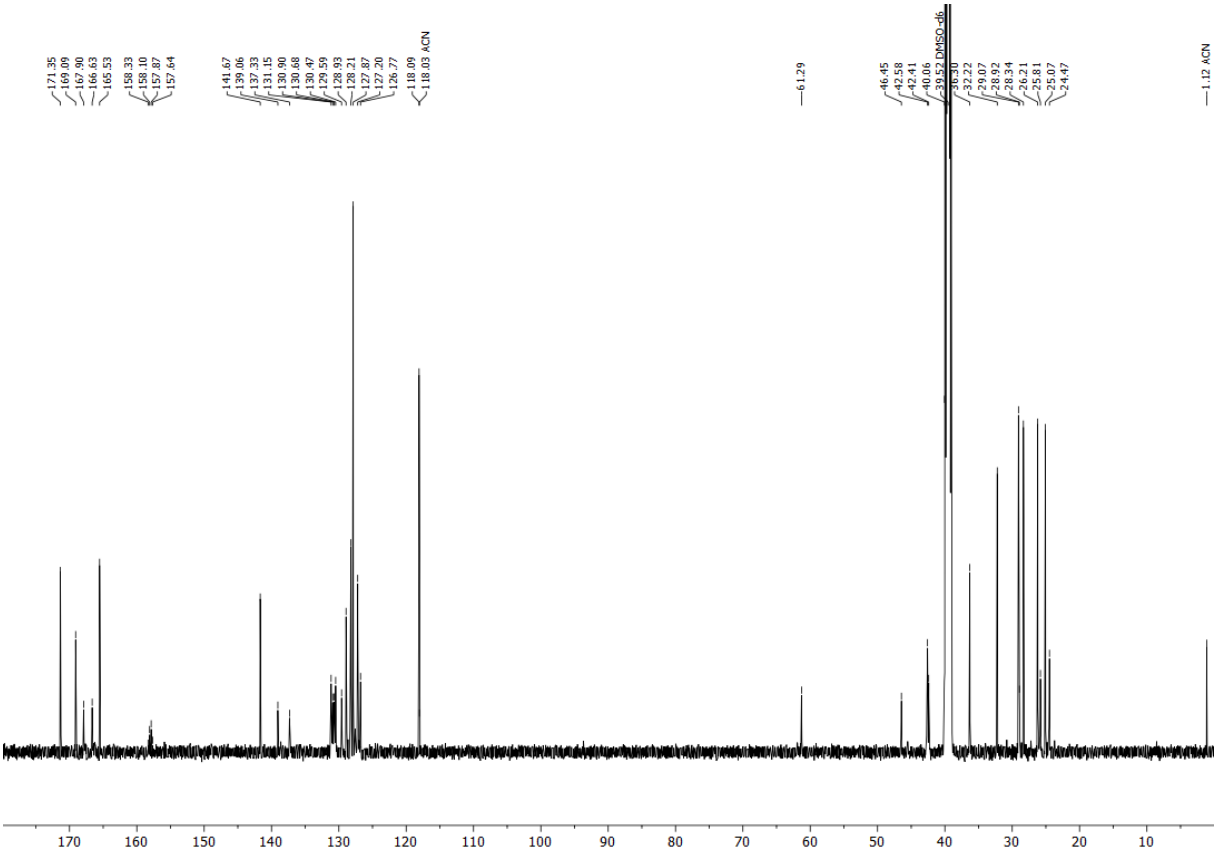

^{13}C NMR spectrum of **1h** (151 MHz, DMSO-d_6).

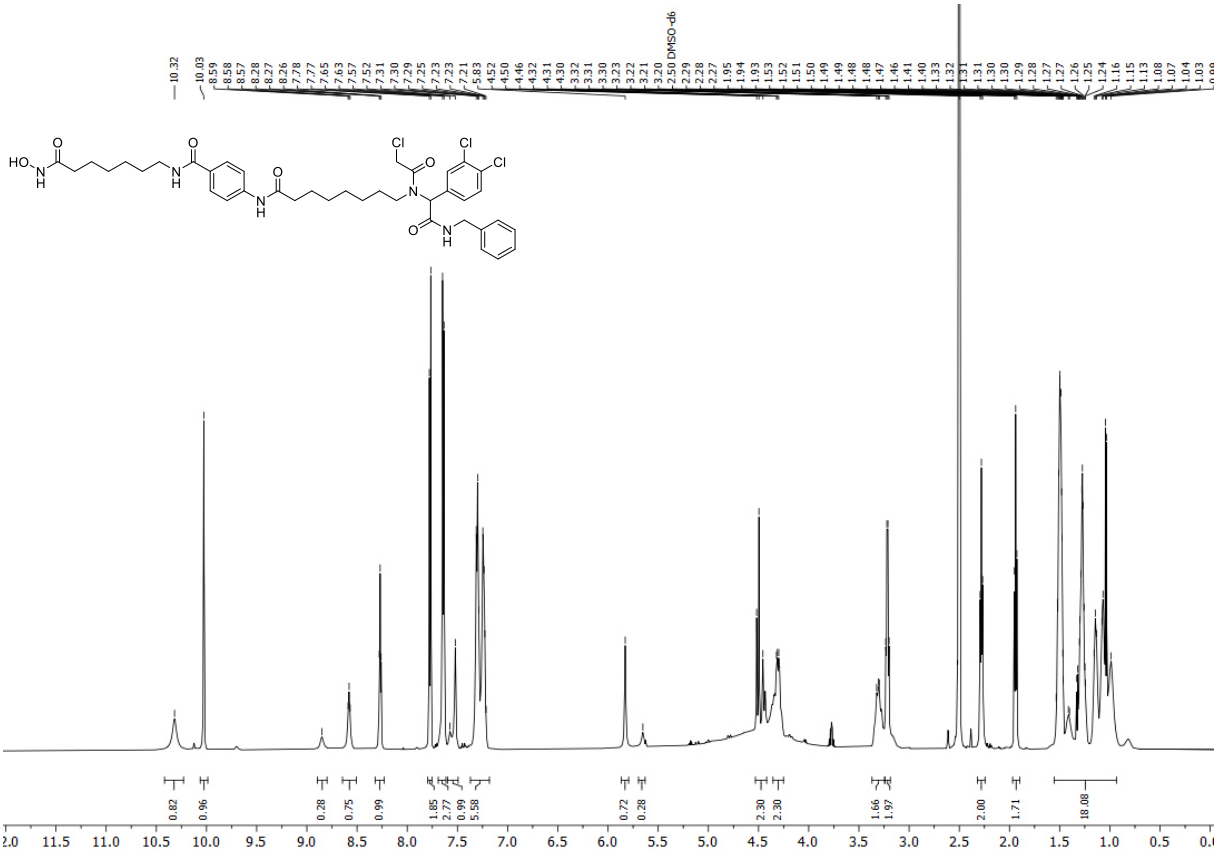

^{1}H NMR spectrum of **1i** (600 MHz, DMSO-d_6).

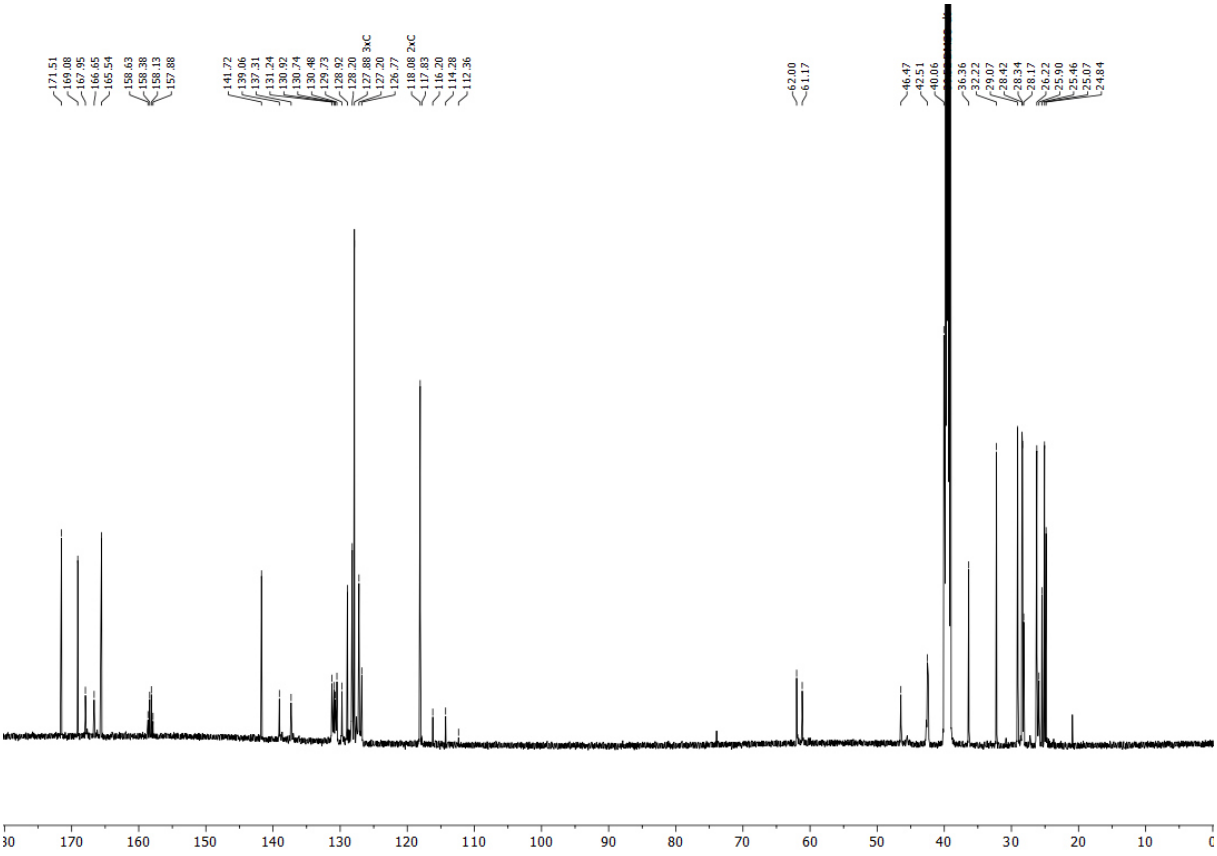

^{13}C NMR spectrum of **1i** (151 MHz, DMSO-d_6).

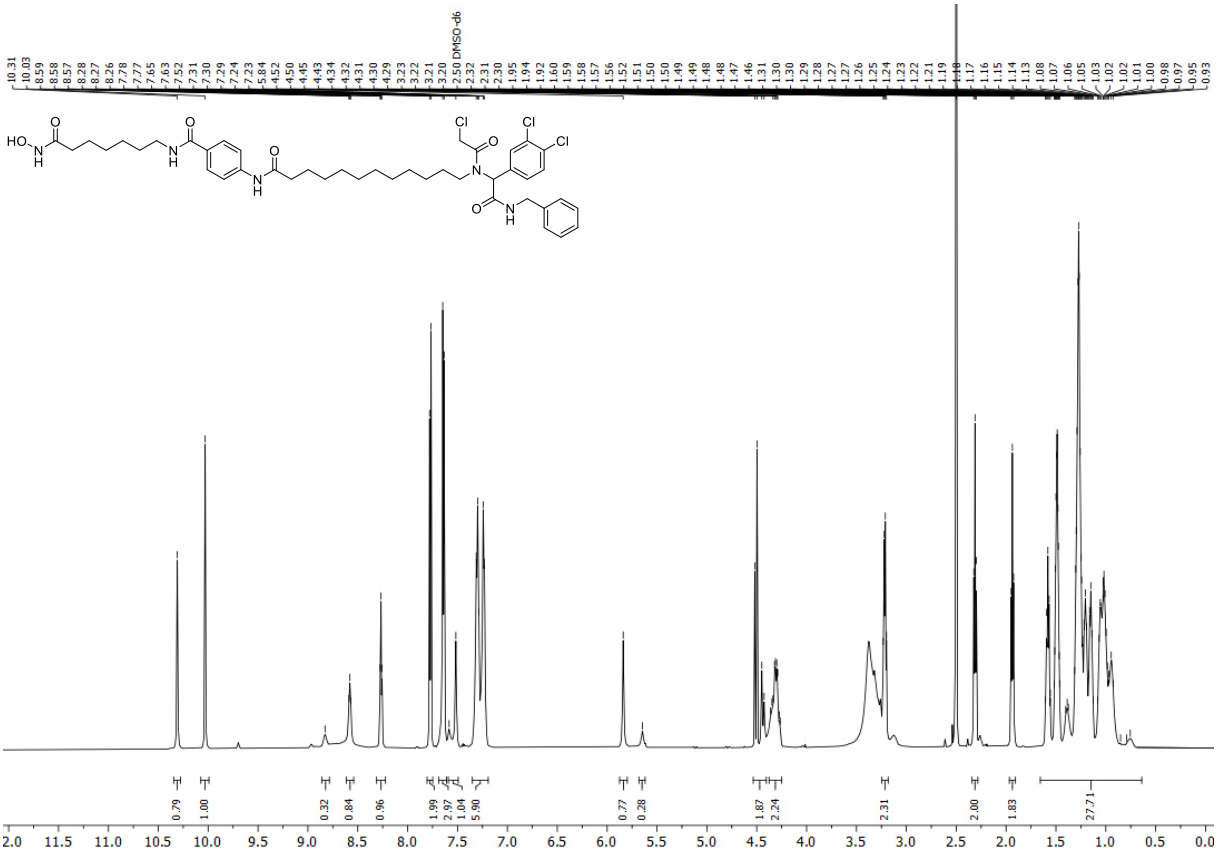

^{1}H NMR spectrum of **1j** (600 MHz, DMSO-d_6).

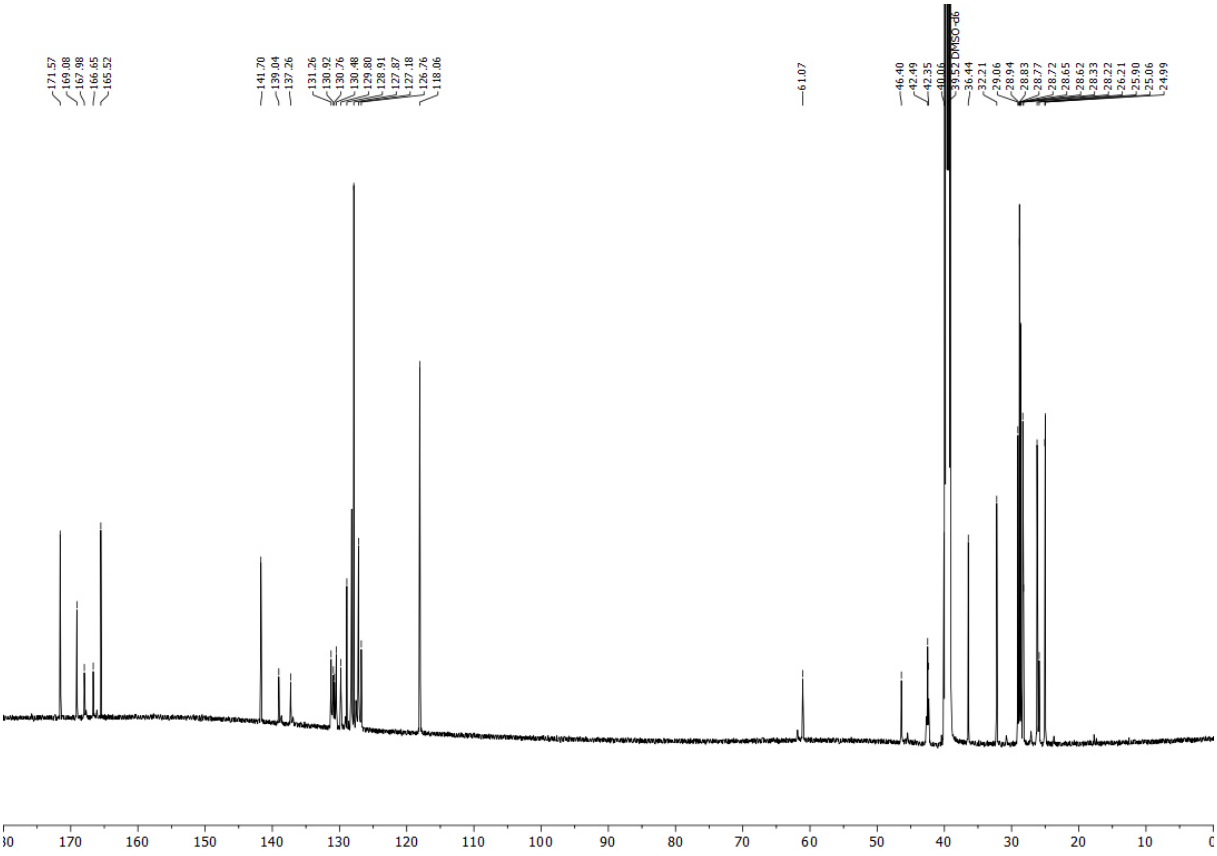

^{13}C NMR spectrum of **1j** (151 MHz, DMSO-d_6).

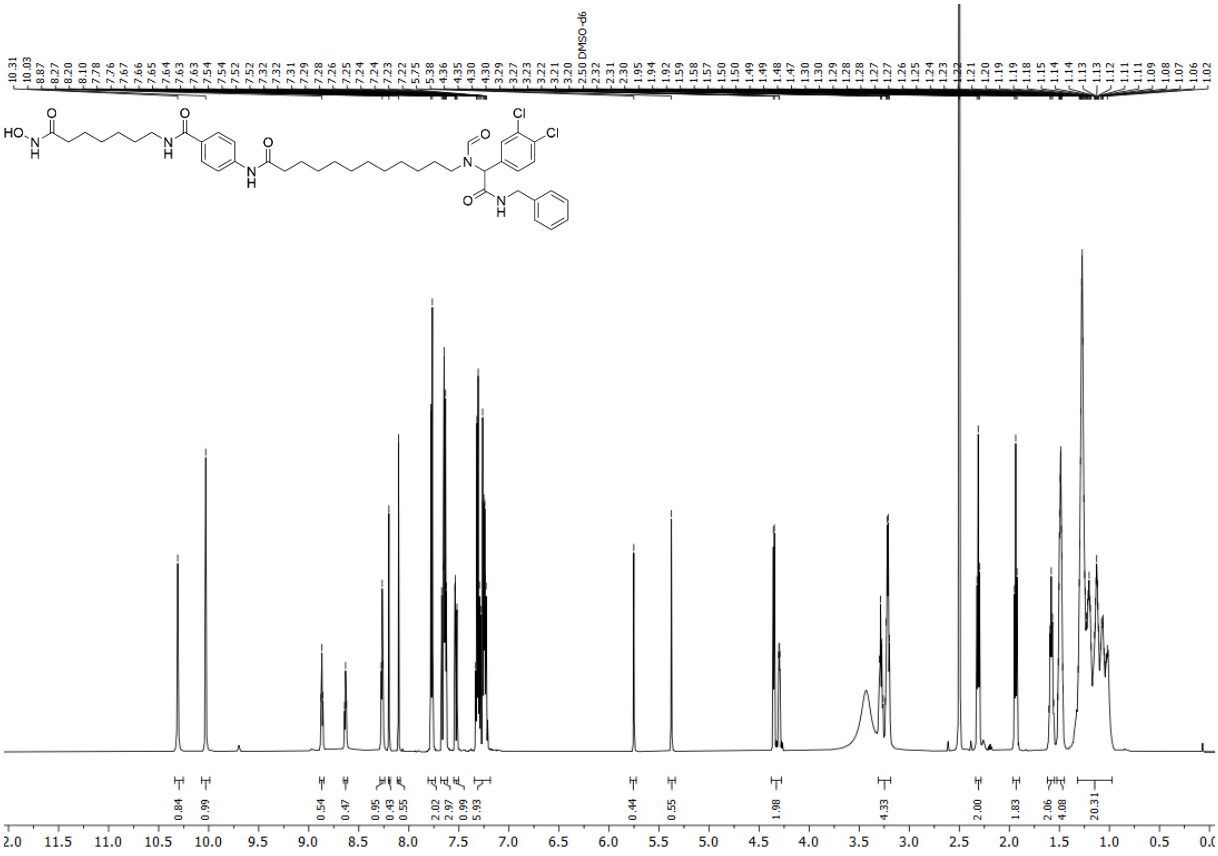

^{1}H NMR spectrum of **1j-nc** (600 MHz, DMSO-d_6).

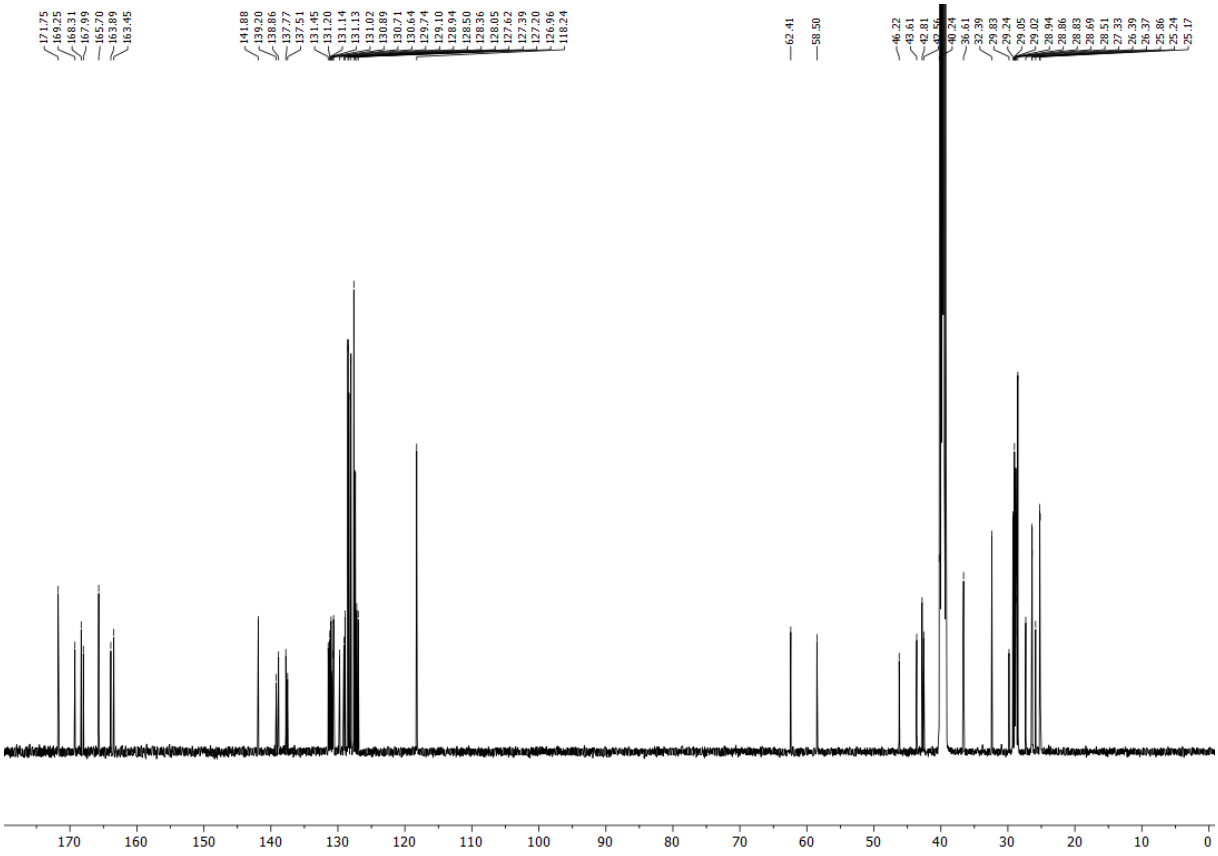

^{13}C NMR spectrum of **1j-nc** (151 MHz, DMSO-d_6).

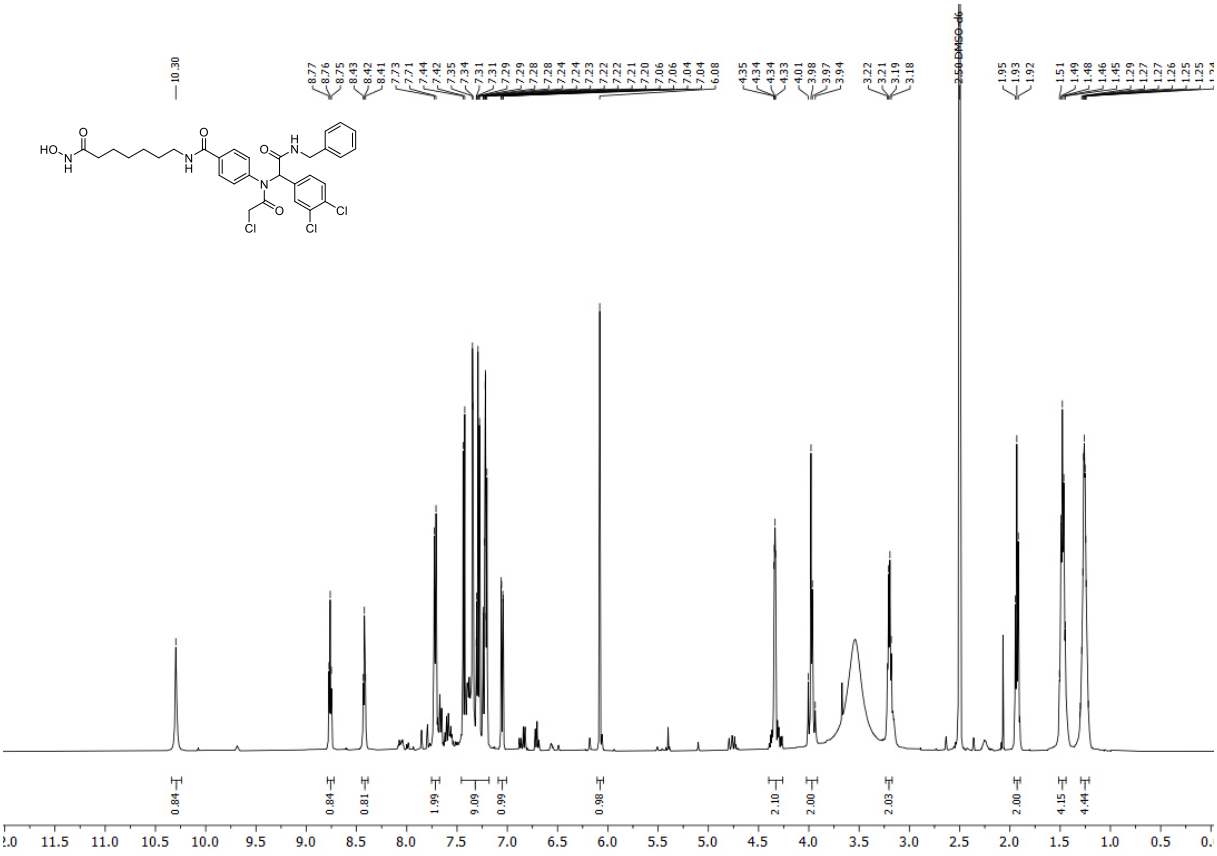

^{1}H NMR spectrum of **2** (500 MHz, DMSO-d_6).

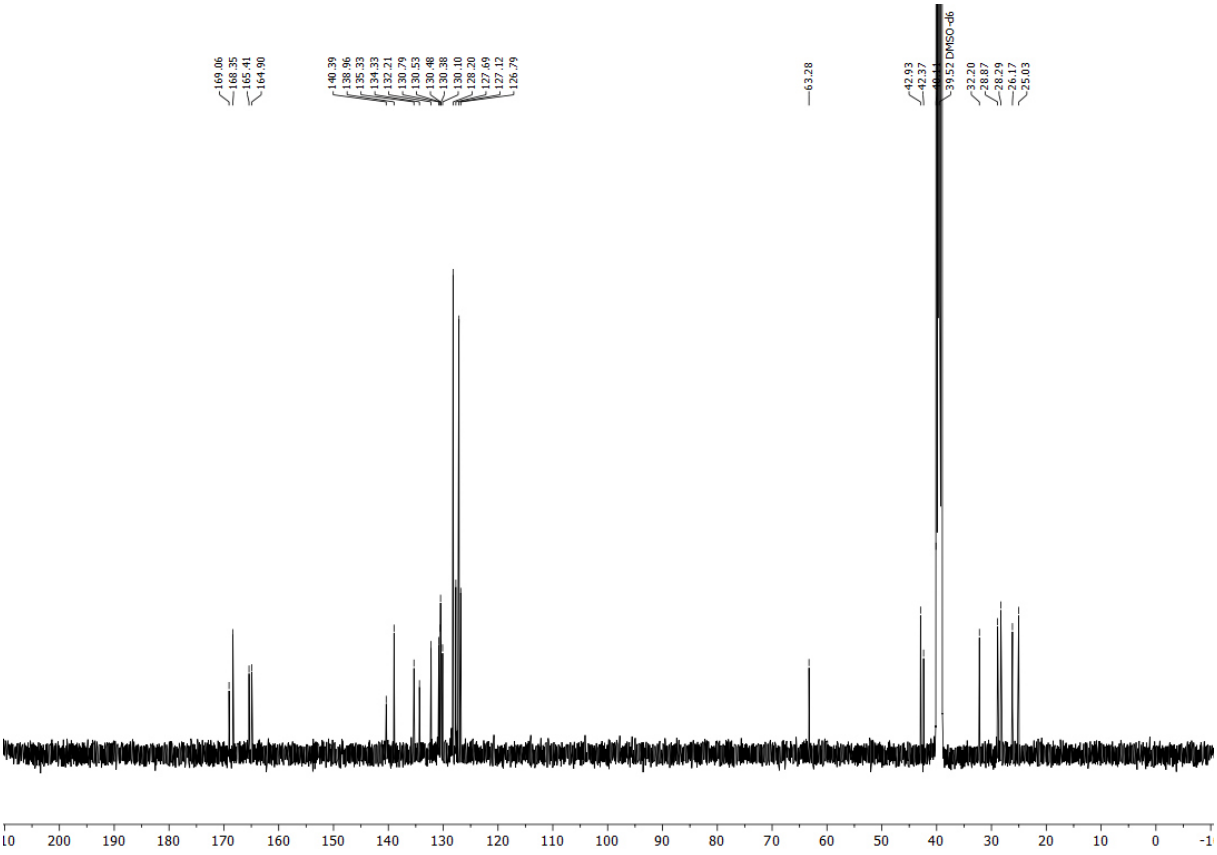

^{13}C NMR spectrum of **2** (126 MHz, DMSO-d_6).

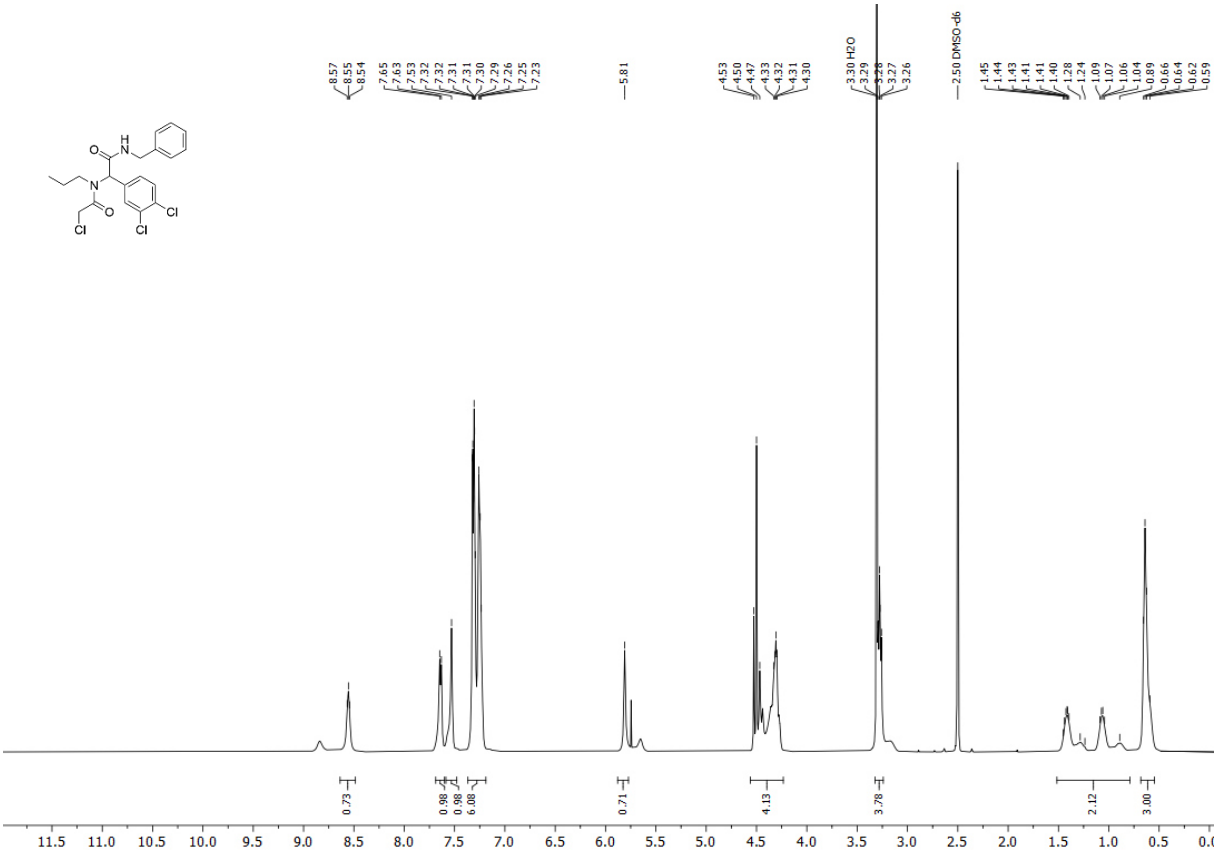

^{1}H NMR spectrum of **6** (500 MHz, DMSO-d_6).

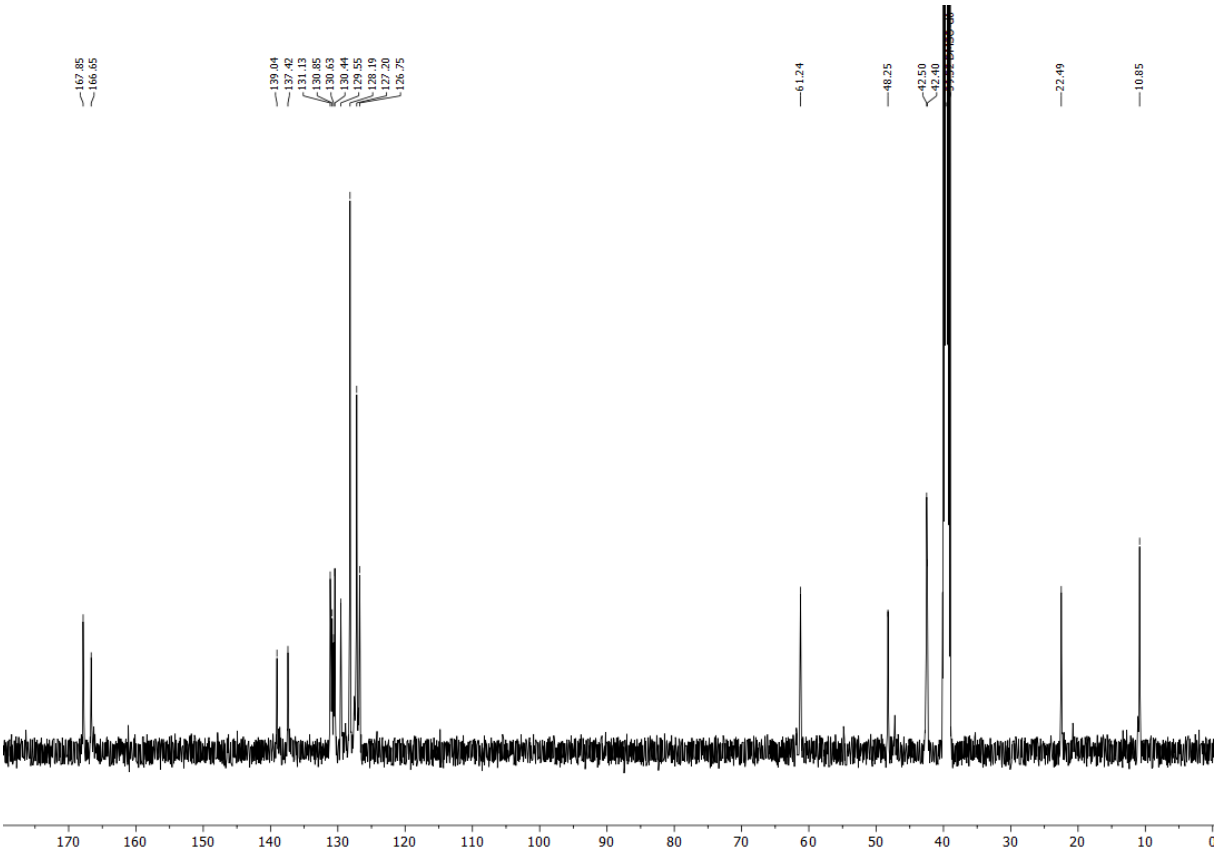

^{13}C NMR spectrum of **6** (126 MHz, DMSO-d_6).

3.5. HPLC chromatograms of target compounds

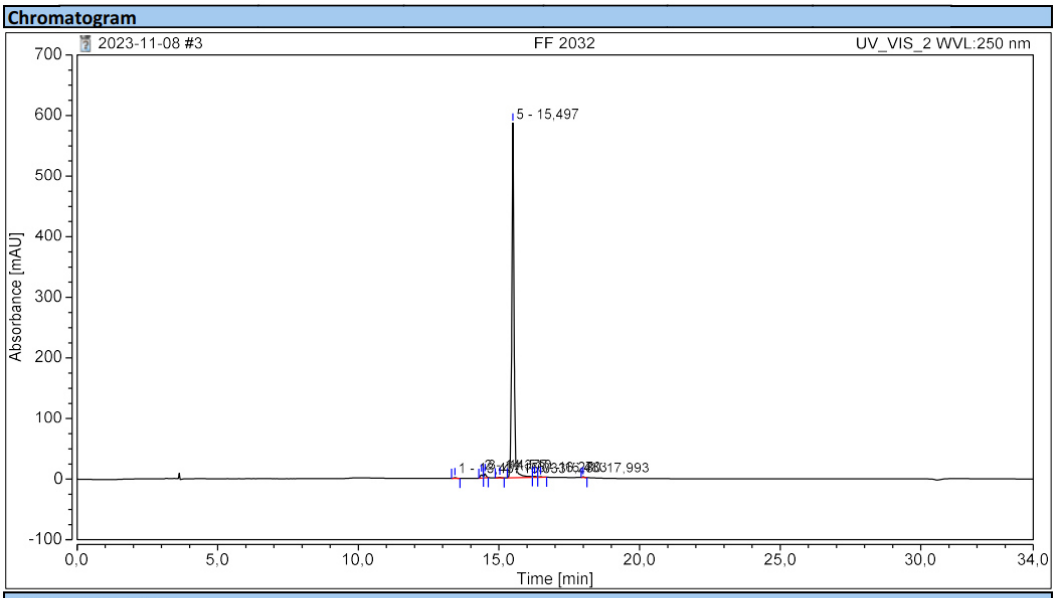

Integration Results

No.	Peak Name	Retention Time min	Area mAU*min	Height mAU	Relative Area %	Relative Height %	Amount n.a.
1		13,437	0,118	1,401	0,22	0,23	n.a.
2		14,377	0,512	6,725	0,94	1,11	n.a.
3		14,510	0,551	6,906	1,01	1,14	n.a.
4		15,033	0,100	1,108	0,18	0,18	n.a.
5		15,497	52,540	585,140	96,74	96,62	n.a.
6		16,270	0,254	1,929	0,47	0,32	n.a.
7		16,483	0,146	1,083	0,27	0,18	n.a.
8		17,993	0,093	1,338	0,17	0,22	n.a.
Total:			**54,313**	**605,630**	**100,00**	**100,00**	

HPLC chromatogram of **1a** (gradient B, purity: 96.7%).

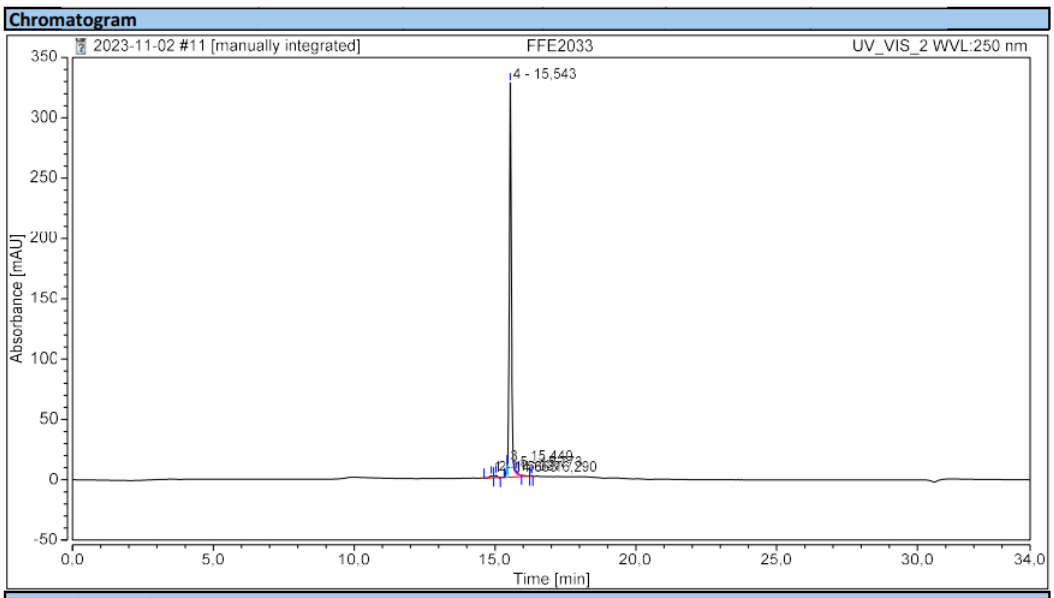

Integration Results

No.	Peak Name	Retention Time min	Area mAU*min	Height mAU	Relative Area %	Relative Height %	Amount n.a.
1		14,863	0,217	1,712	0,72	0,50	n.a.
2		15,037	0,220	2,127	0,74	0,62	n.a.
3		15,440	0,543	10,363	1,81	3,02	n.a.
4		15,543	28,790	326,830	96,04	95,13	n.a.
5		15,773	0,182	2,123	0,61	0,62	n.a.
6		16,290	0,024	0,392	0,08	0,11	n.a.
Total:			**29,977**	**343,547**	**100,00**	**100,00**	

HPLC chromatogram of **1b** (gradient B, purity: 96.0%).

Chromatogram

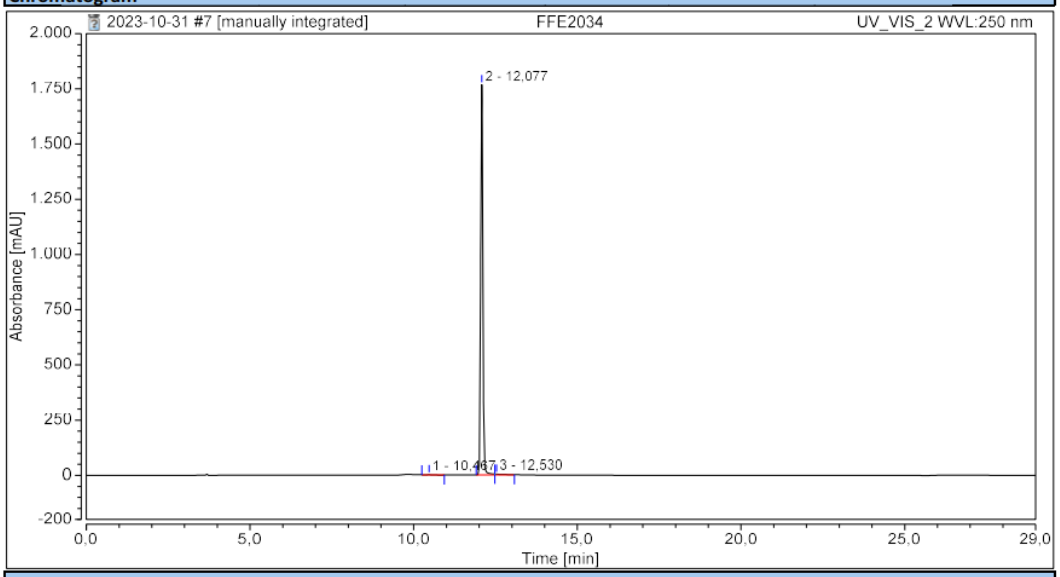

Integration Results

No.	Peak Name	Retention Time min	Area mAU*min	Height mAU	Relative Area %	Relative Height %	Amount n.a.
1		10,467	0,021	0,438	0,02	0,02	n.a.
2		12,077	133,190	1766,184	99,24	99,79	n.a.
3		12,530	0,998	3,251	0,74	0,18	n.a.
Total:			**134,209**	**1769,873**	**100,00**	**100,00**	

HPLC chromatogram of **1c** (gradient A, purity: 99.2%).

Chromatogram

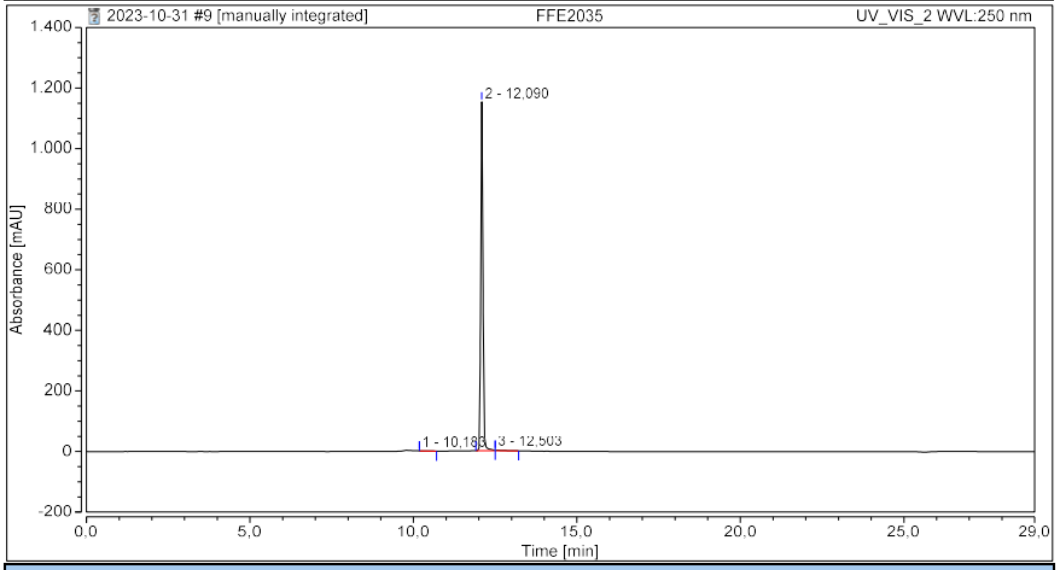

Integration Results

No.	Peak Name	Retention Time min	Area mAU*min	Height mAU	Relative Area %	Relative Height %	Amount n.a.
1		10,183	0,306	0,751	0,34	0,07	n.a.
2		12,090	89,258	1151,844	98,91	99,74	n.a.
3		12,503	0,678	2,252	0,75	0,19	n.a.
Total:			**90,242**	**1154,847**	**100,00**	**100,00**	

HPLC chromatogram of **1d** (gradient A, purity: 98.9%).

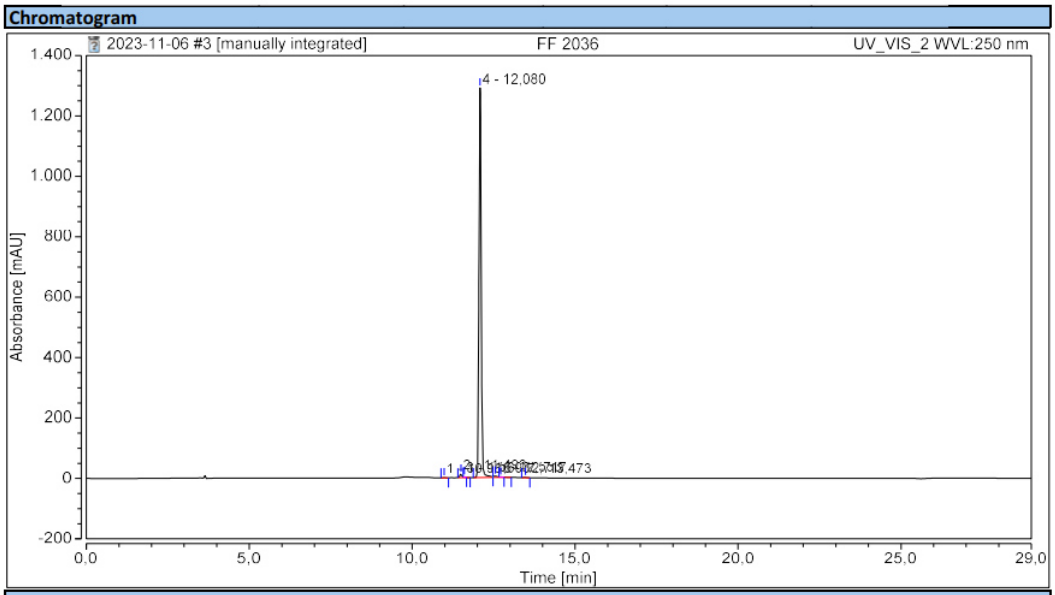

Integration Results

No.	Peak Name	Retention Time min	Area mAU*min	Height mAU	Relative Area %	Relative Height %	Amount n.a.
1		10,980	0,057	0,791	0,06	0,06	n.a.
2		11,493	1,007	12,469	1,00	0,95	n.a.
3		11,603	0,079	1,562	0,08	0,12	n.a.
4		12,080	98,773	1290,418	97,93	98,36	n.a.
5		12,553	0,780	4,846	0,77	0,37	n.a.
6		12,717	0,031	0,508	0,03	0,04	n.a.
7		13,473	0,135	1,315	0,13	0,10	n.a.
Total:			**100,862**	**1311,908**	**100,00**	**100,00**	

HPLC chromatogram of **1e** (gradient A, purity: 97.9%).

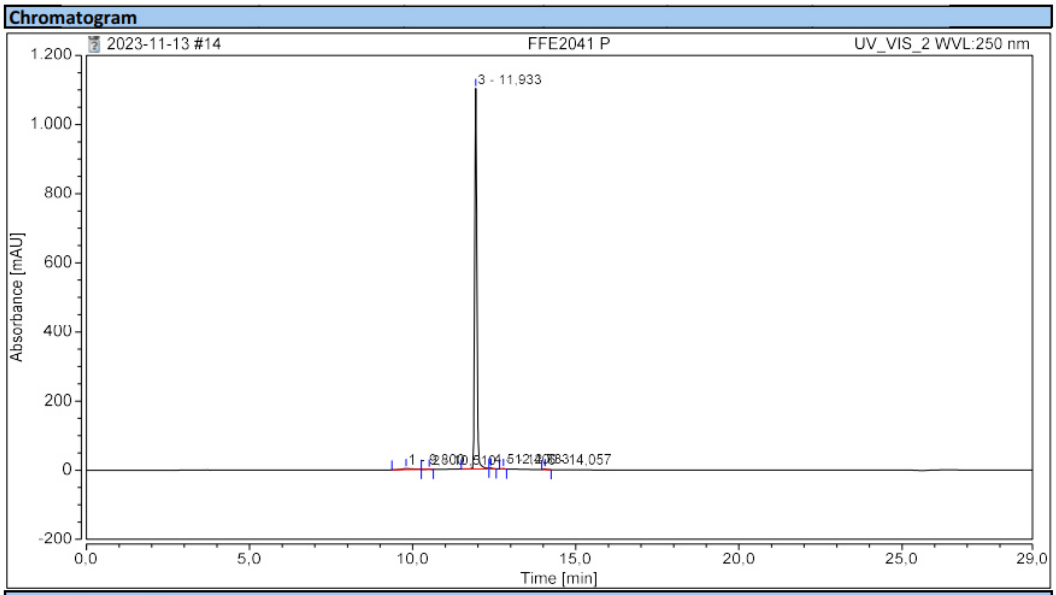

Integration Results

No.	Peak Name	Retention Time min	Area mAU*min	Height mAU	Relative Area %	Relative Height %	Amount n.a.
1		9,800	1,104	3,127	1,28	0,28	n.a.
2		10,510	0,107	0,786	0,12	0,07	n.a.
3		11,933	84,662	1101,043	97,94	99,04	n.a.
4		12,400	0,243	2,365	0,28	0,21	n.a.
5		12,783	0,119	1,693	0,14	0,15	n.a.
6		14,057	0,211	2,711	0,24	0,24	n.a.
Total:			**86,446**	**1111,726**	**100,00**	**100,00**	

HPLC chromatogram of **1f** (gradient A, purity: 97.9%).

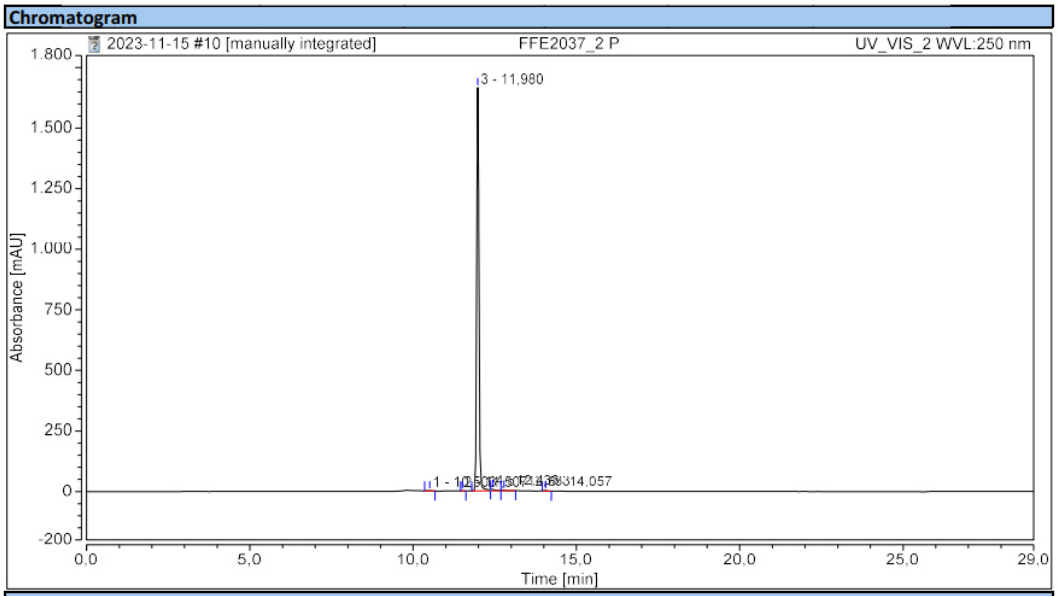

Integration Results

No.	Peak Name	Retention Time min	Area mAU*min	Height mAU	Relative Area %	Relative Height %	Amount n.a.
1		10,503	0,105	0,681	0,08	0,04	n.a.
2		11,507	0,035	0,605	0,03	0,04	n.a.
3		11,980	128,061	1664,337	98,69	99,23	n.a.
4		12,433	0,974	6,297	0,75	0,38	n.a.
5		12,783	0,364	2,427	0,28	0,14	n.a.
6		14,057	0,226	2,881	0,17	0,17	n.a.
Total:			**129,766**	**1677,228**	**100,00**	**100,00**	

HPLC chromatogram of **1g** (gradient A, purity: 98.7%).

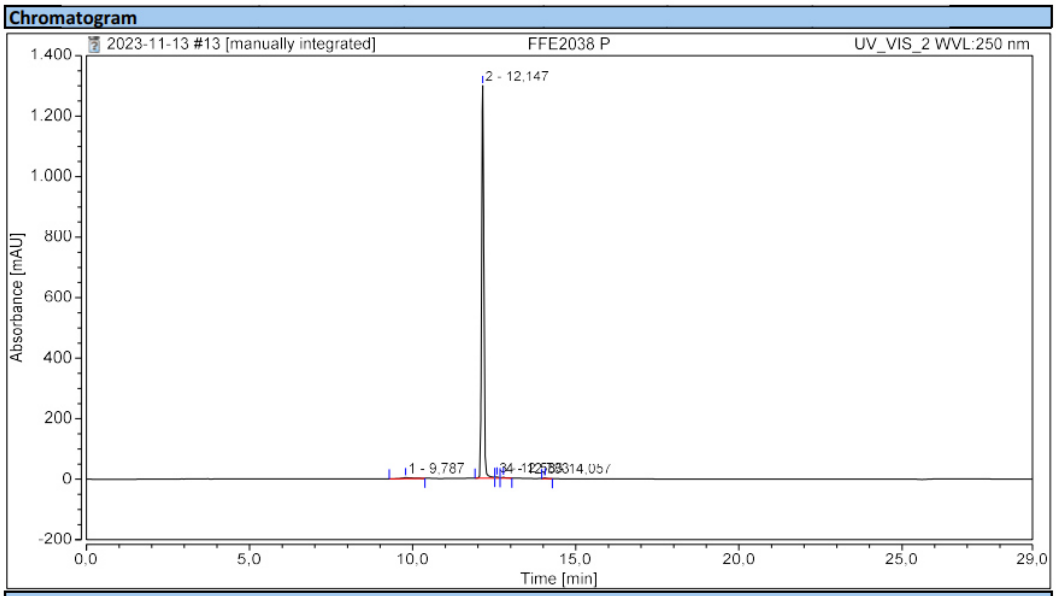

Integration Results

No.	Peak Name	Retention Time min	Area mAU*min	Height mAU	Relative Area %	Relative Height %	Amount n.a.
1		9,787	1,180	3,192	1,13	0,24	n.a.
2		12,147	102,423	1297,680	97,90	99,03	n.a.
3		12,583	0,471	4,115	0,45	0,31	n.a.
4		12,783	0,336	2,733	0,32	0,21	n.a.
5		14,057	0,214	2,701	0,20	0,21	n.a.
Total:			**104,623**	**1310,421**	**100,00**	**100,00**	

HPLC chromatogram of **1h** (gradient A, purity: 97.9%).

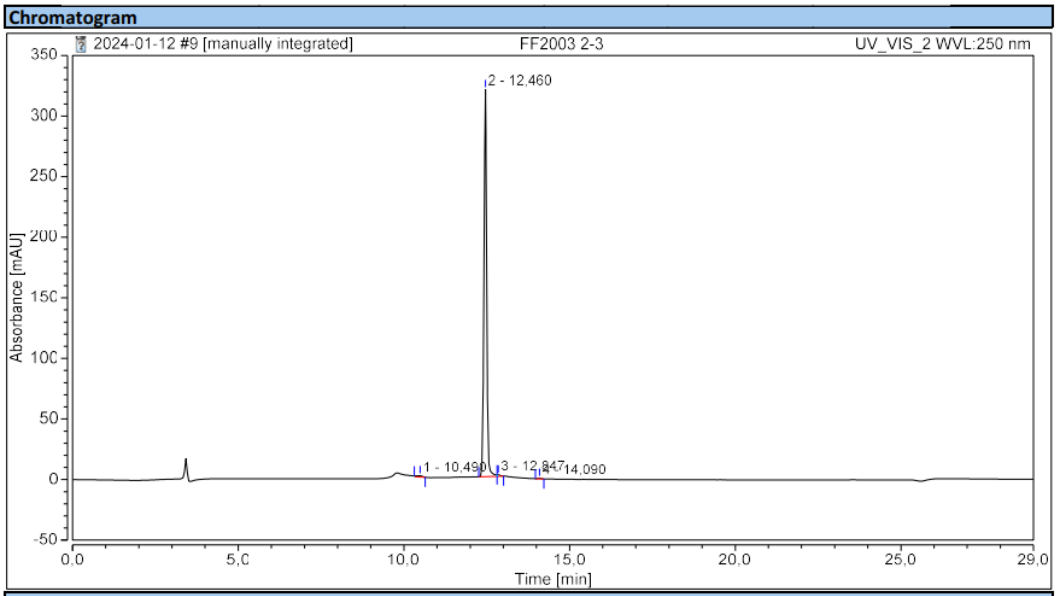

Integration Results

No.	Peak Name	Retention Time min	Area mAU*min	Height mAU	Relative Area %	Relative Height %	Amount n.a.
1		10,490	0,235	1,073	0,75	0,33	n.a.
2		12,460	31,039	319,464	98,74	99,20	n.a.
3		12,847	0,124	1,148	0,39	0,36	n.a.
4		14,090	0,037	0,365	0,12	0,11	n.a.
Total:			**31,436**	**322,050**	**100,00**	**100,00**	

HPLC chromatogram of **1i** (gradient A, purity: 98.7%).

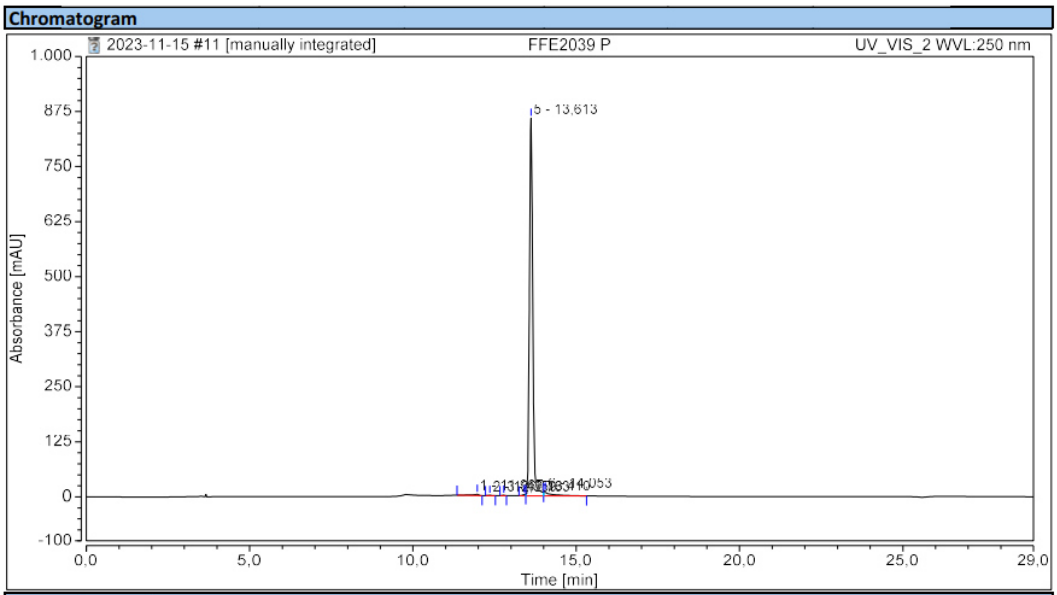

Integration Results

No.	Peak Name	Retention Time min	Area mAU*min	Height mAU	Relative Area %	Relative Height %	Amount n.a.
1		11,967	0,775	2,829	0,75	0,32	n.a.
2		12,350	0,096	0,711	0,09	0,08	n.a.
3		12,783	0,069	0,941	0,07	0,11	n.a.
4		13,410	0,272	2,680	0,26	0,31	n.a.
5		13,613	100,077	857,180	96,47	98,21	n.a.
6		14,053	2,450	8,502	2,36	0,97	n.a.
Total:			**103,738**	**872,843**	**100,00**	**100,00**	

HPLC chromatogram of **1j** (gradient A, purity: 96.5%).

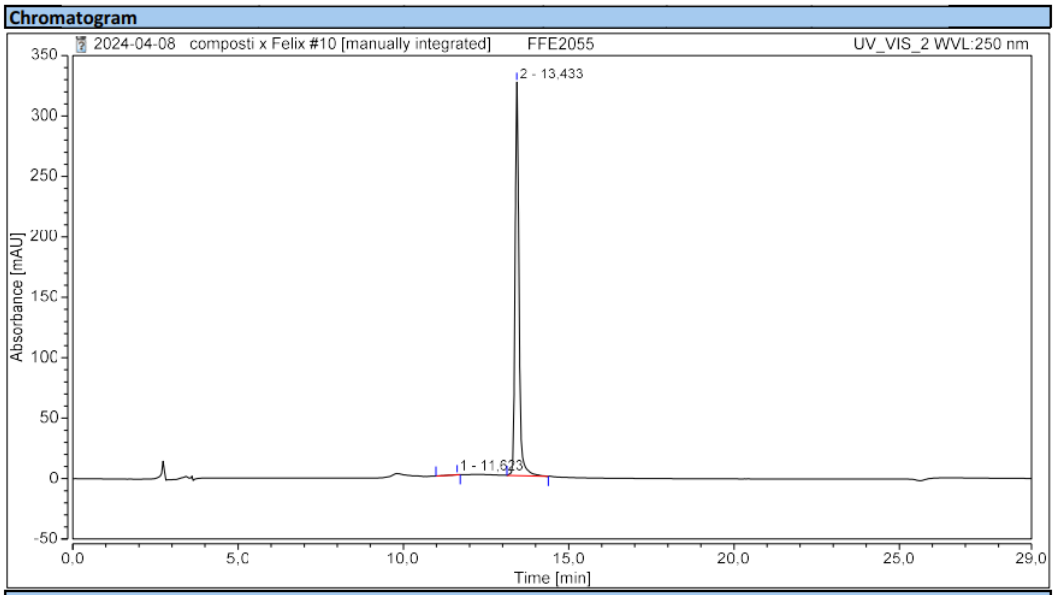

Integration Results

No.	Peak Name	Retention Time min	Area mAU*min	Height mAU	Relative Area %	Relative Height %	Amount n.a.
1		11,623	0,058	0,210	0,13	0,06	n.a.
2		13,433	44,914	325,351	99,87	99,94	n.a.
Total:			**44,972**	**325,561**	**100,00**	**100,00**	

HPLC chromatogram of **1j-nc** (gradient A, purity: 99.9%).

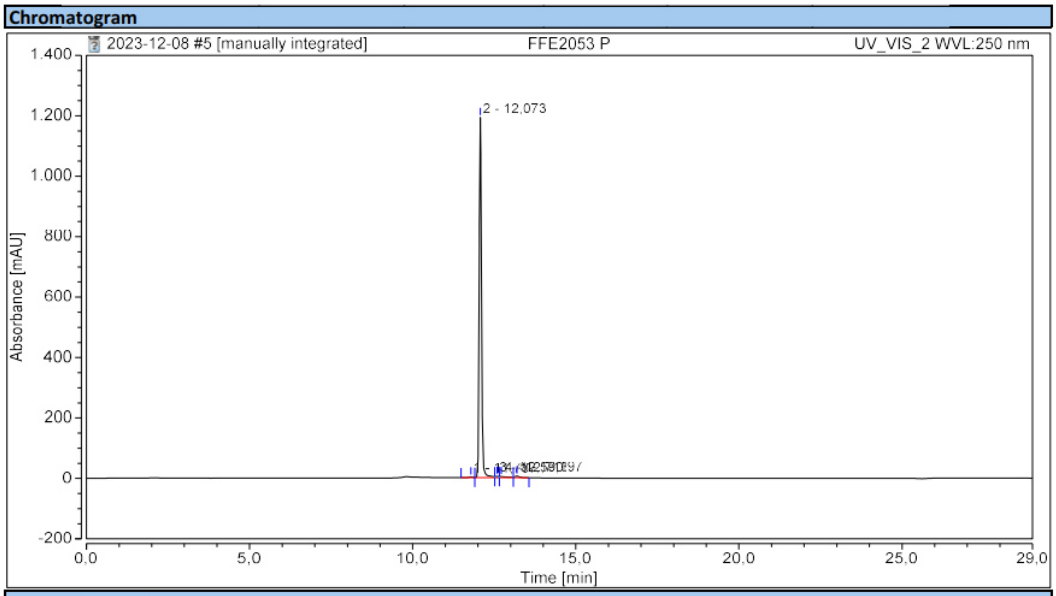

Integration Results

No.	Peak Name	Retention Time min	Area mAU*min	Height mAU	Relative Area %	Relative Height %	Amount n.a.
1		11,787	0,304	2,173	0,31	0,18	n.a.
2		12,073	95,726	1191,763	97,13	98,57	n.a.
3		12,590	0,550	4,756	0,56	0,39	n.a.
4		12,713	1,074	4,347	1,09	0,36	n.a.
5		13,197	0,896	6,060	0,91	0,50	n.a.
Total:			**98,550**	**1209,099**	**100,00**	**100,00**	

HPLC chromatogram of **2** (gradient A, purity: 97.1%).

Chromatogram

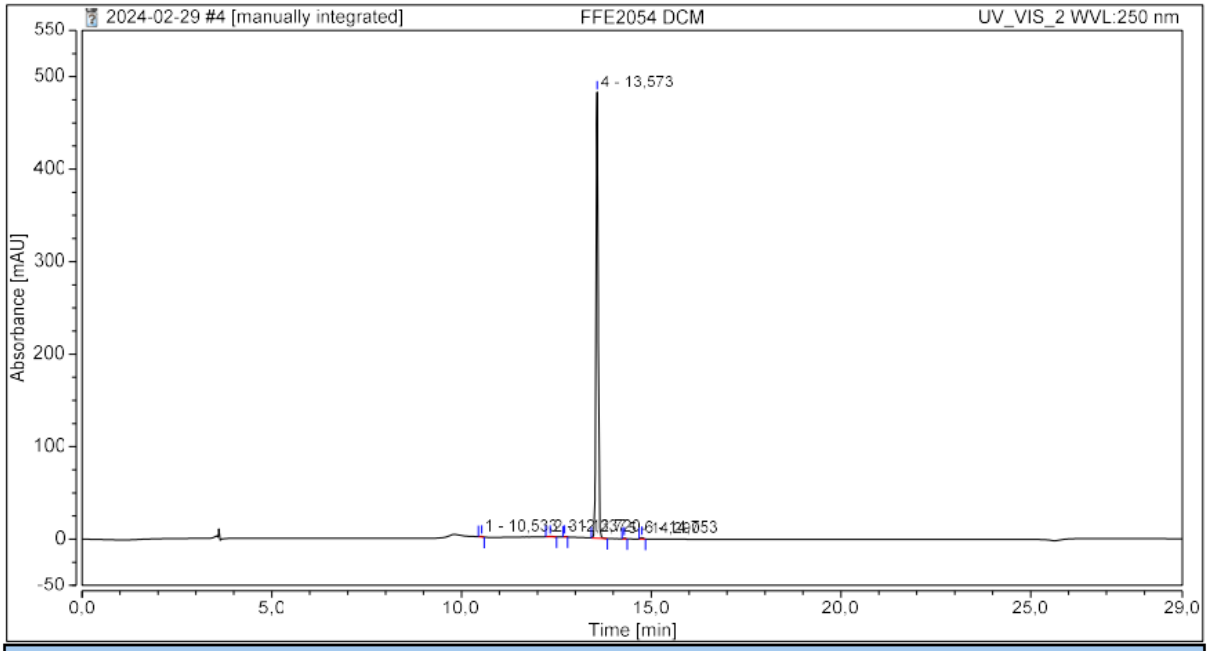

Integration Results

No.	Peak Name	Retention Time min	Area mAU*min	Height mAU	Relative Area %	Relative Height %	Amount n.a.
1		10,533	0,044	0,562	0,14	0,12	n.a.
2		12,337	0,086	0,560	0,27	0,12	n.a.
3		12,720	0,029	0,527	0,09	0,11	n.a.
4		13,573	31,576	482,366	98,96	99,17	n.a.
5		14,290	0,057	0,837	0,18	0,17	n.a.
6		14,753	0,118	1,561	0,37	0,32	n.a.
Total:			**31,909**	**486,412**	**100,00**	**100,00**	

HPLC chromatogram of **6** (gradient A, purity: 99.0%).

4. References

[1] T. Ciossek, H. Julius, H. Wieland, T. Maier, T. Beckers, *Anal. Biochem.* **2008**, *372*, 72–81.

[2] C. Bonfils, A. Kalita, M. Dubay, L. L. Siu, M. A. Carducci, G. Reid, R. E. Martell, J. M. Besterman, Z. Li, *Clin. Cancer Res.* **2008**, *14*, 3441–3449.

[3] L. Schäker-Hübner, R. Warstat, H. Ahlert, P. Mishra, F. B. Kraft, J. Schliehe-Diecks, A. Schöler, A. Borkhardt, B. Breit, S. Bhatia, M. Hügle, S. Günther, F. K. Hansen, *J. Med. Chem.* **2021**, *64*, 14620–14646.

[4] N. Reßing, J. Schliehe-Diecks, P. R. Watson, M. Sönnichsen, A. D. Cragin, A. Schöler, J. Yang, L. Schäker-Hübner, A. Borkhardt, D. W. Christianson, S. Bhatia, F. K. Hansen, *J. Med. Chem.* **2022**, *65*, 15457–15472.

[5] F. B. Kraft, M. Hanl, F. Feller, L. Schäker-Hübner, F. K. Hansen, *Pharmaceuticals* **2023**, *16*, 356.

[6] J. V Watson, S. H. Chambers, P. J. Smith, *Cytometry* **1987**, *8*, 1–8.

[7] L. Sinatra, J. J. Bandolik, M. Roatsch, M. Sönnichsen, C. T. Schoeder, A. Hamacher, A. Schöler, A. Borkhardt, J. Meiler, S. Bhatia, M. U. Kassack, F. K. Hansen, *Angew. Chemie Int. Ed.* **2020**, *59*, 22494–22499.

[8] V. Krieger, A. Hamacher, F. Cao, K. Stenzel, C. G. W. Gertzen, L. Schäker-Hübner, T. Kurz, H. Gohlke, F. J. Dekker, M. U. Kassack, F. K. Hansen, *J. Med. Chem.* **2019**, *62*, 11260–11279.

[9] F. Feller, F. K. Hansen, *ACS Med. Chem. Lett.* **2023**, *14*, 1863–1868.

7.3 Appendix III. Publication 3. Targeted Protein Degradation of Histone Deacetylases by Hydrophobically Tagged Inhibitors

The following pages include the full text and supplementary information of the article "Targeted Protein Degradation of Histone Deacetylases by Hydrophobically Tagged Inhibitors", as it was published in ACS Medicinal Chemistry Letters by the American Chemical Society.

Felix Feller and Finn K. Hansen.

Targeted Protein Degradation of Histone Deacetylases by Hydrophobically Tagged Inhibitors. *ACS Med. Chem. Lett.* **2023**, *14*, 1863–1868. https://doi.org/10.1021/acsmedchemlett.3c00468.

ACS Medicinal Chemistry Letters

pubs.acs.org/acsmedchemlett Letter

Targeted Protein Degradation of Histone Deacetylases by Hydrophobically Tagged Inhibitors

Felix Feller and Finn K. Hansen*

Cite This: ACS Med. Chem. Lett. 2023, 14, 1863−1868 Read Online

ACCESS | Metrics & More | Article Recommendations | Supporting Information

ABSTRACT: There is a growing interest in alternative strategies for targeted protein degradation. In this work, we present the development of histone deacetylase (HDAC) degraders based on hydrophobic tagging technology. To this end, a library of hydrophobically tagged HDAC inhibitors was synthesized via efficient solid-phase protocols utilizing pre-loaded resins. The subsequent biological evaluation led to the identification of our best degrader, **1a**, which significantly decreased HDAC1 levels in MM.1S multiple myeloma cells.

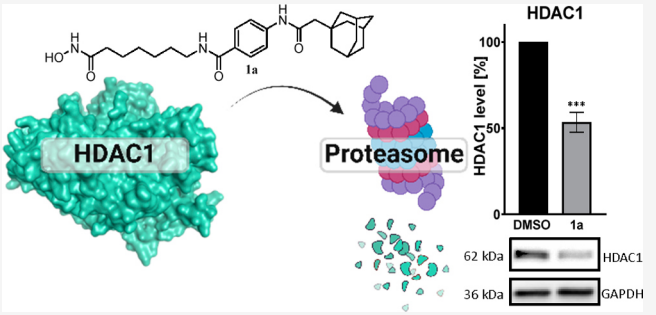

KEYWORDS: *Hydrophobic tagging, targeted protein degradation, histone deacetylase, solid-phase synthesis*

Histone deacetylases (HDACs) are intriguing targets for tumor therapy due to their high expression in many tumor entities. In hematological malignancies like multiple myeloma, HDAC overexpression is associated with bad prognosis.[1] Knockdown of HDAC1 results in inhibition of cell proliferation and cell cycle arrest and induces apoptosis.[2,3] Furthermore, the inhibition of HDAC activity leads to cell differentiation, decreased migration, and reduced angiogenesis of cancer cells as well as sensitizes tumors to chemotherapy.[4,5]

Recent research has demonstrated numerous advantages associated with targeted protein degradation (TPD) of the protein of interest (POI) over the conventional approach of inhibiting the POI: a catalytic mode of action, prolonged pharmacological effects, overcoming of target upregulation, and enhanced specificity.[6] A commonly used example of TPD is proteolysis-targeting chimeras (PROTACs). These bifunctional molecules recruit the POI and an E3 ligase for polyubiquitination and degradation of the POI via the ubiquitin−proteasome system (UPS). Currently, only a few E3 ligases are addressed by PROTACs, and the ligands for those have narrow structure−activity relationships. In addition, thalidomide derivatives, which are the most common E3 ligase recruiters, are associated with possible toxicity and teratogenicity issues.[7] Furthermore, the susceptibility of PROTACs to the development of resistance in tumors is a significant concern, primarily due to their heavy reliance on multiple associated proteins required for degradation. Additionally, these compounds are restricted by the known limitations of the so-called hook effect.[8,9]

Hydrophobic tagging represents an emerging alternative for PROTACs. It takes advantage of the cellular unfolded protein response. Partly unfolded proteins show hydrophobic areas on the surface. This can be recognized by chaperones that stabilize and refold these proteins. The hydrophobic areas of unfolded proteins can be mimicked by hydrophobic tags (HyT's). In the case of hydrophobic tagging, refolding fails and degradation occurs.[10] Another proposed mechanism of hydrophobic tagging suggests that the binding of a hydrophobically tagged ligand results in the destabilization of the target protein, subsequently facilitating its degradation by the proteasome.[11] In this scenario, a target protein with greater stability would be less vulnerable to hydrophobic tagging.[11] In general, our understanding of the degradation mechanism involving HyT's is still in its early stages, making it challenging to predict whether a specific POI can be effectively degraded using the hydrophobic tagging approach.[11] The first HyT's utilized the Halo-Tag ligand to degrade transmembrane proteins as well as the tumor target Hras1^{G12V}.[12] In the past years, the hydrophobic tagging method was successfully employed with many proteins, including the androgen receptor,[13] E3 ligases cereblon[14] and MDM2,[15] Plk1,[16] and PARP.[17] In this work, we used hydrophobic tagging for the targeted degradation of HDACs. To this end, we prepared new HDAC inhibitors (HDACi's) through solid-phase synthesis and fused them with different HyT's. Subsequently, we assessed the anticancer

Received: October 18, 2023
Revised: November 10, 2023
Accepted: November 13, 2023
Published: November 15, 2023

https://doi.org/10.1021/acsmedchemlett.3c00468
ACS Med. Chem. Lett. 2023, 14, 1863−1868

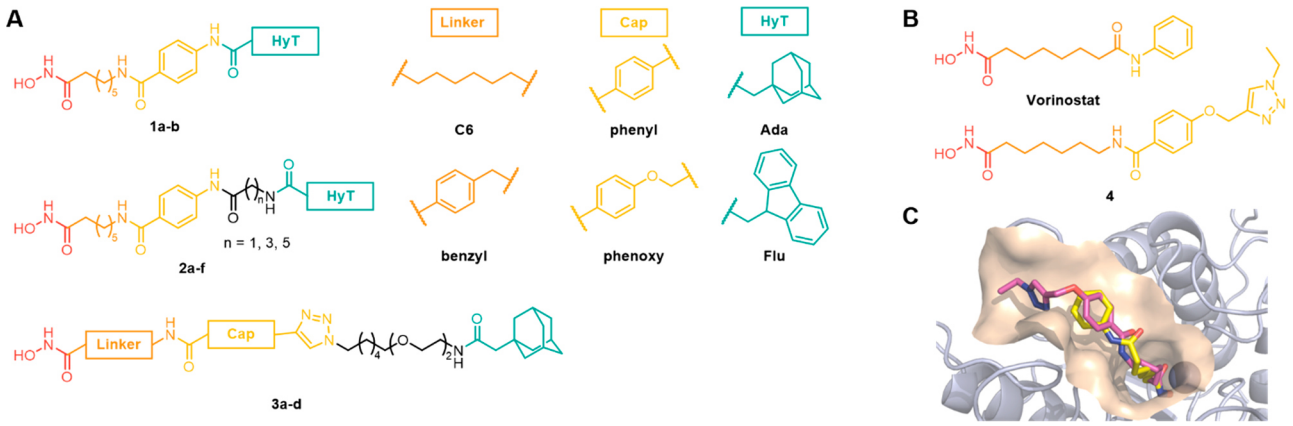

Figure 1. (A) Hydrophobically tagged HDACi's with zinc binding group (red), HDACi linker (orange), HDACi cap (yellow), optional spacer (black), and HyT (cyan). (B) Chemical structures of vorinostat and ligand−triazole conjugate **4** with zinc binding group (red), HDACi linker (orange), and HDACi cap (yellow). (C) Overlay of the crystal structure of vorinostat and the docking pose of ligand−triazole conjugate **4** in HDAC2 (PDB: 4LXZ).[19] The catalytic Zn^{2+}-ion is shown as a gray sphere.

efficacy, target engagement, and degradation ability of these compounds.

To investigate whether HDACs can be degraded by the hydrophobic tagging approach, we designed two series of hydrophobically tagged HDACi's (Figure 1). In the first set of compounds, we utilized a vorinostat-like HDAC ligand based on a hydroxamic acid as a zinc-binding group (ZBG), an alkyl linker, and a phenyl-based cap (Figure 1A). Due to the incomplete understanding of the recognition and degradation mechanisms of hydrophobic tagging, we incorporated various HyT combinations with or without spacers into the HDACi scaffold. Building upon our prior research on selective HDAC6 PROTACs, we postulated that the spacer and HyT could be introduced into the *para*-position of the phenyl cap using an amide group as the connecting unit.[18]

In the second subset of compounds, we introduced additional modifications to the HDACi linker and cap group to assess the influence of different HDACi scaffolds. These modifications were designed based on the established HyT concept reported by Crews and co-workers,[12] and we planned to introduce the HyT−spacer conjugate by a Huisgen 1,3-cycloaddition. To verify that a triazole can serve as a suitable connecting unit between the HDACi and the HyT, we conducted docking studies (see Supporting Information for details) utilizing the crystal structure of HDAC2 in complex with vorinostat (SAHA; PDB 4LXZ).[19] Our docking studies with the ligand−triazole conjugate **4** (Figure 1B) indicated a similar binding mode of **4** compared to the native ligand vorinostat and that the ethyl-substituted triazole is sufficiently solvent-exposed to serve as an exit vector to install the HyT (Figure 1C).

The solid-phase synthesis of the designed target compounds is summarized in Schemes 1 and 2. In detail, the preparation of the HyT degraders was performed on a 2-chlorotrityl chloride (2-CTC) resin, as established by Sinatra et al.,[18,20] to take advantage of this fast and modular approach. In the first step, all building blocks containing an amine were Fmoc-protected (not shown) before being used for solid-phase synthesis. Next, the 2-CTC resin was reacted with *N*-hydroxyphthalimide to immobilize hydroxylamine as a precursor for the hydroxamic acid (Scheme 1). Subsequently, the phthaloyl group was deprotected via the treatment with hydrazine monohydrate followed by the attachment of the respective Fmoc-protected

Scheme 1. Synthesis of a Hydrophobically Tagged HDACi via Amide Coupling Reactions[a]

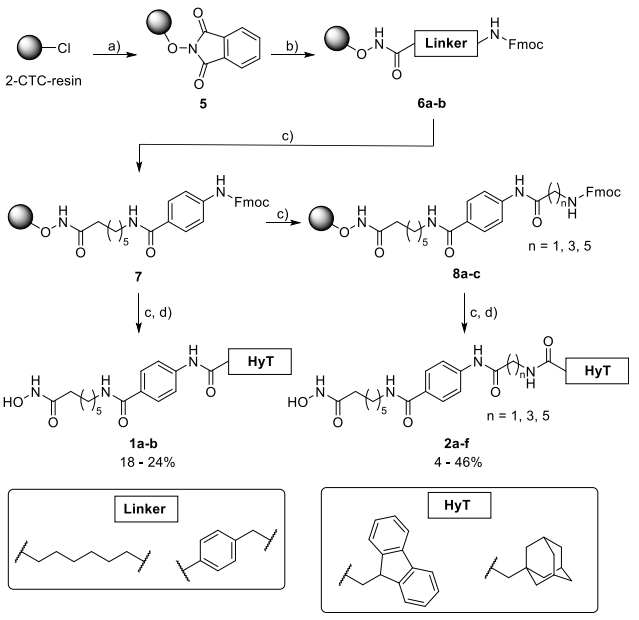

[a]Reaction conditions: (a) PhthN-OH, Et_3N, DMF, rt, 48 h; (b) 1) 5% hydrazine monohydrate, MeOH, rt, 2 × 15 min, 2) Fmoc-Linker-COOH, HATU, HOBt·H_2O, DIPEA, DMF, rt, 20 h, loading determined: 0.42−0.69 mmol/g; (c) 1) 20% piperidine, DMF, rt, 2 × 5 min, 2) Fmoc-4-aminobenzoic acid or Fmoc-Spacer-COOH or HyT-COOH, HATU, HOBt·H_2O, EDC, DIPEA, DMF, rt, 20 h; (d) 5% TFA, CH_2Cl_2, rt, 1 h.

linker through an amide coupling reaction, thereby resulting in the pre-loaded resins **6a,b**. For the first series of compounds, only **6a** was employed as the HDACi linker. The target compounds were subsequently synthesized through iterative cycles of Fmoc deprotection and amide coupling of the HDACi cap, spacer, and HyT part of the molecule. After cleavage from the resin by the treatment with TFA, this route enabled the synthesis of the adamantyl (**1a**, **2a−c**) and fluorenyl (**1b**, **2d−f**) tagged HDACi's with direct attachment of the HyT (**1a,b**) or alkyl spacers of different chain length (**2a−f**).

https://doi.org/10.1021/acsmedchemlett.3c00468
ACS Med. Chem. Lett. 2023, 14, 1863−1868

Scheme 2. Synthesis of Triazole-Connected, Hydrophobically Tagged HDACi's[a]

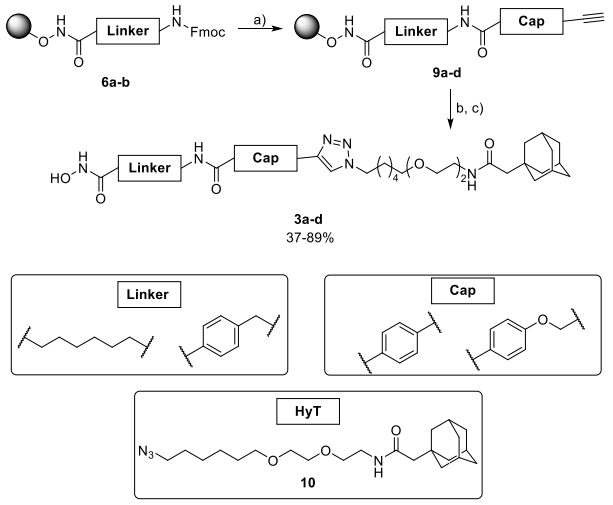

[a]Reaction conditions: (a) 1) 20% piperidine, DMF, rt, 2 × 5 min, 2) Cap-COOH, HATU, HOBt·H_2O, EDC, DIPEA, DMF, rt, 20 h; (b) HyT (**10**), TBTA, $CuSO_4 \cdot 5H_2O$, ascorbic acid, *t*-BuOH, DMF, rt, 18 h; (c) 5% TFA, CH_2Cl_2, rt, 1 h.

For the second series of compounds, **6a**,**b** were utilized as HDACi linkers, and two distinct alkyne-bearing cap groups were installed through amide couplings (Scheme 2). Subsequently, the HyT **10** (see Scheme 2, bottom), which was synthesized following known literature procedures,[16] was introduced to the resin-bound intermediates **9a**−**d** by means of a Cu(I)-catalyzed Huisgen cycloaddition. Finally, the cleavage from the resin yielded the target compounds **3a**−**d**. Before the biological evaluation, all compounds were further purified by preparative RP-HPLC to >95% purity, yielding the final hydrophobically tagged HDACi's in total yields of 4−89%.

To access the biological properties of the synthesized inhibitors, all compounds were first screened for their antiproliferative activity against the multiple myeloma cell line MM.1S. Based on the data summarized in Table 1, compounds **1a**, **2a**, **2d**, and **3a** emerged as the most promising compounds. Consequently, these four compounds were selected for a detailed biological evaluation. The cellular HDAC inhibitory activity was assessed by a whole-cell HDAC assay followed by biochemical HDAC1, 2, and 6 enzyme inhibition assays (Table 1). HDAC1, 2, and 6 were selected as they are the most relevant isoforms in the context of cancer.[21] Compound **2d**, bearing the fluorenyl HyT, showed similar inhibition of cellular HDAC activity as well as comparable IC_{50} values against HDAC1 and 2 compared to vorinostat. Intriguingly, the hydrophobically tagged HDACi's **1a**, **2a**, **2d**, and **3a** (HDAC6 IC_{50} range: 5.2−17.7 nM) outperformed vorinostat (HDAC6 IC_{50}: 36.5 nM) in regard to HDAC6 inhibitory activity.

To investigate the HDAC degradation capability of the hydrophobically tagged HDACi's, the MM.1S cell line was treated with 20 μM samples of the selected compounds for 24 h. Subsequently, the protein levels of the different HDAC isoforms were analyzed by immunoblotting. These experiments confirmed significant HDAC1 degradation by compounds **1a**, **2a**, **2d**, and **3a** (Figure 2A). A slight reduction of HDAC2 can also be observed for **1a** and **2a**. Interestingly, despite all compounds being highly potent HDAC6 inhibitors, HDAC6 levels are unaffected by our hydrophobically tagged inhibitors. Hence, the cellular target engagement was examined by determining the acetylation levels of HDAC target proteins. Hyperacetylation of histone H3 indicates HDAC1−3 inhibition, while HDAC6 inhibition results in a hyperacetylation of α-tubulin. In the case of all compounds under study, immunoblot analysis demonstrated pronounced hyperacetylation of α-tubulin, thereby confirming intracellular HDAC6 target engagement (Figure 2B). Since compounds **1a**, **2a**, **2d**, and **3a** engage but do not degrade HDAC6, it is plausible to speculate that the HyT is not recognized in the relatively wide CD2 pocket of HDAC6.[22] To investigate whether our hydrophobically tagged HDACi's can degrade class IIb HDACs, we chose HDAC4 as a representative isoform and screened compounds **1a**, **2a**, **2d**, and **3a** for their ability to inhibit and degrade HDAC4. All compounds showed low inhibitory activity against HDAC4 and no significant

Table 1. Antiproliferative Activities and HDAC Inhibition of Hydrophobically Tagged HDACi's

Compound	Linker	Cap Group	Spacer	HyT	IC_{50} [μM] cell viability MM.1S[a]	IC_{50} [μM] HDAC cell MM.1S [b]	IC_{50} [nM] HDAC1 [c]	IC_{50} [nM] HDAC2 [c]	IC_{50} [nM] HDAC6 [c]
1a	C6	phenyl	-	Ada	3.97 ± 0.70	1.12± 0.12	192.3 ± 11.0	295.0 ± 49.4	5.2 ± 0.4
1b	C6	phenyl	-	Flu	n.e.	n.d.	n.d.	n.d.	n.d.
2a	C6	phenyl	C1	Ada	7.23 ± 3.48	0.58 ± 0.07	132.6 ± 5.8	245.6 ± 5.2	5.9 ± 1.5
2b	C6	phenyl	C3	Ada	23.76 ± 3.61	n.d.	n.d.	n.d.	n.d.
2c	C6	phenyl	C5	Ada	22.77 ± 4.96	n.d.	n.d.	n.d.	n.d.
2d	C6	phenyl	C1	Flu	11.55 ± 4.55	0.54 ± 0.05	86.4 ± 10.9	157.2 ± 14.2	3.3 ± 0.6
2e	C6	phenyl	C3	Flu	68.07 ± 8.49	n.d.	n.d.	n.d.	n.d.
2f	C6	phenyl	C5	Flu	n.e.	n.d.	n.d.	n.d.	n.d.
3a	C6	phenyl			10.31 ± 0.89	1.17 ± 0.24	349.9 ± 12.2	433.8 ± 0.5	17.7 ± 3.5
3b	benzyl	phenyl			n.e.	n.d.	n.d.	n.d.	n.d.
3c	C6	phenoxy			43.81 ± 11.05	n.d.	n.d.	n.d.	n.d.
3d	benzyl	phenoxy			n.e.	n.d.	n.d.	n.d.	n.d.
vorinostat	-	-	-	-	0.73 ± 0.24	0.40 ± 0.05	102.8 ± 15.7	147.2 ± 5.5	36.5 ± 3.8

[a]At least three independent experiments, each in triplicate. [b]At least three independent experiments, each in duplicate. [c]At least two independent experiments, each in duplicate. In all cases, mean ± standard deviation is shown; n.e. = no effect up to 100 μM, n.d. = not determined.

https://doi.org/10.1021/acsmedchemlett.3c00468
ACS Med. Chem. Lett. 2023, 14, 1863−1868

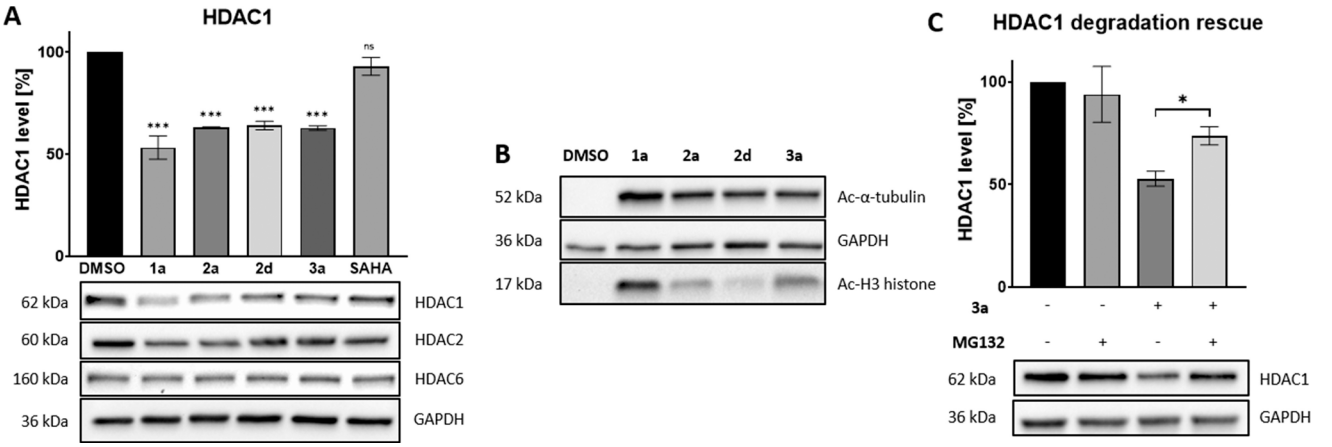

Figure 2. Immunoblot analysis of MM.1S cell lysates. (A) Degradation level of HDAC1: MM.1S lysates after 24 h of treatment with 20 μM of the respective hydrophobically tagged HDACi, vehicle (DMSO), or vorinostat (10 μM). (B) Protein levels of acetyl-α-tubulin and acetyl-histone H3: MM.1S lysates after 24 h of treatment with 20 μM of the respective compound or vehicle (DMSO). (C) Rescue experiment: MM.1S lysates after 0.5 h of pre-treatment with 0.1 μM MG132 or vehicle (DMSO) followed by 24 h of treatment with **3a** (10 μM) or vehicle (DMSO). Mean ± standard deviation of $n \geq 3$ replicates is shown. Significance: ns = $p \geq 0.05$; * = $p \leq 0.05$; *** = $p \leq 0.001$.

degradation of HDAC4 in MM.1S cells (Figure S1, Supporting Information). To confirm that HDAC1 degradation occurs via the proteasome, a pre-treatment with the proteasome inhibitor MG132 was performed. **3a** was selected as a representative compound. The pre-treatment resulted in a partial but significant rescue of HDAC1 degradation, thus confirming that the proteasomal system is involved in the degradation of HDAC1 (Figure 2C).

We further investigated whether our hydrophobically tagged inhibitors are capable of inducing apoptosis. After incubation of MM.1S cells with **1a**, **2a**, **2d**, **3a**, and vorinostat as positive control, apoptosis induction was examined by annexin V-FITC/propidium iodide (PI) staining followed by flow cytometry analysis (Figure 3). As expected, all compounds

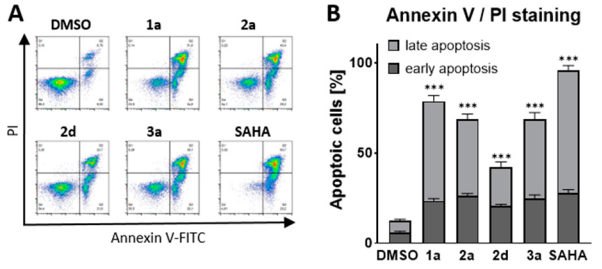

Figure 3. (A) Flow cytometry analysis of MM.1S cells stained by annexin V-FITC/PI after incubation with 20 μM of the indicated compound, vorinostat, or vehicle (DMSO) for 48 h; representative images are shown. (B) Quantification of early and late apoptotic cells. The percentage of cells that were annexin V positive but PI negative were considered as early apoptotic, and the percentage of cells that were both annexin V and PI positive were considered as late apoptotic. Representative blots are depicted. For normalization: Mean ± standard deviation of $n \geq 3$ replicates is shown. Significance: *** = $p \leq 0.001$.

significantly increased the amount of early and late apoptotic cells. The observed potency sequence of inducing apoptosis agreed with the results obtained from the cell viability assays (Table 1). Finally, we could validate these findings by assessing the activity of caspase 3/7 (Figure S2, Supporting Information).

In summary, we have designed and synthesized the first hydrophobically tagged HDACi's capable of degrading HDAC1. The hydrophobically tagged inhibitors displayed significant degradation of HDAC1, with a D_{max} of up to 47% in MM.1S cells. Intriguingly, degradation of HDAC6 was not observable, although all selected compounds demonstrated comparable hyperacetylation of α-tubulin and showed even stronger inhibition of HDAC6 than vorinostat. It is a well-known phenomenon in the field of PROTACs that degraders utilizing a promiscuous POI warhead can achieve selective degradation, thereby indicating that successful degradation requires more than target engagement.[23] One plausible explanation for the enhanced selectivity seen in PROTACs as compared to inhibitors involves the need for a productive ternary complex that is dependent on the linker and the recruited E3 ligase. Although this effect has been predominantly observed in the case of kinase PROTACs, recent reports disclosed selective HDAC6 degraders based on the unselective HDACi's vorinostat and crebinostat.[18,24] Similarly, selective HDAC3 degradation was accomplished through the application of a propyl hydrazide warhead with the ability to inhibit HDAC1−3.[25] While the precise degradation pathway of hydrophobic tagging remains not fully elucidated, it is reasonable to speculate that, due to distinct structural variations in the binding sites and differences in the protein stability, a HyT might effectively mimic an unfolded protein upon engaging HDAC1, but not in the case of HDAC6. Possible ways to achieve HDAC6 degradation via the hydrophobic tagging approach could include the use of selective HDAC6 ZBGs with tight-binding properties and long residence times, such as 2-(difluoromethyl)-1,3,4-oxadiazoles (DFMOs) in combination with the optimization of both the linker and the HyT.[26,27]

Taken together, in this proof-of-concept study, we demonstrated for the first time that the hydrophobic tagging approach is suitable for the targeted degradation of HDAC1. Further optimization studies of the prototypical compounds reported in this work are underway.

https://doi.org/10.1021/acsmedchemlett.3c00468
ACS Med. Chem. Lett. 2023, 14, 1863−1868

■ ASSOCIATED CONTENT

Supporting Information

The Supporting Information is available free of charge at https://pubs.acs.org/doi/10.1021/acsmedchemlett.3c00468.

Supplementary figures, docking protocols, experimental procedures, ^{1}H NMR, ^{13}C NMR, and HPLC data (PDF)

■ AUTHOR INFORMATION

Corresponding Author

Finn K. Hansen − *Department of Pharmaceutical and Cell Biological Chemistry, Pharmaceutical Institute, University of Bonn, 53121 Bonn, Germany;* orcid.org/0000-0001-9765-5975; Email: finn.hansen@uni-bonn.de

Author

Felix Feller − *Department of Pharmaceutical and Cell Biological Chemistry, Pharmaceutical Institute, University of Bonn, 53121 Bonn, Germany;* orcid.org/0009-0007-1820-772X

Complete contact information is available at: https://pubs.acs.org/10.1021/acsmedchemlett.3c00468

Notes

The authors declare no competing financial interest.

■ ACKNOWLEDGMENTS

Immunoblot support by Svenja Henze is gratefully acknowledged. The TOC entry was partially created with Biorender.com.

■ ABBREVIATIONS

2-CTC resin, 2-chlorotrityl chloride resin; Ada, adamantyl; CD2, catalytic domain 2; D_{max}, maximal degradation; DMSO, dimethyl sulfoxide; FITC, fluorescein isothiocyanate; Flu, fluorenyl; HDAC, histone deacetylase; HDACi, histone deacetylase inhibitor; Hras1, GTPase HRas1; HyT, hydrophobic tag; IC_{50}, half-maximal inhibitory concentration; MDM2, mouse double minute 2 homolog; MS, mass spectrometry; NMR, nuclear magnetic resonance; PARP, poly ADP ribose polymerase; PDB, Protein Data Bank; Plk1, polo-like kinase 1; PI, propidium iodide; POI, protein of interest; RP-HPLC, reverse-phase high-performance liquid chromatography; PROTAC, proteolysis-targeting chimera; SAHA, suberoylanilide hydroxamic acid, or vorinostat; TFA, trifluoroacetic acid; TPD, targeted protein degradation; UPS, ubiquitin−proteasome system

■ REFERENCES

(1) Milazzo, G.; Mercatelli, D.; Di Muzio, G.; Triboli, L.; De Rosa, P.; Perini, G.; Giorgi, F. M. Histone Deacetylases (HDACs): Evolution, Specificity, Role in Transcriptional Complexes, and Pharmacological Actionability. *Genes* **2020**, *11*, 556.

(2) Glaser, K. B.; Li, J.; Staver, M. J.; Wei, R.-Q.; Albert, D. H.; Davidsen, S. K. Role of Class I and Class II histone deacetylases in carcinoma cells using siRNA. *Biochem. Biophys. Res. Commun.* **2003**, *310*, 529−536.

(3) Senese, S.; Zaragoza, K.; Minardi, S.; Muradore, I.; Ronzoni, S.; Passafaro, A.; Bernard, L.; Draetta, G. F.; Alcalay, M.; Seiser, C.; Chiocca, S. Role for Histone Deacetylase 1 in Human Tumor Cell Proliferation. *Mol. Cell. Biol.* **2007**, *27*, 4784−4795.

(4) Witt, O.; Deubzer, H. E.; Milde, T.; Oehme, I. HDAC family: What are the cancer relevant targets? *Cancer Lett.* **2009**, *277*, 8−21.

(5) Krieger, V.; Hamacher, A.; Cao, F.; Stenzel, K.; Gertzen, C. G. W.; Schäker-Hübner, L.; Kurz, T.; Gohlke, H.; Dekker, F. J.; Kassack, M. U.; Hansen, F. K. Synthesis of Peptoid-Based Class I-Selective Histone Deacetylase Inhibitors with Chemosensitizing Properties. *J. Med. Chem.* **2019**, *62*, 11260−11279.

(6) Neklesa, T. K.; Winkler, J. D.; Crews, C. M. Targeted protein degradation by PROTACs. *Pharmacol. Ther.* **2017**, *174*, 138−144.

(7) Hughes, S. J.; Testa, A.; Thompson, N.; Churcher, I. The rise and rise of protein degradation: Opportunities and challenges ahead. *Drug Discovery Today* **2021**, *26*, 2889−2897.

(8) Ottis, P.; Palladino, C.; Thienger, P.; Britschgi, A.; Heichinger, C.; Berrera, M.; Julien-Laferriere, A.; Roudnicky, F.; Kam-Thong, T.; Bischoff, J. R.; Martoglio, B.; Pettazzoni, P. Cellular Resistance Mechanisms to Targeted Protein Degradation Converge Toward Impairment of the Engaged Ubiquitin Transfer Pathway. *ACS Chem. Biol.* **2019**, *14*, 2215−2223.

(9) Douglass, E. F.; Miller, C. J.; Sparer, G.; Shapiro, H.; Spiegel, D. A. A Comprehensive Mathematical Model for Three-Body Binding Equilibria. *J. Am. Chem. Soc.* **2013**, *135*, 6092−6099.

(10) Neklesa, T. K.; Crews, C. M. Greasy tags for protein removal. *Nature* **2012**, *487*, 308−309.

(11) Xie, S.; Zhu, J.; Li, J.; Zhan, F.; Yao, H.; Xu, J.; Xu, S. Small-Molecule Hydrophobic Tagging: A Promising Strategy of Druglike Technology for Targeted Protein Degradation. *J. Med. Chem.* **2023**, *66*, 10917−10933.

(12) Neklesa, T. K.; Tae, H. S.; Schneekloth, A. R.; Stulberg, M. J.; Corson, T. W.; Sundberg, T. B.; Raina, K.; Holley, S. A.; Crews, C. M. Small-molecule hydrophobic tagging−induced degradation of HaloTag fusion proteins. *Nat. Chem. Biol.* **2011**, *7*, 538−543.

(13) Gustafson, J. L.; Neklesa, T. K.; Cox, C. S.; Roth, A. G.; Buckley, D. L.; Tae, H. S.; Sundberg, T. B.; Stagg, D. B.; Hines, J.; McDonnell, D. P.; Norris, J. D.; Crews, C. M. Small-Molecule-Mediated Degradation of the Androgen Receptor through Hydrophobic Tagging. *Angew. Chem., Int. Ed.* **2015**, *54*, 9659−9662.

(14) Steinebach, C.; Sosič, I.; Lindner, S.; Bricelj, A.; Kohl, F.; Ng, Y. L. D.; Monschke, M.; Wagner, K. G.; Krönke, J.; Gütschow, M. A. A MedChem toolbox for cereblon-directed PROTACs. *MedChemComm* **2019**, *10*, 1037−1041.

(15) Nietzold, F.; Rubner, S.; Berg, T. The hydrophobically-tagged MDM2-p53 interaction inhibitor Nutlin-3a-HT is more potent against tumor cells than Nutlin-3a. *Chem. Commun.* **2019**, *55*, 14351−14354.

(16) Rubner, S.; Schubert, S.; Berg, T. Poloxin-2HT+: Changing the hydrophobic tag of Poloxin-2HT increases Plk1 degradation and apoptosis induction in tumor cells. *Org. Biomol. Chem.* **2019**, *17*, 3113−3117.

(17) Go, A.; Jang, J. W.; Lee, W.; Ha, J. Du; Kim, H. J.; Nam, H. J. Augmentation of the antitumor effects of PARP inhibitors in triple-negative breast cancer via degradation by hydrophobic tagging modulation. *Eur. J. Med. Chem.* **2020**, *204*, 112635.

(18) Sinatra, L.; Yang, J.; Schliehe-Diecks, J.; Dienstbier, N.; Vogt, M.; Gebing, P.; Bachmann, L. M.; Sönnichsen, M.; Lenz, T.; Stühler, K.; Schöler, A.; Borkhardt, A.; Bhatia, S.; Hansen, F. K. Solid-Phase Synthesis of Cereblon-Recruiting Selective Histone Deacetylase 6 Degraders (HDAC6 PROTACs) with Antileukemic Activity. *J. Med. Chem.* **2022**, *65*, 16860−16878.

(19) Lauffer, B. E.L.; Mintzer, R.; Fong, R.; Mukund, S.; Tam, C.; Zilberleyb, I.; Flicke, B.; Ritscher, A.; Fedorowicz, G.; Vallero, R.; Ortwine, D. F.; Gunzner, J.; Modrusan, Z.; Neumann, L.; Koth, C. M.; Lupardus, P. J.; Kaminker, J. S.; Heise, C. E.; Steiner, P. Histone deacetylase (HDAC) inhibitor kinetic rate constants correlate with cellular histone acetylation but not transcription and cell viability. *J. Biol. Chem.* **2013**, *288*, 26926−26943.

(20) Sinatra, L.; Bandolik, J. J.; Roatsch, M.; Sönnichsen, M.; Schoeder, C. T.; Hamacher, A.; Schöler, A.; Borkhardt, A.; Meiler, J.; Bhatia, S.; Kassack, M. U.; Hansen, F. K. Hydroxamic Acids Immobilized on Resins (HAIRs): Synthesis of Dual-Targeting HDAC Inhibitors and HDAC Degraders (PROTACs). *Angew. Chem., Int. Ed.* **2020**, *59*, 22494−22499.

(21) Jenke, R.; Reßing, N.; Hansen, F. K.; Aigner, A.; Büch, T. Anticancer Therapy with HDAC Inhibitors: Mechanism-Based Combination Strategies and Future Perspectives. *Cancers (Basel)* **2021**, *13*, 634.
(22) Hai, Y.; Christianson, D. W. Histone deacetylase 6 structure and molecular basis of catalysis and inhibition. *Nat. Chem. Biol.* **2016**, *12*, 741−747.
(23) Bondeson, D. P.; Smith, B. E.; Burslem, G. M.; Buhimschi, A. D.; Hines, J.; Jaime-Figueroa, S.; Wang, J.; Hamman, B. D.; Ishchenko, A.; Crews, C. M. Lessons in PROTAC Design from Selective Degradation with a Promiscuous Warhead. *Cell Chem. Biol.* **2018**, *25*, 78−87.
(24) Yang, K.; Song, Y.; Xie, H.; Wu, H.; Wu, Y. T.; Leisten, E. D.; Tang, W. Development of the First Small Molecule Histone Deacetylase 6 (HDAC6) Degraders. *Bioorg. Med. Chem. Lett.* **2018**, *28*, 2493−2497.
(25) Xiao, Y.; Wang, J.; Zhao, L. Y.; Chen, X.; Zheng, G.; Zhang, X.; Liao, D. Discovery of Histone Deacetylase 3 (HDAC3)-Specific PROTACs. *Chem. Commun.* **2020**, *56*, 9866−9869.
(26) Keuler, T.; König, B.; Bückreiß, N.; Kraft, F. B.; König, P.; Schäker-Hübner, L.; Steinebach, C.; Bendas, G.; Gütschow, M.; Hansen, F. K. Development of the First Non-Hydroxamate Selective HDAC6 Degraders. *Chem. Commun.* **2022**, *58*, 11087−11090.
(27) König, B.; Watson, P. R.; Reßing, N.; Cragin, A. D.; Schäker-Hübner, L.; Christianson, D. W.; Hansen, F. K. Difluoromethyl-1,3,4-Oxadiazoles Are Selective, Mechanism-Based, and Essentially Irreversible Inhibitors of Histone Deacetylase 6. *J. Med. Chem.* **2023**, *66*, 13821−13837.

https://doi.org/10.1021/acsmedchemlett.3c00468
ACS Med. Chem. Lett. 2023, 14, 1863−1868

Supplementary Information

Targeted Protein Degradation of Histone Deacetylases by Hydrophobically Tagged Inhibitors

Felix Feller[a] and Finn K. Hansen[a, *]

[a] Department of Pharmaceutical and Cell Biological Chemistry, Pharmaceutical Institute, University of Bonn, An der Immenburg 4, 53121 Bonn, Germany.

[*] Correspondence to: finn.hansen@uni-bonn.de

Table of contents

1. Supplementary Figures

Compound	HDAC4 inhibition at 10 µM [%]
1a	71 ± 11
2a	34 ± 24
2d	22 ± 10
3a	58 ± 14

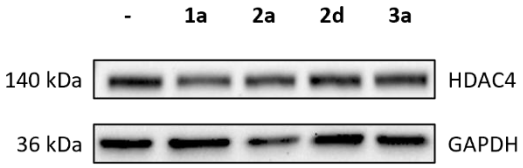

Figure S1. Evaluation of the HDAC4 inhibition and degradation by **1a**, **2a**, **2d**, and **3a**. (A) HDAC4 inhibition at 10 µM of the selected hydrophobically tagged HDACi. Mean ± standard deviation is shown. Data from two independent experiments, each performed in duplicates. (B) Immunoblot analysis of HDAC4 levels in MM.1S cells after 24 h of treatment with 20 µM of the respective hydrophobically tagged HDACi or vehicle (DMSO). Representative images of n = 4 replicates.

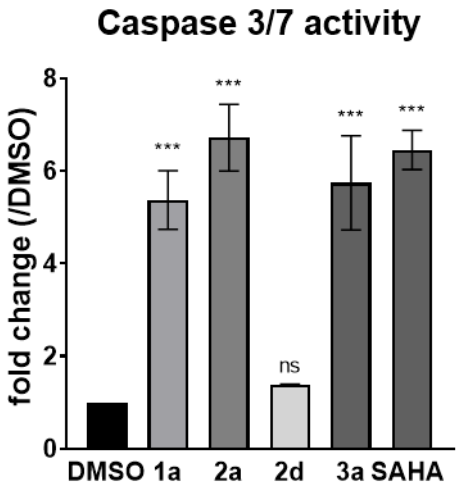

Figure S2. Caspase 3/7 activity analysis of MM.1S cells after incubation with compounds **1a**, **2a**, **2d**, and **3a**, vorinostat (SAHA) (20 µM) or vehicle (DMSO) for 48 h. Mean ± standard deviation is shown. Data from three independent experiments in duplicates.

2. Molecular Docking

The structures of the ligands were prepared using the software ChemDraw 19.1 (PerkinElmer Inc., Waltham, MA, USA), minimized in ChemDraw 3D pro version using the MM2 force field, and used as input for AutoDock tools version 1.5.6. The crystal structure of HDAC2 (PDB: 4LXZ)[1] was downloaded from the Protein Data Base. The native ligand vorinostat, buffer, non-interacting ions, and all waters molecules, except water 606, were removed. AutodockTools-1.5.6 program[2] was used to add all hydrogen atoms, modify histidine protonation (H145 and H146, adding only HD1)[3], compute gasteiger charges, and merge all non-polar hydrogens. After the generation of the pdbqt output file, the charge of the zinc atom was manually changed to +2.

Autogrid 4.2.6[2] was utilized to generate the grid files using a grid box with the following settings: spacing of 0.375 Å, grid box size of 50 × 50 × 50 centered around the coordinates of the native ligand vorinostat. Autodock 4.2.6[2] was used to perform the docking calculations. The generated pdbqt file of the enzyme was set as a rigid macromolecule. The genetic algorithm search parameters were set to 100 GA runs for each ligand with a population size of 150, a maximum number of 2.5×10^6 energy evaluations, a maximum number of 2.7×10^4 generations, a mutation rate of 0.02, and a crossover rate of 0.8. The lowest-energy conformer of the first cluster showing Zn^{2+} binding was used as the representative predicted binding pose.

3. Biological Experiments

No unexpected or unusually high safety hazards were encountered.

3.1. Cell Culture

The human multiple myeloma cell line MM.1S (CRL-2974) was obtained from ATCC (Manassas, VA, USA). MM.1S cells were cultivated in RPMI 1640 medium (PAN Biotech GmbH; Aidenbach, Germany) supplemented with 10% FBS (PAN Biotech GmbH; Aidenbach, Germany), 100 IU/mL penicillin, 0.1 mg/mL streptomycin (PAN Biotech GmbH; Aidenbach, Germany) and 1 mM sodium pyruvate (ThermoFisher Scientific Inc.; Waltham, MA, USA) at 37 °C in a 5% CO_2 atmosphere. The semi-adherent cells were detached mechanically by using a cell scraper.

3.2. Cell Viability Assay

MM.1S cells were seeded (10×10^3 cells/well) in 90 µL in F-bottom 96-well plates (Starlab GmbH, Hamburg, Germany) and grown over night at 37 °C in a 5% CO_2 atmosphere. The treatment was performed by the addition of 10 µL containing the 10 × concentrate of the indicated concentration, DMSO or PBS. After 72 h of incubation at cell culture conditions, 20 µL/well of 2-(4,5-dimethylthiazol-2-yl)-3,5-diphenyl-2*H*-tetrazol-3-ium bromide (5 mg/mL in PBS) was added and developed for 1 h under cell culture conditions. Before the addition of 200 µL/well DMSO, the plates were centrifuged at 1000 × g for 5 min at 4 °C and the medium was carefully aspirated. Absorbance was determined at 570 nm with background subtraction at 690 nm by a microplate photometer (Thermo Scientific Multiskan EX, Thermo Fisher Sceintific). The half-maximal inhibitory concentration (IC_{50}) was determined by plotting dose response curves and nonlinear regression with GraphPad Prism (GraphPad Software, San Diego, CA, USA).

3.3. HDAC Cell Inhibition Assay

The HDAC whole cell assay is based on the assay established by Ciossek et al.[4] and Bonfils et al.[5] with minor changes. Multiple myeloma cells MM.1S were seeded in a concentration of 75×10^3 cells/well (total volume of 189 µL) in 96-well cell culture microplates (Catalog# 655086, Greiner Bio-One) and cultured for 24 h. The DMSO stock solutions were used to perform a serial dilution in DMSO. Next, the cells were treated with 1 µL of the serial dilution (190 × concentrate) for 18 h. For visualization of HDAC activity 10 µL of substrate solution, containing 3 mM Boc-Lys(ε-Ac)-AMC (Catalog# 233691-67-3, BLD pharma) and 0,5% IGEPAL CA-630 (Catalog# J61055, Alfa Aesar), was added and the mixture incubated for 3 h under cell culture conditions. The reaction was stopped with 100 µL of stop solution (50 mM Tris-HCl, 137 mM NaCl, 2.7 mM KCl, 1 mM $MgCl_2$, 1 % IGEPAL CA-630, 10 µM vorinostat, 2.0 mg/mL trypsin) and developed for 1.5 h under cell culture conditions. Fluorescence (excitation $\lambda = 355$ nm, emission $\lambda = 460$ nm) was measured using a Spark multimode microplate reader

(Tecan Group AG, Maennedorf, Swiss). The half-maximal inhibitory concentration (IC_{50}) was determined by plotting dose response curves and nonlinear regression with GraphPad Prism (GraphPad Software, San Diego, CA, USA).

3.4. HDAC Enzyme Inhibition Assay

In vitro inhibitory activities against HDAC1, 2 and HDAC6 were measured using a previously published protocol.[6] In vitro inhibitory activities against HDAC4 were measured using a previously published protocol with slight modifications.[7] For test compounds and controls, serial dilutions of the respective DMSO stock solution in assay buffer (50 mM Tris−HCl, pH 8.0, 137 mM NaCl, 2.7 mM KCl, 1.0 mM $MgCl_2 \cdot 6H_2O$, 0.1 mg/mL BSA) were prepared, and 5.0 µL of this serial dilution were transferred into OptiPlate-96 black microplates (PerkinElmer). In the case of HDAC1-3 and HDAC6, a volume of 35 µL of the fluorogenic substrate ZMAL (Z- Lys(Ac)-AMC,[8] 21.43 µM in assay buffer) and 10 µL enzyme solution were added. In the case of HDAC4, 35 µL of the fluorogenic substrate Boc-Lys(Tfa)-AMC (Bachem, Catalog# 4060676, 42.86 µM in assay buffer) were added, followed by 10 µL of enzyme solution. Human recombinant HDAC1 (BPS Bioscience, Catalog# 50051), HDAC2 (BPS Bioscience, Catalog# 50052), HDAC4 (BPS Bioscience, Catalog# 50004), or HDAC6 (BPS Bioscience, Catalog# 50006) were used. The total assay volume of 50 µL (HDAC4 and 6 max. 1% DMSO; HDAC1 and 2 max. 5% DMSO) was incubated at 37 °C for 90 min. Subsequently, 50 µL of trypsin (0.4 mg/mL) in trypsin buffer (50 mM Tris−HCl, pH 8.0, 100 mM NaCl) was added, followed by additional 30 min of incubation at 37 °C. Fluorescence (excitation λ = 355 nm, emission λ = 460 nm) was measured using a FLUOstar OPTIMA microplate reader (BMG labtech, Ortenburg, Germany). The half-maximal inhibitory concentration (IC_{50}) was determined by plotting dose response curves and nonlinear regression with GraphPad Prism (GraphPad Software, San Diego, CA, USA).

3.5. Immunoblot

MM.1S cells (3×10^6 cells/mL) were seeded to cell culture flasks and after 48 h treated with the indicated concentration of compound or vehicle (DMSO) for the given time. Cell lysis was performed with Cell Extraction Buffer (10 mM Tris, pH 7.4, 100 mM NaCl, 1 mM EDTA, 1 mM EGTA, 1 mM NaF, 20 mM $Na_4P_2O_7$, 2 mM Na_3VO_4, 1% Triton™ ×-100, 10% glycerol, 0.1% SDS, 0.5% deoxycholate; Catalog# FNN0011, Thermo Fisher Scientific Inc., Waltham, MA, USA) and addition of Halt Protease Inhibitor Cocktail (100×) (Catalog# 78429, Life Technologies GmbH, Carlsbad, CA, USA) and phenylmethanesulfonyl fluoride (Catalog# 10837091001, Sigma-Aldrich, St. Louis, MO, USA) according to manufacturer instructions. Protein content was determined by Pierce™ BCA Protein Assay Kit (Catalog# 23225, Thermo Fisher Scientific Inc., Waltham, MA, USA) according to manufacturer guidelines. Samples were denatured by Laemmli 2× Concentrate (Catalog# S3401-10VL, Sigma-Aldrich, St. Louis, MO, USA), and Precision Plus Protein Unstained Standard was used as molecular weight marker (Catalog# 1610363, Bio-Rad, Hercules, CA, USA). SDS-PAGE was performed with

10% Mini-PROTEAN TGX Stain-Free Gel (Catalog# 458035, Bio-Rad, Hercules, CA, USA) at 200 V for 50 min (Catalog# 458035, Bio-Rad). Afterwards, proteins were transferred with the Trans-Blot Turbo Transfer System (Catalog# 1704150, Bio-Rad, Hercules, CA, USA) to Immobilon-FL PVDF membranes (Catalog# IPFL00005, Millipore Merck, Burlington, MA, USA) at 1.0 A for 30 min and incubated with 5% milk-powder solution for 1 h at room temperature under slight agitation. Subsequently, the membranes were incubated with anti-HDAC1 (Catalog# 5356S, Cell Signaling Technology, Denver, MA, USA), anti-HDAC2 (Catalog# 9959S, Cell Signaling Technology, Denver, MA, USA), anti-HDAC4 (Catalog#7628S, Cell Signaling Technology, Denver, MA, USA), anti-HDAC6 (Catalog#7558S, Cell Signaling Technology, Denver, MA, USA), anti-acetyl-histone H3 (Catalog# 9677S, Cell Signaling Technology, Denver, MA, USA), anti-acetyl-α-tubulin (Catalog#5335, Cell Signaling Technology, Denver, MA, USA) or anti-GAPDH (Catalog# T0004, Affinity Biosciences, Cincinnati, OH, USA) antibody solutions in 1:1000–1:20000 dilutions at 4 °C, overnight. Incubation with HRP-conjugated secondary anti-mouse (Catalog# sc-516102, Santa Cruz, Dallas, TX, USA) and anti-rabbit (Catalog# HAF008, R&D Systems, Inc., Minneapolis, MN, USA) antibody solution was performed for 1.5 h, and membranes were developed with clarity western ECL substrate (Catalog# 1705061, Bio-Rad, Hercules, CA, USA). The ChemiDoc XRS+ System (Catalog# 1708265, Bio-Rad, Hercules, CA, USA) was used for detection and Image Lab Software 6.1 (Bio-Rad, Hercules, CA, USA) for quantification. GraphPad Prism (GraphPad Software, San Diego, CA, USA) was used for normalization, statistical analysis and bar graph creation. Significance testing was performed with a one-way analysis of variance (ANOVA). Dunnett's post-hoc test was employed to obtain significance levels of each mean compared to a reference mean value.

3.6. Annexin V/PI Assay

MM.1S cells (3×10^5 cells/well) were seeded in 24-well plates (Starlab GmbH, Hamburg, Germany) and treated with indicated concentration of compound or vehicle (DMSO) for 48 h under cell culture conditions. Subsequently, cells were washed with cell staining buffer (HEPES 0.1 M, NaCl 1.4 M, $CaCl_2 \times 3\ H_2O$ 25 mM), resuspended in 300 µL and 150 µL was transferred in a 96-well plate. The staining was performed using 5 µL/well annexin V-FITC (catalog# 640945, BioLegend, San Diego, CA, USA) and 10 µL/well propidium iodide (catalog# 421301, BioLegend, San Diego, CA, USA), incubated for 15 min and analyzed by flow cytometry (Guava® easyCyteTM, Luminex, Austin, TX, USA). GraphPad Prism (GraphPad Software, San Diego, CA, USA) was used for normalization, statistical analysis and bar graph creation. Significance testing was performed with a one-way analysis of variance (ANOVA). Dunnett's post-hoc test was employed to obtain significance levels of each mean compared to a reference mean value.

3.7. Caspase-Glo 3/7 Assay

MM.1S cells (10×10^3 cells/well) were seeded in white sterile 96-well plates (ThermoFisher Scientific, Waltham, MA, USA, #136102). The cells were treated with the indicated concentration of compound or vehicle (DMSO) for 48 h under culture conditions. The cells were subsequently incubated with Caspase-Glo 3/7 substrate (Promega, Madison, WI, USA, #G8091) for 1 h at 22 °C, according to the manufacturer´s protocol. Luminescence was detected at 22 °C using a FLUOstar OPTIMA microplate reader (BMG labtech, Ortenburg, Germany). GraphPad Prism (GraphPad Software, San Diego, CA, USA) was used for normalization, statistical analysis and bar graph creation. Significance testing was performed with a one-way analysis of variance (ANOVA). Dunnett's post-hoc test was employed to obtain significance levels of each mean compared to a reference mean value.

4. Chemical Experiments

No unexpected or unusually high safety hazards were encountered.

4.1. General Information

Chemicals were purchased from ABCR, Acros Organics, BLDpharm, Carl Roth, Fisher Scientific, Fluorochem, Sigma Aldrich, Tokyo Chemical Industry, and VWR Chemicals. Fmoc protection was performed according to Sinatra et al.[9] Technical grade solvents were distilled prior to use. For all HPLC purposes, acetonitrile in HPLC-grade quality (HiPerSolv CHROMANORM, VWR) was used. Water was purified with a PURELAB flex® (ELGA VEOLIA). Thin layer chromatography was carried out with pre-coated silica gel (60 F_{254}) aluminium sheets from Merck. Detection was performed with UV light at 254 and 360 nm or with $KMnO_4$, bromcresol green or ninhydrin staining. Acros Organics silica gel 60 (70–230 mesh) was taken for preparative column chromatography. Uncorrected melting points were measured on a Büchi 510 oil bath apparatus or on a Büchi Melting Point M-565 apparatus. A Thermo Fisher Scientific UltiMateTM 3000 UHPLC system with a Nucleodur 100-5 C18 (250 × 4.6 mm, Macherey Nagel) with a flow rate of 1 mL/min and a temperature of 25 °C or a 100-5 C18 (100 × 3 mm, Macherey Nagel) with a flow rate of 0.5 mL/min and a temperature of 25 °C with an appropriate gradient were used. For preparative purposes a AZURA Prep. 500/1000 gradient system with a Nucleodur 110-5 C18 HTec (150 × 32 mm, Macherey Nagel) column with 20 mL/min was used. Detection was implemented by UV absorption measurement at a wavelength of λ = 220 nm and λ = 250 nm. Bidest. H_2O (A) and MeCN (B) were used as eluents with an addition of 0.1% TFA for eluent A. The purity of all final compounds was 95% or higher. Purity was determined *via* HPLC with the Nucleodur 100-5 C18 (250 x 4.6 mm, Macherey Nagel) at 250 nm. The following gradients were applied: A (95% A and 5% B for 5 min, to 5% A and 95% B in 5 min, 5% A and 95% B for 12 min), B (95% A and 5% B for 5 min, to 5% A and 95% B in 10 min, 5% A and 95% B for 12 min), C (95% A and 5% B for 5 min, to 5% A and 95% B in 15 min, 5% A and 95% B for 10 min). Low resolution electrospray ionisation mass spectra (LRMS) were acquired with an Advion expression compact mass spectrometer coupled with an automated Advion TLC plate reader Plate Express (Advion, Ithaca, NY, USA). HR-ESI-MS spectra were recorded on a Bruker micrOTOF-Q mass spectrometer coupled with a HPLC Dionex UltiMate 3000 or a LTQ Orbitrap XL. NMR spectra were recorded on a Bruker Avance DRX 500 (500 MHz ^{1}H NMR, 126 MHz ^{13}C NMR) and a Bruker Avance III 600 (600 MHz ^{1}H NMR, 151 MHz ^{13}C NMR). Chemical shifts are given in parts per million (ppm) referring to the signal centre using the solvent peaks for reference, DMSO-d_6 (2.49/39.7), $CDCl_3$ (7.26/77.1) or methanol-d_4 (3.31/49.0). The multiplicity of each signal is reported as singlet (s), doublet (d), triplet (t), multiplet (m) or combinations thereof. Multiplicities and coupling constants are reported as measured and might disagree with the expected values.

4.2. General Procedures

General Procedure A (Resin modification)

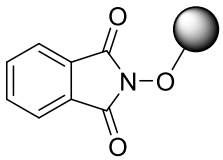

The resin modification was performed as established by Sinatra et al.[9] The amounts of reagents and solvents used in the following synthesis protocol correspond to a 3.00−4.00 mmol scale. After swelling of the 2-chlorotrityl chloride resin (2.00 g, 3.20 mmol, 1.00 eq, loading 1.60 mmol/g) for 30 min in DMF, a solution of *N*-hydroxyphthalimide (1.88 g, 11.5 mmol, 3.50 eq) and Et_3N (1.60 mL, 11.5 mmol, 3.50 eq) in DMF (1.5 mL/g resin) was added to the resin and reacted for 48 h. Afterwards, the resin was washed with DMF (10 × 5 mL) and CH_2Cl_2 (10 × 5 mL). Capping of the modified resin was performed by treatment with a capping solution (CH_2Cl_2/MeOH/DIPEA, 80/15/5 *v*/*v*) two times for 15 min. Subsequently, the resin was washed with CH_2Cl_2 (10 × 5 mL) and dried in *vacuo* to afford the modified resin **11**.

General Procedure B (HAIR synthesis)

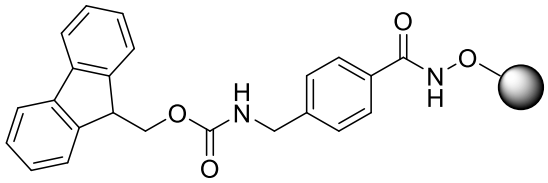

HAIR A

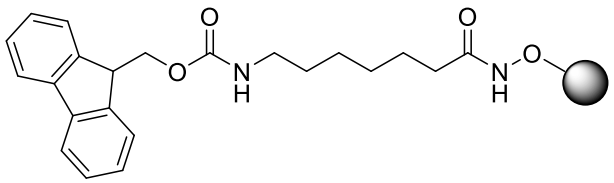

HAIR D

The **HAIR A** and **D** synthesis was performed as established by Sinatra et al.[9] Resin **(11)** was swelled for 1 h in DMF and washed with MeOH (4 × 5 mL) to incubate it with hydrazine (5% in MeOH, 2 × 20 min). Afterwards the resin was washed with DMF (4 × 5 mL), MeOH (4 × 5 mL) and DMF (4 × 5 mL). In parallel the Fmoc protected acid (2.00 eq), HATU (3.00 eq), HOBt*H_2O (3.00 eq) and DIPEA (5.00 eq) were dissolved in DMF and stirred for 5 min. The solution was added to the resin and the amid coupling was performed for 18 h at room temperature. Subsequently, the resin was washed with DMF (5 × 5 mL) and CH_2CL_2 (10 × 5 mL) and the completion of the reaction was confirmed *via* TNBS test, conducted according to manufacturer protocol, and HPLC. The preloaded resin **HAIR A and D** were dried *in vacuo*. The loading was determined photometrically (**general produce F**).

Loadings **HAIR A** 0.42 mmol/g and **D** 0.69 mmol/g

General Procedure C (Amide coupling on resin)

This procedure was performed as established by Sinatra et al.[9] This reaction was performed in a scale of 0.42 – 0.69 mmol/g. The preloaded resin was swelled in DMF for 1 h. After deprotection of the Fmoc group by deprotection solution (20% piperidine in DMF) two times for 5 min, the resin was washed with DMF (4 × 5 mL), MeOH (4 × 5 mL) and DMF (4 × 5 mL). In parallel, the Fmoc protected acid (2.00 eq),

HATU (3.00 eq), HOBt*H_2O (3.00 eq), EDC*HCl (3.00 eq) and DIPEA (5.00 eq) were dissolved in DMF and stirred for 5 min. This solution was added to the resin and the amid coupling was performed for 18 h. Subsequently, the resin was washed with DMF (5 × 5 mL) and CH_2CL_2 (10 × 5 mL) and the completion of the reaction was confirmed *via* TNBS test, conducted according to manufacturer protocol, and HPLC. The loaded resin was dried *in vacuo*.

General Procedure D (On resin *Huisgen* 1,3-cycloaddition)

This reaction was performed in a scale of 0.42 – 0.69 mmol/g. On resin alkine was swelled in DMF (5 mL) for 60 min. In parallel, the following solutions were prepared: **10** (2.00 eq.) in DMF (0.10 M), tris[(1-benzyl-4-triazolyl)methyl]amine (TBTA) (0.25 eq.) in DMF (0.10 M), 0.10 M aqueous $CuSO_4$*5 H_2O solution (0.25 eq.) in DMF (0.05 M), 0.20 M aqueous ascorbic (0.50 eq.) acid solution in DMF (0.10 M) and *t*-BuOH (1 mL) were added to the resin and shaken for 20 h at room temperature. Subsequently, the resin was washed with DMF (5 × 5 mL) and CH_2CL_2 (10 × 5 mL) and dried *in vacuo*.

General Procedure E (Cleavage from resin)

This procedure was performed as established by Sinatra et al.[9] For confirmation of completion of the reaction dried resin (2-3 mg) was shaken with cleaving solution (CH_2CL_2/TFA, 95/5 *v*/*v*; 100 µL/mg) for 1 h at room temperature. After filtration the solution was adjusted to 1 mL with MeCN the and analysed by the HPLC.

The large scale cleavage, for purification of the final compounds, was carried out in the same way, but after 1 h of incubation the cleaving solution was removed under reduced pressure and the crude was dissolved in MeOH or cleavage solution for preparative HPLC.

General Procedure F (Resin loading determination)

This procedure was performed as established by Sinatra et al.[9] The indicated resin (**HAIR A** or **D**, 3-5 mg) was incubated with deprotection solution (500 µL) two times for 5 min and the combined solutions were collected. The concentration of the cleaved Fmoc-group was determined photometrically ($\varepsilon_{300\ nm}$(dibenzofulvene adduct) = 7800 $M^{-1}cm^{-1}$) using Lambert-Beer law.

$$A = \varepsilon * c * l$$

where A = absorbance; ε = molar extinction coefficient; c = concentration; l = optical path length.

The loading was calculated by the concentration of the cleaved Fmoc-group and the resin mass.

4.3. Preparation of Compounds

4-(Prop-2-yn-1-yloxy)benzoic acid (12)

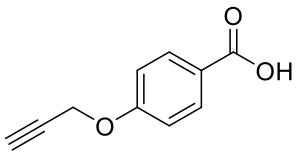

12

4-Hydroxybenzoic acid (150 mg, 1.09 mmol, 1.00 eq) was dissolved in MeOH:H_2O (3 mL, 1/1 *v*/*v*) and Na_2CO_3 (253 mg, 2.39 mmol, 2.20 eq) was added. After the addition of KI (36.0 mg, 0.22 mmol, 0.20 eq) and propagyl bromide (80% in toluene, 236 µL, 2.17 mmol, 2.00 eq), the mixture was stirred for 72 h at 50 °C. Subsequently, the solvent was removed under reduced pressure, H_2O was added and washed with CH_2Cl_2 (3 × 20 mL). The inorganic layer was acidified with 6 M HCl (pH ~ 1) and the resulting precipitate was purified by silica gel column chromatography (CH_2Cl_2/MeOH, 93/7 *v*/*v*) to provide **12** as a white solid (98.2 mg, 0.557 mmol).

Yield 51%; mp. 217-218 °C; R_f = 0.60 (CH_2Cl_2/MeOH, 9/1 *v*/*v*); **^{1}H NMR** (500 MHz, DMSO-d_6) δ = 3.60 (t, *J* = 2.4 Hz, 1H), 4.89 (d, *J* = 2.4 Hz, 2H), 7.04 – 7.11 (m, 2H), 7.88 – 7.94 (m, 2H), 12.64 (s, 1H); **^{13}C NMR** (126 MHz, DMSO-d_6) δ = 55.6, 78.6, 78.7, 114.6, 123.7, 131.2, 160.7, 166.8.

***tert*-Butyl [2-(2-hydroxyethoxy)ethyl]carbamate (13)**

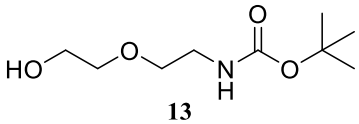

13

2-(2-Aminoethoxy)ethanol (1.00 g, 9.42 mmol, 1.00 eq) was dissolved in ethanol (25 ml) and cooled on ice to 0 °C. Boc_2O (2.30 g, 10.4 mmol, 1.10 eq) was added and the solution was stirred for 16 h at room temperature. The solvent was removed under reduced pressure. 20 mL water was added to the residue and the inorganic layer extracted with CH_2Cl_2 (4 x 20 mL). The combined organic layers were washed with brine, dried over Na_2SO_4 and concentrated under reduced pressure. Purification by silica gel column chromatography (EtOAc) provided **13** as a colourless oil (1.93 g, 9.39 mmol).

Yield 99%; R_f = 0.57 (EtOAc); **^{1}H NMR** (600 MHz, $CDCl_3$) δ = 1.42 (s, 9H), 3.31 (t, *J* = 5.1 Hz, 2H), 3.53 (t, *J* = 5.2 Hz, 2H), 3.54 – 3.58 (m, 2H), 3.69 – 3.74 (m, 2H), 5.28 (s, 1H); **^{13}C NMR** (151 MHz, $CDCl_3$) δ = 28.5, 40.6, 61.8, 70.4, 72.3, 79.5, 156.3.

***tert*-Butyl (2-{2-[(6-chlorohexyl)oxy]ethoxy}ethyl)carbamate (14)**

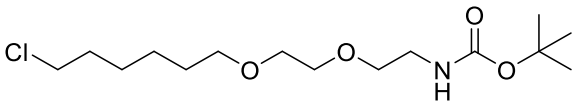

14

In a round bottom flask, NaH (60% in mineral oil, 273 mg, 6.82 mmol, 1.40 eq) was suspended in DMF (5 mL) and cooled to 0 °C. Compound **13** (1.00 g, 4.87 mmol, 1.00 eq) dissolved in THF (15 mL) was

added to the NaH suspension and stirred for 45 min at room temperature. The mixture was cooled to 0 °C and 1-chloro-6-iodhexane (1.20 mL, 7.80 mmol, 1.60 eq) was added dropwise. The reaction mixture was stirred for 18 h at room temperature. Subsequently, aqueous ammonium chloride (20 mL) was added, and the mixture was extracted three times with CH_2Cl_2 (20 mL). The combined organic layers were washed with brine (1 × 20 mL), dried over Na_2SO_4 and concentrated under reduced pressure. Purification by silica gel column chromatography (cyclohexane/EtOAc, 80/20 *v*/*v*) provided **14** as a pale-yellow oil (661 g, 2.04 mmol).

Yield 42%; R_f = 0.59 (cyclohexane/EtOAc, 80/30 *v*/*v*); **^{1}H NMR** (600 MHz, $CDCl_3$) δ = 1.34 – 1.40 (m, 2H), 1.42 – 1.49 (m, 11H), 1.56 – 1.64 (m, 2H), 1.73 – 1.81 (m, 2H), 3.31 (t, *J* = 5.2 Hz, 2H), 3.45 (t, *J* = 6.7 Hz, 2H), 3.51 – 3.57 (m, 6H), 3.58 – 3.61 (m, 2H), 4.99 (s, 1H); **^{13}C NMR** (151 MHz, $CDCl_3$) δ = 25.5, 26.8, 28.5, 29.6, 32.7, 40.5, 45.2, 70.2, 70.3, 70.4, 71.4, 79.3, 156.1; **LRMS (ESI)** *m/z* $[M+H_3O]^+$ calcd for $C_{15}H_{30}ClNO_4$ 342.2, found 342.1.

2-{2-[(6-Chlorohexyl)oxy]ethoxy}ethan-1-amine trifluoromethyl acetate (15)

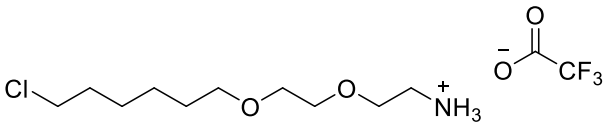

15

Compound **14** (630 mg, 1.95 mmol, 1.00 eq) was dissolved in CH_2Cl_2 (7 mL) and cooled 0°C. Afterwards, TFA (2.30 mL, 29.2 mmol, 15.0 eq) was added dropwise over 10 min. After stirring for 2 h at the indicated temperature (0 °C), the solvent was removed under reduced pressure. Compound **15** was yielded as a yellow oil (639 mg, 1.89 mmol).

Yield 97%; R_f = 0.11 (cyclohexane/EtOAc/TFA, 79/19/2 *v*/*v*); **^{1}H NMR** (600 MHz, DMSO-d_6) δ = 1.28 – 1.34 (m, 2H), 1.36 – 1.42 (m, 2H), 1.47 – 1.53 (m, 2H), 1.68 – 1.74 (m, 2H), 2.95 – 3.00 (m, 2H), 3.38 (t, *J* = 6.6 Hz, 2H), 3.49 – 3.52 (m, 2H), 3.55 – 3.60 (m, 4H), 3.62 (t, *J* = 6.6 Hz, 2H), 7.82 (s, 3H); **^{13}C NMR** (151 MHz, DMSO-d_6) δ = 24.9, 26.1, 29.0, 32.0, 38.6, 45.3, 66.7, 69.3, 69.7, 70.2; **LRMS (ESI)** *m/z* $[M]^+$ calcd for $C_{10}H_{23}ClNO_2^+$ 224.1, found 224.0.

2-[(3*r*,5*r*,7*r*)-Adamantan-1-yl]-*N*-(2-{2-[(6-chlorohexyl)oxy]ethoxy}ethyl)acetamide (16)

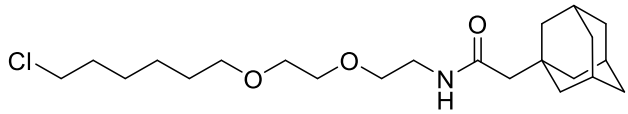

16

2-(Adamantan-1-yl)acetic acid (381 mg, 1.94 mmol, 1.00 eq) was dissolved in CH_2Cl_2 (3.3 mL) and DIPEA (1.12 mL, 3.97 mmol, 3.00 eq). Afterwards, HATU (887 mg, 2.31 mmol, 1.20 eq) was added and the solution was stirred for 10 min. In parallel, **15** (650 mg, 1.92 mmol, 1.00 eq) was dissolved in CH_2Cl_2 (1.5 mL) and DIPEA (340 µL, 1.92 mmol, 1.00 eq). The solution was added dropwise to the acid solution and the mixture stirred for 19 h at room temperature. Finally, H_2O (15 mL) was added, the

inorganic layer was washed with CH_2Cl_2 (3 x 15 mL). The combined organic phases were washed with brine (1 × 15 mL), dried over Na_2SO_4 and concentrated under reduced pressure. Purification by silica gel column chromatography (EtOAc) provided **16** as a yellow oil (751 g, 1.88 mmol).

Yield 98%; R_f = 0.75 (CH_2Cl_2/MeOH, 95/5 *v*/*v*); **^{1}H NMR** (600 MHz, $CDCl_3$) δ = 1.33 – 1.40 (m, 2H), 1.41 – 1.49 (m, 2H), 1.57 – 1.64 (m, 11H), 1.66 – 1.71 (m, 3H), 1.73 – 1.80 (m, 2H), 1.92 (s, 2H), 1.93 – 1.98 (m, 3H), 3.42 – 3.48 (m, 4H), 3.50 – 3.57 (m, 6H), 3.58 – 3.61 (m, 2H), 5.90 (t, *J* = 5.6 Hz, 1H); **^{13}C NMR** (151 MHz, $CDCl_3$) δ = 25.5, 26.8, 28.8, 29.6, 32.6, 32.9, 36.9, 39.2, 42.7, 45.1, 51.8, 70.1, 70.1, 70.4, 71.4, 171.2; **LRMS (ESI)** *m/z* $[M+H]^+$ calcd for $C_{22}H_{38}ClNO_3$ 400.2, found 400.2.

2-[(3*r*,5*r*,7*r*)-Adamantan-1-yl]-*N*-(2-{2-[(6-azidohexyl)oxy]ethoxy}ethyl)acetamide (10)

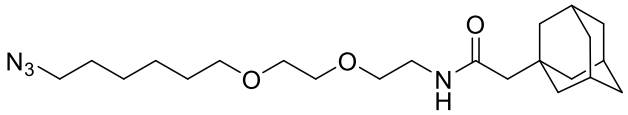

10

Compound **16** (356 mg, 0.890 mmol, 1.00 eq) was dissolved in DMF (2.2 mL) and NaN_3 (87.0 mg, 1.34 mmol, 1.50 eq) was added. The mixture was stirred at 90 °C for 19 h. Afterwards, it was diluted with H_2O (10 mL) and the inorganic layer extracted with EtOAc (4 × 10 mL). The combined organic layers were washed with brine (10 mL), dried over Na_2SO_4 and concentrated under reduced pressure. Purification by silica gel column chromatography (EtOAc) provided **10** as a pale-yellow oil (297 g, 0.731 mmol).

Yield 82%; R_f = 0.49 (EtOAc); **^{1}H NMR** (600 MHz, $CDCl_3$) δ = 1.33 – 1.42 (m, 4H), 1.56 – 1.64 (m, 13H), 1.66 – 1.72 (m, 3H), 1.90 – 1.97 (m, 5H), 3.25 (t, J = 6.9 Hz, 2H), 3.41 – 3.47 (m, 4H), 3.52 – 3.57 (m, 4H), 3.58 – 3.61 (m, 2H), 5.93 (t, *J* = 5.8 Hz, 1H); **^{13}C NMR** (151 MHz, $CDCl_3$) δ = 25.8, 26.7, 28.8, 28.9, 29.6, 32.8, 36.9, 39.1, 42.7, 51.5, 51.8, 70.1, 70.1, 70.3, 71.4, 171.1; **LRMS (ESI)** *m/z* $[M+H]^+$ calcd for $C_{22}H_{38}N_4O_3$ 407.3, found 407.3.

4-{2-[(3*r*,5*r*,7*r*)-Adamantan-1-yl]acetamido}-*N*-[7-(hydroxyamino)-7-oxoheptyl]benzamide (1a)

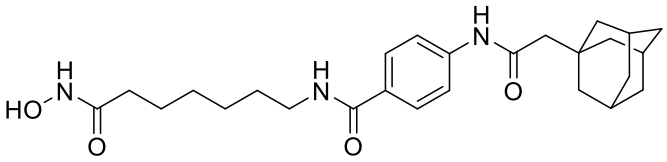

1a

Synthesized according to **general procedure C** using **HAIR D** (1.18 g, 1.02 mmol, 1.00 eq), Fmoc protected 4-aminobenzoic acid (733 mg, 2.04 mmol, 2.00 eq), HATU (1.16 g, 3.06 mmol, 3.00 eq), HOBt*H_2O (468 mg, 3.06 mmol, 3.00 eq), EDC*HCl (592 mg, 3.06 mmol, 3.00 eq) and DIPEA (888 µL, 5.10 mmol, 5.00 eq) in DMF (2.5 mL). The second coupling cycle was also performed according to **general procedure C** using the precursor (210 mg, 0.17 mmol, 1.00 eq), 1-adamantaneacetic acid (67 mg, 0.34 mmol, 2.00 eq), HATU (196 mg, 0.51 mmol, 3.00 eq), HOBt*H_2O

(79 mg, 0.51 mmol, 3.00 eq), EDC*HCl (99 mg, 0.51 mmol, 3.00 eq) and DIPEA (150 µL, 0.91 mmol, 5.00 eq) in DMF (500 µL). Cleavage according to **general procedure E** and purification by preparative HPLC afforded **1a** as an amorphous withe powder (17.8 mg, 39 µmol).

Yield: 23%; **^{1}H NMR** (600 MHz, DMSO-d_6) δ = 1.23 – 1.32 (m, 4H), 1.45 – 1.52 (m, 4H), 1.57 – 1.69 (m, 12H), 1.89 – 1.98 (m, 5H), 2.07 (s, 2H), 3.19 – 3.24 (m, 2H), 7.64 (d, *J* = 8.7 Hz, 2H), 7.77 (d, *J* = 8.7 Hz, 2H), 8.26 (t, *J* = 5.6 Hz, 1H), 9.94 (s, 1H), 10.31 (s, 1H), C-N*H*-OH signal could not be detected due to solvent exchange; **^{13}C NMR** (151 MHz, DMSO-d_6) δ = 25.1, 26.2, 28.0, 28.3, 29.1, 32.2, 32.7, 36.4, 40.1, 42.0, 50.8, 118.1, 127.8, 129.0, 141.6, 165.5, 169.1, 169.5.; **HRMS (ESI)** *m/z* $[M+Na]^+$ calcd for $C_{26}H_{37}N_3O_4$ 478.2676, found 478.2674; **HPLC** (gradient A), t_R = 12.40 min, 97.7% purity.

4-[2-(9*H*-Fluoren-9-yl)acetamido]-*N*-[7-(hydroxyamino)-7-oxoheptyl]benzamide (1b)

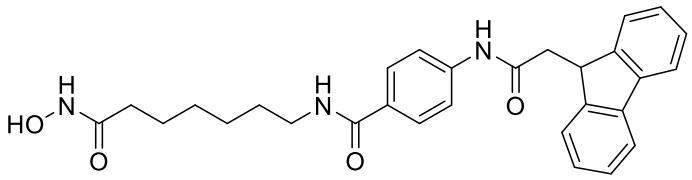

1b

Synthesized according to **general procedure C** using **HAIR D** (1.18 g, 1.02 mmol, 1.00 eq), Fmoc protected 4-aminobenzoic acid (733 mg, 2.04 mmol, 2.00 eq), HATU (1.16 g, 3.06 mmol, 3.00 eq), HOBt*H_2O (468 mg, 3.06 mmol, 3.00 eq), EDC*HCl (592 mg, 3.06 mmol, 3.00 eq) and DIPEA (888 µL, 5.10 mmol, 5.00 eq) in DMF (2.5 mL). The second coupling cycle was also performed according to **general procedure C** using the precursor (211 mg, 0.17 mmol, 1.00 eq), 9-fluoreneacetic acid (67 mg, 0.34 mmol, 2.00 eq), HATU (195 mg, 0.51 mmol, 3.00 eq), HOBt*H_2O (78 mg, 0.51 mmol, 3.00 eq), EDC*HCl (98 mg, 0.51 mmol, 3.00 eq) and DIPEA (149 µL, 0.91 mmol, 5.00 eq) in DMF (500 µL). Cleavage according to **general procedure E** and purification by preparative HPLC afforded **1b** as an amorphous withe powder (20.4 mg, 39 µmol).

Yield: 25%; **^{1}H NMR** (600 MHz, DMSO-d_6) = δ 1.25 – 1.34 (m, 4H), 1.46 – 1.55 (m, 4H), 1.95 (t, *J* = 7.4 Hz, 2H), 2.82 (d, *J* = 7.6 Hz, 2H), 3.21 – 3.27 (m, 2H), 4.46 (t, *J* = 7.5 Hz, 1H), 7.28 – 7.32 (m, 2H), 7.37 – 7.41 (m, 2H), 7.56 (d, *J* = 7.5 Hz, 2H), 7.72 (d, *J* = 8.7 Hz, 2H), 7.84 (d, *J* = 8.7 Hz, 2H), 7.89 (d, *J* = 7.5 Hz, 2H), 8.32 (t, *J* = 5.6 Hz, 1H), 10.23 (s, 1H), 10.33 (s, 1H), C-N*H*-OH signal could not be detected due to solvent exchange; **^{13}C NMR** (151 MHz, DMSO-d_6) δ = 25.1, 26.2, 28.4, 29.1, 32.2, 40.1, 40.6, 43.5, 118.4, 120.1, 124.4, 127.2, 127.3, 128.1, 129.4, 140.1, 141.3, 146.5, 165.6, 169.1, 170.2; **HRMS (ESI)** *m/z* $[M+Na]^+$ calcd for $C_{29}H_{31}N_3O_4$ 508.2207, found 508.2192; **HPLC** (gradient A), t_R = 12.21 min, 98.6% purity.

4-(2-{2-[(3*r*,5*r*,7*r*)-Adamantan-1-yl]acetamido}acetamido)-*N*-[7-(hydroxyamino)-7-oxoheptyl]benzamide (2a)

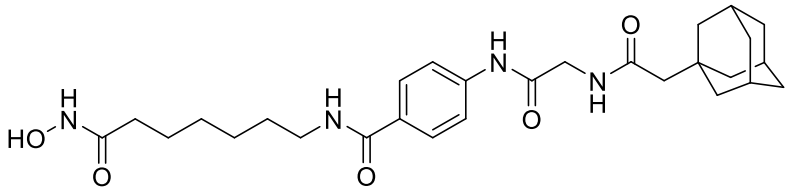

2a

Synthesized according to **general procedure C** using **HAIR D** (1.27 g, 0.93 mmol, 1.00 eq), Fmoc protected 4-aminobenzoic acid (689 mg, 1.86 mmol, 2.00 eq), HATU (1.06 g, 2.79 mmol, 3.00 eq), HOBt*H_2O (427 mg, 2.79 mmol, 3.00 eq), EDC*HCl (540 mg, 2.79 mmol, 3.00 eq) and DIPEA (810 µL, 4.65 mmol, 5.00 eq) in DMF (2.3 mL). The second coupling cycle was also performed according to **general procedure C** using the precursor (681 mg, 0.47 mmol, 1.00 eq), Fmoc-Gly-OH (286 mg, 0.93 mmol, 2.00 eq), HATU (591 mg, 1.40 mmol, 3.00 eq), HOBt*H_2O (238 mg, 1.40 mmol, 3.00 eq), EDC*HCl (271 mg, 1.40 mmol, 3.00 eq) and DIPEA (451 µL, 2.33 mmol, 5 eq) in DMF (1.2 mL). The third coupling cycle was also performed according to **general procedure C** using the precursor (308 mg, 0.21 mmol, 1.00 eq), 1-adamantaneacetic acid (84 mg, 0.42 mmol, 2.00 eq), HATU (241 mg, 0.63 mmol, 3.00 eq), HOBt*H_2O (97 mg, 0.63 mmol, 3.00 eq), EDC*HCl (122 mg, 0.63 mmol, 3.00 eq) and DIPEA (184 µL, 1.05 mmol, 5.00 eq) in DMF (600 µL). Cleavage according to **general procedure E** and purification by preparative HPLC afforded **2a** as an amorphous withe powder (46.0 mg, 90 µmol).

Yield: 46%; **^{1}H NMR** (600 MHz, DMSO-d_6) δ = 1.26 – 1.33 (m, 4H), 1.47 – 1.54 (m, 4H), 1.55 – 1.61 (m, 8H), 1.63 – 1.68 (m, 3H), 1.90 – 1.93 (m, 4H), 2.29 (t, *J* = 7.4 Hz, 2H), 3.20 – 3.24 (m, 2H), 3.57 (s, 2H), 3.86 (d, *J* = 5.8 Hz, 2H), 7.63 (d, *J* = 8.8 Hz, 2H), 7.79 (d, *J* = 8.8 Hz, 2H), 8.02 (t, *J* = 5.8 Hz, 1H), 8.28 (t, *J* = 5.7 Hz, 1H), 10.12 (s, 1H), C-N*H*-O*H* signals could not be detected due to solvent exchange; **^{13}C NMR** (151 MHz, DMSO-d_6) δ = 24.4, 26.1, 28.0, 28.2, 29.0, 32.2, 33.2, 36.4, 42.0, 42.7, 49.7, 51.1, 118.1, 128.0, 129.2, 141.3, 165.5, 168.2, 170.5, 173.3.; **HRMS (ESI)** *m/z* $[M+Na]^+$ calcd for $C_{28}H_{40}N_4O_5$ 535.2891, found 535.2894; **HPLC** (gradient B), t_R = 14.28 min, 98.5% purity.

4-(4-{2-[(3*r*,5*r*,7*r*)-Adamantan-1-yl]acetamido}butanamido)-*N*-[7-(hydroxyamino)-7-oxoheptyl]benzamide (2b)

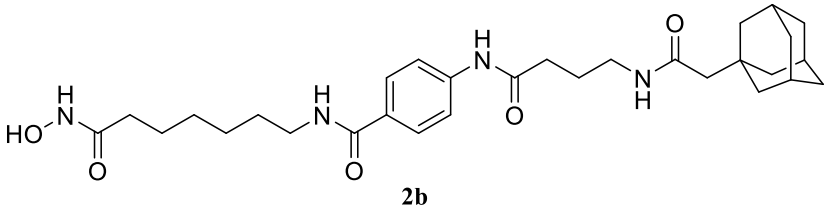

2b

Synthesized according to **general procedure C** using **HAIR D** (1.27 g, 0.93 mmol, 1.00 eq), Fmoc protected 4-aminobenzoic acid (689 mg, 1.86 mmol, 2.00 eq), HATU (1.06 g, 2.79 mmol, 3.00 eq), HOBt*H_2O (427 mg, 2.79 mmol, 3.00 eq), EDC*HCl (540 mg, 2.79 mmol, 3.00 eq) and DIPEA

(810 µL, 4.65 mmol, 5.00 eq) in DMF (2.3 mL). The second coupling cycle was also performed according to **general procedure C** using the precursor (334 mg, 0.23 mmol, 1.00 eq), Fmoc-GABA-OH (154 mg, 0.46 mmol, 2.00 eq), HATU (290 mg, 0.69 mmol, 3.00 eq), HOBt*H_2O (117 mg, 0.69 mmol, 3.00 eq), EDC*HCl (133 mg, 0.69 mmol, 3.00 eq) and DIPEA (221 µL, 1.14 mmol, 5.00 eq) in DMF (600 µL). The third coupling cycle was also performed according to **general procedure C** using the precursor (349 mg, 0.23 mmol, 1.00 eq), 1-adamantaneacetic acid (90 mg, 0.46 mmol, 2.00 eq), HATU (264 mg, 0.69 mmol, 3.00 eq), HOBt*H_2O (106 mg, 0.69 mmol, 3.00 eq), EDC*HCl (133 mg, 0.69 mmol, 3.00 eq) and DIPEA (201 µL, 1.15 mmol, 5.00 eq) in DMF (600 µL). Cleavage according to **general procedure E** and purification by preparative HPLC afforded **2b** as an amorphous withe powder (14.3 mg, 26 µmol).

Yield: 12%; **^{1}H NMR** (500 MHz, DMSO-d_6) δ = 1.23 – 1.32 (m, 4H), 1.46 – 1.52 (m, 4H), 1.53 – 1.60 (m, 9H), 1.61 – 1.67 (m, 3H), 1.67 – 1.74 (m, 2H), 1.82 (s, 2H), 1.87 – 1.97 (m, 5H), 2.34 (t, *J* = 7.4 Hz, 2H), 3.04 – 3.09 (m, 2H), 3.19 – 3.24 (m, 2H), 7.64 (d, *J* = 8.8 Hz, 2H), 7.69 (t, *J* = 5.6 Hz, 1H), 7.77 (d, *J* = 8.8 Hz, 2H), 8.26 (t, *J* = 5.6 Hz, 1H), 10.08 (s, 1H), 10.30 (s, 1H) C-N*H*-OH signals could not be detected due to solvent exchange; **^{13}C NMR** (126 MHz, DMSO-d_6) δ = 25.0, 25.2, 26.2, 28.0, 28.3, 29.0, 32.1, 32.2, 33.9, 36.4, 37.9, 40.1*, 42.1, 50.0, 118.1, 127.9, 129.0, 141.6, 165.5, 169.1, 169.9, 171.2, *overlapping with DMSO signal; **HRMS (ESI)** *m/z* $[M+Na]^+$ calcd for $C_{30}H_{44}N_4O_5$ 563.3204, found 563.3198; **HPLC** (gradient B), t_R = 14.28 min, 96.7% purity.

4-(6-{2-[(3*r*,5*r*,7*r*)-Adamantan-1-yl]acetamido}hexanamido)-*N*-[7-(hydroxyamino)-7-oxoheptyl]benzamide (2c)

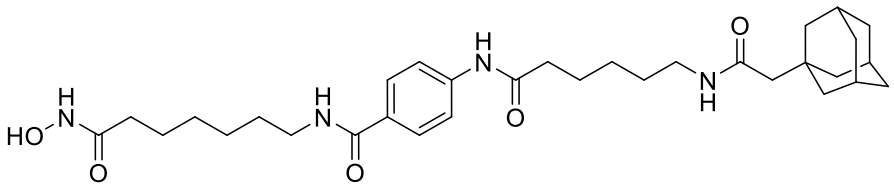

2c

Synthesized according to **general procedure C** using **HAIR D** (1.27 g, 0.93 mmol, 1.00 eq), Fmoc protected 4-aminobenzoic acid (689 mg, 1.86 mmol, 2.00 eq), HATU (1.06 g, 2.79 mmol, 3.00 eq), HOBt*H_2O (427 mg, 2.79 mmol, 3.00 eq), EDC*HCl (540 mg, 2.79 mmol, 3.00 eq) and DIPEA (810 µL, 4.65 mmol, 5.00 eq) in DMF (2.3 mL). The second coupling cycle was also performed according to **general procedure C** using the precursor (334 mg, 0.23 mmol, 1.00 eq), Fmoc-6-Ahx-OH (167 mg, 0.46 mmol, 2.00 eq), HATU (290 mg, 0.69 mmol, 3.00 eq), HOBt*H_2O (117 mg, 0.69 mmol, 3.00 eq), EDC*HCl (133 mg, 0.69 mmol, 3.00 eq) and DIPEA (221 µL, 1.14 mmol, 5.00 eq) in DMF (600 µL). The third coupling cycle was also performed according **to general procedure C** using the precursor (355 mg, 0.23 mmol, 1.00 eq), 1-adamantaneacetic acid (90 mg, 0.46 mmol, 2.00 eq), HATU (264 mg, 0.69 mmol, 3.00 eq), HOBt*H_2O (106 mg, 0.69 mmol, 3.00 eq), EDC*HCl (133 mg, 0.69 mmol, 3.00 eq) and DIPEA (201 µL, 1.15 mmol, 5.00 eq) in DMF (600 µL). Cleavage according

to **general procedure E** and purification by preparative HPLC afforded **2c** as an amorphous withe powder (31 mg, 55 µmol).

Yield: 24%; **^{1}H NMR** (500 MHz, DMSO-d_6) δ = 1.21 – 1.34 (m, 6H), 1.36 – 1.45 (m, 2H), 1.45 – 1.53 (m, 4H), 1.53 – 1.67 (m, 14H), 1.79 (s, 2H), 1.86 – 1.91 (m, 3H), 1.94 (t, *J* = 7.4 Hz, 2H), 2.31 (t, *J* = 7.4 Hz, 2H), 2.98 – 3.05 (m, 2H), 3.18 – 3.25 (m, 2H), 7.60 (t, *J* = 5.7 Hz, 1H), 7.64 (d, *J* = 8.8 Hz, 2H), 7.77 (d, *J* = 8.7 Hz, 2H), 8.25 (t, *J* = 5.6 Hz, 1H), 10.02 (s, 1H), 10.30 (s, 1H) C-N*H*-OH signals could not be detected due to solvent exchange; **^{13}C NMR** (126 MHz, DMSO-d_6) δ = 24.7, 25.0, 26.1, 26.2, 28.0, 28.3, 29.0, 29.0, 32.1, 32.2, 36.3, 36.4, 38.1, 39.0*, 42.1, 50.0, 118.1, 127.8, 128.9, 141.7, 165.5, 169.1, 169.6, 171.5, *overlapping with DMSO signal; **HRMS (ESI)** *m/z* $[M+Na]^+$ calcd for $C_{32}H_{48}N_4O_5$ 591.3517, found 591.3519; **HPLC** (gradient B), t_R = 14.62 min, 97.7% purity.

4-{2-[2-(9*H*-Fluoren-9-yl)acetamido]acetamido}-*N*-[7-(hydroxyamino)-7-oxoheptyl]benzamide (2d)

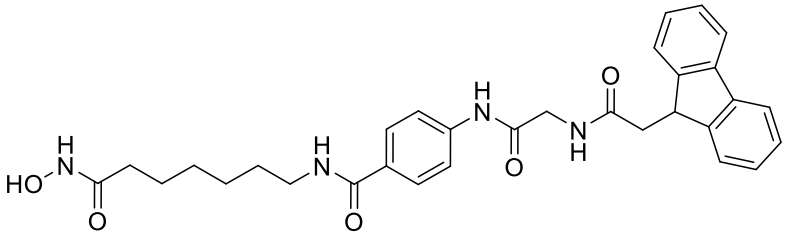

2d

Synthesized according to **general procedure C** using **HAIR D** (1.27 g, 0.93 mmol, 1.00 eq), Fmoc protected 4-aminobenzoic acid (689 mg, 1.86 mmol, 2.00 eq), HATU (1.06 g, 2.79 mmol, 3.00 eq), HOBt*H_2O (427 mg, 2.79 mmol, 3.00 eq), EDC*HCl (540 mg, 2.79 mmol, 3.00 eq) and DIPEA (810 µL, 4.65 mmol, 5 eq) in DMF (2.3 mL). The second coupling cycle was also performed according to **general procedure C** using the precursor (681 mg, 0.47 mmol, 1.00 eq), Fmoc-Gly-OH (286 mg, 0.93 mmol, 2.00 eq), HATU (591 mg, 1.40 mmol, 3.00 eq), HOBt*H_2O (238 mg, 1.40 mmol, 3.00 eq), EDC*HCl (271 mg, 1.40 mmol, 3.00 eq) and DIPEA (451 µL, 2.33 mmol, 5.00 eq) in DMF (1.2 mL). The third coupling cycle was also performed according to **general procedure C** using the precursor (336 mg, 0.229 mmol, 1.00 eq), 9-fluoreneacetic acid (106 mg, 0.46 mmol, 2.00 eq), HATU (263 mg, 0.69 mmol, 3.00 eq), HOBt*H_2O (106 mg, 0.69 mmol, 3.00 eq), EDC*HCl (133 mg, 0.69 mmol, 3.00 eq) and DIPEA (149 µL, 1.14 mmol, 5.00 eq) in DMF (600 µL). Cleavage according to **general procedure E** and purification by preparative HPLC afforded **2d** as an amorphous withe powder (47 mg, 86 µmol).

Yield: 37%; **^{1}H NMR** (500 MHz, DMSO-d_6) δ = 1.24 – 1.34 (m, 4H), 1.46 – 1.55 (m, 4H), 1.95 (t, *J* = 7.4 Hz, 2H), 2.64 (d, *J* = 7.6 Hz, 2H), 3.20 – 3.26 (m, 2H), 4.04 (d, *J* = 5.7 Hz, 2H), 4.38 (t, *J* = 7.6 Hz, 1H), 7.26 – 7.32 (m, 2H), 7.36 – 7.40 (m, 2H), 7.58 – 7.62 (m, 2H), 7.69 (d, *J* = 8.8 Hz, 2H), 7.83 (d, *J* = 8.8 Hz, 2H), 7.85 – 7.89 (m, 2H), 8.30 (t, *J* = 5.6 Hz, 1H), 8.41 (t, *J* = 5.8 Hz, 1H), 10.24 (s, 1H),

10.31 (s, 1H), C-N*H*-OH signal could not be detected due to solvent exchange; **^{13}C NMR** (126 MHz, DMSO-d_6) δ = 25.1, 26.2, 28.3, 29.0, 32.2, 39.1*, 40.1*, 43.0, 43.5, 118.3, 119.9, 124.7, 127.1, 127.2, 128.0, 129.3, 140.0, 141.3, 146.6, 165.5, 168.1, 169.1, 171.4, *overlapping with DMSO signal; **HRMS (ESI)** *m/z* $[M+Na]^+$ calcd for $C_{31}H_{34}N_4O_5$ 565.2421, found 565.2420; **HPLC** (gradient B), t_R = 14.26 min, 99.4% purity.

4-[4-[2-(9*H*-Fluoren-9-yl)acetamido]butanamido}-*N*-[7-(hydroxyamino)-7-oxoheptyl]benzamide (2e)

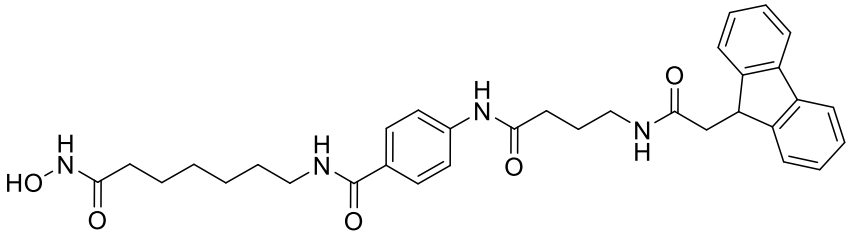

2e

Synthesized according to **general procedure C** using **HAIR D** (790 mg, 0.69 mmol, 1.00 eq), Fmoc protected 4-aminobenzoic acid (492 mg, 1.37 mmol, 2.00 eq), HATU (781 mg, 2.06 mmol, 3.00 eq), HOBt*H_2O (315 mg, 2.06 mmol, 3.00 eq), EDC*HCl (398 mg, 2.06 mmol, 3.00 eq) and DIPEA (597 µL, 3.43 mmol, 5.00 eq) in DMF (1.7 mL). The second coupling cycle was also performed according to **general procedure C** using the precursor (374 mg, 0.27 mmol, 1.00 eq), Fmoc-GABA-OH (184 mg, 0.55 mmol, 2.00 eq), HATU (313 mg, 0.82 mmol, 3.00 eq), HOBt*H_2O (126 mg, 0.82 mmol, 3.00 eq), EDC*HCl (159 mg, 0.82 mmol, 3.00 eq) and DIPEA (239 µL, 1.37 mmol, 5.00 eq) in DMF (700 µL). The third coupling cycle was also performed according to **general procedure C** using the precursor (424 mg, 0.28 mmol, 1.00 eq), 9-fluoreneacetic acid (125 mg, 0.55 mmol, 2.00 eq), HATU (318 mg, 0.83 mmol, 3.00 eq), HOBt*H_2O (128 mg, 0.83 mmol, 3.00 eq), EDC*HCl (160 mg, 0.83 mmol, 3.00 eq) and DIPEA (243 µL, 1.38 mmol, 5.00 eq) in DMF (700 µL). Cleavage according to **general procedure E** and purification by preparative HPLC afforded **2e** as an amorphous withe powder (14 mg, 25 µmol).

Yield: 9%; **^{1}H NMR** (500 MHz, DMSO-d_6) δ = 1.24 – 1.33 (m, 4H), 1.45 – 1.54 (m, 4H), 1.76 – 1.85 (m, 2H), 1.94 (t, *J* = 7.4 Hz, 2H), 2.39 (t, *J* = 7.4 Hz, 2H), 2.50 – 2.53 (m, 2H), 3.20 – 3.27 (m, 4H), 4.36 (t, *J* = 7.6 Hz, 1H), 7.26 – 7.32 (m, 2H), 7.34 – 7.39 (m, 2H), 7.49 – 7.53 (m, 2H), 7.67 (d, *J* = 8.8 Hz, 2H), 7.79 (d, *J* = 8.8 Hz, 2H), 7.84 – 7.88 (m, 2H), 8.00 (t, *J* = 5.6 Hz, 1H), 8.27 (t, *J* = 5.6 Hz, 1H), 8.62 (s, 1H), 10.10 (s, 1H), 10.30 (s, 1H); **^{13}C NMR** (126 MHz, DMSO-d_6) δ = 25.0, 25.0, 26.2, 28.3, 29.1, 32.2, 33.8, 38.2, 39.1*, 39.9*, 43.5, 118.1, 119.9, 124.5, 127.0, 127.2, 127.9, 129.0, 140.0, 141.6, 146.7, 165.5, 169.1, 170.7, 171.1, *overlapping with DMSO signal; **HRMS (ESI)** *m/z* $[M+Na]^+$ calcd for $C_{33}H_{38}N_4O_5$ 593.2734, found 593.2745; **HPLC** (gradient C), t_R = 16.66 min, 96.5% purity.

4-{6-[2-(9*H*-Fluoren-9-yl)acetamido]hexanamido}-*N*-[7-(hydroxyamino)-7-oxoheptyl]benzamide (2f)

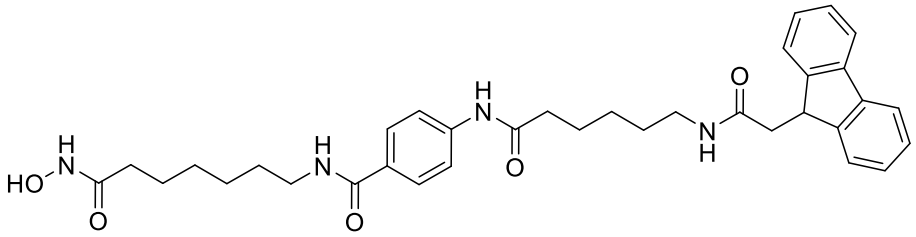

2f

Synthesized according to **general procedure C** using **HAIR D** (790 mg, 0.69 mmol, 1.00 eq), Fmoc protected 4-aminobenzoic acid (492 mg, 1.37 mmol, 2.00 eq), HATU (781 mg, 2.06 mmol, 3.00 eq), HOBt*H_2O (315 mg, 2.06 mmol, 3.00 eq), EDC*HCl (398 mg, 2.06 mmol, 3.00 eq) and DIPEA (597 µL, 3.43 mmol, 5.00 eq) in DMF (1.7 mL). The second coupling cycle was also performed according to **general procedure C** using the precursor (382 mg, 0.28 mmol, 1.00 eq), Fmoc-6-Ahx-OH (204 mg, 0.56 mmol, 2.00 eq), HATU (319 mg, 0.84 mmol, 3.00 eq), HOBt*H_2O (129 mg, 0.84 mmol, 3.00 eq), EDC*HCl (163 mg, 0.84 mmol, 3.00 eq) and DIPEA (244 µL, 1.40 mmol, 5.00 eq) in DMF (700 µL). The third coupling cycle was also performed according to **general procedure C** using the precursor (367 mg, 0.28 mmol, 1.00 eq), 9-fluoreneacetic acid (125 mg, 0.55 mmol, 2.00 eq), HATU (318 mg, 0.83 mmol, 3.00 eq), HOBt*H_2O (128 mg, 0.83 mmol, 3.00 eq), EDC*HCl (160 mg, 0.83 mmol, 3.00 eq) and DIPEA (243 µL, 1.38 mmol, 5.00 eq) in DMF (700 µL). Cleavage according to **general procedure E** and purification by preparative HPLC afforded **2f** as an amorphous withe powder (8 mg, 13 µmol).

Yield: 5%; **^{1}H NMR** (600 MHz, DMSO-d_6) δ = 1.24 – 1.37 (m, 6H), 1.45 – 1.53 (m, 6H), 1.60 – 1.66 (m, 2H), 1.94 (t, *J* = 7.4 Hz, 2H), 2.35 (t, *J* = 7.4 Hz, 2H), 2.48 – 2.49 (m, 2H), 3.16 – 3.20 (m, 2H), 3.20 – 3.24 (m, 2H), 4.35 (t, *J* = 7.7 Hz, 1H), 7.27 – 7.31 (m, 2H), 7.34 – 7.39 (m, 2H), 7.51 (d, *J* = 7.5 Hz, 2H), 7.65 (d, *J* = 8.8 Hz, 2H), 7.78 (d, *J* = 8.7 Hz, 2H), 7.86 (d, *J* = 7.5 Hz, 2H), 7.93 (t, *J* = 5.6 Hz, 1H), 8.27 (t, *J* = 5.6 Hz, 1H), 10.06 (s, 1H), 10.31 (s, 1H), C-N*H*-OH signal could not be detected due to solvent exchange; **^{13}C NMR** (151 MHz, DMSO-d_6) δ = 24.7, 25.1, 26.2, 26.2, 28.3, 28.9, 29.1, 32.2, 36.4, 38.5, 39.1*, 40.1*, 43.6, 118.1, 119.9, 124.5, 127.0, 127.2, 127.9, 128.9, 140.0, 141.7, 146.7, 165.5, 169.1, 170.5, 171.5, *overlapping with DMSO signal; **HRMS (ESI)** *m/z* $[M+Na]^+$ calcd for $C_{35}H_{42}N_4O_5$ 621.3047, found 621.3062; **HPLC** (gradient C), t_R = 20.08 min, 95.5% purity.

4-(1{6-[2-(2-{2-[(3*r*,5*r*,7*r*)-Adamantan-1-yl]acetamido}ethoxy)ethoxy]hexyl}-1*H*-1,2,3-triazol-4-yl)-*N*-[7-(hydroxyamino)-7-oxoheptyl]benzamide (3a)

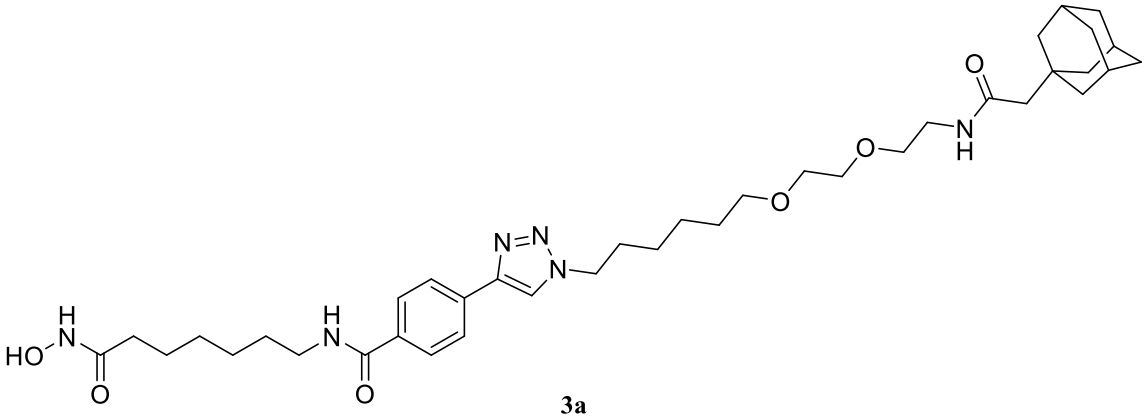

3a

Synthesized according to **general procedure C** using **HAIR D** (253 mg, 0,11 mmol, 1.00 eq), 4-ethynylbenzoic acid (33 mg, 0.21 mmol, 2.00 eq), HATU (121 mg, 0.32 mmol, 3.00 eq), HOBt*H_2O (49 mg, 0.32 mmol, 3.00 eq), EDC*HCl (61 mg, 0.32 mmol, 3.00 eq) and DIPEA (92 µL, 0.53 mmol, 5.00 eq) in DMF (400 µL). The *Huisgen* 1,3-cycloaddition was performed according to **general procedure D** using the azide **10** (77 mg, 0.19 mmol, 2.00 eq), TBTA (12 mg, 0.02 mmol, 0.25 eq), 0.1 M $CuSO_4$ solution (234 µL, 0.02 mmol, 0.25 eq), 0.2 M ascorbic acid solution (234 µL, 0.05 mmol, 0.50 eq) and *t*-BuOH (1 mL). Cleavage according to **general procedure E** and purification by preparative HPLC afforded **3a** as an amorphous withe powder (24.4 mg, 35 µmol).

Yield: 37%; **^{1}H NMR** (600 MHz, methanol-d_4) δ = 1.35 – 1.45 (m, 8H), 1.55 – 1.66 (m, 15H), 1.67 – 1.72 (m, 3H), 1.89 – 1.93 (m, 5H), 1.94 – 2.00 (m, 2H), 2.10 (t, *J* = 7.4 Hz, 2H), 3.33 (t, *J* = 5.5 Hz, 2H), 3.38 (t, *J* = 7.1 Hz, 2H), 3.46 (t, *J* = 6.5 Hz, 2H), 3.51 (t, *J* = 5.4 Hz, 2H), 3.54 – 3.59 (m, 4H), 4.47 (t, *J* = 7.0 Hz, 2H), 7.89 (d, *J* = 8.3 Hz, 2H), 7.92 (d, *J* = 8.3 Hz, 2H), 8.44 (s, 1H), C-N*H*-O*H* signals and CO-N*H* signals could not be detected due to solvent exchange; **^{13}C NMR** (151 MHz, methanol-d_4) δ = 26.5, 26.6, 27.2, 27.7, 29.8, 30.1, 30.3, 30.4, 31.2, 33.7, 33.7, 37.8, 40.2, 40.9, 43.6, 51.5, 51.8, 70.6, 71.1, 72.1, 123.0, 126.5, 129.0, 134.8, 135.3, 147.8, 169.6, 173.0, 173.9; **HRMS (ESI)** *m/z* $[M+H]^+$ calcd for $C_{38}H_{58}N_6O_6$ 695.4491, found 695.4527; **HPLC** (gradient A), t_R = 12.39 min, 98.8% purity.

4-(1-{6-[2-(2-{2-[(3*r*,5*r*,7*r*)-Adamantan-1-yl]acetamido}ethoxy)ethoxy]hexyl}-1*H*-1,2,3-triazol-4-yl)-*N*-[4-(hydroxycarbamoyl)benzyl]benzamide (3b)

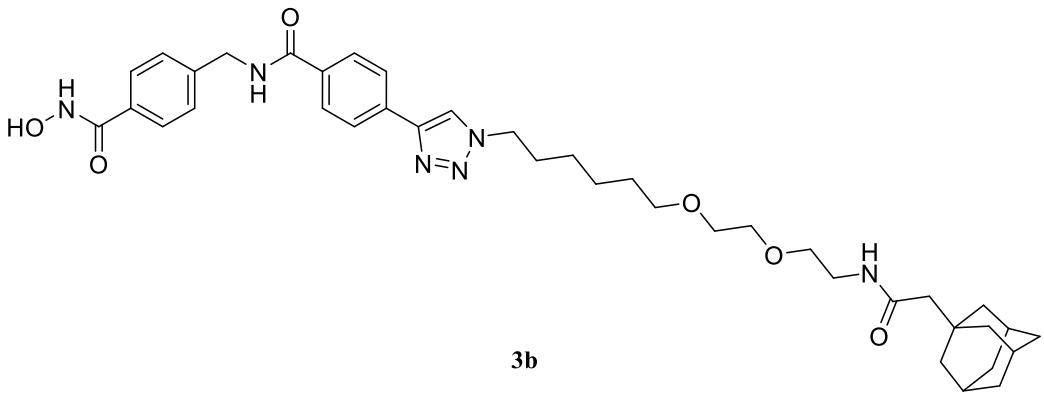

3b

Synthesized according to **general procedure C** using **HAIR A** (219 mg, 0,09 mmol, 1.00 eq), 4-ethynylbenzoic acid (28 mg, 0.18 mmol, 2.00 eq), HATU (104 mg, 0.27 mmol, 3.00 eq), HOBt*H_2O (42 mg, 0.27 mmol, 3.00 eq), EDC*HCl (53 mg, 0.27 mmol, 3.00 eq) and DIPEA (80 µL, 0.46 mmol, 5.00 eq) in DMF (400 µL). The *Huisgen* 1,3-cycloaddition was performed according to **general procedure D** using the azide **10** (75 mg, 0.18 mmol, 2.00 eq), TBTA (12 mg, 0.02 mmol, 0.25 eq), 0.1 M $CuSO_4$ solution (229 µL, 0.02 mmol, 0.25 eq), 0.2 M ascorbic acid solution (229 µL, 0.05 mmol, 0.50 eq) and *t*-BuOH (1 mL). Cleavage according to **general procedure E** and purification by preparative HPLC afforded **3b** as an amorphous withe powder (39.7 mg, 57 µmol).

Yield: 62%; **^{1}H NMR** (600 MHz, DMSO-d_6) δ = 1.24 – 1.37 (m, 4H), 1.44 – 1.51 (m, 2H), 1.51 – 1.57 (m, 9H), 1.59 – 1.65 (m, 3H), 1.81 (s, 2H), 1.83 – 1.91 (m, 5H), 3.14 – 3.19 (m, 2H), 3.35 (t, *J* = 6.5 Hz, 2H), 3.38 (t, *J* = 5.9 Hz, 2H), 3.43 – 3.46 (m, 2H), 3.46 – 3.50 (m, 2H), 4.40 (t, *J* = 7.1 Hz, 2H), 4.50 – 4.56 (m, 2H), 7.40 (d, *J* = 8.1 Hz, 2H), 7.66 (t, *J* = 5.7 Hz, 1H), 7.72 (d, *J* = 8.2 Hz, 2H), 7.95 (d, *J* = 8.3 Hz, 2H), 7.99 (d, *J* = 8.4 Hz, 2H), 8.69 (s, 1H), 9.11 (t, *J* = 6.0 Hz, 1H), 11.16 (s, 1H) C-N*H*-OH signal could not be detected due to solvent exchange; **^{13}C NMR** (151 MHz, DMSO-d_6) δ = 25.1, 25.7, 28.0, 29.0, 29.5, 32.1, 36.4, 38.3, 42.1, 42.4, 49.5, 50.0, 69.2, 69.4, 69.5, 70.2, 122.0, 124.8, 126.9, 127.1, 127.9, 131.3, 133.2, 133.6, 142.9, 145.5, 164.1, 165.8, 169.9; **HRMS (ESI)** *m/z* $[M+H]^+$ calcd for $C_{39}H_{52}N_6O_6$ 701.4021, found 701.4053; **HPLC** (gradient A), t_R = 12.35 min, 98.4% purity.

4-[(1-{6-[2-(2-{2-[(3*r*,5*r*,7*r*)-Adamantan-1-yl]acetamido}ethoxy)ethoxy]hexyl}-1*H*-1,2,3-triazol-4-yl)methoxy]-*N*-[7-(hydroxyamino)-7-oxoheptyl]benzamide (3c)

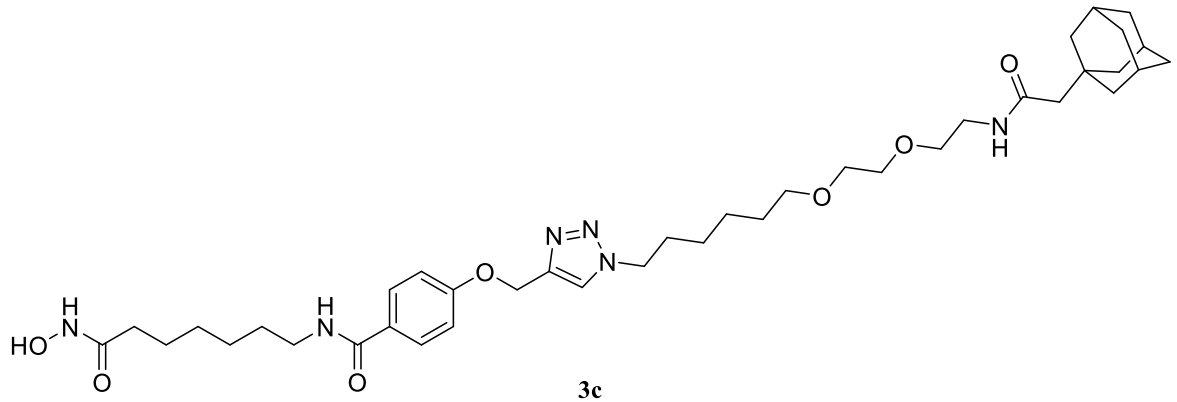

3c

Synthesized according to **general procedure C** using **HAIR D** (200 mg, 0,08 mmol, 1 eq), **12** (29 mg, 0.17 mmol, 2.00 eq), HATU (95 mg, 0.25 mmol, 3.00 eq), HOBt*H_2O (38 mg, 0.25 mmol, 3.00 eq), EDC*HCl (49 mg, 0.25 mmol, 3.00 eq) and DIPEA (73 µL, 0.42 mmol, 5.00 eq) in DMF (300 µL). The *Huisgen* 1,3-cycloaddition was performed according to **general procedure D** using the azide **10** (63 mg, 0.15 mmol, 2.00 eq), TBTA (10 mg, 0.02 mmol, 0.25 eq), 0.1 M $CuSO_4$ solution (192 µL, 0.02 mmol, 0.25 eq), 0.2 M ascorbic acid solution (192 µL, 0.04 mmol, 0.50 eq) and *t*-BuOH (800 µL). Cleavage according to **general procedure E** and purification by preparative HPLC afforded **3c** as an amorphous withe powder (35.3 mg, 49 µmol).

Yield: 63%; **^{1}H NMR** (600 MHz, methanol-d_4) δ = 1.27 – 1.34 (m, 2H), 1.35 – 1.43 (m, 6H), 1.52 – 1.58 (m, 2H), 1.58 – 1.66 (m, 13H), 1.69 – 1.74 (m, 3H), 1.88 – 1.95 (m, 7H), 2.10 (t, *J* = 7.4 Hz, 2H), 3.35 (q, *J* = 5.9 Hz, 4H), 3.45 (t, *J* = 6.5 Hz, 2H), 3.52 (t, *J* = 5.5 Hz, 2H), 3.54 – 3.60 (m, 4H), 4.42 (t, *J* = 7.0 Hz, 2H), 5.23 (s, 2H), 7.07 (d, *J* = 8.8 Hz, 2H), 7.80 (d, *J* = 8.8 Hz, 2H), 8.09 (s, 1H), C-N*H*-O*H* signals and CO-N*H* signals could not be detected due to solvent exchange; **^{13}C NMR** (151 MHz, methanol-d_4) δ = 26.5, 26.6, 27.1, 27.6, 29.8, 30.1, 30.3, 30.4, 31.1, 33.7, 33.8, 37.9, 40.2, 40.9, 43.7, 51.4, 51.8, 62.4, 70.6, 71.1, 71.1, 72.1, 115.6, 125.4, 128.4, 130.1, 144.5, 162.3, 169.6, 173.0, 173.9; **HRMS (ESI)** *m/z* $[M+H]^+$ calcd for $C_{39}H_{60}N_6O_7$ 725.4596, found 725.4618; **HPLC** (gradient A), t_R = 12.30 min, 97.8% purity.

4-[(1-{6-[2-(2-{2-[(3*r*,5*r*,7*r*)-Adamantan-1-yl]acetamido}ethoxy)ethoxy]hexyl}-1*H*-1,2,3-triazol-4-yl)methoxy]-*N*-[4-(hydroxycarbamoyl)benzyl]benzamide (3d)

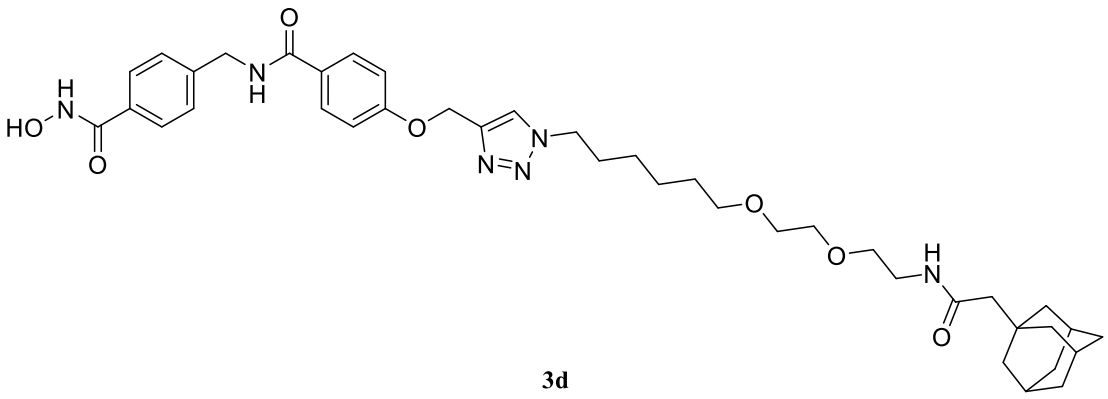

3d

Synthesized according to **general procedure C** using **HAIR A** (200 mg, 0,08 mmol, 1.00 eq), **12** (29 mg, 0.17 mmol, 2.00 eq), HATU (95 mg, 0.25 mmol, 3.00 eq), HOBt*H_2O (38 mg, 0.25 mmol, 3.00 eq), EDC*HCl (48 mg, 0.25 mmol, 3.00 eq) and DIPEA (73 µL, 0.42 mmol, 5.00 eq) in DMF (300 µL). The *Huisgen* 1,3-cycloaddition was performed according to **general procedure D** using the azide **10** (61 mg, 0.15 mmol, 2.00 eq), TBTA (10 mg, 0.02 mmol, 0.25 eq), 0.1 M $CuSO_4$ solution (187 µL, 0.02 mmol, 0.25 eq), 0.2 M ascorbic acid solution (187 µL, 0.04 mmol, 0.50 eq) and *t*-BuOH (800 µL). Cleavage according to **general procedure E** and purification by preparative HPLC afforded **3d** as an amorphous withe powder (48.6 mg, 66 µmol) in >95% purity.

Yield: 89%; **^{1}H NMR** (600 MHz, methanol-d_4) δ = 1.26 – 1.33 (m, 2H), 1.34 – 1.41 (m, 2H), 1.51 – 1.57 (m, 2H), 1.58 – 1.65 (m, 9H), 1.68 – 1.73 (m, 3H), 1.86 – 1.95 (m, 7H), 3.34 (t, *J* = 5.5 Hz, 2H), 3.43 (t, *J* = 6.5 Hz, 2H), 3.51 (t, *J* = 5.5 Hz, 2H), 3.53 – 3.59 (m, 4H), 4.41 (t, *J* = 7.0 Hz, 2H), 4.60 (s, 2H), 5.23 (s, 2H), 7.08 (d, *J* = 8.7 Hz, 2H), 7.42 (d, *J* = 8.1 Hz, 2H), 7.71 (d, *J* = 8.1 Hz, 2H), 7.85 (d, *J* = 8.6 Hz, 2H), 8.09 (s, 1H), C-N*H*-O*H* signals and CO-N*H* signals could not be detected due to solvent exchange; **^{13}C NMR** (151 MHz, methanol-d_4) δ = 26.5, 27.1, 30.1, 30.3, 31.1, 33.8, 37.8, 40.2, 43.6, 44.1, 51.4, 51.8, 62.4, 70.6, 71.1, 71.1, 72.1, 115.7, 125.5, 128.0, 128.3, 128.6, 130.3, 132.2, 144.4, 144.5, 162.5, 167.9, 169.6, 173; **HRMS (ESI)** *m/z* $[M+H]^+$ calcd for $C_{40}H_{54}N_6O_7$ 731.4127, found 731.4153; **HPLC** (gradient A), t_R = 12.27 min, 97.8% purity

4.4. NMR Data of compounds in biological testing

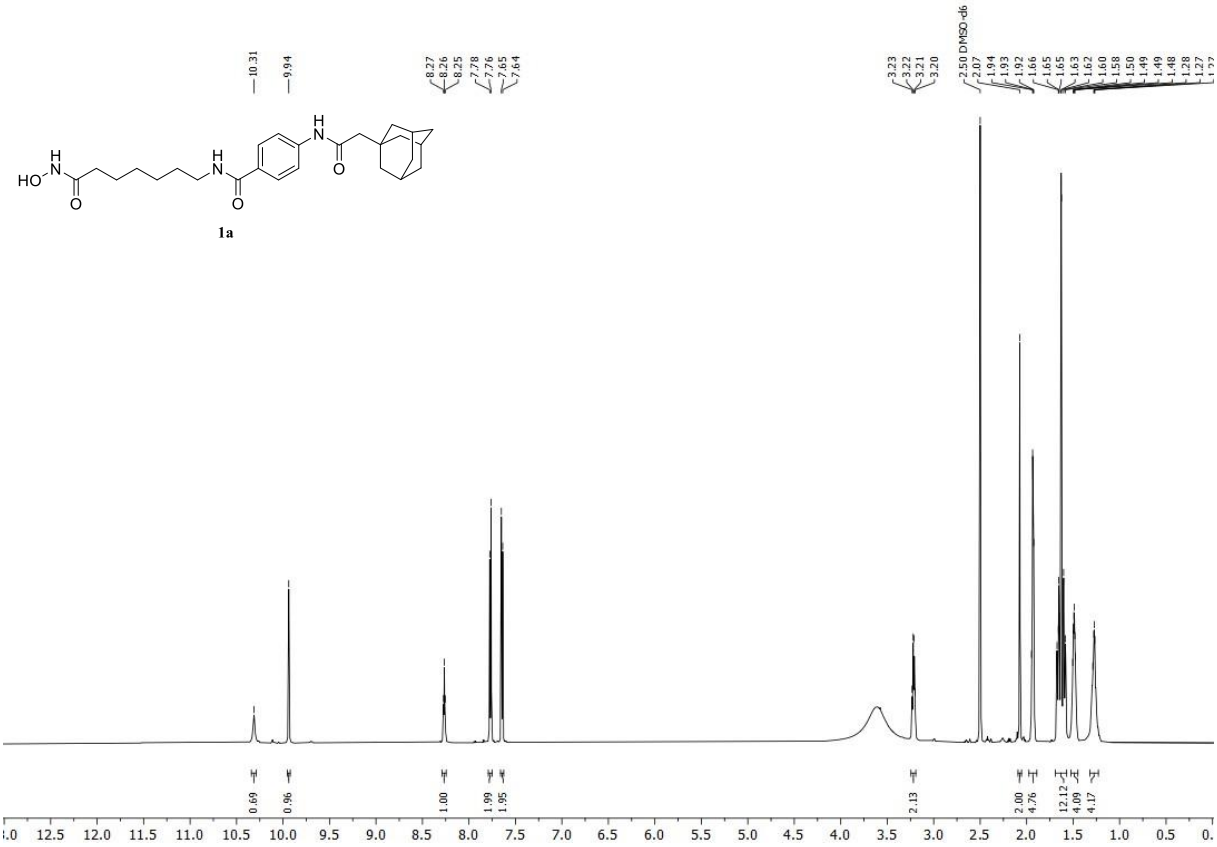

^{1}H NMR spectrum of **1a** (600 MHz, DMSO-d_6).

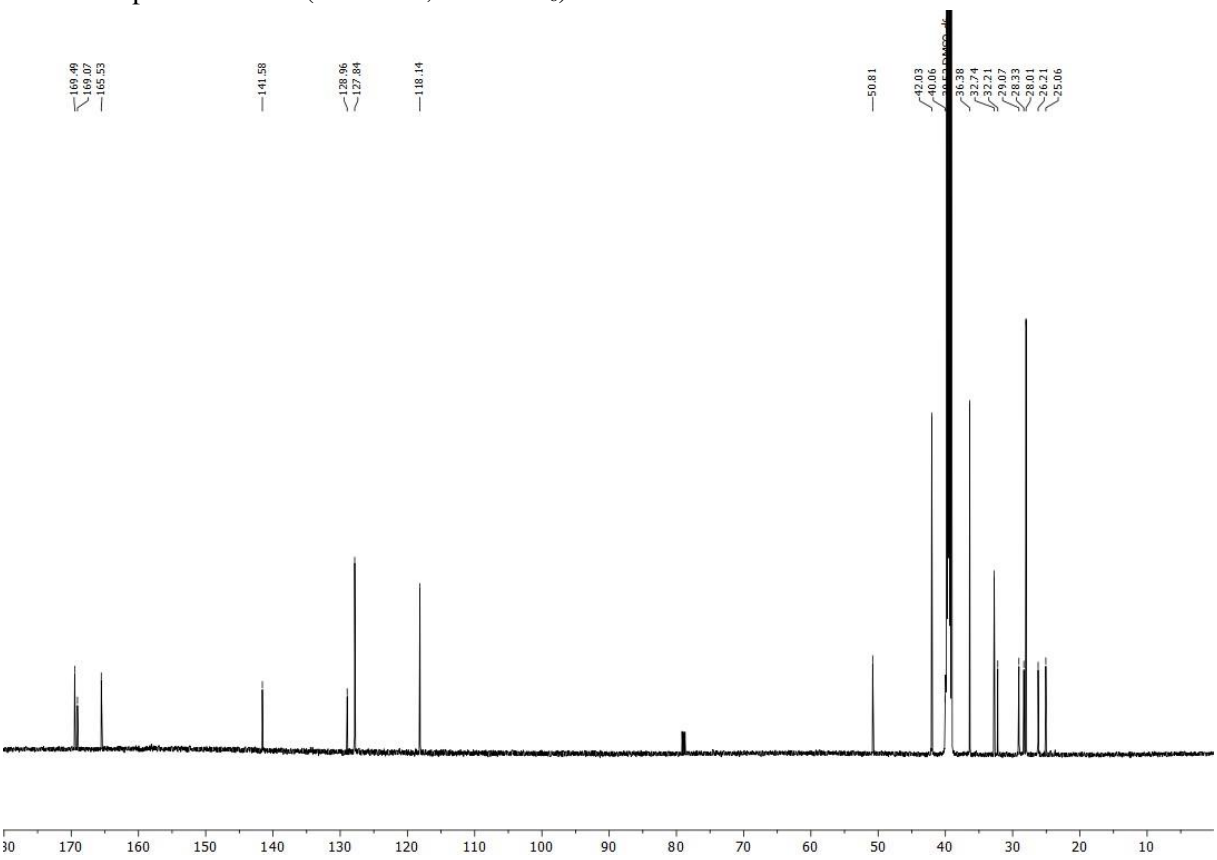

^{13}C NMR spectrum of **1a** (151 MHz, DMSO-d_6).

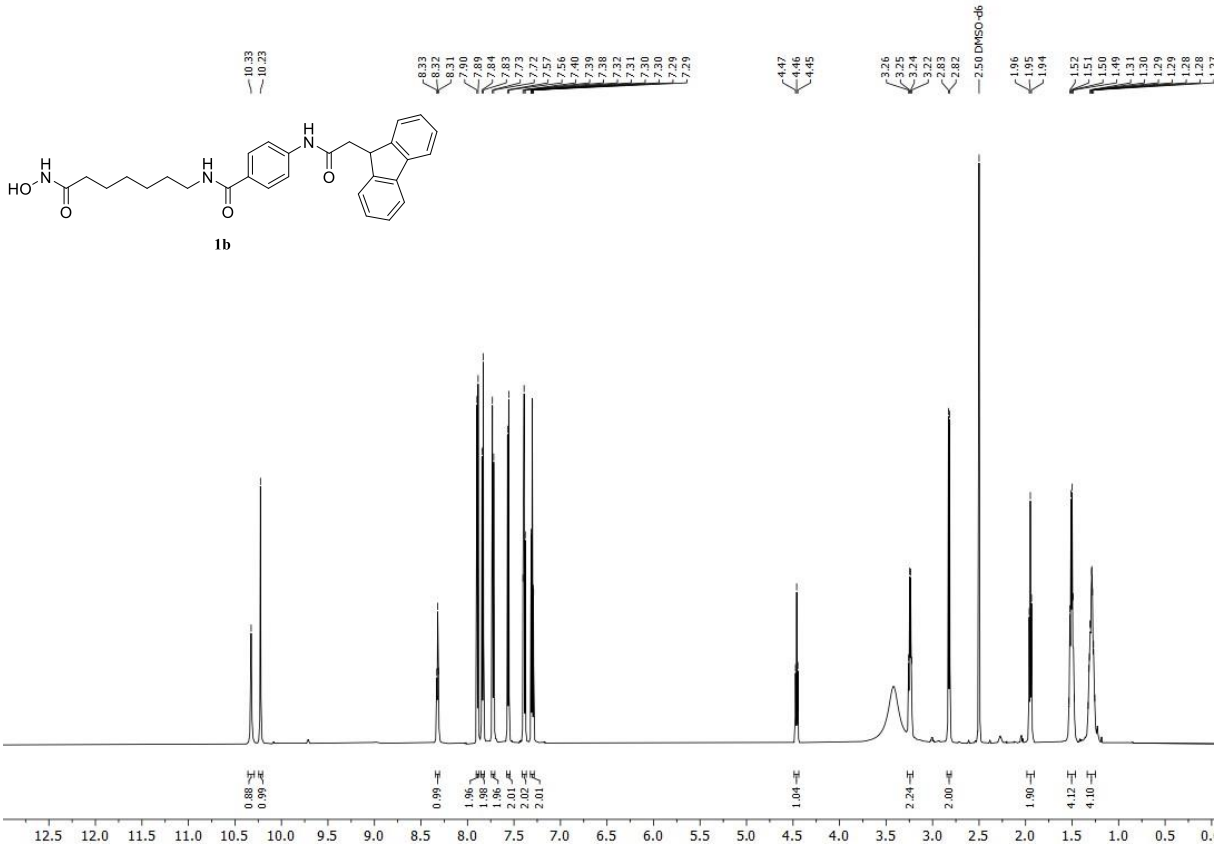

^{1}H NMR spectrum of **1b** (600 MHz, DMSO-d_6).

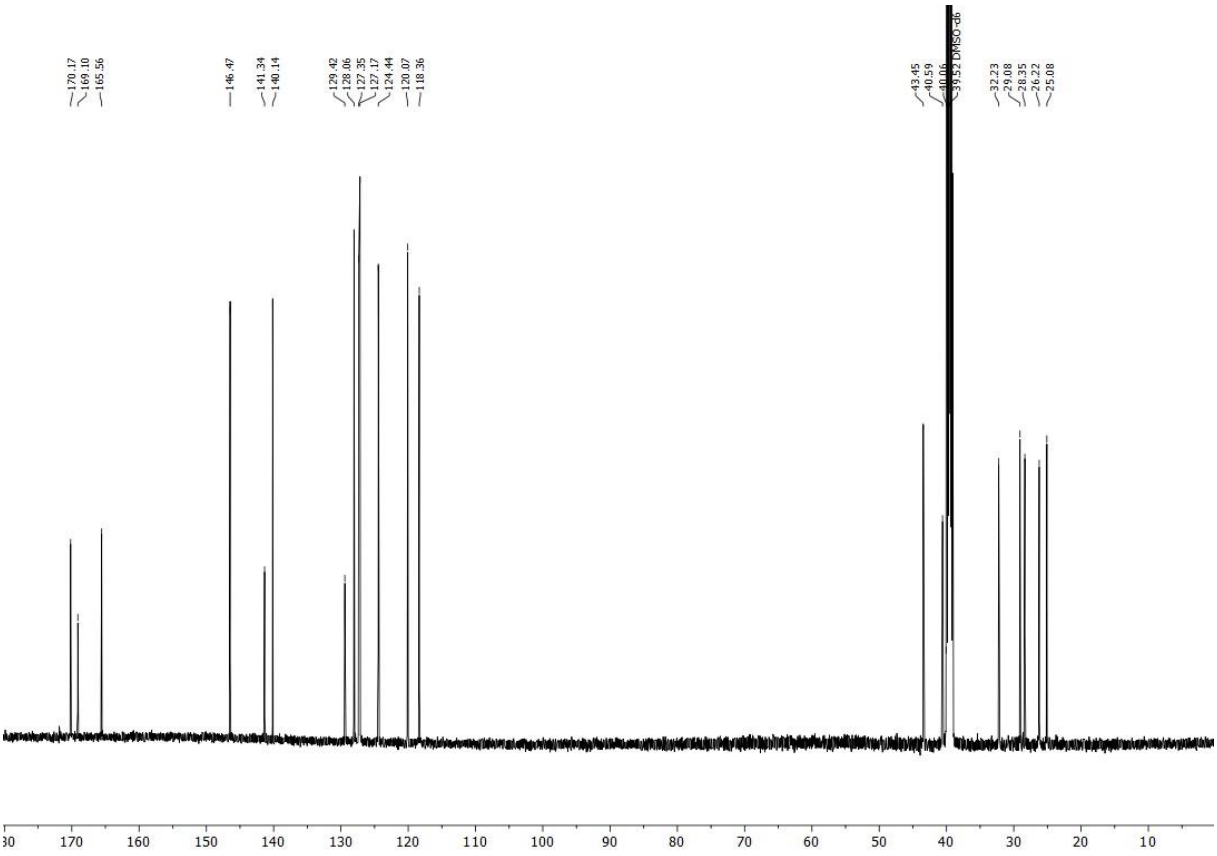

^{13}C NMR spectrum of **1b** (151 MHz, DMSO-d_6).

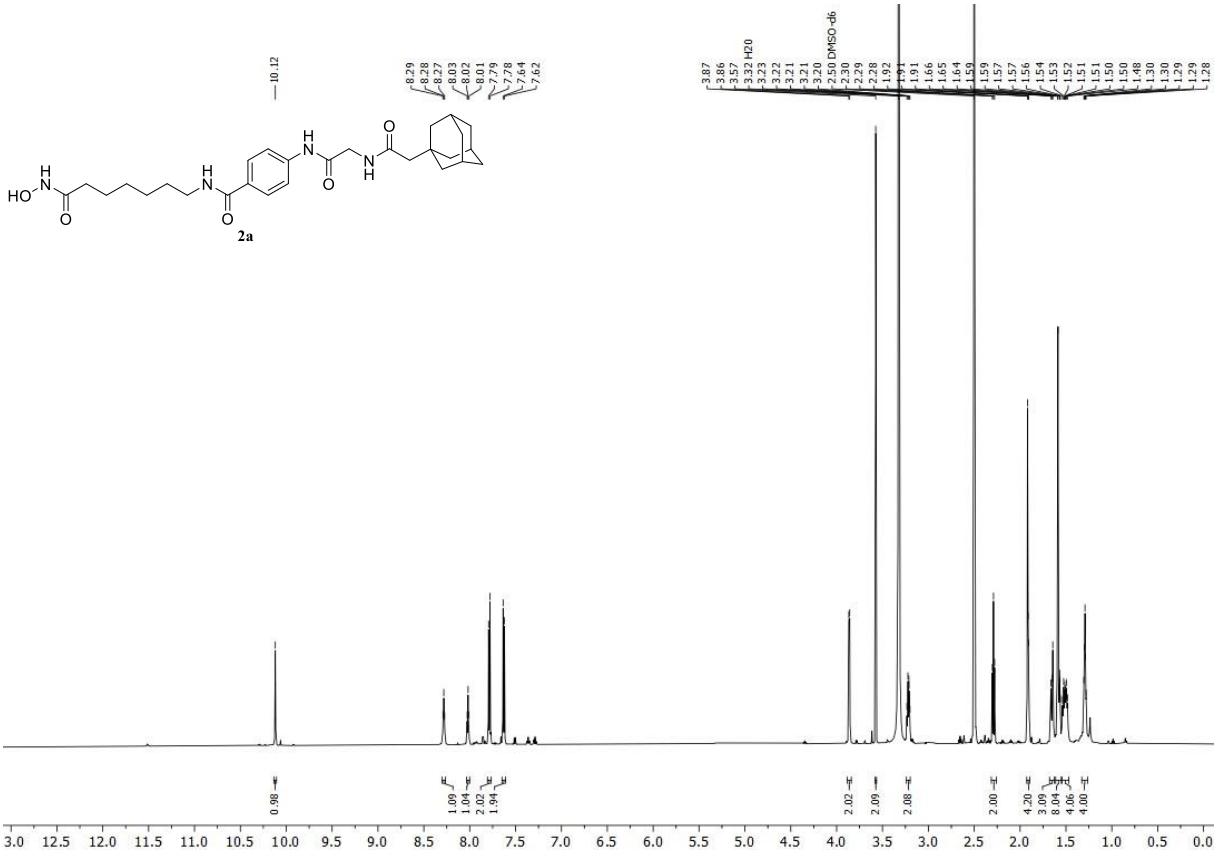

^{1}H NMR spectrum of **2a** (600 MHz, DMSO-d_6).

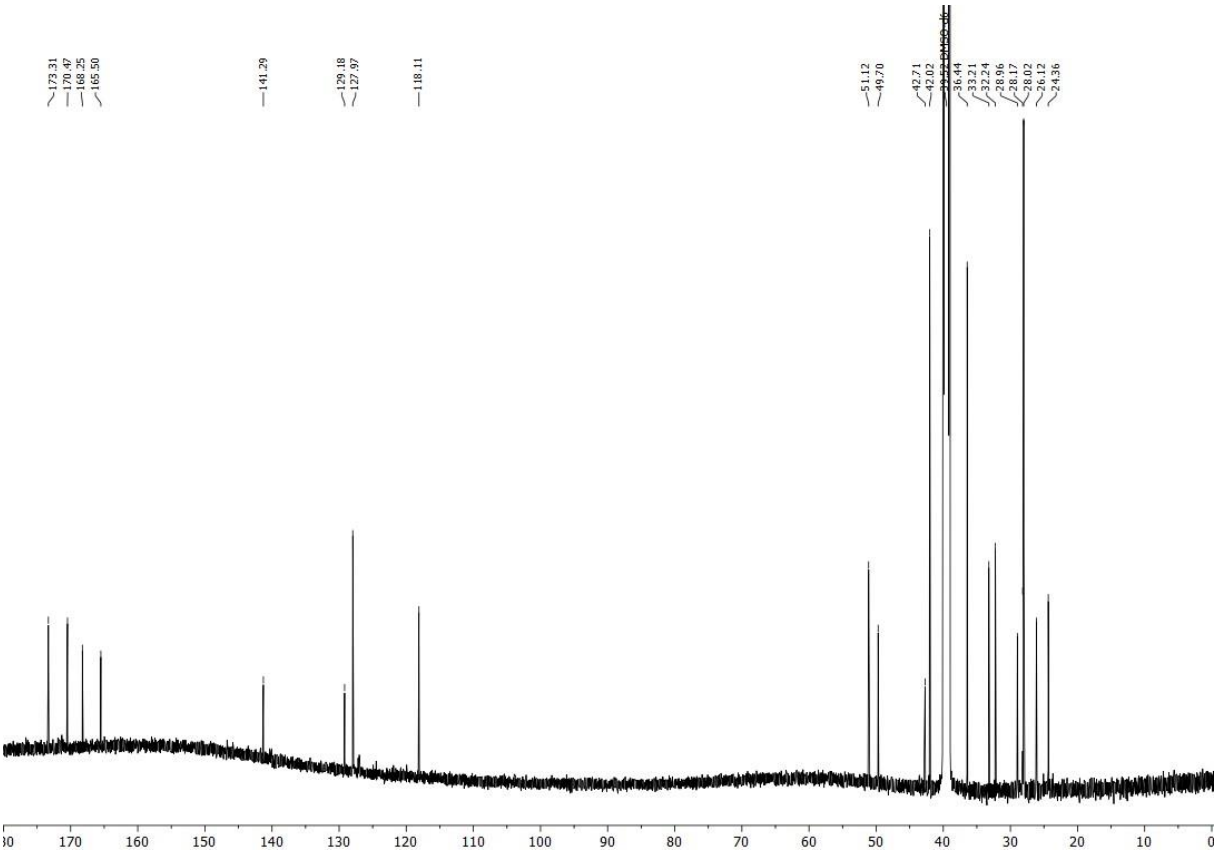

^{13}C NMR spectrum of **2a** (151 MHz, DMSO-d_6).

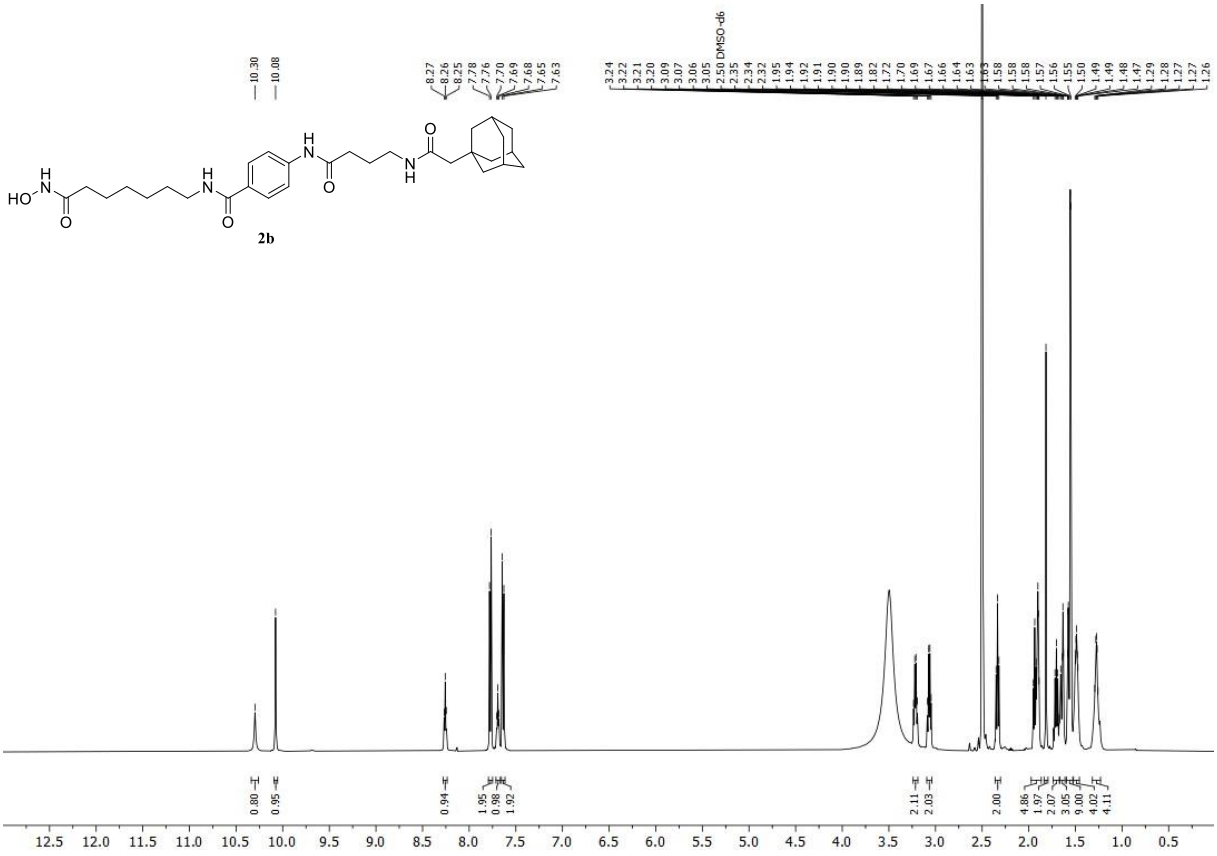

[1]H NMR spectrum of **2b** (500 MHz, DMSO-d_6).

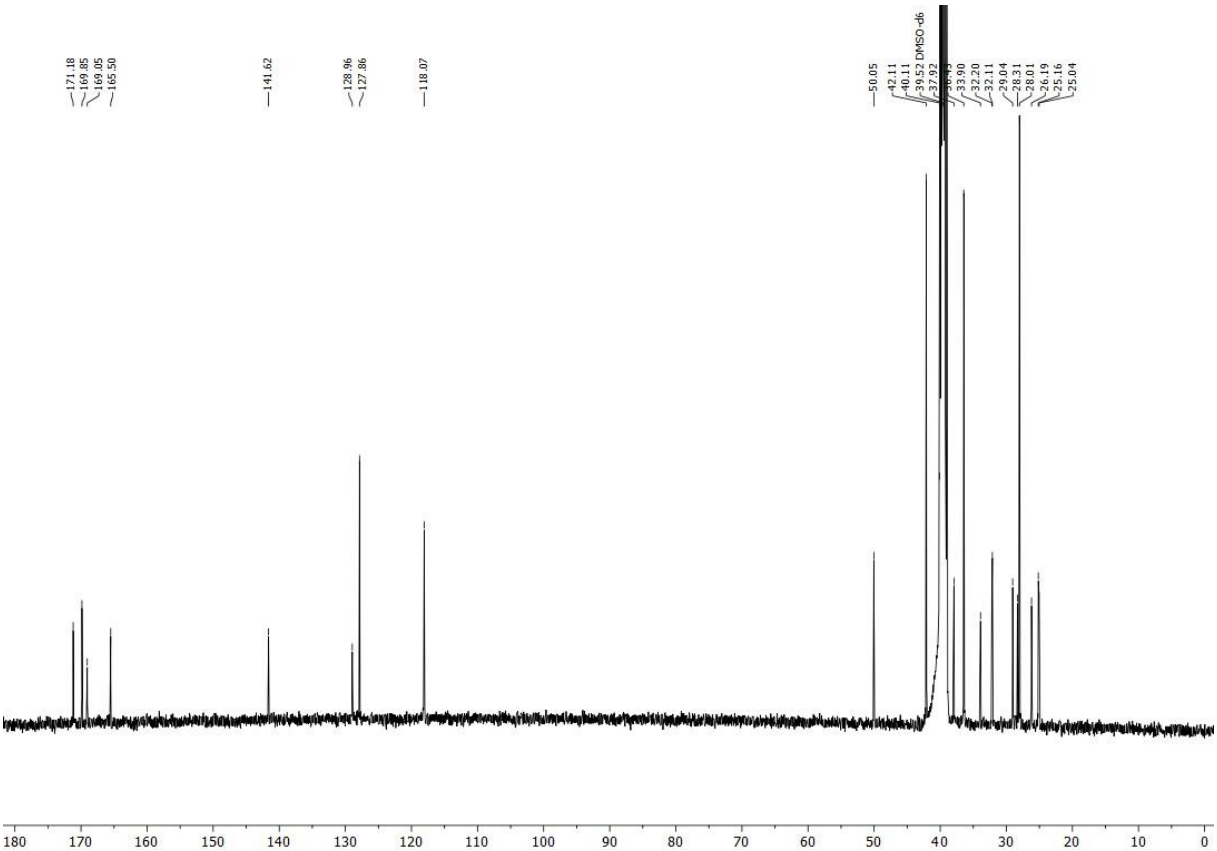

[13]C NMR spectrum of **2b** (126 MHz, DMSO-d_6).

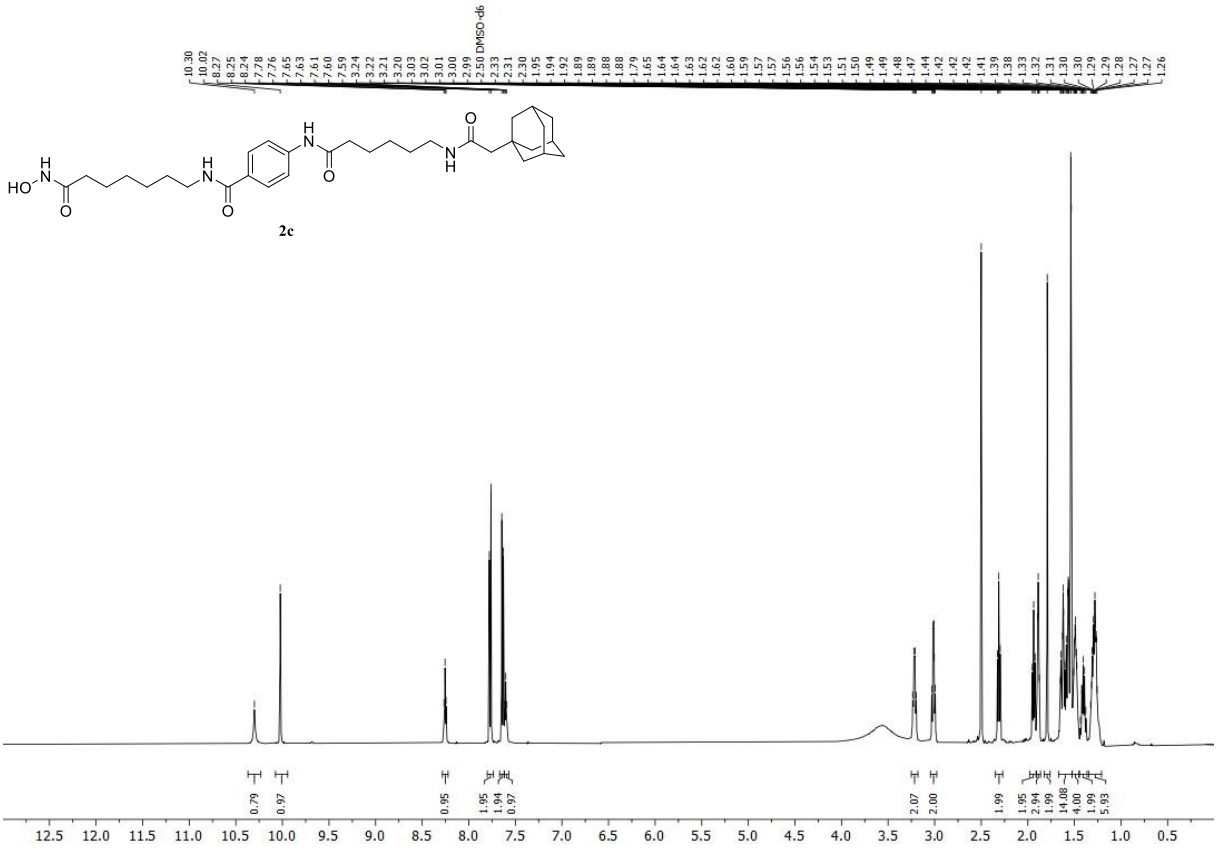

^{1}H NMR spectrum of **2c** (500 MHz, DMSO-d_6).

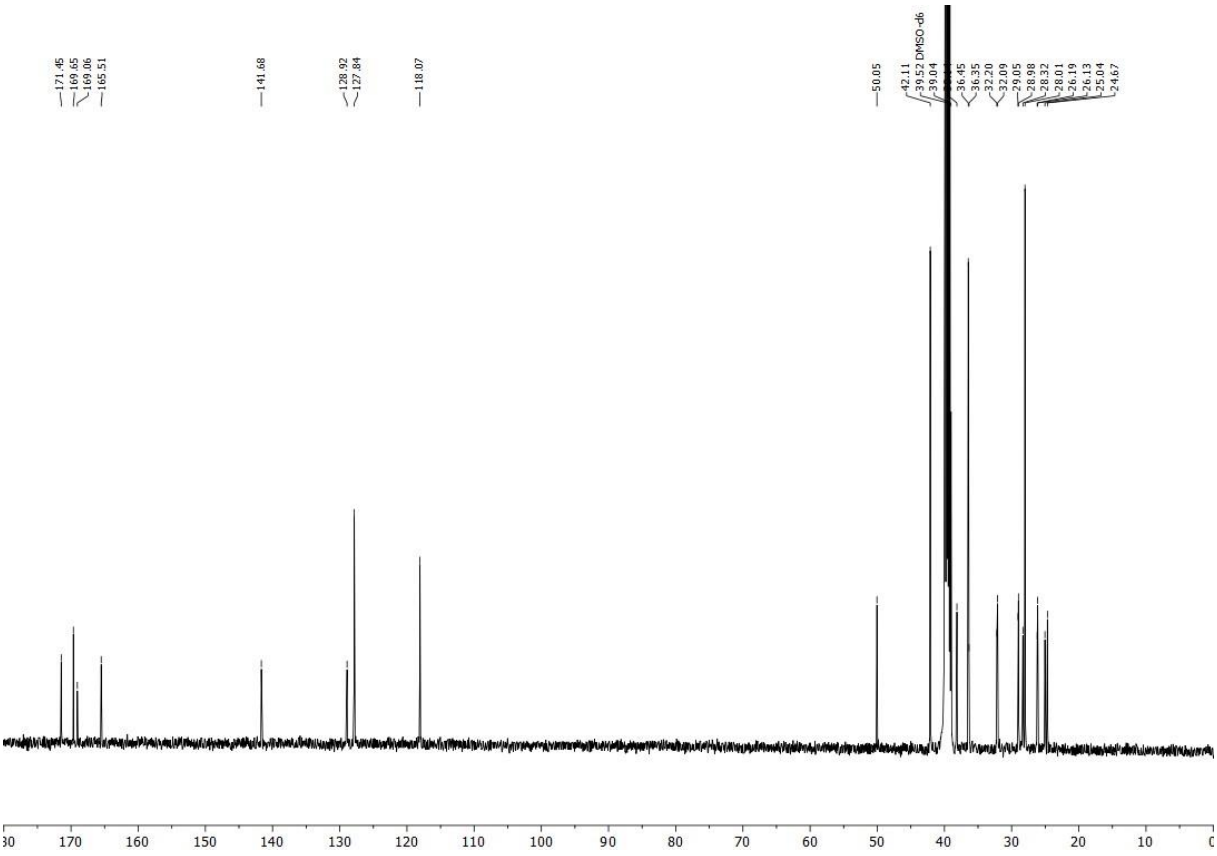

^{13}C NMR spectrum of **2c** (126 MHz, DMSO-d_6).

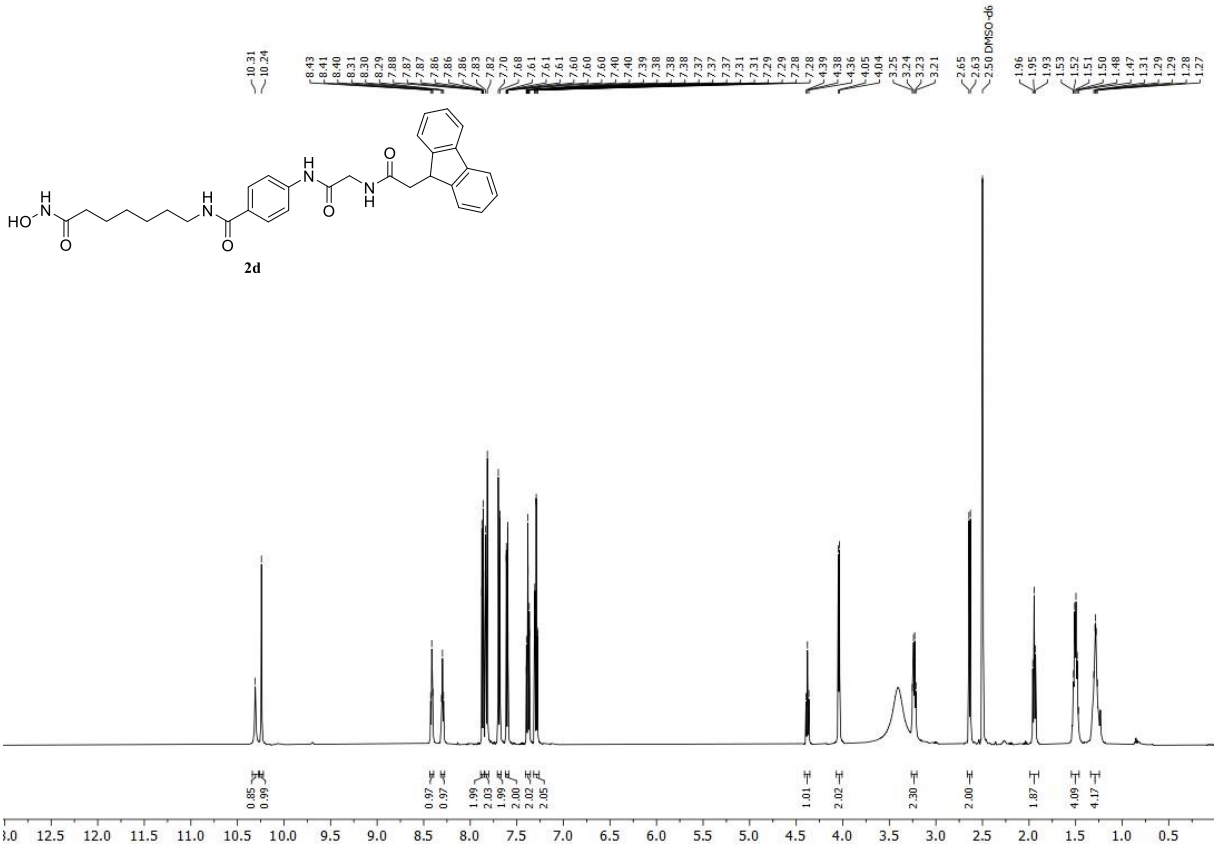

2d

^{1}H NMR spectrum of **2d** (500 MHz, DMSO-d_6).

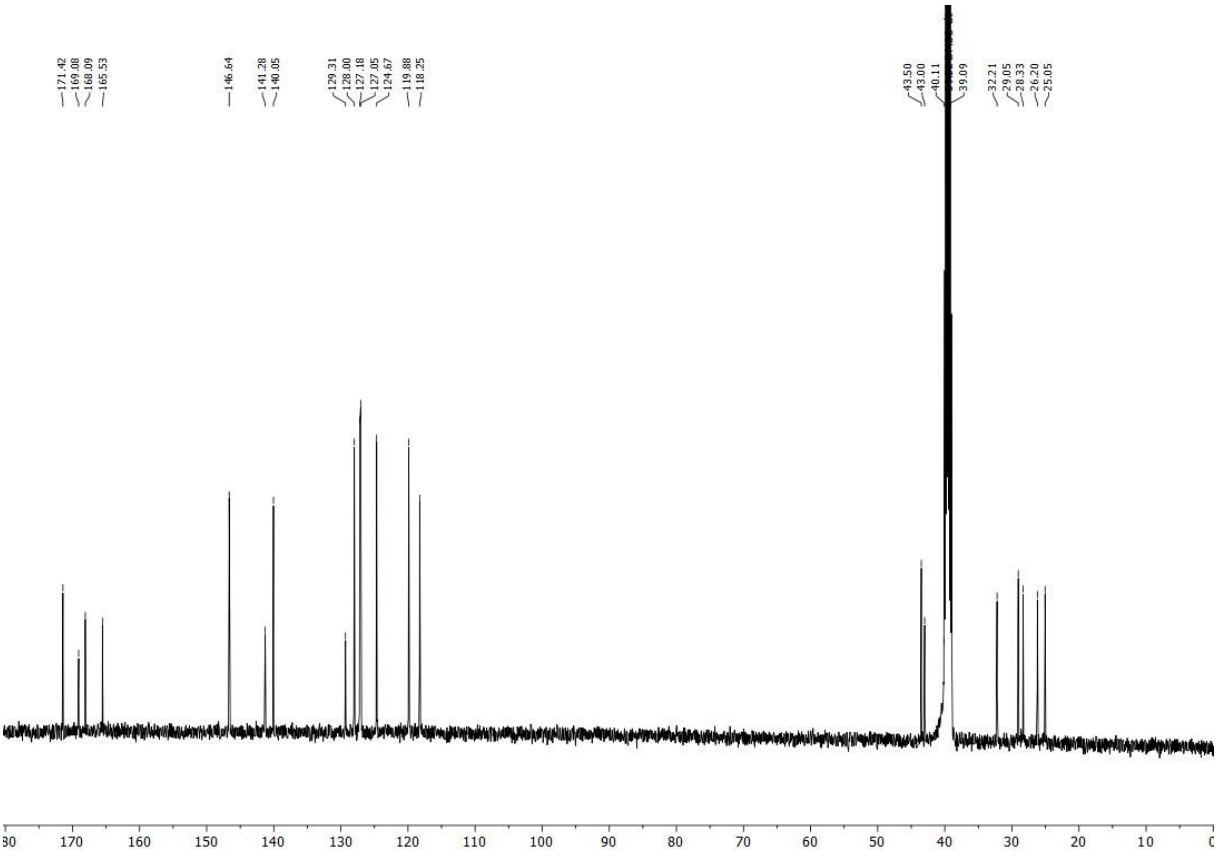

^{13}C NMR spectrum of **2d** (126 MHz, DMSO-d_6).

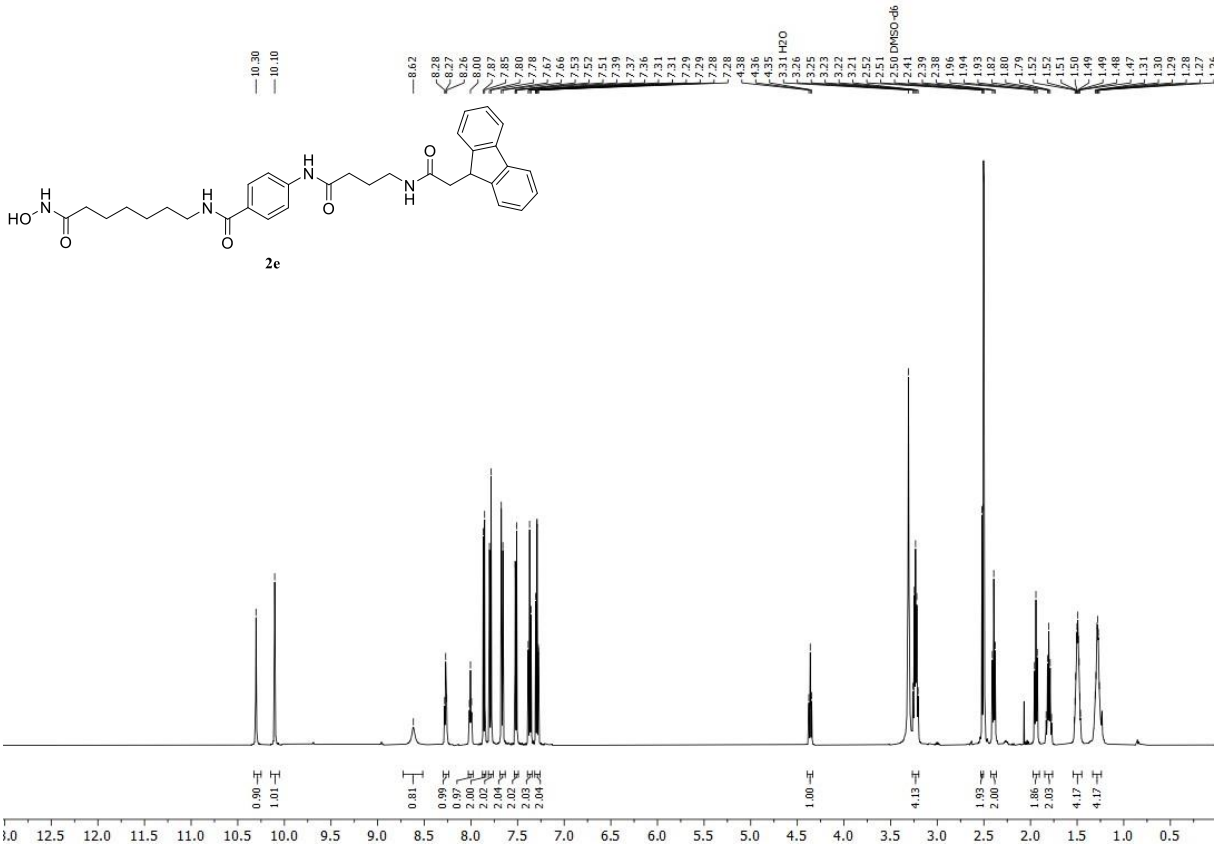

2e

^{1}H NMR spectrum of **2e** (500 MHz, DMSO-d_6).

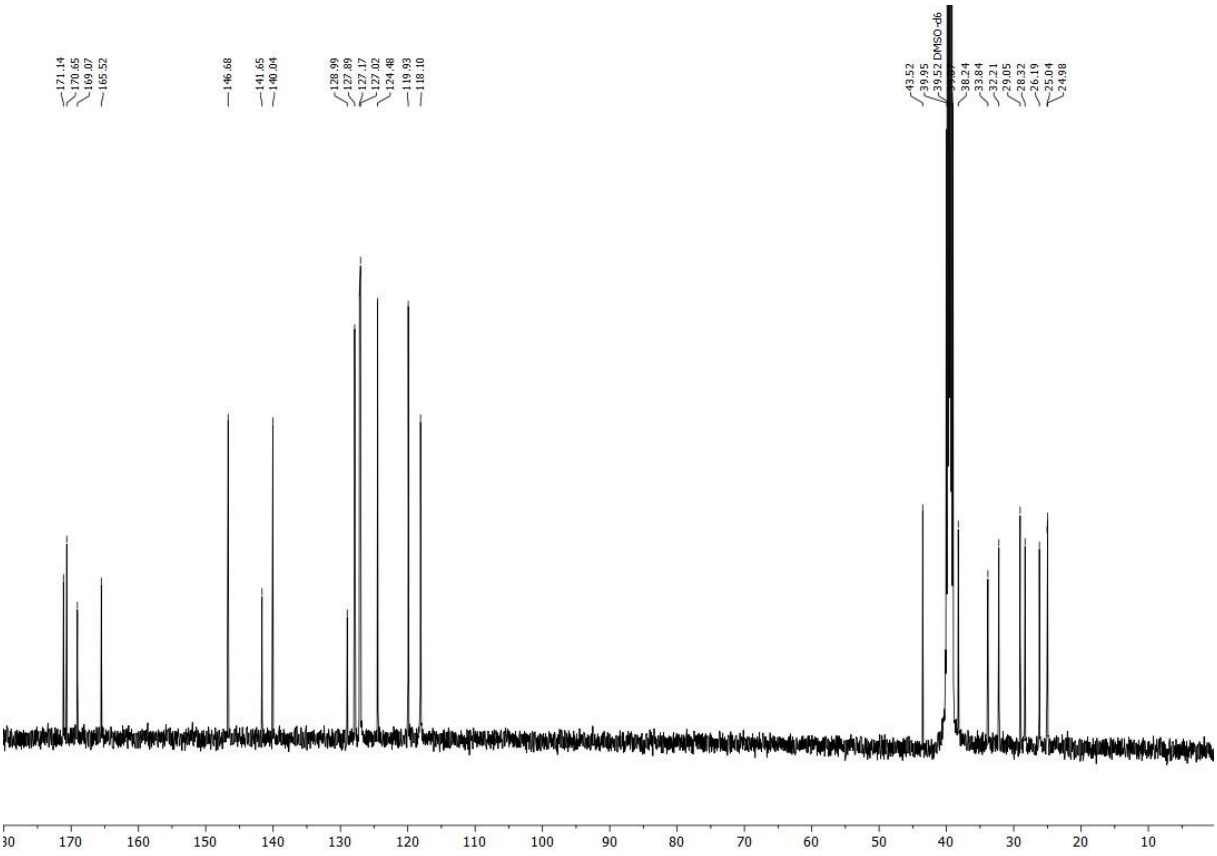

^{13}C NMR spectrum of **2e** (126 MHz, DMSO-d_6).

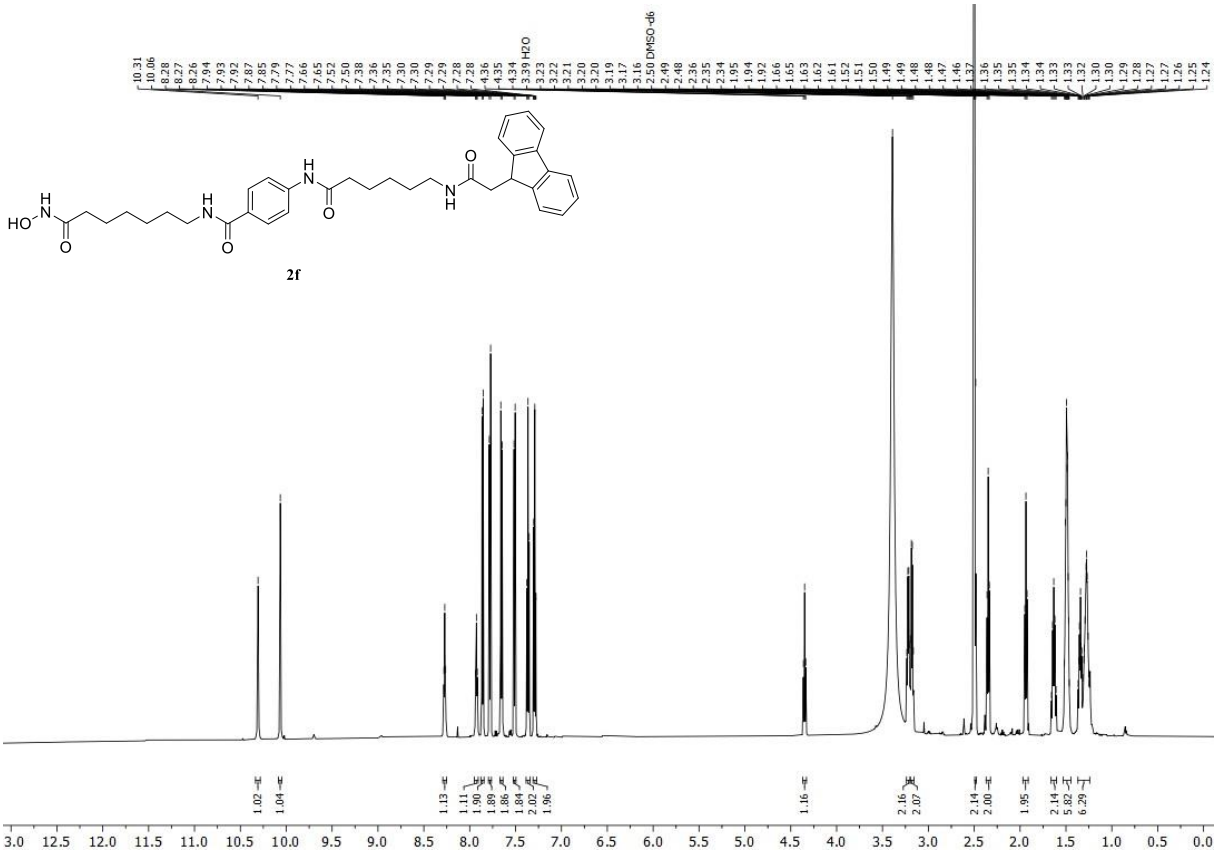

^{1}H NMR spectrum of **2f** (600 MHz, DMSO-d_6).

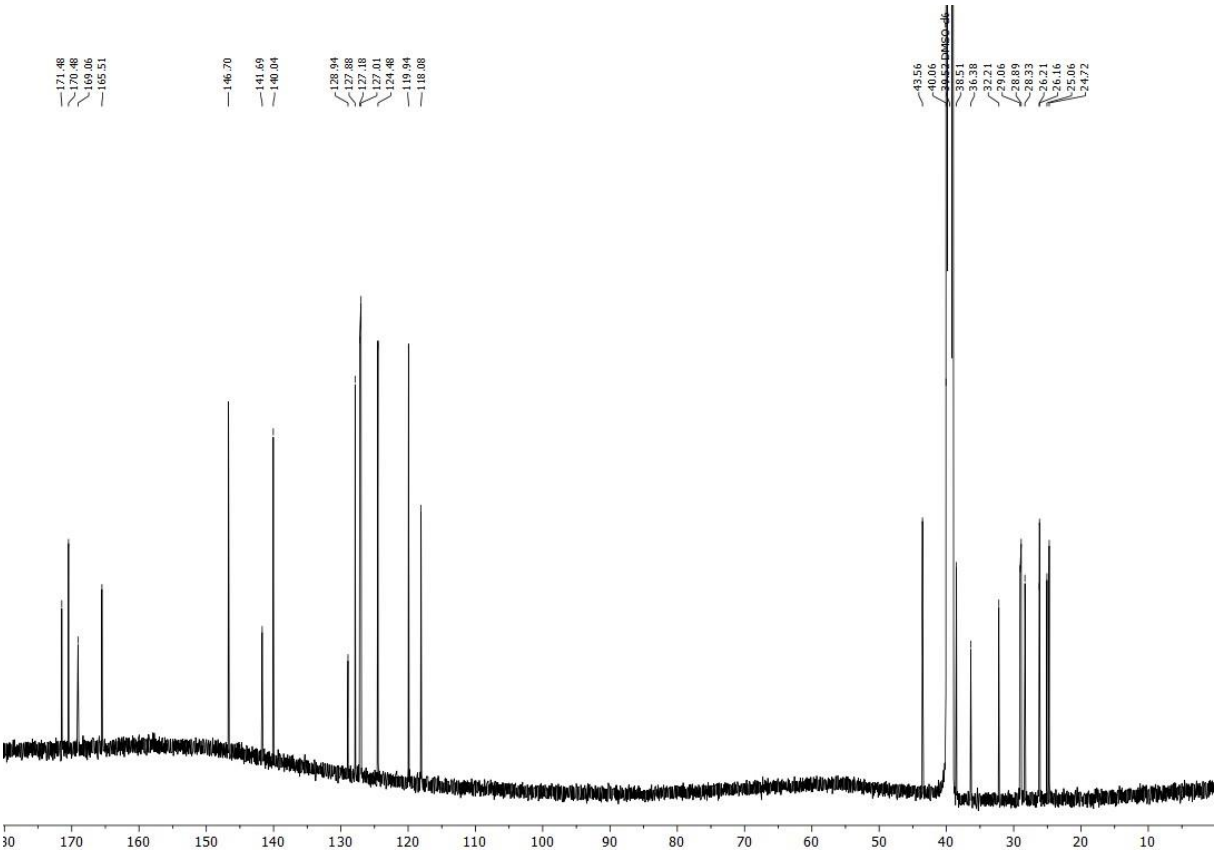

^{13}C NMR spectrum of **2f** (151 MHz, DMSO-d_6).

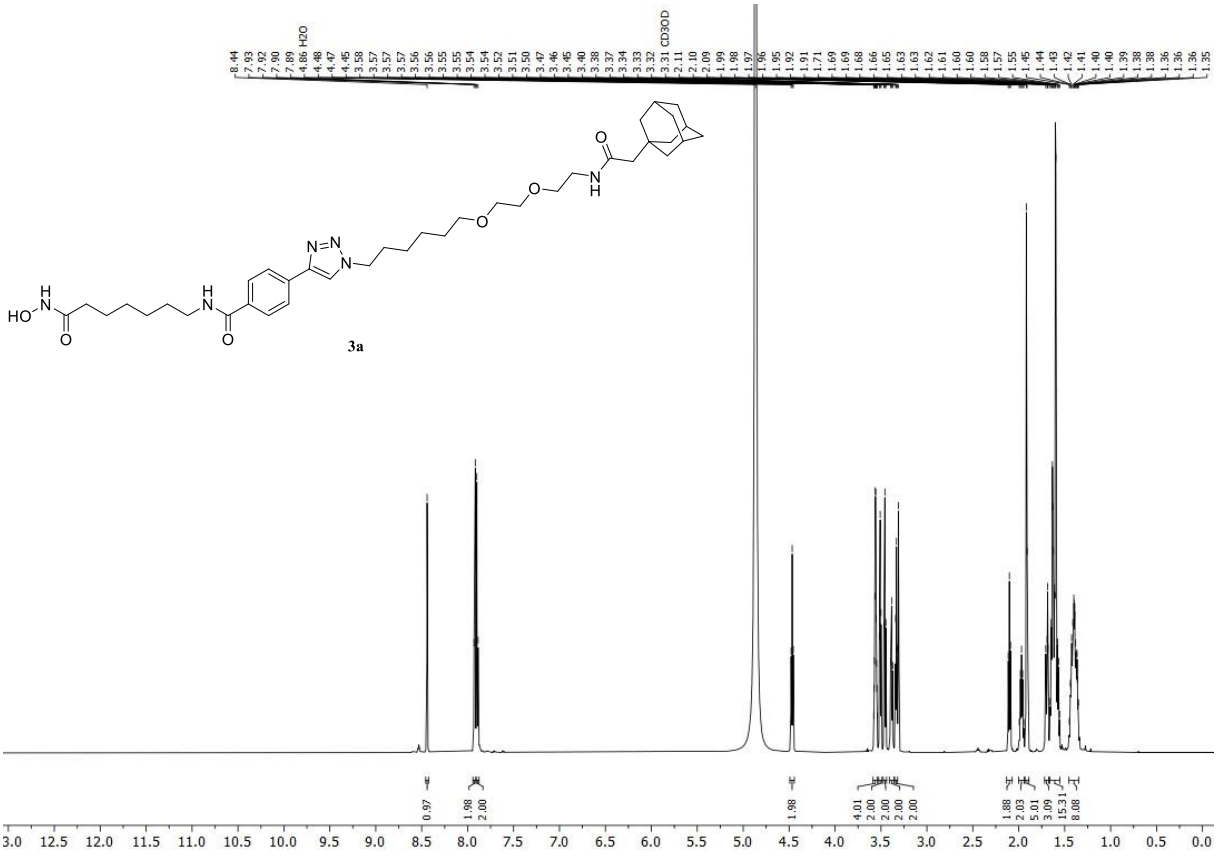

^{1}H NMR spectrum of **3a** (600 MHz, methanol-d_4).

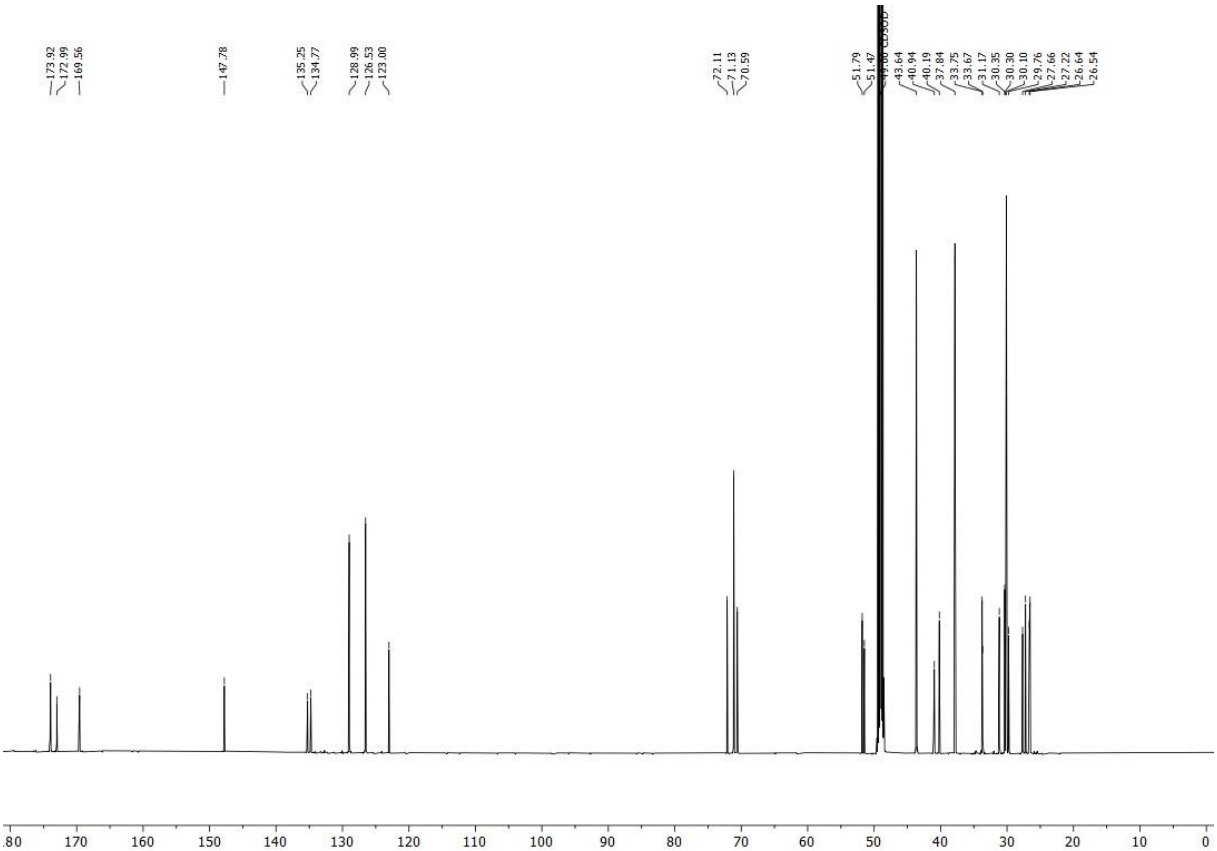

^{13}C NMR spectrum of **3a** (151 MHz, methanol-d_4).

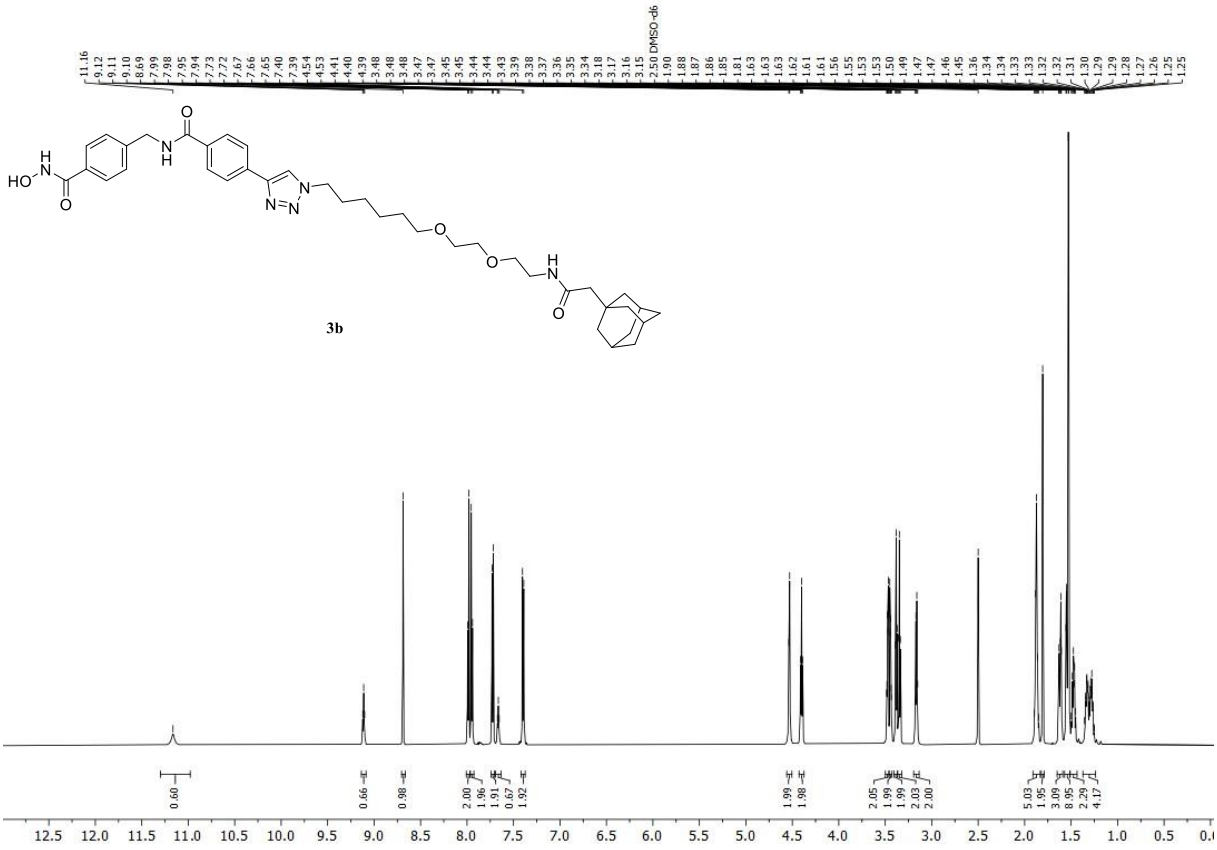

^{1}H NMR spectrum of **3b** (600 MHz, DMSO-d_6).

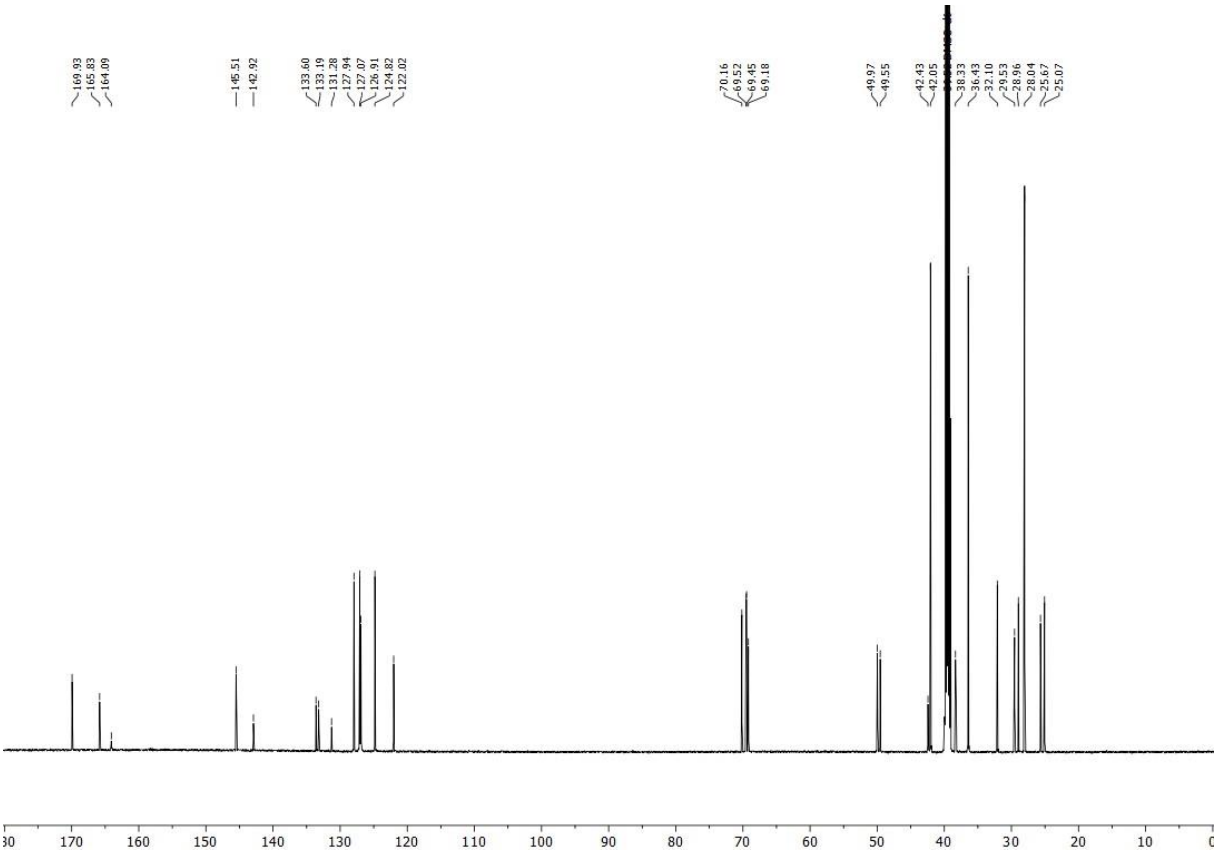

^{13}C NMR spectrum of **3b** (151 MHz, DMSO-d_6).

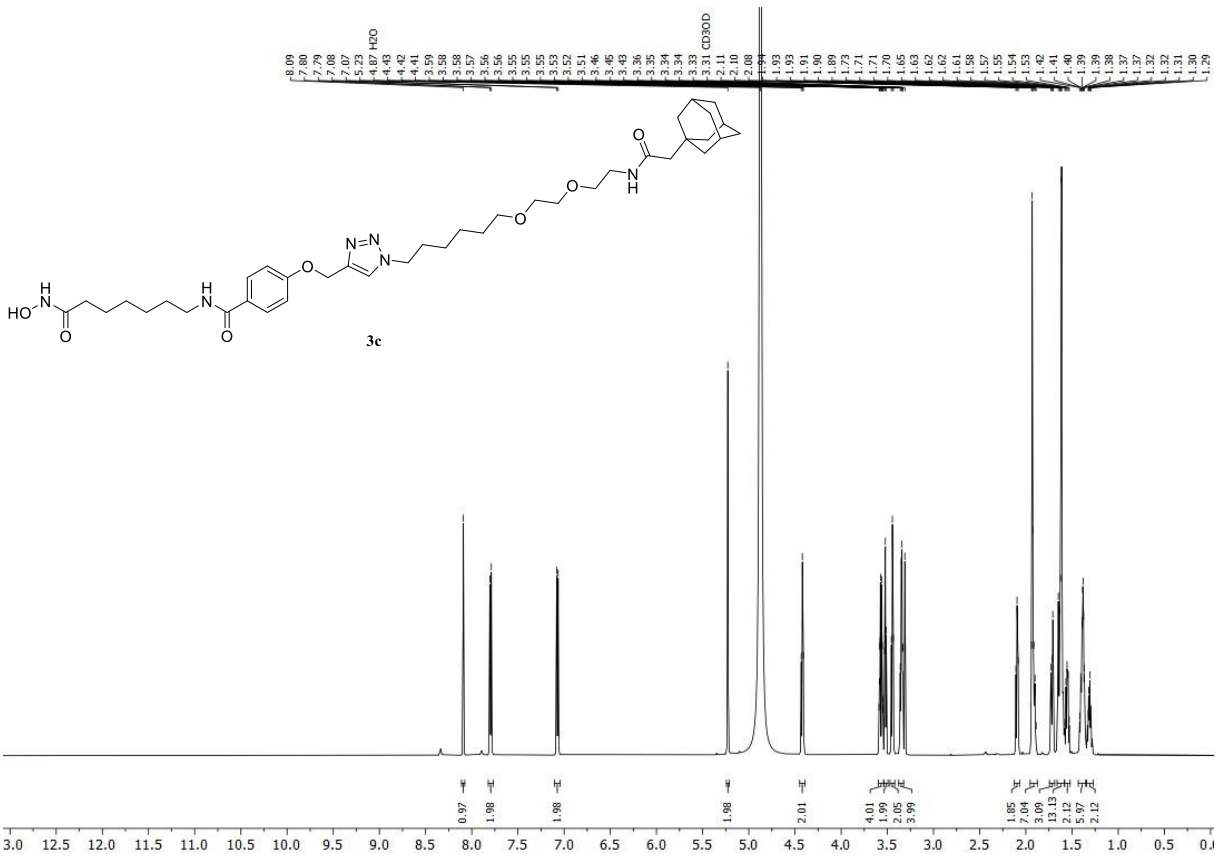

^{1}H NMR spectrum of **3c** (600 MHz, methanol-d_4).

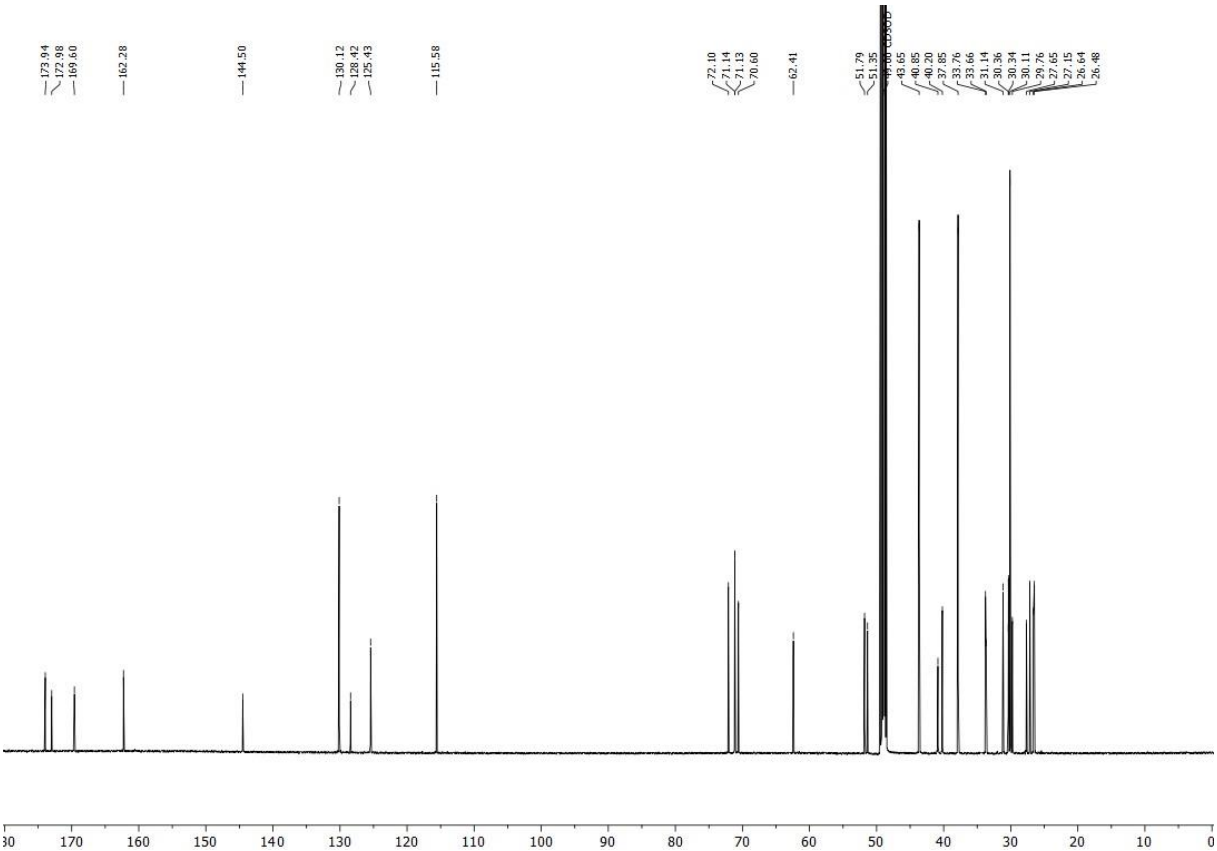

^{13}C NMR spectrum of **3c** (151 MHz, methanol-d_4).

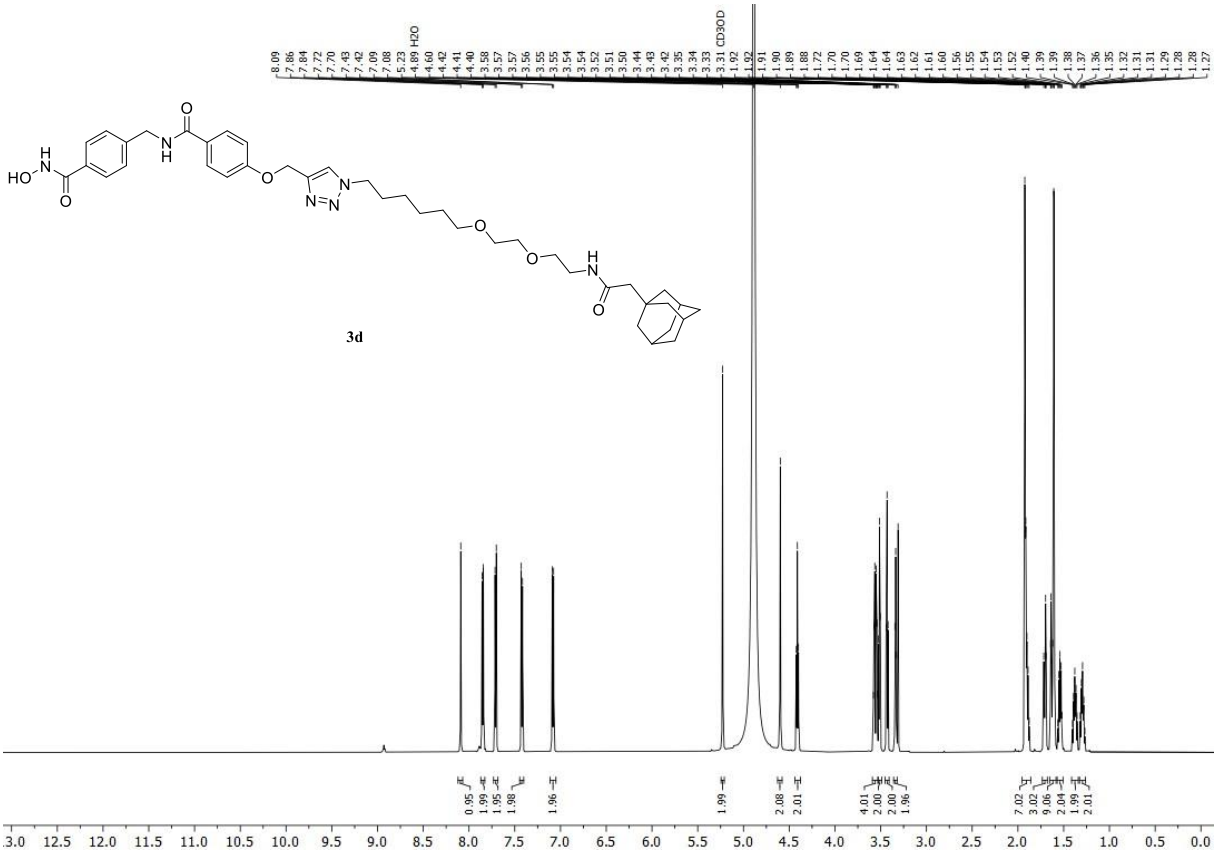

[1]H NMR spectrum of **3d** (600 MHz, methanol-d_4).

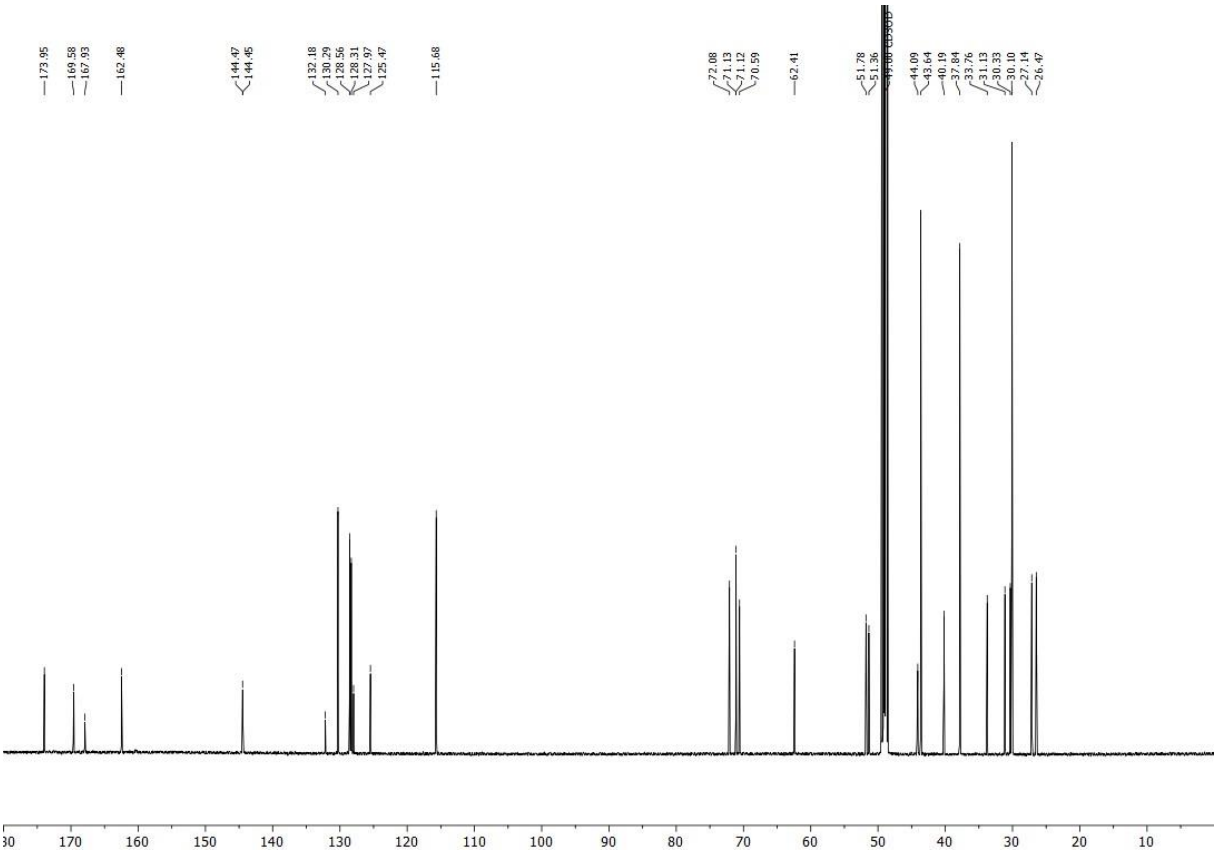

[13]C NMR spectrum of **3d** (151 MHz, methanol-d_4).

4.5. HPLC chromatograms of target compounds

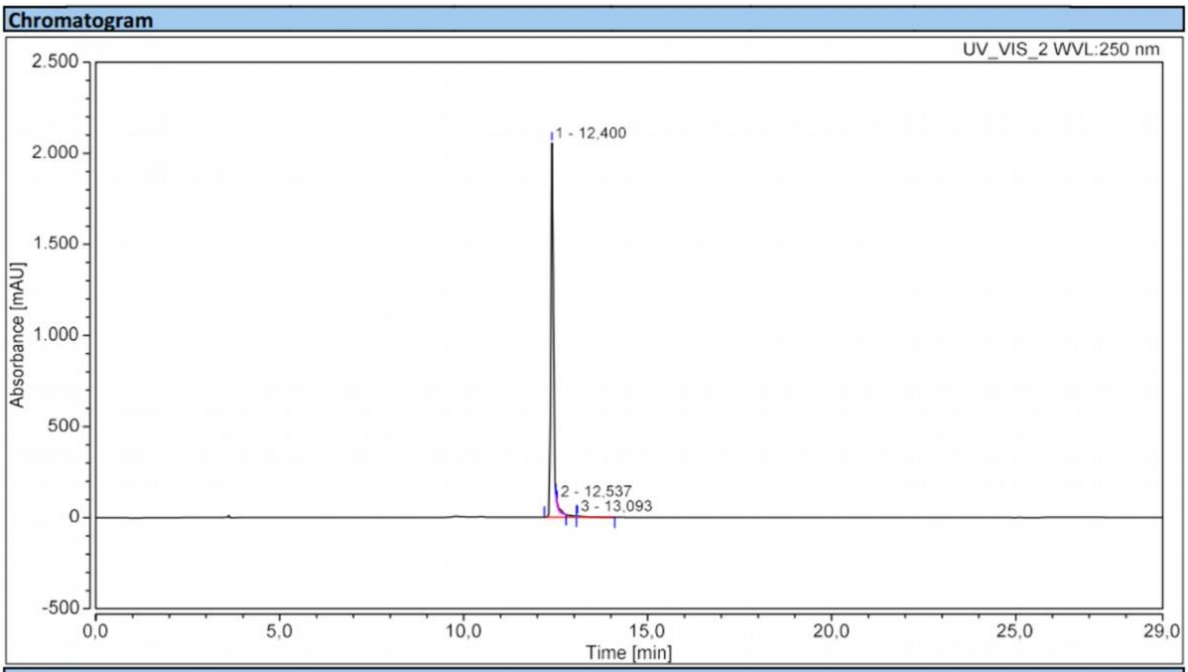

Integration Results

No.	Peak Name	Retention Time min	Area mAU*min	Height mAU	Relative Area %	Relative Height %	Amount n.a.
1		12,400	181,166	2053,321	97,73	99,00	n.a.
2		12,537	2,231	14,601	1,20	0,70	n.a.
3		13,093	1,979	6,050	1,07	0,29	n.a.
Total:			**185,377**	**2073,972**	**100,00**	**100,00**	

HPLC chromatogram of **1a** (gradient A, purity: 97.7%).

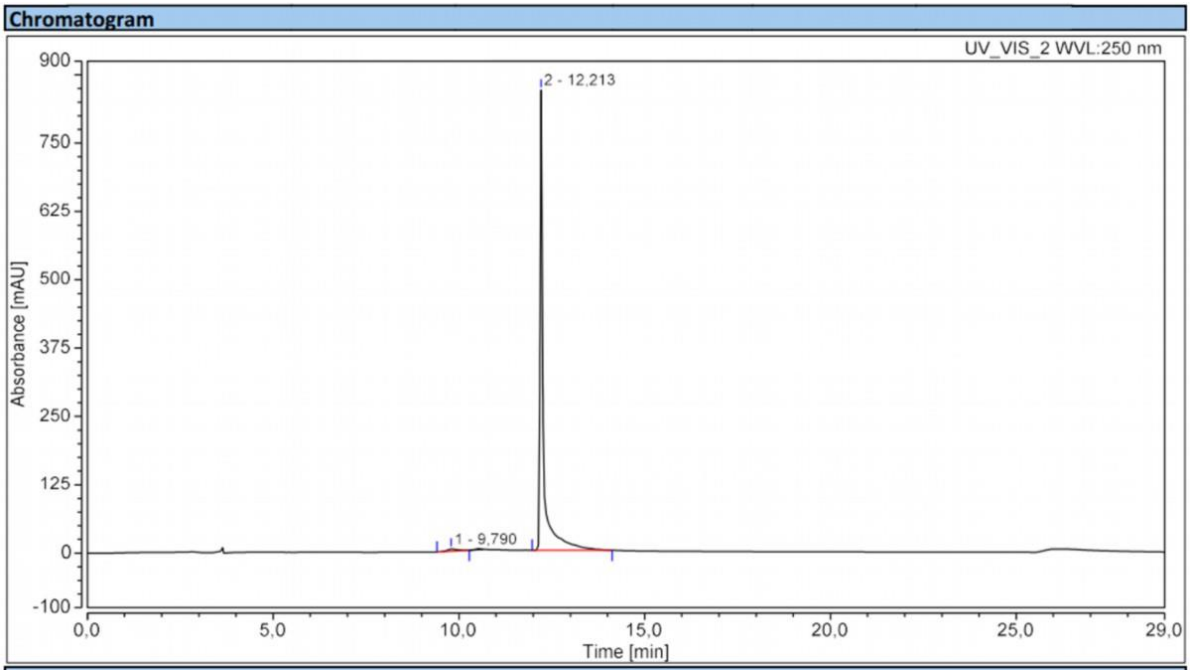

Integration Results

No.	Peak Name	Retention Time min	Area mAU*min	Height mAU	Relative Area %	Relative Height %	Amount n.a.
1		9,790	1,333	3,861	1,45	0,46	n.a.
2		12,213	90,849	841,878	98,55	99,54	n.a.
Total:			**92,183**	**845,739**	**100,00**	**100,00**	

HPLC chromatogram of **1b** (gradient A, purity: 98.6%).

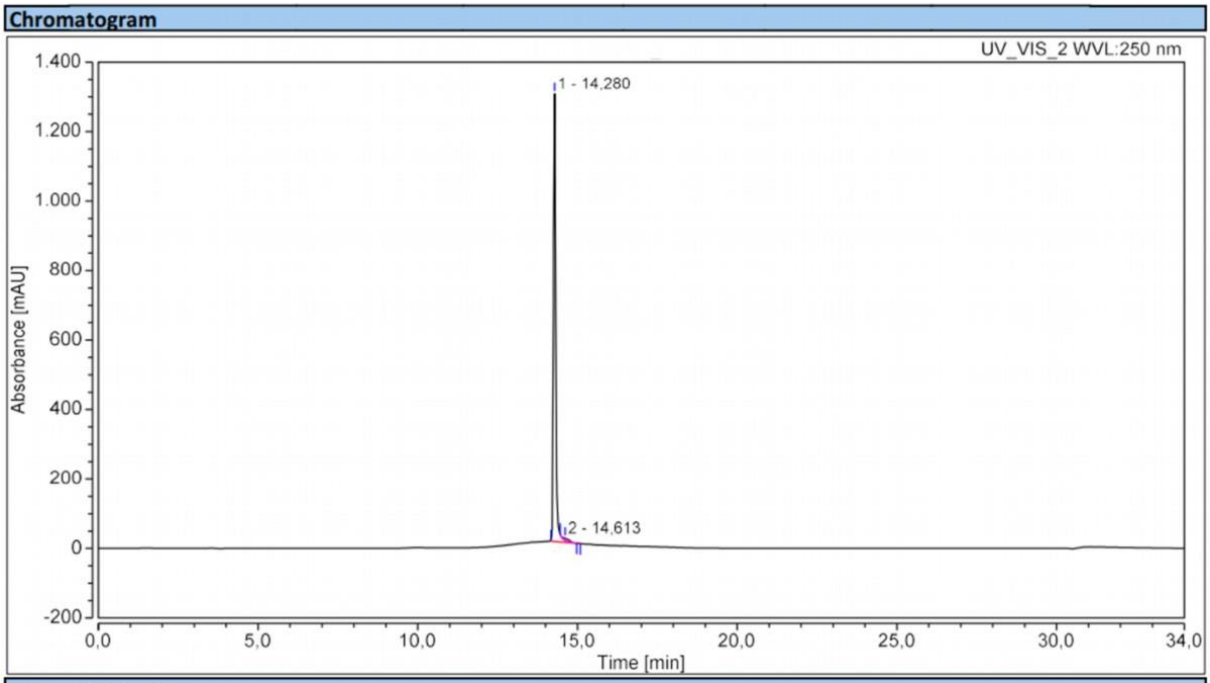

Integration Results

No.	Peak Name	Retention Time min	Area mAU*min	Height mAU	Relative Area %	Relative Height %	Amount n.a.
1		14,280	105,874	1289,525	98,54	99,40	n.a.
2		14,613	1,572	7,738	1,46	0,60	n.a.
Total:			**107,445**	**1297,263**	**100,00**	**100,00**	

HPLC chromatogram of **2a** (gradient B, purity: 98.5%).

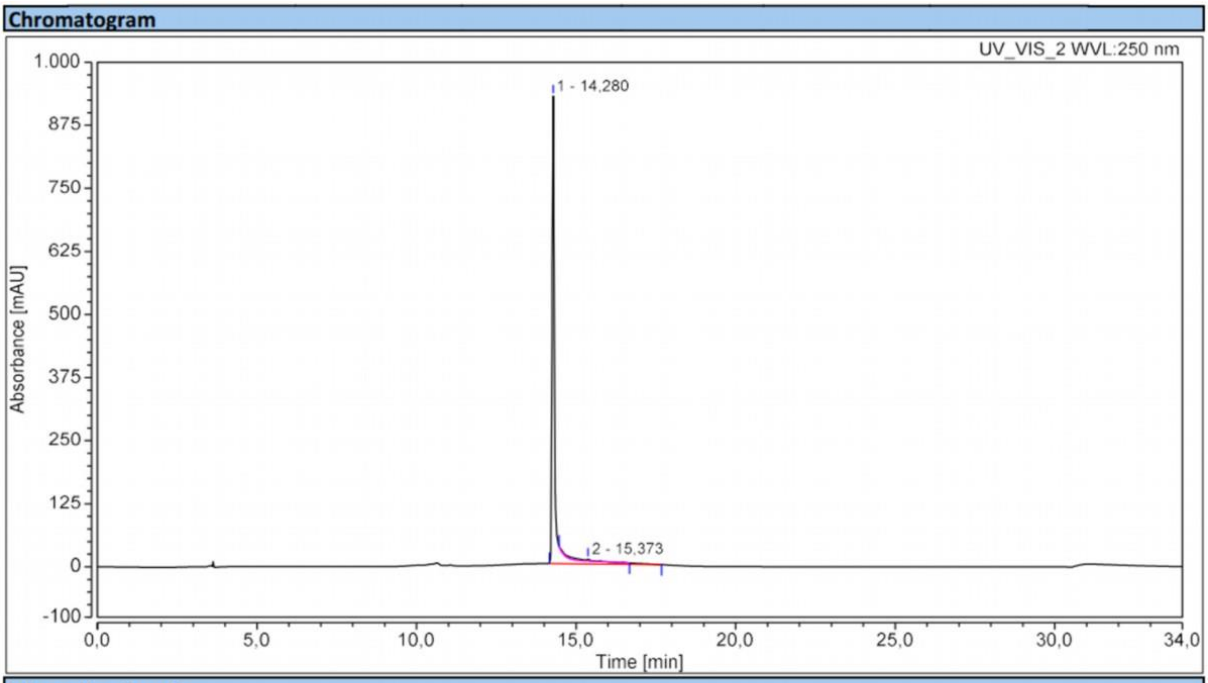

Integration Results

No.	Peak Name	Retention Time min	Area mAU*min	Height mAU	Relative Area %	Relative Height %	Amount n.a.
1		14,280	91,480	926,837	96,68	99,55	n.a.
2		15,373	3,146	4,174	3,32	0,45	n.a.
Total:			**94,626**	**931,011**	**100,00**	**100,00**	

HPLC chromatogram of **2b** (gradient B, purity: 96.7%).

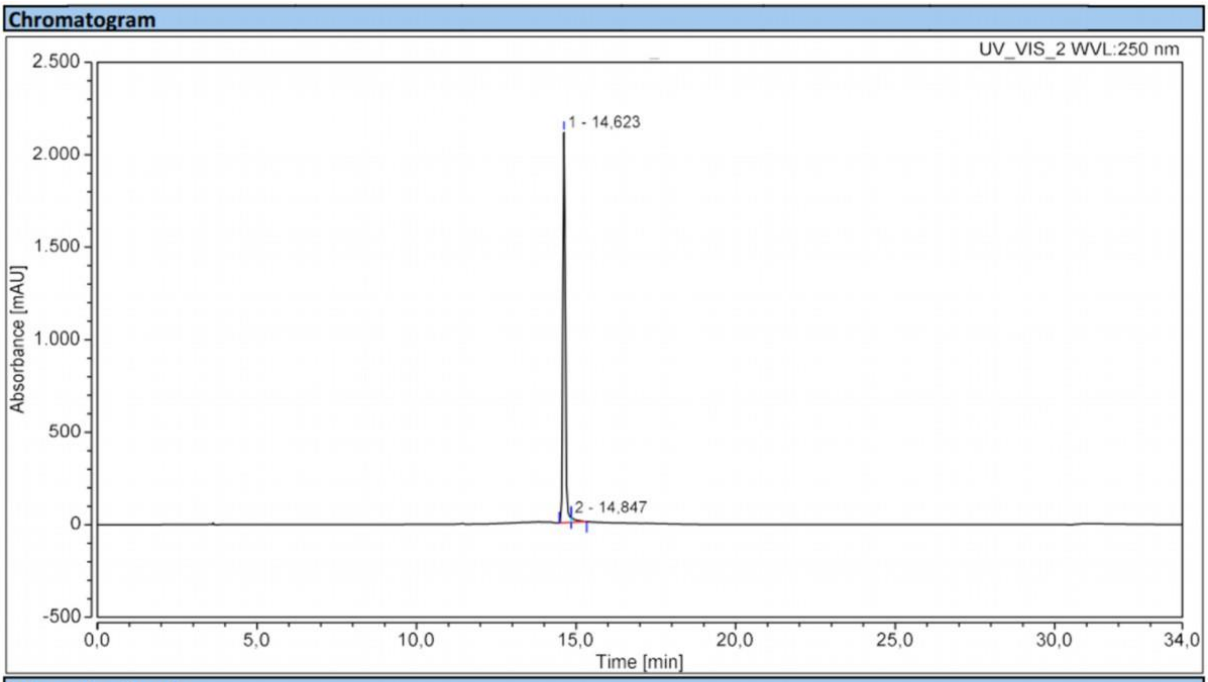

Integration Results

No.	Peak Name	Retention Time min	Area mAU*min	Height mAU	Relative Area %	Relative Height %	Amount n.a.
1		14,623	181,519	2108,619	97,73	98,83	n.a.
2		14,847	4,225	24,903	2,27	1,17	n.a.
Total:			**185,744**	**2133,523**	**100,00**	**100,00**	

HPLC chromatogram of **2c** (gradient B, purity: 97.7%).

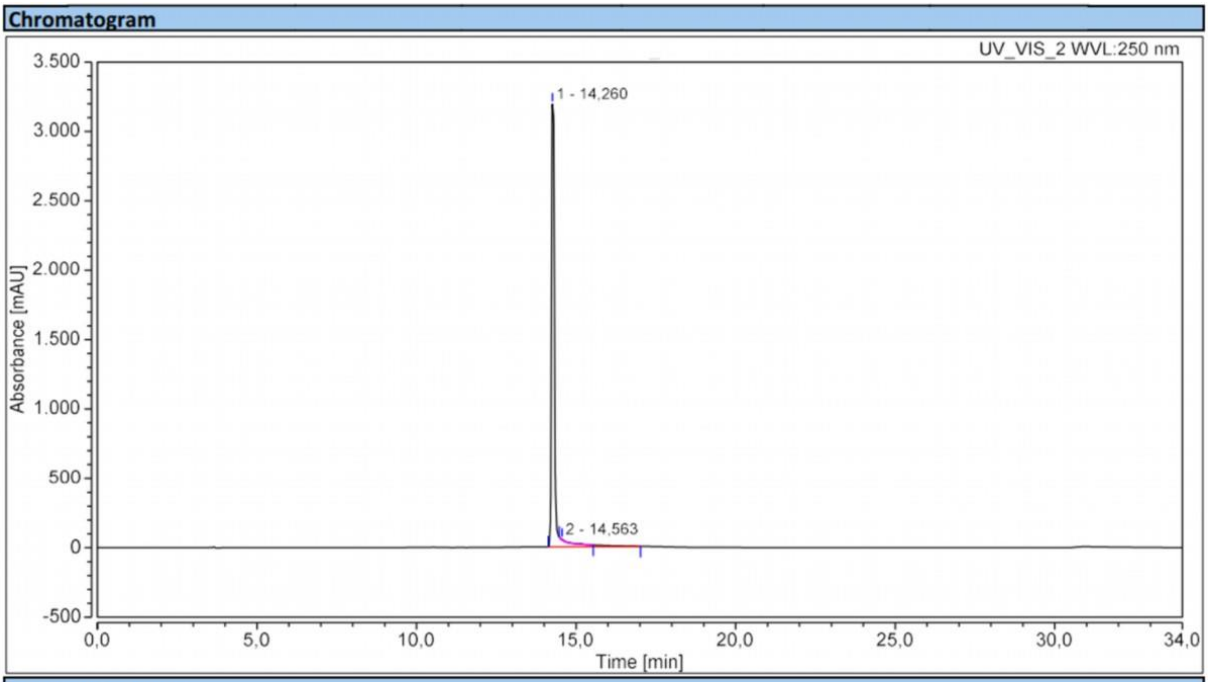

Integration Results

No.	Peak Name	Retention Time min	Area mAU*min	Height mAU	Relative Area %	Relative Height %	Amount n.a.
1		14,260	381,742	3189,003	99,44	99,84	n.a.
2		14,563	2,135	5,009	0,56	0,16	n.a.
Total:			**383,878**	**3194,012**	**100,00**	**100,00**	

HPLC chromatogram of **2d** (gradient B, purity: 99.4%).

Chromatogram

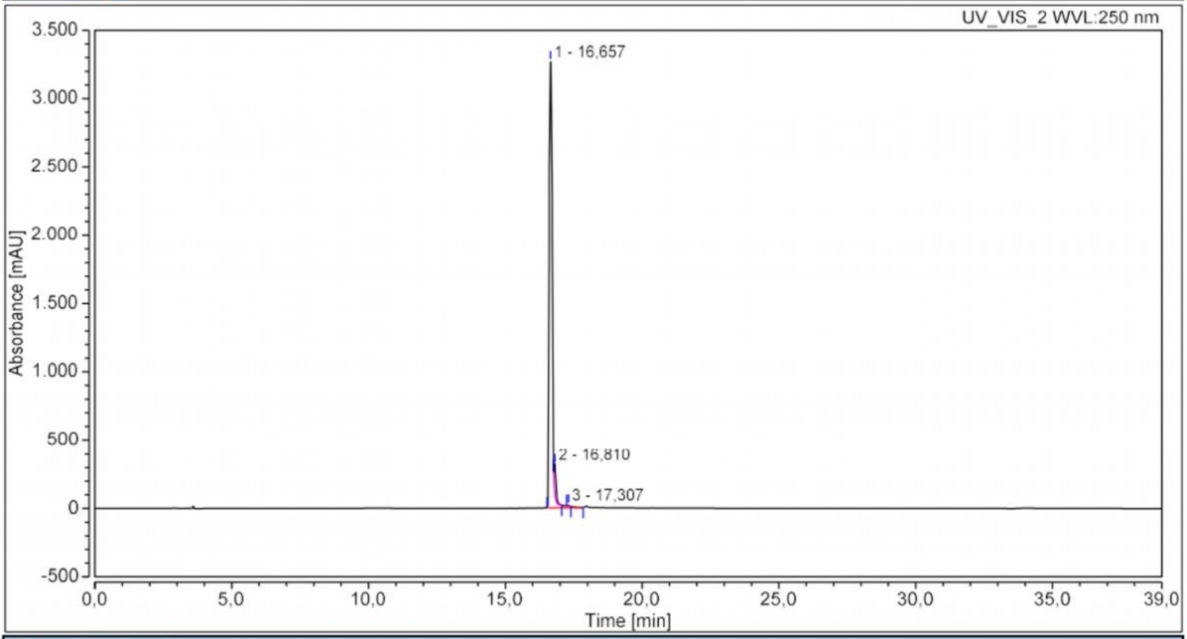

Integration Results

No.	Peak Name	Retention Time min	Area mAU*min	Height mAU	Relative Area %	Relative Height %	Amount n.a.
1		16,657	441,604	3263,437	96,53	93,87	n.a.
2		16,810	15,265	205,439	3,34	5,91	n.a.
3		17,307	0,603	7,589	0,13	0,22	n.a.
Total:			**457,472**	**3476,465**	**100,00**	**100,00**	

HPLC chromatogram of **2e** (gradient C, purity: 96.5%).

Chromatogram

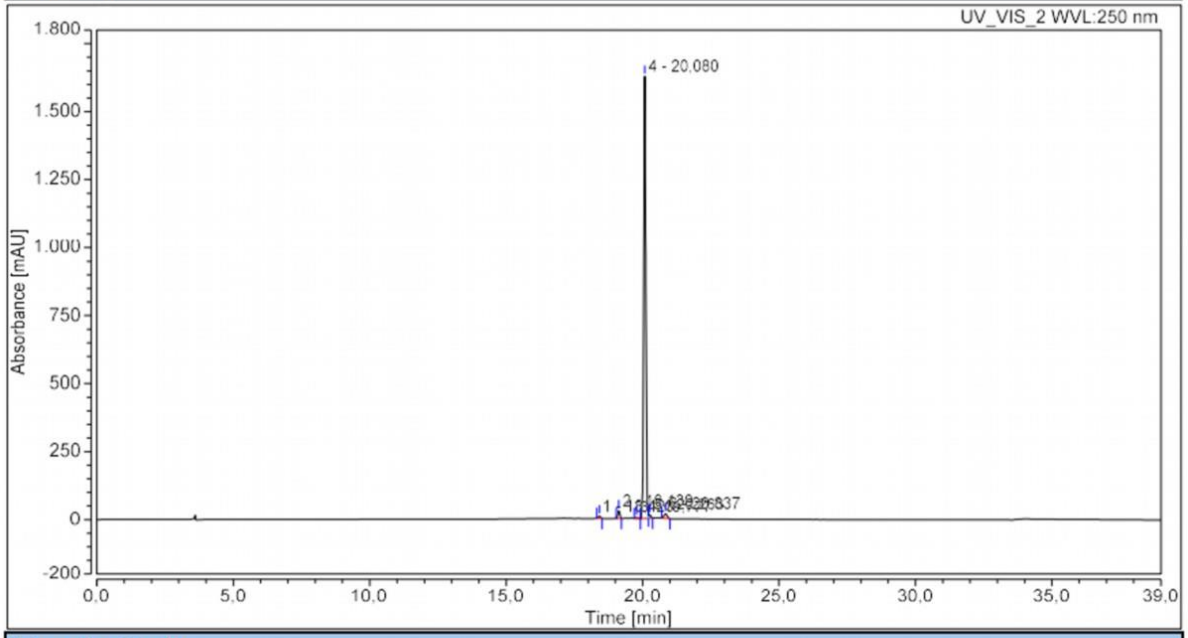

Integration Results

No.	Peak Name	Retention Time min	Area mAU*min	Height mAU	Relative Area %	Relative Height %	Amount n.a.
1		18,423	0,763	9,405	0,51	0,55	n.a.
2		19,130	2,082	28,717	1,39	1,69	n.a.
3		19,777	0,506	4,587	0,34	0,27	n.a.
4		20,080	143,235	1625,557	95,52	95,62	n.a.
5		20,263	1,125	13,491	0,75	0,79	n.a.
6		20,837	2,239	18,272	1,49	1,07	n.a.
Total:			**149,950**	**1700,028**	**100,00**	**100,00**	

HPLC chromatogram of **2f** (gradient C, purity: 95.5%).

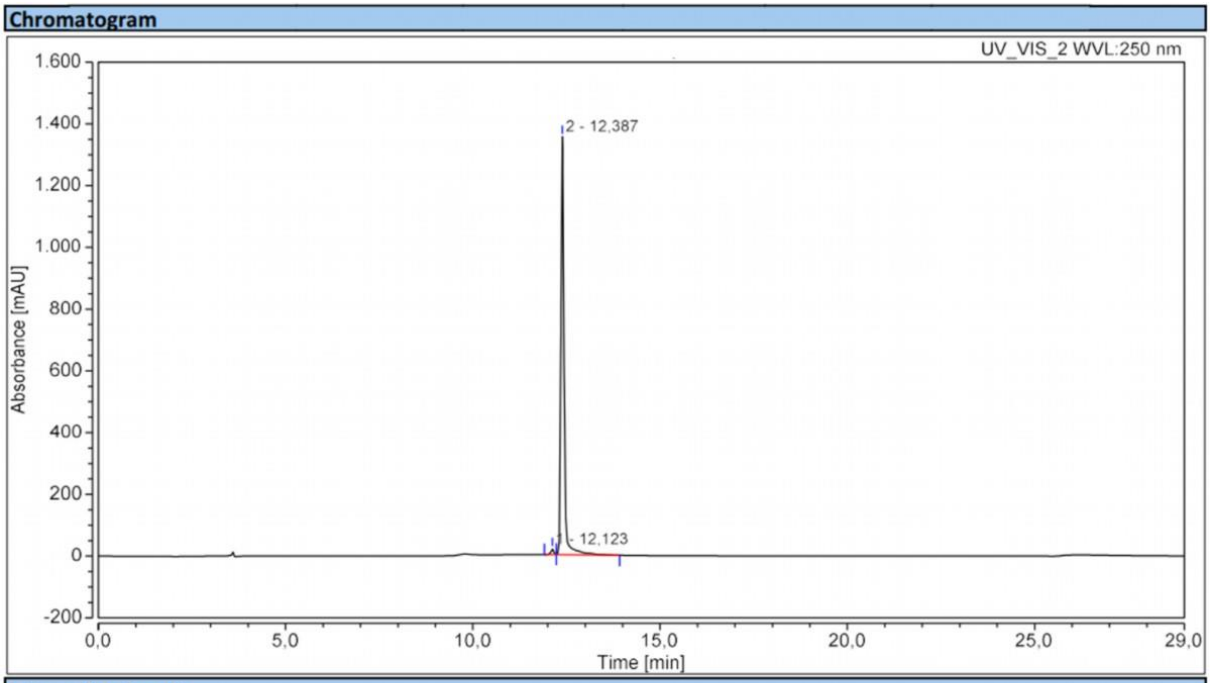

Integration Results

No.	Peak Name	Retention Time min	Area mAU*min	Height mAU	Relative Area %	Relative Height %	Amount n.a.
1		12,123	1,663	18,760	1,22	1,37	n.a.
2		12,387	134,084	1354,573	98,78	98,63	n.a.
Total:			**135,747**	**1373,332**	**100,00**	**100,00**	

HPLC chromatogram of **3a** (gradient A, purity: 98.8%).

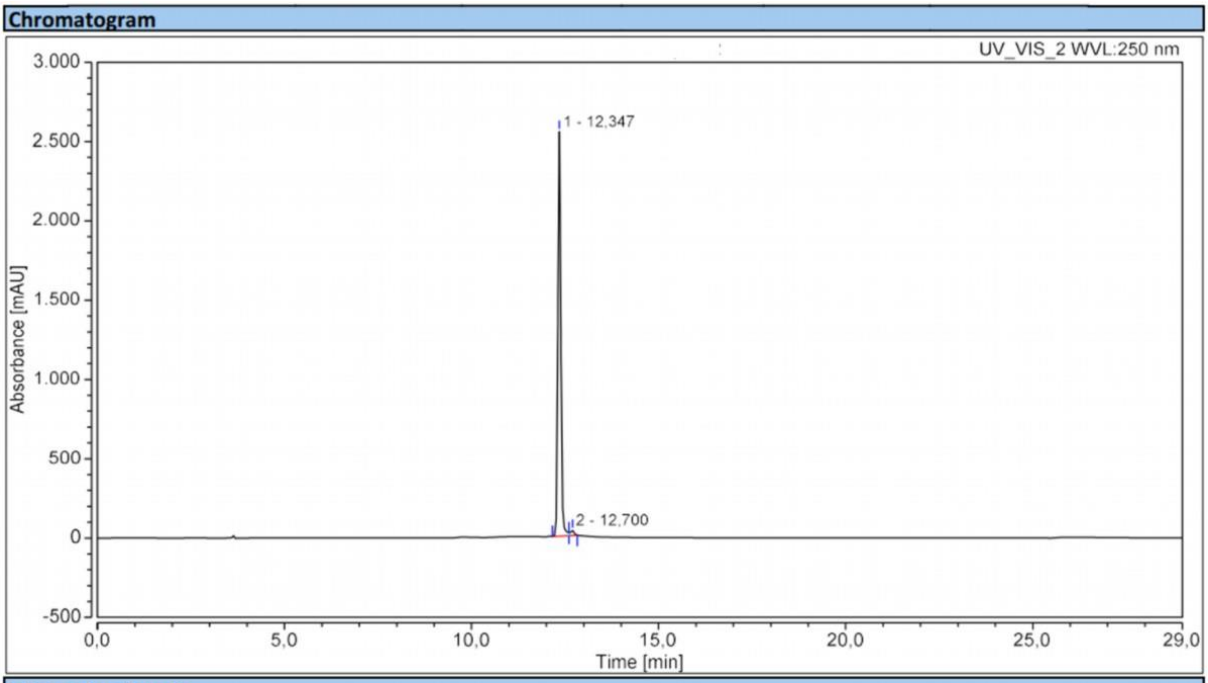

Integration Results

No.	Peak Name	Retention Time min	Area mAU*min	Height mAU	Relative Area %	Relative Height %	Amount n.a.
1		12,347	235,619	2550,242	98,43	98,79	n.a.
2		12,700	3,764	31,116	1,57	1,21	n.a.
Total:			**239,383**	**2581,358**	**100,00**	**100,00**	

HPLC chromatogram of **3b** (gradient A, purity: 98.4%).

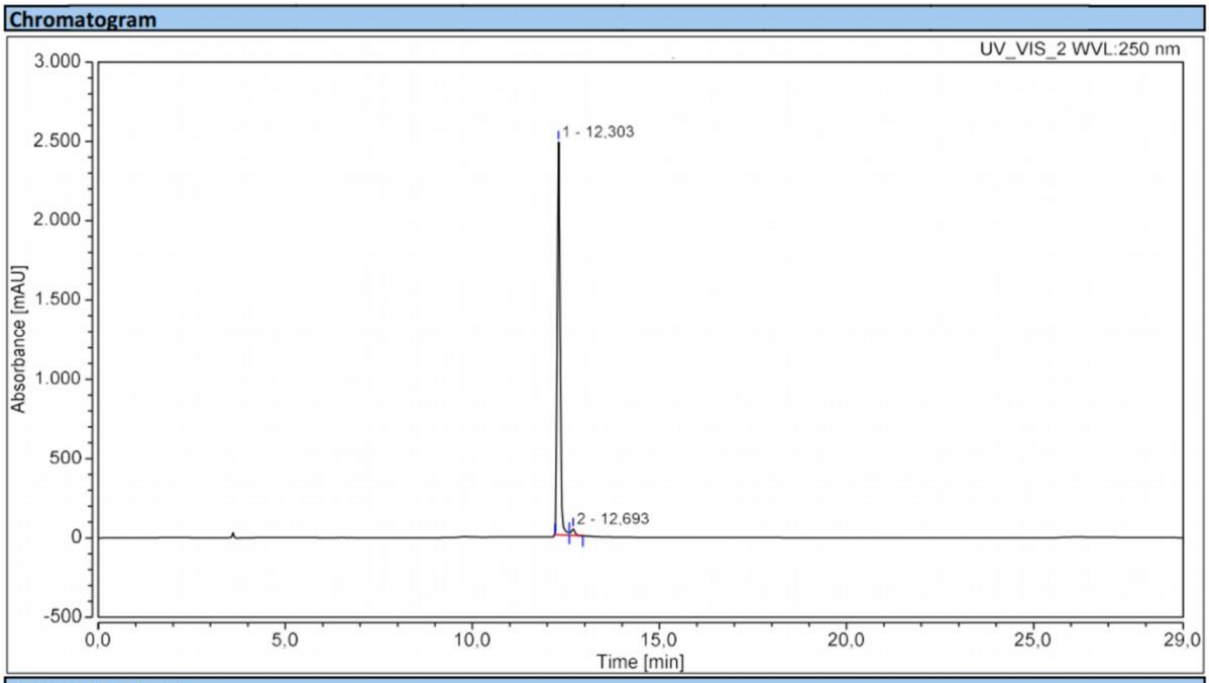

Integration Results

No.	Peak Name	Retention Time min	Area mAU*min	Height mAU	Relative Area %	Relative Height %	Amount n.a.
1		12,303	221,518	2476,576	97,84	98,38	n.a.
2		12,693	4,888	40,825	2,16	1,62	n.a.
Total:			**226,406**	**2517,402**	**100,00**	**100,00**	

HPLC chromatogram of **3c** (gradient A, purity: 97.8%).

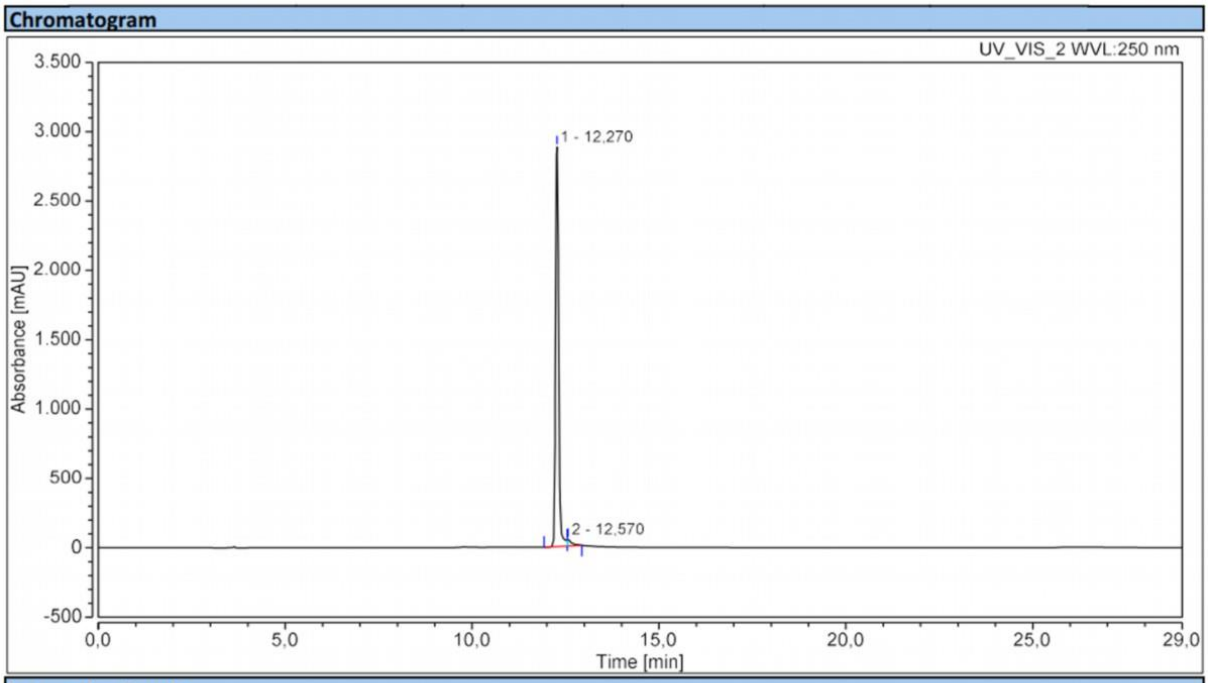

Integration Results

No.	Peak Name	Retention Time min	Area mAU*min	Height mAU	Relative Area %	Relative Height %	Amount n.a.
1		12,270	282,270	2881,157	97,75	98,35	n.a.
2		12,570	6,511	48,469	2,25	1,65	n.a.
Total:			**288,781**	**2929,625**	**100,00**	**100,00**	

HPLC chromatogram of **3d** (gradient A, purity: 97.8%).

5. References

1 Lauffer, B. E. L.; Mintzer, R.; Fong, R.; Mukund, S.; Tam, C.; Zilberleyb, I.; Flicke, B.; Ritscher, A.; Fedorowicz, G.; Vallero, R.; Ortwine, D. F.; Gunzner, J.; Modrusan, Z.; Neumann, L.; Koth, C. M.; Lupardus, P. J.; Kaminker, J. S.; Heise, C. E.; Steiner, P. Histone Deacetylase (HDAC) Inhibitor Kinetic Rate Constants Correlate with Cellular Histone Acetylation but Not Transcription and Cell Viability. *J. Biol. Chem.* **2013**, *288*, 26926–26943.

2 Morris, G. M.; Huey, R.; Lindstrom, W.; Sanner, M. F.; Belew, R. K.; Goodsell, D. S.; Olson, A. J. AutoDock4 and AutoDockTools4: Automated docking with selective receptor flexibility. *J. Comput. Chem.* **2009**, *30*, 2785–2791.

3 Wambua, M. K.; Nalawansha, D. A.; Negmeldin, A. T.; Pflum, M. K. H. Mutagenesis Studies of the 14 Å Internal Cavity of Histone Deacetylase 1: Insights toward the Acetate-Escape Hypothesis and Selective Inhibitor Design. *J. Med. Chem.* **2014**, *57*, 642–650.

4 Ciossek, T.; Julius, H.; Wieland, H.; Maier, T.; Beckers, T. A homogeneous cellular histone deacetylase assay suitable for compound profiling and robotic screening. *Anal. Biochem.* **2008**, *372*, 72–81.

5 Bonfils, C.; Kalita, A.; Dubay, M.; Siu, L. L.; Carducci, M. A.; Reid, G.; Martell, R. E.; Besterman, J. M.; Li, Z. Evaluation of the Pharmacodynamic Effects of MGCD0103 from Preclinical Models to Human Using a Novel HDAC Enzyme Assay. *Clin. Cancer Res.* **2008**, *14*, 3441–3449.

6 Schäker-Hübner, L.; Warstat, R.; Ahlert, H.; Mishra, P.; Kraft, F. B.; Schliehe-Diecks, J.; Schöler, A.; Borkhardt, A.; Breit, B.; Bhatia, S.; Hügle, M.; Günther, S.; Hansen, F. K. 4-Acyl Pyrrole Capped HDAC Inhibitors: A New Scaffold for Hybrid Inhibitors of BET Proteins and Histone Deacetylases as Antileukemia Drug Leads. *J. Med. Chem.* **2021**, *64*, 14620–14646.

7 Reßing, N.; Schliehe-Diecks, J.; Watson, P. R.; Sönnichsen, M.; Cragin, A. D.; Schöler, A.;Yang, J.; Schäker-Hübner, L.; Borkhardt, A.; Christianson, D. W.; Bhatia, S.; Hansen, F. K. Development of Fluorinated Peptoid-Based Histone Deacetylase (HDAC) Inhibitors for Therapy-Resistant Acute Leukemia. *J. Med. Chem.* **2022**, *65*, 15457–15472.

8 Kraft, F. B.; Hanl, M.; Feller, F.; Schäker-Hübner, L.; Hansen, F. K. Photocaged Histone Deacetylase Inhibitors as Prodrugs in Targeted Cancer Therapy. *Pharmaceuticals,* **2023**, *16*, 356.

9 Sinatra, L.; Bandolik, J. J.; Roatsch, M.; Sönnichsen, M.; Schoeder, C. T.; Hamacher, A.; Schöler, A.; Borkhardt, A.; Meiler, J.; Bhatia, S.; Kassack, M. U.; Hansen, F. K. Hydroxamic Acids Immobilized on Resins (HAIRs): Synthesis of Dual-Targeting HDAC Inhibitors and HDAC Degraders (PROTACs). *Angew. Chemie Int. Ed.* **2020**, *59*, 22494–22499.

Danksagung

Bei der Erstellung dieser Arbeit haben mich viele Menschen unterstützt und begleitet, denen ich von Herzen danken möchte. Zuallererst gilt mein besonderer Dank meinem Betreuer und Erstgutachter Prof. Dr. Finn K. Hansen für die Überlassung dieses spannenden Forschungsthemas, die hervorragende Betreuung, das entgegengebrachte Vertrauen, die Entsendung zu großartigen Konferenzen sowie den stets persönlichen und wertschätzenden Umgang.

Mein Dank gilt außerdem Prof. Dr. Gerd Bendas für die Übernahme des Zweitgutachtens und die freundliche Zusammenarbeit, sei es bei der Nutzung der gemeinsamen Labore oder bei den Treffen der beiden Arbeitskreise. Ebenso bedanke ich mich bei Prof. Dr. Martin Baunach für die Leitung der Promotionskommission sowie bei Prof. Dr. Maja Köhn für die Teilnahme als weiteres Mitglied der Kommission.

Ein herzliches Dankeschön richte ich an meine Mitautor*innen für ihren Beitrag zu den Publikationen und den bereichernden wissenschaftlichen Austausch. Darüber hinaus möchte ich allen Mitgliedern des Arbeitskreises Hansen danken, für das kollegiale, freundschaftliche und stets von gegenseitiger Unterstützung geprägte Miteinander. Ich danke euch für die gemeinsamen Kartenspiele in der Mittagspause, den Mensa-Mittwoch und den Blauen-Donnerstag. Ein besonderer Dank geht an Dr. Daniel Stopper, Dr. Beate König, Dr. Fabian Kraft und Dr. Kathrin Tan für den gemeinsamen Aufbau des Arbeitskreises, die inhaltliche wie praktische Unterstützung und die vielen geteilten Erlebnisse, die mir in bester Erinnerung bleiben werden.

Mein Dank gilt ebenfalls Dr. Kathrin Tan und Dr. Linda Schäker-Hübner für die gemeinsame Leitung der Instrumentellen Analytik als Doppel- bzw. Trippelspitze, sowie den bereichernden Austausch, der mir in Zukunft sehr fehlen wird. Den Assistent*innen der Arzneibuchanalytik sowie der Instrumentellen Analytik, besonders Irina Honin und Katrin Nekipelov, danke ich für die vielen gemeinsamen Stunden bei der Betreuung der Praktika.

Ich bedanke mich bei allen Mitreisenden zu den nationalen und internationalen Konferenzen, die für mich unvergessliche und inspirierende Erlebnisse waren. Mein Dank gilt auch allen Mitgliedern des Arbeitskreises Bendas für die gute Stimmung im Labor, die gemeinsamen Mittagessen, Weinwanderungen und all die anderen Momente, die meine Zeit hier bereichert haben.

Ein besonderer Dank geht an die technischen Mitarbeiter*innen Iris Jusen, Dieter Baumert und Svenja Hezel, die mich vor allem bei organisatorischen Fragen stets unterstützt haben. Ein herzliches Dankeschön an Svenja auch für die gemeinsame Zeit und Unterstützung im Blot-Labor.

Ich danke der Bonn International Graduate School of Drug Sciences (BIGS DrugS) für die finanzielle Unterstützung und meiner BIGS-Klasse für die spannenden und unterhaltsamen gemeinsamen Stunden. Ebenso bedanke ich mich bei meinen langjährigen Bürokollegen Silas Wurnig für die gemeinsame Zeit im Büro.

Mein tiefster Dank gilt schließlich meiner Familie, allen voran meiner Frau Fenja Feller. Ohne eure beständige Unterstützung und Geduld wäre diese Arbeit nicht möglich gewesen. Sie hat es mir erst ermöglicht diese Promotion zu wagen, und mich auf diesem Weg in jeder Hinsicht begleitet.